

Towards superior cancer drugs by modeling approaches:
Modification and prediction of the mode of action

by

Mahshad Moshari

A thesis submitted in partial fulfillment of the requirements for the degree of

Doctor of Philosophy

Department of Chemistry
University of Alberta

© Mahshad Moshari, 2021

Abstract

Cancer is a leading cause of death that imposes significant economic and social suffering on a global scale. Based on the projected growth and aging of populations, the global burden of cancer is set to increase. Despite the vast investment in cancer research, the rate of translation of research developments into clinical practice and drug discovery is still low, mainly because drug development is a lengthy, expensive, and complicated process. Computer-aided, *in silico*, drug discovery is a powerful technology that offers a more effective, cheaper, and faster alternative for drug design. Based on the known structure of biomacromolecules and small targeting molecules, computational methods employ virtual screening techniques for a broad range of applications, from hit identification to lead optimization, and to drug target prediction.

In terms of cancer research, microtubules are a key component of anti-cancer drug design approaches. Microtubule dynamics play a critical role during cell division making these biopolymers and their subunits superb targets for anti-cancer therapy. Diverse chemotherapeutic agents with the potential to target microtubules are currently among the most effective group of anticancer drugs available. Colchicine is an effective anti-mitotic drug that tightly binds between α , β tubulins and inhibits their assembly into microtubules; however, its application as an anti-cancer drug is limited due to its serious drug interactions and toxicity. Regardless,

colchicine, due to its effective antiproliferation activity, has been used as a lead compound to generate potential chemotherapeutic drugs with desired pharmacological profiles.

In this thesis, several computational techniques including *ab initio* quantum chemistry calculations, molecular docking, and virtual screening were employed to identify libraries of colchicine derivatives with highest binding affinities towards β tubulin. Good R^2 values of linear regression between the binding affinities and IC_{50} values of compounds against different human cancer cell lines including breast cancer (MCF7), lung carcinoma (A549), and colon cancer (LoVo) were achieved.

Computational studies on the novel derivatives were conducted on different groups of colchicine analogues including a group of double-modified 4-halothiocolchicines derivatives, a series of triple-modified 4-chloro-7-carbamatethiocolchicines, 4-bromothiocolchicine, and 4-chlorothiocolchicine analogues. A library of double-modified carbamate or thiocarbamate derivatives of 10-demethoxy-10-methylaminocolchicine, 7-deacetyl-10-thiocolchicine, and 4-iodo-7-deacetyl-10-thiocolchicine were also studied.

Moreover, a 3D QSAR model was generated that has the ability to predict the IC_{50} values for 70 novel derivatives of colchicine based on their binding affinities. The IC_{50} values of these colchicine analogues were predicted against two commonly-used cell lines including MCF7 and A549. The chemical structure of a library of 50

new compounds and their corresponding *in vitro* activities (IC₅₀ values) were used as input data to construct two models for the cell lines mentioned above. The input data was split into training and test sets using a Kohonen map. External independent validation was done using 15 independent compounds. Docking was used to estimate the binding and electrostatic energies between the colchicine derivatives library and β II tubulin. The identified estimates were used as two novel descriptors. The models were generated using a commonly used Artificial Neural Network. The generated QSAR models showed good performance on the test set for both A549 and MCF7 cancer cell lines (assessed through the high values of q^2 and R^2). Besides, it was shown that these models had predictive ability and desired generalization on the independent validation set of compounds.

In an effort to discover new chemotherapeutic agents, the mode of action of a novel microtubule inhibitor scoulerine, was evaluated using a combination of computational approaches. To the best of our knowledge, this is the first time that the computational prediction and experimental validation of the molecular mode of action of scoulerine as a potential anticancer drug was investigated. Human tubulin structures at both free and microtubule states were modeled. Docking of the optimized structure of scoulerine was subsequently performed and the highest affinity binding sites located in both the free tubulin and in a microtubule were identified. Our findings show that binding in the vicinity of the colchicine binding

site and near the laulimalide binding site are the most likely locations for scoulerine. These computational predictions were confirmed by thermophoresis assays using scoulerine and tubulin in both free and polymerized form. These results suggest a unique property of a dual mode of action for scoulerine with both microtubule stabilization and tubulin polymerization inhibition ability.

Preface

This Thesis contains material that has been previously published by Mahshad Moshari and supervisors M. Klobukowski and J.A. Tuszynski.

Chapter 2 of the thesis has been published as research article as G. Klejborowska, A. Urbaniak, E. Maj, J. Wietrzyk, M. Moshari, J. Preto, J. A. Tuszynski, T. C. Chambers, and A. Huczyński. 2021. Synthesis, anticancer activity and molecular docking studies of N-deacetylthiocolchicine and 4-iodo-N-deacetylthiocolchicine derivatives. *Bioorg. Med. Chem.* 32, (February 2021), 116014. Published by Elsevier Ltd. All rights reserved. I was in charge of the entire computational aspect of the project, which included *ab initio* quantum chemistry computations, molecular docking, and analysis. I also wrote the computational part of the manuscript. G. Klejborowska, A. Urbaniak, E. Maj, and J. Wietrzyk were responsible for the chemical synthesis of new analogues as well as their biological characterization. All the mentioned writers contributed to the development of the manuscript. J.A Tuszynski, T. C Chambers, and A. Huczyński were the supervisory authors. A. Huczyński also designed the project and is the corresponding author.

Chapter 3 has been published as research article as U. Majcher, G. Klejborowska, M. Moshari, E. Maj, J. Wietrzyk, F. Bartl, J. A. Tuszynski, and A. Huczyński, 2018. Antiproliferative Activity and Molecular Docking of Novel Double-Modified Colchicine Derivatives. *Cells* 7, 11, 192. Published by MDPI. All rights reserved. I performed all *ab initio* quantum chemistry computations, molecular docking and analyzed the results. I also wrote the computational part of the manuscript. Urszula Majcher and Greta Klejborowska worked on the chemical synthesis of new analogues and E. Maj, J. Wietrzyk, F. Bartl carried out the biological characterization of the compounds. All these authors contributed to draft the manuscript. J.A

Tuszynski, and A. Huczyński were the supervisory authors. A. Huczyński also designed the project and is the corresponding author.

Chapter 4 has been published as research article as G. Klejborowska, M. Moshari, E. Maj, U. Majcher, J. Preto, J. Wietrzyk, J. A. Tuszynski, and A. Huczyński, 2020. Synthesis, antiproliferative activity, and molecular docking studies of 4-chlorothiocolchicine analogues. *Chem. Biol. Drug Des.* 95, 1, 182–191. Published by John Wiley & Sons, Inc. All rights reserved. I carried out *ab initio* quantum chemistry computations and molecular docking calculations. J. Preto generated the raw data of MM/GBSA and MM/PBSA binding free energies of the compounds. All of the computational analysis and results discussions were performed by me. I also wrote the computational part of the manuscript. G. Klejborowska and U. Majcher synthesized the library of chemical analogues and E. Maj administered the biological characterization of the compounds. All of these authors contributed to the draft of the manuscript. J. Wietrzyk, J.A. Tuszynski, and A. Huczyński were the supervisory authors. A. Huczyński also designed the project and is the corresponding author.

Chapter 5 was published as research article as U. Majcher , G. Klejborowska , M. Kaik , E. Maj , J. Wietrzyk, M. Moshari , J. Preto, J. A. Tuszynski , and A. Huczyński, 2018. Synthesis and Biological Evaluation of Novel Triple-Modified Colchicine Derivatives as Potent Tubulin-Targeting Anticancer Agents. *Cells* 7, 11, 216. Published by MDPI. All rights reserved. I carried out *ab initio* quantum chemistry computations and molecular docking calculations. J. Preto generated the raw data of MM/GBSA and MM/PBSA binding free energies of the compounds. All of the computational analysis and results discussions were performed by me. I also wrote the computational part of the manuscript. U. Majcher and G. Klejborowska, M. Kaik , E. Maj, and J. Wietrzyk synthesized the library of chemical analogues and E. Maj administered the biological characterization of the compounds. All of these authors contributed to the draft of the manuscript. J.A. Tuszynski, and A. Huczyński were

the supervisory authors. A. Huczyński also designed the project and is the corresponding author.

Chapter 6 has been published as research article as U. Majcher, A. Urbaniak, E. Maj, M. Moshari, M. Delgado, J. Wietrzyk, F. Bartl, T. C Chambers, J. A Tuszynski, and A. Huczyński, 2018. Synthesis, antiproliferative activity and molecular docking of thiocolchicine urethanes. *Bioorg. Chem.* 81, 553–566. Published by Elsevier Ltd. All rights reserved. I was in charge of the entire computational aspect of the project, which included *ab initio* quantum chemistry computations, molecular docking, and analysis. A. Urbaniak, E. Maj, M. Delgado, J. Wietrzyk, and F. Bartl were responsible for the chemical synthesis of new analogues as well as their biological characterization. All the mentioned writers contributed to the development of the manuscript. T. C Chambers, J. A. Tuszynski, and A. Huczyński were the supervisory authors. A. Huczyński also designed the project and is the corresponding author.

Chapter 7 of the thesis was written in research article format entitled: Prediction of the inhibitory concentrations of colchicine derivatives for specific cancer cell lines by 3D quantitative structure-activity relationship (QSAR) modelling. The paper is submitted and is under review. The authors of the paper include M. Moshari, L. Pallante, E. A. Zizzi, M. A. Deriu, G. Klejborowska, A. Huczynski, M. Klobukowski, and J.A. Tuszynski. I was responsible for the project design, as well as computational work such as *ab initio* quantum chemistry calculations, and molecular docking. I also generated the theoretical input data (different properties of the colchicine derivatives) and 3QSAR models by ADMET predictor and modeler. I also wrote the manuscript. G. Klejborowska and A. Huczynski synthesized the library of the colchicine derivatives and provided the *in vitro* activities (IC₅₀ values) of the compounds. L. Pallante, E. A. Zizzi, and M. A. Deriu contributed with the editing of the manuscript. J.A Tuszynski and M. Klobukowski were the supervisory author and were responsible for project design, manuscript composition, and editing.

Chapter 8 of the thesis was written in research article format entitled: Computational prediction and experimental validation of the unique molecular mode of action of scoulerine. The paper is submitted. The authors of the paper include M. Moshari, Q. Wang, M. Michalak, M. Klobukowski and J. A. Tuszynski. I was in charge of the project design, as well as computational work such as *ab initio* quantum chemistry calculations, molecular docking, and molecular dynamic simulations. The analysis and writing of the manuscript also carried out by me. The supervisory authors, J.A. Tuszynski and M. Klobukowski designed the project and were involved in manuscript composition and editing.

To my Family

Acknowledgement

I would like to express my sincere gratitude to both my supervisors Dr. Jack Tuszynski and Dr. Mariusz Klobukowski for their advice, guidance, and encouragement throughout this work. I am grateful for their insightful comments and suggestions throughout my Ph.D. program. I also will be forever thankful to them for their heart-warming unconditional support for me as a mom-student during the pandemic. Dr. Klobukowski, you are exceptionally kind and insightful, and a brilliant scientist and a teacher. My Ph.D. program was a considerable journey from illness to a pandemic and I have to admit your words of encouragement and support were sometimes the only ones that helped me overcome obstacles. Dr. Tuszynski, with no doubt you are one of the best scientists working in the field of computational calculations. Your mind and ideas always amaze me. Each of our brainstorming meetings was a testament to how lucky I am to find an opportunity to be in your group. Your knowledge, your collaborative spirit and your respect for their trainees are the best qualities that a mentor can have.

I would like to thank all the present and former friends and labmates in Tuszynski and Klobukowski group, Sara Omar, Sahar Arbabimoghadam, Philip Winter, Niloofar Nayebi, Holly Freeman, Francesco Gentile, Jordane Preto, Aarat Kalra, Douglas Friesen, Cassandra Churchill, Ahmed Ayoub, Megan Oakley, Dylan Hennessey, Miriam Van Hoeve and for their friendship and support and for making such a friendly, enjoyable, and supportive environment to be.

To My guardian angels, Maman Marjan and Baba Bijan, whoever I am and all that I accomplished is because of your fierce support and unconditional love. You gave me the happiest childhood that a person can imagine and now I am a parent who can understand how difficult it is and you make it look so easy and natural, thank you for leading me on the right path.

To My Mehdi, you are the reviewer of my articles, the editor of my thesis, my intelligent colleague, my best friend, my first and last love, and last but not least my rock! You are the definition of gender equality and unconditional love. You are an extraordinary team player and going through the journey of life with you is my blessing. May we grow old together.

To My Roham, you experience the pressure of the academic life in your sweet life more than most adults ever will experience. You lived in a house that your mom was getting ready for her candidacy and your dad was writing his thesis to defence.

You went to university as young as 10-month old. You have played in help rooms, offices, meeting rooms. I am sorry for disturbing your relaxing childhood by being busy all the time. I want to thank you for being patient with me, you are an incredible toddler. I will forever love you.

Table of Contents

Abstract.....	ii
Preface	vi
Acknowledgement	xi
List of Tables	xix
List of Figures.....	xxiv
Chapter 1: Introduction.....	1
1.1 Cancer.....	2
1.2 Microtubules.....	3
1.3 The cell cycle and mitosis	6
1.3.1 Cell division cycle.....	6
1.4 Mitosis.....	7
1.4.1 Drugs and cell cycle regulation.....	9
1.4.2 Anti-microtubular therapeutic agents.....	10
1.4.3 Laulimalide binding site	11
1.4.4 Colchicine binding site	12
1.5 Scope and computational methodology	15
1.6 References	16
Chapter 2: Synthesis, anticancer activity and molecular docking studies of <i>N</i>-deacetylthiocolchicine and 4-iodo-<i>N</i>-deacetylthiocolchicine derivatives.....	24
2.1 Introduction	25
2.2 Materials and methods	26
General	26
2.2.1 Spectroscopic measurements	26
2.2.2 Synthesis	27
Synthesis of thiocolchicine (2)	27
Synthesis of <i>N</i> -deacetylthiocolchicine (3).....	28
General procedure for the synthesis of colchicine derivatives (4–10).....	28
Synthesis of 4-iodocolchicine (11)	31
Synthesis of 4-iodothiocolchicine (12).....	32
Synthesis of 4-iododeacetylthiocolchicine (13).....	32
General procedure for the synthesis of colchicine derivatives (14–20).....	33
2.2.3 Cell lines and culturing conditions.....	36
2.2.4 Cell viability assays	37

SRB assay	37
MTT assay	38
2.2.5 DNA content analysis	40
2.2.6 Western blot analysis	40
2.2.7 Statistical analysis	41
2.2.8 Docking simulations	41
2.3 Results and discussion.....	42
2.3.1 Chemistry	42
2.3.2 <i>In vitro</i> cytotoxic activity evaluation	43
2.3.3 The effect of colchicine and its double- and triple-modified analogues on cell cycle progression in ALL-5 and MCF-7 cells.....	46
2.3.4 The effect of colchicine, double-modified analogue 7 and triple-modified analogue 17 on PARP cleavage in primary ALL-5 cells	49
2.3.5 Molecular docking	51
2.4 Conclusions	59
References	60
Chapter 3: Antiproliferative Activity and Molecular Docking of Novel Double-Modified Colchicine Derivatives.....	68
3.1 Introduction	69
3.2 Materials and Methods	70
3.2.1 General.....	70
3.2.2 Spectroscopic Measurements.....	71
3.2.3 Synthesis	72
Synthesis of 2	72
Synthesis of 3	73
Synthesis of 5	74
Synthesis of 7	75
3.2.4 Antiproliferative activity of colchicine and its derivatives	75
The antiproliferative assays <i>in vitro</i>	76
Sulforhodamine B assay (SRB).....	77
3.2.5 Molecular Docking Simulations	77
3.3 Results	78
3.3.1 Chemistry	78
3.3.2 <i>In vitro</i> Determination of Drug-Induced Inhibition of Human Cancer Cell Line Growth.....	79
3.3.3 Molecular Docking: <i>in Silico</i> Determination of Drug-Induced Inhibition of β I Tubulin	82
3.4 Discussion	88

References	91
Chapter 4: Synthesis, antiproliferative activity, and molecular docking studies of 4-chlorothiocolchicine analogues	98
4.1 Introduction	99
4.2 Results and discussion.....	101
4.2.1 Chemistry	101
4.2.2 Antiproliferative effect toward both human cancer cells and normal cells	101
4.2.3 Molecular docking: <i>in silico</i> determination of the molecular mode of action.....	104
4.3 Conclusions	112
References	113
Chapter 5: Synthesis and Biological Evaluation of Novel Triple-Modified Colchicine Derivatives as Potent Tubulin-Targeting Anticancer Agents.....	117
Introduction	117
5.1 Materials and Methods	119
5.1.1 General.....	119
5.1.2 Spectroscopic Measurements	120
5.1.3 Synthesis	121
Synthesis of 2	121
Synthesis of 3	122
Synthesis of 4	123
5.1.4 General Procedure for the Synthesis of Colchicine Derivatives (5–12)	124
Compound 5	124
Compound 6	125
Compound 7	126
Compound 8	126
Compound 9	127
Compound 10	128
Compound 11	129
Compound 12	129
5.1.5 Antiproliferative Activity of Colchicine and Its Derivatives	130
5.1.6 The Antiproliferative Assays <i>In vitro</i>	131
SRB.....	132
5.1.7 Molecular Docking Simulations	133
5.2 Results	133
5.2.1 Chemistry	133

5.2.2 <i>In vitro</i> Determination of Drug-Induced Inhibition of Human Cancer Cell Line Growth.....	135
5.2.3 Molecular Docking: <i>In Silico</i> Determination of Drug-Induced Inhibition of β I Tubulin	138
5.2.4 Linear regression with two independent variables.....	143
5.2.5 MM/PBSA and MM/GBSA: <i>In Silico</i> Determination of Drug-Induced Inhibition of β Tubulin Isotypes.....	145
5.2.6 Linear Regression with Two Independent Variables	150
5.3 Conclusions	152
References	154
Chapter 6: Synthesis, Antiproliferative Activity And Molecular Docking of Thiocolchicine Urethanes	160
Introduction	160
6.1 Experimental	163
6.1.1 General.....	163
6.1.2 Synthesis	164
General procedure for the synthesis of 7-deacetyl-10-thiocolchicine derivatives (4–14).....	164
Compound 4	164
Compound 5	165
Compound 6	165
Compound 7	166
Compound 8	166
Compound 9	167
Compound 10	167
Compound 11	167
Compound 12	168
Compound 13	168
Compound 14	169
6.1.3 Antiproliferative activity of colchicine and its derivatives	169
6.1.4 Molecular docking simulations.....	171
6.1.5 Flow cytometry and immunofluorescence microscopy	171
Cell cultures.....	171
6.1.6 Effects of the compounds on cell cycle progression.....	172
6.1.7 Statistical analysis.....	173
6.1.8 Immunofluorescence microscopy	174
6.2 Results and discussion.....	174
6.2.1 Chemistry.....	174

6.2.2 Inhibition of human cancer cell line growth	176
6.2.3 Molecular docking: <i>in silico</i> determination of the molecular mode of action.....	179
6.2.4 Colchicine and its analogs induce G ₂ /M arrest in MCF-7 cells	188
6.2.5 Effect of colchicine and compound 5 on microtubule depolymerization	191
6.3 Conclusions	191
References	193
Chapter 7: Prediction of the Inhibitory Concentrations of Colchicine Derivatives for Specific Cancer Cell Lines by 3D Quantitative Structure-Activity Relationship (QSAR) Modelling	198
7.1 Introduction	199
7.2 Materials and methods	203
7.2.1 Dataset collection.....	203
7.2.2 Docking.....	204
7.2.3 Descriptor Calculations.....	205
7.2.4 3-Dimensional Quantitative-Structure-Activity-Relationship Models	206
7.2.5 Statistical Evaluation/Validation of the Model	207
7.2.6 External Validation	208
7.3 Results and Discussion.....	209
7.3.1 3D-QSAR Model Development and Validation	209
7.3.2 External Validation	214
7.3.3 Regression Uncertainty	216
7.4 Conclusions	220
References	222
Chapter 8: Computational Prediction and Experimental Validation of the Unique Molecular Mode of Action of Scoulerine	227
Introduction	228
8.1 Materials and methods	230
8.1.1 3D structure preparation of the ligand.	230
8.1.2 Blind docking.....	230
8.1.3 3D structure preparation of complexes for MD simulation	231
Scoulerine in the colchicine binding.....	231
Scoulerine in the laulimalide binding sites of microtubule	231
8.1.4 Molecular dynamic simulation.....	232
8.1.5 Clustering analysis	232
8.1.6 Binding affinities and pose analysis of potential scoulerine binding sites	233

8.1.7 Microscale thermophoresis	235
8.2 Result and discussion	235
8.2.1 Protonated or deprotonated scoulerine in cancer cell	235
8.2.2 Analysis of potential scoulerine binding sites on β tubulin	236
8.2.3 Colchicine site.....	238
8.2.4 Potential scoulerine binding site (S_1).....	239
8.2.5 Conformational analysis	241
RMSD analysis on S_1 site	241
Clustering analysis.....	242
8.2.6 Laulimalide sites on β tubulin.....	245
8.2.7 Potential scoulerine binding site (S_2).....	246
8.2.8 Conformational analysis	248
RMSD analysis on scoulerine bound between protofilament (laulimalide binding sites).....	248
Clustering Analysis.....	250
Experimental validation.....	252
8.3 Conclusions	254
References	257
Chapter 9: Major conclusions	262
9.1 Conclusion.....	263
9.2 Future work	266
References.....	267
Appendix A.....	315
Appendix B.....	349
Appendix C.....	363
Appendix D.....	392
Appendix E.....	416

List of Tables

Table 2-1. Antiproliferative activity (IC_{50}) and resistance index (RI) values of colchicine (1) and its derivatives (2–20) compared with antiproliferative activity of standard anticancer drugs doxorubicin and cisplatin [32–35].	39
Table 2-2. Summary of the calculated binding energies for the interactions between β I tubulin and <i>N</i> -deacetylthiocolchicine and 4-iodo- <i>N</i> -deacetylthiocolchicine analogues, the values of compounds' Moriguchi octanol-water partition coefficient (MlogP), which have been investigated in this chapter. The active residues (residues interacting with each ligand <i>via</i> hydrogen bonding or π -interactions) in the binding pocket of β I tubulin are listed in the last column.	53
Table 2-3. Exemplary 3D representations of the interactions between β I tubulin, colchicine and its derivatives (7 and 17).	54
Table 2-4. 3D molecular electrostatic potential maps of compound 3 and 13 and 15 . The blue color represents negative charges and the red color represents positive charges.	57
Table 2-5. The docking binding free energy values for the ligand-tubulin complexes and the MlogP predicted values for the ligands are two independent variables in the linear regression calculations with $\log IC_{50}$ [nM] for different cancer cell lines. The bolded value indicates the highest linear regression values.	59
Table 3-1. Antiproliferative activity (IC_{50}) of colchicine (1) and its derivatives (2–8) compared with antiproliferative activity of standard anticancer drugs doxorubicin and cisplatin and the calculated values of the resistance index (RI) and selectivity index (SI) of tested compounds [19,43].	81
Table 3-2. Binding energies interactions between eight different colchicine derivatives and β I tubulin and the estimated Moriguchi octanol-water partition coefficient, MlogP for each colchicine derivative.	83

Table 3-3. Heat map of binding energies interactions between the eight different colchicine derivatives and β I, β III β IIa, β IIb, β IVa, β IVb, β V and β VI tubulin isotypes.....	86
Table 3-4. Binding energies interactions between compound 8 and β IIa and β VI tubulin as well as the estimated Moriguchi octanol-water partition coefficient, MlogP for compound 8	87
Table 4-1. Antiproliferative activity of colchicine and its derivatives (2-9) compared with antiproliferative activity of standard anticancer drugs doxorubicin and cisplatin.	102
Table 4-2. Summary of the calculated binding energies for the interactions between β I tubulin and 4-chlorothiocolchicine analogues, the compounds' molecular weights, the values of their Moriguchi octanol-water partition coefficient (MlogP), which have been investigated in this chapter. The active residues of the binding pocket of β I tubulin are listed in the last column.	107
Table 4-3. The docking binding free energy of ligands-tubulin and MlogP of the ligands are the two independent variables in linear regression that are correlated with log IC ₅₀ [μ M] in different cancer cell lines.	109
Table 4-4. Binding energies of novel colchicine derivative versus different tubulin isotypes were calculated by MM/PBSA and MM/GPSA methods.	111
Table 4-5. The MM/PBSA binding free energy of the ligand-tubulin complex and the values of the MlogP for the ligands are the two independent variables in our linear regression calculations that are obtained with respect to log IC ₅₀ [μ M] in different cancer cell lines.	111
Table 4-6. The MM/GBSA binding free energy of the ligand-tubulin complex and the values of the MlogP for the ligands are the two independent variables in our linear regression calculations that are obtained with respect to log IC ₅₀ [μ M] in different cancer cell lines.	111
Table 5-1. Antiproliferative activity of colchicine (1) and its derivatives (2–12) compared with antiproliferative activity of standard anticancer drugs doxorubicin and cisplatin and the calculated values of resistance index (RI) and selectivity index (SI) of tested compounds.	137

Table 5-2. Calculated binding energies for the interactions between the new colchicine derivatives investigated in this chapter and β I tubulin, and also the values of the Moriguchi octanol-water partition coefficient, MlogP, calculated for the same colchicine derivatives.	139
Table 5-3. Linear regressions involving two independent variables (the binding free energy obtained from the docking method and MlogP) of the investigated colchicine derivatives versus $\log IC_{50}$ [μ M] in different cancer cell lines.....	144
Table 5-4. Binding energies (kcal/mol) were calculated by MM/PBSA and MM/GPSA methods.....	149
Table 5-5. Linear regressions involving two independent variables (binding energy by MM/PBSA method and MlogP) of the investigated colchicine derivatives versus $\log IC_{50}$ (μ M) in different cancer cell lines.	151
Table 5-6. Linear regressions involving two independent variables (binding energy by MM/GBSA method and MlogP) of the investigated colchicine derivatives versus $\log IC_{50}$ (μ M) in different cancer cell lines.	151
Table 6-1. Antiproliferative activity (IC_{50}) [μ M] of 1 and its derivatives 2–14 compared with that of standard anticancer drugs doxorubicin and cisplatin. The calculated values of the resistance index (<i>RI</i>) for LoVo/DX versus LoVo cells are also shown.	173
Table 6-2. Selectivity indexes.....	179
Table 6-3. Computational predictions of the interactions between thiocolchicine derivatives and β I tubulin. Binding energy values in kcal/mol, graphical representation of the ligand-protein interactions, molecular weight, partition coefficient and the length of the aliphatic chains involved are tabulated.....	182
Table 6-4. Linear regressions two independent (binding energy and M log P) and $\log IC_{50}$ [μ M].....	188
Table 7-1. Novel colchicine derivatives were used in training and internal and external test sets. R_1 , R_2 and, R_3 represent the modification on for C_4 , C_{10} , and C_7 respectively. pIC_{50} values for MCF7 and A549 cell lines are reported.	201

Table 7-2. Binding energies (kcal/mol) and electrostatic energies (kcal/mol) between β II tubulin and referred derivatives, polarizability (\AA^3) and sum of absolute values of Hückel pi atomic charges on O atoms, used to build two QSAR models for MCF7 and A549 cells.	210
Table 7-3. Values of R^2 , RMSE, RMSU, and MAE were reported for each of the training and internal test sets of model 1 (for MCF7 cell line) and model 2 (for A459cell line).	214
Table 7-4. validation parameters for the external test on A549 and MCF7 models: R^2 , the squared correlation coefficient of predicted versus observed activities; R_0^2 the squared correlation coefficient calculated by using regression through the origin (RTO) for graphs of predicted versus observed activities; K, the slope of the regression through the origin (RTO).	215
Table 8-1. (A) Binding energies of scoulerine and colchicine docked in the colchicine binding site (1SA0). (B) scoulerine and laulimalide docked in the laulimalide binding site (4O4H).	234
Table 8-2. RMSD values for scoulerine in S1 and S2 with respect to the reference of crystal structures of colchicine, colchicine derivative, CN2 and laulimalide form 5NM5,1SA0 and 4O4H PDB files respectively.	234
Table 8-3. Total energy of protonated and non-protonated scoulerine by quantum mechanical calculations in 8 different systems. (A) scoulerine and hydronium in vacuum and water. (B) protonated scoulerine with H_2O in water and vacuum. (C) scoulerine with H_2O in water and vacuum. (D) protonated scoulerine with hydroxy in water and vacuum.	236
Table A-1. 2D interaction diagrams for the interactions between β I tubulin and N-deacetylthiocolchicine and 4-iodo-N-deacetylthiocolchicine analogues.	338
Table A-2. 3D interaction diagrams for the interactions between β I tubulin and N-deacetylthiocolchicine and 4-iodo-N-deacetylthiocolchicine analogues.	341
Table A-3. RMSD values of the 20 colchicine derivatives with respect to the X-ray structure of colchicine (5NM5).	345
Table A-4. A. contact preference map to predict non-bonded contact preferences, the preferred locations of hydrophobic and hydrophilic ligand atoms (hyd green, HPL red) and	

electrostatic feature maps that predict the electrostatically preferred locations of hydrophobic from the solutions of the Poisson-Boltzmann equation (yellow) B. 2D scheme of ligand-protein interaction C. The protein-ligand interaction fingerprints (PLIF) based on surface contact interactions between each of our derivatives and beta-tubulin (H: hydrophobic surface contact Q: charged surface contact and P: partial hydrophobic contact).	346
Table A-5. Values of H-bonding, atomic charges, solubility, etc calculated for the colchicine derivatives by ADMET predictors.....	347

List of Figures

Figure 1-1. (A) Representative structure of a MT and its tubulin heterodimers. Each MT subunit is a heterodimer of α - and β -tubulin monomers that assemble and form MT protofilaments. (B) each MT is a hollow cylindrical structure formed from 13 protofilamen. (From <i>Cell Biology, Thomas D. Pollard et al.</i> , 3rd ed., ISBN 9780323341264, page 596, Reprinted with permission from Elsevier).....	5
Figure 1-2. The four phases of the cell cycle. G1 and G2 phases separate the main events of M phase and S phase. G1 phase is the gap between S phase and M phase, and G2 phase is the gap between M phase and S phase. M phase consists of two main processes, mitosis and cytokinesis. (From <i>Cell Biology, Thomas D. Pollard et al.</i> , 3rd ed., ISBN 9780323341264, page 698, Reprinted with permission from Elsevier).	7
Figure 1-3. Schematic diagram of stages of mitosis. At interphase, chromosomes become duplicated in S phase. During prophase, chromatins condense into dense mitotic chromosomes. At prometaphase, spindle MTs attach to kinetochores of chromosomes, and chromosomes start moving towards the midplane. In metaphase, chromosomes are lined up at the equator of the spindle. At anaphase, the sister chromosomes separate, and are pulled toward the pole of mitotic spindle. At telophase, chromosomes start to decondense and new nuclear envelopes begin to assemble around them. (From <i>Cell Biology, Thomas D. Pollard et al.</i> , 3rd ed., ISBN 9780323341264, page 755, Reprinted with permission from Elsevier).	8
Figure 1-4. (A) Schematic structure of sister chromatids that are attached to each other at the centromere region. MTs attach to a multi-protein region on each chromatid called kinetochore. (B) Orientation of MTs in metaphase. (From <i>Cell Biology, Thomas D. Pollard et al.</i> , 3rd ed., ISBN 9780323341264, pages 758 and 760, Reprinted with permission from Elsevier).....	9
Figure 1-5. (A) MTA binding sites on tubulin heterodimer. (B) Binding sites and mechanism of action of each group of MTAs. ((A) reprinted with permission from Elsevier, Trends in	

cell biology, from [58], Copyright 2018, B reprinted with permission from <i>Springer Nature</i> , Pharmaceutical Research, from [57], Copyright 2012).	11
Figure 1-6. Chemical structure of laulimalide. (Reprinted with permission from <i>Elsevier</i> , European Journal of Medicinal Chemistry, from [13], Copyright 2018).	12
Figure 1-7. (A) Binding modes and mechanism of targeting of ligands targeting colchicine site. (B) Upon binding of MT-binding agents to colchicine-site, the curved-to-straight conformational transition in $\alpha\beta$ -tubulin heterodimer is inhibited which results in MT destabilization [58]. (Reprinted with permission from <i>Elsevier</i> , Trends in cell biology, from [58], Copyright 2018).	14
Figure 2-1. Synthesis of colchicine derivatives (2–20). Reagents and conditions: (a) NIS, AcOH, 70°C, 20 h (b) MeOH/H ₂ O, CH ₃ SNa, RT; (c) 2 N HCl, 90°C, 72 h; (d) Et ₃ N, DMAP, respective acyl/carbamoyl chloride, THF, 0°C → RT.....	43
Figure 2-2. Comparison of selectivity index (SI) values for the tested compounds. SI was calculated for each compound using the formula: $SI = IC_{50}$ for normal cell line BALB/3T3/ IC_{50} for respective cancerous cell line. A beneficial $SI > 1.0$ indicates a drug with efficacy against tumor cells greater than the toxicity against normal cells.	46
Figure 2-3. ALL-5 (A) or MCF-7 (B) cells were treated with DMSO (vehicle), 1, or its selected double- and triple-modified analogues for 24, 48 or 72 h and subjected to propidium iodide staining and flow cytometry. Percent of cells observed in different phases of cell cycle, determined by PI staining, is shown. Data are presented as a mean \pm SD (n = 3 for all ALL-5 time points and MCF-7 at 72 h; for MCF-7 at 24 and 48 h, n = 1) $P < 0.0001$, $P <$ 0.001 , $P < 0.01$, * $P < 0.05$ control versus dose. See (Appendix A, Figure A9) for a full set of representative cytograms.	48
Figure 2-4. (A) Cleavage of PARP. ALL-5 cells were treated with 43 nM compound 1, 23 nM compound 7, 45 nM compound 17, 0.2 μ M doxorubicin (DX), or 0.1% DMSO (vehicle) for the times indicated, and extracts were prepared and subjected to immunoblotting for PARP. The intact (116 kDa) and cleaved (85 kDa) forms of PARP are shown. GAPDH was used as a loading control. Images were quantified by measuring the band intensity using ImageJ software. (B) Bar diagram showing the fold changes of PARP normalized to	

GAPDH. Data represented as mean \pm S.D. of three independent determinations (n = 3); 24 h treatment was compared with 48 h for respective compound. **P < 0.005, *P < 0.05.... 50

Figure 2-5. A. The colchicine derivatives numbered 6, 17, 14, 5 and 7 show the strongest binding energies of -9.30, -9.30, -9.20, -8.78 and -8.70 kcal/mol, sequentially, unmodified colchicine added to the picture in white for comparison. B. compounds 13 and 19 have the highest binding energies, -6.90 and -7.05 kcal/mol, colchicine is added in blue..... 51

Figure 3-1. Synthesis of colchicine derivatives (**2-8**). Reagents and conditions: (a) for **3**, NCS, acetonitrile, RT; (b) for **5**, NBS, acetonitrile, RT; (c) for **7**, NIS, AcOH, 70°C; (d) MeOH/H₂O, CH₃SNa, RT. 79

Figure 4-1. Chemical structure of colchicine..... 99

Figure 4-2. Synthesis of 4-chlorothiocolchicine derivatives (**1-9**). Reagents and conditions: (a) 2M HCl, 90°C, 72h; (b) triphosgene, Et₃N, respective alcohol, THF, 0°C \rightarrow RT..... 100

Figure 4-3. Comparison of selectivity index (SI) values of tested compounds. SI was calculated for each compound using the formula: SI = IC₅₀ for normal cell line BALB/3T3 / IC₅₀ for respective cancerous cell line..... 103

Figure 4-4. Comparison of resistance index (RI) values of tested compounds. The RI indicates how many times the chemoresistance of a resistant subline was higher relative to its parental cell line. The RI was calculated for each compound using the formula: RI = IC₅₀ for LoVoDX / IC₅₀ for LoVo cell line..... 104

Figure 5-1. Structure of colchicine (**1**)..... 118

Figure 5-2. Structure of compound **2**..... 121

Figure 5-3. Structure of compound **3**..... 122

Figure 5-4. Structure of compound **4**..... 123

Figure 5-5. Structure of compound **5**..... 125

Figure 5-6. Structure of compound **6**..... 125

Figure 5-7. Structure of compound **7**..... 126

Figure 5-8. Structure of compound **8**..... 127

Figure 5-9. Structure of compound **9**..... 128

Figure 5-10. Structure of compound **10**..... 128

Figure 5-11. Structure of compound 11	129
Figure 5-12. Structure of compound 12	130
Figure 5-13. Synthesis of colchicine derivatives (2–12). Reagents and conditions: (a) N-bromosuccinimide (NBS), acetonitrile, room temperature; (b) MeOH/H ₂ O, CH ₃ SNa, room temperature; (c) 2M HCl, 90°C, 72 h; (d) triphosgene, Et ₃ N, respective alcohol, tetrahydrofuran (THF), 0°C → room temperature.....	134
Figure 5-14. Tubulin β I structure in 3D with (Top) 5 colchicine derivatives with binding energies of –8.40 kcal/mol and higher, and (bottom) with 6 colchicine derivatives with binding energies lower than –8.40 kcal/mol.....	146
Figure 6-1. Synthesis of colchicine derivatives (2–14). Reagents and conditions: (a) MeOH/H ₂ O, CH ₃ SNa, RT; (b) 20% HCl, MeOH, reflux; (c) triphosgene, THF, Et ₃ N, 0°C; primary or secondary alcohols, RT.....	162
Figure 6-2. Illustration in 3D of the interaction modes of the tubulin β I structure with: (a) 8 thiocolchicine derivatives with binding energies of –8 kcal/mol and higher; (b) with 6 thiocolchicine derivatives with binding energies lower than –8 kcal/mol.....	181
Figure 6-3. Colchicine (1), starting compounds (2–3) and derivatives (4–6, 14) induced G ₂ /M arrest in MCF-7 cells. MCF-7 cells were treated with the indicated compounds for 24, 48 or 72 h and subjected to propidium iodide staining and flow cytometry. Percent of cells with 4N DNA (G ₂ /M phases) was determined (mean \pm SD, n = 3). (**p < 0.01, ***p < 0.001, *p < 0.05 vs. control). See Appendix E for a full set of representative data.	188
Figure 6-4. Effects of 1 and 5 on microtubule structures in HeLa (A) and MCF-7 (B) cells. HeLa and MCF-7 cells were incubated for 12 h without (vehicle, 0.1% DMSO) or with 1 (120 nM), 5 (80 nM) (concentrations corresponding with 10 \times IC ₅₀ values) or 100 nM VCR (positive control). Bar equals 5 μ m (A) or 10 μ m (B).	190
Figure 7-1. (A) Colchicine. (B) Double modification in C-4 and C-10 positions and triple modification in C-4, C-7 and C-10 positions on colchicine., R ₁ = H, Cl, I and Br, R ₃ = mentioned above and R ₂ = S-CH ₃ and O-CH ₃ . (C) Triple modification R ₁ = H, Cl, I and Br, R ₂ = S-CH ₃ and R ₄ = NH ₃	201
Figure 7-2. Linear regression graph of predicted vs observed values of IC ₅₀ for both A549 and MCF7 cancer cell lines for training and internal test sets.....	213

Figure 7-3. (A) Linear regression graph of predicted vs observed values of pIC ₅₀ for A549 cancer cell lines in external test sets. (B) Linear regression graph of predicted vs observed values of pIC ₅₀ for MCF7 cancer cell lines in external test sets.	216
Figure 7-4. Associated regression uncertainty models of 3D-QSAR model both A549 and MCF7 cancer cell lines.	217
Figure 7-5. Associated squared error and standard deviation distributions Q-Q plots of 3D-QSAR models for A549 and MCF7 cancer cell lines.	219
Figure 7-6. Outlier structures of internal test sets of 3D-QSAR models for A549 and MCF7 cancer cell lines.	220
Figure 8-1. Scoulerine structure	229
Figure 8-2. S ₁ , S ₂ and S ₃ represent the three predicted potential binding sites by blink docking of scoulerine (blue) to α (green) and β (red) tubulins of 1SA0 PDB structure. Colchicine derivative from 1SA0 in S ₁ and Laulimalide from 404H in S ₂ shown in white.	238
Figure 8-3. Interactions between the pharmacophoric points and the tubulin structure [21].	239
Figure 8-4. (A) 2D-interaction scheme of superimposed colchicine crystal structure from 5NM5 PDB file (green) on scoulerine in the S ₁ site (red). (B) 2D-interaction scheme of scoulerine in the S ₁ site. (C) Surface patches identifying regions of hydrophobicity (yellow) around scoulerine. Residues Leu255, Ala316, Val318, and Ile378 of β tubulin that involve in hydrophobic interaction colored in teal.	241
Figure 8-5. RMSD of scoulerine to the colchicine binding site (S ₁ -1SA0).	242
Figure 8-6. Mass-weighted root mean squared deviation (Å) of the binding site of colchicine to tubulin, classified according to cluster number, with occupancy indicated. The binding site includes scoulerine and residues having atoms within 8 Å of scoulerine. The dark blue part of the graph illustrates the equilibration.	243
Figure 8-7. (A) Representative structures of scoulerine in cluster B (purple) versus colchicine (yellow) (B) 2D- interaction scheme of scoulerine in colchicine binding site. (C) Representative structures of cluster A (red), cluster B (purple) and cluster C (dark pink) in colchicine binding site, α tubulin colored in teal and β I tubulin colored in light pink. (D) Colchicine (yellow) in colchicine binding site, α tubulin colored in teal and β I tubulin colored	

in light pink. (E) surface patches identifying regions of hydrophobicity (yellow) around scoulerine, residues Leu255, Val318, and Ile378 of β tubulin that involve in hydrophobic interaction colored in teal.	244
Figure 8-8. Laulimalide in the laulimalide binding site of β tubulin (green) in 4O4H PDB file. Residues in blue have hydrogen bonding interaction with laulimalide (purple).	246
Figure 8-9. (A) 2D-interaction scheme of scoulerine in the S ₂ site <i>via</i> blind docking. (B) 2D-interaction scheme of superimposed laulimalide crystal structure from 4O4H PDB file (green) on scoulerine (red) in the S ₂ site. (C) 2D- interaction scheme of scoulerine in the S ₃ site <i>via</i> blind docking.....	248
Figure 8-10. RMSD of scoulerine to the laulimalide binding site (S1-1SA0).....	249
Figure 8-11. Mass-weighted root mean squared deviation (Å) of the binding sites of laulimalide to tubulin, classified according to cluster number, with occupancy indicated. The binding site includes scoulerine and residues having atoms within 8 Å of scoulerine. The purple part of the graph illustrates the equilibration.	250
Figure 8-12. (A) 3D-interaction scheme of scoulerine (blue) and superimposed laulimalide crystal structure from 4O4H PDB file (purple) between microtubules. Residues in light green are in laulimalides's site on β_A tubulin and residues in dark green are in laulimalides's site on β_B tubulin. (B) 2D-interaction scheme of Scoulerine in laulimalide binding sites on β_A tubulin and β_B tubulin. (C) Representative structures of cluster A (purple) and cluster B (pink) in laulimalide binding sites. α_A and α_B tubulins colored in light and dark pink and β_A and β_B tubulins colored in light and dark green respectively.....	252
Figure 8-13. (A) K _d values for scoulerin bound to labelled α and β tubulin (colchicine binding site) and microtubule (laulimalide binding site) obtained by microscale thermophoresis. (B) K _d value of colchicine bound to labelled α and β tubulin (colchicine binding site) used as a control.....	254
Figure A-1. The ¹³ C-NMR spectrum of 6 in CDCl ₃	325
Figure A-2. The ¹ H-NMR spectrum of 6 in CDCl ₃	326
Figure A-3. The ¹³ C-NMR spectrum of 7 in CDCl ₃	326
Figure A-4. The ¹ H-NMR spectrum of 7 in CDCl ₃	327

Figure A-5. The ¹³ C-NMR spectrum of 14 in CDCl ₃	328
Figure A-6. The ¹ H-NMR spectrum of 14 in CDCl ₃	329
Figure A-7. The ¹³ C-NMR spectrum of 15 in CDCl ₃	329
Figure A-8. The ¹ H-NMR spectrum of 15 in CDCl ₃	330
Figure A-9. Sensitivity of primary ALL cells to 1 and its derivatives. Cell viability was assessed by MTT assay employing ALL-5 cells. Cells were treated with vehicle (100% viability) or increasing concentrations of investigated compounds for 120 h. Results are given as mean ± SD (n = 4) and IC ₅₀ values are indicated. See Figure 1 for structures....	333
Figure A-10. DNA content of treated cells. ALL-5 (A) or MCF-7 (B) cells were treated with 5 x IC ₅₀ values of 1 , its analogs or 0.1% of DMSO (vehicle) for 24, 48 or 72 h (panel A, ALL-5, as indicated) or 72 h (panel B, MCF-7), and subjected to propidium iodide staining and flow cytometry, as described in Materials and Methods. The proportion of cells in different cell cycle phases or with sub-G1 DNA is indicated numerically and by the bars. Data shown are representative of three independent experiments.....	337
Figure B-1. The ¹³ C NMR spectrum of 2 in CDCl ₃	349
Figure B-2. The ¹ H NMR spectrum of 2 in CDCl ₃	350
Figure B-3. The ¹³ C NMR spectrum of 3 in CDCl ₃	351
Figure B-4. The ¹ H NMR spectrum of 3 in CDCl ₃	352
Figure B-5. The ¹³ C NMR spectrum of 4 in CDCl ₃	353
Figure B-6. The ¹ H NMR spectrum of 4 in CDCl ₃	354
Figure B-7. The ¹³ C NMR spectrum of 5 in CDCl ₃	355
Figure B-8. The ¹ H NMR spectrum of 5 in CDCl ₃	356
Figure B-9. The ¹³ C NMR spectrum of 6 in CDCl ₃	357
Figure B-10. The ¹ H NMR spectrum of 6 in CDCl ₃	358
Figure B-11. The ¹³ C NMR spectrum of 7 in CDCl ₃	359
Figure B-12. The ¹ H NMR spectrum of 7 in CDCl ₃	360
Figure B-13. The ¹³ C NMR spectrum of 8 in CDCl ₃	361
Figure B-14. The ¹ H NMR spectrum of 8 in CDCl ₃	362
Figure C-1. The ¹³ C NMR spectrum of 1 in CDCl ₃	365
Figure C-2. The ¹ H NMR spectrum of 1 in CDCl ₃	366

Figure C-3. The ^{13}C NMR spectrum of 2 in CDCl_3	368
Figure C-4. The ^1H NMR spectrum of 2 in CDCl_3	369
Figure C-5. The ^{13}C NMR spectrum of 3 in CDCl_3	370
Figure C-6. The ^1H NMR spectrum of 3 in CDCl_3	371
Figure C-7. The ^{13}C NMR spectrum of 4 in CDCl_3	372
Figure C-8. The ^1H NMR spectrum of 4 in CDCl_3	373
Figure C-9. The ^{13}C NMR spectrum of 5 in CDCl_3	374
Figure C-10. The ^1H NMR spectrum of 5 in CDCl_3	375
Figure C-11. The ^{19}F NMR spectrum of 5 in CDCl_3	376
Figure C-12. The ^{13}C NMR spectrum of 6 in CDCl_3	377
Figure C-13. The ^1H NMR spectrum of 6 in CDCl_3	378
Figure C-14. The ^{13}C NMR spectrum of 7 in CDCl_3	379
Figure C-15. The ^1H NMR spectrum of 7 in CDCl_3	380
Figure C-16. The ^{13}C NMR spectrum of 8 in CDCl_3	381
Figure C-17. The ^1H NMR spectrum of 8 in CDCl_3	382
Figure C-18. The ^{13}C NMR spectrum of 9 in CDCl_3	383
Figure C-19. The ^1H NMR spectrum of 9 in CDCl_3	384
Figure D-1. The ^{13}C NMR spectrum of 2 in CDCl_3	392
Figure D-2. The ^1H NMR spectrum of 2 in CDCl_3	393
Figure D-3. The ^{13}C NMR spectrum of 3 in CDCl_3	394
Figure D-4. The ^1H NMR spectrum of 3 in CDCl_3	395
Figure D-5. The ^{13}C NMR spectrum of 4 in CDCl_3	396
Figure D-6. The ^1H NMR spectrum of 4 in CDCl_3	397
Figure D-7. The ^{13}C NMR spectrum of 5 in CDCl_3	398
Figure D-8. The ^1H NMR spectrum of 5 in CDCl_3	399
Figure D-9. The ^{13}C NMR spectrum of 6 in CDCl_3	400
Figure D-10. The ^1H NMR spectrum of 6 in CDCl_3	401
Figure D-11. The ^{13}C NMR spectrum of 7 in CDCl_3	402
Figure D-12. The ^1H NMR spectrum of 7 in CDCl_3	403
Figure D-13. The ^{13}C NMR spectrum of 8 in CDCl_3	404

Figure D-14. The ¹ H NMR spectrum of 8 in CDCl ₃	405
Figure D-15. The ¹⁹ F NMR spectrum of 8 in CDCl ₃	406
Figure D-16. The ¹³ C NMR spectrum of 9 in CDCl ₃	407
Figure D-17. The ¹ H NMR spectrum of 9 in CDCl ₃	408
Figure D-18. The ¹³ C NMR spectrum of 10 in CDCl ₃	409
Figure D-19. The ¹ H NMR spectrum of 10 in CDCl ₃	410
Figure D-20. The ¹³ C NMR spectrum of 11 in CDCl ₃	411
Figure D-21. The ¹ H NMR spectrum of 11 in CDCl ₃	412
Figure D-22. The ¹³ C NMR spectrum of 12 in CDCl ₃	413
Figure D-23. The ¹ H NMR spectrum of 12 in CDCl ₃	414
Figure D-24. 3D plots of the linear regression results for the binding energies (BE) vs MlogP vs log IC ₅₀ [μM] values for LoVo cell line.	415
Figure D-25. 3D plots of the linear regression results for the binding energies (BE) vs MlogP vs log IC ₅₀ [μM] values for LoVo/DX cell line.	415
Figure E-1. Spectroscopic characterization of compound 2	416
Figure E-2. Spectroscopic characterization of compound 3	417
Figure E-3. Spectroscopic characterization of compound 3	418
Figure E-4. Spectroscopic characterization of compound 4	419
Figure E-5. Spectroscopic characterization of compound 5	420
Figure E-6. Spectroscopic characterization of compound 6	421
Figure E-7. Spectroscopic characterization of compound 7	422
Figure E-8. Spectroscopic characterization of compound 8	423
Figure E-9. Spectroscopic characterization of compound 9	424
Figure E-10. Spectroscopic characterization of compound 10	425
Figure E-11. Spectroscopic characterization of compound 11	426
Figure E-12. Spectroscopic characterization of compound 12	427
Figure E-13. Spectroscopic characterization of compound 13	428
Figure E-14. Spectroscopic characterization of compound 14	429
Figure E-15. 3D plots of the linear regression results for the binding energies (BE) vs MlogP vs log IC ₅₀ [μM] values for MCF-7 cell line.	430

Figure E-16. 3D plots of the linear regression results for the binding energies (BE) vs MlogP vs $\log IC_{50}$ [μM] values for <i>LoVo</i> cell line.	430
Figure E-17. 3D plots of the linear regression results for the binding energies (BE) vs MlogP vs $\log IC_{50}$ [μM] values for <i>LoVo/DX</i> cell line.	430
Figure E-18. 3D plots of the linear regression results for the binding energies (BE) vs MlogP vs $\log IC_{50}$ [μM] values for <i>A-549</i> cell line.	430
Figure E-19. 3D plots of the linear regression results for the binding energies (BE) vs MlogP vs $\log IC_{50}$ [μM] values for <i>BALB/3T3</i> cell line.	431
Figure E-20. Colchicine and its analogs, induce G ₂ /M phase arrest. MCF-7 cells were treated with 10 x IC_{50} values of the indicated compounds, for 24, 48 or 72 h, and subjected to propidium iodide staining and flow cytometry, as described in Experimental section. The proportion of cells in different cell cycle phases or with sub-G1 DNA is indicated numerically and by the bars. Data shown are representative of three independent experiments.....	433

Chapter 1:

Introduction

1.1 Cancer

Cancer is a multifactorial pathology entailing a complex family of diseases which reflects uncontrolled events turning a normal cell into a cancer cell [1–3]. Cancer is a leading cause of death globally. According to GLOBOCAN estimates of cancer incidence and mortality reported by the International Agency for Research on Cancer, over 19 million new cancer cases and nearly 10 million cancer deaths occurred in 2020 [4]. From this, more than 220,000 new cases and over 80,000 cancer deaths were reported in 2020 in Canada [5]. With an estimated rise of 47% from 2020, the global burden of cancer is projected to be 28.4 million cases in 2040 [1]. Besides, it is estimated that within the next three decades, nearly 20.5% of all cancer cases will be diagnosed in adults aged 80 and older, where due to the complexity of cancer management in aged patients, economic and social impact of cancer is expected to grow dramatically worldwide [6].

Cancer is characterized by loss of cellular regulation where uncontrolled cell proliferation within a certain tissue gives rise to the destructive cancer phenotype [7]. The process of cancer forming also known as oncogenesis or tumorigenesis, involves a series of abnormal changes in cell machinery that induce unregulated cellular proliferation that could generate a progressive and rapid dividing cell type that escapes normal growth checkpoints, leading to growing the clones of cells into a tumor [7].

Given the higher rate of growth and division of malignant tumor-composing cells compared to the normal cells, they are prone to invade the nearby tissues. This invasion occurs with no significant change in the proliferation rate of cancer cells, where at progressive stages, tumor cells could spread into surrounding tissues and get into the circulation system of the body, leading to the establishment of secondary regions of proliferation, a process known as metastasis [7]. Once cancer has progressed to a metastatic stage, it is much more difficult to treat [8].

Conventional cancer treatment approaches include surgery, radiation therapy, proton therapy, and chemotherapy. Despite their application in the treatment and management of different types of cancer, each of these therapy methods is associated with risks that limit their effective use. Surgery is effective in the removal of the clearly localized tumor; however, it is location-dependent and is limited, with some complications such as the risk of spread of tumor cells into other tissues, high possibility of recurrence, and

permanent disfigurement. Despite being a key component of cancer treatment, radiation therapy also has various side effects due to indiscriminate destruction of normal cells and damage to healthy tissues caused by undesirable energy placement pattern. In chemotherapy, the cytotoxic drugs are utilized to kill tumor cells, however, due to the lack of targeting, healthy tissues surrounding the tumor are also damaged [9,10]. Chemotherapeutic agents are designed to destroy cells having a high rate of proliferation and regeneration, however, normal non-tumor cells with rapid proliferating characteristics residing in certain tissues such as bone marrow and gastrointestinal tract epithelium are damaged as well. Due to this, high levels of toxicity are associated with such treatments [11].

Cancer research is constantly evolving to discover novel treatment strategies. Innovative therapeutic approaches such as photodynamic therapy, photothermal therapy, gene therapy, and nanoparticle-based therapy have shown promising potential to treat cancer [10]. It is believed that these novel therapeutic strategies combined with traditional approaches could greatly improve the overall outcome of cancer treatment [12]. Thus, finding new therapeutic agents with specific targeting ability of cancer cells with a reduced affinity towards non-tumor cells could more effectively treat different types of cancer [13–16].

1.2 Microtubules

Microtubules (MTs) are a major component of the cytoskeleton which, along with two other types of cytoskeletal filaments including microfilaments and intermediate filaments, each playing a different role, take part in spatial organization and mechanical properties of cells [7,17]. MTs are found in eukaryotic cells and are involved in certain cell movements. They direct intracellular transport and play a key role in mitosis, where MTs assemble mitotic spindles around chromosomes and segregate them during cell division [17]. As MTs play such a critical role in cell division, they are a very suitable target for development of chemotherapeutics against rapidly dividing cancer cells [18].

MTs are long, hollow cylinder-shaped polymers made of globular tubulin protein. A tubulin subunit is a heterodimer of α - and β -tubulin (Figure 1-1). The amino acid

sequences of these monomers are highly conserved in all eukaryotic cells and share 40% identity [7,19]. Several studies using different techniques such as cryo-electron microscopy (cryo-EM) [20,21], electron, and X-ray crystallography [22] have identified the three-dimensional structures of MTs and tubulins. Atomic coordinates are available in the Protein Data Base (PDB) (<https://www.rcsb.org/>). However, in electron crystallographic data, the structure of α - and β -tubulin are not distinguishable beyond a resolution of 6 Å [19, 23]. With Cryo-EM the structure of MTs has been obtained with resolutions between 30 Å and 3.5 Å [20, 21, 24–28]. As of 2020, the majority of the protein structures determined by Cryo-EM are at a higher resolution of 3–4 Å [29]. This electron microscopy technique has been recently possible to obtain ligand–protein coordinates at near atomic-resolution (2.2 Å) by cryo-EM [30,31]. However, the best to date Cryo-EM resolutions are approaching 1.5 Å, [32] making it a fair competitor in resolution in some cases.

All $\alpha\beta$ -tubulin heterodimers are identical, as α - and β -tubulins always combine with each other through a specific interfacial surface region. By convention, in each heterodimer, the β -tubulin is considered as the ‘top’ unit and α -tubulin as the ‘bottom’ unit. Thus, along the longitudinal axis of the MT, the bottom of each α -tubulin molecule interacts with the top of the β -tubulin molecule in the adjacent heterodimer (Figure 1-1A) [17]. The heterodimers assemble *via* non-covalent interactions. The approximate size of one dimer is 4 nm × 5 nm × 8 nm with a molecular weight of about 100 kDa [33].

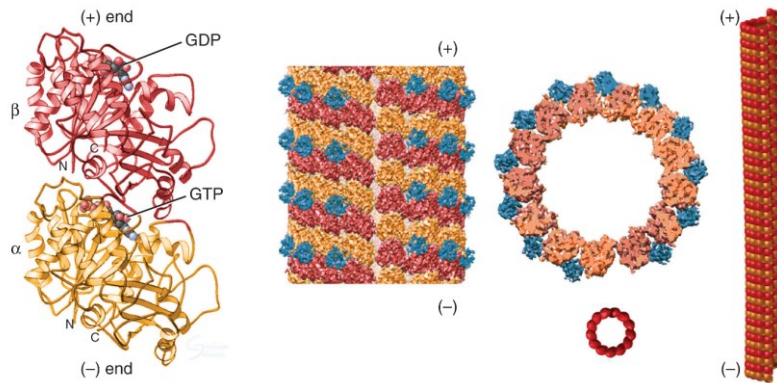


Figure 1-1. (A) Representative structure of a MT and its tubulin heterodimers. Each MT subunit is a heterodimer of α - and β -tubulin monomers that assemble and form MT protofilaments. (B) each MT is a hollow cylindrical structure formed from 13 protofilamen. (From *Cell Biology*, Thomas D. Pollard et al., 3rd ed., ISBN 9780323341264, page 596, Reprinted with permission from Elsevier).

Tubulin subunits ($\alpha\beta$ -heterodimers) form long protofilaments through end-to-end interactions, where all subunits have the same orientation. Upon protofilament formation, they interact laterally with each other and associate into a curved sheet which eventually rolls into an MT. Each MT is composed of 13 parallel-aligned protofilaments (Figure 1-1B) [7,17].

The head-to-tail assembly of $\alpha\beta$ -heterodimers in a protofilament gives an overall structural polarity to an MT, and since all protofilaments have the same orientation in the MT structure, one end of MT will always be a ring of α -tubulin, whereas the other end will be a ring of β -tubulins. Two ends of MT have a different rate of assembly giving rise to a complex dynamic behavior in which an MT alternates between growing and shortening phases. The two ends of an MT are designated as plus and minus ends where the plus end corresponds to the β -tubulin exposed end. The plus end of an MT grows and shortens more rapidly. This interchanging behavior of MTs between growth and shortening phases is referred to as ‘dynamic instability’. The abrupt transition from the growth phase to shortening phase is called ‘catastrophe’, while the change to growth phase is called ‘rescue’. The growth rate and shortening rates as well as the catastrophe and rescue frequencies are the parameters that determine the stability of an MT. In addition to dynamic instability, MTs exhibit another dynamic behavior called ‘treadmilling’ where one end

grows due to the addition of subunits and one end shrinks at the other end due to the loss of subunits [7,34,35].

1.3 The cell cycle and mitosis

1.3.1 Cell division cycle

Reproduction of a cell involves an ordered series of events in which the content of the parent cell is duplicated and then divides into two daughter cells. This cycle of sequential steps of content duplication and division is called the 'cell cycle' [36]. The cell cycle comprises two distinct phases including interphase and mitotic (M) phase. The M phase consists of two main processes, mitosis and cytokinesis. Mitosis is the division of the nucleus, and during cytokinesis which generally begins before completion of mitosis, the cytoplasm of the cell splits to form two cells. Interphase is the period between one M phase and the next. As the duration of the M phase is a small fraction of the total time of the cell cycle, a typical mammalian cell spends most of its life in interphase (Figure 1-2) [36,37].

The cells that have the reproduction ability are highly active during interphase. Although no cell division is occurring during interphase, all required materials for cell division and growth are synthesised in this time. Interphase comprises the three remaining phases of the cell cycle including S phase, G1 phase, and G2 phase. During the S phase (S stands for the synthesis) nuclear DNA is replicated indicating that the cell will have a duplicated copy of each chromosome which is a necessary pre-requirement for cell division. Upon completion of mitosis, cells enter the G1 phase (G stands for gap) which continues until the beginning of the S phase. During this interval of time between the end of the M phase and starting the S phase, cells grow and synthesize enzymes and proteins required for mitosis. The second gap occurs between the completion of the S phase and beginning of the M phase called G2 phase. In the G2 phase, cell keeps growing in mass, expressing more proteins, and duplicating more cellular organelles which all prepare a cell for mitosis. Depending on the cell type and extracellular conditions, the progress of the cell cycle could be delayed or even permanently stopped in the G1 phase, a resting phase that is called G0 phase [36–38].

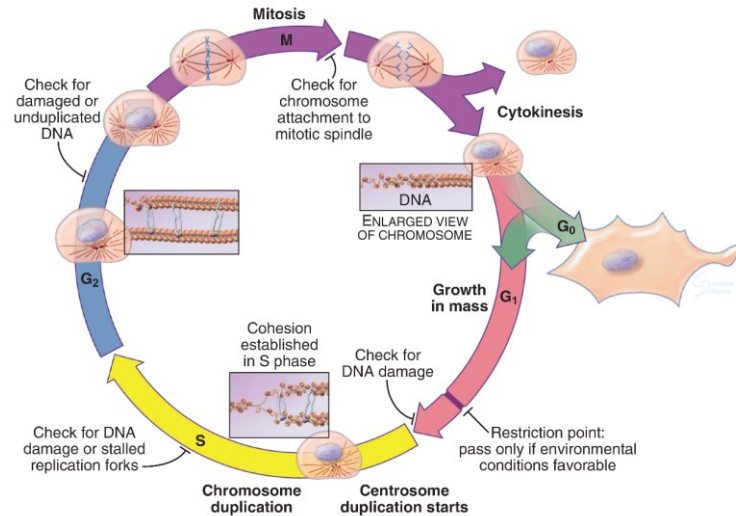


Figure 1-2. The four phases of the cell cycle. G₁ and G₂ phases separate the main events of M phase and S phase. G₁ phase is the gap between S phase and M phase, and G₂ phase is the gap between M phase and S phase. M phase consists of two main processes, mitosis and cytokinesis. (From *Cell Biology*, Thomas D. Pollard et al., 3rd ed., ISBN 9780323341264, page 698, Reprinted with permission from Elsevier).

1.4 Mitosis

During mitosis, the replicated chromosomes separate and so after completion of cell division, each new daughter cell gets a copy of each chromosome. Mitosis is a continuous process that based on the early microscopy studies is divided into five stages: prophase, prometaphase, metaphase, anaphase, and telophase. During prophase, long chromatin molecules start to condense into short, compact, and *disentangled* chromosomes, where each is composed of two sister chromatids that are linked to each other at a region called centromeres. A highly dynamic and complex division machinery called mitotic spindle also begins to assemble in prophase. The mitotic spindle is a bipolar assembly of MTs, where the minus end of each MT is at the poles of the spindle, and the plus end is oriented outwards from each pole (Figure 1-4B) [36,37].

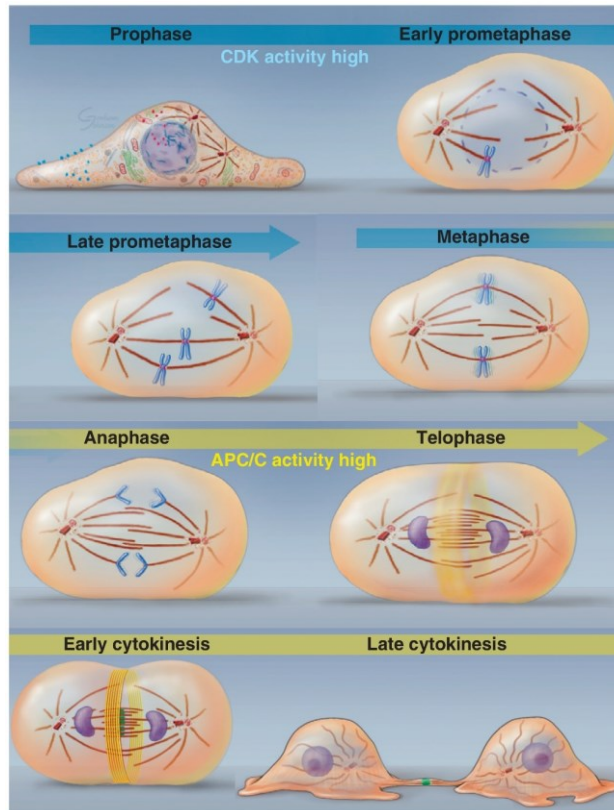


Figure 1-3. Schematic diagram of stages of mitosis. At interphase, chromosomes become duplicated in S phase. During prophase, chromatin condenses into dense mitotic chromosomes. At prometaphase, spindle MTs attach to kinetochores of chromosomes, and chromosomes start moving towards the midplane. In metaphase, chromosomes are lined up at the equator of the spindle. At anaphase, the sister chromosomes separate, and are pulled toward the pole of mitotic spindle. At telophase, chromosomes start to decondense and new nuclear envelopes begin to assemble around them. (From *Cell Biology*, Thomas D. Pollard et al., 3rd ed., ISBN 9780323341264, page 755, Reprinted with permission from Elsevier).

Prometaphase begins with breaking down the nuclear envelope and progresses with the completion of mitotic spindle. The dynamic instability at the plus end is essential for MTs forming mitotic spindle apparatus so they could capture the chromosomes. High rate of growing and shortening at the plus end, allows them to move into the chromosome-rich region of the cell in which these MTs could attach to a multi-protein region on each chromosome called kinetochore (Figure 1-4A) [7,17].

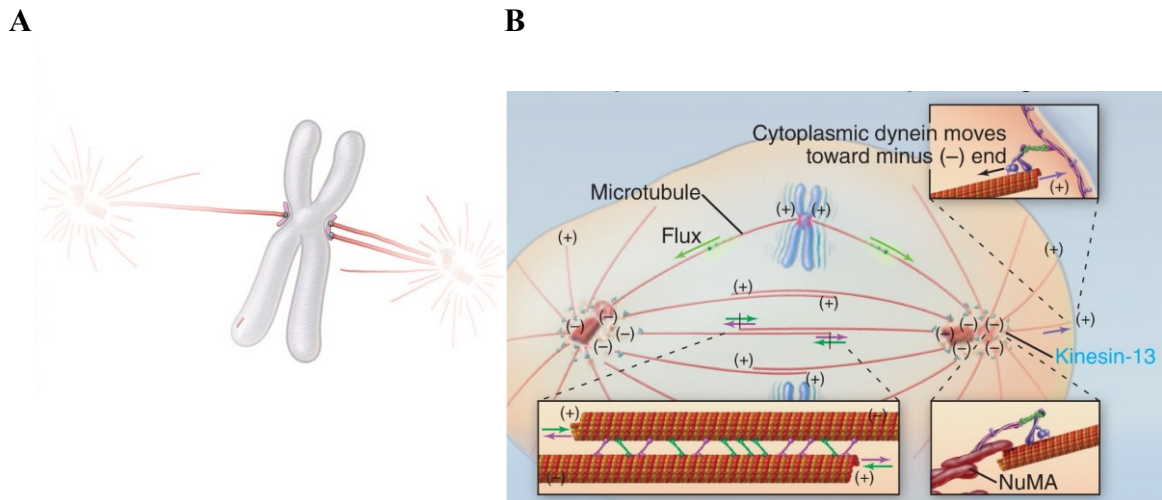


Figure 1-4. (A) Schematic structure of sister chromatids that are attached to each other at the centromere region. MTs attach to a multi-protein region on each chromatid called kinetochore. (B) Orientation of MTs in metaphase. (From *Cell Biology*, Thomas D. Pollard et al., 3rd ed., ISBN 9780323341264, pages 758 and 760, Reprinted with permission from Elsevier).

At the metaphase step of mitosis, chromosomes line up at the equator of the spindle with MTs attached to their kinetochores. Subsequently, at anaphase, the sister chromosomes separate, and each formed daughter chromosome is pulled toward the pole of mitotic spindle. Chromosome segregation and pulling towards the poles takes place due to two contributing factors: (i) the shrinking of kinetochore-attached MTs at their plus end; (ii) two poles of the spindle moving apart from each other. MTs and MT-associated motor proteins (kinesins) play the key role in movement of poles and spindle elongation. During telophase, while two groups of chromosomes arrive at the poles, they start to decondense and new nuclear envelopes begin to assemble around them (Figure 1-3) [7,17,37,39].

1.4.1 Drugs and cell cycle regulation

Studies investigating the effect of drugs and molecules on polymerization or depolymerization of MTs have had a major contribution in finding the role of these biopolymers in the cell, and given the critical role played by MTs in mitotic spindle assembly, any physical or chemical agents that destabilize the MTs could disrupt mitosis. Early studies using MT-destabilizing agents such as colchicine and vinblastine showed that cells treated with these drugs entered a state of prolonged mitotic arrest (hours or even

days) [17,40]. These studies led to the identification of the spindle-assembly checkpoint that is a control mechanism monitoring the metaphase-to-anaphase transition [17,41,42]. Even if only a single kinetochore of a chromosome fails to properly associate with spindle MTs, the spindle-assembly checkpoint will prevent entry into anaphase. MT-destabilizing drugs can activate this regulatory mechanism resulting in mitosis inhibition [7,43].

Due to the essential role of MTs in mitosis, antimetabolic agents that disrupt MT dynamics play an important role in anticancer drug discovery, where some MT-targeted drugs such as paclitaxel (Taxol) and vinblastine have shown effective therapeutic outcomes [44,45].

1.4.2 Anti-microtubular therapeutic agents

The fragility of cancer cells during division serves as a critical target point in chemotherapy. With an established track record of clinical efficacy, classically, MT-targeting agents (MTAs) play the most reliable role as antimetabolic agents [44,46]. MTAs are generally classified into two types based on their interaction with MTs or tubulin subunits; “MT-stabilizing agents” that stabilize MT polymers, and “MT-destabilizing agents” that inhibit MT polymerization. Both MT-stabilizer and MT-destabilizer drugs or chemical agents could interfere with MT dynamics and hence inhibit their function in mitosis. For example, colchicine acts as an anti-mitotic agent by interacting with tubulin subunits that leads to MT depolymerization [47], whereas Taxol binds to MTs and hyper-stabilizes them leading to inhibition of spindle function and cell death [48]. Thus, MTs are superb therapeutic targets for cancer treatment, where through blocking of mitosis, drugs activate the spindle-assembly checkpoint that eventually can trigger apoptotic tumour cell death [49–53]. MTAs target different binding sites on the tubulin heterodimer. The most common binding sites are taxane/epothilone-, vinca alkaloid-, colchicine-, and laulimalide-binding sites (Figure 1-5B) [52,54–57].

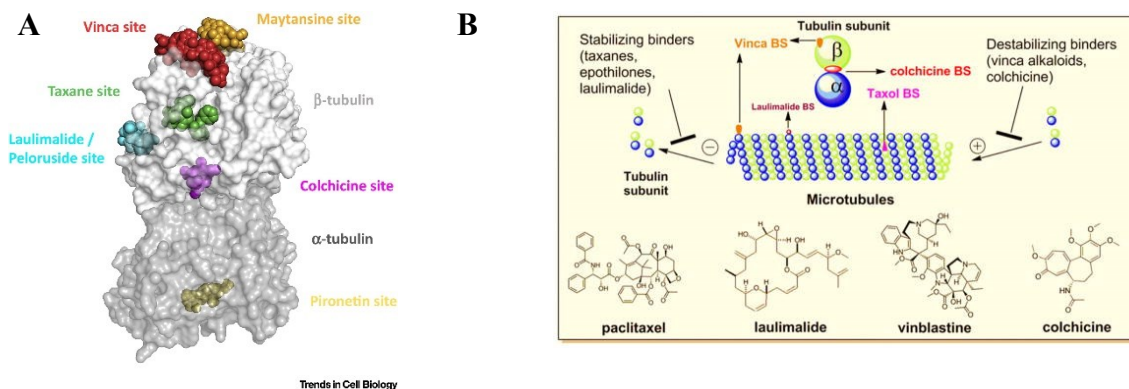


Figure 1-5. (A) MTA binding sites on tubulin heterodimer. (B) Binding sites and mechanism of action of each group of MTAs. ((A) reprinted with permission from *Elsevier*, Trends in cell biology, from [58], Copyright 2018, B reprinted with permission from *Springer Nature*, Pharmaceutical Research, from [57], Copyright 2012).

1.4.3 Lauimalide binding site

Laulimalide and peloruside A are MT-stabilizing agents that exhibit significant cytotoxic effects against a diverse range of cancer cell lines [59,60]. Like the cancer chemotherapy drug taxol, both laulimalide and peloruside A stimulate MT polymerization leading to mitotic arrest and apoptotic cell death. However, these two compounds have several unique characteristics that may provide an advantage over clinically used chemotherapy drugs such as Taxol. Compared to Taxol, they are more hydrophilic, which eliminates the need for formulation vehicle required to improve the solubility of poorly-water soluble drugs, thus reducing the toxicity caused by vehicle. Besides, it has been shown that Lauimalide and peloruside A are less susceptible than Taxol to multi-drug resistance caused by overexpressed drug efflux pump (P-glycoprotein efflux pump) in some cancer cells [61–63].

High-resolution studies, using X-ray crystallography and cryo-EM have recently identified the laulimalide/peloruside A binding site on β -tubulin, which is different from the taxane site. The binding pocket of taxane-site ligands located at the luminal side of the MT, whereas laulimalide and peloruside A target a pocket on β -tubulin that faces the outside of the MT [58,64,65].

Two β -tubulin loops including H9–H9' and H10–S9, and polar and hydrophobic residues of helices H9 and H10 form the laulimalide/peloruside site. This site is located on

the outer surface of the MT near the lateral interface between protofilaments [58]. Both ligands could bind at the interface of two nearby β -tubulin molecules making a lateral contact with helix H3 of the juxtaposed tubulin subunit in the neighbouring protofilament, thus acting like molecular clamps that strengthen interactions across adjacent protofilaments and therefore, preventing MT disassembly [58,64]. In the structure of the laulimalide molecule, the C19 side chain, methyl group of C30, and hydroxyl group of C15 play the key role in its activity (Figure 1-6) [66].

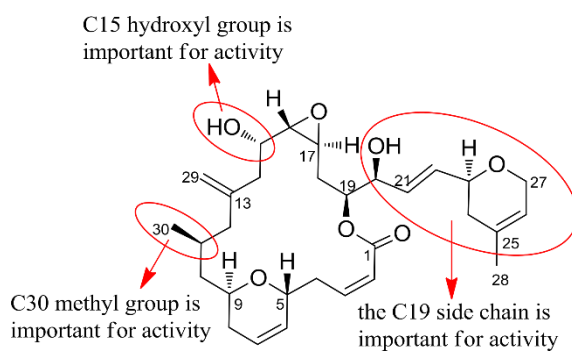


Figure 1-6. Chemical structure of laulimalide. (Reprinted with permission from *Elsevier*, *European Journal of Medicinal Chemistry*, from [13], Copyright 2018).

1.4.4 Colchicine binding site

Colchicine is the first MT destabilizing agent to be discovered. It is a tricyclic alkaloid derived from poisonous meadow saffron *Colchicum autumnale* L. Colchicine is an ancient remedy that still is used today. Therapeutic use of *Colchicum autumnale* has a 3000-year-old history, and for many years, as an unapproved drug, colchicine has been used to treat gout, pericarditis, familial Mediterranean fever, and Behçet's disease. In 2009, colchicine was approved as a monotherapy drug by U.S. Food and Drug Administration (FDA) for the treatment of acute gout flares and familial Mediterranean fever [57]. Over the past few years, there has been emerging research indicating potential therapeutic applications for colchicine in different areas such as oncology, cardiology, immunology, and dermatology [67]. For instance, the most recent research on COVID-19 has shown that colchicine could reduce the risk of death or hospitalizations in patients with COVID-19 by 21 percent [68].

It has been shown that, compared to normal cells, colchicine is more effective in killing cancerous cells, however, its pharmaceutical application for cancer treatment is limited by its low therapeutic index due to complications raised from its toxicity in higher doses and undesired drug interactions [69,70]. However, due to colchicine's ability to halt mitosis, it is believed that the synthesis of the colchicine analogues could offer effective drugs with desired pharmacological profiles for cancer treatment [69,71].

In terms of MT-binding agents, colchicine-site ligands have probably received the most attention in cancer research; however, none of them have made it to the commercial phase yet [72]. The first atomic-level description of tubulin in complex with colchicine was obtained in 2004, and since then, binding of a wide range of colchicine-site ligands to tubulin having various structures and origins (synthetic or natural) has been studied using X-ray crystallography [58,73].

The colchicine site is located close to the intradimer interface between two subunits of an $\alpha\beta$ -heterodimer where it is mostly buried deep in the intermediate domain of β -tubulin [19,73,74]. Upon binding a colchicine domain molecule, the T7 loop, the H7 and H8 α -helices, and the S8 and S9 strands of β -tubulin all interact with the ligand. These structures mostly contribute to the core of the colchicine site and T5 loop of α -tubulin completes the colchicine pocket [58,75]. It has been shown that the colchicine-site ligands occupy different parts of this site, and based upon this, this site is subdivided into three zones: i) zone 2 or the main zone which is a hydrophobic pocket and located at the center of the domain (i.e. β -tubulin subunit), ii) zone 1: an accessory pocket near zone 2 that is face the α -tubulin subunit interface, iii) zone 3: the second accessory pocket near zone 2 that is buried deeper in β -tubulin subunit (Figure 1-7A). The colchicine-site ligands studied so far occupy either zones 1 and 2, or zones 2 and 3, and a ligand simultaneously occupying all three zones has not yet been identified [58,76,77].

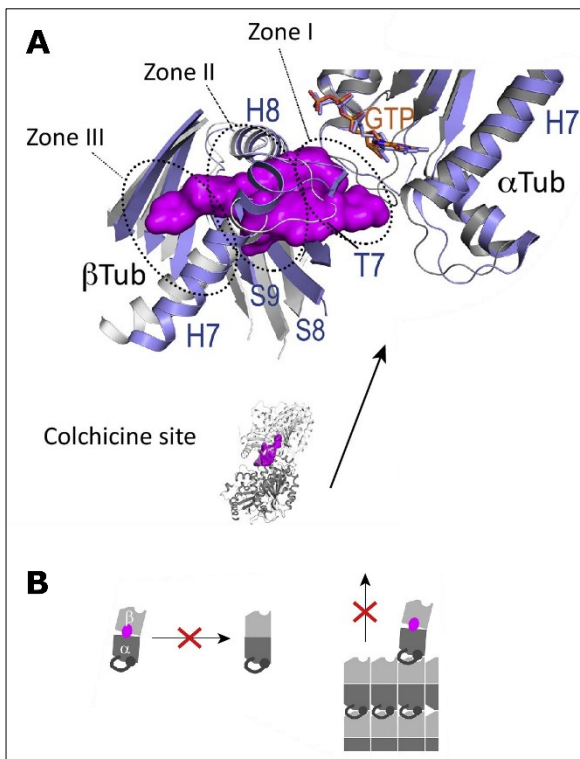


Figure 1-7. (A) Binding modes and mechanism of targeting of ligands targeting colchicine site. (B) Upon binding of MT-binding agents to colchicine-site, the curved-to-straight conformational transition in $\alpha\beta$ -tubulin heterodimer is inhibited which results in MT destabilization [58]. (Reprinted with permission from *Elsevier*, Trends in cell biology, from [58], Copyright 2018).

In the ligand-bound state, the hydrophobic contacts between the secondary structures of colchicine site and the ligand molecule play the main role. A few polar interactions are also involved in this process. During ligand binding, a conformational switch occurs in the T7 loop that frees up space for the entering ligand. The tubulin heterodimers have a curved-shaped conformation at their free state that upon assembling into MT polymer, switches into a straight conformation. This conformational transition from curved to straight is associated with movement of intradimer domain intermediating α and β subunits, where strands S8 and S9 could get closer to helix H8. *Along with this conformational* change, a translation of helix H7 also occurs that all together results in an overall contraction of the colchicine site. Given the role of this conformational transition in MT assembly, when a ligand binds to colchicine site, it prevents this curved-to-straight conformational change leading to inhibition of MT formation [19,73–75,78].

1.5 Scope and computational methodology

There is an extensive research effort directed toward the synthesis of modified derivatives of colchicine which could be as effective as colchicine with less side effects. However, the synthesis protocol of these derivatives is usually very complex, expensive, and time-consuming, which makes it very difficult to develop those compounds. Over the past three decades, computational-based drug discovery has played a significant role in the development of small molecules as therapeutic agents. Besides, computer-aided methods could be applied for toxicity prediction and optimization methods, which can speed the process and guide the experimental approaches [79].

In this thesis, we simulated several libraries of colchicine derivatives and studied their effects on tubulin and their free energies of binding. We also developed a QSAR model to predict the IC_{50} values of novel derivatives of colchicine based on their binding affinities. Moreover, the mode of action of a novel MT inhibitor, scoulerine was investigated by a combination of computational approaches.

In these studies, we employed several computational techniques, including similarity-based virtual screening, molecular docking [80], molecular dynamics simulations [81–83], *ab initio* quantum chemistry calculations [84–86], and QSAR modelling [87].

1.6 References

- [1] R. W. Ruddon, *Cancer Biology*. Oxford University Press, USA, 2007.
- [2] D. Hanahan and R. A. Weinberg, “Hallmarks of Cancer: The Next Generation,” *Cell*, vol. 144, no. 5, pp. 646–674, Mar. 2011, doi: 10.1016/j.cell.2011.02.013.
- [3] H. F. M. Kamel and H. S. B. Al-Amodi, “Cancer Biomarkers,” in *Role of Biomarkers in Medicine*, InTech, 2016.
- [4] H. Sung *et al.*, “Global cancer statistics 2020: GLOBOCAN estimates of incidence and mortality worldwide for 36 cancers in 185 countries,” *CA. Cancer J. Clin.*, p. caac.21660, Feb. 2021, doi: 10.3322/caac.21660.
- [5] A. A. Demers, D. R. Brenner, L. Smith, and A. Shaw, “At-a-glance, Cancer trends in Canada, 1984 to 2015,” *Heal. Promot. Chronic Dis. Prev. Canada*, vol. 39, no. 11, pp. 310–314, Nov. 2019, doi: 10.24095/hpcdp.39.11.04.
- [6] S. Pilleron *et al.*, “Estimated global cancer incidence in the oldest adults in 2018 and projections to 2050,” *Int. J. Cancer*, vol. 148, no. 3, pp. 601–608, Feb. 2021, doi: 10.1002/ijc.33232.
- [7] H. Lodish *et al.*, *Molecular Cell Biology*, 8th ed. W. H. Freeman, 2016.
- [8] S. Chakraborty and T. Rahman, “The difficulties in cancer treatment,” *Ecancermedicalscience*, vol. 6, p. ed16, 2012, doi: 10.3332/ecancer.2012.ed16.
- [9] D. Schaue and W. H. McBride, “Opportunities and challenges of radiotherapy for treating cancer,” *Nat. Rev. Clin. Oncol.*, vol. 12, no. 9, pp. 527–40, Sep. 2015, doi: 10.1038/nrclinonc.2015.120.
- [10] E. Bidram *et al.*, “A concise review on cancer treatment methods and delivery systems,” *J. Drug Deliv. Sci. Technol.*, vol. 54, p. 101350, Dec. 2019, doi: 10.1016/j.jddst.2019.101350.
- [11] P. M. Gunjal, G. Schneider, A. A. Ismail, S. S. Kakar, M. Kucia, and M. Z. Ratajczak, “Evidence for induction of a tumor metastasis-receptive microenvironment for ovarian cancer cells in bone marrow and other organs as an unwanted and underestimated side effect of chemotherapy/radiotherapy,” *J. Ovarian Res.*, vol. 8, p. 20, Mar. 2015, doi: 10.1186/s13048-015-0141-7.
- [12] S. Charmsaz, D. M. Collins, A. S. Perry, and M. Prencipe, “Novel Strategies for Cancer Treatment: Highlights from the 55th IACR Annual Conference,” *Cancers*

- (Basel)., vol. 11, no. 8, Aug. 2019, doi: 10.3390/cancers11081125.
- [13] V. Emuss, “The Molecular Biology of Cancer,” *Br. J. Cancer*, vol. 95, no. 8, pp. 1128–1128, Oct. 2006, doi: 10.1038/sj.bjc.6603379.
- [14] Komala M, Sathesh Kumar S, and Padmavathy J, “Novel Drug Formulation for the Treatment of Hepatic Cancer- A Review,” *Int. J. Res. Pharm. Sci.*, vol. 11, no. 3, pp. 4395–4401, Jul. 2020, doi: 10.26452/ijrps.v11i3.2658.
- [15] P. Ravi, Z. Bakouny, A. Schmidt, and T. K. Choueiri, “Novel Therapeutic Approaches and the Evolution of Drug Development in Advanced Kidney Cancer.,” *Cancer J.*, vol. 26, no. 5, pp. 464–470, doi: 10.1097/PPO.0000000000000477.
- [16] U. Hani *et al.*, “Recent advances in novel drug delivery systems and approaches for management of breast cancer: A comprehensive review,” *J. Drug Deliv. Sci. Technol.*, vol. 56, p. 101505, Apr. 2020, doi: 10.1016/j.jddst.2020.101505.
- [17] B. Alberts, *Molecular Biology of the Cell*. W.W. Norton, 2017.
- [18] J. Zhou and P. Giannakakou, “Targeting microtubules for cancer chemotherapy.,” *Curr. Med. Chem. Anticancer. Agents*, vol. 5, no. 1, pp. 65–71, Jan. 2005, doi: 10.2174/1568011053352569.
- [19] E. Nogales, S. G. Wolf, and K. H. Downing, “Structure of the alpha beta tubulin dimer by electron crystallography.,” *Nature*, vol. 391, no. 6663, pp. 199–203, Jan. 1998, doi: 10.1038/34465.
- [20] M. Auer, “Three-dimensional electron cryo-microscopy as a powerful structural tool in molecular medicine.,” *J. Mol. Med. (Berl.)*, vol. 78, no. 4, pp. 191–202, 2000, doi: 10.1007/s001090000101.
- [21] T. Allen, *Introduction to electron microscopy for biologists*. Elsevier Science, 2008.
- [22] Y. Fujiyoshi, “Structural physiology based on electron crystallography.,” *Protein Sci.*, vol. 20, no. 5, pp. 806–17, May 2011, doi: 10.1002/pro.621.
- [23] J. Torin Huzil, R. F. Ludueña, and J. Tuszynski, “Comparative modelling of human β tubulin isotypes and implications for drug binding.,” *Nanotechnology*, vol. 17, no. 4, pp. S90–S100, Feb. 2006, doi: 10.1088/0957-4484/17/4/014.
- [24] M. P. M. H. Benoit, A. B. Asenjo, and H. Sosa, “Cryo-EM reveals the structural basis of microtubule depolymerization by kinesin-13s.,” *Nat. Commun.*, vol. 9, no. 1, p. 1662, Apr. 2018, doi: 10.1038/s41467-018-04044-8.

- [25] E. Nogales, M. Whittaker, R. A. Milligan, and K. H. Downing, “High-resolution model of the microtubule.,” *Cell*, vol. 96, no. 1, pp. 79–88, Jan. 1999, doi: 10.1016/s0092-8674(00)80961-7.
- [26] H. Sosa *et al.*, “A model for the microtubule-Ncd motor protein complex obtained by cryo-electron microscopy and image analysis.,” *Cell*, vol. 90, no. 2, pp. 217–24, Jul. 1997, doi: 10.1016/s0092-8674(00)80330-x.
- [27] F. J. Fourniol *et al.*, “Template-free 13-protofilament microtubule-MAP assembly visualized at 8 Å resolution.,” *J. Cell Biol.*, vol. 191, no. 3, pp. 463–70, Nov. 2010, doi: 10.1083/jcb.201007081.
- [28] G. M. Alushin, G. C. Lander, E. H. Kellogg, R. Zhang, D. Baker, and E. Nogales, “High-Resolution Microtubule Structures Reveal the Structural Transitions in $\alpha\beta$ -Tubulin upon GTP Hydrolysis,” *Cell*, vol. 157, no. 5, pp. 1117–1129, May 2014, doi: 10.1016/j.cell.2014.03.053.
- [29] K. M. Yip, N. Fischer, E. Paknia, A. Chari, and H. Stark, “Atomic-resolution protein structure determination by cryo-EM.,” *Nature*, vol. 587, no. 7832, pp. 157–161, Nov. 2020, doi: 10.1038/s41586-020-2833-4.
- [30] A. Bartesaghi *et al.*, “2.2 Å resolution cryo-EM structure of β -galactosidase in complex with a cell-permeant inhibitor.,” *Science*, vol. 348, no. 6239, pp. 1147–51, Jun. 2015, doi: 10.1126/science.aab1576.
- [31] E. Binshtein and M. D. Ohi, “Cryo-electron microscopy and the amazing race to atomic resolution.,” *Biochemistry*, vol. 54, no. 20, pp. 3133–41, May 2015, doi: 10.1021/acs.biochem.5b00114.
- [32] D. Bhella, “Cryo-electron microscopy: an introduction to the technique, and considerations when working to establish a national facility.,” *Biophysical reviews*, vol. 11, no. 4, pp. 515–519, Aug. 2019, doi: 10.1007/s12551-019-00571-w.
- [33] J. A. Tuszynski and M. Kurzynski, *Introduction to Molecular Biophysics*. CRC Press, 2003.
- [34] T. Mitchison and M. Kirschner, “Dynamic instability of microtubule growth,” *Nature*, vol. 312, no. 5991, pp. 237–242, 1984, doi: 10.1038/312237a0.
- [35] R. A. Walker *et al.*, “Dynamic instability of individual microtubules analyzed by video light microscopy: rate constants and transition frequencies.,” *J. Cell Biol.*, vol.

- 107, no. 4, pp. 1437–48, Oct. 1988, doi: 10.1083/jcb.107.4.1437.
- [36] B. Alberts *et al.*, *Essential Cell Biology*, 6th ed. Garland Science, 2009.
- [37] L. R. B. Eldra P. Solomon, Diana W. Martin, *Biology*, 8th ed. Brooks/Cole, 2007.
- [38] J. J. Blow and T. U. Tanaka, “The chromosome cycle: coordinating replication and segregation. Second in the cycles review series.,” *EMBO Rep.*, vol. 6, no. 11, pp. 1028–34, Nov. 2005, doi: 10.1038/sj.embor.7400557.
- [39] S. Ruchaud, M. Carmena, and W. C. Earnshaw, “Chromosomal passengers: conducting cell division.,” *Nat. Rev. Mol. Cell Biol.*, vol. 8, no. 10, pp. 798–812, Oct. 2007, doi: 10.1038/nrm2257.
- [40] J. Zhou, D. Panda, J. W. Landen, L. Wilson, and H. C. Joshi, “Minor alteration of microtubule dynamics causes loss of tension across kinetochore pairs and activates the spindle checkpoint.,” *J. Biol. Chem.*, vol. 277, no. 19, pp. 17200–8, May 2002, doi: 10.1074/jbc.M110369200.
- [41] C. L. Rieder and R. E. Palazzo, “Colcemid and the mitotic cycle.,” *J. Cell Sci.*, vol. 102 (Pt 3, pp. 387–392, Jul. 1992.
- [42] O. J. Eigsti and P. Dustin, *Colchicine in agriculture, medicine, biology, and chemistry*. Ames,: Iowa State College Press, 1955.
- [43] A. Musacchio and E. D. Salmon, “The spindle-assembly checkpoint in space and time.,” *Nat. Rev. Mol. Cell Biol.*, vol. 8, no. 5, pp. 379–93, May 2007, doi: 10.1038/nrm2163.
- [44] M. A. Jordan and K. Kamath, “How do microtubule-targeted drugs work? An overview.,” *Curr. Cancer Drug Targets*, vol. 7, no. 8, pp. 730–742, 2007, doi: 10.2174/156800907783220417.
- [45] Q. Shi, K. Chen, S. L. Morris-Natschke, and K. H. Lee, “Recent progress in the development of tubulin inhibitors as antimitotic antitumor agents.,” *Curr. Pharm. Des.*, vol. 4, no. 3, pp. 219–248, Jun. 1998.
- [46] K.-S. Chan, C.-G. Koh, and H.-Y. Li, “Mitosis-targeted anti-cancer therapies: where they stand.,” *Cell Death Dis.*, vol. 3, no. 10, p. e411, Oct. 2012, doi: 10.1038/cddis.2012.148.
- [47] B. Bhattacharyya, D. Panda, S. Gupta, and M. Banerjee, “Anti-mitotic activity of colchicine and the structural basis for its interaction with tubulin.,” *Med. Res. Rev.*,

- vol. 28, no. 1, pp. 155–183, Jan. 2008, doi: 10.1002/med.20097.
- [48] B. A. Weaver, “How Taxol/paclitaxel kills cancer cells.,” *Mol. Biol. Cell*, vol. 25, no. 18, pp. 2677–2681, Sep. 2014, doi: 10.1091/mbc.E14-04-0916.
- [49] U. Majcher *et al.*, “Synthesis, antiproliferative activity and molecular docking of thiocolchicine urethanes.,” *Bioorg. Chem.*, vol. 81, pp. 553–566, 2018, doi: 10.1016/j.bioorg.2018.09.004.
- [50] M. A. Jordan and L. Wilson, “Microtubules as a target for anticancer drugs.,” *Nat. Rev. Cancer*, vol. 4, no. 4, pp. 253–65, Apr. 2004, doi: 10.1038/nrc1317.
- [51] C. Dumontet and M. A. Jordan, “Microtubule-binding agents: a dynamic field of cancer therapeutics.,” *Nat. Rev. Drug Discov.*, vol. 9, no. 10, pp. 790–803, Oct. 2010, doi: 10.1038/nrd3253.
- [52] J. J. Field, J. F. Díaz, and J. H. Miller, “The binding sites of microtubule-stabilizing agents.,” *Chem. Biol.*, vol. 20, no. 3, pp. 301–15, Mar. 2013, doi: 10.1016/j.chembiol.2013.01.014.
- [53] E. Mukhtar, V. M. Adhami, and H. Mukhtar, “Targeting microtubules by natural agents for cancer therapy.,” *Mol. Cancer Ther.*, vol. 13, no. 2, pp. 275–284, Feb. 2014, doi: 10.1158/1535-7163.MCT-13-0791.
- [54] K. E. Arnst *et al.*, “Current advances of tubulin inhibitors as dual acting small molecules for cancer therapy.,” *Med. Res. Rev.*, vol. 39, no. 4, pp. 1398–1426, Jul. 2019, doi: 10.1002/med.21568.
- [55] A. R. Ranade *et al.*, “Characterizing the Epothilone Binding Site on β -Tubulin by Photoaffinity Labeling: Identification of β -Tubulin Peptides TARGSQY and TSRGSQY as Targets of an Epothilone Photoprobe for Polymerized Tubulin.,” *J. Med. Chem.*, vol. 59, no. 7, pp. 3499–514, Apr. 2016, doi: 10.1021/acs.jmedchem.6b00188.
- [56] L. A. Amos, “What tubulin drugs tell us about microtubule structure and dynamics.,” *Semin. Cell Dev. Biol.*, vol. 22, no. 9, pp. 916–26, Dec. 2011, doi: 10.1016/j.semcdb.2011.09.014.
- [57] Y. Lu, J. Chen, M. Xiao, W. Li, and D. D. Miller, “An overview of tubulin inhibitors that interact with the colchicine binding site.,” *Pharm. Res.*, vol. 29, no. 11, pp. 2943–71, Nov. 2012, doi: 10.1007/s11095-012-0828-z.

- [58] M. O. Steinmetz and A. E. Prota, "Microtubule-Targeting Agents: Strategies To Hijack the Cytoskeleton.," *Trends Cell Biol.*, vol. 28, no. 10, pp. 776–792, Oct. 2018, doi: 10.1016/j.tcb.2018.05.001.
- [59] L. M. West, P. T. Northcote, and C. N. Battershill, "Peloruside A: a potent cytotoxic macrolide isolated from the new zealand marine sponge *Mycale* sp.," *J. Org. Chem.*, vol. 65, no. 2, pp. 445–449, Jan. 2000, doi: 10.1021/jo991296y.
- [60] D. G. Corley, R. Herb, R. E. Moore, P. J. Scheuer, and V. J. Paul, "Laulimalides. New potent cytotoxic macrolides from a marine sponge and a nudibranch predator," *J. Org. Chem.*, vol. 53, no. 15, pp. 3644–3646, Jul. 1988, doi: 10.1021/jo00250a053.
- [61] A. Kanakkanthara, M. R. Rowe, J. J. Field, P. T. Northcote, P. H. Teesdale-Spittle, and J. H. Miller, " β I-tubulin mutations in the laulimalide/peloruside binding site mediate drug sensitivity by altering drug–tubulin interactions and microtubule stability," *Cancer Lett.*, vol. 365, no. 2, pp. 251–260, Sep. 2015, doi: 10.1016/j.canlet.2015.06.001.
- [62] T. N. Gaitanos *et al.*, "Peloruside A does not bind to the taxoid site on beta-tubulin and retains its activity in multidrug-resistant cell lines.," *Cancer Res.*, vol. 64, no. 15, pp. 5063–5067, Aug. 2004, doi: 10.1158/0008-5472.CAN-04-0771.
- [63] D. E. Pryor *et al.*, "The microtubule stabilizing agent laulimalide does not bind in the taxoid site, kills cells resistant to paclitaxel and epothilones, and may not require its epoxide moiety for activity.," *Biochemistry*, vol. 41, no. 29, pp. 9109–9115, Jul. 2002, doi: 10.1021/bi020211b.
- [64] E. H. Kellogg *et al.*, "Insights into the Distinct Mechanisms of Action of Taxane and Non-Taxane Microtubule Stabilizers from Cryo-EM Structures," *J. Mol. Biol.*, vol. 429, no. 5, pp. 633–646, 2017, doi: 10.1016/j.jmb.2017.01.001.
- [65] A. E. Prota *et al.*, "Structural basis of microtubule stabilization by laulimalide and peloruside A.," *Angew. Chem. Int. Ed. Engl.*, vol. 53, no. 6, pp. 1621–5, Feb. 2014, doi: 10.1002/anie.201307749.
- [66] Y.-N. Cao, L.-L. Zheng, D. Wang, X.-X. Liang, F. Gao, and X.-L. Zhou, "Recent advances in microtubule-stabilizing agents.," *Eur. J. Med. Chem.*, vol. 143, pp. 806–828, Jan. 2018, doi: 10.1016/j.ejmech.2017.11.062.
- [67] B. Dasgeb, D. Kornreich, K. McGuinn, L. Okon, I. Brownell, and D. L. Sackett,

- “Colchicine: an ancient drug with novel applications.,” *Br. J. Dermatol.*, vol. 178, no. 2, pp. 350–356, Feb. 2018, doi: 10.1111/bjd.15896.
- [68] M. I. Lopes *et al.*, “Beneficial effects of colchicine for moderate to severe COVID-19: a randomised, double-blinded, placebo-controlled clinical trial.,” *RMD open*, vol. 7, no. 1, 2021, doi: 10.1136/rmdopen-2020-001455.
- [69] A. Kumar, P. R. Sharma, and D. M. Mondhe, “Potential anticancer role of colchicine-based derivatives: an overview.,” *Anticancer. Drugs*, vol. 28, no. 3, pp. 250–262, 2017, doi: 10.1097/CAD.0000000000000464.
- [70] Z.-Y. Lin, C.-H. Kuo, D.-C. Wu, and W.-L. Chuang, “Anticancer effects of clinically acceptable colchicine concentrations on human gastric cancer cell lines.,” *Kaohsiung J. Med. Sci.*, vol. 32, no. 2, pp. 68–73, Feb. 2016, doi: 10.1016/j.kjms.2015.12.006.
- [71] K. Larocque, P. Ovadje, S. Djurdjevic, M. Mehdi, J. Green, and S. Pandey, “Novel analogue of colchicine induces selective pro-death autophagy and necrosis in human cancer cells.,” *PLoS One*, vol. 9, no. 1, p. e87064, 2014, doi: 10.1371/journal.pone.0087064.
- [72] Y. Finkelstein *et al.*, “Colchicine poisoning: the dark side of an ancient drug.,” *Clin. Toxicol. (Phila.)*, vol. 48, no. 5, pp. 407–14, Jun. 2010, doi: 10.3109/15563650.2010.495348.
- [73] R. B. G. Ravelli *et al.*, “Insight into tubulin regulation from a complex with colchicine and a stathmin-like domain.,” *Nature*, vol. 428, no. 6979, pp. 198–202, Mar. 2004, doi: 10.1038/nature02393.
- [74] J. Löwe, H. Li, K. . Downing, and E. Nogales, “Refined structure of $\alpha\beta$ -tubulin at 3.5 Å resolution 1 1Edited by I. A. Wilson,” *J. Mol. Biol.*, vol. 313, no. 5, pp. 1045–1057, Nov. 2001, doi: 10.1006/jmbi.2001.5077.
- [75] A. Dorléans, B. Gigant, R. B. G. Ravelli, P. Mailliet, V. Mikol, and M. Knossow, “Variations in the colchicine-binding domain provide insight into the structural switch of tubulin.,” *Proc. Natl. Acad. Sci. U. S. A.*, vol. 106, no. 33, pp. 13775–9, Aug. 2009, doi: 10.1073/pnas.0904223106.
- [76] M.-J. Pérez-Pérez, E.-M. Priego, O. Bueno, M. S. Martins, M.-D. Canela, and S. Liekens, “Blocking Blood Flow to Solid Tumors by Destabilizing Tubulin: An

- Approach to Targeting Tumor Growth.,” *J. Med. Chem.*, vol. 59, no. 19, pp. 8685–8711, 2016, doi: 10.1021/acs.jmedchem.6b00463.
- [77] A. Massarotti, A. Coluccia, R. Silvestri, G. Sorba, and A. Brancale, “The tubulin colchicine domain: a molecular modeling perspective.,” *ChemMedChem*, vol. 7, no. 1, pp. 33–42, Jan. 2012, doi: 10.1002/cmdc.201100361.
- [78] A. Akhmanova and M. O. Steinmetz, “Control of microtubule organization and dynamics: two ends in the limelight.,” *Nat. Rev. Mol. Cell Biol.*, vol. 16, no. 12, pp. 711–26, Dec. 2015, doi: 10.1038/nrm4084.
- [79] G. Sliwoski, S. Kothiwale, J. Meiler, and E. W. J. Lowe, “Computational methods in drug discovery.,” *Pharmacol. Rev.*, vol. 66, no. 1, pp. 334–395, 2014, doi: 10.1124/pr.112.007336.
- [80] D. B. Kitchen, H. Decornez, J. R. Furr, and J. Bajorath, “Docking and scoring in virtual screening for drug discovery: methods and applications.,” *Nat. Rev. Drug Discov.*, vol. 3, no. 11, pp. 935–949, Nov. 2004, doi: 10.1038/nrd1549.
- [81] C. J. Cramer, *Essentials of Computational Chemistry Theories and Models*. Wiley, 2004.
- [82] S. A. Adcock and J. A. McCammon, “Molecular Dynamics: Survey of Methods for Simulating the Activity of Proteins,” *Chem. Rev.*, vol. 106, no. 5, pp. 1589–1615, May 2006, doi: 10.1021/cr040426m.
- [83] M. Karplus and J. A. McCammon, “Molecular dynamics simulations of biomolecules,” *Nat. Struct. Biol.*, vol. 9, no. 9, pp. 646–652, Sep. 2002, doi: 10.1038/nsb0902-646.
- [84] I. N. Levine, *Quantum chemistry*. Englewood Cliffs, NJ: Prentice Hall, 1991.
- [85] F. Jensen, *Introduction to Computational Chemistry*. Hoboken: John Wiley and Sons Ltd, 2006.
- [86] R. A. Friesner, “Ab initio quantum chemistry: Methodology and applications,” *Proceedings of the National Academy of Sciences*, vol. 102, no. 19, pp. 6648–6653, 2005.
- [87] J. Verma, V. M. Khedkar, and E. C. Coutinho, “3D-QSAR in drug design--a review.,” *Curr. Top. Med. Chem.*, vol. 10, no. 1, pp. 95–115, 2010, doi: 10.2174/156802610790232260.

Chapter 2:

Synthesis, anticancer activity and molecular docking studies of *N*-deacetylthiocolchicine and 4-iodo-*N*-deacetylthiocolchicine derivatives*

*The paper in this chapter is included by permission from the publisher (Elsevier) and the journal (*Bioorganic & Medicinal Chemistry*). All authors of the paper were notified about its inclusion in the thesis.

Greta Klejborowska, Alicja Urbaniak, Ewa Maj, Joanna Wietrzyk, Mahshad Moshari, Jordane Preto, Jack A Tuszynski, Timothy C Chambers, and Adam Huczyński. 2021. Synthesis, anticancer activity and molecular docking studies of *N*-deacetylthiocolchicine and 4-iodo-*N*-deacetylthiocolchicine derivatives. *Bioorg. Med. Chem.* 32, 116014. DOI:<https://doi.org/10.1016/j.bmc.2021.116014>

2.1 Introduction

Colchicine isolated from *Colchicum autumnale* [1]. It is used for the treatment of acute gout, familial Mediterranean fever, Behçet's disease, pericarditis, and other medical conditions [2-12]. It also acts as an anticancer agent and its mechanism of action is well-described in the scientific literature and is linked to its ability to inhibit mitosis. Specifically, colchicine binds to β -tubulin and forms complexes with tubulin dimers, which destabilizes microtubules and suppresses microtubule dynamics preventing mitotic spindle formation. This consequently leads to mitotic arrest and cell death typically *via* apoptosis [13–16]. Despite numerous pre-clinical findings highlighting beneficial effects of colchicine treatment for various types of cancers, its clinical application remains limited mainly to anti-inflammatory indications, due to its associated side-effects. To overcome those limitations, efforts are focused on developing more clinically-applicable colchicine derivatives [17-40].

Brossi *et al.* synthesized a series of N-acyl and N-aroyl derivatives prepared from deacetylcolchicine. Several compounds showed high potency in the lymphocytic leukemia P388 screens *in vitro* and *in vivo* [41]. Later Kerekes *et al.* synthesized analogues of thiocolchicine, a very potent inhibitor of tubulin polymerization and cell growth, including N-acyldeacetylthiocolchicines, N-(alkoxycarbonyl)deacetylthiocolchicines, thiodemecolchicine and its methyl carbamate, as well as O-ethyl ethers of demethylthiocolchicines [42]. Both novel and previously described analogues were evaluated *in vitro* in a tubulin binding assay, *in vivo* in mice for acute toxicity, and in the P388 lymphocytic leukemia model [42]. Sun *et al.* subsequently reported three series of novel thiocolchicine analogs, N-acyl-, N-aroyl-, and N-(substituted benzyl)-deacetylthiocolchicinoids [43]. Those derivatives were evaluated for their cytotoxicity against various tumor cell lines, with particular emphasis on solid tumor cell lines, and for their inhibitory effects on tubulin polymerization *in vitro*. In 2011, Takayama's research group published results of their studies on C-4 halogen substituted colchicine derivatives, including 4-iodocolchicine [29]. 4-iodocolchicine showed *in vitro* similar potency against A549, HT29 and HCT116 cancerous cell lines to other halogenated colchicine derivatives in the C-4 position. Despite satisfactory results, to the best of our knowledge, it has not been implemented in *in vivo* studies or has not been further modified. In our previous

research, we developed the concept of double- [33] and triple-modified colchicine analogs with diversified carbamate [34,35,44] or amide [45,46], substituents in the C-7 position. 4-iodothiocolchicine, double-modified colchicine derivative in the C-4 and C-10 position, showed very high potency against A549, MCF-7 and LoVo cancerous cell lines in the nanomolar range, higher than the activity of unmodified colchicine or 4-iodocolchicine. Interestingly, the high antiproliferative activity of 4-iodothiocolchicine was combined with beneficial selectivity index values [33]. Also the majority of novel triple-modified derivatives showed antiproliferative activity in the nanomolar range together with beneficial selectivity index values when tested against normal cells. Encouraged by the previously reported results, we sought to synthesize two series of novel double-modified derivatives of N-deacetylthiocolchicine and triple-modified derivatives of 4-iodo-N-deacetylthiocolchicine. In this study, we describe their synthesis, molecular docking, and anti-proliferative activities against several cancer cell lines.

2.2 Materials and methods

General

All precursors and solvents for the synthesis were obtained from Sigma Aldrich (Merck KGaA, Saint Louis, MO, USA) and were used without further purification. CDCl_3 spectral grade solvent was stored over 3 Å molecular sieves for several days. TLC was performed on precoated plates (TLC silica gel 60 F254, Aluminium Plates Merck, Merck KGaA, Saint Louis, MO, USA) visualized by illumination with an UV lamp. HPLC grade solvents (without further purification) were used for flash chromatography (CHROMASOLV from Sigma Aldrich, Merck KGaA, Saint Louis, MO, USA). The elemental analysis of compounds was performed on Vario ELIII (Elementar, Langensfeld, Germany).

2.2.1 Spectroscopic measurements

The ^1H , ^{13}C spectra were recorded on a Varian VNMR-S 400 MHz spectrometer (Varian, Inc., Palo Alto, CA, USA). ^1H NMR measurements of **2–20** (0.07 mol dm^{-3}) in

CDCl₃ were carried out at the operating frequency 402.64 MHz. The error of the chemical shift value was 0.01 ppm. The ¹³C NMR spectra were recorded at the operating frequency 101.25 MHz. The error of chemical shift value was 0.1 ppm. All spectra were locked to deuterium resonance of CDCl₃. The ¹H and ¹³C NMR spectra are shown in the Appendix A.

The FT-IR spectra of **2–20** in the mid infrared region were recorded in KBr. The spectra were taken with an IFS 113v FT-IR spectrophotometer (Bruker, Karlsruhe, Germany) equipped with a DTGS detector; resolution 2 cm⁻¹, NSS = 64. The Happ-Genzel apodization function was used. The ESI (Electrospray Ionisation) mass spectra were recorded also on a Waters/Micromass (Waters Corporation, Manchester, UK) ZQ mass spectrometer equipped with a Harvard Apparatus syringe pump. The samples were prepared in dry acetonitrile (5 × 10⁻⁵ mol dm⁻³). The sample was infused into the ESI source using a Harvard pump at a flow rate of 20 ml min⁻¹. The ESI source potentials were: capillary 3 kV, lens 0.5 kV, extractor 4 V. The standard ESI mass spectra were recorded at the cone voltages: 10 and 30 V. The source temperature was 120°C and the desolvation temperature was 300°C. Nitrogen was used as the nebulizing and desolvation gas at flow-rates of 100 dm³ h⁻¹. Mass spectra were acquired in the positive ion detection mode with unit mass resolution at a step of 1 *m/z* unit. The mass range for ESI experiments was from *m/z* = 100 to *m/z* = 1000, as well as from *m/z* = 200 to *m/z* = 1500.

2.2.2 Synthesis

Synthesis of thiocolchicine (2)

To a mixture of **1** (500 mg, 1.25 mmol) in MeOH/water (1/1, *v/v*, 5 ml), the sodium methanethiolate (solution 21% in H₂O, 0.83 ml, 2.5 mmol) was added. The mixture was stirred in at RT for 72 h. Reaction time was determined by TLC. After that time, the reaction mixture was quenched by the addition of water (150 ml). The whole mixture was extracted four times with CH₂Cl₂, and the combined organic layers were dried over MgSO₄, filtered, and evaporated under reduced pressure. The residue was purified by CombiFlash® (hexane/EtOAc (1/1), then EtOAc/MeOH, increasing concentration gradient) to give **2** (C₂₂H₂₅NO₅S, MW = 415.5 g/mol) with yield 78% [47]. ¹H NMR (403 MHz, CDCl₃) δ 7.92 (s, 1H), 7.46 (s, 1H), 7.33 (d, *J* = 10.4 Hz, 1H), 7.10 (d, *J* = 10.5 Hz, 1H), 6.55 (s, 1H),

4.72–4.64 (m, 1H), 3.95 (s, 3H), 3.91 (s, 3H), 3.67 (s, 3H), 2.54 (dd, $J = 13.0, 5.8$ Hz, 1H), 2.45 (s, $J = 5.7$ Hz, 3H), 2.43–2.26 (m, 2H), 1.99 (s, 3H), 1.94 (dd, $J = 11.8, 5.5$ Hz, 1H) ppm. ^{13}C -NMR (101 MHz, CDCl_3) δ 182.4, 170.0, 158.1, 153.6, 151.8, 151.1, 141.6, 138.6, 134.8, 134.4, 128.3, 126.7, 125.6, 107.3, 61.6, 61.4, 56.1, 52.3, 36.4, 29.9, 22.8, 15.1 ppm. FT-IR (KBr pellet): 3283, 2935, 1660, 1605, 1541, 1485, 1461, 1425, 1404, 1349, 1321, 1286, 1236, 1195, 1155, 1138, 1095, 1023 cm^{-1} . ESI-MS (m/z): $[\text{M}+\text{H}]^+$ calcd. 416, found 416, $[\text{M}+\text{Na}]^+$ calcd. 438, found 438, $[\text{M}+\text{K}]^+$ calcd. 454 found 454, $[2\text{M}+\text{Na}]^+$ calcd. 853, found 853, $[3\text{M}+\text{Na}]^+$ calcd. 1268, found 1268.

Synthesis of N-deacetylthiocolchicine (3)

Compound **3** was prepared from **2** by hydrolysis with 2 M HCl. To a solution of compound **2** (500 mg, 1.20 mmol) in MeOH (3 ml), the 2 N HCl solution (5 ml) was added. The mixture was stirred at 90°C for 72 h. Reaction time was determined by TLC. After that time the reaction mixture was quenched by the addition of water (100 ml). The whole mixture was extracted four times with CH_2Cl_2 , and the combined organic layers were dried over MgSO_4 , filtered, and evaporated under reduced pressure. The residue was purified by CombiFlash® (EtOAc/MeOH, increasing concentration gradient) to give **3** ($\text{C}_{20}\text{H}_{23}\text{NO}_4\text{S}$, MW = 373.5 g/mol) with yield 86% [42]. ^1H NMR (403 MHz, CDCl_3) δ 7.58 (s, 1H), 7.19 (d, $J = 10.3$ Hz, 1H), 7.03 (d, $J = 10.7$ Hz, 1H), 6.54 (s, 1H), 3.91 (s, 3H), 3.91 (s, 3H), 3.75–3.69 (m, 1H), 3.66 (s, 3H), 2.52–2.26 (m, 6H), 1.65–1.57 (m, 3H) ppm. ^{13}C NMR (101 MHz, CDCl_3) δ 182.5, 157.8, 153.7, 153.4, 150.6, 141.1, 138.1, 135.2, 134.1, 129.3, 125.9, 125.4, 106.9, 61.1, 61.0, 56.0, 53.6, 40.2, 30.5, 15.1 ppm. FT-IR (KBr pellet): 3365, 3293, 2931, 2852, 2838, 1603, 1546, 1485, 1458, 1422, 1402, 1347, 1318, 1138, 1094, 1017 cm^{-1} . ESI-MS (m/z): $[\text{M}+\text{H}]^+$ calcd 374, found 374.

General procedure for the synthesis of colchicine derivatives (4–10)

Compounds **4–10** were obtained directly from compound **3**. To a solution of compound **4** (100 mg, 0.27 mmol) in tetrahydrofuran (THF, 5 ml) cooled to the 0 °C temperature, the following compounds were added: Et_3N (2 ml, 14 mmol) and DMAP (catalytic amount). The mixture was first stirred at 0 °C temperature for a few minutes and

then the solution of respective acyl chloride (**4–9**) or diethylcarbamoyl chloride (**10**) in THF (0.81 mmol in 2.5 ml) was added dropwise. The mixture was stirred at RT for the next 24 h. The solution was filtered to remove triethylamine hydrochloride. The THF was evaporated and the residue was purified by CombiFlash® (hexane/ethyl acetate, increasing concentration gradient) to give respective compounds as amorphous yellow solids with yield from 38% to 82% (**4–10**).

Compound **4**: ^1H NMR (403 MHz, CDCl_3) δ 7.26 (d, $J = 10.3$ Hz, 1H), 7.18 (s, 1H), 7.09 (d, $J = 7.5$ Hz, 1H), 7.02 (d, $J = 10.6$ Hz, 1H), 6.52 (s, 1H), 4.65 (dt, $J = 11.8$, 6.9 Hz, 1H), 3.92 (s, 3H), 3.88 (s, 3H), 3.83 (d, $J = 4.3$ Hz, 2H), 3.63 (s, 3H), 3.41 (s, 3H), 2.59–2.51 (m, 1H), 2.48–2.37 (m, 4H), 2.22 (tt, $J = 13.0$, 6.6 Hz, 1H), 1.88 (ddd, $J = 11.9$, 8.9, 5.8 Hz, 1H) ppm. ^{13}C NMR (101 MHz, CDCl_3) δ 182.3, 167.0, 158.2, 153.5, 151.2, 150.0, 141.6, 137.7, 134.4, 134.1, 128.5, 126.1, 125.6, 107.3, 71.6, 61.4, 61.3, 59.1, 56.0, 51.2, 36.8, 29.8, 15.1 ppm. FT-IR: 3287, 2937, 1672, 1607, 1552, 1486, 1462, 1426, 1403, 1350, 1323, 1287, 1264, 1236, 1195, 1154, 1138, 1096, 1022 cm^{-1} . ESI-MS (m/z): $[\text{M}+\text{Na}]^+$ calcd 468, found 468. Anal. Calcd. for C, 62.00; H, 6.11; N, 3.14; O, 21.55; S, 7.20; found C, 61.89; H, 6.05; N, 3.19; S, 7.35.

Compound **5**: ^1H NMR (403 MHz, CDCl_3) δ 7.55 (d, $J = 7.4$ Hz, 1H), 7.45 (s, 1H), 7.34–7.29 (m, 1H), 7.08 (d, $J = 10.8$ Hz, 1H), 6.53 (s, 1H), 4.70 (dt, $J = 11.8$, 6.9 Hz, 1H), 3.94 (s, 3H), 3.90 (s, 3H), 3.66 (s, 3H), 3.51 (td, $J = 6.6$, 1.1 Hz, 2H), 2.55–2.47 (m, 1H), 2.45–2.33 (m, 6H), 2.26 (dt, $J = 18.6$, 6.3 Hz, 1H), 2.08–1.99 (m, 2H), 1.94–1.86 (m, 1H) ppm. ^{13}C NMR (101 MHz, CDCl_3) δ 182.4, 171.5, 158.2, 153.6, 151.5, 151.1, 141.6, 138.4, 134.7, 134.3, 128.6, 126.6, 125.6, 107.3, 61.6, 61.4, 56.1, 51.9, 44.4, 36.8, 33.0, 30.0, 28.1, 15.12 ppm. FT-IR: 3273, 2937, 1669, 1604, 1531, 1486, 1461, 1428, 1403, 1368, 1346, 1320, 1282, 1234, 1194, 1156, 1138, 1092, 1020 cm^{-1} . ESI-MS (m/z): $[\text{M}+\text{Na}]^+$ calcd 500, found 500. Anal. Calcd. for C, 60.30; H, 5.90; Cl, 7.42; N, 2.93; O, 16.74; S, 6.71; found C, 60.46; H, 6.01; Cl, 7.44; N, 2.98; S, 6.69.

Compound **6**: ^1H NMR (403 MHz, CDCl_3) δ 7.83–7.79 (m, 2H), 7.68 (d, $J = 7.3$ Hz, 1H), 7.49 (s, 1H), 7.40–7.28 (m, 4H), 7.08 (d, $J = 10.8$ Hz, 1H), 6.56 (s, 1H), 4.91 (dt, $J = 11.7$, 6.8 Hz, 1H), 3.96 (s, 3H), 3.91 (s, 3H), 3.74 (s, 3H), 2.57 (dd, $J = 13.3$, 5.9 Hz, 1H), 2.50–2.40 (m, 4H), 2.35 (td, $J = 12.4$, 6.2 Hz, 1H), 2.07 (td, $J = 11.7$, 5.4 Hz, 1H) ppm. ^{13}C NMR (101 MHz, CDCl_3) δ 182.2, 166.8, 158.2, 153.6, 151.2, 141.6, 138.3, 134.6,

134.4, 133.5, 131.5, 128.7, 128.4, 127.1, 126.4, 125.7, 107.3, 61.7, 61.4, 56.1, 52.5, 36.6, 30.0, 15.1 ppm. FT-IR: 3334, 2937, 1658, 1605, 1545, 1528, 1485, 1461, 1424, 1404, 1350, 1322, 1287, 1235, 1195, 1154, 1137, 1095, 1020 cm^{-1} . ESI-MS (m/z): $[\text{M}+\text{H}]^+$ calcd 478, found 478, $[\text{M}+\text{Na}]^+$ calcd 500, found 500. Anal. Calcd. for C, 67.90; H, 5.70; N, 2.93; O, 16.75; S, 6.71; found C, 67.81; H, 5.78; N, 2.89; S, 6.79.

Compound 7: ^1H NMR (403 MHz, CDCl_3) δ 7.39 (s, 1H), 7.30 (d, $J = 10.3$ Hz, 1H), 7.07 (d, $J = 10.6$ Hz, 1H), 6.52 (s, $J = 4.6$ Hz, 1H), 4.67 (dt, $J = 11.8, 6.7$ Hz, 1H), 3.93 (s, 3H), 3.89 (s, 3H), 3.66 (s, 3H), 2.51 (dd, $J = 13.3, 6.2$ Hz, 1H), 2.45–2.33 (m, 4H), 2.30–2.22 (m, 3H), 1.95–1.84 (m, 1H), 1.09 (t, $J = 7.6$ Hz, 3H) ppm. ^{13}C NMR (101 MHz, CDCl_3) δ 182.4, 173.6, 158.1, 153.5, 151.6, 151.1, 141.6, 138.4, 134.6, 134.4, 128.4, 126.6, 125.7, 107.3, 61.7, 61.3, 56.1, 51.9, 36.6, 29.9, 29.2, 15.1, 9.5 ppm. FT-IR: 3303, 2937, 1660, 1607, 1543, 1486, 1462, 1425, 1404, 1349, 1321, 1283, 1235, 1196, 1154, 1138, 1096, 1022 cm^{-1} . ESI-MS (m/z): $[\text{M}+\text{H}]^+$ calcd 430, found 430, $[\text{M}+\text{Na}]^+$ calcd 552, found 552 $[\text{M}+\text{K}]^+$ calcd 468, found 468. Anal. Calcd. for C, 64.31; H, 6.34; N, 3.26; O, 18.62; S, 7.42; found C, 64.41; H, 6.46; N, 3.22; S, 7.48.

Compound 8: ^1H NMR (403 MHz, CDCl_3) δ 7.45 (s, 1H), 7.41 (d, $J = 7.6$ Hz, 1H), 7.32–7.28 (m, 1H), 7.06 (d, $J = 10.8$ Hz, 1H), 6.52 (s, 1H), 4.69 (dt, $J = 11.8, 7.0$ Hz, 1H), 3.93 (s, 3H), 3.89 (s, 3H), 3.67 (s, 3H), 2.51 (dt, $J = 13.5, 6.8$ Hz, 2H), 2.44–2.32 (m, 4H), 2.25 (dt, $J = 18.6, 6.3$ Hz, 1H), 1.89 (td, $J = 11.8, 6.1$ Hz, 1H), 1.12 (dd, $J = 6.9, 4.0$ Hz, 6H). ^{13}C NMR (101 MHz, CDCl_3) δ 182.3, 176.8, 158.0, 153.5, 151.7, 151.2, 141.6, 138.4, 134.5, 134.4, 128.6, 126.5, 125.7, 107.3, 61.7, 61.3, 56.1, 51.5, 36.7, 35.2, 30.0, 19.5, 19.5, 15.1 ppm. FT-IR: 3312, 2968, 2935, 1669, 1607, 1544, 1486, 1461, 1425, 1404, 1349, 1322, 1283, 1235, 1196, 1154, 1137, 1096, 1021 cm^{-1} . ESI-MS (m/z): $[\text{M}+\text{Na}]^+$ calcd 466, found 466. Anal. Calcd. for C, 64.99; H, 6.59; N, 3.16; O, 18.04; S, 7.23; found C, 64.87; H, 6.56; N, 3.15; S, 7.31.

Compound 9: ^1H NMR (403 MHz, CDCl_3) δ 7.56 (d, $J = 7.4$ Hz, 1H), 7.45 (s, 1H), 7.31 (d, $J = 10.4$ Hz, 1H), 7.08 (d, $J = 10.8$ Hz, 1H), 6.54 (s, 1H), 4.71 (dt, $J = 11.8, 6.9$ Hz, 1H), 3.95 (s, 3H), 3.91 (s, 3H), 3.67 (s, 3H), 2.52 (dd, $J = 13.3, 6.1$ Hz, 1H), 2.46–2.34 (m, 4H), 2.30–2.21 (m, 3H), 1.89 (td, $J = 11.9, 6.2$ Hz, 1H), 1.58 (dd, $J = 14.6, 7.2$ Hz, 2H), 1.30–1.19 (m, 12H), 0.86 (t, $J = 6.9$ Hz, 3H) ppm. ^{13}C NMR (101 MHz, CDCl_3) δ 182.3, 173.0, 158.0, 153.5, 151.7, 151.1, 141.5, 138.4, 134.6, 134.4, 128.6, 126.5, 125.7,

107.3, 61.6, 61.3, 56.0, 51.8, 36.6, 36.3, 31.8, 30.0, 29.3, 29.3, 29.2, 29.2, 25.5, 22.6, 15.1, 14.0 ppm. FT-IR: 3298, 2927, 2853, 1655, 1607, 1543, 1485, 1461, 1425, 1404, 1348, 1321, 1282, 1235, 1195, 1154, 1137, 1097, 1022 cm^{-1} . ESI-MS (m/z): $[\text{M}+\text{Na}]^+$ calcd 550, found 550. Anal. Calcd. for C, 68.28; H, 7.83; N, 2.65; O, 15.16; S, 6.08; found C, 68.21; H, 7.98; N, 2.68; S, 5.98.

Compound **10**: ^1H NMR (403 MHz, CDCl_3) δ 7.48 (s, 1H), 7.26 (d, $J = 10.4$ Hz, 1H), 7.03–6.99 (d, $J = 10.8$ Hz, 1H), 6.50 (s, 1H), 5.90 (d, $J = 7.1$ Hz, 1H), 4.66 (dt, $J = 11.7, 6.7$ Hz, 1H), 3.91 (s, 3H), 3.87 (s, 3H), 3.67 (s, 3H), 3.32–3.25 (m, 4H), 2.48 (dd, $J = 13.3, 5.7$ Hz, 1H), 2.41–2.20 (m, 5H), 1.97–1.86 (m, 1H), 1.11 (t, $J = 7.1$ Hz, 6H) ppm. ^{13}C NMR (101 MHz, CDCl_3) δ 182.2, 157.8, 156.0, 153.3, 152.6, 151.1, 141.5, 138.4, 134.6, 134.3, 129.2, 126.2, 125.8, 107.2, 61.7, 61.3, 56.0, 53.1, 40.9, 37.2, 30.2, 15.0, 13.9 ppm. FT-IR: 3372, 2970, 2935, 1641, 1607, 1550, 1523, 1486, 1460, 1425, 1404, 1349, 1322, 1282, 1269, 1236, 1195, 1152, 1138, 1096, 1021 cm^{-1} . ESI-MS (m/z): $[\text{M}+\text{H}]^+$ calcd 473, found 473, $[\text{M}+\text{Na}]^+$ calcd 495, found 495, $[\text{M}+\text{K}]^+$ calcd 511, found 511. Anal. Calcd. for C, 63.54; H, 6.82; N, 5.93; O, 16.93; S, 6.78; found C, 63.41; H, 6.77; N, 6.01; S, 6.61.

Synthesis of 4-iodocolchicine (11)

A mixture of *N*-iodosuccinimide (560 mg, 2.49 mmol) and **1** (500 mg, 1.25 mmol) in AcOH was stirred at 70°C under nitrogen atmosphere for the 20 h. Reaction time was determined by TLC. The reaction was quenched with saturated aqueous $\text{Na}_2\text{S}_2\text{O}_3$. The whole mixture was extracted four times with CH_2Cl_2 , and the combined organic layers were dried over MgSO_4 , filtered, and evaporated under reduced pressure. The residue was purified by CombiFlash® (EtOAc/MeOH, increasing concentration gradient) to give **11** with yield 95% [29]. ^1H NMR (403 MHz, CDCl_3) δ 8.22 (d, $J = 5.6$ Hz, 1H), 7.61 (s, 1H), 7.30 (d, $J = 10.7$ Hz, 1H), 6.89 (d, $J = 11.2$ Hz, 1H), 4.55–4.47 (m, 1H), 4.04 (s, 3H), 3.97 (s, 3H), 3.95 (s, 3H), 3.63 (s, 3H), 3.21–3.15 (m, 1H), 2.40 (dd, $J = 12.7, 5.0$ Hz, 1H), 1.99 (s, 3H), 1.87–1.81 (m, 1H) ppm. ^{13}C NMR (101 MHz, CDCl_3) δ 179.5, 170.2, 164.4, 153.4, 152.0, 151.4, 145.6, 136.7, 136.2, 135.6, 130.1, 129.5, 112.5, 92.1, 61.5, 61.3, 60.7, 56.5, 52.6, 34.4, 34.4, 22.7 ppm. FT-IR (KBr pellet): 3274, 2934, 1662, 1617, 1588, 1563, 1461,

1406, 1393, 1346, 1318, 1266, 1249, 1171, 1136, 1078, 1015 cm^{-1} . ESI-MS (m/z): $[\text{M}+\text{H}]^+$ calcd 526, found 526 $[\text{M}+\text{Na}]^+$ calcd 548, found 548.

Synthesis of 4-iodothiocolchicine (12)

To a mixture of **11** (500 mg, 0.95 mmol) in MeOH/water (1/1, v/v, 5 ml), the sodium methanethiolate (solution 21% in H_2O , 0.72 ml, 1.9 mmol) was added. The mixture was stirred in at RT for 72 h. Reaction time was determined by TLC. After that time the reaction mixture was quenched by the addition of water (150 ml). The whole mixture was extracted four times with CH_2Cl_2 , and the combined organic layers were dried over MgSO_4 , filtered, and evaporated under reduced pressure. The residue was purified by CombiFlash® (hexane/EtOAc (1/1), then EtOAc/MeOH, increasing concentration gradient) to give **12** ($\text{C}_{22}\text{H}_{24}\text{INO}_5\text{S}$, MW = 541.4 g/mol) as amorphous yellow solid with yield 71% [33,47]. ^1H NMR (403 MHz, CDCl_3) δ 7.75 (d, J = 6.9 Hz, 1H), 7.42 (s, 1H), 7.25 (d, J = 10.3 Hz, 1H), 7.09 (d, J = 10.8 Hz, 1H), 4.58–4.50 (m, 1H), 3.97 (s, 3H), 3.95 (s, 3H), 3.63 (s, 3H), 3.18 (dd, J = 13.7, 5.0 Hz, 1H), 2.46 (s, 3H), 2.40 (dd, J = 13.6, 6.2 Hz, 1H), 2.32–2.23 (m, 1H), 2.01 (s, 3H), 1.85–1.79 (m, 1H) ppm. ^{13}C NMR (101 MHz, CDCl_3) δ 182.4, 170.1, 159.1, 153.5, 151.4, 151.1, 145.6, 137.8, 136.8, 134.7, 129.7, 128.1, 126.3, 92.2, 61.6, 61.4, 60.8, 52.1, 34.5, 34.4, 22.9, 15.2 ppm. FT-IR (KBr pellet): 3288, 2936, 1660, 1607, 1547, 1461, 1406, 1346, 1318, 1288, 1262, 1197, 1138, 1081, 1019 cm^{-1} . ESI-MS (m/z): $[\text{M}+\text{H}]^+$ calcd 542, found 542, $[\text{M}+\text{Na}]^+$ calcd 564, found 564, $[\text{M}+\text{K}]^+$ calcd 580, found 580.

Synthesis of 4-iododeacetylothiocolchicine (13)

Compound **13** was prepared from **12** by hydrolysis with 2 N HCl. To a solution of compound **12** (500 mg, 0.92 mmol) in MeOH (3 ml), the 2 N HCl solution (5 ml) was added. The mixture was stirred at 90°C for 72 h. Reaction time was determined by TLC. After that time the reaction mixture was quenched by the addition of water (100 ml). The whole mixture was extracted four times with CH_2Cl_2 , and the combined organic layers were dried over MgSO_4 , filtered, and evaporated under reduced pressure. The residue was purified by CombiFlash® (EtOAc/MeOH, increasing concentration gradient) to give **13** ($\text{C}_{20}\text{H}_{22}\text{INO}_4\text{S}$, MW = 499.4 g/mol) with yield 83% [42]. ^1H NMR (403 MHz, CDCl_3) δ

7.59 (s, 1H), 7.11 (d, $J = 10.3$ Hz, 1H), 7.01 (d, $J = 10.7$ Hz, 1H), 3.93 (s, 6H), 3.62 (s, 3H), 3.57 (dd, $J = 10.8, 6.2$ Hz, 1H), 3.15–3.08 (m, 1H), 2.48–2.39 (m, 4H), 2.33–2.24 (m, 1H), 1.53–1.46 (m, 3H) ppm. ^{13}C NMR (101 MHz, CDCl_3) δ 182.5, 158.7, 153.4, 153.1, 150.9, 145.1, 137.7, 137.5, 133.8, 129.5, 129.2, 125.5, 91.7, 61.2, 61.0, 60.8, 53.4, 38.2, 35.1, 15.1 ppm. FT-IR (KBr pellet): 3375, 3309, 2932, 1605, 1553, 1460, 1405, 1343, 1313, 1246, 1195, 1136, 1081, 1014 cm^{-1} . ESI-MS (m/z): $[\text{M}+\text{H}]^+$ calcd 500, found 500. Anal. Calcd. for C, 48.10; H, 4.44; I, 25.41; N, 2.80; O, 12.82; S, 6.42; found C, 48.18; H, 4.54; I, 25.43; N, 2.75; S, 6.49.

General procedure for the synthesis of colchicine derivatives (14–20)

Compounds **14–20** were obtained directly from compound **13**. To a solution of compound **13** (100 mg, 0.20 mmol) in tetrahydrofuran (THF, 5 ml) cooled to the 0 °C temperature, the following compounds were added: Et_3N (2 ml, 14 mmol) and DMAP (catalytic amount). The mixture was first stirred at 0 °C temperature for a few minutes and then the solution of respective acyl chloride (**4–9**) or diethylcarbamoyl chloride (**10**) in THF (0.75 mmol in 2.5 ml) was added dropwise. The mixture was stirred at RT for the next 24 h. The solution was filtered to remove triethylamine hydrochloride. The THF was evaporated and the residue was purified by CombiFlash® (hexane/ethyl acetate, increasing concentration gradient) to give respective compounds as amorphous yellow solids with yield from 25% to 67% (**14–20**).

Compound **14**: ^1H NMR (403 MHz, CDCl_3) δ 7.20 (d, $J = 7.6$ Hz, 1H), 7.19 (s, 1H), 7.16 (d, $J = 6.6$ Hz, 1H), 7.03 (d, $J = 10.6$ Hz, 1H), 4.53 (dt, $J = 11.8, 6.9$ Hz, 1H), 3.97 (s, 3H), 3.94 (s, 3H), 3.87 (q, $J = 15.0$ Hz, 2H), 3.62 (s, 3H), 3.43 (s, 3H), 3.20 (dd, $J = 13.9, 5.1$ Hz, 1H), 2.52–2.42 (m, 4H), 2.28–2.17 (m, 1H), 1.80 (td, $J = 12.0, 6.5$ Hz, 1H) ppm. ^{13}C NMR (101 MHz, CDCl_3) δ 182.2, 169.2, 159.2, 153.4, 151.5, 149.4, 145.6, 137.0, 136.6, 134.3, 129.7, 128.3, 125.7, 92.1, 71.6, 61.4, 61.3, 60.7, 59.1, 51.1, 34.8, 34.4, 15.1 ppm. FT-IR: 3339, 2998, 2929, 1674, 1605, 1547, 1516, 1465, 1449, 1425, 1408, 1373, 1347, 1316, 1292, 1262, 1190, 1156, 1134, 1107, 1081, 1056, 1018 cm^{-1} . ESI-MS (m/z): $[\text{M}+\text{Na}]^+$ calcd 594, found 594. Anal. Calcd. for C, 48.34; H, 4.59; I, 22.21; N, 2.45; O, 16.80; S, 5.61; found C, 48.22; H, 4.51; I, 22.36; N, 2.46; S, 5.66.

Compound **15**: ^1H NMR (403 MHz, CDCl_3) δ 7.47 (d, $J = 7.3$ Hz, 1H), 7.42 (s, 1H), 7.23 (d, $J = 10.4$ Hz, 1H), 7.07 (d, $J = 10.7$ Hz, 1H), 4.57 (dt, $J = 11.8, 6.9$ Hz, 1H), 3.96 (s, 3H), 3.95 (s, 3H), 3.63 (s, 3H), 3.53 (t, $J = 6.4$ Hz, 2H), 3.16 (dd, $J = 13.7, 5.0$ Hz, 1H), 2.52–2.35 (m, 7H), 2.29–2.18 (m, 1H), 2.11–2.02 (m, 2H), 1.78 (td, $J = 12.0, 5.6$ Hz, 1H) ppm. ^{13}C NMR (101 MHz, CDCl_3) δ 182.3, 171.7, 159.2, 153.5, 151.4, 150.8, 145.6, 137.6, 136.7, 134.7, 129.6, 128.4, 126.2, 92.2, 61.6, 61.4, 60.8, 51.7, 44.4, 34.8, 34.5, 33.0, 28.1, 15.2 ppm. FT-IR: 3301, 2937, 1674, 1607, 1544, 1461, 1406, 1346, 1318, 1283, 1262, 1244, 1196, 1154, 1137, 1081, 1054, 1019 cm^{-1} . ESI-MS (m/z): $[\text{M}+\text{Na}]^+$ calcd 626, found 626. Anal. Calcd. for C, 47.73; H, 4.51; Cl, 5.87; I, 21.01; N, 2.32; O, 13.25; S, 5.31; found C, 47.74; H, 4.53; I, 20.89; N, 2.26; S, 5.27.

Compound **16**: ^1H NMR (403 MHz, CDCl_3) δ 7.93 (d, $J = 7.1$ Hz, 1H), 7.81 (dt, $J = 8.5, 1.7$ Hz, 2H), 7.52 (s, 1H), 7.37–7.32 (m, 1H), 7.29–7.23 (m, 3H), 7.10–7.05 (m, 1H), 4.79 (dt, $J = 11.8, 6.9$ Hz, 1H), 3.98 (s, 3H), 3.95 (s, 3H), 3.71 (s, 3H), 3.20 (dd, $J = 13.7, 4.8$ Hz, 1H), 2.52–2.42 (m, 4H), 2.31 (dt, $J = 17.1, 4.9$ Hz, 1H), 2.05 – 1.96 (m, 1H) ppm. ^{13}C NMR (101 MHz, CDCl_3) δ 182.2, 167.1, 159.2, 153.5, 151.5, 150.9, 145.6, 137.7, 136.9, 134.6, 133.3, 131.6, 129.8, 128.5, 128.4, 127.1, 126.1, 92.2, 61.7, 61.4, 60.8, 52.3, 34.7, 34.5, 15.2 ppm. FT-IR: 3323, 3058, 2935, 1659, 1606, 1549, 1487, 1461, 1406, 1346, 1319, 1289, 1262, 1197, 1152, 1081, 1019 cm^{-1} . ESI-MS (m/z): $[\text{M}+\text{H}]^+$ calcd 604, found 604, $[\text{M}+\text{Na}]^+$ calcd 626, found 626. Anal. Calcd. for C, 53.74; H, 4.34; I, 21.03; N, 2.32; O, 13.26; S, 5.31; found C, 53.79; H, 4.46; I, 20.97; N, 2.28; S, 5.33.

Compound **17**: ^1H NMR (403 MHz, CDCl_3) δ 7.53–7.48 (m, 1H), 7.40 (s, 1H), 7.24 (dd, $J = 9.1, 4.0$ Hz, 1H), 7.10–7.05 (m, 1H), 4.56 (dt, $J = 11.9, 6.8$ Hz, 1H), 3.97 (s, 3H), 3.95 (s, 3H), 3.64 (s, 3H), 3.17 (dd, $J = 14.0, 4.6$ Hz, 1H), 2.49–2.37 (m, 4H), 2.35–2.20 (m, 3H), 1.79 (td, $J = 12.0, 5.2$ Hz, 1H), 1.11 (dd, $J = 9.8, 5.3$ Hz, 3H) ppm. ^{13}C NMR (101 MHz, CDCl_3) δ 182.3, 173.8, 159.1, 153.4, 151.4, 151.0, 145.6, 137.7, 136.8, 134.6, 129.7, 128.2, 126.2, 92.2, 61.6, 61.4, 60.8, 51.7, 34.6, 34.5, 29.2, 15.2, 9.6 ppm. FT-IR: 3301, 2938, 1660, 1608, 1567, 1462, 1406, 1346, 1319, 1283, 1262, 1231, 1198, 1138, 1081, 1019 cm^{-1} . ESI-MS (m/z): $[\text{M}+\text{H}]^+$ calcd 556, found 556, $[\text{M}+\text{Na}]^+$ calcd 578, found 578. Anal. Calcd. for C, 50.62; H, 4.96; I, 22.29; N, 2.46; O, 14.05; S, 5.63; found C, 50.69; H, 4.91; I, 22.36; N, 2.41; S, 5.67.

Compound **18**: ^1H NMR (403 MHz, CDCl_3) δ 7.47 (d, $J = 8.3$ Hz, 2H), 7.23 (d, $J = 10.3$ Hz, 1H), 7.06 (d, $J = 10.6$ Hz, 1H), 4.58 (dt, $J = 11.8, 7.0$ Hz, 1H), 3.97 (s, 3H), 3.95 (s, 3H), 3.65 (s, 3H), 3.16 (dd, $J = 13.8, 5.1$ Hz, 1H), 2.55 (dt, $J = 13.8, 6.9$ Hz, 1H), 2.48–2.36 (m, 4H), 2.28–2.16 (m, 1H), 1.80 (td, $J = 11.9, 5.3$ Hz, 1H), 1.16 (dd, $J = 6.9, 3.6$ Hz, 6H) ppm. ^{13}C NMR (101 MHz, CDCl_3) δ 182.2, 177.0, 159.0, 153.4, 151.5, 151.1, 145.6, 137.7, 136.8, 134.5, 129.7, 128.5, 126.1, 92.2, 61.7, 61.3, 60.8, 51.3, 35.2, 34.7, 34.6, 19.5, 19.4, 15.1 ppm. FT-IR: 3331, 2970, 2935, 1669, 1608, 1552, 1461, 1406, 1345, 1319, 1284, 1262, 1239, 1198, 1153, 1137, 1081, 1019 cm^{-1} . ESI-MS (m/z): $[\text{M}+\text{H}]^+$ $[\text{M}+\text{Na}]^+$ calcd 592, found 592. Anal. Calcd. for C, 50.62; H, 4.96; I, 22.29; N, 2.46; O, 14.05; S, 5.63; found C, 50.71; H, 4.99; I, 22.31; N, 2.40; S, 5.59.

Compound **19**: ^1H NMR (403 MHz, CDCl_3) δ 7.40 (s, 1H), 7.23 (d, $J = 10.3$ Hz, 1H), 7.15 (d, $J = 7.1$ Hz, 1H), 7.06 (d, $J = 10.8$ Hz, 1H), 4.57 (dt, $J = 11.9, 7.0$ Hz, 1H), 3.97 (s, 3H), 3.95 (s, 3H), 3.63 (s, 3H), 3.17 (dd, $J = 13.9, 5.0$ Hz, 1H), 2.47–2.18 (m, 7H), 1.75 (td, $J = 12.0, 5.2$ Hz, 1H), 1.60 (td, $J = 14.8, 7.3$ Hz, 2H), 1.35–1.20 (m, 12H), 0.86 (t, $J = 7.2$ Hz, 3H) ppm. ^{13}C NMR (101 MHz, CDCl_3) δ 182.3, 173.2, 159.1, 153.4, 151.5, 150.9, 145.6, 137.6, 136.7, 134.5, 129.7, 128.3, 126.2, 92.2, 61.6, 61.3, 60.8, 51.6, 36.4, 34.8, 34.5, 31.8, 29.4, 29.3, 29.3, 29.2, 25.5, 22.6, 15.1, 14.1 ppm. FT-IR: 3298, 2927, 2856, 1656, 1607, 1547, 1461, 1406, 1346, 1319, 1283, 1262, 1246, 1198, 1154, 1138, 1081, 1019 cm^{-1} . ESI-MS (m/z): $[\text{M}+\text{H}]^+$ calcd 654, found 654. Anal. Calcd. for C, 55.13; H, 6.17; I, 19.42; N, 2.14; O, 12.24; S, 4.91; found C, 55.02; H, 6.19; I, 19.44; N, 2.19; S, 4.86.

Compound **20**: ^1H NMR (403 MHz, CDCl_3) δ 7.48 (s, 1H), 7.21–7.17 (m, 1H), 7.03–6.99 (m, 1H), 5.89–5.85 (m, 1H), 4.53 (dt, $J = 11.7, 6.7$ Hz, 1H), 3.94 (s, 3H), 3.92 (s, 3H), 3.64 (s, 3H), 3.30 (q, $J = 7.1$ Hz, 4H), 3.12 (dd, $J = 13.8, 4.7$ Hz, 1H), 2.44–2.33 (m, 4H), 2.28–2.18 (m, 1H), 1.81 (td, $J = 12.0, 5.3$ Hz, 1H), 1.12 (t, $J = 7.1$ Hz, 6H) ppm. ^{13}C NMR (101 MHz, CDCl_3) δ 182.2, 158.8, 156.0, 153.2, 152.1, 151.4, 145.5, 137.6, 137.0, 134.3, 129.9, 128.9, 125.9, 92.1, 61.7, 61.3, 60.7, 52.9, 41.0, 35.2, 34.8, 15.1, 13.9 ppm. FT-IR: 3383, 2973, 2935, 1639, 1608, 1553, 1525, 1492, 1460, 1425, 1406, 1344, 1318, 1284, 1264, 1216, 1183, 1152, 1137, 1080, 1018 cm^{-1} . ESI-MS (m/z): $[\text{M}+\text{H}]^+$ calcd 599, found 599, $[\text{M}+\text{Na}]^+$ calcd 621, found 621. Anal. Calcd. for C, 50.17; H, 5.22; I, 21.20; N, 4.68; O, 13.37; S, 5.36; found C, 50.08; H, 5.19; I, 21.21; N, 4.70; S, 5.41.

2.2.3 Cell lines and culturing conditions

Primary ALL-5 cells were derived from the bone marrow of a 37-year old patient as previously described [48,49]. Although these cells can be cultured up to 6 months with no obvious change in their properties [48], in the present study they were exclusively used at low passage for all experiments, and are thus referred to as primary cells. Primary ALL-5 cells were routinely maintained at 37°C in a humidified 5% CO₂ incubator in IMDM Modified (SH30228, HyClone) media supplemented with 10 µg mL⁻¹ cholesterol (C3045, Sigma-Aldrich), 6 mg mL⁻¹ human serum albumin (HA1000, Golden West Biologicals), 2 mM L-glutamine (25-005, Corning), 2% v/v amphotericin-B/penicillin/streptomycin (A2942, Sigma-Aldrich, 30-002, Corning), 1 µg mL⁻¹ insulin (128-100, Cell Applications), 200 µg mL⁻¹ apo-transferrin (T1147, Sigma-Aldrich), and 50 µM β-mercaptoethanol, and were subcultured to maintain a density of 1–3 × 10⁶ cells mL⁻¹. Human MCF-7 mammary gland adenocarcinoma cells originally isolated from a 69 year old Caucasian woman with several characteristics of differentiated mammary epithelium were cultured in Eagle's Minimum Essential Medium (EMEM) (30-2003, ATCC, USA) supplemented with 10% (v/v) heat-inactivated fetal bovine serum (FBS) (FP-0500-A, Atlas Biologicals, USA), and 1% Penicillin/Streptomycin Solution 100x (30-002-C1, Corning, USA). MCF-7 cell line was tested *via* short tandem repeat profiling in July 2018 by Genetica DNA Laboratories (Burlington, NC) and verified as authentic, giving a 100% match when compared to the known reference profile [50]. Both primary ALL-5 cells and MCF-7 cell line for cell cycle analysis were maintained in the Department of Biochemistry & Molecular Biology at University of Arkansas for Medical Sciences, USA.

The BALB/3T3 cell line was purchased from the American Type Culture Collection (ATCC Manassas, VA, USA), A549 and MCF-7 cell lines – from European Collection of Authenticated Cell Cultures (Salisbury, UK), LoVo cell line was purchased from the American Type Culture Collection (ATCC, Manassas, VA, USA), and LoVo/DX received courtesy of Prof. E. Borowski (Technical University of Gdańsk, Gdańsk, Poland). All of the above-listed cell lines were maintained in the Institute of Immunology and Experimental Therapy (IJET), Wrocław, Poland. Human lung adenocarcinoma cell line (A549) was cultured in the mixture of OptiMEM and RPMI 1640 (1:1) medium (IJET, Wrocław, Poland), supplemented with 5% fetal bovine serum (GE Healthcare, Logan UT,

USA) and 2 mM L-glutamine (Sigma-Aldrich, Merck KGaA, Saint Louis, MO, USA). Human colon adenocarcinoma cell lines (LoVo) were cultured in mixture of OptiMEM and RPMI 1640 (1:1) medium (IET, Wroclaw, Poland), supplemented with 5% fetal bovine serum (GE Healthcare, Logan, UT, USA), 2 mM L-glutamine, 1 mM sodium pyruvate (Sigma-Aldrich, Merck KGaA, Saint Louis, MO, USA) and 10 µg/100 ml doxorubicin for LoVo/DX (Sigma-Aldrich, Merck KGaA, Saint Louis, MO, USA). Murine embryonic fibroblast cells (BALB/3T3) were cultured in Dulbecco medium (Life Technologies Limited, Paisley, UK), supplemented with 10% fetal bovine serum (GE Healthcare, Logan, UT, USA) and 2 mM glutamine (Sigma-Aldrich, Merck KGaA, Saint Louis, MO, USA). All cell culture media contained antibiotics: 100 U/ml penicillin and 100 µg/ml streptomycin (Polfa-Tarchomin, Warsaw, Poland). All cell lines were cultured during entire experiment in humid atmosphere at 37°C and 5% CO₂. Cells were tested for mycoplasma contamination by mycoplasma detection kit for conventional PCR: Venor GeM Classic (Minerva Biolabs GmbH, Berlin, Germany) and negative results were obtained. The procedure is repeated every year or in the case of less frequently used lines after thawing.

2.2.4 Cell viability assays

SRB assay

Sulforhodamine B (SRB) assay was performed to assess about cytotoxic activity of studied compounds towards adherent cell lines. Cells (10⁴ per well) were seeded in 96-well plates (Sarstedt, Nümbrecht, Germany) in appropriate complete cell culture media and after 24 h prior addition of tested compounds. Cells were subjected to the treatment with tested agents or cisplatin (Teva Pharmaceuticals Polska, Warsaw, Poland) or doxorubicin (Accord Healthcare Limited, Middlesex, UK) in the concentration range 100–0.01 µg/ml for 72 h. Treatment with DMSO (POCh, Gliwice, Poland) at concentrations corresponding to these present in tested agents' dilutions was applied as a control (100% cell viability). After 72 h of incubation with the tested compounds, cells were fixed *in situ* by gently adding of 50 µL per well of cold 50% trichloroacetic acid TCA (POCh, Gliwice, Poland) following incubation at 4°C for one hour [51]. Next, wells were washed four times with

water and air dried. 50 μ L of 0.1% solution of sulforhodamine B (Sigma–Aldrich, Merck KGaA, Saint Louis, MO, USA) in 1% acetic acid (POCh, Gliwice, Poland) were added to each well and plates were incubated at room temperature for 0.5 h. Unbounded dye was removed by washing plates four times with 1% acetic acid. Stained cells were solubilized with 10 mM Tris base (Sigma–Aldrich, Merck KGaA, Saint Louis, MO, USA). Absorbance of each solution was read at Synergy H4 Hybrid Multi-Mode Microplate Reader (BioTek Instruments, Inc., Winooski VT, USA) at the 540 nm wavelength.

Results are presented as mean IC_{50} (concentration of the tested compound, that inhibits cell proliferation by 50%) \pm standard deviation. IC_{50} values were calculated in Cheburator 0.4, Dmitry Nevozhay software (version 1.2.0 software by Dmitry Nevozhay, 2004–2014, <http://www.cheburator.nevozhay.com>, freely available) for each experiment [52]. Compounds at each concentration were tested in triplicate in individual experiment and each experiment was repeated at least three times independently.

MTT assay

A 3-(4,5-dimethylthiazol-2-yl)-2,5-dimethylthiazol-2-yl)-2,5-diphenyltetrazolium bromide (MTT)-based assay [53], was used to evaluate the effect of drugs on the viability of primary ALL-5 cells. Cells (10^5 /well) in 100 μ L of complete IMDM Modified medium were seeded in 96-well plates (TPP, Switzerland) and treated with drugs at concentrations up to 10 μ M for 120 h with control cells receiving vehicle (0.1% DMSO) alone. After treatment, 10 μ L of MTT solution (5 mg/mL) was added to each well, and the plate was incubated at 37°C for 24 h in a humidified 5% CO₂ incubator. Then 100 μ L of 10% SDS in 0.01 M HCl was added to each well and the plate was incubated at 37°C for a further 24 h. The experiment was performed in quadruplicate (n = 4). Absorbance was recorded at 540 nm using a BioTek Plate Reader. Inhibition of formation of colored MTT formazan was taken as an index of cytotoxicity activity. IC_{50} values were determined by non-linear regression analysis using GraphPad Prism 6 for Windows (GraphPad Software).

Selectivity index (SI) was calculated by dividing the IC_{50} value for BALB/3T3 cells by the IC_{50} value for individual cancer cell lines, and resistance index (RI) was calculated by dividing the IC_{50} for LoVo/DX cells by the IC_{50} for LoVo cells. The Resistance Index

(RI) was defined as the ratio of IC₅₀ for a given compound calculated for resistant cell line to that measured for its parental drug sensitive cell line (Table 2-1).

Table 2-1. Antiproliferative activity (IC₅₀) and resistance index (RI) values of colchicine (**1**) and its derivatives (**2–20**) compared with antiproliferative activity of standard anticancer drugs doxorubicin and cisplatin [32–35].

Compound	ALL-5 IC ₅₀ (nM)	A549 IC ₅₀ (nM)	MCF-7 IC ₅₀ (nM)	LoVo IC ₅₀ (nM)	LoVo/DX IC ₅₀ (nM)	RI	BALB/3T3 IC ₅₀ (nM)
1	8.6 ± 0.2	125 ± 13	20.7 ± 2.4	108 ± 25	1,694 ± 275	15.7	106 ± 23
2	3.1 ± 1.3	11.3 ± 1.4	9.6 ± 2.4	21.0 ± 5.5	398 ± 75	19.0	137 ± 59
3	16.3 ± 4.9	24.1 ± 2.7	14.2 ± 1.6	16.9 ± 4.0	145 ± 21	8.6	223 ± 32
4	8.5 ± 0.2	13.5 ± 0.1	12.7 ± 1.3	8.2 ± 1.3	132 ± 44	16.0	12.0 ± 1.3
5	5.9 ± 0.1	13.3 ± 1.2	11.9 ± 1.2	8.4 ± 0.1	102 ± 15	12.2	20.2 ± 10.5
6	5.7 ± 1.9	11.2 ± 1.2	11.2 ± 1.2	5.6 ± 3.2	57.9 ± 13.5	10.4	21.6 ± 17.6
7	4.6 ± 0.6	13.2 ± 1.3	12.4 ± 1.3	8.5 ± 1.3	163 ± 51	19.1	17.9 ± 1.3
8	5.5 ± 0.1	15.8 ± 3.9	13.5 ± 0.02	9.0 ± 0.1	174 ± 46	19.3	69.9 ± 24.4
9	27.3 ± 0.5	13.3 ± 0.2	66.3 ± 25.5	7.6 ± 0.1	84.6 ± 1.1	11.2	87.2 ± 25.1
10	17.4 ± 5.1	133 ± 6	113 ± 7	69.1 ± 11.7	1,105 ± 191	16.0	88.2 ± 10.0
11	15.5 ± 1.6	93.9 ± 5.8	97.7 ± 29.3	10.2 ± 2.2	2,776 ± 449	278.0	135 ± 56
12	8.7 ± 0.2	11.1 ± 1.8	16.6 ± 6.4	7.4 ± 1.8	642 ± 84	91.7	115 ± 44
13	135 ± 35	866 ± 320	1,705 ± 361	126 ± 43	844 ± 52	6.7	1,424 ± 304
14	15.0 ± 5.9	10.5 ± 1.8	10.5 ± 1.8	7.0 ± 0.1	92.2 ± 19.3	13.2	51.2 ± 20.0
15	47.5 ± 9.0	82.8 ± 4.4	89.4 ± 6.6	39.2 ± 5.8	529 ± 77	13.5	87.8 ± 23.2
16	25.4 ± 0.8	13.3 ± 4.4	47.5 ± 14.9	7.2 ± 1.0	72.9 ± 5.0	10.2	76.2 ± 16.3
17	9.0 ± 1.1	11.4 ± 1.0	10.8 ± 1.8	7.2 ± 0.1	168 ± 66	23.3	39.6 ± 13.9
18	19.9 ± 5.2	62.6 ± 5.6	44.5 ± 23.6	7.0 ± 0.1	91.3 ± 16.8	13.0	69.7 ± 18.4
19	615 ± 181	833 ± 60	846 ± 117	568 ± 43	3,866 ± 1,328	6.8	305 ± 138
20	81.9 ± 16.5	81.3 ± 17.6	94.7 ± 7.5	64.6 ± 1.0	794 ± 134	12.3	107 ± 32
Doxorubicin	39.1 ± 7.0	258 ± 44	386 ± 118	92.0 ± 18.0	4,7500 ± 990	51.6	166 ± 74
Cisplatin	—*	6,367 ± 1,413	10,700 ± 753	4,370 ± 73	5,700 ± 630	1.3	3,900 ± 1,500

The IC₅₀ value is defined as the concentration of a compound at which 50% growth inhibition is observed.

*Inhibition of proliferation did not exceed 50% at the highest concentration tested of 10 μM.

The RI indicates how many times a resistant subline is chemoresistant relative to its parental cell line. The RI was calculated for each compound using the formula: RI = IC₅₀ for LoVoDX/IC₅₀ for LoVo cell line. When RI is 0–2, the cells are sensitive to the compound tested, RI in the range 2–

10 means that the cell shows moderate sensitivity to the drug tested, RI above 10 indicates strong drug-resistance.

2.2.5 DNA content analysis

ALL-5 (1.5×10^6) and MCF-7 (0.2×10^6) cells were seeded in 100 mm Petri dishes (Corning, NY) and incubated in the presence of vehicle (0.1% DMSO) or compounds, at concentrations specified in the text, for 24, 48 or 72 h at 37°C in a humidified 5% CO₂ incubator. Cells were then washed with 1 ml phosphate-buffer saline (PBS), fixed with 1–3 ml of 70% ice-cold ethanol and stored at 4°C prior to flow cytometric analysis. Cells were centrifuged, treated with 500 µL propidium iodide/RNase Staining buffer (BD Biosciences, San Jose, CA, USA) and stored in the dark for 1 h at RT. The stained cells were subjected to a FACS Aria IIIu Flow Cytometer (BD Biosciences, San Jose, CA, USA) performed by UAMS Flow Cytometry Core Facility and data were analyzed using FlowJo software.

2.2.6 Western blot analysis

ALL-5 cells (15×10^6 cells/dish) were treated for 24 and 48 h with **1** and **5** at $5 \times IC_{50}$ values concentration or with vehicle (0.1% DMSO) or DX (0.2 µM) for 24 h. Cells were washed in PBS and lysed in lysis buffer (25 mM HEPES, pH 7.5, 300 mM NaCl, 0.1% Triton X-100, 1.5 mM MgCl₂, 0.2 mM EDTA, 0.5 mM DTT, EDTA-free complete protease inhibitor tablets (Roche), 20 µg ml⁻¹ aprotinin, 50 µg ml⁻¹ leupeptin, 10 µM pepstatin, 1 mM phenylmethylsulfonyl fluoride, 20 mM β-glycerophosphate, 1 mM Na₃VO₄, and 1 µM okadaic acid. Protein content was measured by Bradford assay and equal amounts (20 µg) were separated by electrophoresis using Mini-PROTEAN® precast gels (Bio-Rad). Proteins were electrophoretically transferred onto a PVDF membrane (Immobilon-FL, Merck Millipore) and next stained with Ponceau S to assess transfer efficiency and verify equal loading. The membrane was blocked with 5% nonfat milk in Tris-buffered saline containing 0.1% TWEEN-20 (TBS-T) for 1 h at RT and incubated overnight at 4°C with primary antibodies (Santa Cruz Biotechnology) against PARP (9532) (1:2500 dilution) and GAPDH (2118) (1:10000 dilution). After washing with TBS-T for 5

× 5 min the membrane was incubated with secondary HRP-conjugated goat anti-rabbit IgG (H+L) antibody (1:5000 dilution) (Bio-Rad) for 1 h at RT. After washing in TBS-T the membrane was exposed to Clarity™ Western ECL Substrate luminol enhancer solution and peroxide solution (Bio-Rad) for 5 min and visualized and quantified using Image J software.

2.2.7 Statistical analysis

Unpaired t test with Welch's correction was performed for the significance and p values of <0.05 were considered significant.

2.2.8 Docking simulations

Docking of the *N*-deacetylthiocolchicine and 4-iodo-*N*-deacetylthiocolchicine derivatives was performed using AutoDock 4 software package. AutoDock4 includes AutoGrid calculation that pre-calculate atomic affinity potentials in the ligand docked binding site and predict poses for ligand with up to 10 flexible bonds with combination of grid values, the Lamarckian Genetic Algorithm and empirical free energy scoring function [54]. For our docking simulations, a cubic box with size 44.0 × 44.0 × 60.0 Å³ centered at the center of mass of the bound colchicine was considered. All cofactors, namely, GTP, GDP, colchicine, and the magnesium ion were removed during docking. The protein was kept rigid but the compounds were chosen to be flexible. The ligand structures were fully optimized based on the RHF/cc-pVDZ level [55] of theory implemented in the software package GAMESS-US, version 2010-10-01 [56-58]. Since there is no crystal structure for human βI tubulin (UniProt ID: P07437) available in the Protein Data Bank (PDB), the bovine tubulin structure 1SA0.pdb was used as a template to construct a homology model for human βI tubulin using the software package MOE2015. Note that this particular structure is appropriate for colchicine-derivative binding because it corresponds to a co-crystallized complex of tubulin with colchicine. Other β tubulin isotypes used for computational studies were: βIIa (UniProt ID: Q13885), βIIb (UniProt ID: Q9BVA1), βIII

(UniProt ID: Q13509), β IVa (UniProt ID: P04350), β IVb (UniProt ID: P68371), and β VI (UniProt ID: Q9H4B7).

For every compound, docking was run separately on each of the tubulin representative structures obtained from clustering. The ligand poses were eventually rescored using AutoDock's scoring function. For every derivative, the pose with the best AutoDock score over all representative structures of each tubulin isotype was kept for further analysis, especially to investigate the correlation with experimental pIC_{50} values. Besides AutoDock scores, the Moriguchi octanol-water partition coefficient (MLogP) of every compound was calculated using the ADMET Predictor 8.0 package (ADMET Predictor, Simulations Plus, Lancaster, CA, USA). Both Vina scores and MlogP values were used as inputs to build a two-variable linear regression model for every tubulin isotype.

2.3 Results and discussion

2.3.1 Chemistry

Compounds **2–3**, **11–13** were obtained according to previously described procedures [29,33,42]. Double-modified (**4–10**) derivatives were synthesized in one pot reactions of compound **3** with respective acyl (**4–9**) or carbamoyl (**10**) chloride in the presence of triethylamine and 4-dimethylaminopyridine (DMAP) (see Figure 2-1). Compound **6** was previously synthesized by Kerekes *et al.* [42]. Triple-modified derivatives (**14–20**) were synthesized analogously starting with the compound **13** (see Figure 2-1). The structures and purity of all products **2–20** were determined using the ESI-MS, FT-IR, 1H NMR and ^{13}C NMR methods (see exemplary NMR spectra, Appendix A, Figure A1-A8).

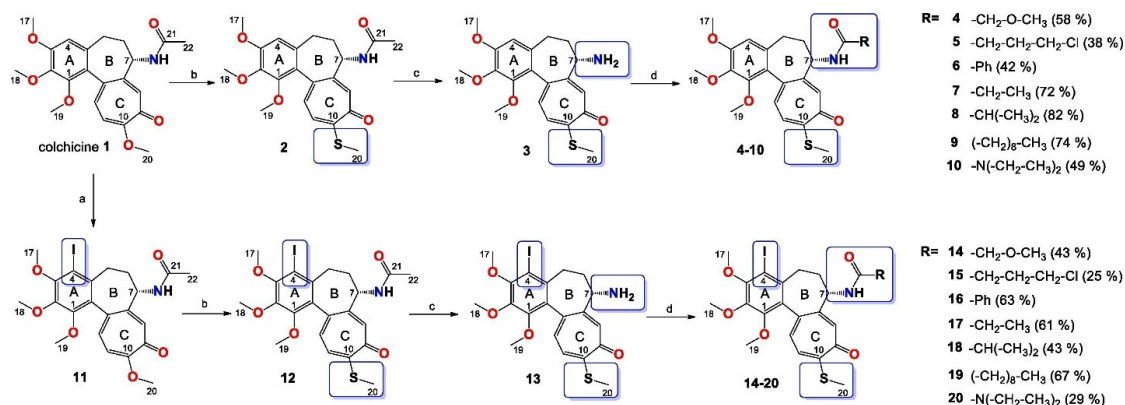


Figure 2-1. Synthesis of colchicine derivatives (2–20). Reagents and conditions: (a) NIS, AcOH, 70°C, 20 h (b) MeOH/H₂O, CH₃SNa, RT; (c) 2 N HCl, 90°C, 72 h; (d) Et₃N, DMAP, respective acyl/carbamoyl chloride, THF, 0°C → RT.

2.3.2 *In vitro* cytotoxic activity evaluation

The seven double-modified derivatives (4–10), triple-modified colchicine derivatives (14–20), other colchicine derivatives (2–3, 11–13), and the starting material (1) were evaluated for their *in vitro* antiproliferative effect on acute lymphoblastic leukemia cells (ALL-5) and four human cancer cell lines: human lung adenocarcinoma (A549), human breast adenocarcinoma (MCF-7), human colon adenocarcinoma (LoVo) and its doxorubicin-resistant subline (LoVo/DX) as well as on normal murine embryonic fibroblasts (BALB/3T3). The data, expressed as IC₅₀ ± SD of the tested compounds, are presented in Table 2-1 [51,52]. and the viability curves for ALL cells are shown in (Appendix A, Figure A9). Some general conclusions based on these data can be drawn. First, the majority of novel double-modified analogs of 7-deacetyl-10-thiocolchicine showed activity greater than or comparable to the unmodified colchicine towards primary ALL-5, A549, MCF-7 and LoVo cells (exception are compounds 9 and 10). Although the compounds 4–8 have different substituents in the C-7 position, that does not seem to have a significant impact on the activity of these derivatives, since the IC₅₀ values against all the tested cancer cell lines are quite similar. The situation is different in case of triple-modified 4-iodo-7-deacetyl-10-thiocolchicine analogs. Compounds 14 and 17 showed the highest activity toward primary ALL-5, A549, MCF-7 and LoVo cells, and 16 showed moderate activity. The structural differences in the C-7 position have bigger impact on the IC₅₀ values

of triple-modified derivatives comparing to double-modified ones. Second, the greatest improvement in the activity of the new derivatives, in comparison to the colchicine, was observed for the A549, LoVo and LoVo/DX cell lines. The most active compounds were the following: against A549, **4–9, 14, 16–17** (approx. 9–12 fold more active than **1**); against LoVo, **4–9, 14, 16–18** (approx. 12–15 fold more active than **1**, compound **6** had even 19 times lower IC₅₀); against LoVo/DX, **4–9, 14, 16–18** (approx. 10–20 fold more active than **1**, compound **6** had even 30 times lower IC₅₀). For the primary acute lymphoblastic leukemia cells (ALL-5) and MCF-7 cells only the moderate improvement in the activity of the new derivatives was observed and the most active compounds were the following: against ALL-5, **5–8** (approx. 1.5-fold more active than **1**); and against MCF-7, **4–8, 14, 17** (approx. 1.5–2 fold more active than **1**). All of the above-listed compounds had very low, single- or double-nanomolar IC₅₀ values, which are lower, than those presented for doxorubicin and cisplatin, currently widely used as antitumor agents in cancer chemotherapy. Third, all of the tested derivatives were more active against LoVo cell line in comparison to its drug-resistant cell line LoVo/DX. Compounds **13** and **19** showed the weakest activity against all cancer cell lines tested (with the exception of **13** on LoVo/DX). When comparing double- (**4–10**) and triple-modified (**14–20**) derivatives, in many cases the derivatives with the same substituents in C-7 position showed similar IC₅₀ values as for compounds **4** and **14** (except BALB/3T3 against which compound **14** turned out to be less potent), compounds **7** and **17**, and compounds **10** and **20** (except ALL-5 against which compound **20** turned out to be less potent). However, some differences between corresponding pairs should be highlighted. Compound **15** showed, depending on the cell line, 4–8 times higher IC₅₀ in comparison to compound **5**. Compounds **6** and **16** showed similar IC₅₀ against A549, LoVo and LoVo/DX cell lines, but compound **16** was 4–5 times less potent against ALL-5, MCF-5 and BALB/3T3 cell lines than **6**. Compounds **8** and **18** showed similar IC₅₀ against LoVo and BALB/3T3, but compound **18** was about 4 times less potent against ALL-5, A549 and MCF-7 cell lines. Surprisingly, compound **18** was more active against LoVo/DX than **8**. The biggest difference can be observed between derivatives **9** and **19**; the derivative of *N*-deacetylthiocolchicine bearing long alkyl chain (**9**) proved to be much more active than the corresponding derivative of 4-iodo-*N*-deacetylthiocolchicine (**19**). These differences are further discussed in the molecular

docking section in terms of binding affinities to the colchicine-binding pocket and structural differences between colchicine derivatives.

In a previous report, analogues of 4-chloro-*N*-deacetylthiocolchicine [45] and 4-bromo- *N*-deacetylthiocolchicine [46] were described. The less potent derivatives in all 4-halo series were amides with long hydrophilic alkyl chains (like **19** from 4-iodo derivatives). Interestingly, the same substituent in the C-7 position did not decrease significantly the activity of double-modified derivative (**9**). The moderate potency, in all series, was also shown by ureas (like **10**, **20**), derivatives with 4-chlorobutanamide moiety in the C-7 position (like **5**, **15**), and for 4-iodo series also benzamide derivative (**16**). The highest activity, in all series, showed compounds bearing given moieties in the C-7 position: methoxyacetamide (like **4**, **14**), benzamide (like **6**, except 4-iodo derivative **16**), propionamide (like **7**, **17**) and isobutyramide (like **8**, **18**).

In order to evaluate the activity of the new analogs against cells with an MDR (multidrug resistance) phenotype, one drug resistant cancer cell line, LoVo/DX, was tested, and the resistance index (RI) values were calculated, as described in Materials and Methods and presented in Table 2-1. However, none of the derivatives was able to overcome the drug resistance of the LoVo/DX cell line, indicated by RI values ranging from 6.7 to 278. Comparison of IC₅₀ values between cancer cell lines and normal murine fibroblasts (BALB/3T3) was made to calculate the Selectivity Index (SI) as an initial indication of the compound's therapeutic potential (Figure 2-2). Standard cancer chemotherapeutics utilized in this study (doxorubicin and cisplatin) are characterized by very low SI values < 1 (with the exception of doxorubicin on ALL-5, SI = 4.2 and on LoVo, SI = 1.8). The majority of double- and triple-modified analogues as well as their precursors showed favorable SI > 1.0 towards ALL-5 cells and A549, MCF-7 and LoVo cell lines. The exceptions are compounds: **4** on A549 and MCF-7; **10** on A549 and MCF-7; **13** on MCF-7; **19** on all cells studied. A beneficial SI on LoVo/DX cell line was observed only for compounds **3** and **13**. In general, the parent (unmodified) colchicine is characterized by higher SI values than doxorubicin and cisplatin (except doxorubicin on the LoVo cell line). Despite that, the following analogues showed higher SI values than parent colchicine: **2**, **3**, **8**, **12** on ALL-5; **2**, **3**, **5-9**, **11-18**, **20** on A549; **2**, **3**, **12**, on MCF-7; **2-18**, **20** on LoVo; **2**, **3**, **5**, **6**, **8**, **9**, **12-16**, **18** on LoVo/DX. This is important since high SI values result from large differences

between the cytotoxicity against cancer versus normal cells, which might indicate that cancer cells will be affected to a greater extent than normal cells.

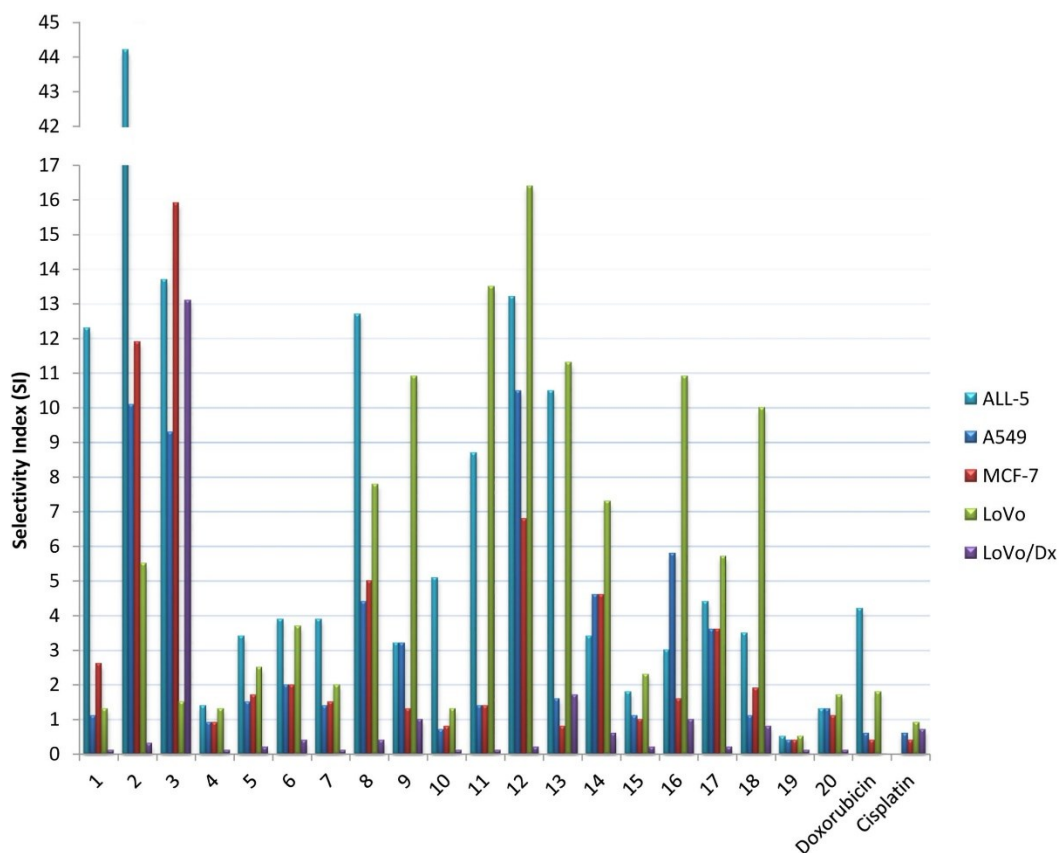


Figure 2-2. Comparison of selectivity index (SI) values for the tested compounds. SI was calculated for each compound using the formula: $SI = IC_{50}$ for normal cell line BALB/3T3/ IC_{50} for respective cancerous cell line. A beneficial $SI > 1.0$ indicates a drug with efficacy against tumor cells greater than the toxicity against normal cells.

2.3.3 The effect of colchicine and its double- and triple-modified analogues on cell cycle progression in ALL-5 and MCF-7 cells

In order to further investigate the mechanism behind the favorable activity of colchicine (**1**) and its analogues towards primary ALL-5 cells, we assessed DNA content and DNA fragmentation *via* flow cytometry. Specifically, propidium iodide staining was employed to determine DNA content and cells with sub-G1 (<2N) DNA were assessed as dead. Primary ALL-5 cells were treated for 24, 48 or 72 h with unmodified **1**, the most active synthesis precursors **2** and **12** (characterized by the lowest IC_{50} values, see Table

2-1) as well as double- and triple-modified analogues (**4–8** and **17**, respectively), each at concentrations equal to $5 \times IC_{50}$ values. Treatment with 0.1% DMSO (vehicle) or 0.2 μ M DX at equivalent time intervals served as negative and positive controls, respectively. For the full set of representative cytograms, see (Appendix A, Figure A10.A). A graphical representation of cells in different phases of the cell cycle has been summarized from the mean of 3 experiments and presented in Figure 2-3A. Statistically significant increases in sub-G1 DNA content were observed after 48 h of treatment with all of the compounds and further increased after 72 h (Figure 2-3A, orange bars). However, double-modified analogues **5**, **8** and synthesis precursor **12** induced DNA fragmentation more rapidly, as indicated by significant sub-G1 DNA after 24 h. The increase in sub-G1 DNA (Figure 2-3A, orange bars) coincided with a decrease of the pool of cells in the G1 phase of the cell cycle (Figure 2-3A, green bars), suggesting that in response to treatments ALL cells in G1 were susceptible to death. Since **1** is typically considered to induce cell death in the M phase [59], it was of interest to investigate whether it, and the novel analogues, caused mitotic arrest in these cells. As shown in Figure 2-3A (red bars) the total amount of cells in the G2/M phases (4N DNA) was maintained at a relatively low level throughout, with a maximum of 20%, and no evidence of overt mitotic arrest was observed. Thus it appears that **1** and the analogues developed here induce death of primary ALL cells directly from the G1 not M phase, a finding consistent with previous results where we reported that two other microtubule destabilizing agents, vincristine and eribulin, exhibited this same property [60]. In contrast, when tested in MCF-7 cells, treatment with **1** and its analogues caused mitotic arrest, as indicated by accumulation of cells with 4N DNA (Figure 2-3B, red bars; Appendix A, Figure A10.B). Noteworthy also was the lack of significant sub-G1 DNA in treated MCF-7 cells, suggesting delayed death kinetics after arrest, or that they may die through a mechanism independent of DNA fragmentation, perhaps due to caspase-3 deficiency [61].

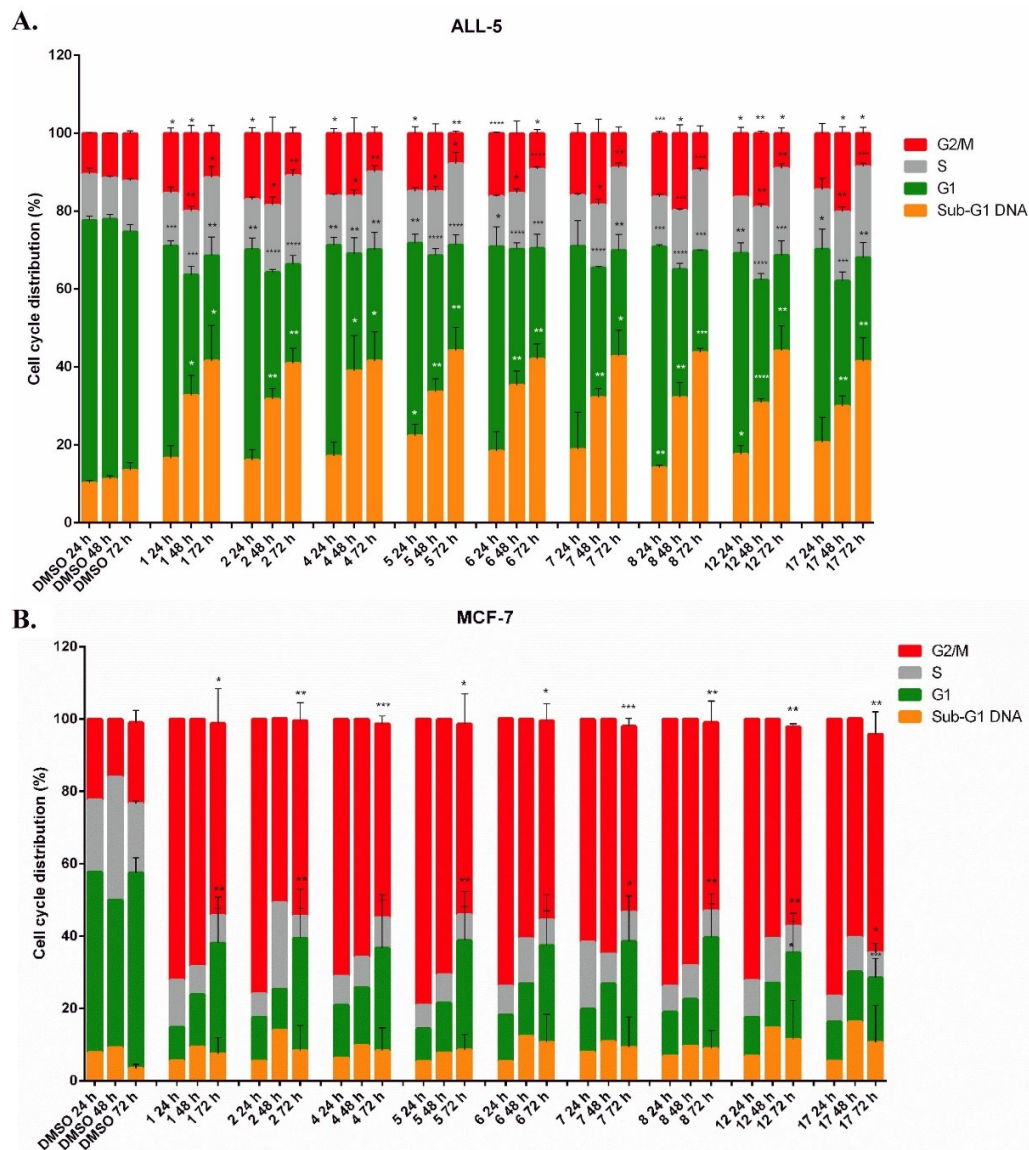


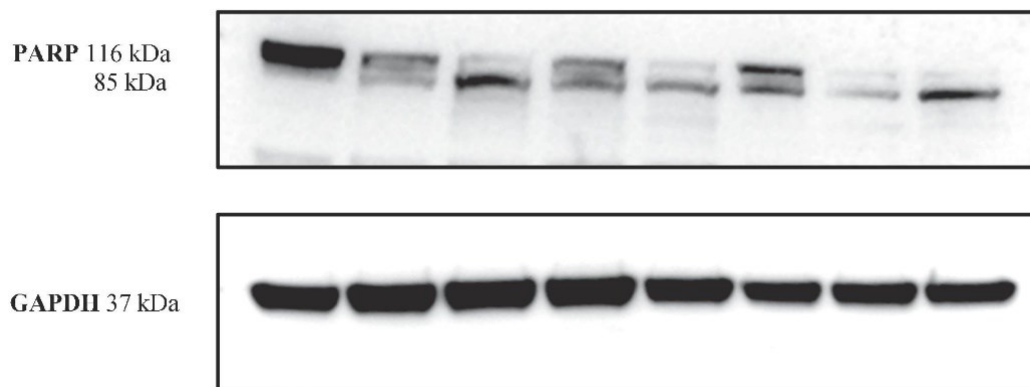
Figure 2-3. ALL-5 (A) or MCF-7 (B) cells were treated with DMSO (vehicle), 1, or its selected double- and triple-modified analogues for 24, 48 or 72 h and subjected to propidium iodide staining and flow cytometry. Percent of cells observed in different phases of cell cycle, determined by PI staining, is shown. Data are presented as a mean \pm SD (n = 3 for all ALL-5 time points and MCF-7 at 72 h; for MCF-7 at 24 and 48 h, n = 1) P < 0.0001, P < 0.001, P <

0.01, *P < 0.05 control versus dose. See (Appendix A, Figure A9) for a full set of representative cytograms.

2.3.4 The effect of colchicine, double-modified analogue 7 and triple-modified analogue 17 on PARP cleavage in primary ALL-5 cells

In order to further assess apoptotic cell death we investigated poly (ADP-ribose) polymerase (PARP) cleavage by immunoblotting. Primary ALL-5 cells were treated with parent colchicine (**1**) or the most active double- or triple-modified analogues (based on the lowest IC₅₀ values, Table 2-1), namely compounds **7** and **17**, respectively, for 24 and 48 h. Treatment with 0.1% DMSO (vehicle) or 0.2 μM DX represented negative and positive controls, respectively. Representative immunoblots are shown in Figure 2-4A and quantitation of PARP band intensities in Figure 2-4B. All of the studied compounds induced loss of 116 kDa PARP over 48 h (Figure 2-4A, top panel and Figure 2-4B). The characteristic 85 kDa product of PARP degradation can be clearly observed for each treatment condition with **1** and its analogues. Treatment of ALL-5 cells with DX also induced PARP cleavage as we previously reported [62,63]. Glyceraldehyde 3-phosphate dehydrogenase (GAPDH) was used as a loading control (Figure 2-4A, lower panel).

A.



Compound	vehicle	1	1	7	7	17	17	DX
Harvest time (h)	24	24	48	24	48	24	48	24

B.

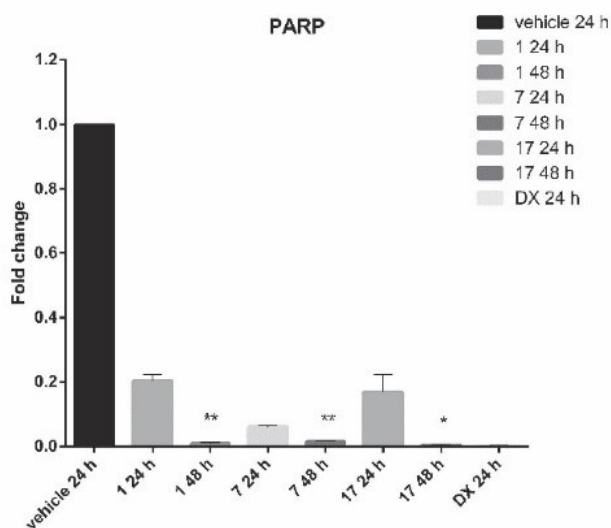


Figure 2-4. (A) Cleavage of PARP. ALL-5 cells were treated with 43 nM compound 1, 23 nM compound 7, 45 nM compound 17, 0.2 μ M doxorubicin (DX), or 0.1% DMSO (vehicle) for the times indicated, and extracts were prepared and subjected to immunoblotting for PARP. The intact (116 kDa) and cleaved (85 kDa) forms of PARP are shown. GAPDH was used as a loading control. Images were quantified by measuring the band intensity using ImageJ software. (B) Bar diagram showing the fold changes of PARP normalized to GAPDH. Data represented as mean \pm S.D. of three independent determinations ($n = 3$); 24 h treatment was compared with 48 h for respective compound. ** $P < 0.005$, * $P < 0.05$.

described in section 2.2, the most active synthetic precursors are **2**, **12**, **4–8**, **14** and **17**, respectively.

While in agreement with compounds **4** to **8** having the highest potency toward the investigated cell lines, the binding energies of compounds **5** to **7** show the lowest values but not in the same order. Compound **6** with -9.30 kcal/mol has the lowest binding energy and compounds **5** and **7** with values of -8.78 kcal/mol and -8.70 kcal/mol come after. Compounds **4** and **8** also have stronger binding energies, -8.30 and -8.25 kcal/mol, respectively compared with the unmodified colchicine, -8.09 kcal/mol.

Based on the *in silico* results, Compounds **17** and **14** with a triplet modification have the shared first and second position of the lowest binding energies of modified derivatives, -9.30 and -9.20 kcal/mol, respectively. As previously described, the above-mentioned compounds also show two of the highest potency with regards to the LoVo, LoVo/DX, A549 and MCF-7 cell lines.

Compounds **15**, **16** and **18** also show strong activity toward LoVo, LoVo/DX, A549 cell lines, although just compounds **16** and **18** were reported with the binding energy values lower than that for colchicine, i.e. -8.30 kcal/mol.

Table 2-2. Summary of the calculated binding energies for the interactions between β I tubulin and *N*-deacetylthiocolchicine and 4-iodo-*N*-deacetylthiocolchicine analogues, the values of compounds' Moriguchi octanol-water partition coefficient (MlogP), which have been investigated in this chapter. The active residues (residues interacting with each ligand *via* hydrogen bonding or π -interactions) in the binding pocket of β I tubulin are listed in the last column.

Compound	Binding energy (kcal/mol)	MlogP	Active residues
1	-8.09	1.368	Asn258, Met259
2	-8.13	2.127	Met259, Asn258, Lys352
3	-8.25	2.129	Asn258, Met259
4	-8.30	1.583	Ala 316, Lys352, Asn 258, Met 259
5	-8.78	2.761	Val 315, Met259, Lys254
6	-9.30	2.944	Val 315, Met259, Ala250
7	-8.70	2.342	Val 238, Met259, Lys352
8	-8.25	2.553	Cys 241, Ala316
9	-8.36	3.753	Val315
10	-7.40	2.813	Lys352, Met259, Asn258, Val238
11	-7.53	1.794	Ala317, Cys241
12	-8.13	2.553	Met259, Lys352
13	-6.90	2.570	Asn258, Cys241, Lys352
14	-9.20	2.001	Lys 352, Met259 Ala316, Ala317
15	-7.94	3.166	Lys 352, Met 259, Ala 250, Lys254, Cys241
16	-8.31	3.338	Asn258, Ala250, Lys254, Val238, Met259
17	-9.30	2.761	Lys 352, Met259, Ala316
18	-8.30	2.965	Cys241
19	-7.05	4.131	Lys254, Leu248
20	-7.63	3.219	Lys352, Asn258, Met259

Consistent with the *in vitro* cytotoxic activity experiment results, compounds **13** and **19** have been found to have the highest binding energies, -6.90 and -7.05 kcal/mol.

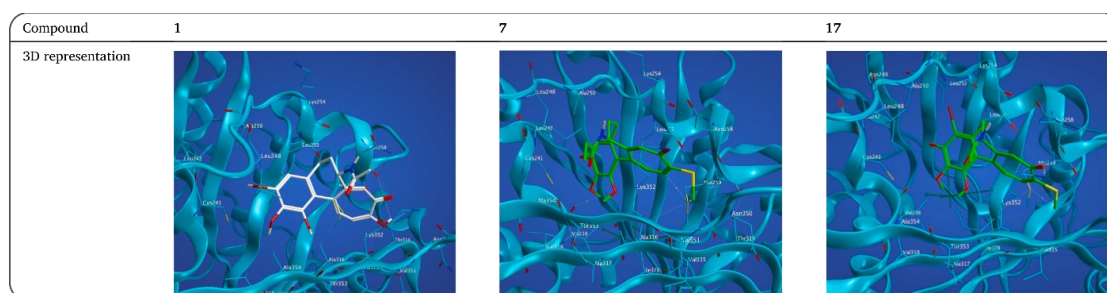
None among the **2**, **3**, **11** and **12** compounds that show high potency toward different cell lines are amongst compounds with the lowest binding energies group. It is worth noting that except compound **11** that has a higher binding energy than -8.09 the rest of the compounds still have stronger binding energies, -8.13, -8.25 and -8.13 kcal/mol respectively, than the binding energies of unmodified colchicine compounds.

To sum up, as predicted by our *in silico* calculations, we conclude that the colchicine derivatives numbered **6**, **17**, **14**, **5** and **7** show the strongest binding energies of -9.30, -9.30, -9.20, -8.78 and -8.70 kcal/mol, respectively.

The two Met 259 and Lys 352 residues present in the binding pocket of β I tubulin are most strongly involved in the ligand-tubulin interactions. Met 259 and Lys 352 residues

mostly interact with the hydrogen of C-20 (side chain H-acceptor) and oxygen of the carbonyl group (side chain H-donor) on ring C of the new colchicine derivatives, respectively. Previous research showed that substituting the *N*-acetyl group with an aliphatic, straight-chain acyl moiety group or an aromatic group on the acetamido group of the B ring might show some strong hydrophobic interactions with β tubulins. However, for example, adding hydrophilic ether function to the chain of the acetamido group can decrease the compound's hydrophobicity [20,66]. Table 2-3 and Table A2 depict these interactions (see Table A1. for 2D-ligand-protein interactions representation).

Table 2-3. Exemplary 3D representations of the interactions between β I tubulin, colchicine and its derivatives (**7** and **17**).



In the 2D ligand-protein interactions scheme, see Table A1, greasy residues, which do not have a polar or charged sidechain, are shown in green. These residues are more likely to show hydrophobic interactions either with other protein residues or ligands. A proximity contour, shown as a dashed line, shows how deep a ligand is buried in the receptor cavity and if the ligand is surrounded by greasy residues, the most probable interactions between the ligand and greasy residues are hydrophobic reactions. The other parameter that plays a key role in the hydrophobic reactions is the ligand and receptor exposure, which shows the exposed part of a ligand or a residue to the water.

In the case of compound **6** and **16**, an aromatic functional group was substituted in the C-7 position that might induce the hydrophobic interactions between aromatic rings and greasy residues and result in a stronger interaction with β I tubulin. According to the *in vitro* cytotoxic activity experiments reported here, compound **6** has 5 and 4 times smaller IC₅₀ values toward ALL-5 and LoVo cell lines than the IC₅₀ values for compound **16**, respectively. Here, in the computational part, compound **6** also shows the lowest binding energy among the novel colchicine derivatives. It should be emphasized that while

compound **16** has a binding energy which is weaker than that for colchicine, the novel derivative is not in the group of top 5 compounds with the lowest binding energies. A side-by-side analysis of the 2D ligand-protein interactions schemes of compounds **6** and **16** shows that the aromatic group of compound **6** unlike that for compound **16**, is close to the proximity contour and deep in the receptor cavity, which might increase its hydrophobic interactions with hydrophobic side chains of the residues such as Ala 317, Leu248 and Leu252. For compound **16**, however, the blue circle around the aliphatic carbons represents the exposure of water to the functional group.

To investigate in more detail the non-bonded interactions of compound **6**, a contact preference map, electrostatic feature maps and the protein-ligand interaction fingerprints (PLIF) based on surface contact interactions were calculated (see Table A-1). The data illustrate that Leu248 and Leu252 present hydrophobic interactions with an aromatic functional group in the C-7 position that might result in stronger binding energy with β I tubulin and a lower value of IC_{50} again for ALL-5 and LoVo cell lines.

Triple-modified compound **17** also has the highest binding energy and shares the first position in terms of the lowest binding energies for the modified derivatives. The binding energy of double-modified compound **7** also has the last position in the top 5 compounds with the lowest binding energies. Replacing the methyl group of acetamido group on carbon 7 on the B ring with ethyl group in compounds **7** and **17** improves the strength of their binding energies significantly. Based on the 3D ligand-protein interactions scheme, , the rings C and B of both compounds are in the same poses. Met259 has a sidechain H-acceptor with the hydrogen of carbon 20 on ring C and Lys352 has a sidechain H-donor with the oxygen of carbonyl on the same ring. The residues that interact with ring A of compound **17** and **7**, however, are different and this might be the reason for the 0.6 kcal/mol difference between their binding energies.

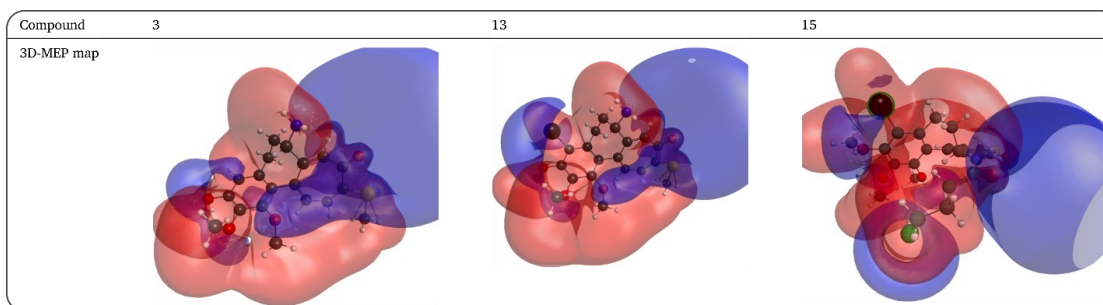
Compound **14** ranks in the second position among the compounds with the strongest interaction with β I tubulin. Adding hydrophilic ether groups to the chain of a functional group can decrease the hydrophobicity, so theoretically the binding energies of compound **4** and **14** should be lower than those for compound **7** and **17**. The binding energy of compound **4** is still lower than that for colchicine, but is not among the best modified compounds. To our surprise, the binding energy for compound **14** is almost as good as

those for compounds **6** and **17**. A possible explanation of this finding could be that the interaction between the iodine atom at carbon atom 4 of ring A and Ala 317 put the modified functional group of ring B in a position that can have a sidechain H-acceptors interacting with Lysine 352, a residue with an electrostatically-charged side chain, and Methionine 259. The above-mentioned interactions cause the added ether group to be less exposed to water and buried deeper into the cavity. It should be recalled that the IC₅₀ values for compounds **17** and **14** are almost the same for the MCF-7, A549 and LoVo cell lines.

Compound **5** is placed in the third position among the top 5 tubulin-binding compounds. Despite the fact that in both compounds **5** and **15**, methyl of acetamido group is replaced with 3-chloropropyl, the binding energies of double-modified, ligand **5**, and triple-modified, ligand **15**, are different as are their values of IC₅₀ against all of the cell lines investigated here. Either in experimental or theoretical results, compound **5** shows to be a more desirable novel derivative than compound **15**. In a side-by-side comparison of the 2D interaction scheme for compound **5** and **15**, it can be found that sulfur of the Cysteine residue exhibits an interaction with sulfur of the substituted functional group on ring B for compound **5**. It is worth noting, that the interaction between sulfurs is not a disulfide bridge due to the fact that the two sulfurs are 3.68 Å apart which is longer than 2.05 Å of the disulfide bond length and hence can be categorized as a weak sulfur-sulfur interaction. Compound **15** has weaker binding energies than compound **5** even though it has a few hydrogen donors and acceptors interacting with residues, Lys352, Met259, Ala250, Lys 254 and Cys 241. The sidechain hydrogen acceptor interaction between Cys241 and hydrogen of carbon 7 in the 4-iodosubstituted compound is caused by inducing electronegativity on the ortho position of the subtitled iodine. This effect, puts the functional group of ring B in a position that is more exposed to water and hence engages in stronger hydrophilic interactions. The 3D molecular electrostatic potential map included in Table 2-4 shows a larger negative charge cloud over the oxygen of the ether group in the ortho position of iodine on the A ring. In compound **5**, the modified functional group is

positioned in the receptor cavity and has less interface with water, which leads to a stronger interaction with the binding pocket of β I tubulin.

Table 2-4. 3D molecular electrostatic potential maps of compound **3** and **13** and **15**. The blue color represents negative charges and the red color represents positive charges.



Consistent with experimental data, compound **13** and compound **19** are the weakest modified derivatives of colchicine that interact with β I tubulin. To investigate in detail the poor performance of compound **13**, 3D molecular electrostatic potential maps for compounds **3** and **13** were created for comparison. As is illustrated in Table 2-4, there is an enlarged negative charge cloud around the substituted iodine on carbon 4 of ring A and the ether group in its ortho position. The intensified negative charge on ring A enhanced the hydrophilic interaction of ring A with water and resulted in weaker binding energies with β I tubulin.

A comparison of 2D and 3D interaction schemes between compound **9** and **19** in Table A1 and Table A2 shows that the only differences in their poses are the positions of their long hydrophobic aliphatic chains. The long functional group on ring B of compound **9** is surrounded by greasy residues and might result in an increased hydrophobic interaction, which might also explain higher cytotoxicity of compound **9** in comparison to compound **19**. It should be noted that long hydrophobic aliphatic chains can cause a steric effect which could jeopardize the cytotoxic activity of the novel derivatives, which is particularly confirmed by experimental data of compound **19**.

To provide a comparison between the computational and experimental results, linear regression coefficients were calculated. However, in numerous cases, the binding affinity alone is insufficient to arrive at a close correlation between the results of biological assays (and the values of IC_{50} given by them) and the binding free energies between the

ligands and their protein targets obtained from docking computations. In order to account for the novel compounds' properties other than the affinity for the target, the Moriguchi octanol-water partition coefficients (MLogP) were calculated. MlogP is a useful factor to estimate and compare the distribution of drugs within biological systems such as the human body.

Thus, the two independent variables chosen in the compounds' characterization have been: MlogP values and the binding free energies with the tubulin β I isotype. Linear regression between IC_{50} values and these two variables was then performed and analyzed. A value of 0.5 is a good regression coefficient that has been found using this method for $\log IC_{50}$ of BALB/3T3 and LoVo cell lines. An acceptable value of 0.4 was obtained for LoVo/DX cell lines and the binding affinities for our compounds and tubulin β I isotype. The regression coefficient values obtained for the MCF-7, A549 and ALL-5 cell lines are very low. This may be due to off-target interactions, P-glycoprotein-based efflux of these compounds or additional complexities involved in the response of these cells to the compounds tested.

To take into account the fact that, regardless of their redundancy, all tubulin isotypes are expressed in a cell-based assay, the interaction energies involving the novel derivatives and the remaining isotypes of tubulin, namely: β IIa, β IIb, β III, β IVa, β IVb, and β VI were calculated using the same docking method and comparisons of experimental data with computational results were made. It is worth noting that the ALL-5 cell line shows an acceptable linear regression coefficient 0.4 with β IIa and β VI isotypes (see Table 2-5). Low values of regression coefficients have been found for the remaining tubulin isotypes. While these biological assays include millions of cells in a culture, computational work only focuses on a single protein at a time and its interaction with the pharmacological agent binding to it. Other biopharmaceutical properties should also be taken into account when theoretical and experimental results are compared. The upregulation of MDR proteins that act as efflux pumps for the tested compounds may be the main reason for some discrepancies between computation and experiment. Another possibility could involve off-target interactions whereby not only tubulin but also other proteins present in the tested cell lines bind these compounds lowering their measured potency.

Table 2-5. The docking binding free energy values for the ligand-tubulin complexes and the MlogP predicted values for the ligands are two independent variables in the linear regression calculations with log IC₅₀ [nM] for different cancer cell lines. The bolded value indicates the highest linear regression values.

Linear regression of colchicine derivatives (R ²)	ALL-5	MCF-7	LoVo	LoVo/DX	A549	BALB/3T3
βI	0.090	0.200	0.500	0.400	0.004	0.500
βIIa	0.400	0.100	0.040	0.100	0.040	0.001
βIIb	0.300	0.200	0.030	0.090	0.040	0.040
βIII	0.300	0.200	0.090	0.090	0.040	0.040
βIVa	0.20	0.300	0.200	0.020	0.200	0.200
βIVb	0.200	0.040	0.002	0.040	0.010	0.001
βV	0.200	0.100	0.110	0.020	0.040	0.002
βVI	0.400	0.100	0.060	0.002	0.090	0.010

2.4 Conclusions

We synthesized and characterized a set of 7-deacetyl-10-thiocolchicine and 4-iodo-7-deacetyl-10-thiocolchicine analogues. In total 19 colchicine derivatives, including 13 novel amide derivatives, were developed with moderate to good yields. Most of the derivatives showed activity against primary leukemia ALL-5 and established cancer cell lines (MCF-7, LoVo, LoVo/DX) in the low nanomolar range. In general, we conclude that 7-deacetyl-10-thiocolchicine analogues were more active towards ALL-5 cells while 4-iodo-7-deacetyl-10-thiocolchicine analogues were slightly more active toward the LoVo cell line. Most of the synthesized compound showed favorable selectivity index values, especially for ALL-5 and LoVo cell lines. Cell cycle progression studies revealed that colchicine and its derivatives induce death of primary ALL cells directly from G1 phase, as do other microtubule destabilizing agents such as vincristine and eribulin. In contrast, a lack of sub-G1 DNA after treatment of MCF-7 cells suggests delayed death kinetics after mitotic arrest. *In silico* calculations demonstrated that colchicine derivatives **6**, **17**, **14**, **5** and **7** show the strongest binding energies of -9.30 , -9.30 , -9.20 , 8.78 and -8.70 kcal/mol, respectively. These also exhibited very low nanomolar IC₅₀ values in experimental assays. Favourable linear regression coefficients ($R^2 = 0.5$) were obtained for βI tubulin and LoVo as well as BALB/3T3 cell lines emphasizing the utility of molecular docking methodology for anticancer drug development.

References

- [1] S. L. Wallace, "Colchicine," *Semin. Arthritis Rheum.*, vol. 3, no. 4, pp. 369–381, 1974, doi: [https://doi.org/10.1016/0049-0172\(74\)90006-7](https://doi.org/10.1016/0049-0172(74)90006-7).
- [2] E. S. Shchegravina, D. I. Knyazev, I. P. Beletskaya, E. V Svirshchevskaya, H.-G. Schmalz, and A. Y. Fedorov, "Synthesis of Nonracemic Pyrrolo-allocolchicinoids Exhibiting Potent Cytotoxic Activity," *European J. Org. Chem.*, vol. 2016, no. 34, pp. 5620–5623, 2016, doi: <https://doi.org/10.1002/ejoc.201601069>.
- [3] D. Zemer, A. Livneh, Y. L. Danon, M. Pras, and E. Sohar, "Long-term colchicine treatment in children with familial Mediterranean fever.," *Arthritis Rheum.*, vol. 34, no. 8, pp. 973–7, Aug. 1991, doi: [10.1002/art.1780340806](https://doi.org/10.1002/art.1780340806).
- [4] M. Imazio *et al.*, "Colchicine for recurrent pericarditis (CORP): a randomized trial.," *Ann. Intern. Med.*, vol. 155, no. 7, pp. 409–414, Oct. 2011, doi: [10.7326/0003-4819-155-7-201110040-00359](https://doi.org/10.7326/0003-4819-155-7-201110040-00359).
- [5] E. Ben-Chetrit and M. Levy, "Colchicine prophylaxis in familial Mediterranean fever: Reappraisal after 15 years," *Semin. Arthritis Rheum.*, vol. 20, no. 4, pp. 241–246, 1991, doi: [https://doi.org/10.1016/0049-0172\(91\)90019-V](https://doi.org/10.1016/0049-0172(91)90019-V).
- [6] C. Cerquaglia, M. Diaco, G. Nucera, M. La Regina, M. Montalto, and R. Manna, "Pharmacological and clinical basis of treatment of Familial Mediterranean Fever (FMF) with colchicine or analogues: an update.," *Curr. Drug Targets. Inflamm. Allergy*, vol. 4, no. 1, pp. 117–124, Feb. 2005, doi: [10.2174/1568010053622984](https://doi.org/10.2174/1568010053622984).
- [7] K. Masuda, A. Nakajima, A. Urayama, K. Nakae, M. Kogure, and G. Inaba, "Double-masked trial of cyclosporin versus colchicine and long-term open study of cyclosporin in Behçet's disease.," *Lancet (London, England)*, vol. 1, no. 8647, pp. 1093–1096, May 1989, doi: [10.1016/s0140-6736\(89\)92381-7](https://doi.org/10.1016/s0140-6736(89)92381-7).
- [8] M. M. Kaplan, "New strategies needed for treatment of primary biliary cirrhosis?," *Gastroenterology*, vol. 104, no. 2. United States, pp. 651–653, Feb. 1993, doi: [10.1016/0016-5085\(93\)90440-n](https://doi.org/10.1016/0016-5085(93)90440-n).
- [9] Y. Gong and C. Gluud, "Colchicine for primary biliary cirrhosis: a Cochrane Hepato-Biliary Group systematic review of randomized clinical trials.," *Am. J. Gastroenterol.*, vol. 100, no. 8, pp. 1876–1885, Aug. 2005, doi: [10.1111/j.1572-0241.2005.41522.x](https://doi.org/10.1111/j.1572-0241.2005.41522.x).

- [10] R. J. McKendry, G. Kraag, S. Seigel, and A. al-Awadhi, "Therapeutic value of colchicine in the treatment of patients with psoriatic arthritis.," *Ann. Rheum. Dis.*, vol. 52, no. 11, pp. 826–828, Nov. 1993, doi: 10.1136/ard.52.11.826.
- [11] R. A. Kyle *et al.*, "A trial of three regimens for primary amyloidosis: colchicine alone, melphalan and prednisone, and melphalan, prednisone, and colchicine.," *N. Engl. J. Med.*, vol. 336, no. 17, pp. 1202–1207, Apr. 1997, doi: 10.1056/NEJM199704243361702.
- [12] M. Imazio and F. Gaita, "Colchicine for cardiovascular medicine.," *Future Cardiol.*, vol. 12, no. 1, pp. 9–16, Jan. 2016, doi: 10.2217/fca.15.59.
- [13] R. C. Weisenberg, G. G. Borisy, and E. W. Taylor, "The colchicine-binding protein of mammalian brain and its relation to microtubules.," *Biochemistry*, vol. 7, no. 12, pp. 4466–4479, Dec. 1968, doi: 10.1021/bi00852a043.
- [14] J. Seligmann and C. Twelves, "Tubulin: an example of targeted chemotherapy.," *Future Med. Chem.*, vol. 5, no. 3, pp. 339–52, Mar. 2013, doi: 10.4155/fmc.12.217.
- [15] C. D. Katsetos and P. Dráber, "Tubulins as therapeutic targets in cancer: from bench to bedside.," *Curr. Pharm. Des.*, vol. 18, no. 19, pp. 2778–92, 2012, doi: 10.2174/138161212800626193.
- [16] C. Avendaño and J. C. Menéndez, "Chapter 1 - Introduction," in *Medicinal Chemistry of Anticancer Drugs*, C. Avendaño and J. C. Menéndez, Eds. Amsterdam: Elsevier, 2008, pp. 1–8.
- [17] X. Zhang *et al.*, "Design, synthesis and biological evaluation of colchicine derivatives as novel tubulin and histone deacetylase dual inhibitors," *Eur. J. Med. Chem.*, vol. 95, pp. 127–135, 2015, doi: <https://doi.org/10.1016/j.ejmech.2015.03.035>.
- [18] K. C. Nicolaou, R. A. Valiulin, J. K. Pokorski, V. Chang, and J. S. Chen, "Bio-inspired synthesis and biological evaluation of a colchicine-related compound library," *Bioorg. Med. Chem. Lett.*, vol. 22, no. 11, pp. 3776–3780, 2012, doi: <https://doi.org/10.1016/j.bmcl.2012.04.007>.
- [19] D.-J. Chang *et al.*, "Design, synthesis and identification of novel colchicine-derived immunosuppressant," *Bioorg. Med. Chem. Lett.*, vol. 19, no. 15, pp. 4416–4420, 2009, doi: <https://doi.org/10.1016/j.bmcl.2009.05.054>.

- [20] A. Marzo-Mas *et al.*, “Interactions of long-chain homologues of colchicine with tubulin,” *Eur. J. Med. Chem.*, vol. 126, pp. 526–535, 2017, doi: <https://doi.org/10.1016/j.ejmech.2016.11.049>.
- [21] L. Johnson *et al.*, “Novel Colchicine Derivatives and their Anti-cancer Activity.,” *Curr. Top. Med. Chem.*, vol. 17, no. 22, pp. 2538–2558, 2017, doi: [10.2174/1568026617666170104143618](https://doi.org/10.2174/1568026617666170104143618).
- [22] B. Kumar *et al.*, “Synthesis and biological evaluation of pyrimidine bridged combretastatin derivatives as potential anticancer agents and mechanistic studies,” *Bioorg. Chem.*, vol. 78, pp. 130–140, 2018, doi: <https://doi.org/10.1016/j.bioorg.2018.02.027>.
- [23] A. Kumar, P. R. Sharma, and D. M. Mondhe, “Potential anticancer role of colchicine-based derivatives,” *Anticancer. Drugs*, vol. 28, no. 3, pp. 250–262, Mar. 2017, doi: [10.1097/CAD.0000000000000464](https://doi.org/10.1097/CAD.0000000000000464).
- [24] E. S. Shchegravina *et al.*, “Synthesis and biological evaluation of novel non-racemic indole-containing allocolchicinoids,” *Eur. J. Med. Chem.*, vol. 141, pp. 51–60, 2017, doi: <https://doi.org/10.1016/j.ejmech.2017.09.055>.
- [25] D. Bartusik, B. Tomanek, E. Lattová, H. Perreault, J. Tuszynski, and G. Fallone, “Derivatives of thiocolchicine and its applications to CEM cells treatment using 19F Magnetic Resonance ex vivo,” *Bioorg. Chem.*, vol. 38, no. 1, pp. 1–6, 2010, doi: <https://doi.org/10.1016/j.bioorg.2009.10.002>.
- [26] G. Raspaglio *et al.*, “Thiocolchicine dimers: a novel class of topoisomerase-I inhibitors,” *Biochem. Pharmacol.*, vol. 69, no. 1, pp. 113–121, 2005, doi: <https://doi.org/10.1016/j.bcp.2004.09.004>.
- [27] T. Kozaka *et al.*, “Antitumor agents 273. Design and synthesis of N-alkyl-thiocolchicinoids as potential antitumor agents,” *Bioorg. Med. Chem. Lett.*, vol. 20, no. 14, pp. 4091–4, Jul. 2010, doi: [10.1016/j.bmcl.2010.05.081](https://doi.org/10.1016/j.bmcl.2010.05.081).
- [28] K. Nakagawa-Goto *et al.*, “Antitumor agents. Part 236: Synthesis of water-soluble colchicine derivatives.,” *Bioorg. Med. Chem. Lett.*, vol. 15, no. 1, pp. 235–238, Jan. 2005, doi: [10.1016/j.bmcl.2004.07.098](https://doi.org/10.1016/j.bmcl.2004.07.098).
- [29] N. Yasobu *et al.*, “Design, Synthesis, and Antitumor Activity of 4-Halocolchicines and Their Pro-drugs Activated by Cathepsin B.,” *ACS Med. Chem. Lett.*, vol. 2, no.

- 5, pp. 348–352, May 2011, doi: 10.1021/ml100287y.
- [30] N. Hiroyuki *et al.*, “Synthesis and biological evaluation of 4-chlorocolchicine derivatives as potent anticancer agents with broad effective dosage ranges,” *Medchemcomm*, vol. 3, pp. 1500–1504, 2012.
- [31] A. Huczyński *et al.*, “Synthesis, antiproliferative and antibacterial evaluation of C-ring modified colchicine analogues,” *Eur. J. Med. Chem.*, vol. 90, pp. 296–301, Jan. 2015, doi: 10.1016/j.ejmech.2014.11.037.
- [32] A. Huczyński *et al.*, “Synthesis, antiproliferative activity and molecular docking of Colchicine derivatives,” *Bioorg. Chem.*, vol. 64, pp. 103–112, 2016, doi: <https://doi.org/10.1016/j.bioorg.2016.01.002>.
- [33] U. Majcher *et al.*, “Antiproliferative Activity and Molecular Docking of Novel Double-Modified Colchicine Derivatives,” *Cells*, vol. 7, no. 11, p. 192, Nov. 2018, doi: 10.3390/cells7110192.
- [34] U. Majcher *et al.*, “Synthesis and Biological Evaluation of Novel Triple-Modified Colchicine Derivatives as Potent Tubulin-Targeting Anticancer Agents,” *Cells*, vol. 7, no. 11, Nov. 2018, doi: 10.3390/cells7110216.
- [35] U. Majcher *et al.*, “Synthesis, antiproliferative activity and molecular docking of thiocolchicine urethanes,” *Bioorg. Chem.*, vol. 81, pp. 553–566, 2018, doi: 10.1016/j.bioorg.2018.09.004.
- [36] J. Kurek *et al.*, “7-Deacetyl-10-alkylthiocolchicine derivatives-new compounds with potent anticancer and fungicidal activity,” *Medchemcomm*, vol. 9, no. 10, pp. 1708–1714, 2018, doi: 10.1039/C8MD00352A.
- [37] H. Alkadi, M. J. Khubeiz, and R. Jbeily, “Colchicine: A Review on Chemical Structure and Clinical Usage,” *Infect. Disord. Drug Targets*, vol. 18, no. 2, pp. 105–121, 2018, doi: 10.2174/1871526517666171017114901.
- [38] A. A. Ghawanmeh, K. F. Chong, S. M. Sarkar, M. A. Bakar, R. Othaman, and R. M. Khalid, “Colchicine prodrugs and codrugs: Chemistry and bioactivities,” *Eur. J. Med. Chem.*, vol. 144, pp. 229–242, 2018, doi: <https://doi.org/10.1016/j.ejmech.2017.12.029>.
- [39] A. A. Ghawanmeh, H. M. Al-Bajalan, M. M. Mackeen, F. Q. Alali, and K. F. Chong, “Recent developments on (–)-colchicine derivatives: Synthesis and structure-

- activity relationship,” *Eur. J. Med. Chem.*, vol. 185, p. 111788, 2020, doi: <https://doi.org/10.1016/j.ejmech.2019.111788>.
- [40] I. A. Gracheva, E. S. Shchegravina, H.-G. Schmalz, I. P. Beletskaya, and A. Y. Fedorov, “Colchicine Alkaloids and Synthetic Analogues: Current Progress and Perspectives,” *J. Med. Chem.*, vol. 63, no. 19, pp. 10618–10651, Oct. 2020, doi: [10.1021/acs.jmedchem.0c00222](https://doi.org/10.1021/acs.jmedchem.0c00222).
- [41] A. Brossi *et al.*, “Biological effects of modified colchicines. 2. Evaluation of catecholic colchicines, colchifolines, colchicide, and novel N-acyl- and N-aroyldeacetylcolchicines,” *J. Med. Chem.*, vol. 26, no. 10, pp. 1365–1369, Oct. 1983, doi: [10.1021/jm00364a006](https://doi.org/10.1021/jm00364a006).
- [42] P. Kerekes, P. N. Sharma, A. Brossi, C. F. Chignell, and F. R. Quinn, “Synthesis and biological effects of novel thiocolchicines. 3. Evaluation of N-acyldeacetylthiocolchicines, N-(alkoxycarbonyl) deacetylthiocolchicines, and O-ethyl demethylthiocolchicines. New synthesis of thiodemecolcine and antileukemic effects of 2-deme,” *J. Med. Chem.*, vol. 28, no. 9, pp. 1204–1208, Sep. 1985, doi: [10.1021/jm00147a014](https://doi.org/10.1021/jm00147a014).
- [43] L. Sun, E. Hamel, C. M. Lin, S. B. Hastie, A. Pyluck, and K. H. Lee, “Antitumor agents. 141. Synthesis and biological evaluation of novel thiocolchicine analogs: N-acyl-, N-aroyl-, and N-(substituted benzyl)deacetylthiocolchicines as potent cytotoxic and antimetabolic compounds,” *J. Med. Chem.*, vol. 36, no. 10, pp. 1474–1479, May 1993, doi: [10.1021/jm00062a021](https://doi.org/10.1021/jm00062a021).
- [44] G. Klejborowska *et al.*, “Synthesis, antiproliferative activity, and molecular docking studies of 4-chlorothiocolchicine analogues,” *Chem. Biol. Drug Des.*, vol. 95, no. 1, pp. 182–191, Jan. 2020, doi: [10.1111/cbdd.13618](https://doi.org/10.1111/cbdd.13618).
- [45] G. Klejborowska *et al.*, “Synthesis, biological evaluation and molecular docking studies of new amides of 4-chlorothiocolchicine as anticancer agents,” *Bioorg. Chem.*, vol. 97, p. 103664, 2020, doi: [10.1016/j.bioorg.2020.103664](https://doi.org/10.1016/j.bioorg.2020.103664).
- [46] G. Klejborowska *et al.*, “Synthesis, biological evaluation and molecular docking studies of new amides of 4-bromothiocolchicine as anticancer agents,” *Bioorg. Med. Chem.*, vol. 27, no. 23, p. 115144, 2019, doi: [10.1016/j.bmc.2019.115144](https://doi.org/10.1016/j.bmc.2019.115144).
- [47] Q. Shi, P. Verdier-Pinard, A. Brossi, E. Hamel, and K. H. Lee, “Antitumor agents--

- CLXXV. Anti-tubulin action of (+)-thiocolchicine prepared by partial synthesis.,” *Bioorg. Med. Chem.*, vol. 5, no. 12, pp. 2277–2282, Dec. 1997, doi: 10.1016/s0968-0896(97)00171-5.
- [48] B. A. Nijmeijer *et al.*, “Long-term culture of primary human lymphoblastic leukemia cells in the absence of serum or hematopoietic growth factors.,” *Exp. Hematol.*, vol. 37, no. 3, pp. 376–385, Mar. 2009, doi: 10.1016/j.exphem.2008.11.002.
- [49] A. Kothari, W. N. Hittelman, and T. C. Chambers, “Cell Cycle-Dependent Mechanisms Underlie Vincristine-Induced Death of Primary Acute Lymphoblastic Leukemia Cells.,” *Cancer Res.*, vol. 76, no. 12, pp. 3553–3561, Jun. 2016, doi: 10.1158/0008-5472.CAN-15-2104.
- [50] W. G. Dirks *et al.*, “Cell line cross-contamination initiative: an interactive reference database of STR profiles covering common cancer cell lines.,” *International journal of cancer*, vol. 126, no. 1. United States, pp. 303–304, Jan. 2010, doi: 10.1002/ijc.24999.
- [51] P. Skehan *et al.*, “New colorimetric cytotoxicity assay for anticancer-drug screening.,” *J. Natl. Cancer Inst.*, vol. 82, no. 13, pp. 1107–1112, Jul. 1990, doi: 10.1093/jnci/82.13.1107.
- [52] D. Nevozhay, “Cheburator software for automatically calculating drug inhibitory concentrations from in vitro screening assays.,” *PLoS One*, vol. 9, no. 9, p. e106186, 2014, doi: 10.1371/journal.pone.0106186.
- [53] M. C. Alley *et al.*, “Feasibility of drug screening with panels of human tumor cell lines using a microculture tetrazolium assay.,” *Cancer Res.*, vol. 48, no. 3, pp. 589–601, Feb. 1988.
- [54] O. Trott and A. J. Olson, “AutoDock Vina: Improving the speed and accuracy of docking with a new scoring function, efficient optimization, and multithreading,” *J. Comput. Chem.*, vol. 31, no. 2, pp. 455–461, Jan. 2009, doi: 10.1002/jcc.21334.
- [55] T. H. Dunning, “Gaussian basis sets for use in correlated molecular calculations. I. The atoms boron through neon and hydrogen,” *J. Chem. Phys.*, vol. 90, no. 2, pp. 1007–1023, Jan. 1989, doi: 10.1063/1.456153.
- [56] M. W. Schmidt *et al.*, “General atomic and molecular electronic structure system,” *J. Comput. Chem.*, vol. 14, no. 11, pp. 1347–1363, Nov. 1993, doi:

10.1002/jcc.540141112.

- [57] M. S. Gordon and M. W. Schmidt, “Advances in electronic structure theory: GAMESS a decade later,” in *Theory and Applications of Computational Chemistry*, C. E. Dykstra, G. Frenking, K. S. Kim, and G. E. Scuseria, Eds. Amsterdam: Elsevier, 2005, pp. 1167–1189.
- [58] G. M. J. Barca *et al.*, “Recent developments in the general atomic and molecular electronic structure system.,” *J. Chem. Phys.*, vol. 152, no. 15, p. 154102, Apr. 2020, doi: 10.1063/5.0005188.
- [59] M. A. Jordan and L. Wilson, “Microtubules as a target for anticancer drugs.,” *Nat. Rev. Cancer*, vol. 4, no. 4, pp. 253–65, Apr. 2004, doi: 10.1038/nrc1317.
- [60] M. Delgado, A. Urbaniak, and T. C. Chambers, “Contrasting effects of microtubule destabilizers versus stabilizers on induction of death in G1 phase of the cell cycle.,” *Biochem. Pharmacol.*, vol. 162, pp. 213–223, Apr. 2019, doi: 10.1016/j.bcp.2018.12.015.
- [61] R. U. Jänicke, M. L. Sprengart, M. R. Wati, and A. G. Porter, “Caspase-3 is required for DNA fragmentation and morphological changes associated with apoptosis.,” *J. Biol. Chem.*, vol. 273, no. 16, pp. 9357–9360, Apr. 1998, doi: 10.1074/jbc.273.16.9357.
- [62] M. Antoszczak *et al.*, “Biological activity of doubly modified salinomycin analogs - Evaluation in vitro and ex vivo.,” *Eur. J. Med. Chem.*, vol. 156, pp. 510–523, Aug. 2018, doi: 10.1016/j.ejmech.2018.07.021.
- [63] A. Urbaniak, M. Delgado, M. Antoszczak, A. Huczyński, and T. C. Chambers, “Salinomycin derivatives exhibit activity against primary acute lymphoblastic leukemia (ALL) cells in vitro.,” *Biomed. Pharmacother.*, vol. 99, pp. 384–390, Mar. 2018, doi: 10.1016/j.biopha.2018.01.081.
- [64] P. G. Morris and M. N. Fornier, “Microtubule active agents: beyond the taxane frontier.,” *Clin. Cancer Res.*, vol. 14, no. 22, pp. 7167–72, Nov. 2008, doi: 10.1158/1078-0432.CCR-08-0169.
- [65] L. J. Leandro-García *et al.*, “Tumoral and tissue-specific expression of the major human beta-tubulin isotypes.,” *Cytoskeleton (Hoboken)*, vol. 67, no. 4, pp. 214–223, Apr. 2010, doi: 10.1002/cm.20436.

- [66] S. Mons *et al.*, “The interaction between lipid derivatives of colchicine and tubulin: consequences of the interaction of the alkaloid with lipid membranes.,” *Biochim. Biophys. Acta*, vol. 1468, no. 1–2, pp. 381–395, Sep. 2000, doi: 10.1016/s0005-2736(00)00279-0.

Chapter 3:

Antiproliferative Activity and Molecular Docking of Novel Double-Modified Colchicine Derivatives*

*The paper in this chapter is included by permission from the publisher (MDPI) and the journal (*Cells*). All authors of the paper were notified about its inclusion in the thesis.

Urszula Majcher, Greta Klejborowska, Mahshad Moshari, Ewa Maj, Joanna Wietrzyk, Franz Bartl, Jack A Tuszynski, and Adam Huczyński. 2018. Antiproliferative Activity and Molecular Docking of Novel Double-Modified Colchicine Derivatives. *Cells* 7, 11, 192. DOI:<https://doi.org/10.3390/cells7110192>

3.1 Introduction

Microtubules, present in all eukaryotic cells, are cylindrical polymers composed of α/β -tubulin heterodimers. They are involved in a wide range of key cellular processes, such as the maintenance of cellular morphology and the active motor transport of cellular components throughout the cytoplasm [1]. Another essential role microtubules play is the formation of mitotic spindles and force generation during mitosis with the purpose of separating chromosomes [2]. A failure within this mitotic spindle apparatus leads to mitotic arrest and eventually apoptosis. This results in cell death, which is a desirable outcome for cancer cells, but not for healthy tissues. With the objective of promoting the former and avoiding the latter effect, microtubules have become the target for a large number of antimitotic agents that act by either favoring or inhibiting microtubule polymerization by binding at specific sites on the exposed surface of α/β -tubulin heterodimers [3-7]. Although there are multiple distinct binding sites on a tubulin heterodimer, β -tubulin is the main binding partner for all major microtubule-targeting drug families [8-10].

Among them colchicine (**1**), a well-known tropolone alkaloid isolated from *Colchicum autumnale*, is of particular interest due to its powerful antimitotic properties. It has played an important role in studies of mitosis and the therapeutic potential of using the colchicine binding site on β -tubulin in chemotherapy applications has generated much interest [5-7,11-16]. However, colchicine itself as well as many of its derivatives, have not yet been used as successful drugs in long-term treatment because of their detrimental side effects [6,7,11]. Up to now, many structure-activity relationship studies have been performed to elucidate the structural features required for tubulin binding. These studies have demonstrated great importance of the 9-keto function and the methoxy groups at C-1, C-2, and C-10 as well as the importance of stereochemistry of the 7-acetamido center, which is critical for antimitotic activity. Ring B appears to be responsible for the irreversible nature of colchicine binding to tubulin, although it may also contribute to its toxic effects [11,17]. Therefore, currently much interest has focused on structural modification of **1** in the hope of improving its anticancer activity [18-33].

In 2011 Yasobu et al. published results of their studies on C-4 halogen substituted colchicine derivatives [32]. On the evaluation of cell-growth inhibitory activity using mice transplanted with the HCT116 human colorectal carcinoma cell line, some of the derivatives exhibited less toxicity in mice and more potent cell-growth inhibitory activity than **1**. Moreover, another colchicine derivative with thiomethyl group at C-10 called thiocolchicine, is also a potent inhibitor of tubulin polymerization and cell growth, and binds to tubulin more rapidly than colchicine [34-36]. Thiocolchicine is not only easily available from colchicine after treatment with sodium methanethiolate, but also is more stable, which allows for using harsher reaction conditions without formation of isomers.

Inspired by these reports, we decided to verify how double modification in C-4 and C-10 positions influences the activity and selectivity of colchicine. Below, we report the synthesis and spectroscopic analysis of a series of seven compounds, of which three are entirely novel compounds synthesized for the first time. We also provide an evaluation of these derivatives as cytotoxic, tubulin-targeting agents. The antiproliferative effect of seven colchicines derivatives (**2–8**) was tested *in vitro* using four cancer cell lines and one normal murine embryonic fibroblast cell line. To better understand the interactions between these colchicine derivatives and various isotypes of β -tubulin, we investigated potential binding modes of novel double-modified derivatives, 4-halocolchicines as well as colchicine docked into the colchicine binding site (CBS) of eight different isotypes of β -tubulin using AutoDock4 software (version 2018.2.0, Tableau Research, Stanford University, Seattle, WA, USA) under flexible ligand and rigid receptor condition. A detailed discussion regarding differences between the structures of the synthesized compounds and their ability to form complexes with the CBS is provided below.

3.2 Materials and Methods

3.2.1 General

All precursors for the synthesis and solvents were obtained from Sigma-Aldrich (Merck KGaA, Saint Louis, MO, USA) and were used as received without further purification. CDCl_3 spectral grade solvent was stored over 3 Å molecular sieves for several days. Thin layer chromatography was carried out on precoated plates (TLC silica gel 60

F254, Aluminum Plates Merck (Merck KGaA Saint Louis, MO, USA)) and spots were detected by illumination with an ultra-violet (UV) lamp. All the solvents used in flash chromatography were of HPLC grade (CHROMASOLV from Sigma-Aldrich, Merck KGaA, Saint Louis, MO, USA) and were used as received. The elemental analysis of compounds was carried out on Vario ELIII (Elementar, Langensfeld, Germany).

3.2.2 Spectroscopic Measurements

The ^1H , ^{13}C spectra were recorded on a Varian VNMR-S 400 MHz spectrometer (Varian, Inc., Palo Alto, CA, USA). ^1H NMR measurements of **2–8** (0.07 mol dm^{-3}) in CDCl_3 were carried out at the operating frequency 402.64 MHz. The error of the chemical shift value was 0.01 ppm. The ^{13}C NMR spectra were recorded at the operating frequency 101.25 MHz. The error of chemical shift value was 0.1 ppm. All spectra were locked to deuterium resonance of CDCl_3 . The ^1H and ^{13}C NMR spectra are shown in the Appendix B.

The FT-IR spectra of **2–8** in the mid-infrared region were recorded in KBr pallet. The spectra were taken with an IFS 113v FT-IR spectrophotometer (Bruker, Karlsruhe, Germany) equipped with a deuterated triglycine sulfate detector (DTGS) detector; resolution 2 cm^{-1} , NSS = 64. The Happ-Genzel apodization function was used.

The ESI (Electrospray Ionization) mass spectra were recorded also on a Waters/Micromass (Waters Corporation, Manchester, UK) ZQ mass spectrometer equipped with a Harvard Apparatus syringe pump. The samples were prepared in dry acetonitrile ($5 \times 10^{-5} \text{ mol dm}^{-3}$). The sample was infused into the ESI source using a Harvard pump at a flow rate of 20 mL min^{-1} . The ESI source potentials were: capillary 3 kV, lens 0.5 kV, extractor 4 V. The standard ESI mass spectra were recorded at the cone voltages: 10 and 30 V. The source temperature was 120°C and the desolvation temperature was 300°C . Nitrogen was used as the nebulizing and desolvation gas at flow-rates of $100 \text{ dm}^3 \text{ h}^{-1}$. Mass spectra were acquired in the positive ion detection mode with unit mass resolution at a step of 1 m/z unit. The mass range for ESI experiments was from $m/z = 100$ to $m/z = 1000$, as well as from $m/z = 200$ to $m/z = 1500$.

3.2.3 Synthesis

Synthesis of 2

To a mixture of **1** (500 mg, 1.25 mmol) in MeOH/water (1/1, v/v, 5 mL), the sodium methanethiolate (21% in H₂O, 0.83 mL, 2.5 mmol) was added. The mixture was stirred in at RT for 72 h. Reaction time was determined by TLC. After that time, the reaction mixture was quenched by the addition of water (150 mL). The whole mixture was extracted four times with CH₂Cl₂, and the combined organic layers were dried over MgSO₄, filtered, and evaporated under reduced pressure. The residue was purified by CombiFlash[®] (hexane/EtOAc (1/1), then EtOAc/MeOH, increasing concentration gradient) to give **2** with yield 78% [34].

The synthesis of compounds **4**, **6** and **8** was carried out analogously to the above starting respectively from the compounds **3**, **5** and **7**.

Compound 2, ¹H-NMR (403 MHz, CDCl₃) δ 7.92 (s, 1H), 7.46 (s, 1H), 7.33 (d, *J* = 10.4 Hz, 1H), 7.10 (d, *J* = 10.5 Hz, 1H), 6.55 (s, 1H), 4.72–4.64 (m, 1H), 3.95 (s, 3H), 3.91 (s, 3H), 3.67 (s, 3H), 2.54 (dd, *J* = 13.0, 5.8 Hz, 1H), 2.45 (s, *J* = 5.7 Hz, 3H), 2.43–2.26 (m, 2H), 1.99 (s, 3H), 1.94 (dd, *J* = 11.8, 5.5 Hz, 1H) ppm; ¹³C-NMR (101 MHz, CDCl₃) δ 182.4, 170.0, 158.1, 153.6, 151.8, 151.1, 141.6, 138.6, 134.8, 134.4, 128.3, 126.7, 125.6, 107.3, 61.6, 61.4, 56.1, 52.3, 36.4, 29.9, 22.8, 15.1 ppm. FT-IR (KBr pellet): 3283, 2935, 1660, 1605, 1541, 1485, 1461, 1425, 1404, 1349, 1321, 1286, 1236, 1195, 1155, 1138, 1095, 1023 cm⁻¹. ESI-MS (*m/z*): [M + H]⁺ calcd. 416, found 416, [M + Na]⁺ calcd. 438, found 438, [M + K]⁺ calcd. 454 found 454, [2M + Na]⁺ calcd. 853, found 853, [3M + Na]⁺ calcd. 1268, found 1268.

Compound 4, Amorphous yellow solid. ¹H-NMR (403 MHz, CDCl₃) δ 7.98 (d, *J* = 6,7 Hz, 1H), 7.44 (s, 1H), 7.26 (d, *J* = 10.3 Hz, 1H), 7.08 (d, *J* = 10.8 Hz, 1H), 4.58 (dt, *J* = 13.1, 6.7 Hz, 1H), 3.98 (s, 3H), 3.96 (s, 3H), 3.61 (s, 3H), 3.24 (dd, *J* = 13.5, 4.8 Hz, 1H), 2.44 (s, 3H), 2.27 (ddd, *J* = 18.0, 12.1, 6.0 Hz, 1H), 2.14 (td, *J* = 13.4, 6.2 Hz, 1H), 2.00 (s, 3H), 1.92–1.80 (m, 1H); ¹³C-NMR (101 MHz, CDCl₃) δ 182.4, 170.1, 159.1, 151.3, 150.2, 149.7, 146.6, 137.3, 134.8, 131.7, 129.9, 128.1, 126.4, 122.1, 61.6, 61.5, 61.1, 52.2, 34.5, 25.9, 22.8, 15.1 ppm. FT-IR (KBr pellet): 3290, 2936, 1661, 1608, 1550, 1464, 1413, 1349, 1327, 1288, 1267, 1197, 1140, 1086, 1023 cm⁻¹. ESI-MS (*m/z*): [M + H]⁺ calcd. 450, found 450, [M + Na]⁺ calcd. 472, found 472, [2M + H]⁺ calcd. 889, found 889, [2M + Na]⁺ calcd.

921, found 921. Anal. Calcd. for C, 58.73; H, 5.38; Cl, 7.88; N, 3.11; O, 17.78; S, 7.13; found: C, 58.61; H 5.35; Cl, 7.93; N, 3.01; S, 7.25.

6, Amorphous yellow solid. ¹H-NMR (403 MHz, CDCl₃) δ 7.68 (d, *J* = 6.6 Hz, 1H), 7.42 (s, 1H), 7.26 (d, *J* = 9.6 Hz, 1H), 7.08 (d, *J* = 10.8 Hz, 1H), 4.61–4.52 (m, 1H), 3.99 (s, 3H), 3.97 (s, 3H), 3.63 (s, 3H), 3.27 (d, *J* = 8.0 Hz, 1H), 2.45 (s, 3H), 2.25 (dt, *J* = 13.4, 7.9 Hz, 2H), 2.01 (s, *J* = 1.6 Hz, 3H), 1.85 (dd, *J* = 6.7, 4.1 Hz, 1H) ppm; ¹³C-NMR (101 MHz, CDCl₃) δ 182.4, 170.0, 159.2, 151.2, 151.0, 150.4, 146.6, 137.4, 134.8, 133.4, 130.2, 128.1, 126.3, 113.5, 61.6, 61.5, 61.0, 52.2, 34.5, 29.0, 22.9, 15.2 ppm. FT-IR (KBr pellet): 3267, 2930, 1659, 1603, 1559, 1462, 1410, 1347, 1138, 1074, 1053, 1014 cm⁻¹. ESI-MS (*m/z*): [M + H]⁺ calcd. 494, found 494, [M + 2 + H]⁺ 496, found 496, [M + Na]⁺ calcd. 516, found 516, [M + 2 + Na]⁺ calcd. 518, found 518, [2M + H]⁺ calcd. 989, found 989, [2M + 2 + H]⁺ calcd. 991, found 991, [2M + Na]⁺ calcd. 1011, found 1011, [2M + 2 + Na]⁺ calcd. 1013, found 1013. Anal. Calcd. for C, 53.45; H, 4.89; Br, 16.16; N, 2.83; O, 16.18; S, 6.49; found: C, 53.56; H 4.81; Br, 16.28; N, 2.89; S, 6.55.

8, Amorphous yellow solid. ¹H-NMR (403 MHz, CDCl₃) δ 7.75 (d, *J* = 6.9 Hz, 1H), 7.42 (s, 1H), 7.25 (d, *J* = 10.3 Hz, 1H), 7.09 (d, *J* = 10.8 Hz, 1H), 4.58–4.50 (m, 1H), 3.97 (s, 3H), 3.95 (s, 3H), 3.63 (s, 3H), 3.18 (dd, *J* = 13.7, 5.0 Hz, 1H), 2.46 (s, 3H), 2.40 (dd, *J* = 13.6, 6.2 Hz, 1H), 2.32–2.23 (m, 1H), 2.01 (s, 3H), 1.85–1.79 (m, 1H); ¹³C-NMR (101 MHz, CDCl₃) δ 182.4, 170.1, 159.1, 153.5, 151.4, 151.1, 145.6, 137.8, 136.8, 134.7, 129.7, 128.1, 126.3, 92.2, 61.6, 61.4, 60.8, 52.1, 34.5, 34.4, 22.9, 15.2 ppm. FT-IR (KBr pellet): 3288, 2936, 1660, 1607, 1547, 1461, 1406, 1346, 1318, 1288, 1262, 1197, 1138, 1081, 1019 cm⁻¹. ESI-MS (*m/z*): [M + H]⁺ calcd. 542, found 542, [M + Na]⁺ calcd. 564, found 564, [M + K]⁺ calcd. 580, found 580. Anal. Calcd. for C, 48.81; H, 4.47; I, 23.44; N, 2.59; O, 14.78; S, 5.92; found: C, 48.67; H 4.55; I, 23.59; N, 2.64; S, 5.98.

Synthesis of 3

A mixture of *N*-chlorosuccinimide (175 mg, 1.31 mmol) and **1** (500 mg, 1.25 mmol) in acetonitrile was stirred at RT under nitrogen atmosphere for the 72 h. Reaction time was determined by TLC. The reaction was quenched with saturated aqueous Na₂S₂O₃. The whole mixture was extracted four times with CH₂Cl₂, and the combined organic layers

were dried over MgSO₄, filtered, and evaporated under reduced pressure. The residue was purified by CombiFlash[®] (EtOAc/MeOH, increasing concentration gradient) to give **3** with yield 75% [32].

¹H-NMR (403 MHz, CDCl₃) δ 8.29 (d, *J* = 6.2 Hz, 1H), 7.59 (s, 1H), 7.30 (d, *J* = 10.7 Hz, 1H), 6.87 (d, *J* = 11.2 Hz, 1H), 4.60–4.49 (m, 1H), 4.01 (s, 3H), 3.97 (s, 3H), 3.95 (s, 3H), 3.61 (s, 3H), 3.23 (dd, *J* = 13.7, 5.1 Hz, 1H), 2.31 (dq, *J* = 18.7, 6.2 Hz, 1H), 2.18–2.09 (m, 1H), 1.96 (s, 3H), 1.93–1.82 (m, 1H) ppm; ¹³C-NMR (101 MHz, CDCl₃) δ 179.5, 170.2, 164.3, 152.0, 150.1, 149.7, 146.6, 135.8, 135.8, 131.7, 130.1, 129.8, 122.1, 112.5, 61.5, 61.5, 61.1, 56.5, 52.7, 34.5, 25.8, 22.7 ppm. FT-IR (KBr pellet): 3256, 2935, 1663, 1618, 1591, 1556, 1456, 1412, 1397, 1351, 1290, 1272, 1243, 1171, 1136, 1080, 1021 cm⁻¹. ESI-MS (*m/z*): [M + H]⁺ calcd. 434, found 434, [M + Na]⁺ calcd. 456, found 456, [2M + Na]⁺ calcd. 889, found 889.

Synthesis of 5

A mixture of *N*-bromosuccinimide (279 mg, 1.57 mmol) and **1** (500 mg, 1.25 mmol) in acetonitrile was stirred at RT under nitrogen atmosphere for the 72 h. Reaction time was determined by TLC. The reaction was quenched with saturated aqueous Na₂S₂O₃. The whole mixture was extracted four times with CH₂Cl₂, and the combined organic layers were dried over MgSO₄, filtered, and evaporated under reduced pressure. The residue was purified by CombiFlash[®] (EtOAc/MeOH, increasing concentration gradient) to give **5** with yield 95% [32].

¹H-NMR (403 MHz, CDCl₃) δ 8.02 (s, 1H), 7.58 (s, 1H), 7.30 (d, *J* = 10.7 Hz, 1H), 6.88 (d, *J* = 11.1 Hz, 1H), 4.59–4.49 (m, 1H), 4.03 (s, 3H), 3.99 (s, 3H), 3.96 (s, 3H), 3.63 (s, 3H), 3.27 (dd, *J* = 13.0, 4.3 Hz, 1H), 2.26 (dd, *J* = 13.1, 5.2 Hz, 1H), 2.18 (d, *J* = 2.4 Hz, 1H), 1.99 (s, 3H), 1.78 (s, 1H) ppm; ¹³C-NMR (101 MHz, CDCl₃) δ 179.5, 170.2, 164.4, 151.8, 151.1, 150.4, 146.6, 135.8, 135.7, 133.4, 130.2, 130.0, 113.5, 112.4, 61.5, 61.5, 61.0, 56.5, 52.6, 34.5, 28.9, 22.8 ppm. FT-IR (KBr pellet): 3274, 2936, 1662, 1617, 1589, 1565, 1462, 1411, 1398, 1350, 1270, 1250, 1172, 1137, 1080, 1018 cm⁻¹. ESI-MS (*m/z*): [M + Na]⁺ calcd. 500, found 500, [M + 2 + Na]⁺ calcd. 502, found 502, [2M + 2 +

Na]⁺ calcd. 979, found 979, [2M + Na]⁺ calcd. 977, found 977, [2M + 4 + Na]⁺ calcd. 981, found 981.

Synthesis of 7

A mixture of *N*-iodosuccinimide (560 mg, 2.49 mmol) and **1** (500 mg, 1.25 mmol) in AcOH was stirred at 70°C under nitrogen atmosphere for the 20 h. Reaction time was determined by TLC. The reaction was quenched with saturated aqueous Na₂S₂O₃. The whole mixture was extracted four times with CH₂Cl₂, and the combined organic layers were dried over MgSO₄, filtered, and evaporated under reduced pressure. The residue was purified by CombiFlash[®] (EtOAc/MeOH, increasing concentration gradient) to give **7** with yield 95% [32].

¹H-NMR (403 MHz, CDCl₃) δ 8.22 (d, *J* = 5.6 Hz, 1H), 7.61 (s, 1H), 7.30 (d, *J* = 10.7 Hz, 1H), 6.89 (d, *J* = 11.2 Hz, 1H), 4.55–4.47 (m, 1H), 4.04 (s, 3H), 3.97 (s, 3H), 3.95 (s, 3H), 3.63 (s, 3H), 3.21–3.15 (m, 1H), 2.40 (dd, *J* = 12.7, 5.0 Hz, 1H), 1.99 (s, 3H), 1.87–1.81 (m, 1H); ¹³C-NMR (101 MHz, CDCl₃) δ 179.5, 170.2, 164.4, 153.4, 152.0, 151.4, 145.6, 136.7, 136.2, 135.6, 130.1, 129.5, 112.5, 92.1, 61.5, 61.3, 60.7, 56.5, 52.6, 34.4, 34.4, 22.7 ppm; FT-IR (KBr pellet): 3274, 2934, 1662, 1617, 1588, 1563, 1461, 1406, 1393, 1346, 1318, 1266, 1249, 1171, 1136, 1078, 1015 cm⁻¹. ESI-MS (*m/z*): [M + H]⁺ calcd. 526, found 526 [M + Na]⁺ calcd. 548, found 548.

3.2.4 Antiproliferative activity of colchicine and its derivatives

Four human cancer cell lines and one murine normal cell line were used to evaluate antiproliferative activity of colchicine and its derivatives: human lung adenocarcinoma (A549), human breast adenocarcinoma (MCF-7), human colon adenocarcinoma cell lines sensitive and resistant to doxorubicin (LoVo) and (LoVo/DX) respectively, and normal murine embryonic fibroblast cell line (BALB/3T3). The BALB/3T3 cell line was purchased from the American Type Culture Collection (ATCC, Manassas, VA, USA), A549 and MCF-7 cell lines—from European Collection of Authenticated Cell Cultures (Salisbury, UK), LoVo cell line was purchased from the ATCC (ATCC, Manassas, VA, USA), and LoVo/DX by courtesy of Prof. E. Borowski (Technical University of Gdańsk,

Gdańsk, Poland). All the cell lines are maintained in the Institute of Immunology and Experimental Therapy (IET), Wrocław, Poland. Human lung adenocarcinoma cell line was cultured in mixture of OptiMEM and RPMI 1640 (1:1) medium (IET, Wrocław, Poland), supplemented with 5% fetal bovine serum (GE Healthcare, Logan, UT, USA) and 2 mM l-glutamine (Sigma-Aldrich, Merck KGaA, Saint Louis, MO, USA). Human breast adenocarcinoma cell line was cultured in mixture of Eagle medium (IET, Wrocław, Poland), supplemented with 10% fetal bovine serum, 2 mM l-glutamine, 8 µg/mL insulin and 1% amino-acids (Sigma-Aldrich, Merck KGaA, Saint Louis, MO, USA). Human colon adenocarcinoma cell lines were cultured in mixture of OptiMEM and RPMI 1640 (1:1) medium (IET, Wrocław, Poland), supplemented with 5% fetal bovine serum (GE Healthcare, Logan UT, USA), 2 mM l-glutamine, 1 mM sodium pyruvate (Sigma-Aldrich, Merck KGaA, Saint Louis, MO, USA) and 10 µg/100 mL doxorubicin for LoVo/DX (Sigma-Aldrich, Merck KGaA, Saint Louis, MO, USA). Murine embryonic fibroblast cells were cultured in Dulbecco medium (Life Technologies Limited, Paisley, UK), supplemented with 10% fetal bovine serum (GE Healthcare, Logan, UT, USA) and 2 mM glutamine (Sigma-Aldrich, Merck KGaA, Saint Louis, MO, USA). All culture media contained antibiotics: 100 U/mL penicillin and 100 µg/mL streptomycin (Polfa-Tarchomin, Warsaw, Poland). All cell lines were cultured during entire experiment in humid atmosphere at 37°C and 5% CO₂. Cells were tested for mycoplasma contamination by mycoplasma detection kit for conventional PCR: Venor GeM Classic (Minerva Biolabs GmbH, Berlin, Germany) and negative results was obtained. The procedure is repeated every year or in the case of less frequently used lines, after thawing.

The antiproliferative assays in vitro

Twenty-four hours before adding the tested compounds, all cell lines were seeded in 96-well plates (Sarstedt, Nümbrecht, Germany) in appropriate media with 10⁴ cells per well. All cell lines were exposed to each tested agent at four different concentrations in the range 100–0.01 µg/mL for 72 h. Cells were also exposed to the reference drug cisplatin (Teva Pharmaceuticals Polska, Warsaw, Poland) and doxorubicin (Accord Healthcare Limited, Middlesex, UK). Additionally, all cell lines were exposed to DMSO (solvent used

for tested compounds) (POCh, Gliwice, Poland) at concentrations corresponding to those present in tested agents' dilutions. After 72 h sulforhodamine B assay (SRB) was performed [37].

Sulforhodamine B assay (SRB)

After 72 h of incubation with the tested compounds, cells were fixed in situ by gently adding of 50 μ L per well of cold 50% trichloroacetic acid (TCA) (POCh, Gliwice, Poland) and were incubated at 4°C for one hour. Following, wells were washed four times with water and air dried. Next, 50 μ L of 0.1% solution of sulforhodamine B (Sigma-Aldrich, Merck KGaA, Saint Louis, MO, USA) in 1% acetic acid (POCh, Gliwice, Poland) were added to each well and plates were incubated at room temperature for 0.5 h. After incubation time, unbound dye was removed by washing plates four times with 1% acetic acid whereas stain bound to cells was solubilized with 10 mM Tris base (Sigma-Aldrich, Steinheim, Germany). Absorbance of each solution was read at Synergy H4 Hybrid Multi-Mode Microplate Reader (BioTek Instruments, Inc., Winooski, VT, USA) at the 540 nm wavelength.

Results are presented as mean IC_{50} (concentration of the tested compound, that inhibits cell proliferation by 50%) \pm standard deviation. IC_{50} values were calculated in Cheburator 0.4, Dmitry Nevozhay software (version 1.2.0 software by Dmitry Nevozhay, 2004–2014, <http://www.cheburator.nevozhay.com>, freely available) for each experiment [38]. Compounds at each concentration were tested in triplicates in single experiment and each experiment was repeated at least three times independently. Results are summarized in Table 3-1. The Resistance Index (*RI*) was defined as the ratio of IC_{50} for a given compound calculated for resistant cell line to that measured for its parental drug sensitive cell line (Table 3-1).

3.2.5 Molecular Docking Simulations

A combination of different theoretical methods was used to explore ligand-tubulin interactions. The ligand structures were fully optimized based on the RHF/cc-pVDZ [39] level of theory in GAMESS-US version 2010-10-01 [40-42]. Since there is no crystal

structure available for human β I tubulin (TBB5_HUMAN), we obtained its sequence from UniProt (ID: Q13509). We used the tubulin structure 1SA0.pdb as a template to construct the homology model for β I tubulin using MOE2015. We then docked the small library of colchicine derivatives to the protein using the AutoDock4 program under flexible ligand and rigid receptor conditions (Table 3-2). AutoDock4 software (version 2018.2.0, Tableau Research, Standford University, Seattle, WA, USA) is designed to predict how drug candidates bind to a receptor of a known 3D structure and consists of two main programs: AutoDock performs the docking of the ligand to a set of grids describing the target protein; AutoGrid pre-calculates these grids. The estimated Moriguchi octanol-water partition coefficient, MlogP, of the compounds were calculated by ADMET Predictor 8.0 (ADMET Predictor, Simulations Plus, Lancaster, CA, USA).

3.3 Results

3.3.1 Chemistry

The synthetic routes to colchicines derivatives **2–8** are outlined in Figure 3-1. Colchicine (**1**) was treated with sodium methanethiolate to give thiocolchicine (**2**) with yield 78% according to the previously described method [34]. 4-chlorocolchicine (**3**), 4-bromocolchicine (**5**), and 4-iodocolchicine (**7**) were synthesized from **1** by treatment with NCS, NBS, and NIS with yields from 75% up to 95%, respectively, based on the methods developed earlier [32]. For 4-chlorocolchicine (**3**) and 4-bromocolchicine (**5**), the application of milder conditions, i.e., the replacement of acetic acid (the solvent) by acetonitrile followed by reacting at room temperature, also allowed to obtain the same final yields. Compounds **3**, **5**, **7** were then treated with sodium methanethiolate to give double-modified derivatives (**4**, **6**, **8**) with yields from 71% to 75%.

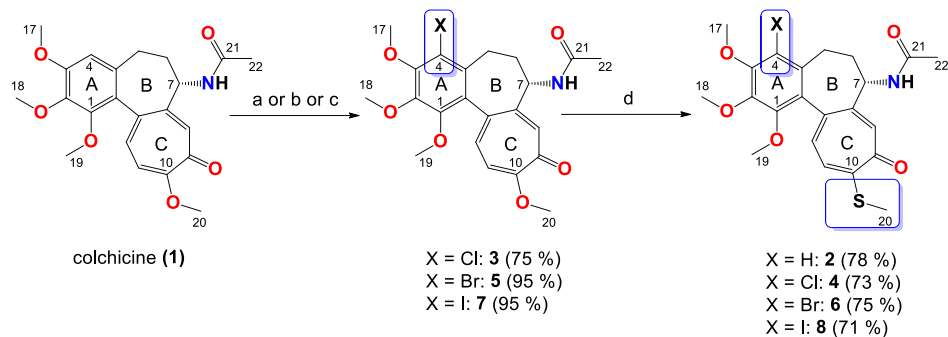


Figure 3-1. Synthesis of colchicine derivatives (**2–8**). Reagents and conditions: (a) for **3**, NCS, acetonitrile, RT; (b) for **5**, NBS, acetonitrile, RT; (c) for **7**, NIS, AcOH, 70°C; (d) MeOH/H₂O, CH₃SNa, RT.

The structures of all products **2–8** were determined using the elemental analysis, ESI-MS, FT-IR, ¹H- and ¹³C-NMR methods and are shown in (Appendix B). In the ¹³C-NMR spectra of the 4-halo derivatives a resonance for the C-4 carbon atom of the A aromatic ring was observed at 122.1 ppm for **3**, at 113.5 ppm for **5** and at 92.1 ppm for **7**, while in **1** it was observed at 107.3 ppm. After the introduction of thiomethyl group in C-10 positions shifts of the signal for the C-20 carbon atom in compounds **2**, **4**, **6** and **8** were observed in the range 15.1–15.2 ppm, while in unmodified **1** as well as 4-halo derivatives (**3**, **5**, **7**) shifts of the signal for the C-20 carbon atom were observed in the range 56.1–56.5 ppm.

3.3.2 *In vitro* Determination of Drug-Induced Inhibition of Human Cancer Cell Line Growth

The synthesized colchicine derivatives (**2–8**) and starting material (**1**) were evaluated for their *in vitro* antiproliferative effect on normal and cancer cells. Each compound was tested on four human cancer cell lines, including one cell line displaying various level of drug resistance, namely human lung adenocarcinoma (A549), human breast adenocarcinoma (MCF-7), human colon adenocarcinoma cell line (LoVo) and doxorubicin-resistant subline (LoVo/DX). The antiproliferative effect was also studied on normal murine embryonic fibroblast cell line (BALB/3T3) for better description of cytotoxic activity of the compounds studied. The mean values of IC₅₀ ± SD of the tested

compounds are collected in Table 3-1. To evaluate the agents' activity against the cells with MDR (multidrug resistance) phenotype, one drug resistant cancer cell line, i.e., LoVo/DX, was tested and the indexes of resistance (RI) were calculated (see Table 3-1). The RI values indicate how many times more resistant is the subline in comparison to its parental cell line.

All obtained derivatives with single modification at either the C-4 or C-10 position as well as double-modified compounds showed better antiproliferative activity against all tested cancer cell lines than unmodified **1** and some common chemotherapeutics such as doxorubicin and cisplatin. The IC₅₀ values of novel 4-halothiocolchines are better than for single-modified colchicines in C-4 positions and remain at a level similar to the cytotoxicity of **2** for the A549 and MCF-7 cell lines.

As many as three of the compounds tested on the LoVo cell line (**6–8**), including two novel double-modified derivatives (**6,8**), exhibited extremely high activity (IC₅₀ = 0.007–0.014 μM), which is even better than the activity of **2** (IC₅₀ = 0.021 μM). During the tests on the doxorubicin-resistant subline (LoVo/DX), compounds **4** and **6** showed the best activity among all tested compounds. However, the RI values of the tested compounds indicated that colchicines did not break the drug resistance of LoVo/DX (RI = 9.64–278). Comparison between the cancer cell lines and the normal cell line (BALB/3T3) was made to define the Selectivity Index (SI) as a measure of therapeutic potential. This parameter seems to be especially important for drug-like molecules based on a scaffold of a toxic compound. The SI values showed that compounds **2**, **6** and **8** mostly targeted cancer cells, and fewer targeted normal cells (SI = 10.08–10.45, SI = 6.76–11.85, SI = 5.45–16.43 for A549, MCF-7, LoVo cancer cell lines, respectively). Also compounds **3** and **5** indicated good SI values for MCF-7 cell line (SI = 6.00, SI = 5.26, respectively), as well as compound **7** indicated good SI value for LoVo cell line (SI = 13.5).

Table 3-1. Antiproliferative activity (IC_{50}) of colchicine (**1**) and its derivatives (**2–8**) compared with antiproliferative activity of standard anticancer drugs doxorubicin and cisplatin and the calculated values of the resistance index (RI) and selectivity index (SI) of tested compounds [19,43].

Compound	A549		MCF-7		LoVo		LoVo/DX			BALB/3T3
	IC_{50} (μ M)	SI	RI	IC_{50} (μ M)						
1	0.149 ± 0.009	1.4	0.128 ± 0.135	1.6	0.108 ± 0.025	1.9	2.65 ± 0.96	0.1	24.5	0.208 ± 0.042
2	0.011 ± 0.001	10.1	0.010 ± 0.002	11.9	0.021 ± 0.006	5.5	0.398 ± 0.075	0.3	19.0	0.114 ± 0.072
3	0.046 ± 0.035	3.0	0.023 ± 0.005	6.0	0.069 ± 0.012	2.0	0.784 ± 0.28	0.2	11.4	0.138 ± 0.069
4	0.022 ± 0.002	1.0	0.022 ± 0.002	1.0	0.022 ± 0.002	1.0	0.111 ± 0.044	0.2	5.1	0.022 ± 0.002
5	0.105 ± 0.008	1.4	0.027 ± 0.008	5.3	0.084 ± 0.021	1.7	1.55 ± 0.17	0.1	18.5	0.142 ± 0.073
6	0.010 ± 0.0001	10.3	0.015 ± 0.002	6.9	0.014 ± 0.004	7.4	0.135 ± 0.012	0.8	9.6	0.103 ± 0.089
7	0.094 ± 0.006	1.4	0.098 ± 0.029	1.4	0.010 ± 0.002	13.5	2.78 ± 0.45	0.1	278.0	0.135 ± 0.056
8	0.011 ± 0.002	10.5	0.017 ± 0.006	6.8	0.007 ± 0.002	16.4	0.642 ± 0.084	0.2	91.7	0.115 ± 0.044
Doxorubicin	0.258 ± 0.044	0.6	0.386 ± 0.118	0.4	0.092 ± 0.018	1.8	4.75 ± 0.99	<0.1	51.6	0.166 ± 0.074
Cisplatin	6.367 ± 1.413	0.6	10.70 ± 0.753	0.4	4.37 ± 0.73	0.9	5.70 ± 0.63	0.7	1.3	3.90 ± 1.50

The IC_{50} value is defined as the concentration of a compound at which 50% growth inhibition is observed. Human lung adenocarcinoma (A549), human breast adenocarcinoma (MCF-7), human colon adenocarcinoma cell line (LoVo) and doxorubicin resistant subline (LoVo/DX), normal murine embryonic fibroblast cell line (BALB/3T3). The SI (Selectivity Index) was calculated for each compound using the formula: $SI = IC_{50}$ for normal cell line BALB/3T3 / IC_{50} for respective cancerous cell line. A beneficial SI > 1.0 indicates a drug with efficacy against tumor cells greater than the toxicity against normal cells. The RI (Resistance Index) indicates how many times a resistant subline is chemoresistant relative to its parental cell line. The RI was calculated for each compound using the formula: $RI = IC_{50}$ for LoVo/DX / IC_{50} for LoVo cell line. When RI is 0–2, the cells are sensitive to the compound tested, RI in the range 2–10 means that the cell shows moderate sensitivity to the drug tested, RI above 10 indicates strong drug-resistance.

3.3.3 Molecular Docking: *in Silico* Determination of Drug-Induced Inhibition of β I Tubulin

To further investigate the ability to inhibit tubulin aggregation by the new colchicine derivatives in cancer cell growth assays, binding energies between the new compounds and β I tubulin, one of the subunits of microtubules in the cytoskeleton structure of every eukaryotic cell, were calculated using docking methodology. The eight structures of colchicine and its derivatives described above were docked into the β I tubulin CBS and ranked according to their binding affinity (Table 3-2).

Since the binding energy shows how strong the interaction between the distributed drug in the cell and β -tubulin protein can be, the partition coefficient (MlogP) values were calculated and considered for the ability of the drugs to diffuse into the cells (Table 3-2). The MlogP values can be a beneficial factors in estimating and comparing the distribution of the novel drugs within the cells, organs and the body [44].

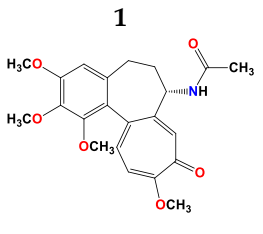
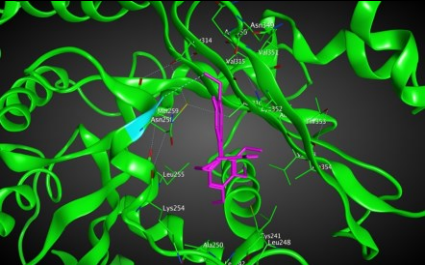
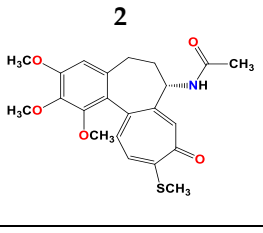
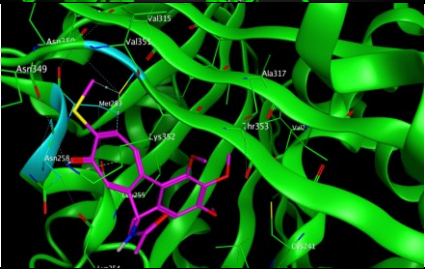
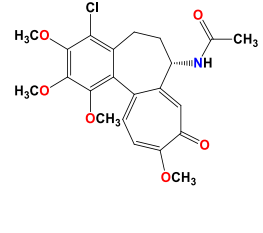
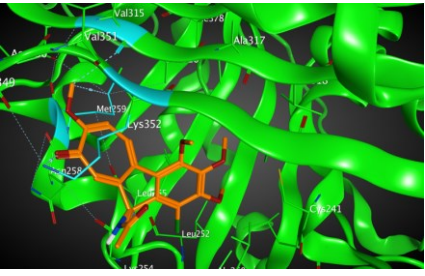
Based on our computational predictions, compounds **6**, **4**, **5** and **3** show the lowest binding energies of -8.6 , -8.6 , -8.4 and -8.3 kcal/mol, respectively. In the experimental part of the study, the lowest IC_{50} values showed **4**, **6**, **8** compounds having higher activity than **3**, **5**, **7** (Table 3-1). To investigate in more detail why the computational results did not show better binding energies of compound **8** than **3** and **5**, the interactions between double-modified colchicine derivatives and the CBS of β I tubulin were studied.

As shown in the diagrams representing schematic interactions of the **4** and **6** compounds with the CBS of β I tubulin Lys 352, Met 259 and Asn 258 residues interact with oxygen of the carbonyl of the C ring (sidechain acceptor), with hydrogen of thiomethyl group on ring C and hydrogen of C-11 on ring C (sidechain donor) and with ring C (arene-H), respectively.

However, Lys 352, Met 259 and Val 315 residues of the CBS of β I tubulin interact with oxygen of the carbonyl of the C ring (sidechain acceptor), with hydrogen

of C-11 on ring C (sidechain donor) and with hydrogens of methoxyl groups on ring C (backbone donors) of the **3** and **5** compounds, respectively.

Table 3-2. Binding energies interactions between eight different colchicine derivatives and β I tubulin and the estimated Moriguchi octanol-water partition coefficient, MlogP for each colchicine derivative.

Structure	Interactions	Binding energy (Kcal/mol)	MlogP	Active residues
 <p>1</p>		-8.09	1.37	Asn258
 <p>2</p>		-8.13	1.56	Met259 Asn258 Lys352
 <p>3</p>		-8.33	1.58	Met 259 Lys352 Val315

<p style="text-align: center;">4</p>		-8.57	2.34	Met259 Asn258 Lys352
<p style="text-align: center;">5</p>		-8.40	1.93	Met259 Val315 Lys352
<p style="text-align: center;">6</p>		- 8.60	2.69	Met259 Asn258 Lys352
<p style="text-align: center;">7</p>		-7.53	1.50	Ala317 Cys241
<p style="text-align: center;">8</p>		-7.33	2.00	Ala316 Ala317 Cys241

The study was continued for compound **8** with the highest binding energy for better understanding over the effect of interaction of β I tubulin's residues with novel

derivatives on better activities of the derivatives. Compound **8** interacts with Ala317 residue of β I tubulin, iodine on ring A (backbone donor) and Cys241 residue of β I tubulin, hydrogen of methoxyl group on ring A (sidechain donor) and Ala 316 residue of β I tubulin, the oxygen of carbonyl on ring B (sidechain acceptor).

Since the IC_{50} is a cell-based assay and the β I tubulin isotype is not the only isotype of tubulin expressed in the cell, we decided to check interactions of the synthesized compounds with the other tubulin isotypes present in the referred cell lines. Tubulin isotypes are highly conserved in all mammals as discussed by Luduena [45]. As is commonly the case, both normal and cancer cells in humans contain the same tubulin isotypes. However, their expression levels differ and specifically β III (TUBB3) tubulin is very narrowly distributed in normal cells while it is almost always found in cancer cells and it is often correlated with drug resistance [46-48]. Furthermore, β I isotype (TUBB) is the most abundant isotype in most tumors, followed by, β IVb (TUBB4B), β IIa (TUBB2A), β V (TUBB6), and β III (TUBB3) with 47%, 38%, 8.9%, 3.1%, and 2.2% respectively and with β IVa (TUBB4), β IIb (TUBB2B) and β VI (TUBB1) levels below 0.5% of the total β tubulin [46]. Interestingly, the binding sites for common tubulin-binding agents do not vary significantly between tubulin isotypes except for the CBS [8].

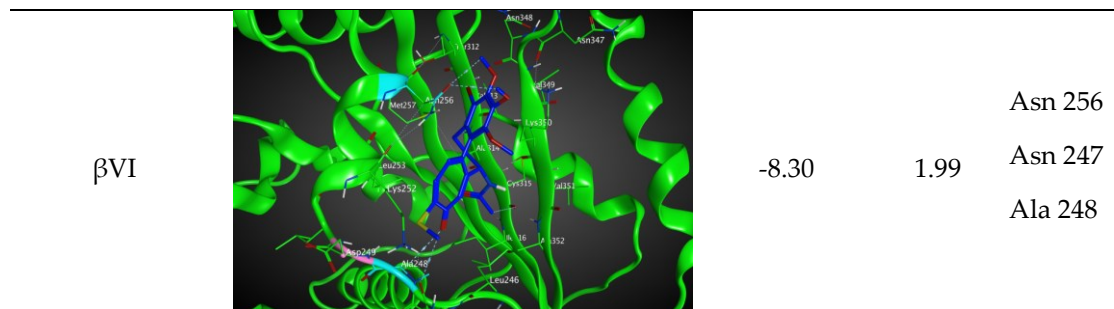
Tubulin isotype classes β IVa and β IVb comprised more than 50% of the total β tubulin in breast cancer (MCF-7) and colon cancer cells. The expression of β I, β III and β IV (a and b) in the MCF-7 cell line has been reported as 39.1%, 2.5% and 58.4% respectively [49]. In another study, the ratio for MCF-7 cell line was reported as 55% to 6% to 39% [50]. In colon cancer cells, the percentage expression of the referred tubulin isotypes is 61.8%, 0.2% and 38%, respectively. The ratio of the isotype expression in lung cancer cells (A549) is given as 71.9% to 1.6% to 26.5% [49]. Consequently, each of the cell lines investigated has a distinct distribution of tubulin isotypes, which affects the overall response to a cytotoxic agent whose affinity for each of these isotypes is different making the problem of computational prediction complex.

To quantify the assumption that these compounds have different binding free energies for each of the tubulin isotypes, docking simulations between the novel colchicine derivatives and β I (UniProt ID: P07437), β IIa (UniProt ID: Q13885), β IIb (UniProt ID: Q9BVA1), β III (UniProt ID: Q13509), β IVa (UniProt ID: P04350), β IVb (UniProt ID: P68371), β V (UniProt ID: Q9BUF5), and β VI (UniProt ID: Q9H4B7), isotypes were performed. Tubulin structure 1SA0.pdb was used as the homology model template for all tubulin isotypes using MOE2015. To visualize the results, a heat map was prepared to better illustrate the comparison of binding energies between the investigated compounds and the different tubulin isotypes using AutoDock Tableau Desktop (version 2018.2.0, Tableau Research, Stanford University, Seattle, WA, USA) (see Table 3-3).

Table 3-3. Heat map of binding energies interactions between the eight different colchicine derivatives and β I, β III β IIa, β IIb, β IVa, β IVb, β V and β VI tubulin isotypes.

	1	2	3	4	5	6	7	8
β I	-8.090	-8.130	-8.330	-8.570	-8.400	-8.600	-7.530	-7.330
β IIa	-7.420	-7.190	-7.890	-7.640	-8.000	-7.460	-8.300	-8.200
β IIb	-7.050	-6.680	-6.800	-6.900	-6.890	-7.050	-6.430	-7.040
β III	-7.490	-7.150	-7.470	-7.620	-7.850	-7.780	-8.200	-7.710
β IVa	-7.610	-7.300	-7.100	-7.300	-7.210	-7.430	-6.970	-7.010
β IVb	-7.260	-7.210	-7.420	-7.610	-7.370	-7.620	-7.180	-6.340
β V	-7.480	-7.180	-7.320	-7.260	-7.250	-7.340	-6.500	-7.190
β VI	-7.730	-7.050	-7.270	-7.710	-7.590	-7.870	-8.320	-8.300

As can be seen in the heat map above, the binding energy between compound **8** and tubulin isotype β IIa as well as β VI are good examples of high binding energies while for compounds **3** and **5** their interaction with β I tubulin and β IIa dominates. For compound **7** β VI, β IIa and β III are the strongest binding tubulin isotypes. These differences might be the reasons of a discrepancy between experimental and computational data. However, even data concerning the level of tubulin isotypes



The analysis of interactions between compounds **4**, **6** with β I and compound **8** and β Ila and β VI shows that an arene-H interaction between the ring C Asn256 or Asn258 and a sidechain acceptor interaction between the oxygen of carbonyl on ring C and either Lys352 or Ala248 can result in a strong binding effect. As mentioned before, the probability of the expression of β Ila in most tumors is approximately 9% versus less than 0.5% for each isotype in the group of β IVa, β VI and β I Ib [46].

To the best of the authors' knowledge of the literature, ligands binding to alpha and β tubulin are exclusive, except of course of ATP, and therefore, we do not expect any cross-interactions of our compounds with alpha tubulin [52]. Concerning interactions with ABC transporters, it is quite possible that our compounds are substrates for these multidrug resistance enzymes, but this is common to many chemotherapy drugs, including taxanes. Therefore, in order to inhibit this interaction, it would most advantageous to use our compounds in combination with some of their modulators, e.g., verapamil [53].

3.4 Discussion

We synthesized three novel double-modified 4-halothiocolchicines (**4**, **6**, **8**) and evaluated their biological activity according to the *in vitro* antiproliferative tests as well as the molecular docking. For a better comparison, also the activity of single-modified colchicine derivatives (**2**, **3**, **5**, **7**) as well as colchicine itself (**1**) was evaluated on four

human cancer cell lines and normal murine embryonic fibroblast cell line. The results of our study clearly showed that the antiproliferative activity of novel 4-halothiocolchines (**4**, **6**, **8**) is better than the activity of 4-halocolchicines (**3**, **5**, **7**) and remain at a level similar to the cytotoxicity of **2** for the A549, MCF-7 and LoVo cell lines. Furthermore, the cytotoxicity of compounds **4**, **6** and **8** is higher than cytotoxicity of unmodified colchicine (**1**) and commonly used chemotherapeutics such as doxorubicin and cisplatin.

The introduction of thiomethyl group in C-10 position significantly increased the cytotoxicity in comparison to single-modified 4-halo derivatives (**3**, **5**, **7**) as well as allowed to reduce the toxicity for 4-bromo and 4-iodo derivatives. Compounds 4-bromothiocolchine (**6**) and 4-iodothiocolchicine (**8**) proved to be less toxic to normal murine fibroblast cells than the currently used anticancer drugs, such as cisplatin and doxorubicin, which is confirmed by their high SI values. The appropriate modification of colchicine molecule and synthesis of its analogs might overcome the toxicity, which is a major challenge in designing a potential colchicine-based drug candidate. However, it is still challenging to draw clear conclusions from the molecular-level calculations. Compounds **6**, **4**, **5** and **3** showed the lowest binding energies of -8.6 , -8.6 , -8.4 and -8.3 kcal/mol, respectively. The results only partially correlate with *in vitro* determined IC_{50} values. This may be explained by several additional effects taking place in living cells compared to the computational simulations that focus only on the binding mode of the compounds to the target. Specifically, off-target interactions involving efflux pumps with different affinities for the individual compounds may explain the observed partial correlation between IC_{50} values and binding free energies. Additionally, differences in the solubility values and membrane permeability may have to be accounted for when ranking the various compounds in biological assays and comparing them to computational predictions based on binding affinity for the target alone. We have partially addressed this issue by performing docking simulations for the remaining tubulin isotypes, several of them may be expressed in cancer cells in a manner different than in normal cells. We have demonstrated that a higher affinity for βVI tubulin of the

compounds investigated may explain the differences in their biological activities. Our studies clearly show the potential of the obtained double-modified compounds. In particular, 4-halothiocolchicines are worthwhile for a continuation of the search for strong and broad-spectrum anticancer agents. Inspired by these preliminary results we plan subsequent modifications in C-7 position to obtain a series of triple-modified derivatives. Further evaluation should help to find more detailed structure-activity relationships of microtubule-targeting drugs and CBS inhibitors, which can help in rational drug design in the future.

References

- [1] J. Hyams and H. Stebbings, "The mechanism of microtubule associated cytoplasmic transport," *Cell Tissue Res.*, vol. 196, no. 1, Jan. 1979, doi: 10.1007/BF00236351.
- [2] P. Dustin, Ed., *Microtubules*, 2nd ed. Berlin: Springer-Verlag, 1984.
- [3] M. A. Jordan and L. Wilson, "Microtubules as a target for anticancer drugs.," *Nat. Rev. Cancer*, vol. 4, no. 4, pp. 253–65, Apr. 2004, doi: 10.1038/nrc1317.
- [4] S. K. Dutcher, "The tubulin fraternity: alpha to eta," *Curr. Opin. Cell Biol.*, vol. 13, no. 1, pp. 49–54, Feb. 2001, doi: 10.1016/S0955-0674(00)00173-3.
- [5] N. G. Vindya, N. Sharma, M. Yadav, and K. R. Ethiraj, "Tubulins - the target for anticancer therapy.," *Curr. Top. Med. Chem.*, vol. 15, no. 1, pp. 73–82, 2015, doi: 10.2174/1568026615666150112115805.
- [6] J. Seligmann and C. Twelves, "Tubulin: an example of targeted chemotherapy.," *Future Med. Chem.*, vol. 5, no. 3, pp. 339–52, Mar. 2013, doi: 10.4155/fmc.12.217.
- [7] C. D. Katsetos and P. Dráber, "Tubulins as therapeutic targets in cancer: from bench to bedside.," *Curr. Pharm. Des.*, vol. 18, no. 19, pp. 2778–92, 2012, doi: 10.2174/138161212800626193.
- [8] J. Torin Huzil, R. F. Ludueña, and J. Tuszynski, "Comparative modelling of human β tubulin isotypes and implications for drug binding.," *Nanotechnology*, vol. 17, no. 4, pp. S90–S100, Feb. 2006, doi: 10.1088/0957-4484/17/4/014.
- [9] S. Ravanbakhsh, M. Gajewski, R. Greiner, and J. A. Tuszynski, "Determination of the optimal tubulin isotype target as a method for the development of individualized cancer chemotherapy.," *Theor. Biol. Med. Model.*, vol. 10, no. 29, p. 29, May 2013, doi: 10.1186/1742-4682-10-29.
- [10] B. Kumar, R. Kumar, I. Skvortsova, and V. Kumar, "Mechanisms of Tubulin Binding Ligands to Target Cancer Cells: Updates on their Therapeutic Potential and Clinical Trials.," *Curr. Cancer Drug Targets*, vol. 17, no. 4, pp. 357–375, 2017, doi: 10.2174/1568009616666160928110818.

- [11] C. Avendaño and J. C. Menéndez, *Medicinal Chemistry of Anticancer Drugs*. 2008.
- [12] A. Slobodnick, B. Shah, M. H. Pillinger, and S. Krasnokutsky, “Colchicine: old and new.,” *Am. J. Med.*, vol. 128, no. 5, pp. 461–70, May 2015, doi: 10.1016/j.amjmed.2014.12.010.
- [13] N. Nerlekar, A. Beale, and R. W. Harper, “Colchicine — a short history of an ancient drug,” *Med. J. Aust.*, vol. 201, no. 11, pp. 687–688, Dec. 2014, doi: 10.5694/mja14.00846.
- [14] I. Grattagliano, L. Bonfrate, V. Ruggiero, G. Scaccianoce, G. Palasciano, and P. Portincasa, “Novel therapeutics for the treatment of familial Mediterranean fever: from colchicine to biologics.,” *Clin. Pharmacol. Ther.*, vol. 95, no. 1, pp. 89–97, Jan. 2014, doi: 10.1038/clpt.2013.148.
- [15] G. Cocco, D. C. C. Chu, and S. Pandolfi, “Colchicine in clinical medicine. A guide for internists.,” *Eur. J. Intern. Med.*, vol. 21, no. 6, pp. 503–8, Dec. 2010, doi: 10.1016/j.ejim.2010.09.010.
- [16] L. P. H. Yang, “Oral Colchicine (Colcrys®),” *Drugs*, vol. 70, no. 12, pp. 1603–1613, 2010, doi: 10.2165/11205470-000000000-00000.
- [17] J. Marangon *et al.*, “Tools for the rational design of bivalent microtubule-targeting drugs,” *Biochem. Biophys. Res. Commun.*, vol. 479, no. 1, pp. 48–53, 2016, doi: <https://doi.org/10.1016/j.bbrc.2016.09.022>.
- [18] A. Huczyński *et al.*, “Synthesis, antiproliferative and antibacterial evaluation of C-ring modified colchicine analogues.,” *Eur. J. Med. Chem.*, vol. 90, pp. 296–301, Jan. 2015, doi: 10.1016/j.ejmech.2014.11.037.
- [19] A. Huczyński *et al.*, “Synthesis, antiproliferative activity and molecular docking of Colchicine derivatives,” *Bioorg. Chem.*, vol. 64, pp. 103–112, 2016, doi: <https://doi.org/10.1016/j.bioorg.2016.01.002>.

- [20] A. Kumar, P. R. Sharma, and D. M. Mondhe, "Potential anticancer role of colchicine-based derivatives," *Anticancer. Drugs*, vol. 28, no. 3, pp. 250–262, Mar. 2017, doi: 10.1097/CAD.0000000000000464.
- [21] E. S. Shchegravina *et al.*, "Synthesis and biological evaluation of novel non-racemic indole-containing allocolchicinoids," *Eur. J. Med. Chem.*, vol. 141, pp. 51–60, 2017, doi: <https://doi.org/10.1016/j.ejmech.2017.09.055>.
- [22] D. Bartusik, B. Tomanek, E. Lattová, H. Perreault, J. Tuszynski, and G. Fallone, "Derivatives of thiocolchicine and its applications to CEM cells treatment using 19F Magnetic Resonance ex vivo," *Bioorg. Chem.*, vol. 38, no. 1, pp. 1–6, 2010, doi: <https://doi.org/10.1016/j.bioorg.2009.10.002>.
- [23] G. Raspaglio *et al.*, "Thiocolchicine dimers: a novel class of topoisomerase-I inhibitors," *Biochem. Pharmacol.*, vol. 69, no. 1, pp. 113–121, 2005, doi: <https://doi.org/10.1016/j.bcp.2004.09.004>.
- [24] T. Kozaka *et al.*, "Antitumor agents 273. Design and synthesis of N-alkyl-thiocolchicinoids as potential antitumor agents," *Bioorg. Med. Chem. Lett.*, vol. 20, no. 14, pp. 4091–4094, 2010, doi: 10.1016/j.bmcl.2010.05.081.
- [25] K. Nakagawa-Goto *et al.*, "Antitumor agents. Part 236: Synthesis of water-soluble colchicine derivatives.," *Bioorg. Med. Chem. Lett.*, vol. 15, no. 1, pp. 235–238, Jan. 2005, doi: 10.1016/j.bmcl.2004.07.098.
- [26] N. Yasobu *et al.*, "Design, Synthesis, and Antitumor Activity of 4-Halocolchicines and Their Pro-drugs Activated by Cathepsin B.," *ACS Med. Chem. Lett.*, vol. 2, no. 5, pp. 348–352, May 2011, doi: 10.1021/ml100287y.
- [27] E. S. Shchegravina, D. I. Knyazev, I. P. Beletskaya, E. V. Svirshchevskaya, H.-G. Schmalz, and A. Y. Fedorov, "Synthesis of Nonracemic Pyrrolo-allocolchicinoids Exhibiting Potent Cytotoxic Activity," *European J. Org. Chem.*, vol. 2016, no. 34, pp. 5620–5623, 2016, doi: <https://doi.org/10.1002/ejoc.201601069>.

- [28] X. Zhang *et al.*, “Design, synthesis and biological evaluation of colchicine derivatives as novel tubulin and histone deacetylase dual inhibitors,” *Eur. J. Med. Chem.*, vol. 95, pp. 127–135, 2015, doi: <https://doi.org/10.1016/j.ejmech.2015.03.035>.
- [29] K. C. Nicolaou, R. A. Valiulin, J. K. Pokorski, V. Chang, and J. S. Chen, “Bio-inspired synthesis and biological evaluation of a colchicine-related compound library,” *Bioorg. Med. Chem. Lett.*, vol. 22, no. 11, pp. 3776–3780, 2012, doi: <https://doi.org/10.1016/j.bmcl.2012.04.007>.
- [30] D.-J. Chang *et al.*, “Design, synthesis and identification of novel colchicine-derived immunosuppressant,” *Bioorg. Med. Chem. Lett.*, vol. 19, no. 15, pp. 4416–4420, 2009, doi: <https://doi.org/10.1016/j.bmcl.2009.05.054>.
- [31] A. Marzo-Mas *et al.*, “Interactions of long-chain homologues of colchicine with tubulin,” *Eur. J. Med. Chem.*, vol. 126, pp. 526–535, 2017, doi: <https://doi.org/10.1016/j.ejmech.2016.11.049>.
- [32] L. Johnson *et al.*, “Novel Colchicine Derivatives and their Anti-cancer Activity.,” *Curr. Top. Med. Chem.*, vol. 17, no. 22, pp. 2538–2558, 2017, doi: [10.2174/1568026617666170104143618](https://doi.org/10.2174/1568026617666170104143618).
- [33] B. Kumar *et al.*, “Synthesis and biological evaluation of pyrimidine bridged combretastatin derivatives as potential anticancer agents and mechanistic studies,” *Bioorg. Chem.*, vol. 78, pp. 130–140, 2018, doi: <https://doi.org/10.1016/j.bioorg.2018.02.027>.
- [34] Q. Shi, P. Verdier-Pinard, A. Brossi, E. Hamel, and K. H. Lee, “Antitumor Agents-CLXXV. Anti-tubulin action of (+)-thiocolchicine prepared by partial synthesis,” *Bioorg. Med. Chem.*, vol. 5, no. 12, pp. 2277–2282, 1997, doi: [10.1016/S0968-0896\(97\)00171-5](https://doi.org/10.1016/S0968-0896(97)00171-5).
- [35] A. Banerjee, L. T. Kasmala, E. Hamel, L. Sun, and K.-H. Lee, “Interaction of Novel Thiocolchicine Analogs with the Tubulin Isoforms from Bovine Brain 1,” vol. 337, pp. 334–337, 1999, doi: [10.1006/bbrc.1998.9943](https://doi.org/10.1006/bbrc.1998.9943).

- [36] P. B. Prajapati, K. B. Bodiwala, and B. P. Marolia, "Oxidative Degradation Kinetic Study of Thiocolchicoside using Stability Indicating High Performance Thin Layer Chromatographic Method," *Pharm. Methods*, vol. 5, no. 2, pp. 1–10, 2014, doi: 10.5530/phm.2014.2.5.
- [37] P. Skehan et al., "New colorimetric cytotoxicity assay for anticancer-drug screening," *J. Natl. Cancer Inst.*, vol. 82, no. 13, pp. 1107–1112, Jul. 1990, doi: 10.1093/jnci/82.13.1107.
- [38] D. Nevozhay, "Cheburator software for automatically calculating drug inhibitory concentrations from in vitro screening assays.," *PLoS One*, vol. 9, no. 9, p. e106186, 2014, doi: 10.1371/journal.pone.0106186.
- [39] T. H. Dunning, "Gaussian basis sets for use in correlated molecular calculations. I. The atoms boron through neon and hydrogen," *J. Chem. Phys.*, vol. 90, no. 2, pp. 1007–1023, Jan. 1989, doi: 10.1063/1.456153.
- [40] M. W. Schmidt et al., "General atomic and molecular electronic structure system," *J. Comput. Chem.*, vol. 14, no. 11, pp. 1347–1363, Nov. 1993, doi: 10.1002/jcc.540141112.
- [41] M. S. Gordon and M. W. Schmidt, "Advances in electronic structure theory: GAMESS a decade later," in *Theory and Applications of Computational Chemistry*, C. E. Dykstra, G. Frenking, K. S. Kim, and G. E. Scuseria, Eds. Amsterdam: Elsevier, 2005, pp. 1167–1189.
- [42] G. M. J. Barca et al., "Recent developments in the general atomic and molecular electronic structure system.," *J. Chem. Phys.*, vol. 152, no. 15, p. 154102, Apr. 2020, doi: 10.1063/5.0005188.
- [43] U. Majcher et al., "Synthesis, antiproliferative activity and molecular docking of thiocolchicine urethanes.," *Bioorg. Chem.*, vol. 81, pp. 553–566, 2018, doi: 10.1016/j.bioorg.2018.09.004.

- [44] H. Devalapally, A. Chakilam, and M. M. Amiji, "Role of nanotechnology in pharmaceutical product development.," *J. Pharm. Sci.*, vol. 96, no. 10, pp. 2547–2565, Oct. 2007, doi: 10.1002/jps.20875.
- [45] R. F. Ludueña, "Multiple Forms of Tubulin: Different Gene Products and Covalent Modifications," in *International review of cytology* vol. 173, 1st Editio., Academic Press, 1997, pp. 207–275.
- [46] L. J. Leandro-García et al., "Tumoral and tissue-specific expression of the major human beta-tubulin isotypes," *Cytoskeleton*, vol. 67, no. 4, pp. 214–223, 2010, doi: 10.1002/cm.20436.
- [47] S. Mozzetti et al., "Class III beta-tubulin overexpression is a prominent mechanism of paclitaxel resistance in ovarian cancer patients.," *Clin. Cancer Res.*, vol. 11, no. 1, pp. 298–305, Jan. 2005.
- [48] P. Sève and C. Dumontet, "Is class III β -tubulin a predictive factor in patients receiving tubulin-binding agents?," *Lancet Oncol.*, vol. 9, no. 2, pp. 168–175, Feb. 2008, doi: 10.1016/S1470-2045(08)70029-9.
- [49] L. Hiser et al., "Comparison of beta-tubulin mRNA and protein levels in 12 human cancer cell lines," *Cell Motil. Cytoskeleton*, vol. 63, no. 1, pp. 41–52, 2006, doi: 10.1002/cm.20109.
- [50] A. Davis, S. Martinez, D. Nelson, and K. Middleton, "A tubulin polymerization microassay used to compare ligand efficacy," in *Methods in Cell Biology*, First edit., vol. 95, no. C, L. Wilson and J. J. Correia, Eds. Elsevier, 2010, pp. 331–351.
- [51] C. Y. Tseng et al., "Quantitative analysis of the effect of tubulin isotype expression on sensitivity of cancer cell lines to a set of novel colchicine derivatives," *Mol. Cancer*, vol. 9, pp. 1–19, 2010, doi: 10.1186/1476-4598-9-131.
- [52] C. Dumontet and M. A. Jordan, "Microtubule-binding agents: a dynamic field of cancer therapeutics.," *Nat. Rev. Drug Discov.*, vol. 9, no. 10, pp. 790–803, Oct. 2010, doi: 10.1038/nrd3253.

[53] Y. H. Choi and A.-M. Yu, “ABC transporters in multidrug resistance and pharmacokinetics, and strategies for drug development.,” *Curr. Pharm. Des.*, vol. 20, no. 5, pp. 793–807, 2014.

Chapter 4:

Synthesis, antiproliferative activity, and molecular docking studies of 4-chlorothiocolchicine analogues*

*The paper in this chapter is included by permission from the publisher (John Wiley) and the journal (*Chemical Biology & Drug Design*). All authors of the paper were notified about its inclusion in the thesis

Greta Klejborowska, Mahshad Moshari, Ewa Maj, Urszula Majcher, Jordane Preto, Joanna Wietrzyk, Jack A. Tuszynski, and Adam Huczyński. 2020. Synthesis, antiproliferative activity, and molecular docking studies of 4-chlorothiocolchicine analogues. *Chem. Biol. Drug Des.* 95, 1, 182–191. DOI:<https://doi.org/10.1111/cbdd.13618>

4.1 Introduction

Colchicine (Figure 4-1) has been used in medicine for a long time. It is a medication administered orally to treat gout and familial Mediterranean fever, as well as to prevent Behçet's disease and pericarditis. Mostly unsuccessful attempts to implement colchicine in the treatment of inflammatory disorders prone to fibrosis have been undertaken. This well-known bioactive alkaloid shows also antiproliferative impact through the inhibition of microtubule formation, leading to mitotic arrest, vascular disruption, and cell death by apoptosis [1-11]. However, when administered intravenously, causes severe side effects. Wherefore, colchicine has not been clinically used to treat cancer [12-14]. Although much effort has been made to devise colchicine derivatives as potential anticancer agents, no generally acceptable solution has been found yet [15-21]. In 2011, Hiromitsu Takayama's research group published results of studies on C-4 halogen substituted colchicine derivatives [22]. Some of them exhibited more potent cytotoxicity toward tumor cells than unmodified colchicine. In 2012, they published extended results on 4-chlorocolchicine derivatives bearing an amide moiety at the C-7 position [23].

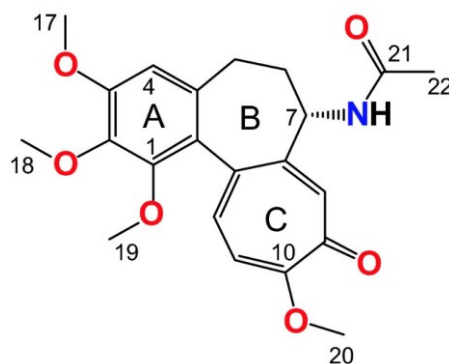


Figure 4-1. Chemical structure of colchicine.

4-Chlorocolchicine and some of the double-modified derivatives with trifluoroacetyl or propionyl amide substituents at the C-7 exhibited strong antitumor

activities over broad effective dosage ranges *in vivo*, but their metabolic stabilities were poorer than that of colchicine. It is well known that substitution of methoxyl group at the C-10 position by a thiomethyl group is a good way to increase molecular stability of colchicine [15,20,24].

In our previous studies, we prepared double-modified colchicine derivatives, at the C-4 and C-10 positions as well as at the C-7 and C-10 positions [25] as well as at the C-7 and C-10 positions [26] and evaluated their cytotoxicity. We have also prepared a series of triple-modified 4-bromo-7-carbamatethiocolchicines bearing different substituents at the C-7 position [27] and most of the compounds showed cytotoxicity at the nanomolar range. Since in drug design even a small change in molecular structure can significantly affect biologic properties, as well as sulfur and chlorine, are the most common elements (except carbon, hydrogen, oxygen, and nitrogen) in Food and Drug Administration approved pharmaceuticals [28], we decided to develop the concept and synthesize a series of novel triple-modified 4-chloro-7-carbamatethiocolchicines (compounds **2–9**, Figure 4-2) with diversified substituents at the C-7 position as well as to perform *in vitro* and *in silico* studies.

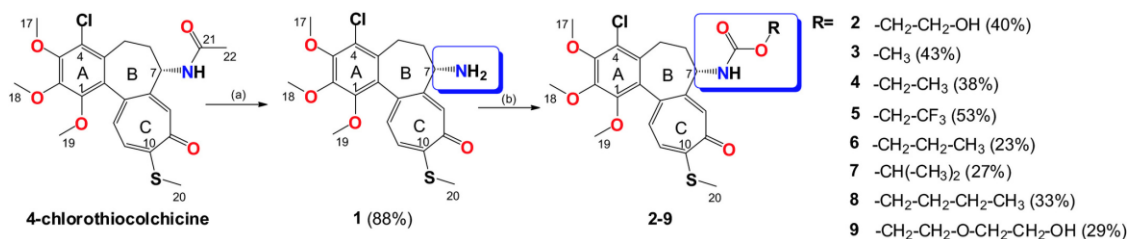


Figure 4-2. Synthesis of 4-chlorothiocolchicine derivatives (**1-9**). Reagents and conditions: (a) 2M HCl, 90°C, 72h; (b) triphosgene, Et₃N, respective alcohol, THF, 0°C → RT.

4.2 Results and discussion

4.2.1 Chemistry

The aim of this project was the synthesis and evaluation of the cytotoxic activity of novel 4-chlorothiocolchicine derivatives. The synthesis of 4-chlorothiocolchicine was previously reported by our group [25]. N-deacetylation followed by the reaction with respective alcohol in the presence of triphosgene led to a series of eight novel triple-modified colchicine derivatives (2–9) with diversified substituents in C-7 position. The structures of all products were characterized by spectroscopic (FT-IR, ^1H NMR, ^{13}C NMR) and spectrometric (ESI-MS) methods. The experimental and full spectral data for compounds (1–9) are given in Appendix C.

4.2.2 Antiproliferative effect toward both human cancer cells and normal cells

The cytotoxic activity of 4-chlorothiocolchicine analogues (1–9) was screened on human lung adenocarcinoma (A549), human breast adenocarcinoma (MCF-7), human colon adenocarcinoma cell line (LoVo), and doxorubicin-resistant subline (LoVo/DX) as well as normal murine embryonic fibroblast cell line (BALB/3T3). The mean $\text{IC}_{50} \pm \text{SD}$ of the tested compounds are collected in Table 4-1.

The highest cytotoxic activity from among the triple-modified colchicine derivatives against respective cancerous cell lines showed compounds **3–7** against A549 ($\text{IC}_{50} = 0.009\text{--}0.021 \mu\text{M}$), compounds **3–6** against MCF-7 ($\text{IC}_{50} = 0.019\text{--}0.021 \mu\text{M}$), compounds **3–8** against LoVo ($\text{IC}_{50} = 0.008\text{--}0.020 \mu\text{M}$), and compounds **3–8** against LoVo/DX ($\text{IC}_{50} = 0.021\text{--}0.081 \mu\text{M}$). The mentioned IC_{50} values are at least several times lower than those obtained for unmodified colchicine and common anticancer agents such as doxorubicin and cisplatin. The majority of colchicine derivatives demonstrated cytotoxic activity at submicromolar concentrations. In comparison, corresponding 4-

bromothicolchicine analogues bearing same substituents at the C-7 and C-10 positions, but bromine instead of chlorine at the C-4 positions, have shown slightly different antiproliferative activity. The most active brominated derivatives were those with methyl, ethyl, and propyl carbamate moieties at the C-7 position and trifluoroethyl, as well as isopropyl carbamate derivatives, exhibited lower cytotoxicity comparing to the corresponding chlorinated derivatives [27].

Table 4-1. Antiproliferative activity of colchicine and its derivatives (2-9) compared with antiproliferative activity of standard anticancer drugs doxorubicin and cisplatin.

Compound	A549	MCF-7	LoVo	LoVo/DX	BALB/3T3
	IC ₅₀ (μM)				
Colchicine	0.125 ± 0.013	0.054 ± 0.028	0.108 ± 0.025	1.69 ± 0.28	0.139 ± 0.073
1	0.147 ± 0.027	0.221 ± 0.022	0.098 ± 0.010	0.172 ± 0.049	0.270 ± 0.069
2	0.081 ± 0.008	0.040 ± 0.016	0.081 ± 0.004	0.847 ± 0.140	0.141 ± 0.014
3	0.021 ± 0.002	0.021 ± 0.002	0.011 ± 0.001	0.021 ± 0.011	0.021 ± 0.002
4	0.010 ± 0.001	0.021 ± 0.002	0.008 ± 0.002	0.042 ± 0.013	0.083 ± 0.017
5	0.009 ± 0.001	0.019 ± 0.004	0.007 ± 0.0002	0.056 ± 0.006	0.094 ± 0.026
6	0.010 ± 0.001	0.020 ± 0.002	0.008 ± 0.002	0.081 ± 0.020	0.101 ± 0.004
7	0.020 ± 0.012	0.040 ± 0.020	0.020 ± 0.002	0.081 ± 0.020	0.121 ± 0.018
8	0.059 ± 0.033	0.098 ± 0.039	0.020 ± 0.012	0.079 ± 0.020	0.118 ± 0.010
9	0.093 ± 0.006	0.167 ± 0.019	0.315 ± 0.172	7.944 ± 3.020	0.130 ± 0.031
Doxorubicin	0.258 ± 0.044	0.386 ± 0.118	0.092 ± 0.018	4.75 ± 0.99	0.166 ± 0.074
Cisplatin	6.367 ± 1.413	10.70 ± 0.753	4.37 ± 0.73	5.70 ± 0.63	3.90 ± 1.50

Note: The IC₅₀ value is defined as the concentration of a compound at which 50% growth inhibition is observed.

Comparison between the IC₅₀ values obtained for cancer cell lines and the normal murine fibroblasts (BALB/3T3) was made to calculate the selectivity index (SI) as a measure of therapeutic potential (Figure 4-3). SI values calculated for A549 and LoVo cell lines are especially high for compounds 4–7. These compounds showed also moderate SI values on MCF-7. High SI values result from large differences between the cytotoxicity against cancer and normal cells, which might indicate that cancer cells will

be affected by the cytotoxic agents prior to the normal cells. These values are much higher than the SI values of commonly used drugs, such as doxorubicin and cisplatin. Moreover, compounds 4–7 showed very high antiproliferative activity against A549, MCF-7 and LoVo cell lines, which in combination with high SI values make them good candidates for further studies. Previous calculations of SI values for corresponding 4-brominated analogues indicate some interesting differences between chlorinated and brominated colchicine derivatives, for example, compound 3 showed very low selectivity while the corresponding 4-bromo-7-methylcarbamatethiocolchicine showed moderate SI values on A549, MCF-7 and LoVo cell lines [27].

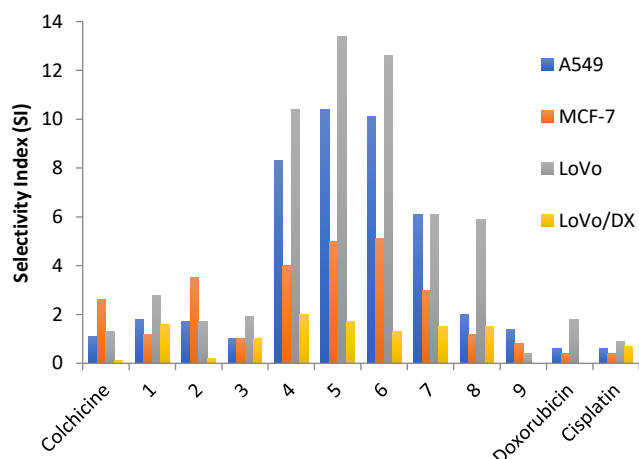


Figure 4-3. Comparison of selectivity index (SI) values of tested compounds. SI was calculated for each compound using the formula: $SI = IC_{50}$ for normal cell line BALB/3T3 / IC_{50} for respective cancerous cell line.

To evaluate the agents' activity against the cells with MDR (multidrug resistance) phenotype, one drug resistant cancer cell line, that is, LoVo/DX was tested and the resistance index (RI) values were calculated (Figure 4-4). Only compounds 1 and 3 were able to efficiently overcome the drug resistance of the LoVo/DX cell line, simultaneously showing high antiproliferative activity (RI = 1.8, IC_{50} = 0.172 μ M and RI = 1.9, IC_{50} = 0.021 μ M, respectively).

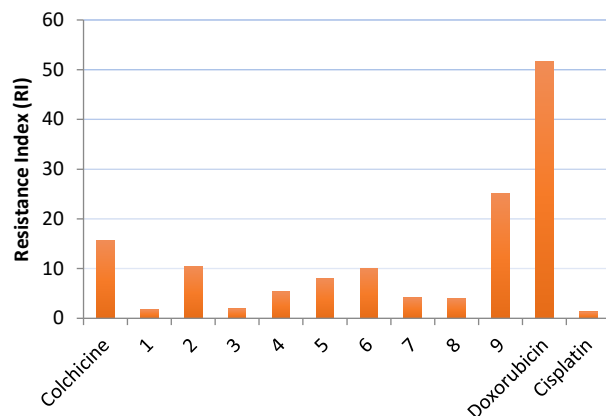


Figure 4-4. Comparison of resistance index (RI) values of tested compounds. The RI indicates how many times the chemoresistance of a resistant subline was higher relative to its parental cell line. The RI was calculated for each compound using the formula: $RI = IC_{50} \text{ for LoVoDX} / IC_{50} \text{ for LoVo cell line}$.

4.2.3 Molecular docking: *in silico* determination of the molecular mode of action

Numerous well-known chemotherapeutic drugs are known to bind to human β tubulin isotypes, which are structural subunits of microtubules in the cytoskeleton of eukaryotic cells, in order to inhibit the growth and proliferation of cancer cells. From among all isotypes, β I tubulin is the most abundant and most popular target of tubulin-binding drugs. One of the fast and inexpensive methods to predict the effectiveness of the drugs inhibition of cancer cell proliferation is computational docking. This *in silico* drug discovery method can predict the binding affinity between the colchicine-binding pocket of β I tubulin and new colchicine derivatives. The 3D structures of the human isotypes were built from homology modeling by using the crystallographic structure of the bovine α - β IIb tubulin isotype complexed with colchicine as a template (PDB ID: 1SA0; [29]) The dimer models generated were made of the α IA isotype for α -tubulin

(UniProt ID: Q71U36) and different isoforms of the β -tubulin. Here, molecular docking was combined with other computational methods to explore ligand-tubulin interactions for the compounds discussed in this chapter.

The colchicine derivatives numbered **6**, **2**, **5**, and **7** showed the strongest binding energies of -9.15 , -9.03 , -8.98 , and -8.94 kcal/mol in our *in silico* calculations, respectively. Met 259 and Lys 352 residues in the binding pocket of β I tubulin appear to be involved in the strongest interactions with ligands. Those two residues interact with C-20 (sidechain donor) and oxygen of carbonyl (sidechain acceptor) on ring C of the new colchicine derivatives, respectively. Table 4-2 depicts graphically these interactions in column 3.

In the present article, the interactions of the tested compounds with β I tubulin were evaluated and compared with IC_{50} values obtained in cell-based assays. Since in a cell-based assay, the β I tubulin isoform is not the only isoform of tubulin expressed but several different tubulin isoforms are simultaneously present in given cells, the interactions between novel derivatives and the other key isoforms of tubulins, namely β IIa (UniProt ID: Q13885), β IIb (UniProt ID: Q9BVA1), β III (UniProt ID: Q13509), β IVa (UniProt ID: P04350), β IVb (UniProt ID: P68371), and β VI (UniProt ID: Q9H4B7) were calculated by the same docking method.

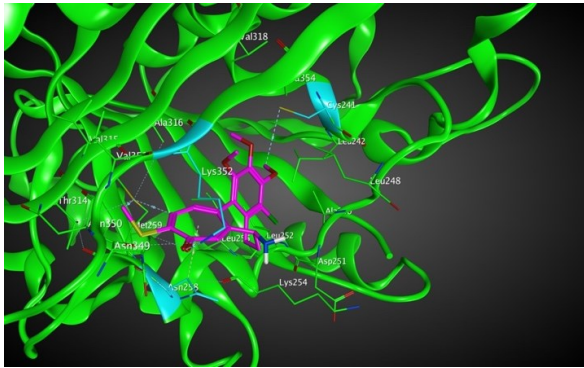
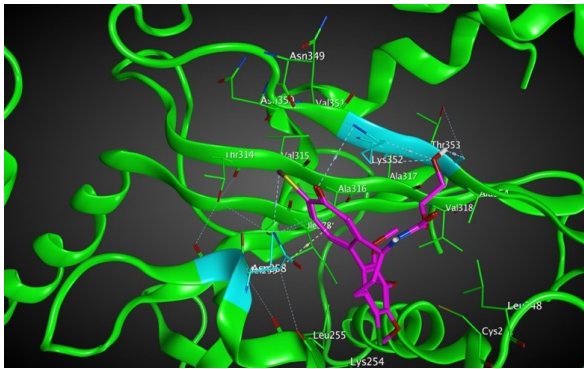
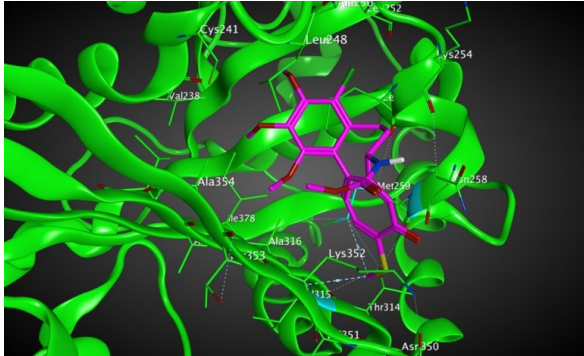
Following the docking simulations, the results of our computational prediction for different β tubulin isoforms were compared with experimental values of IC_{50} by calculating the linear regression coefficients. The physicochemical properties of medicinal chemistry compounds such as permeability and solubility, along with the understanding of transport mechanisms of the drugs *in vivo* [30] should be taken into account when the computational (*in silico*) and experimental (*in vitro*) results are compared. Here, the Moriguchi octanol-water partition coefficient (MLogP), a useful factor in estimating and comparing the distribution of the drugs within the cells, organs, and the body was calculated.

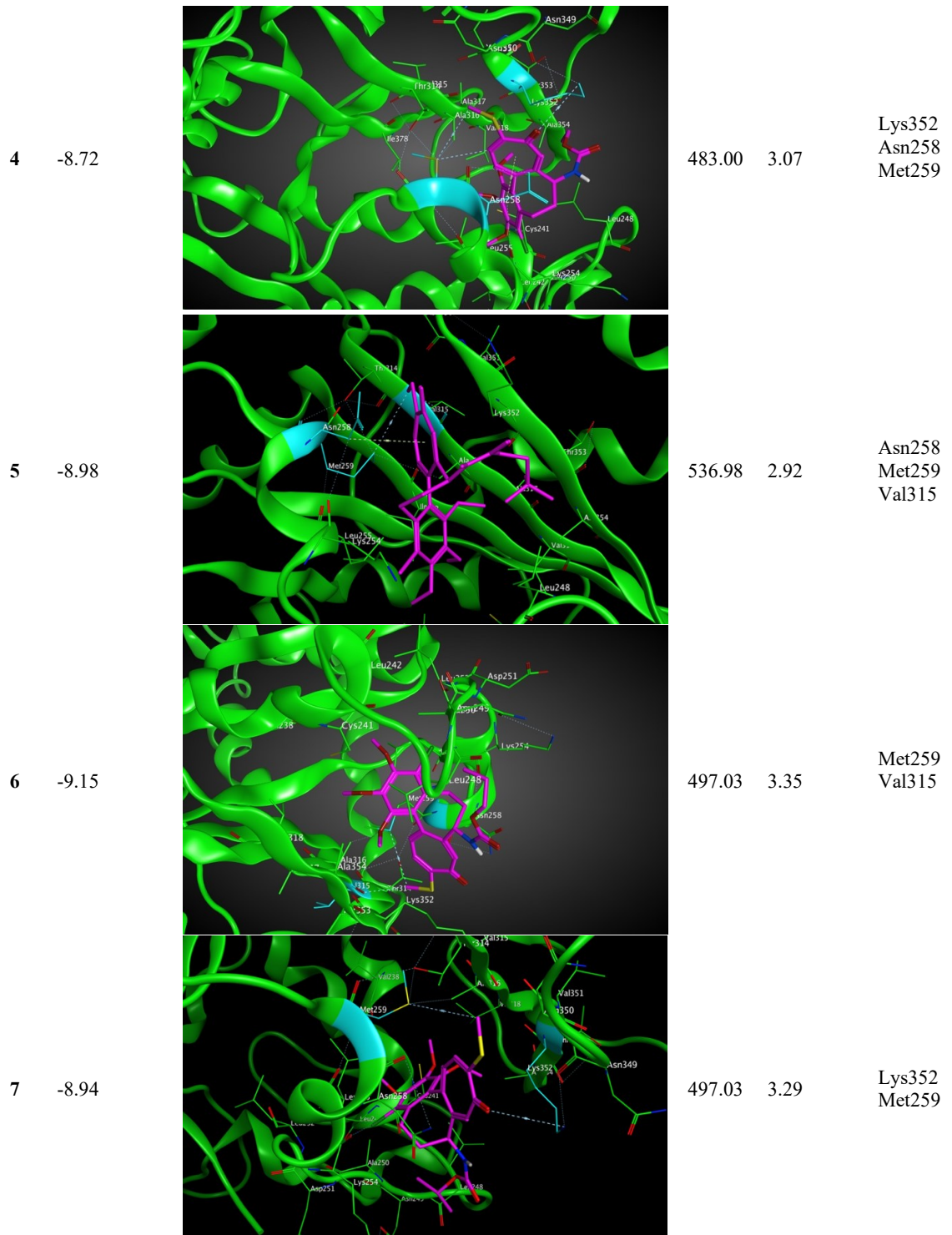
Good regression coefficients for log IC₅₀ of the LoVo/DX and A549 cell lines and an acceptable coefficient for the LoVo cell line were reported as 0.61 and 0.60 and 0.44, respectively. The two independent variables involved in the regression analysis were the compounds' MlogP values and the binding free energies of our compounds with the tubulin β I isotype as the main target. The regression coefficients found for the MCF-7 and BALB/3T3 cell lines are very low (see Table 4-3). The reason for the latter discrepancy between computation and experiment may be due to additional biologic factors, such as the upregulation of MDR proteins that act as efflux pumps and prevent the drugs from exerting their cytotoxic action. Another possibility could involve off-target interactions of the compounds studied.

Comparing the results on 4-chlorothiocolchicine analogues and previously published studies on corresponding 4-bromothiocolchicine analogues, different active residues of the binding pocket of β I tubulin interacting with ligands *via* hydrogen bonding or π -interactions were identified for most of the compounds, also the regression coefficients calculated for the brominated and chlorinated derivatives indicate some specific differences in their interactions with the colchicine-binding site [27].

To further investigate these novel colchicine derivatives, more computationally expensive and time consuming *in silico* methods, namely MM/PBSA and MM/GBSA, were used to calculate the binding free energies between the novel colchicine derivatives and β tubulin isotypes. The linear regression of these binding energies was taken into account under the same conditions as those applied to the docking method. In Table 4-4, the best PBSA and GBSA score out of the three trajectories associated with the three representative structures of the tubulin dimer is shown for each of the tested compounds.

Table 4-2. Summary of the calculated binding energies for the interactions between β I tubulin and 4-chlorothiocolchicine analogues, the compounds' molecular weights, the values of their Moriguchi-octanol-water partition coefficient (MlogP), which have been investigated in this chapter. The active residues of the binding pocket of β I tubulin are listed in the last column.

Compound	Binding energy (kcal/mol)	Interactions	MW	MlogP	Active residues
1	-8.6		413.97	1.80	Lys352 Asn258 Cys 241
2	-9.03		499.00	2.34	Lys352 Thr353 Met259 Asn258
3	-8.95		468.98	2.83	Met259 Val315



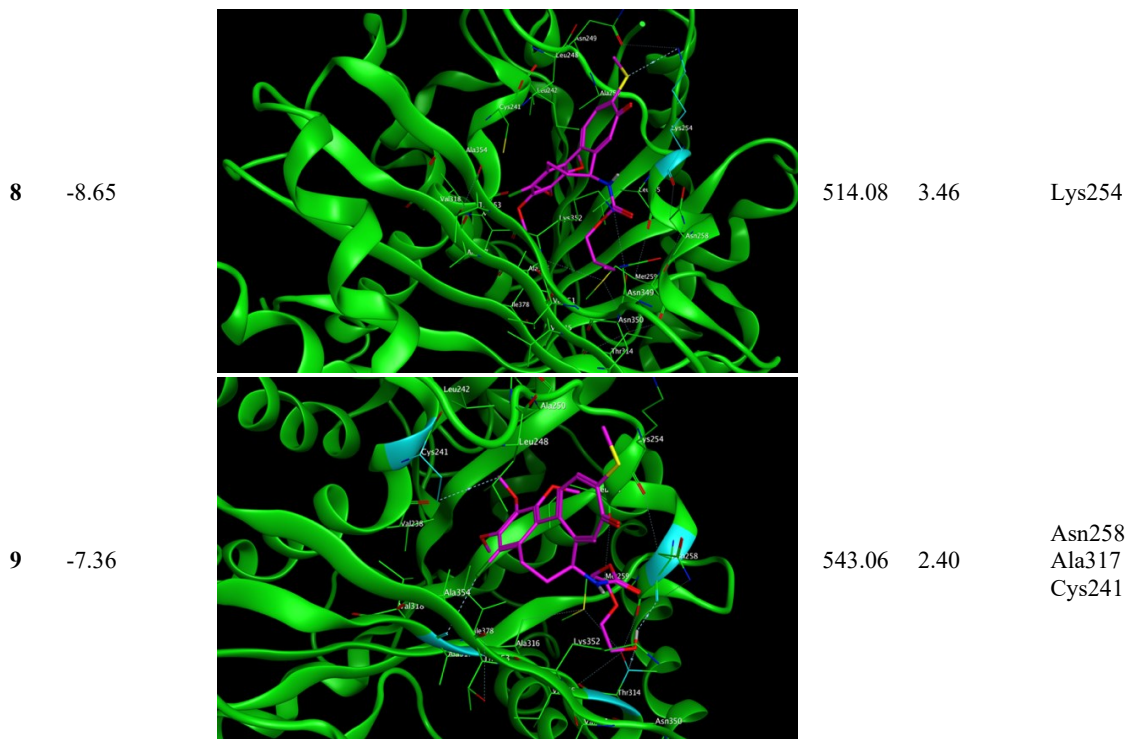


Table 4-3. The docking binding free energy of ligands-tubulin and MlogP of the ligands are the two independent variables in linear regression that are correlated with log IC₅₀ [μM] in different cancer cell lines.

	LogIC ₅₀	MCF-7	LoVo	LoVo/DX	A549	BALB/3T3
Linear regression of colchicine derivatives (R²)	βI	0.01	0.44	0.61	0.60	0.06
	βIIa	0.03	0.21	0.05	0.40	0.14
	βIIb	0.06	0.18	0.06	0.35	0.10
	βIII	0.04	0.25	0.14	0.42	0.15
	βIVa	0.04	0.20	0.08	0.36	0.11
	βIVb	0.03	0.30	0.09	0.38	0.11
	βV	0.04	0.067	0.19	0.41	0.14
βVI	0.04	0.23	0.11	0.42	0.15	

Following the MM/PBSA and MM/GBSA simulations, we calculated the linear regression coefficients between experiment and computational simulations of different β tubulin isotypes (see Table 4-5 and Table 4-6, respectively).

As can be clearly seen in Table 4-5 and Table 4-6, MM/PBSA also shows a good correlation coefficient R^2 of 0.48 with $\log IC_{50}$ of BALB/3T3 cell line but the $\log IC_{50}$ for A549 cell line gives the only experimental value that shows an acceptable linear regression with the MM/PBSA and MM/GBSA calculations of the binding free energy of the ligand-tubulin isotype complexes, which is in the same range for molecular docking results. There are numerous possible reasons for poor correlation between computational predictions and experimental results, most of which include issues such as solubility, membrane permeability, off-target interactions, and *p*-glycoprotein drug removal. What is encouraging in our calculations, however, is that the most common isotypes of β tubulin, namely βI and βII and to some extent βIII , show strong correlation with the compounds' cytotoxicity. To improve our prediction methodology, it would be necessary to obtain precise information about the tubulin isotype expression levels and develop a weighted average for the binding affinity based on the expression values for the contributing isotypes in each cell line separately. This information could then be used to design a compound with optimized binding affinity profile for each cancer cell type.

Table 4-4. Binding energies of novel colchicine derivative versus different tubulin isotypes were calculated by MM/PBSA and MM/GPSA methods.

Ligand	GBSA	PBSA	GBSA	PBSA	GBSA	PBSA	GBSA	PBSA	GBSA	PBSA
	β I	β I	β IIa	β IIa	β III	β III	β IVb	β IVb	β VI	β VI
1	-12.67	-25.58	-15.46	-25.33	0.14	-18.28	-3.71	-24.35	-19.89	-26.75
2	-42.48	-50.56	-46.41	-49.88	-40.23	-46.74	-43.25	-43.7	-48.11	-39.58
3	-33.65	-37.9	-33.95	-39.16	-30.27	-29.17	-28.45	-28.82	-41.31	-38.15
4	-42.19	-46.54	-48.05	-51.07	-36.69	-42.14	-44.09	-53.51	-45.9	-45.25
5	-34.14	-42.48	-31.95	-32.64	-24.14	-24.08	-34.15	-34.84	-39.49	-39.83
6	-37.13	-44.81	-40.44	-44.5	-21.32	-21.59	-34.44	-38.46	-45.35	-44.27
7	-33.57	-46.6	-36.27	-40.36	-26.43	-25.61	-27.54	-31.27	-34.7	-33.34
8	-40.71	-47.21	-36.63	-42.14	-37.12	-39.56	-30.95	-25.16	-40.58	-34.49
9	-47.9	-48.43	-62.18	-42.91	-45.14	-45.09	-44.89	-49.09	-45.9	-36.76

Table 4-5. The MM/PBSA binding free energy of the ligand-tubulin complex and the values of the MlogP for the ligands are the two independent variables in our linear regression calculations that are obtained with respect to $\log IC_{50}$ [μ M] in different cancer cell lines.

	LogIC ₅₀	MCF-7	LoVo	LoVo/DX	A549	BALB/3T3
Linear regression of colchicine derivatives (R ²)	β I	0.03	0.22	0.13	0.36	0.082
	β IIa	0.002	0.20	0.11	0.36	0.093
	β III	0.030	0.23	0.13	0.37	0.11
	β IVb	0.03	0.21	0.13	0.36	0.11
	β VI	0.10	0.14	0.03	0.35	0.48

Table 4-6. The MM/GBSA binding free energy of the ligand-tubulin complex and the values of the MlogP for the ligands are the two independent variables in our linear regression calculations that are obtained with respect to $\log IC_{50}$ [μ M] in different cancer cell lines.

	LogIC ₅₀	MCF-7	LoVo	LoVo/DX	A549	BALB/3T3
Linear regression of colchicine derivatives (R ²)	β I	0.02	0.20	0.14	0.36	0.10
	β IIa	0.17	0.24	0.19	0.37	0.10
	β III	0.03	0.22	0.15	0.36	0.10
	β IVb	0.02	0.21	0.14	0.36	0.10
	β VI	0.0002	0.20	0.15	0.36	0.06

4.3 Conclusions

In this work, we present the design and multistep synthesis of novel triple-modified colchicine derivatives (**2–9**), which are 4-chlorothiocolchicine analogues, as anticancer agents and mitotic inhibitors. All target compounds were screened for their *in vitro* cytotoxicity against MCF-7, LoVo, LoVo/DX, and A549 cancer cell lines. The majority of 4-chlorothiocolchicine derivatives were shown to be active at nanomolar concentrations, lower than those of colchicine, doxorubicin, and cisplatin, against tested cancer cell lines. Four of obtained compounds also showed higher potency against cancer cells over normal cells as confirmed by their high SI values. Molecular docking was performed to reveal the interaction of the obtained active compounds into the colchicine-binding site of tubulin isotopes. These studies revealed that all of the obtained compounds successfully dock in the colchicine-binding site of tubulin. Our calculation results confirm that multistep chemical modification of colchicine is a promising method to obtain new active anticancer agents and improve binding affinity to several human tubulin isotypes. Our studies clearly show the potential of the obtained triple-modified colchicine derivatives, and some of the obtained compounds are suitable candidates for further tests (*ex vivo*, *in vivo*).

References

- [1] E. Ben-Chetrit and M. Levy, “Colchicine prophylaxis in familial Mediterranean fever: Reappraisal after 15 years,” *Semin. Arthritis Rheum.*, vol. 20, no. 4, pp. 241–246, 1991, doi: [https://doi.org/10.1016/0049-0172\(91\)90019-V](https://doi.org/10.1016/0049-0172(91)90019-V).
- [2] C. Cerquaglia, M. Diaco, G. Nucera, M. La Regina, M. Montalto, and R. Manna, “Pharmacological and clinical basis of treatment of Familial Mediterranean Fever (FMF) with colchicine or analogues: an update.,” *Curr. Drug Targets. Inflamm. Allergy*, vol. 4, no. 1, pp. 117–124, Feb. 2005, doi: [10.2174/1568010053622984](https://doi.org/10.2174/1568010053622984).
- [3] Y. Gong and C. Gluud, “Colchicine for primary biliary cirrhosis: a Cochrane Hepato-Biliary Group systematic review of randomized clinical trials.,” *Am. J. Gastroenterol.*, vol. 100, no. 8, pp. 1876–1885, Aug. 2005, doi: [10.1111/j.1572-0241.2005.41522.x](https://doi.org/10.1111/j.1572-0241.2005.41522.x).
- [4] M. Imazio and F. Gaita, “Colchicine for cardiovascular medicine.,” *Future Cardiol.*, vol. 12, no. 1, pp. 9–16, Jan. 2016, doi: [10.2217/fca.15.59](https://doi.org/10.2217/fca.15.59).
- [5] M. Imazio *et al.*, “Colchicine for recurrent pericarditis (CORP): a randomized trial.,” *Ann. Intern. Med.*, vol. 155, no. 7, pp. 409–414, Oct. 2011, doi: [10.7326/0003-4819-155-7-201110040-00359](https://doi.org/10.7326/0003-4819-155-7-201110040-00359).
- [6] M. M. Kaplan, “New strategies needed for treatment of primary biliary cirrhosis?,” *Gastroenterology*, vol. 104, no. 2. United States, pp. 651–653, Feb. 1993, doi: [10.1016/0016-5085\(93\)90440-n](https://doi.org/10.1016/0016-5085(93)90440-n).
- [7] R. A. Kyle *et al.*, “A Trial of Three Regimens for Primary Amyloidosis: Colchicine Alone, Melphalan and Prednisone, and Melphalan, Prednisone, and Colchicine,” *N. Engl. J. Med.*, vol. 336, no. 17, pp. 1202–1207, Apr. 1997, doi: [10.1056/NEJM199704243361702](https://doi.org/10.1056/NEJM199704243361702).
- [8] K. Masuda, A. Nakajima, A. Urayama, K. Nakae, M. Kogure, and G. Inaba, “Double-masked trial of cyclosporin versus colchicine and long-term open study of cyclosporin in Behçet’s disease.,” *Lancet (London, England)*, vol. 1, no. 8647, pp. 1093–1096, May 1989, doi: [10.1016/s0140-6736\(89\)92381-7](https://doi.org/10.1016/s0140-6736(89)92381-7).

- [9] R. J. McKendry, G. Kraag, S. Seigel, and A. al-Awadhi, "Therapeutic value of colchicine in the treatment of patients with psoriatic arthritis.," *Ann. Rheum. Dis.*, vol. 52, no. 11, pp. 826–828, Nov. 1993, doi: 10.1136/ard.52.11.826.
- [10] E. S. Shchegravina, D. I. Knyazev, I. P. Beletskaya, E. V Svirshchevskaya, H.-G. Schmalz, and A. Y. Fedorov, "Synthesis of Nonracemic Pyrrolo-allocholchicinoids Exhibiting Potent Cytotoxic Activity," *European J. Org. Chem.*, vol. 2016, no. 34, pp. 5620–5623, 2016, doi: <https://doi.org/10.1002/ejoc.201601069>.
- [11] D. Zemer, A. Livneh, Y. L. Danon, M. Pras, and E. Sohar, "Long-term colchicine treatment in children with familial mediterranean fever," *Arthritis & Rheum.*, vol. 34, no. 8, pp. 973–977, 1991, doi: <https://doi.org/10.1002/art.1780340806>.
- [12] C. Avendaño and J. C. Menéndez, "Chapter 1 - Introduction," in *Medicinal Chemistry of Anticancer Drugs*, C. Avendaño and J. C. Menéndez, Eds. Amsterdam: Elsevier, 2008, pp. 1–8.
- [13] C. D. Katsetos and P. Dráber, "Tubulins as therapeutic targets in cancer: from bench to bedside.," *Curr. Pharm. Des.*, vol. 18, no. 19, pp. 2778–92, 2012, doi: 10.2174/138161212800626193.
- [14] J. Seligmann and C. Twelves, "Tubulin: an example of targeted chemotherapy.," *Future Med. Chem.*, vol. 5, no. 3, pp. 339–52, Mar. 2013, doi: 10.4155/fmc.12.217.
- [15] A. Banerjee, L. T. Kasmala, E. Hamel, L. Sun, and K. H. Lee, "Interaction of novel thiocolchicine analogs with the tubulin isoforms from bovine brain.," *Biochem. Biophys. Res. Commun.*, vol. 254, no. 2, pp. 334–337, Jan. 1999, doi: 10.1006/bbrc.1998.9943.
- [16] D. Bartusik, B. Tomanek, E. Lattová, H. Perreault, J. Tuszynski, and G. Fallone, "Derivatives of thiocolchicine and its applications to CEM cells treatment using 19F Magnetic Resonance ex vivo," *Bioorg. Chem.*, vol. 38, no. 1, pp. 1–6, 2010, doi: <https://doi.org/10.1016/j.bioorg.2009.10.002>.

- [17] A. Huczyński *et al.*, “Synthesis, antiproliferative activity and molecular docking of Colchicine derivatives,” *Bioorg. Chem.*, vol. 64, pp. 103–112, 2016, doi: <https://doi.org/10.1016/j.bioorg.2016.01.002>.
- [18] T. Kozaka *et al.*, “Antitumor agents 273. Design and synthesis of N-alkyl-thiocolchicinoids as potential antitumor agents.,” *Bioorg. Med. Chem. Lett.*, vol. 20, no. 14, pp. 4091–4, Jul. 2010, doi: 10.1016/j.bmcl.2010.05.081.
- [19] J. Marangon *et al.*, “Tools for the rational design of bivalent microtubule-targeting drugs,” *Biochem. Biophys. Res. Commun.*, vol. 479, no. 1, pp. 48–53, 2016, doi: <https://doi.org/10.1016/j.bbrc.2016.09.022>.
- [20] P. B. Prajapati, K. B. Bodiwala, and B. P. Marolia, “Oxidative Degradation Kinetic Study of Thiocolchicoside using Stability Indicating High Performance Thin Layer Chromatographic Method,” *Pharm. Methods*, vol. 5, no. 2, pp. 1–10, 2014, doi: 10.5530/phm.2014.2.5.
- [21] G. Raspaglio *et al.*, “Thiocolchicine dimers: a novel class of topoisomerase-I inhibitors,” *Biochem. Pharmacol.*, vol. 69, no. 1, pp. 113–121, 2005, doi: <https://doi.org/10.1016/j.bcp.2004.09.004>.
- [22] N. Yasobu *et al.*, “Design, Synthesis, and Antitumor Activity of 4-Halocolchicines and Their Pro-drugs Activated by Cathepsin B.,” *ACS Med. Chem. Lett.*, vol. 2, no. 5, pp. 348–352, May 2011, doi: 10.1021/ml100287y.
- [23] N. Hiroyuki *et al.*, “Synthesis and biological evaluation of 4-chlorocolchicine derivatives as potent anticancer agents with broad effective dosage ranges,” *Medchemcomm*, vol. 3, pp. 1500–1504, 2012.
- [24] Q. Shi *et al.*, “Discovery of a (19)F MRI sensitive salinomycin derivative with high cytotoxicity towards cancer cells.,” *Chem. Commun. (Camb)*, vol. 52, no. 29, pp. 5136–5139, Apr. 2016, doi: 10.1039/c6cc01508e.
- [25] U. Majcher *et al.*, “Antiproliferative Activity and Molecular Docking of Novel Double-Modified Colchicine Derivatives.,” *Cells*, vol. 7, no. 11, p. 192, Nov. 2018, doi: 10.3390/cells7110192.

- [26] U. Majcher *et al.*, “Synthesis, antiproliferative activity and molecular docking of thiocolchicine urethanes,” *Bioorg. Chem.*, vol. 81, pp. 553–566, 2018, doi: 10.1016/j.bioorg.2018.09.004.
- [27] U. Majcher *et al.*, “Synthesis and Biological Evaluation of Novel Triple-Modified Colchicine Derivatives as Potent Tubulin-Targeting Anticancer Agents,” *Cells*, vol. 7, no. 11, Nov. 2018, doi: 10.3390/cells7110216.
- [28] B. R. Smith, C. M. Eastman, and J. T. Njardarson, “Beyond C, H, O, and N! Analysis of the elemental composition of U.S. FDA approved drug architectures,” *J. Med. Chem.*, vol. 57, no. 23, pp. 9764–9773, Dec. 2014, doi: 10.1021/jm501105n.
- [29] R. B. G. Ravelli *et al.*, “Insight into tubulin regulation from a complex with colchicine and a stathmin-like domain,” *Nature*, vol. 428, no. 6979, pp. 198–202, Mar. 2004, doi: 10.1038/nature02393.
- [30] H. Devalapally, A. Chakilam, and M. M. Amiji, “Role of nanotechnology in pharmaceutical product development,” *J. Pharm. Sci.*, vol. 96, no. 10, pp. 2547–2565, Oct. 2007, doi: 10.1002/jps.20875.

Chapter 5:

Synthesis and Biological Evaluation of Novel Triple-Modified Colchicine Derivatives as Potent Tubulin-Targeting Anticancer Agents*

*The paper in this chapter is included by permission from the publisher (MDPI) and the journal (*Cells*). All authors of the paper were notified about its inclusion in the thesis.

Urszula Majcher, Greta Klejborowska, Magdalena Kaik, Ewa Maj, Joanna Wietrzyk, Mahshad Moshari, Jordane Preto, Jack A Tuszynski, and Adam Huczyński. 2018. Synthesis and Biological Evaluation of Novel Triple-Modified Colchicine Derivatives as Potent Tubulin-Targeting Anticancer Agents. *Cells* 7, 11. DOI:<https://doi.org/10.3390/cells7110216>

Introduction

Colchicine (**1**, Figure 5-1) is one of the oldest therapeutic substances known to mankind. Although its medical properties have been known for centuries, the drug was approved for clinical use by the United States Food and Drug Administration only in 2009 [1]. Clinically, colchicine is approved and used for the treatment of familial Mediterranean fever, Behcet's disease, acute gout, chondrocalcinosis, and other types of microcrystalline arthritis [2-6]. Other therapeutic indications include primary biliary cirrhosis, psoriasis, amyloidosis, various forms of dermatitis, relapsing polychondritis, necrotizing vasculitis, Sweet's syndrome, leukocytoclastic vasculitis, and cardiovascular diseases, such as particular pericarditis, atrial fibrillation caused by inflammation, and ischemic episodes [7-12]. Colchicine is of particular interest in a broader context, especially as a cancer chemotherapy agent, due to its antimitotic properties. It has played an important role in studies of mitosis and the therapeutic potential of the colchicine binding site has been investigated for chemotherapy applications. However, its clinical use is often hampered by relatively high general toxicity, which results from its accumulation in the gastrointestinal tract, as well as neurotoxicity [13-15].

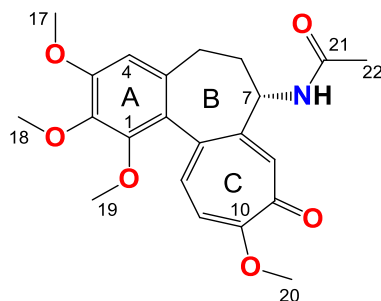


Figure 5-1. Structure of colchicine (**1**).

Many efforts have been made to develop colchicine analogs with the goal of reducing toxicity and increasing bioavailability. Additionally, diverse structure-activity relationship studies have been performed to elucidate the structural features required for

tubulin binding. Substitution of methoxyl group in the C-10 position by a thiomethyl group increases molecular stability and thiocolchicine binds to tubulin more rapidly than colchicine itself [16-21]. In 2011, Hiromitsu Takayama's research group [22] published results of their studies on C-4 halogen substituted colchicine derivatives. Some of them exhibited more potent cytotoxicity for tumor cells compared to **1**. In our previous studies, we prepared double-modified, in the C-7 and C-10 positions, colchicine derivatives and evaluated their cytotoxicity [23]. Encouraged by these results, we decided to further develop the concept of diversified urethane substituents in the C-7 position and combine it with bromination in the C-4 position. We synthesized a series of triple-modified 4-bromo-*N*-deacetyl-7-carbamatethiocolchicines maintaining the stereochemistry of the C-7 center, which is critical for antimitotic activity [15,21].

5.1 Materials and Methods

5.1.1 General

All precursors for the synthesis and solvents were obtained from Sigma-Aldrich (Merck KGaA, Saint Louis, MO, USA) and were used as received without further purification. Spectral grade solvent (CDCl₃) was stored over 3 Å molecular sieves for several days. Thin layer chromatography (TLC) was carried out on precoated plates (TLC silica gel 60 F254, Aluminum Plates Merck, Merck KGaA, Saint Louis, MO, USA) and spots were detected by illumination with a UV lamp. All the solvents used in flash chromatography were of HPLC grade (CHROMASOLV from Sigma-Aldrich, Merck KGaA, Saint Louis, MO, USA) and were used as received. The elemental analysis of compounds was carried out on Vario ELIII (Elementar, Langenselbold, Germany).

5.1.2 Spectroscopic Measurements

The ^1H , ^{13}C spectra were recorded on a Varian VNMR-S 400 MHz spectrometer (Varian, Inc., Palo Alto, CA, USA). ^1H -NMR measurements of **2–8** (0.07 mol dm^{-3}) in CDCl_3 were carried out at the operating frequency 402.64 MHz. The error of the chemical shift value was 0.01 ppm. The ^{13}C -NMR spectra were recorded at the operating frequency 101.25 MHz. The error of chemical shift value was 0.1 ppm. All spectra were locked to deuterium resonance of CDCl_3 . The ^1H - and ^{13}C -NMR spectra are shown in the (Appendix D).

The FT-IR spectra of **2–8** in the mid-infrared region were recorded in KBr. The spectra were taken with an IFS 113v FT-IR spectrophotometer (Bruker, Karlsruhe, Germany) equipped with a DTGS detector; resolution 2 cm^{-1} , NSS = 64. The Happ-Genzel apodization function was used.

The ESI (electrospray ionisation) mass spectra were recorded also on a Waters/Micromass (Waters Corporation, Manchester, UK) ZQ mass spectrometer equipped with a Harvard Apparatus syringe pump. The samples were prepared in dry acetonitrile ($5 \times 10^{-5} \text{ mol dm}^{-3}$). The sample was infused into the ESI source using a Harvard pump at a flow rate of 20 mL min^{-1} . The ESI source potentials were: capillary 3 kV, lens 0.5 kV, and extractor 4 V. The standard ESI mass spectra were recorded at the cone voltages: 10 and 30 V. The source temperature was 120°C and the desolvation temperature was 300°C . Nitrogen was used as the nebulizing and desolvation gas at flow-rates of $100 \text{ dm}^3 \text{ h}^{-1}$. Mass spectra were acquired in the positive ion detection mode with unit mass resolution at a step of 1 m/z unit. The mass range for ESI experiments was from $m/z = 100$ to $m/z = 1000$, as well as from $m/z = 200$ to $m/z = 1500$.

5.1.3 Synthesis

Synthesis of 2

A mixture of N-bromosuccinimide (NBS, 279 mg, 1.57 mmol) and **1** (500 mg, 1.25 mmol) in acetonitrile was stirred at RT under nitrogen atmosphere for the 72 h. Reaction time was determined by TLC. The reaction was quenched with saturated aqueous Na₂S₂O₃. The whole mixture was extracted four times with CH₂Cl₂, and the combined organic layers were dried over MgSO₄, filtered, and evaporated under reduced pressure. The residue was purified by CombiFlash[®] (EtOAc/MeOH, increasing concentration gradient) to give **2** (MW = 478.3 g/mol, Figure 5-2) as amorphous yellow solid with yield 95% (569 mg) [22]. ¹H-NMR (403 MHz, CDCl₃) δ 8.02 (s, 1H), 7.58 (s, 1H), 7.30 (d, *J* = 10.7 Hz, 1H), 6.88 (d, *J* = 11.1 Hz, 1H), 4.59–4.49 (m, 1H), 4.03 (s, 3H), 3.99 (s, 3H), 3.96 (s, 3H), 3.63 (s, 3H), 3.27 (dd, *J* = 13.0, 4.3 Hz, 1H), 2.26 (dd, *J* = 13.1, 5.2 Hz, 1H), 2.18 (d, *J* = 2.4 Hz, 1H), 1.99 (s, 3H), 1.78 (s, 1H) ppm. ¹³C-NMR (101 MHz, CDCl₃) δ 179.5, 170.2, 164.4, 151.8, 151.1, 150.4, 146.6, 135.8, 135.7, 133.4, 130.2, 130.0, 113.5, 112.4, 61.5, 61.5, 61.0, 56.5, 52.6, 34.5, 28.9, 22.8 ppm. FT-IR (KBr pellet): 3274, 2936, 1662, 1617, 1589, 1565, 1462, 1411, 1398, 1350, 1270, 1250, 1172, 1137, 1080, 1018 cm⁻¹. ESI-MS (*m/z*): [M + Na]⁺ calcd. 500, found 500, [M + 2 + Na]⁺ calcd. 502, found 502, [2M + 2 + Na]⁺ calcd. 979, found 979, [2M + Na]⁺ calcd. 977, found 977, [2M + 4 + Na]⁺ calcd. 981, found 981.

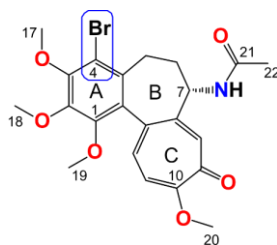


Figure 5-2. Structure of compound **2**.

Synthesis of 3

To a mixture of **2** (500 mg, 1.01 mmol) in MeOH/water (1/1, v/v, 5 mL), the sodium methanethiolate (solution 21% in H₂O, 0.79 mL, 2.1 mmol) was added. The mixture was stirred in at RT for 72 h. Reaction time was determined by TLC. After that time the reaction mixture was quenched by the addition of water (150 mL). The whole mixture was extracted four times with CH₂Cl₂, and the combined organic layers were dried over MgSO₄, filtered, and evaporated under reduced pressure. The residue was purified by CombiFlash[®] (hexane/EtOAc (1/1), then EtOAc/MeOH, increasing concentration gradient) to give **3** (Figure 5-3, MW = 494.4 g/mol) as amorphous yellow solid with yield 75% (388 mg) [24]. ¹H-NMR (403 MHz, CDCl₃) δ 7.68 (d, *J* = 6.6 Hz, 1H), 7.42 (s, 1H), 7.26 (d, *J* = 9.6 Hz, 1H), 7.08 (d, *J* = 10.8 Hz, 1H), 4.61–4.52 (m, 1H), 3.99 (s, 3H), 3.97 (s, 3H), 3.63 (s, 3H), 3.27 (d, *J* = 8.0 Hz, 1H), 2.45 (s, 3H), 2.25 (dt, *J* = 13.4, 7.9 Hz, 2H), 2.01 (s, 3H), 1.85 (dd, *J* = 6.7, 4.1 Hz, 1H) ppm. ¹³C-NMR (101 MHz, CDCl₃) δ 182.4, 170.0, 159.2, 151.2, 151.0, 150.4, 146.6, 137.4, 134.8, 133.4, 130.2, 128.1, 126.3, 113.5, 61.6, 61.5, 61.0, 52.2, 34.5, 29.0, 22.9, 15.2 ppm. FT-IR (KBr pellet): 3267, 2930, 1659, 1603, 1559, 1462, 1410, 1347, 1138, 1074, 1053, 1014 cm⁻¹. ESI-MS (*m/z*): [M + H]⁺ calcd 494, found 494, [M + 2 + H]⁺ 496, found 496, [M + Na]⁺ calcd 516, found 516, [M + 2 + Na]⁺ calcd 518, found 518, [2M + H]⁺ calcd 989, found 989, [2M + 2 + H]⁺ calcd 991, found 991, [2M + Na]⁺ calcd 1011, found 1011, [2M + 2 + Na]⁺ calcd 1013, found 1013.

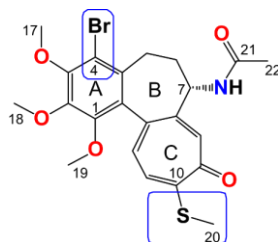


Figure 5-3. Structure of compound **3**.

Synthesis of 4

Compound **4** (Figure 5-4) was prepared from **3** by hydrolysis with 2 N HCl. To a solution of compound **3** (500 mg, 1.01 mmol) in MeOH (3 mL), the 2 N HCl solution (5 mL) was added. The mixture was stirred at 90°C for 72 h. Reaction time was determined by TLC. After that time the reaction mixture was quenched by the addition of water (100 mL). The whole mixture was extracted four times with CH₂Cl₂, and the combined organic layers were dried over MgSO₄, filtered, and evaporated under reduced pressure. The residue was purified by CombiFlash[®] (EtOAc/MeOH, increasing concentration gradient) to give **4** (MW = 452.4 g/mol) as amorphous brownish solid with yield 80% (366 mg) [25]. ¹H-NMR (403 MHz, CDCl₃) δ 7.52 (s, 1H), 7.05 (d, *J* = 10.3 Hz, 1H), 6.94 (d, *J* = 10.7 Hz, 1H), 3.88 (s, 3H), 3.88 (s, 3H), 3.55 (s, 3H), 3.54–3.51 (m, 1H), 3.16–3.10 (m, 1H), 2.37 (s, 3H), 2.24–2.15 (m, 2H), 1.50–1.45 (m, 1H) ppm. ¹³C-NMR (101 MHz, CDCl₃) 182.5, 158.7, 151.1, 149.9, 146.1, 137.1, 134.3, 134.0, 129.9, 129.2, 125.5, 113.2, 61.3, 61.0, 61.0, 53.4, 38.2, 29.6, 15.1 ppm. FT-IR (KBr pellet): 3378, 3315, 2935, 1605, 1557, 1462, 1409, 1345, 1248, 1196, 1138, 1083, 1016 cm⁻¹. ESI-MS (*m/z*): [M + Na]⁺ calcd. 474, found 474, [M + 2 + Na]⁺ calcd. 476, found 476.

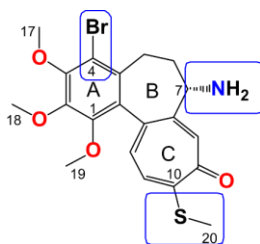


Figure 5-4. Structure of compound **4**.

5.1.4 General Procedure for the Synthesis of Colchicine Derivatives (5–12)

Compounds **5–12** were obtained directly from compound **4**. To a solution of compound **4** (100 mg, 0.22 mmol) in tetrahydrofuran (THF, 5 mL) cooled to the 0°C temperature, the following compounds were added: Et₃N (1 mL, 7 mmol), and triphosgene (69 mg, 0.23 mmol). The mixture was first stirred at 0°C temperature for 20 min and then for the next 20 min at RT. After that time respective alcohol (11 mmol) was added and the mixture was stirred at RT for the next 48 h. Reaction time was determined by TLC. The solution was filtered to remove triethylamine hydrochloride. The THF was evaporated and the residue was quenched by the addition of CH₂Cl₂ (100 mL) and was washed sequentially with a solution of HCl(aq) (0.5 M) and then with water. The organic layer was evaporated to dryness under reduced pressure and purified by CombiFlash® (hexane/ethyl acetate, increasing concentration gradient) to give respective compounds as amorphous yellow solids (**5–12**).

Compound 5

Amorphous yellowish brown solid, yield 55 mg, 46%, MW = 539.1 g/mol (Figure 5-5). ¹H-NMR (403 MHz, CDCl₃) δ 7.43 (s, 1H), 7.23 (d, *J* = 10.3 Hz, 1H), 7.07 (d, *J* = 10.5 Hz, 1H), 6.55 (d, *J* = 6.9 Hz, 1H), 4.38–4.27 (m, 1H), 4.05 (dd, *J* = 8.7, 4.1 Hz, 2H), 3.96 (s, 3H), 3.95 (s, 3H), 3.67–3.63 (m, 2H), 3.59 (s, 3H), 3.29–3.22 (m, 1H), 2.45 (s, 3H), 2.33–2.21 (m, 2H), 1.83 (dd, *J* = 10.4, 6.1 Hz, 1H) ppm. ¹³C-NMR (101 MHz, CDCl₃) δ 182.4, 159.2, 156.0, 151.2, 150.6, 150.3, 146.5, 137.0, 134.7, 133.5, 130.0, 128.5, 126.2, 113.5, 66.9, 61.4, 61.4, 61.1, 61.0, 53.7, 34.9, 29.0, 15.1 ppm. FT-IR (KBr pellet): 3295, 2936, 1719, 1607, 1547, 1463, 1410, 1348, 1324, 1288, 1249, 1154, 1141, 1083, 1062, 1020 cm⁻¹. ESI-MS (*m/z*): [M + H]⁺ calcd. 540, found 540, [M + 2 + H]⁺ calcd. 542, found 542, [M + Na]⁺ calcd. 562, found 562, [M + 2 + Na]⁺ calcd. 564, found 564.

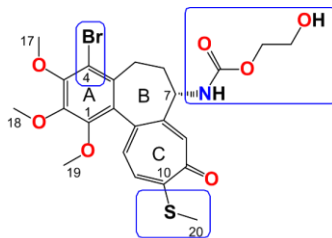


Figure 5-5. Structure of compound **5**.

Compound **6**

Amorphous yellowish brown solid, yield 47 mg, 42%, MW = 509.1 g/mol (Figure 5-6). $^1\text{H-NMR}$ (403 MHz, CDCl_3) δ 7.32 (s, 1H), 7.20 (d, $J = 10.3$ Hz, 1H), 7.03 (d, $J = 10.4$ Hz, 1H), 5.60 (d, $J = 7.2$ Hz, 1H), 4.37–4.27 (m, 1H), 3.97 (s, 3H), 3.95 (s, 3H), 3.60 (s, 3H), 3.59 (s, 3H), 3.25 (d, $J = 8.0$ Hz, 1H), 2.43 (s, 3H), 2.25 (dd, $J = 6.8, 3.4$ Hz, 2H), 1.76–1.66 (m, 1H) ppm. $^{13}\text{C-NMR}$ (101 MHz, CDCl_3) δ 182.3, 159.3, 156.0, 151.2, 150.4, 149.9, 146.6, 136.6, 134.5, 133.4, 130.1, 128.5, 125.8, 113.5, 61.5, 61.4, 61.0, 53.6, 52.3, 35.2, 29.0, 15.2 ppm. FT-IR (KBr pellet): 3297, 2932, 1725, 1608, 1551, 1463, 1410, 1348, 1323, 1289, 1248, 1197, 1153, 1020 cm^{-1} . ESI-MS (m/z): $[\text{M} + \text{H}]^+$ calcd. for 510, found 510, $[\text{M} + 2 + \text{H}]^+$ calcd. 512, found 512, $[\text{M} + \text{Na}]^+$ calcd. 534, found 534, $[\text{M} + 2 + \text{Na}]^+$ calcd. 536, found 536.

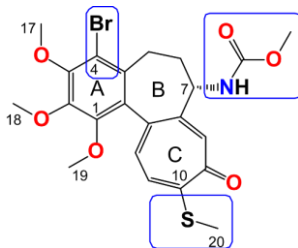


Figure 5-6. Structure of compound **6**.

Compound 7

Amorphous yellowish brown solid, yield 35 mg, 30%, MW = 524.4 g/mol (Figure 5-7). $^1\text{H-NMR}$ (403 MHz, CDCl_3) δ 7.32 (s, 1H), 7.20 (d, $J = 10.3$ Hz, 1H), 7.03 (d, $J = 10.5$ Hz, 1H), 5.35 (d, $J = 7.2$ Hz, 1H), 4.37–4.28 (m, 1H), 4.02 (dd, $J = 7.1, 2.2$ Hz, 1H), 3.98 (s, 3H), 3.96 (s, 3H), 3.94–3.90 (m, 1H), 3.61 (s, 3H), 3.27 (d, $J = 8.9$ Hz, 1H), 2.44 (s, 3H), 2.30–2.24 (m, 2H), 1.72–1.65 (m, 1H), 1.19 (t, $J = 7.1$ Hz, 3H) ppm. $^{13}\text{C-NMR}$ (101 MHz, CDCl_3) δ 182.3, 159.2, 155.5, 151.1, 150.4, 149.9, 146.6, 136.6, 134.5, 133.4, 130.09, 128.5, 125.8, 113.5, 61.5, 61.4, 61.2, 61.0, 53.4, 35.3, 29.0, 15.2, 14.4 ppm. FT-IR (KBr pellet): 3303, 2935, 1716, 1608, 1550, 1460, 1406, 1346, 1322, 1248, 1150, 1084, 1020 cm^{-1} . ESI-MS (m/z): $[\text{M} + \text{H}]^+$ calcd. for 524, found 524, $[\text{M} + 2 + \text{H}]^+$ calcd. 526, found 526, $[\text{M} + \text{Na}]^+$ calcd. 546, found 546, $[\text{M} + 2 + \text{Na}]^+$ calcd. 548, found 548.

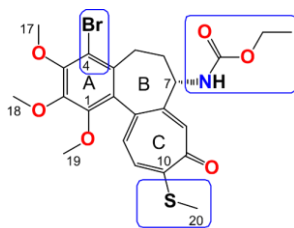


Figure 5-7. Structure of compound 7.

Compound 8

Amorphous yellowish solid, yield 49 mg, 38%, MW = 578.4 g/mol (Figure 5-8). $^1\text{H-NMR}$ (403 MHz, CDCl_3) δ 7.37 (s, 1H), 7.22 (d, $J = 10.3$ Hz, 1H), 7.06 (d, $J = 10.6$ Hz, 1H), 6.18 (d, $J = 7.4$ Hz, 1H), 4.48 (dq, $J = 12.6, 8.5$ Hz, 1H), 4.38–4.29 (m, 1H), 4.17–4.06 (m, 1H), 3.98 (s, 3H), 3.96 (s, 3H), 3.59 (s, 3H), 3.29 (dd, $J = 13.2, 4.3$ Hz, 1H), 2.44 (s, 3H), 2.38–2.23 (m, 2H), 1.82 (dt, $J = 11.0, 4.7$ Hz, 1H) ppm. $^{13}\text{C-NMR}$ (101 MHz, CDCl_3) δ 182.3, 159.6, 153.5, 151.3, 150.4, 149.4, 146.7, 136.5, 134.8, 133.3, 129.9, 128.4, 126.0, 124.2, 121.4, 113.6, 61.5, 61.2, 61.2, 61.0, 60.8, 54.0, 35.1,

28.9, 15.2 ppm. ^{19}F -NMR (379 MHz, CDCl_3) δ -74.8 ppm. FT-IR (KBr pellet): 3221, 2938, 1735, 1610, 1543, 1464, 1411, 1349, 1325, 1283, 1244, 1161, 1100, 1081, 1021 cm^{-1} . ESI-MS (m/z): $[\text{M} + \text{H}]^+$ calcd. for 578, found 578, $[\text{M} + 2 + \text{H}]^+$ calcd. 580, found 580, $[\text{M} + \text{Na}]^+$ calcd. 600, found 600, $[\text{M} + 2 + \text{Na}]^+$ calcd. 602, found 602.

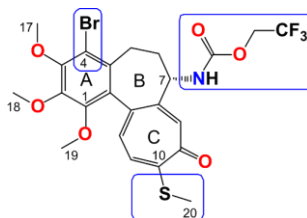


Figure 5-8. Structure of compound **8**.

Compound 9

Amorphous yellowish brown solid, yield 57 mg, 48%, MW = 538.5 g/mol (Figure 5-9). ^1H -NMR (403 MHz, CDCl_3) δ 7.33 (s, 1H), 7.21 (d, $J = 10.3$ Hz, 1H), 7.04 (d, $J = 10.5$ Hz, 1H), 5.39 (d, $J = 7.3$ Hz, 1H), 4.33 (dt, $J = 12.6, 6.4$ Hz, 1H), 3.98 (s, 3H), 3.96 (s, 3H), 3.95–3.90 (m, 2H), 3.61 (s, 3H), 3.27 (d, $J = 9.1$ Hz, 1H), 2.44 (s, 3H), 2.27 (dd, $J = 7.1, 3.6$ Hz, 2H), 1.69 (dd, $J = 15.9, 5.1$ Hz, 1H), 1.63–1.52 (m, 2H), 0.89 (t, $J = 7.4$ Hz, 3H) ppm. ^{13}C -NMR (101 MHz, CDCl_3) δ 182.3, 159.2, 155.6, 151.1, 150.4, 149.9, 146.6, 136.6, 134.5, 133.4, 130.1, 128.5, 125.8, 113.5, 66.9, 61.5, 61.4, 61.0, 53.4, 35.3, 29.0, 22.1, 15.2, 10.2 ppm. FT-IR (KBr pellet): 3300, 2937, 1717, 1608, 1549, 1463, 1410, 1348, 1324, 1288, 1245, 1153, 1083, 1020 cm^{-1} . ESI-MS (m/z): $[\text{M} + \text{Na}]^+$ calcd. 560, found 560, $[\text{M} + 2 + \text{Na}]^+$ calcd. 562, found 562.

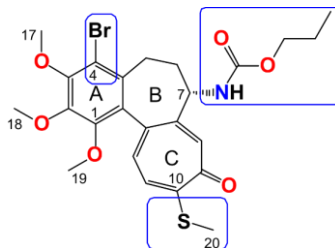


Figure 5-9. Structure of compound **9**.

Compound 10

Amorphous yellowish brown solid, yield 50 mg, 42%. MW = 538.5 g/mol (Figure 5-10). $^1\text{H-NMR}$ (403 MHz, CDCl_3) δ 7.29 (s, 1H), 7.19 (d, $J = 10.3$ Hz, 1H), 7.02 (d, $J = 10.4$ Hz, 1H), 5.15 (d, $J = 6.7$ Hz, 1H), 4.77 (dp, $J = 12.5, 6.2$ Hz, 1H), 4.36–4.26 (m, 1H), 3.97 (s, 3H), 3.95 (s, 3H), 3.60 (s, 3H), 3.29–3.23 (m, 1H), 2.43 (s, 3H), 2.25 (dd, $J = 7.3, 3.9$ Hz, 2H), 1.71–1.62 (m, 1H), 1.16 (dt, $J = 16.2, 8.1$ Hz, 6H) ppm. $^{13}\text{C-NMR}$ (101 MHz, CDCl_3) δ 182.4, 159.2, 155.0, 151.1, 150.4, 149.9, 146.6, 136.6, 134.5, 133.4, 130.1, 128.5, 125.8, 113.5, 68.7, 61.5, 61.4, 61.0, 53.3, 35.4, 29.0, 22.1, 22.1, 15.2. FT-IR (KBr pellet): 3328, 2936, 1715, 1609, 1550, 1464, 1411, 1348, 1323, 1286, 1245, 1153, 1111, 1084, 1021 cm^{-1} . ESI-MS (m/z): $[\text{M} + \text{Na}]^+$ calcd. 560, found 560, $[\text{M} + 2 + \text{Na}]^+$ calcd. 562, found 562.

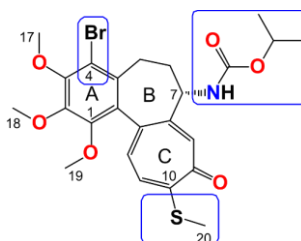


Figure 5-10. Structure of compound **10**.

Compound 11

Amorphous brownish solid, yield 54 mg, 44%. MW = 551.1 g/mol (Figure 5-11). $^1\text{H-NMR}$ (403 MHz, CDCl_3) δ 7.33 (s, 1H), 7.21 (d, $J = 10.3$ Hz, 1H), 7.04 (d, $J = 10.4$ Hz, 1H), 5.40 (d, $J = 7.3$ Hz, 1H), 4.38–4.27 (m, 1H), 3.98 (s, 3H), 3.96 (s, 3H), 3.94–3.90 (m, 2H), 3.61 (s, 3H), 3.27 (d, $J = 8.8$ Hz, 1H), 2.44 (s, 3H), 2.27 (dd, $J = 7.1, 3.5$ Hz, 2H), 1.71 (dd, $J = 19.8, 11.1$ Hz, 1H), 1.56 (ddd, $J = 28.3, 14.4, 7.3$ Hz, 2H), 1.32 (dt, $J = 14.7, 7.4$ Hz, 2H), 0.93–0.86 (m, 3H) ppm. $^{13}\text{C-NMR}$ (101 MHz, CDCl_3) δ 182.3, 159.2, 155.6, 151.1, 150.4, 149.9, 146.6, 136.6, 134.5, 133.4, 130.1, 128.5, 125.8, 113.5, 65.1, 61.5, 61.4, 61.0, 53.4, 35.3, 30.8, 28.9, 19.0, 15.2, 13.7 ppm. FT-IR (KBr pellet): 3288, 2935, 1717, 1608, 1548, 1463, 1410, 1347, 1325, 1246, 1154, 1083, 1020 cm^{-1} . ESI-MS (m/z): $[\text{M} + \text{H}]^+$ calcd. for 552, found 552, $[\text{M} + 2 + \text{H}]^+$ calcd. 554, found 554, $[\text{M} + \text{Na}]^+$ calcd. 574, found 574, $[\text{M} + 2 + \text{Na}]^+$ calcd. 576, found 576.

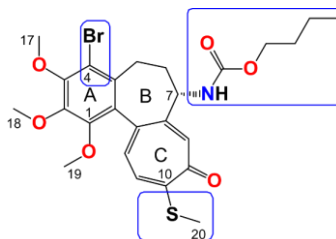


Figure 5-11. Structure of compound 11.

Compound 12

Amorphous orangish solid, yield 54 mg, 42%. MW = 584.5 g/mol (Figure 5-12). $^1\text{H-NMR}$ (403 MHz, CDCl_3) δ 7.36 (s, 1H), 7.22 (d, $J = 10.3$ Hz, 1H), 7.06 (d, $J = 10.6$ Hz, 1H), 5.97 (d, $J = 7.2$ Hz, 1H), 4.35–4.20 (m, 2H), 4.13–4.06 (m, 1H), 3.98 (s, 3H), 3.96 (s, 3H), 3.78–3.70 (m, 2H), 3.65 (dd, $J = 10.0, 5.3$ Hz, 2H), 3.62–3.57 (m, 5H), 3.27 (d, $J = 8.7$ Hz, 1H), 2.44 (s, 3H), 2.27 (dd, $J = 6.6, 3.5$ Hz, 2H), 1.80–1.70 (m, 1H) ppm. $^{13}\text{C-NMR}$ (101 MHz, CDCl_3) δ 182.4, 159.3, 155.4, 151.2, 150.4, 150.2, 146.6,

136.8, 134.7, 133.4, 130.0, 128.3, 126.1, 113.5, 72.4, 69.1, 64.2, 61.5, 61.4, 61.0, 53.7, 34.9, 28.9, 15.2 ppm. FT-IR (KBr pellet): 3285, 2936, 1718, 1607, 1546, 1463, 1410, 1348, 1324, 1249, 1137, 1081, 1020 cm^{-1} . ESI-MS (m/z): $[\text{M} + \text{Na}]^+$ calcd. 606, found 606, $[\text{M} + 2 + \text{Na}]^+$ calcd. 608, found 608.

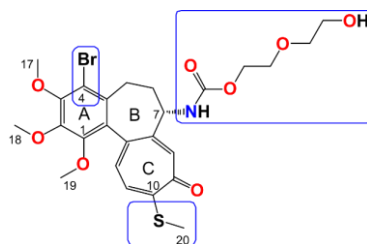


Figure 5-12. Structure of compound 12.

5.1.5 Antiproliferative Activity of Colchicine and Its Derivatives

Four human cancer cell lines and one murine normal cell line were used to evaluate antiproliferative activity of colchicine and its derivatives (2–12): human lung adenocarcinoma (A549), human breast adenocarcinoma (MCF-7), human colon adenocarcinoma cell lines sensitive and resistant to doxorubicin (LoVo) and (LoVo/DX) respectively, and also normal murine embryonic fibroblast cell line (BALB/3T3). The BALB/3T3 cell line was purchased from the American Type Culture Collection (ATCC, Manassas, VA, USA), A549 and MCF-7 cell lines—from European Collection of Authenticated Cell Cultures (Salisbury, UK). The LoVo cell line was purchased from the American Type Culture Collection (ATCC, Manassas, VA, USA), and LoVo/DX by courtesy of Prof. E. Borowski (Technical University of Gdańsk, Gdańsk, Poland). All the cell lines are maintained in the Institute of Immunology and Experimental Therapy (IET), Wrocław, Poland. The human lung adenocarcinoma cell line was cultured in a mixture of OptiMEM and RPMI 1640 (1:1) medium (IET, Wrocław, Poland), supplemented with 5% foetal bovine serum (GE Healthcare, Logan UT, USA) and 2 mM l-glutamine (Sigma-Aldrich, Merck KGaA, Saint Louis, MO, USA). Human breast

adenocarcinoma cell line was cultured in mixture of Eagle's medium (IET, Wrocław, Poland), supplemented with 10% fetal bovine serum, 2 mM l-glutamine, 8 µg/mL insulin, and 1% amino-acids (Sigma-Aldrich, Merck KGaA, Saint Louis, MO, USA). Human colon adenocarcinoma cell lines were cultured in mixture of OptiMEM and RPMI 1640 (1:1) medium (IET, Wrocław, Poland), supplemented with 5% fetal bovine serum (GE Healthcare, Logan, UT, USA), 2 mM l-glutamine, 1 mM sodium pyruvate (Sigma-Aldrich, Merck KGaA, Saint Louis, MO, USA) and 10 µg/100 mL doxorubicin for LoVo/DX (Sigma-Aldrich, Merck KGaA, Saint Louis, MO, USA). Murine embryonic fibroblast cells were cultured in Dulbecco medium (Life Technologies Limited, Paisley, UK), supplemented with 10% foetal bovine serum (GE Healthcare, Logan, UT, USA) and 2 mM glutamine (Sigma-Aldrich, Merck KGaA, Saint Louis, MO, USA). All culture media contained antibiotics: 100 U/mL penicillin and 100 µg/mL streptomycin (Polfa-Tarchomin, Warsaw, Poland). All cell lines were cultured during the entire experiment in a humid atmosphere at 37°C and 5% CO₂. Cells were tested for mycoplasma contamination by mycoplasma detection kit for conventional PCR: Venor GeM Classic (Minerva Biolabs GmbH, Berlin, Germany) and negative results was obtained. The procedure was repeated every year or in the case of less frequently used lines: after thawing.

5.1.6 The Antiproliferative Assays *In vitro*

Twenty-four h before adding the tested compounds, all cell lines were seeded in 96-well plates (Sarstedt, Nümbrecht, Germany) in appropriate media with 10⁴ cells per well. All cell lines were exposed to each tested agent at four different concentrations in the range 100–0.01 µg/mL for 72 h. Cells were also exposed to the reference drug cisplatin (Teva Pharmaceuticals Polska, Warsaw, Poland) and doxorubicin (Accord Healthcare Limited, Middlesex, UK). Additionally, all cell lines were exposed to DMSO (solvent used for tested compounds) (POCh, Gliwice, Poland) at concentrations

corresponding to these present in tested agents' dilutions. After 72 h sulforhodamine B assay (SRB) was performed [26].

SRB

After 72 h of incubation with the tested compounds, cells were fixed in situ by gently adding 50 μ L per well of cold 50% trichloroacetic acid TCA (POCh, Gliwice, Poland) and were incubated at 4°C for one hour. Following, wells were washed four times with water and air dried. Next, 50 μ L of 0.1% solution of sulforhodamine B (Sigma-Aldrich, Merck KGaA, Saint Louis, MO, USA) in 1% acetic acid (POCh, Gliwice, Poland) were added to each well and plates were incubated at room temperature for 0.5 h. After incubation time, unbound dye was removed by washing plates four times with 1% acetic acid whereas stain bound to cells was solubilized with 10 mM Tris base (Sigma-Aldrich, Merck KGaA, Saint Louis, MO, USA). Absorbance of each solution was read at Synergy H4 Hybrid Multi-Mode Microplate Reader (BioTek Instruments, Inc., Winooski, VT, USA) at the 540 nm wavelength.

Results are presented as mean IC_{50} (concentration of the tested compound, that inhibits cell proliferation by 50%) \pm standard deviation. IC_{50} values were calculated in Cheburator 0.4, Dmitry Nevozhay software (version 1.2.0 software by Dmitry Nevozhay, 2004–2014, <http://www.cheburator.nevozhay.com>, freely available) for each experiment [27]. Compounds at each concentration were tested in triplicates in single experiment and each experiment was repeated at least three times independently. Results are summarized in Table 5-1. Antiproliferative activity of colchicine (**1**) and its derivatives (**2–12**) compared with antiproliferative activity of standard anticancer drugs doxorubicin and cisplatin and the calculated values of resistance index (RI) and selectivity index (SI) of tested compounds.. The Resistance Index (RI) was defined as the ratio of IC_{50} for a given compound calculated for resistant cell line to that measured for its parental drug sensitive cell line (Table 5-1).

5.1.7 Molecular Docking Simulations

A combination of different computational methods was used to explore ligand-tubulin interactions. The ligands structures were fully optimized based on the RHF/cc-pVDZ level of theory [28] in GAMESS-US version 2010-10-01 [29-31]. Since there is no crystal structure available for human β I tubulin (TBB5_HUMAN), we obtained its sequence from UniProt (ID: Q13509). We used the tubulin structure 1SA0.pdb as a template to construct the homology model for β I tubulin using MOE2015. We then docked the colchicine library to the protein using the Autodock4 program [32] under flexible ligand and rigid receptor conditions (Table 5-2). To verify the computed binding free energies, we employed two accurate but computationally expensive methods, namely MM/PBSA and MM/GBSA.

5.2 Results

5.2.1 Chemistry

In the present chapter, we report the synthesis and spectroscopic analysis of a series of eight novel triple-modified colchicine derivatives (**5–12**). As shown in Figure 5-13, 4-bromocolchicine (**2**), 4-bromothiocolchicine (**3**), and 4-bromo-*N*-deacetylthiocolchicine (**4**) were prepared according to previously described methods [22,24,25]. Compound **4** became the starting material for the synthesis of triple-modified colchicine derivatives. Compounds **5–12** were readily available from **4** by treatment with triphosgene as an activating reagent in the presence of triethylamine and the excess of respective alcohol or glycol in dry THF with yields from 30% to 48%. The structures of all products **2–12** were determined using the ESI-MS, FT-IR, ^1H and ^{13}C -NMR methods. Spectra are shown in (Appendix D, Figures D1–D23) and the results are also presented in the Materials and Methods section. All the spectroscopic and mass

spectrometry data presented in (Appendix D) confirm the structures of the studied compounds.

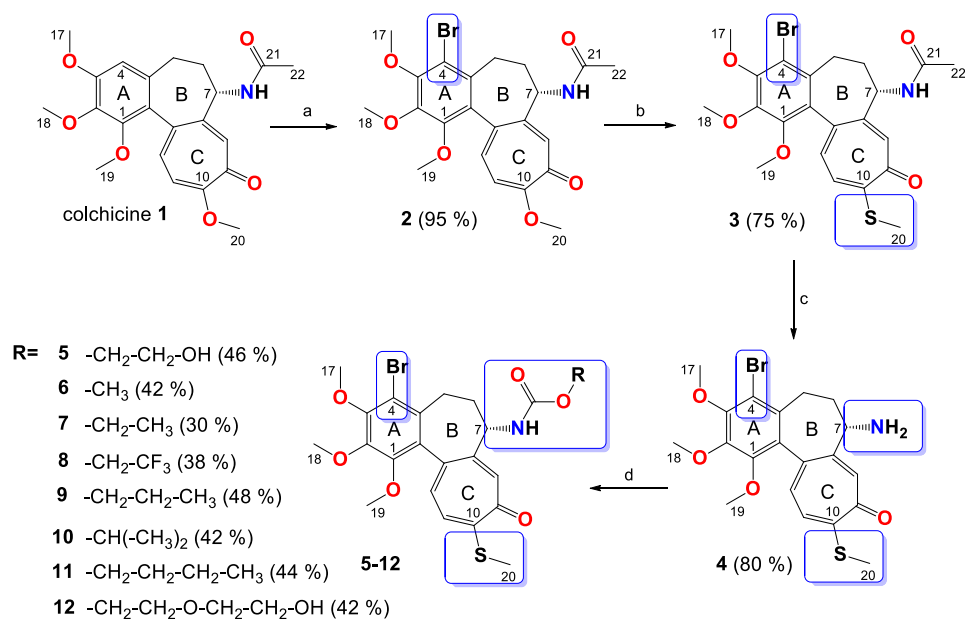


Figure 5-13. Synthesis of colchicine derivatives (**2**–**12**). Reagents and conditions: (a) N-bromosuccinimide (NBS), acetonitrile, room temperature; (b) MeOH/H₂O, CH₃SNa, room temperature; (c) 2M HCl, 90°C, 72 h; (d) triphosgene, Et₃N, respective alcohol, tetrahydrofuran (THF), 0°C → room temperature.

In the ¹³C-NMR spectra of the **2**, a resonance for the C-4 carbon atom of the A aromatic ring was observed at 113.5 ppm, while in **1** it was observed at 107.3 ppm. After the introduction of thiomethyl group in C-10 positions shifts of the signal for the C-20 carbon atom in compound **3** were observed at 15.2 ppm, while in unmodified **1** as well as **2** shifts of the signal for the C-20 carbon atom were observed in the range 56.1–56.5 ppm. In the ¹³C-NMR spectra of the **4** signals for the acetyl group, which were observed at 170.0 and 22.9 ppm in compound **3**, had disappeared. In carbamates (**5**–**12**), shifts of the signal for the carbamate carbon atom were observed in the range 153.5–156.0 ppm.

5.2.2 *In vitro* Determination of Drug-Induced Inhibition of Human Cancer Cell Line Growth

The eight triple-modified colchicine derivatives (**5–12**), three other colchicine derivatives (**2–4**), and starting material (**1**) were evaluated for their *in vitro* antiproliferative effect on normal and cancerous cells. Each compound was tested on four human cancer cell lines, including one cell line displaying various levels of drug resistance, namely human lung adenocarcinoma (A549), human breast adenocarcinoma (MCF-7), human colon adenocarcinoma cell line (LoVo) and doxorubicin-resistant subline (LoVo/DX). The antiproliferative effect was also studied on the normal murine embryonic fibroblast cell line (BALB/3T3) for better evaluation of cytotoxic activity of the compounds studied. The mean values $IC_{50} \pm SD$ of the tested compounds are summarized in Table 5-1

. To evaluate the agents' activity against the cells with MDR (multidrug resistance) phenotype, one drug resistant cancer cell line, i.e., LoVo/DX, was tested and the resistance index values (RI) were calculated (see Table 5-1). The RI values indicate how many times more resistant the subline was in comparison to its parental cell line.

All of the colchicine derivatives (**2–12**) showed higher antiproliferative activity against the A549 cell line than the commonly used cytostatic agents—doxorubicin ($IC_{50} = 0.258 \mu\text{M}$) and cisplatin ($IC_{50} = 6.367 \mu\text{M}$), as well as **1** itself ($IC_{50} = 0.125 \mu\text{M}$). The triple-modified colchicine derivatives (**5–12**) exhibited very significant activity with IC_{50} values ranging from 0.010 to 0.095 μM . As many as five of the compounds tested, including three of the triple-modified derivatives (**6**, $IC_{50} = 0.013 \mu\text{M}$; **7**, $IC_{50} = 0.018 \mu\text{M}$; **9**, $IC_{50} = 0.027 \mu\text{M}$), exhibited better activity against the MCF-7 cell line than **1** ($IC_{50} = 0.054 \mu\text{M}$). All of the colchicine derivatives (**2–12**) as well as **1** showed higher antiproliferative activity against the MCF-7 cell line than doxorubicin ($IC_{50} = 0.386 \mu\text{M}$) and cisplatin ($IC_{50} = 10.70 \mu\text{M}$). As many as nine of the colchicine derivatives (except **4** and **12**) showed better activity against the LoVo cell line, with IC_{50} values in the range

of 0.007–0.085 μM , than **1** ($\text{IC}_{50} = 0.108 \mu\text{M}$) and doxorubicin ($\text{IC}_{50} = 0.092 \mu\text{M}$). All of the colchicine derivatives (**2–12**) as well as **1** showed higher antiproliferative activity against the LoVo cell line than cisplatin ($\text{IC}_{50} = 4.37 \mu\text{M}$).

The data presented in Table 5-1 show that all of the studied compounds including unmodified colchicine and the two reference anticancer drugs less effectively inhibited the proliferation of the resistant LoVo/DX cell line than the sensitive LoVo cell line. However, all of the colchicine derivatives (**2–12**) with IC_{50} values in the range of 0.050–1.550 μM as well as **1** ($\text{IC}_{50} = 1.69 \mu\text{M}$) showed higher antiproliferative activity against the LoVo/DX cell line than doxorubicin ($\text{IC}_{50} = 4.75 \mu\text{M}$) and cisplatin ($\text{IC}_{50} = 5.70 \mu\text{M}$). The calculated values of RI clearly confirmed that only compounds **10** and **11** (RI = 1.7 and 1.5, respectively) are able to efficiently overcome the drug resistance of the LoVo/DX cell line simultaneously showing very high antiproliferative activity ($\text{IC}_{50} = 0.089 \mu\text{M}$ and $0.091 \mu\text{M}$, respectively).

The values of the selectivity index (SI) were calculated to evaluate the toxicity of compounds against normal cells. The SI values calculated for A549, MCF-7, and LoVo cell lines were especially high ($\text{SI} \geq 4.3$) for compounds **6–9** (except SI of **8** for the MCF-7 cell line). These values were much higher than the SI values of commonly used drugs, such as doxorubicin and cisplatin. High SI values result from large differences between the cytotoxicity against cancer and normal cells and this means that cancer cells will be killed at a higher rate than normal ones. Moreover, compounds **6–9** showed very high antiproliferative activity against A549, MCF-7, and LoVo cell lines, which is expressed by very low IC_{50} values ($\text{IC}_{50} = 0.010\text{--}0.030$; $0.013\text{--}0.027$ (without **8**), and $0.007\text{--}0.018$ for A549, MCF-7, and LoVo, respectively).

Table 5-1. Antiproliferative activity of colchicine (**1**) and its derivatives (**2–12**) compared with antiproliferative activity of standard anticancer drugs doxorubicin and cisplatin and the calculated values of resistance index (RI) and selectivity index (SI) of tested compounds.

Compound	Cancer Cells						Normal Cells			
	A549		MCF-7		LoVo		LoVo/DX		RI	BALB/3T3
	IC ₅₀ (μM)	SI	IC ₅₀ (μM)	SI	IC ₅₀ (μM)	SI	IC ₅₀ (μM)	SI		IC ₅₀ (μM)
1	0.125 ± 0.013	1.11	0.054 ± 0.028	2.57	0.108 ± 0.025	1.29	1.69 ± 0.28	0.08	15.65	0.139 ± 0.073
2	0.105 ± 0.008	1.35	0.027 ± 0.008	5.26	0.084 ± 0.021	1.69	1.550 ± 0.170	0.09	18.45	0.142 ± 0.073
3	0.010 ± 0.0001	10.3	0.015 ± 0.002	6.87	0.014 ± 0.004	7.36	0.135 ± 0.012	0.76	9.64	0.103 ± 0.089
4	0.115 ± 0.007	8.13	0.178 ± 0.020	7.08	0.125 ± 0.044	10.08	0.700 ± 0.088	1.80	5.60	1.260 ± 0.796
5	0.074 ± 0.009	1.41	0.057 ± 0.011	1.82	0.074 ± 0.019	1.41	1.010 ± 0.020	0.10	13.65	0.104 ± 0.043
6	0.010 ± 0.0001	6.60	0.013 ± 0.002	5.08	0.007 ± 0.002	9.43	0.050 ± 0.010	1.32	7.14	0.066 ± 0.031
7	0.012 ± 0.004	8.50	0.018 ± 0.002	5.67	0.011 ± 0.004	9.27	0.071 ± 0.010	1.44	6.45	0.102 ± 0.063
8	0.030 ± 0.021	4.60	0.055 ± 0.026	2.51	0.018 ± 0.010	7.67	0.074 ± 0.007	1.86	4.11	0.138 ± 0.010
9	0.012 ± 0.004	9.67	0.027 ± 0.007	4.30	0.011 ± 0.0001	10.55	0.072 ± 0.011	1.61	6.55	0.116 ± 0.009
10	0.089 ± 0.020	1.94	0.132 ± 0.017	1.31	0.054 ± 0.017	3.20	0.089 ± 0.026	1.94	1.65	0.173 ± 0.108
11	0.095 ± 0.005	1.54	0.125 ± 0.014	1.17	0.062 ± 0.013	2.35	0.091 ± 0.009	1.60	1.47	0.146 ± 0.014
12	0.093 ± 0.014	2.14	0.125 ± 0.015	1.08	0.281 ± 0.185	0.48	4.240 ± 1.330	0.03	15.09	0.135 ± 0.015
Doxorubicin	0.258 ± 0.044	0.64	0.386 ± 0.118	0.43	0.092 ± 0.018	1.80	4.75 ± 0.99	0.035	51.60	0.166 ± 0.074
Cisplatin	6.367 ± 1.413	0.61	10.70 ± 0.753	0.36	4.37 ± 0.73	0.89	5.70 ± 0.63	0.68	1.3	3.90 ± 1.50

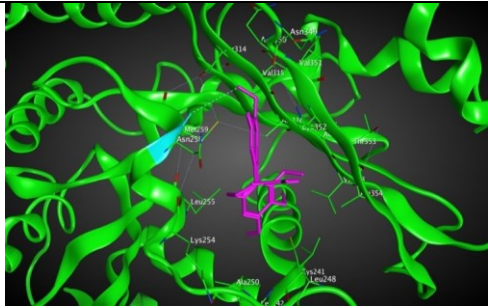
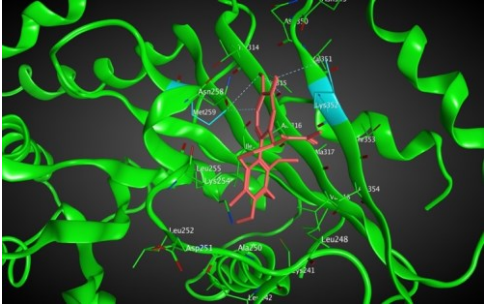
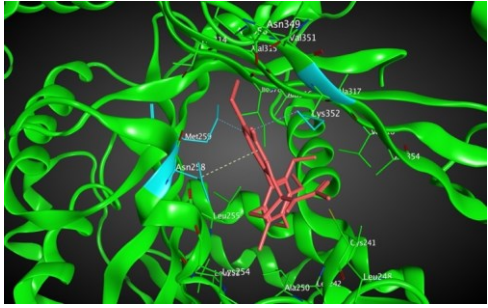
The IC₅₀ value is defined as the concentration of a compound at which 50% growth inhibition is observed. The SI (selectivity index) was calculated for each compound using the formula: SI = IC₅₀ for normal cell line BALB/3T3 / IC₅₀ for respective cancerous cell line. A beneficial SI > 1.0 indicates a drug with efficacy against tumor cells greater than the toxicity against normal cells. The RI (resistance index) indicates how many times a resistant subline is chemo-resistant relative to its parental cell line. The RI was calculated for each compound using the formula: RI = IC₅₀ for LoVoDX / IC₅₀ for LoVo cell line. When RI is 0–2, the cells are sensitive to the compound tested, RI in the range 2–10 means that the cell shows moderate sensitivity to the drug tested, RI above 10 indicates strong drug-resistance.

5.2.3 Molecular Docking: *In Silico* Determination of Drug-Induced Inhibition of β I Tubulin

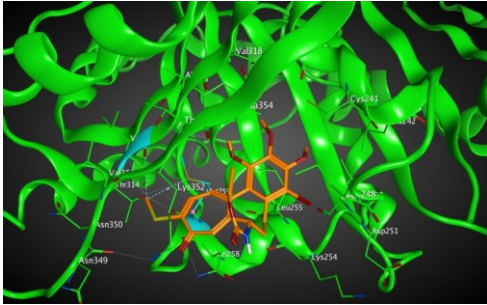
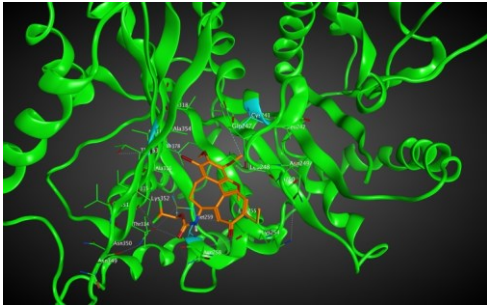
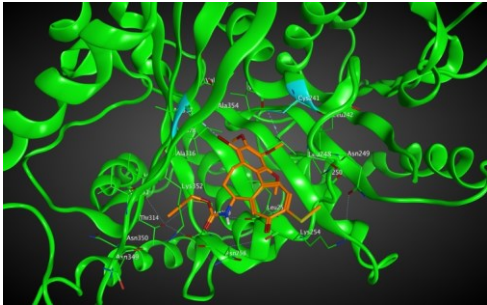
β I tubulin, one of the subunits of microtubules in the cytoskeleton of eukaryotic cells, is a well-known and well-studied target for chemotherapeutic drugs selected to inhibit the growth and proliferation of cancer cells. The computational evaluation of binding energies between drug candidates and β I tubulin performed by docking is a fast and inexpensive prediction method to investigate and rank the ability to arrest cancer cell proliferation by new compounds, which inhibit microtubule assembly. Here, the binding energies of new colchicine derivatives were calculated by docking the referred compounds to the colchicine-binding pocket of β I tubulin.

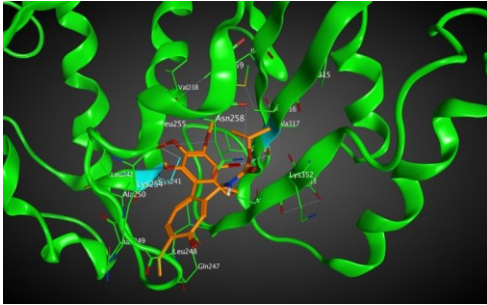
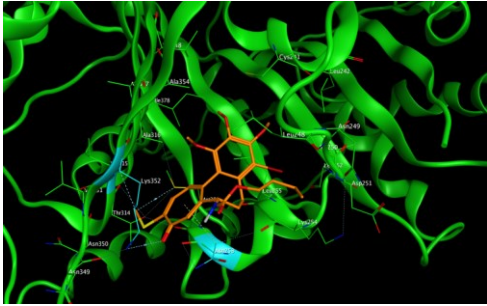
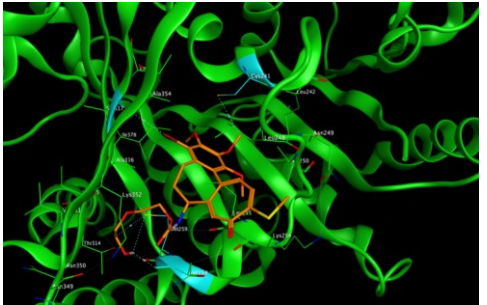
A combination of different computational methods was used to explore ligand-tubulin interactions. The ligand structures were first energy-minimized, then fully optimized based on the RHF/cc-pVDZ level of theory implemented in the software package GAMESS-US, version 2010-10-01. Since there is no crystal structure for human β I tubulin (UniProt ID: P07437) available in the Protein Data Bank (PDB), the bovine tubulin structure 1SA0.pdb was used as a template to construct the homology model for human β I tubulin using the software package MOE2015. Autodock4 program under flexible ligand and rigid receptor conditions was also used to dock the small library of investigated colchicine derivatives to the target protein structure (see Table 5-2). AutoDock4 software is designed to predict how ligands bind to a receptor of a known 3D structure and it consists of two main modules: (1) autodock, which performs the docking of the ligand to a set of grids describing the target protein; and (2) auto grid, which pre-calculates these grids.

Table 5-2. Calculated binding energies for the interactions between the new colchicine derivatives investigated in this chapter and β I tubulin, and also the values of the Moriguchi octanol-water partition coefficient, MlogP, calculated for the same colchicine derivatives.

Compound	Binding Energy (kcal/mol)	Interactions	MW	MlogP	Active Residues
1	-8.09		399.44	1.37	Asn258
2	-8.40		481.37	1.93	Met259 Asn258 Lys352
3	-8.60		497.44	2.69	Met259 Lys352 Val315

4	-8.12		455.40	2.71	Asn349 Met259 Lys352 Cys241
5	-7.68		543.46	2.20	Cys241 Ala317 Val315 Met259
6	-8.99		513.43	2.74	Met259 Lys352 Val315

7	-9.20		527.46	2.95	Met259 Val315
8	-7.61		581.43	3.26	Cys241 Asn258 Ala317
9	-8.21		541.49	3.16	Cys241 Ala317

10	-8.06		541.49	3.16	Cys241 Ala317
11	-9.25		528.51	2.30	Lys352 Asn258 Val315
12	-7.92		587.52	1.87	Ala317 Asn258 Met259 Cys241

Based on our *in silico* calculations, **11**, **7**, **6**, and **3** show the strongest binding energies of -9.25 , -9.20 , -8.99 , and -8.60 kcal/mol, respectively. Note that two Met 259 and Lys 352 residues in the colchicine binding site of β I tubulin interact with C-20 (sidechain donor) and oxygen of carbonyl (sidechain acceptor) on ring C of the new colchicine derivatives, respectively. The diagrams depicting these interactions can be found in Table 5-2.

The evaluation of IC₅₀ values in a cell-based assay involves interactions of the tested compounds with all tubulin expressed by the cell and β I tubulin isotype is not the only isotype of tubulin expressed, although it is expected to be one of the most abundant ones. Even though both normal and cancer cells in humans contain the same tubulin isotypes, their expression levels and distribution of tubulin isotypes in each of the cell lines are different. In particular, the most abundant isotype in most tumors is β I isotype (*TUBB*) followed by, β IVb (*TUBB4B*), β IIa (*TUBB2A*), β V (*TUBB6*), and β III (*TUBB3*), with 47%, 38%, 8.9%, 3.1%, and 2.2%, respectively, and then β IVa (*TUBB4*), β IIIb (*TUBB2B*), and β VI (*TUBB1*) with levels below 0.5% of the total expressed β tubulins. Since the expression levels of tubulin isotypes in each individual cell lines are unique, the binding energies for each of these isotypes would differ and affect the overall response to cytotoxic agents and make the computational prediction fairly complex [33]. To quantify the assumption that isotype expression levels correlate with cytotoxicity of the compounds acting on these isotypes of tubulin, the same docking simulation method was applied between the novel colchicine derivatives and β IIa (UniProt ID: Q13885), β IIIb (UniProt ID: Q9BVA1), β III (UniProt ID: Q13509), β IVa (UniProt ID: P04350), β IVb (UniProt ID: P68371), and β VI (UniProt ID: Q9H4B7) tubulin isotypes.

5.2.4 Linear regression with two independent variables

Following the docking simulations, in order to determine the level of correlation between experiment and computational simulations, we have calculated the linear regression coefficients between experimental values of IC₅₀ and computational prediction for different β tubulin isotypes. To have a more realistic correlation coefficient, a logarithmic value of solubility of the compounds, the Moriguchi octanol-water partition coefficients (MLogP), were calculated using a software package called ADMET Predictor 8.0 (ADMET Predictor, Simulations Plus, Lancaster, CA, USA) and taken into account for predicting the biopharmaceutical properties like permeability and the understanding of transport mechanisms of the drugs *in vivo* [34]. The partition

coefficient is also a useful factor in estimating and comparing the distribution of the drugs within the cells, organs, and the body.

A very good correlation of 0.66 and 0.84 involving log IC₅₀ for LoVo and LoVo/DX cell lines, respectively, was the result of linear regression analysis with two independent variables, namely the compounds' MlogP values and the other being the binding free energies of our compounds and the tubulin β I isotype. These two cell lines have also a good correlation of 0.72 and 0.80 with the binding free energies of the compounds to the β IVb isotype, respectively. MlogP and the experimental IC₅₀ values of 4-bromocolchicine based series are listed in Table 5-3, (Appendix D, Figures D24 and D25). For the A549 cell line, the regression coefficients found were 0.43, 0.43, and 0.51 with binding free energies for β I, β IVb, and β IVa isotypes, respectively. The reported regression coefficient for the A549 cell line is still acceptable, while its value for the MCF-7 and BALB/3T3 cell lines is very low (see Table 5-3). The reason for the latter discrepancy between computation and experiment may be due to additional biological factors, such as the upregulation of MDR proteins that act as efflux pumps and prevent the drugs from exerting their cytotoxic action. Another possibility could involve off-target interactions.

Table 5-3. Linear regressions involving two independent variables (the binding free energy obtained from the docking method and MlogP) of the investigated colchicine derivatives versus log IC₅₀ [μ M] in different cancer cell lines.

		MCF-7	LoVo	LoVo/DX	A549	BALB/3T3
Linear regression of colchicine derivatives (R ²)	β I	0.11	0.66	0.84	0.43	0.02
	β IIa	0.01	0.53	0.68	0.30	0.07
	β IIb	0.15	0.69	0.76	0.42	0.0004
	β III	0.01	0.57	0.71	0.36	0.09
	β IVa	0.16	0.65	0.74	0.51	0.31
	β IVb	0.02	0.72	0.80	0.43	0.01
	β VI	0.03	0.56	0.66	0.38	0.09

To further investigate the accuracy of the reported linear regressions between our computational results obtained using the docking method and the experimentally generated IC_{50} values, more accurate but also more time-consuming computational methods were applied to calculate the binding free energies between the novel colchicine derivatives and β tubulin isotypes. This analysis is described below.

5.2.5 MM/PBSA and MM/GBSA: *In Silico* Determination of Drug-Induced Inhibition of β Tubulin Isotypes

The molecular operating environment (MOE) was used to build a 3D model for the α - β I tubulin heterodimer [35]. Human tubulin protein sequences were obtained from UniProt [36]. The sequence corresponding to the gene *TUBA1A* (UniProt ID: Q71U36) was chosen as a reference sequence for human α -tubulin whereas gene *TUBB* associated to β I isoform (UniProt ID: P07437) was chosen for human β -tubulin. Homology modeling was performed using MOE by setting the number of generated models to 10 and by selecting the final model based on MOE's generalized Born/volume integral (GB/VI) scoring function. As a template, the crystallographic structure of α - β IIb tubulin isotype complexed with colchicine (PDB ID: 1SA0) was used [37]. During the modeling, cofactors including GTP, GDP, colchicine, and the magnesium ion located at the interface between α - and β -monomers were kept as part of the environment and included in the refinement step. The final model was eventually protonated at neutral pH and minimized using a MOE's built-in protocol.

In order to equilibrate our model and get representative conformations, molecular dynamics (MDs) simulations were run using Amber14 [38]. Amber's antechamber utility was applied to generate MD parameters—e.g., partial charges, force constants, etc.—for the four cofactors from the Gasteiger charge method. Amber's tleap program was applied to solvate the system in TIP3P water. Minimization of the structure was carried out in two steps, both using the steepest descent and conjugate gradient

methods successively. First, minimization was done during 2 ps on solvent atoms only, by restraining the protein-ligand complex. Next, minimization was run without the restraint during 10 ps. The structure was then equilibrated in an NVT ensemble during 20 ps and in an NPT ensemble during 40 ps setting the temperature to 298 K and the pressure to 1 bar. Finally, MD production was run for 70 ns. The root-mean-square deviation (RMSD) of both the entire tubulin structure and the colchicine binding site were found to plateau after 40 ns (see Figure 5-14).

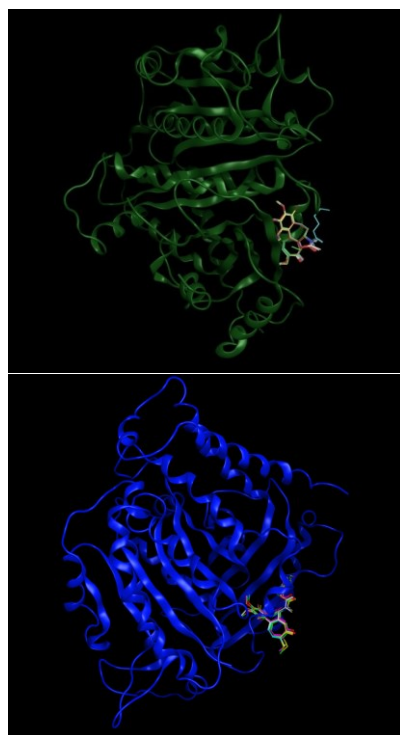


Figure 5-14. Tubulin β I structure in 3D with (**Top**) 5 colchicine derivatives with binding energies of -8.40 kcal/mol and higher, and (**bottom**) with 6 colchicine derivatives with binding energies lower than -8.40 kcal/mol.

Clustering analysis of the last 30 ns of the generated MD trajectory was carried out using Amber's CPPTRAJ program [39] to identify representative conformations of the tubulin dimer. Clustering was done *via* a hierarchical agglomerative using the RMSD

of atoms in the colchicine binding site as a metric. An RMSD cutoff of 1.0 Å was set to differentiate the clusters. From clustering analysis, three representative structures of the tubulin dimer were found. The structures were further used as a rigid target for the screening of 4-bromocolchicine derivatives.

Docking of 4-bromocolchicine derivatives was performed using the AutoDock Vina [40] program, which makes use of an iterated local search global optimizer as a searching method. The Vina scoring function combines aspects from knowledge-based and empirical potentials. Tested on the same set used for Autodock4, Vina was able to identify the correct binding pose in 78% of the cases as compared to 53% for Autodock4 [41]. For our docking simulations, a cubic box with 30.0 Å for each side centered at the center of mass of the bound colchicine was used. All cofactors, namely, GTP, GDP, colchicine, and the magnesium ion were removed during docking while the target was kept rigid. For every compound, docking was run separately on each of the three tubulin representative structures obtained from clustering of the MD trajectory. Every generated pose was energy-minimized using Amber14 by keeping the protein fixed and was re-scored using the Vina software. For each compound/protein-structure pair, the pose with the best score was identified and used as an initial configuration for molecular mechanics Poisson–Boltzmann surface area MM/PBSA computations.

The MM/PBSA technique was used to calculate the free energy associated with the binding of 4-bromocolchicine derivatives [42,43]. This method combines molecular mechanics with continuum solvation models. The binding free energy is estimated as

$$\Delta G_{bind} = \langle \Delta E_{MM} \rangle - T\Delta S + \Delta G_{solv}, \quad (1)$$

where $\langle \Delta E_{MM} \rangle - T\Delta S$ can be regarded as the change in the free energy of the system in vacuum (gas phase); it includes the change in the molecular mechanics energy $\langle \Delta E_{MM} \rangle = \langle E_{MM} \rangle_{bound} - \langle E_{MM} \rangle_{unbound}$ and the change in the conformational entropy ΔS due to the binding. Since our goal was to compare the binding free energy of similar compounds derived from colchicine, ΔS was not estimated when calculating ΔG_{bind} as

each compound is assumed to provide comparable ΔS values. ΔG_{solv} stands for the difference of solvation free energies due to the binding, which is given as $\Delta G_{solv} = \Delta G_{solv}^{complex} - \Delta G_{solv}^{lig} - \Delta G_{solv}^{prot}$ where every term on the right-hand side is given as the sum of polar and nonpolar contributions. The polar parts are obtained by solving the Poisson–Boltzmann (PB) equation or by using the generalized Born (GB) model—resulting in the MM/GBSA method, whereas the nonpolar terms are estimated from a linear relation to the solvent accessible surface area (SASA). The values of $\langle \Delta E_{MM} \rangle$ and ΔG_{solv} are generally computed as ensemble averages requiring a short MD trajectory of the solvated complexed system as input of the MM/PBSA method. In the present case, a 1 ns-duration MD trajectory was run in TIP3P water using Amber14, for every top pose generated at the end of the docking step. The MM/PBSA and MM/GBSA calculations were performed on a subset of 200 frames collected at regular time intervals from the trajectory. For PB calculations, an ionic strength of 0.0 nM ($istrng = 0.0$) and a solvent probe radius of 1.6 Å ($prbrad = 1.6$) were used. For GB calculations, the igb parameter was set to 5 that corresponds to a modified GB model equivalent to model II in reference [44]. For each of the tested compounds, the best PB and GB score out of the three trajectories associated with the three representative structures of the tubulin dimer were collected and reported in Table 5-4.

Table 5-4. Binding energies (kcal/mol) were calculated by MM/PBSA and MM/GPSA methods.

MM/PBSA—Molecular Mechanics Poisson-Boltzmann Surface Area, MM/GBSA—Molecular Mechanics Generalized Born Surface Area, PBSA—Poisson-Boltzmann Surface Area, GBSA—Generalized Born Surface Area.

Ligand	GBSA β I	PBSA β I	GBSA β IIa	PBSA β IIa	GBSA β III	PBSA β III	GBSA β IVb	PBSA β IVb	GBSA β VI	PBSA β VI
1	-40.4	-40.2	-40.8	-45.4	-33.5	-32.0	-39.5	-44.6	-43.1	-35.6
2	-36.6	-44.3	-47.0	-31.0	-33.1	-32.5	-44.8	-36.9	-46.8	-44.0
3	-34.0	-37.2	-33.0	-29.8	-27.7	-28.2	-34.2	-30.9	-33.5	-37.9
4	-37.1	-43.1	-36.5	-41.4	-34.8	-31.9	-40.2	-43.7	-39.1	-33.8
5	-36.8	-44.1	-33.3	-42.7	-29.9	-22.9	-35.0	-39.9	-37.9	-39.2
6	-37.2	-45.7	-38.8	-38.7	-29.3	-29.2	-30.7	-23.0	-34.4	-31.8
7	-40.3	-44.1	-39.3	-45.5	-28.7	-26.9	-41.0	-49.0	-41.9	-42.6
8	-48.2	-51.0	-40.0	-25.4	-45.9	-50.0	-47.4	-50.3	-50.7	-45.6
9	-54.1	-39.5	-58.3	-54.2	-42.8	-41.1	-41.6	-32.4	-61.4	-51.7

10	-58.6	-48.7	-60.9	-37.2	-62.0	-55.6	-58.2	-55.8	-59.4	-49.7
11	-46.8	-49.8	-41.3	-41.5	-29.3	-19.5	-43.0	-23.9	-45.3	-35.5
12	-52.7	-45.5	-55.4	-34.8	-39.0	-26.1	-54.0	-32.1	-50.3	-46.4

5.2.6 Linear Regression with Two Independent Variables

Following the MM/PBSA simulations, we have calculated the linear regression coefficients between experiment and computational simulations of different β tubulin isotypes. The result of linear regression with two independent variables between the binding free energies of β IVb isotypes, MlogP and IC₅₀ for the LoVo and LoVo/DX cell lines is that very good correlation coefficients were found, namely 0.78 and 0.67, respectively. Also, reasonably good correlation of 0.65 and 0.54 was obtained with the binding free energies of β I isotype for these two cell lines, respectively. These correlation coefficients are also consistent with the correlation coefficients calculated using the docking binding energies and these cell lines except for LoVo/DX and β I which were lower but still acceptable. For the A549 cell line, the regression coefficients found were 0.62, 0.58, and 0.48 for the binding free energies with β III, β IVb, and β I isotypes, respectively. The reported regression coefficient for the A549 cell line was improved a little bit by using the more expensive method but the MM/PBSA method could not improve the correlation coefficient values for the MCF-7 and BALB/3T3 cell lines and they are still very low (Table 5-5).

Table 5-5. Linear regressions involving two independent variables (binding energy by MM/PBSA method and MlogP) of the investigated colchicine derivatives versus log IC₅₀ (μM) in different cancer cell lines.

		MCF-7	LoVo	LoVo/DX	A549	BALB/3T3
Linear regression of colchicine derivatives (R ²)	βI	0.18	0.65	0.54	0.48	0.0006
	βIIa	0.09	0.57	0.56	0.41	0.0006
	βIII	0.31	0.61	0.40	0.62	0.03
	βIVb	0.22	0.78	0.67	0.58	0.03
	βVI	0.17	0.64	0.67	0.47	0.0005

The LoVo and LoVo/DX cell line correlation with βI and βIVb isotypes 0.60, 0.66, 0.65, and 0.71 respectively. The result also shows a good correlation of 0.7 between binding energies for βV tubulin and LoVo/DX cell line. For, the regression coefficients of 0.55 and 0.51 with free energies of βI, the isotypes which showed for the A549 cell line were in the same range with docking and MM/GBSA results. There were no improvements for the correlation values for the MCF-7 and BALB/3T3 cell lines with the MM/GBSA simulations (Table 5-6).

Table 5-6. Linear regressions involving two independent variables (binding energy by MM/GBSA method and MlogP) of the investigated colchicine derivatives versus log IC₅₀ (μM) in different cancer cell lines.

		MCF-7	LoVo	LoVo/DX	A549	BALB/3T3
Linear regression of colchicine derivatives (R ²)	βI	0.21	0.60	0.65	0.55	0.0005
	βIIa	0.02	0.54	0.68	0.36	0.0004
	βIII	0.08	0.57	0.59	0.46	0.013
	βIVb	0.12	0.66	0.71	0.51	0.095
	βVI	0.04	0.58	0.70	0.37	0.013

The ranges of correlation coefficients between the IC₅₀ values of all the cell lines and the corresponding binding free energies calculated with three different methods are the same. Reassuringly, the best correlation values from all three methods used were found for βI and βIVb tubulin isotypes, which are reported to be most abundant in these types of cells.

5.3 Conclusions

We synthesized a series of novel triple-modified 4-bromothiocolchicine derivatives (**5–12**) as well as 4-bromocolchicine (**2**), 4-bromothiocolchine (**3**) and 4-bromo-*N*-deacetylthiocolchicine (**4**) and evaluated their biological activity according to the *in vitro* antiproliferative tests as well as *in silico* studies. Biological activity was evaluated on four human cancer cell lines and a normal murine embryonic fibroblast cell line. The results of our study have clearly showed that the cytotoxicity of almost all colchicine derivatives (**2–12**) is higher than the corresponding cytotoxicity of commonly used cytostatic agents—doxorubicin and cisplatin against A549, MCF-7, LoVo (except **4** and **12**) and LoVo/DX cancer cell lines. The majority of the derivatives also exhibit a higher cytotoxicity than unmodified colchicine. Particularly noteworthy are the compounds **6–9**, which show very high antiproliferative activity against A549, MCF-7 and LoVo cell lines, that is expressed by very low IC₅₀ values at nanomolar concentrations (IC₅₀ = 0.010–0.030; 0.013–0.027 (without **8**) and 0.007–0.018 μM for A549, MCF-7 and LoVo, respectively). Moreover, compounds **6–9** were demonstrated to be less toxic to normal murine fibroblast cells than the currently used anticancer drugs, such as cisplatin and doxorubicin, which is confirmed by particularly high selectivity index (SI) values calculated for A549, MCF-7, and LoVo cell lines are (SI ≥ 4.3, except SI of eight for MCF-7 cell line). The toxicity is a major challenge in designing a potential colchicine-based drug candidate. High SI values result from large differences between the cytotoxicity against cancer and normal cells and this means that cancer cells exposed to the same concentration of the compound will be killed at a higher rate than normal ones, which might lead to a potential colchicine-based drug candidate.

Based on our *in silico* calculations, **11**, **7**, **6**, and **3** show the strongest binding energies of –9.25, –9.20, –8.99 and –8.60 kcal/mol, respectively. Two Met 259 and Lys 352 residues in the colchicine binding site of βI tubulin interact with C-20 (sidechain donor) and oxygen of carbonyl (sidechain acceptor) on ring C of the new colchicine derivatives, respectively. In order to determine the level of correlation between

experiment and computational simulations, we have calculated the linear regression coefficients between IC_{50} values and the binding free energies involving the compounds and tubulin isotypes as well as the MlogP coefficients for these compounds. A very good correlation of 0.66 and 0.84 with $\log IC_{50}$ for LoVo and LoVo/DX cell lines, respectively, has been found. For the A549 cell line, the regression coefficient found is 0.43, still acceptable, while its value for the MCF-7 and BALB/3T3 cell lines is very low. This may be explained by a number of additional effects taking place in living cells compared to the computational simulations that focus only on the binding mode of the compounds to the target. Specifically, off-target interactions involving efflux pumps with different affinities for the individual compounds may explain the observed partial correlation between IC_{50} values and binding free energies. Additionally, differences in the solubility values and membrane permeability may have to be accounted for when ranking the various compounds in biological assays and comparing them to computational predictions based on binding affinity alone. We have additionally supported these findings with calculations using two very accurate methods of calculating the binding energies of ligands to proteins, namely MM/PBSA and MM/GBSA. The results using all three *in silico* approaches have been found consistent.

In short, these results confirm that a suitable chemical modification of colchicine aimed for an improved binding affinity to human tubulin βI or βIVb isotypes is a promising approach to finding highly biologically active and less toxic compounds. Some of the obtained compounds are suitable candidates for further tests (*ex vivo*, *in vivo*). The synthesis of new colchicine derivatives with diverse substituents is also a next step in developing structure-activity relationship (SAR) of colchicine-binding site inhibitors.

References

- [1] A. Slobodnick, B. Shah, M. H. Pillinger, and S. Krasnokutsky, "Colchicine: old and new.," *Am. J. Med.*, vol. 128, no. 5, pp. 461–70, May 2015, doi: 10.1016/j.amjmed.2014.12.010.
- [2] E. S. Shchegravina, D. I. Knyazev, I. P. Beletskaya, E. V. Svirshchevskaya, H.-G. Schmalz, and A. Y. Fedorov, "Synthesis of Nonracemic Pyrrolo-allocholchicinoids Exhibiting Potent Cytotoxic Activity," *European J. Org. Chem.*, vol. 2016, no. 34, pp. 5620–5623, 2016, doi: <https://doi.org/10.1002/ejoc.201601069>.
- [3] D. Zemer, A. Livneh, Y. L. Danon, M. Pras, and E. Sohar, "Long-term colchicine treatment in children with familial Mediterranean fever.," *Arthritis Rheum.*, vol. 34, no. 8, pp. 973–7, Aug. 1991, doi: 10.1002/art.1780340806.
- [4] E. Ben-Chetrit and M. Levy, "Colchicine prophylaxis in familial Mediterranean fever: reappraisal after 15 years.," *Semin. Arthritis Rheum.*, vol. 20, no. 4, pp. 241–6, Feb. 1991.
- [5] C. Cerquaglia, M. Diaco, G. Nucera, M. La Regina, M. Montalto, and R. Manna, "Pharmacological and clinical basis of treatment of Familial Mediterranean Fever (FMF) with colchicine or analogues: an update.," *Curr. Drug Targets. Inflamm. Allergy*, vol. 4, no. 1, pp. 117–124, Feb. 2005, doi: 10.2174/1568010053622984.
- [6] K. Masuda, A. Nakajima, A. Urayama, K. Nakae, M. Kogure, and G. Inaba, "Double-masked trial of cyclosporin versus colchicine and long-term open study of cyclosporin in Behçet's disease.," *Lancet (London, England)*, vol. 1, no. 8647, pp. 1093–1096, May 1989, doi: 10.1016/s0140-6736(89)92381-7.
- [7] M. M. Kaplan, "New strategies needed for treatment of primary biliary cirrhosis?," *Gastroenterology*, vol. 104, no. 2, pp. 651–653, Feb. 1993, doi: 10.5555/URI:PII:001650859390440N.
- [8] Y. Gong and C. Gluud, "Colchicine for primary biliary cirrhosis: a Cochrane Hepato-Biliary Group systematic review of randomized clinical trials.," *Am. J.*

Gastroenterol., vol. 100, no. 8, pp. 1876–1885, Aug. 2005, doi: 10.1111/j.1572-0241.2005.41522.x.

[9] R. J. McKendry, G. Kraag, S. Seigel, and A. al-Awadhi, “Therapeutic value of colchicine in the treatment of patients with psoriatic arthritis.,” *Ann. Rheum. Dis.*, vol. 52, no. 11, pp. 826–828, Nov. 1993, doi: 10.1136/ard.52.11.826.

[10] R. A. Kyle *et al.*, “A Trial of Three Regimens for Primary Amyloidosis: Colchicine Alone, Melphalan and Prednisone, and Melphalan, Prednisone, and Colchicine,” *N. Engl. J. Med.*, vol. 336, no. 17, pp. 1202–1207, Apr. 1997, doi: 10.1056/NEJM199704243361702.

[11] M. Imazio and F. Gaita, “Colchicine for cardiovascular medicine.,” *Future Cardiol.*, vol. 12, no. 1, pp. 9–16, Jan. 2016, doi: 10.2217/fca.15.59.

[12] M. Imazio *et al.*, “Colchicine for recurrent pericarditis (CORP): a randomized trial.,” *Ann. Intern. Med.*, vol. 155, no. 7, pp. 409–414, Oct. 2011, doi: 10.7326/0003-4819-155-7-201110040-00359.

[13] J. Seligmann and C. Twelves, “Tubulin: an example of targeted chemotherapy.,” *Future Med. Chem.*, vol. 5, no. 3, pp. 339–52, Mar. 2013, doi: 10.4155/fmc.12.217.

[14] C. D. Katsetos and P. Dráber, “Tubulins as therapeutic targets in cancer: from bench to bedside.,” *Curr. Pharm. Des.*, vol. 18, no. 19, pp. 2778–92, 2012, doi: 10.2174/138161212800626193.

[15] C. Avendaño and J. C. Menéndez, *Medicinal Chemistry of Anticancer Drugs*. 2008.

[16] T. Kozaka *et al.*, “Antitumor agents 273. Design and synthesis of N-alkylthiocolchicinoids as potential antitumor agents.,” *Bioorg. Med. Chem. Lett.*, vol. 20, no. 14, pp. 4091–4, Jul. 2010, doi: 10.1016/j.bmcl.2010.05.081.

[17] G. Raspaglio *et al.*, “Thiocolchicine dimers: a novel class of topoisomerase-I inhibitors,” *Biochem. Pharmacol.*, vol. 69, no. 1, pp. 113–121, 2005, doi: <https://doi.org/10.1016/j.bcp.2004.09.004>.

- [18] D. Bartusik, B. Tomanek, E. Lattová, H. Perreault, J. Tuszynski, and G. Fallone, “Derivatives of thiocolchicine and its applications to CEM cells treatment using ¹⁹F Magnetic Resonance ex vivo,” *Bioorg. Chem.*, vol. 38, no. 1, pp. 1–6, 2010, doi: <https://doi.org/10.1016/j.bioorg.2009.10.002>.
- [19] P. B. Prajapati, K. B. Bodiwala, and B. P. Marolia, “Oxidative Degradation Kinetic Study of Thiocolchicoside using Stability Indicating High Performance Thin Layer Chromatographic Method,” *Pharm. Methods*, vol. 5, no. 2, pp. 1–10, 2014, doi: [10.5530/phm.2014.2.5](https://doi.org/10.5530/phm.2014.2.5).
- [20] A. Banerjee, L. T. Kasmala, E. Hamel, L. Sun, and K. H. Lee, “Interaction of novel thiocolchicine analogs with the tubulin isoforms from bovine brain.,” *Biochem. Biophys. Res. Commun.*, vol. 254, no. 2, pp. 334–337, Jan. 1999, doi: [10.1006/bbrc.1998.9943](https://doi.org/10.1006/bbrc.1998.9943).
- [21] J. Marangon *et al.*, “Tools for the rational design of bivalent microtubule-targeting drugs,” *Biochem. Biophys. Res. Commun.*, vol. 479, no. 1, pp. 48–53, 2016, doi: <https://doi.org/10.1016/j.bbrc.2016.09.022>.
- [22] N. Yasobu *et al.*, “Design, Synthesis, and Antitumor Activity of 4-Halocolchicines and Their Pro-drugs Activated by Cathepsin B.,” *ACS Med. Chem. Lett.*, vol. 2, no. 5, pp. 348–352, May 2011, doi: [10.1021/ml100287y](https://doi.org/10.1021/ml100287y).
- [23] U. Majcher *et al.*, “Synthesis, antiproliferative activity and molecular docking of thiocolchicine urethanes.,” *Bioorg. Chem.*, vol. 81, pp. 553–566, 2018, doi: [10.1016/j.bioorg.2018.09.004](https://doi.org/10.1016/j.bioorg.2018.09.004).
- [24] Q. Shi, P. Verdier-Pinard, A. Brossi, E. Hamel, and K. H. Lee, “Antitumor Agents-CLXXV. Anti-tubulin action of (+)-thiocolchicine prepared by partial synthesis,” *Bioorg. Med. Chem.*, vol. 5, no. 12, pp. 2277–2282, 1997, doi: [10.1016/S0968-0896\(97\)00171-5](https://doi.org/10.1016/S0968-0896(97)00171-5).
- [25] P. Kerkes, P. N. Sharma, A. Brossi, C. F. Chignell, and F. R. Quinn, “Synthesis and biological effects of novel thiocolchicines. 3. evaluation of N-acyldeacetylthiocolchicines, N-(alkoxycarbonyl)deacetylthiocolchicines, and O-

ethyl-demethylthiocolchicines. New synthesis of thiodemecolcine and antileukemic effects of 2-demeth,” *J. Med. Chem.*, vol. 28, no. 9, pp. 1204–1208, Sep. 1985, doi: 10.1021/jm00147a014.

[26] P. Skehan *et al.*, “New colorimetric cytotoxicity assay for anticancer-drug screening,” *J. Natl. Cancer Inst.*, vol. 82, no. 13, pp. 1107–1112, Jul. 1990, doi: 10.1093/jnci/82.13.1107.

[27] D. Nevozhay, “Cheburator software for automatically calculating drug inhibitory concentrations from in vitro screening assays,” *PLoS One*, vol. 9, no. 9, p. e106186, 2014, doi: 10.1371/journal.pone.0106186.

[28] T. H. Dunning, “Gaussian basis sets for use in correlated molecular calculations. I. The atoms boron through neon and hydrogen,” *J. Chem. Phys.*, vol. 90, no. 2, pp. 1007–1023, Jan. 1989, doi: 10.1063/1.456153.

[29] M. W. Schmidt *et al.*, “General atomic and molecular electronic structure system,” *J. Comput. Chem.*, vol. 14, no. 11, pp. 1347–1363, Nov. 1993, doi: 10.1002/jcc.540141112.

[30] M. S. Gordon and M. W. Schmidt, “Advances in electronic structure theory: GAMESS a decade later,” in *Theory and Applications of Computational Chemistry*, C. E. Dykstra, G. Frenking, K. S. Kim, and G. E. Scuseria, Eds. Amsterdam: Elsevier, 2005, pp. 1167–1189.

[31] G. M. J. Barca *et al.*, “Recent developments in the general atomic and molecular electronic structure system,” *J. Chem. Phys.*, vol. 152, no. 15, p. 154102, Apr. 2020, doi: 10.1063/5.0005188.

[32] G. M. Morris *et al.*, “AutoDock4 and AutoDockTools4: Automated docking with selective receptor flexibility,” *J. Comput. Chem.*, vol. 30, no. 16, pp. 2785–91, Dec. 2009, doi: 10.1002/jcc.21256.

[33] L. J. Leandro-García *et al.*, “Tumoral and tissue-specific expression of the major human β -tubulin isotypes,” *Cytoskeleton*, vol. 67, no. 4, pp. 214–223, 2010, doi: 10.1002/cm.20436.

- [34] H. Devalapally, A. Chakilam, and M. M. Amiji, "Role of nanotechnology in pharmaceutical product development.," *J. Pharm. Sci.*, vol. 96, no. 10, pp. 2547–2565, Oct. 2007, doi: 10.1002/jps.20875.
- [35] M. M. Niu et al., "Tubulin inhibitors: Pharmacophore modeling, virtual screening and molecular docking," *Acta Pharmacol. Sin.*, vol. 35, no. 7, pp. 967–979, 2014, doi: 10.1038/aps.2014.34.
- [36] "Update on activities at the Universal Protein Resource (UniProt) in 2013.," *Nucleic Acids Res.*, vol. 41, no. Database issue, pp. D43-7, Jan. 2013, doi: 10.1093/nar/gks1068.
- [37] R. B. G. Ravelli et al., "Insight into tubulin regulation from a complex with colchicine and a stathmin-like domain.," *Nature*, vol. 428, no. 6979, pp. 198–202, Mar. 2004, doi: 10.1038/nature02393.
- [38] R. Salomon-Ferrer, D. A. Case, and R. C. Walker, "An overview of the Amber biomolecular simulation package," *WIREs Comput. Mol. Sci.*, vol. 3, no. 2, pp. 198–210, 2013, doi: <https://doi.org/10.1002/wcms.1121>.
- [39] D. R. Roe and T. E. 3rd Cheatham, "PTRAJ and CPPTRAJ: Software for Processing and Analysis of Molecular Dynamics Trajectory Data.," *J. Chem. Theory Comput.*, vol. 9, no. 7, pp. 3084–3095, Jul. 2013, doi: 10.1021/ct400341p.
- [40] O. Trott and A. J. Olson, "AutoDock Vina: Improving the speed and accuracy of docking with a new scoring function, efficient optimization, and multithreading," *J. Comput. Chem.*, vol. 31, no. 2, pp. 455–461, Jan. 2009, doi: 10.1002/jcc.21334.
- [41] J. Preto, P. Gentile, P. Winter, C. Churchill, S. Omar, and J. A. Tuszynski, "Molecular Dynamics and Related Computational Methods with Applications to Drug Discovery," in *Workshop on Coupled Mathematical Models for Physical and Nanoscale Systems and their Applications*, 2016, pp. 267–285.
- [42] T. Hou, J. Wang, Y. Li, and W. Wang, "Assessing the performance of the MM/PBSA and MM/GBSA methods. 1. The accuracy of binding free energy

calculations based on molecular dynamics simulations.,” *J. Chem. Inf. Model.*, vol. 51, no. 1, pp. 69–82, Jan. 2011, doi: 10.1021/ci100275a.

[43] I. Spasevska et al., “Modeling the *Colchicum autumnale* Tubulin and a Comparison of Its Interaction with Colchicine to Human Tubulin.,” *Int. J. Mol. Sci.*, vol. 18, no. 8, Aug. 2017, doi: 10.3390/ijms18081676.

[44] A. Onufriev, D. Bashford, and D. A. Case, “Exploring protein native states and large-scale conformational changes with a modified generalized born model.,” *Proteins*, vol. 55, no. 2, pp. 383–394, May 2004, doi: 10.1002/prot.20033.

Chapter 6:

Synthesis, Antiproliferative Activity And Molecular Docking of Thiocolchicine Urethanes*

*The paper in this chapter is included by permission from the publisher (Elsevier) and the journal (*Bioorganic Chemistry*).

All authors of the paper were notified about its inclusion in the thesis.

Urszula Majcher, Alicja Urbaniak, Ewa Maj, Mahshad Moshari, Magdalena Delgado, Joanna Wietrzyk, Franz Bartl, Timothy C Chambers, Jack A Tuszynski, and Adam Huczyński. 2018. Synthesis, antiproliferative activity and molecular docking of thiocolchicine urethanes. *Bioorg. Chem.* 81, (2018), 553–566. DOI:<https://doi.org/10.1016/j.bioorg.2018.09.004>

Introduction

Colchicine (**1**), (see Figure 6-1) - a major alkaloid isolated from *Colchicum autumnale* and *Gloriosa superba*, has been in clinical use since 1810 for the treatment of acute gout and is also used for familial Mediterranean fever and other diseases [1,2]. More recently, its relatively high antiproliferative activity generated interest in the development of colchicine and its derivatives as potential anti-cancer drugs [3-5]. The anticancer activity of **1** is related to the formation of a colchicine–tubulin complex, which prevents microtubule polymerization due to a conformational inflexibility making tubulin dimers incompetent for microtubule assembly. As a consequence, the cells exposed to it tend to undergo mitotic arrest during the cell cycle, followed by apoptosis [6-8]. Various families of microtubule-targeting agents have been successfully applied in the treatment of several types of cancer [9,10]. However, the relatively high toxicity of colchicine has prevented its use in cancer therapy thus far [5]. To overcome colchicine's general toxicity problem, numerous colchicine derivatives having high potency and reduced toxicity have been synthesized and tested over the past few decades [8,11-15]. From among a large number of synthetic colchicine analogues, thiocolchicine (**2**) (Figure 6-1) merits special attention. It has a C-10 methylthio group at the tropolone ring C instead of a methoxy group and binds at the colchicine site on tubulin. Previous studies have indicated that the replacement of oxygen by the sulfur atom leads to increased potency of the compound [16-18]. Moreover from the chemical point of view **2** is also highly stable under acidic hydrolytic conditions [16-18].

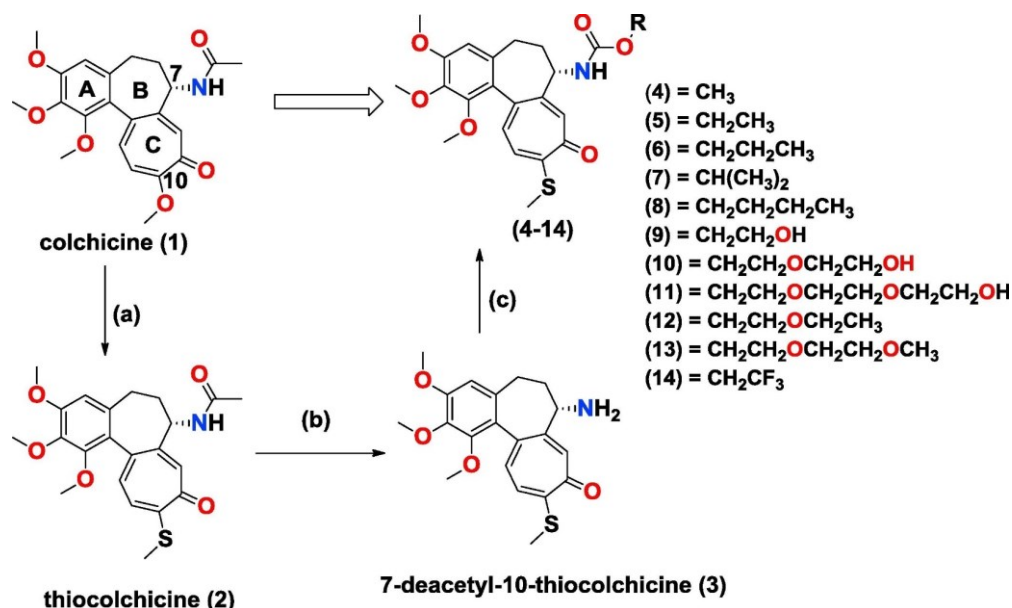


Figure 6-1. Synthesis of colchicine derivatives (2–14). Reagents and conditions: (a) MeOH/H₂O, CH₃SNa, RT; (b) 20% HCl, MeOH, reflux; (c) triphosgene, THF, Et₃N, 0°C; primary or secondary alcohols, RT.

The aim of this work was to develop more selective thicolchicine derivatives while maintaining the potent antiproliferative activity of colchicine. The designed compounds (4–14) shown in Figure 6-3 are carbamates of 7-deacetyl-10-thicolchicine (3). We have chosen carbamate derivatives (urethane) of 7-deacetyl-10-thicolchicine (3) since it has been proved that the carbamate group is a key structural motif in many approved drugs and prodrugs. In fact, the use of carbamate derivatives has been consistently increasing in medicinal chemistry and many derivatives have been specifically designed to cause drug–target interactions through their carbamate moiety [19]. Additionally, some previously described carbamates of 1 have been also shown to be active against gouty arthritis [20].

Herein, we report the synthesis of a series of thicolchicine analogues modified at ring-B and obtained in the reaction of 7-deacetyl-10-thicolchicine (3) with eleven different alcohols in the presence of triphosgene. We also describe the results of *in vitro* antiproliferative activity evaluation of the obtained derivatives against human cancer

cell lines, namely MCF-7, LoVo, LoVo/DX and A-549 as well as normal cells BALB/3T3. To gain more knowledge about the molecular mechanism of action of the synthesized compounds, we also present results of a molecular docking study, flow cytometric cell cycle analyses, and investigation of the effects on microtubules organization using immunofluorescence.

6.1 Experimental

6.1.1 General

All precursors for the synthesis of colchicine derivatives and solvents were obtained from Aldrich or Fluka and were used as received without further purification. CDCl_3 spectral-grade solvents were stored over 3 Å molecular sieves for several days. All the solvents used in flash chromatography were of HPLC grade (CHROMASOLV from Sigma–Aldrich) and were used as received. Reaction mixtures were stirred using Teflon-coated magnetic stir bars. Reactions were monitored by thin layer chromatography (TLC) using aluminum-backed plates (Merck 60F254). TLC plates were visualized in UV-light (254 nm). The ^1H , ^{13}C spectra were recorded on a Varian VNMR-S 400 MHz spectrometer using TMS as the internal standard in both cases. No window function or zero filling was used. ^1H NMR measurements of **1–14** (0.07 mol dm^{-3}) in CDCl_3 were carried out at the operating frequency 402.64 MHz. The error of the chemical shift value was 0.01 ppm. The ^{13}C NMR spectra were recorded at the operating frequency 101.25 MHz. The error of chemical shift value was 0.1 ppm. All spectra were locked to deuterium resonance of CDCl_3 . The ^1H and ^{13}C NMR spectra are shown in the Appendix E. Then, the FT-IR spectra were recorded in the mid infrared region in KBr pallets (2.0/200.0 mg) at 300 K on an IFS 113v FT-IR spectrophotometer (Bruker, Karlsruhe) equipped with a DTGS detector; resolution 2 cm^{-1} , NSS = 64. The Happ-Genzel apodization function was used. Low-resolution EI-mass spectra were recorded using AMD-Intectra GmbH (Harpstedt) D-27243 model 402 double-focusing

sector mass spectrometer (ionizing voltage 70 eV; accelerating voltage 8 kV; resolution 10,000; 10% valley definition). The elemental analyses of 2–6 were carried out on Vario ELIII (Elementar, Germany).

6.1.2 Synthesis

General procedure for the synthesis of 7-deacetyl-10-thiocolchicine derivatives (4–14)

The synthetic routes of target compounds **4–14** are depicted in Figure 6-1. A solution 7-deacetyl-10-thiocolchicine (**3**) (200 mg, 0.5355 mmol) in tetrahydrofuran (15 ml) and 0.7 cm³ triethylamine were stirred at 0°C for 15 min. Triphosgene (158.9 mg, 0.5355 mmol) dissolved in tetrahydrofuran (2 ml) was added dropwise to the cooled solution and stirred at 0°C for 30 min. The solution was then brought to room temperature and from 0.2 ml to 1 ml (5.355 mmol) was added of the suitable primary or secondary alcohols (for example, 0.22 ml methanol). The course of the reaction was followed by silica gel TLC. The mixture was stirred at room temperature for 2 days and then filtered to remove the precipitated triethylamine hydrochloride, and the remaining solution was evaporated under reduced pressure. The resulting mixture was dissolved in CH₂Cl₂ and extracted with 2 N HCl (aq), and then solvated with water. The organic layers were combined and evaporated to dryness under reduced pressure and purified using dry-column flash chromatography (Silica gel 60 from Fluka; chloroform/acetone 10:2) to give respective urethanes derivatives of 7-deacetyl-10-thiocolchicine **4–14**.

Compound 4

Yield 203 mg, 88%; ¹H NMR (403 MHz, CDCl₃) δ 7.34 (s, 1H), 7.28 (d, *J*=0.4 Hz, 1H), 7.26 (s, 1H), 7.05 (d, *J*=10.4 Hz, 1H), 6.55 (s, 1H), 5.30 (s, 1H), 4.43 (dt, *J*=13.3, 6.8 Hz, 1H), 3.94 (s, 3H), 3.91 (s, 3H), 3.64 (s, 3H), 3.58 (s, 3H), 2.54 (m, 1H), 2.44 (s, 3H), 2.28 (m, 1H), 1.84–1.74 (m, 1H); ¹³C NMR (101 MHz, CDCl₃) δ 182.4,

158.3, 155.9, 153.5, 151.1, 150.5, 141.6, 137.7, 134.5, 134.3, 128.6, 126.2, 125.6, 107.3, 61.4, 61.3, 56.0, 53.7, 52.2, 37.0, 29.9, 15.1; FT-IR (KBr pellet, ν_{\max} , cm^{-1}) 3231, 2942, 1727, 1608, 1538, 1486, 1406, 1349, 1321, 1255., 1195, 1137, 1099, 1068, 1023, Anal. calcd. (%) for $\text{C}_{22}\text{H}_{25}\text{NO}_6\text{S}$: C 61.24; H 5.84; N 3.25; S 7.43, Found: C 61.12; H 5.9; 3N 3.21; S 7.29, MS (EI) m/z 431.3 (M).

Compound 5

Yield 200 mg, 84%; ^1H NMR (403 MHz, CDCl_3) δ 7.30 (s, 1H), 7.28 (d, $J=7.3$ Hz, 1H), 7.25 (s, 1H), 7.04 (d, $J=10.5$ Hz, 1H), 6.53 (s, 1H), 5.18 (d, $J=7.5$ Hz, 1H), 4.42 (dt, $J=13.5, 6.8$ Hz, 1H), 4.00 (qd, $J=7.3, 4.2$ Hz, 2H), 3.93 (s, 3H), 3.90 (s, 3H), 3.63 (s, 3H), 2.56–2.48 (m, 1H), 2.43 (s, 3H), 2.33–2.21 (m, 1H), 1.74 (m, 1H), 1.19 (t, $J=7.1$ Hz, 3H); ^{13}C NMR (101 MHz, CDCl_3) δ 182.4, 158.2, 155.4, 153.5, 151.1, 150.6, 141.5, 137.7, 134.4, 134.3, 128.7, 126.2, 125.6, 107.3, 61.4, 61.3, 61.0, 56.0, 53.5, 37.1, 29.9, 15.1, 14.4; FT-IR (KBr pellet, ν_{\max} , cm^{-1}) 3225, 2937, 1718, 1608, 1537, 1486, 1406, 1374, 1348, 1321, 1284, 1256, 1139, 1097, 1065, 1025; Anal. calcd. (%) for $\text{C}_{23}\text{H}_{27}\text{NO}_6\text{S}$: C 62.00; H 6.11; N 3.14; S 7.20, Found: C 62.12; H 6.03; N 3.06; S 7.03, MS (EI) m/z 445.2 (M).

Compound 6

Yield 177 mg, 72%; ^1H NMR (403 MHz, CDCl_3) δ 7.35 (s, 1H), 7.28 (d, $J=2.5$ Hz, 1H), 7.26 (s, 1H), 7.05 (d, $J=10.5$ Hz, 1H), 6.55 (s, 1H), 5.49 (s, 1H), 5.30 (s, 1H), 4.43 (dt, $J=13.3, 6.9$ Hz, 1H), 3.94 (s, 3H), 3.91 (s, 3H), 3.64 (s, 3H), 2.54 (dd, $J=13.4, 6.0$ Hz, 1H), 2.44 (s, 3H), 2.34–2.22 (m, 2H), 1.84–1.75 (m, 1H), 1.55 (dd, $J=14.2, 7.1$ Hz, 2H), 0.87 (t, $J=7.4$ Hz, 3H); ^{13}C NMR (101 MHz, CDCl_3) δ 182.4, 158.2, 155.5, 153.5, 151.1, 150.5, 141.6, 137.7, 134.4, 134.3, 128.7, 126.2, 125.6, 107.3, 66.7, 61.4, 61.3, 56.0, 53.5, 37.1, 29.9, 22.1, 15.1, 10.2; FT-IR (KBr pellet, ν_{\max} , cm^{-1}) 3210, 2936, 1720, 1608, 1539, 1486, 1406, 1348, 1320, 1284, 1255, 1199, 1139, 1097,

1072, 1027; Anal. calcd. (%) for C₂₄H₂₉NO₆S: C 62.73%; H 6.36%; N 3.05%; S 6.98%, Found C 62.66%; H 6.52%; N 3.01%; S 6.75%, MS (EI) 459.2 (M).

Compound 7

Yield 86 mg, 35%; ¹H NMR (403 MHz, CDCl₃) δ 7.32 (s, 1H), 7.28 (d, *J* = 3.0 Hz, 1H), 7.26 (s, 1H), 7.05 (d, *J* = 10.5 Hz, 1H), 6.55 (s, 1H), 5.24 (s, 1H), 4.82–4.70 (m, 1H), 4.43 (dt, *J* = 11.8, 6.8 Hz, 1H), 3.94 (s, 3H), 3.91 (s, 3H), 3.64 (s, 3H), 2.65–2.48 (m, 1H), 2.44 (s, 3H), 2.33–2.23 (m, *J* = 19.4, 12.6, 6.5 Hz, 1H), 2.07–1.98 (m, 1H), 1.86–1.70 (m, 1H), 1.21–1.08 (m, 6H); ¹³C NMR (101 MHz, CDCl₃) δ 182.4, 158.2, 154.9, 153.5, 151.1, 150.5, 141.6, 137.6, 134.4, 134.3, 128.7, 126.2, 125.6, 107.2, 68.5, 61.4, 61.3, 56.0, 53.4, 37.3, 29.9, 22.1, 22.0, 15.1; FT-IR (KBr pellet, *v*_{max}, cm⁻¹) 3243, 2935, 1711, 1608, 1525, 1486, 1439, 1407, 1379, 1346, 1317, 1256, 1139, 1119, 1095, 1027; Anal. calcd. (%) for C₂₄H₂₉NO₆S: C 62.73; H 6.36; N 3.05; S 6.98, Found C 62.67; H 6.44; N 3.15; S 6.78, MS (EI) *m/z* 459.3 (M).

Compound 8

Yield 169 mg, 67%; ¹H NMR (403 MHz, CDCl₃) δ 7.38 (s, 1H), 7.29 (d, *J* = 1.1 Hz, 1H), 7.27 (s, 1H), 7.06 (d, *J* = 10.4 Hz, 1H), 6.55 (s, 1H), 5.68 (s, 1H), 4.43 (dt, *J* = 25.3, 9.5 Hz, 1H), 3.94 (s, 3H), 3.91 (s, 3H), 3.64 (s, 3H), 2.53 (d, *J* = 6.1 Hz, 1H), 2.44 (s, 3H), 2.30 (ddd, *J* = 19.0, 12.4, 6.2 Hz, 1H), 2.05–1.75 (m, 2H), 1.82 (dd, *J* = 17.7, 11.4 Hz, 1H), 1.53–1.44 (m, 2H), 1.35–1.24 (m, 2H), 0.87 (t, *J* = 7.3 Hz, 3H); ¹³C NMR (101 MHz, CDCl₃) δ 182.4, 158.2, 155.6, 153.5, 151.0, 150.7, 141.5, 137.7, 134.4, 134.3, 128.7, 126.2, 125.5, 107.2, 64.9, 61.4, 61.3, 56.0, 53.5, 37.1, 30.7, 29.8, 18.9, 15.0, 13.6; FT-IR (KBr pellet, *v*_{max}, cm⁻¹) 3308, 2934, 1715, 1607, 1546, 1486, 1404, 1349, 1322, 1247, 1137, 1095, 1021 Anal. calcd. (%) for C₂₅H₃₁NO₆S: C 63.40; H 6.60; N 2.96; S 6.77, Found C 63.29; H 6.68; N 2.98; S 6.65, MS (EI) *m/z* 473.2 (M).

Compound 9

Yield 222 mg, 90%; ^1H NMR (403 MHz, CDCl_3) δ 7.46 (s, 1H), 7.31 (d, 1H), 7.28 (s, 1H), 6.65 (d, $J=7.3$ Hz, 1H), 6.56 (s, 1H), 4.40 (dt, 1H), 4.13–4.01 (m, 2H), 3.94 (s, 3H), 3.91 (s, 3H), 3.63 (s, 3H), 3.36 (s, 1H), 2.61–2.49 (m, 1H), 2.44 (s, 3H), 2.35–2.24 (m, $J=18.9, 6.1$ Hz, 1H), 1.96–1.86 (m, 1H); ^{13}C NMR (101 MHz, CDCl_3) δ 182.5, 158.2, 155.9, 153.6, 151.3, 151.0, 141.5, 138.2, 134.7, 134.4, 128.7, 126.7, 125.5, 107.3, 66.8, 61.4, 61.3, 61.0, 56.0, 53.8, 36.8, 29.9, 15.1; FT-IR (KBr pellet, ν_{max} , cm^{-1}) 3314, 2936, 1715, 1606, 1540, 1486, 1404, 1349, 1322, 1238, 1195, 1137, 1095, 1021; Anal. calcd. (%) for $\text{C}_{23}\text{H}_{27}\text{NO}_7\text{S}$: C 59.85; H 5.90; N 3.03; S 6.95, Found C 59.77; H 5.99; N 2.98; S 6.79, MS (EI) m/z 461.2.

Compound 10

Yield 119 mg, 44%; ^1H NMR (403 MHz, CDCl_3) δ 7.36 (s, 1H), 7.29 (d, $J=10.5$ Hz, 1H), 7.27 (s, 1H), 7.07 (d, $J=10.5$ Hz, 1H), 6.55 (s, 1H), 5.85 (s, 1H), 4.40 (dt, 1H), 4.30–4.15 (m, 2H), 4.16–4.02 (m, 2H), 3.94 (s, 3H), 3.91 (s, 3H), 3.74 (d, $J=4.4$ Hz, 2H), 3.63 (s, 3H), 3.60–3.56 (m, 2H), 3.57 (s, 1H), 2.57–2.51 (m, 1H), 2.44 (s, 3H), 2.33–2.24 (m, 1H), 1.85–1.76 (m, 1H); ^{13}C NMR (101 MHz, CDCl_3) δ 182.4, 158.4, 155.3, 153.6, 151.1, 150.7, 141.6, 137.8, 134.7, 134.3, 128.5, 126.4, 125.5, 107.3, 72.4, 69.1, 64.1, 61.5, 61.4, 61.3, 56.1, 53.7, 36.9, 29.8, 15.1; FT-IR (KBr pellet, ν_{max} , cm^{-1}) 3312, 2934, 1716, 1606, 1543, 1486, 1459, 1404, 1349, 1322, 1252, 1137, 1095, 1021; Anal. calcd. (%) for $\text{C}_{25}\text{H}_{31}\text{NO}_8\text{S}$: C 59.39; H 6.18; N 2.77; S 6.34, Found C 59.44; H 6.07; N 2.67; S 6.15 MS (EI) m/z 505.3 (M).

Compound 11

Yield 235 mg, 78%; ^1H NMR (403 MHz, CDCl_3) δ 7.34 (s, 1H), 7.27 (d, $J=9.8$ Hz, 1H), 7.26 (s, 1H), 7.06 (d, $J=10.6$ Hz, 1H), 6.57 (d, $J=14.6$ Hz, 1H), 6.12 (s, 1H), 4.40 (dt, $J=13.3, 6.8$ Hz, 1H), 4.16 (dt, $J=11.8, 4.2$ Hz, 2H), 4.20–4.00 (m,

2H), 3.94 (s, 3H), 3.92 (d, $J=4.6$ Hz, 4H), 3.91 (s, 3H), 3.81–3.73 (m, 2H), 3.70–3.67 (m, 2H), 3.65–3.65 (m, 1H), 3.63 (s, 3H), 2.57–2.49 (m, 1H), 2.44 (s, 3H), 2.32–2.21 (m, 1H), 1.84–1.77 (m, $J=11.6, 5.2$ Hz, 1H); ^{13}C NMR (101 MHz, CDCl_3) δ 182.4, 158.2, 155.3, 153.5, 151.0, 150.6, 141.5, 137.7, 134.5, 134.3, 128.6, 126.3, 125.5, 107.2, 72.3, 70.4, 70.0, 69.2, 63.9, 61.5, 61.4, 61.3, 56.0, 53.6, 36.9, 29.8, 15.1; FT-IR (KBr pellet, ν_{max} , cm^{-1}) 3312, 2934, 1716, 1606, 1543, 1486, 1459, 1404, 1349, 1322, 1252, 1137, 1095, 1021; Anal. calcd. (%) for $\text{C}_{27}\text{H}_{35}\text{NO}_9\text{S}$: C 59.00; H 6.42; N 2.55; S 5.83, Found C 59.18; H 6.36; N 2.64; S 5.65, MS (EI) m/z 549.0 (M).

Compound 12

Yield 111 mg, 41%; ^1H NMR (403 MHz, CDCl_3) δ 7.30 (s, 1H), 7.27 (d, $J=2.6$ Hz, 1H), 7.25 (s, 1H), 7.04 (d, $J=10.7$ Hz, 1H), 6.54 (s, 1H), 5.37 (s, 1H), 4.41 (dt, $J=11.7, 6.7$ Hz, 1H), 4.18–4.07 (m, 2H), 3.94 (s, $J=2.0$ Hz, 3H), 3.92 (s, 1H), 3.91 (s, 3H), 3.63 (s, 3H), 3.56 (ddd, $J=8.9, 5.4, 3.3$ Hz, 2H), 3.53–3.48 (m, 2H), 2.60–2.48 (m, $J=13.6, 5.9$ Hz, 1H), 2.43 (s, $J=4.1$ Hz, 3H), 2.31–2.23 (m, 1H), 1.80–1.73 (m, $J=12.1, 6.5$ Hz, 1H), 1.21 (t, $J=7.0$ Hz, 2H); ^{13}C NMR (101 MHz, CDCl_3) δ 182.4, 158.3, 155.1, 153.5, 151.1, 150.2, 141.6, 137.5, 134.5, 134.2, 128.7, 126.2, 125.6, 107.3, 68.5, 66.6, 64.4, 61.4, 61.4, 56.1, 53.6, 37.2, 29.8, 15.1, 15.0; FT-IR (KBr pellet, ν_{max} , cm^{-1}) 3310, 2932, 1718, 1607, 1548, 1486, 1459, 1404, 1349, 1322, 1285, 1248, 1195, 1137, 1095, 1068, 1022; Anal. calcd. (%) for $\text{C}_{25}\text{H}_{31}\text{NO}_7\text{S}$: C 61.33; H 6.38; N 2.86; S 6.55, Found C 61.27; H 6.48; N 2.76; S 6.51, MS (EI) m/z 489.2 (M).

Compound 13

Yield 145 mg, 52%; ^1H NMR (403 MHz, CDCl_3) δ 7.29 (s, 1H), 7.27 (d, $J=2.6$ Hz, 1H), 7.25 (s, 1H), 7.04 (d, $J=10.7$ Hz, 1H), 6.54 (s, 1H), 5.33 (d, $J=7.3$ Hz, 1H), 4.42 (dt, $J=11.8, 6.8$ Hz, 1H), 4.18 (dd, $J=6.8, 5.1$ Hz, 2H), 4.15–4.08 (m, 2H), 3.94 (s, 3H), 3.91 (s, 3H), 3.63 (s, 3H), 3.62–3.59 (m, 2H), 3.55 (td, $J=4.0, 1.9$ Hz, 2H),

3.38 (s, 3H), 2.58–2.50 (m, 1H), 2.43 (s, 3H), 2.32–2.24 (m, 1H), 1.79–1.72 (m, 1H); ^{13}C NMR (101 MHz, CDCl_3) δ 182.4, 158.3, 155.1, 153.5, 151.1, 150.1, 141.6, 137.5, 134.5, 134.2, 128.7, 126.1, 125.6, 107.3, 71.8, 70.4, 69.4, 64.2, 61.4, 61.4, 59.0, 56.1, 53.6, 37.2, 29.7, 15.1; FT-IR (KBr pellet, ν_{max} , cm^{-1}) 3303, 2920, 1718, 1608, 1551, 1485, 1404, 1349, 1322, 1247, 1195, 1137, 1095, 1021; Anal. calcd. (%) for $\text{C}_{26}\text{H}_{33}\text{NO}_8\text{S}$: C 60.10; H 6.40; N 2.70; S 6.17, Found C 60.28; H 6.58; N 2.61; S 6.00, MS (EI) m/z 519.2 (M).

Compound 14

Yield 115 mg, 43%; ^1H NMR (403 MHz, CDCl_3) δ 7.47 (s, 1H), 7.30 (s, $J=10.4$ Hz, 1H), 7.28 (s, 1H), 7.10 (d, $J=10.6$ Hz, 1H), 6.62 (d, $J=4.9$ Hz, 1H), 6.57 (s, 1H), 4.47 (dt, $J=4.0$ Hz, 2H), 3.95 (s, 3H), 3.92 (s, 3H), 3.62 (s, 3H), 3.59 (s, 1H), 2.55 (s, 1H), 2.45 (s, 3H), 2.05–2.01 (m, 1H), 1.89 (s, 1H); ^{13}C NMR (101 MHz, CDCl_3) δ 182.4, 158.6, 153.6, 153.6, 151.0, 150.3, 141.6, 137.7, 134.8, 134.3, 128.8, 126.5, 125.4, 107.3, 61.3, 61.2, 60.9, 60.6, 56.0, 54.1, 36.9, 29.8, 15.1; FT-IR (KBr pellet, ν_{max} , cm^{-1}) 3314.3, 2938, 1740, 1608, 1546, 1486, 1350, 1322, 1237, 1163, 1097, 1022; Anal. calcd. (%) for $\text{C}_{23}\text{H}_{24}\text{F}_3\text{NO}_6\text{S}$: C 55.30; H 4.84; N 2.80; S 6.42, Found C 55.15; H 4.98; N 2.80; S 6.14, MS (EI) m/z 499.1 (M).

The ^1H , ^{13}C NMR, FT-IR and EI MS spectra all tested compounds are included in Appendix E (Figures E1–E13).

6.1.3 Antiproliferative activity of colchicine and its derivatives

A549, MCF-7 cell lines were obtained from the European Collection of Authenticated Cell Cultures (ECACC, Salisbury, UK), LoVo and BALB/3T3 were obtained from the American Type Culture Collection (ATCC, Manassas VA, USA), and LoVo/DX cells were a gift from Prof. Borowski from Gdańsk University of Technology, Poland. A549 and LoVo cells were cultured in OptiMEM + RPMI (1:1) medium (PChO IIET PAS, Wrocław, Poland) supplemented with 5% fetal bovine serum (FBS) (GE

Healthcare, Logan UT, USA), 2 mM l-glutamine (Sigma-Aldrich, Steinheim, Germany) and for LoVo cell lines also with 1 mM sodium pyruvate (Sigma-Aldrich, Steinheim, Germany). Medium for LoVo/DX contained additionally 10 µg/100 ml doxorubicin hydrochloride (Accord Healthcare Poland, Warsaw, Poland). MCF-7 cells were grown in Eagle medium (PChO IIET PAS, Wroclaw, Poland) supplemented with 10% FBS, 2 mM l-glutamine, 1% amino acids, 8 µg/mL insulin (Sigma-Aldrich, Steinheim, Germany). BALB/3T3 cells were cultured in DMEM (Gibco, Paisley, UK) medium supplemented with 10% FBS (GE Healthcare, Logan UT, USA), 2 mM l-Glutamine (Sigma-Aldrich, Steinheim, Germany). All culture media contained antibiotics: 100 U/mL penicillin and 100 µg/mL streptomycin (Polfa Tarchomin, Warsaw, Poland and Sigma-Aldrich, Steinheim, Germany respectively). 24 h before addition of a tested compound, the cells were seeded in 96-well plates in respective culture media. Next, the compounds were dissolved in DMSO (Avantor, Gliwice, Poland) and serially diluted in culture medium in the range of 100–0.1 µg/mL and added to tested cells for 72 h. The proliferation inhibition was measured by means of sulforhodamine B (SRB) assay: cells were fixed and permeabilized with 50% cold trichloroacetic acid (Avantor, Gliwice, Poland) for 1 h, next were washed with tap water, stained with 0.1% SRB (Sigma-Aldrich, Steinheim, Germany) in 1% acetic acid (Avantor, Gliwice, Poland) for 30 min, followed with washing of unbound dye with the use of 1% acetic acid. Following, SRB was extracted from cells with 10 mM TRIS (tris(hydroxymethyl)aminomethane) (Sigma-Aldrich, Steinheim, Germany) and the absorbance of resulting solution was measured at 540 nm wavelength in universal plate reader Synergy H4 (BioTek Instruments, Winooski VT, USA). The results were calculated as an IC₅₀ – the concentration of tested agent, which inhibits proliferation of 50% of the cancer cells, using Cheburator 0.4, Dmitry Nevozhay software [Nevozhay D: Cheburator Software for Automatically Calculating Drug Inhibitory Concentrations from *In vitro* Screening Assays. Plos One 2014, 9(9):10.]. Cells were also exposed to solvent DMSO in the same serial dilutions as with the tested agents, and to cisplatin and doxorubicin hydrochloride

used as reference drugs (Accord Healthcare Poland, Warsaw, Poland). Experiments were repeated at least three times in separate tests.

6.1.4 Molecular docking simulations

3D structures of thiocolchicine and its 13 derivatives (shown in Figure 6-1) were docked into the colchicine binding site of β I tubulin using the Autodock4.2 program under flexible ligand and rigid receptor conditions. AutoDock4 is designed to predict how drug candidates bind to a receptor of a known 3D structure and consists of two main programs: (a) autodock which performs the docking of the ligand to a set of grids describing the target protein; (b) autogrid which pre-calculates these grids. The initial structures of ligands were first minimized using the Amber12: EHT force field (in MOE2013.0802). Single point energies were calculated in RHF/cc-pVDZ [21] level of theory for those structures and then, they were fully optimized on RHF/RM1 [22] level of theory in GAMESS-US version 2010-10-01 [23-25]. β I Tubulin sequence data (TBB5_HUMAN) were obtained from UniProt ID and a homology model was constructed for β I tubulin on the basis of the bovine tubulin structure in RCSB Protein Data Bank (1SA0.pdb) by MOE2013.0802.

6.1.5 Flow cytometry and immunofluorescence microscopy

Cell cultures

Human MCF-7 mammary gland adenocarcinoma cells were cultured in Eagle's Minimum Essential Medium (EMEM) (30-2003, ATCC, USA) supplemented with 10% (v/v) heat-inactivated fetal bovine serum (FBS) (FP-0500-A, Atlas Biologicals, USA), and 1% Penicillin/Streptomycin Solution 100 \times (30-002-C1, Corning, USA). MCF-7 cell line was tested *via* STR profiling in July 2018 by Genetica DNA Laboratories (a LabCorp brand; Burlington, NC); and verified as authentic by using a 100% match when compared to the known reference profile [26].

Human HeLa cell line was cultured in Dulbecco's Modified Eagle Medium (DMEM) (11995-065, Gibco) supplemented with 10% (v/v) heat-inactivated fetal bovine serum (FBS) (FP-0500-A, Atlas Biologicals, USA), and 1% Penicillin/Streptomycin Solution 100× (30-002-C1, Corning, USA).

6.1.6 Effects of the compounds on cell cycle progression

In order to determine the effect of compounds **1-6** and **14** on cell cycle progression, MCF-7 cells were grown for 48 h (one cell cycle) in 6-well plates (92006, TPP, Switzerland) (0.4×10^6 cells/well) in the absence of the drug studied. After 48 h, cells were treated with 0.1% DMSO (vehicle) or compounds **1-6**, **14** at concentrations equal to $10 \times IC_{50}$ values determined *via* cell viability assay on MCF-7 cell line (Table 6-1) for 24, 48 and 72 h in triplicate ($n = 3$) at 37°C in a humidified 5% CO₂ incubator. Cells were then washed with 1 ml phosphate-buffer saline (PBS) (Corning, USA), trypsinized with 1 ml of 0.05% trypsin (25-052-C1, Corning, USA), fixed with 3 ml of 70% ice-cold ethanol and stored at 4°C prior to flow cytometric analysis. In the next step, cells were centrifuged, treated with 400 µL propidium iodide/RNase Staining buffer (BD Biosciences, San Jose, CA, USA) and stored in the dark for 1 h at RT according to our previously published protocol [27,28]. The stained cells were analyzed by FacsAria IIIu Flow Cytometer (BD Biosciences, San Jose, CA, USA) using FlowJo software to determine DNA content.

Table 6-1. Antiproliferative activity (IC_{50}) [μ M] of **1** and its derivatives **2–14** compared with that of standard anticancer drugs doxorubicin and cisplatin. The calculated values of the

Compound	MCF-7	LoVo	LoVo/DX	<i>RI</i>	A-549	BALB/3T3
	$IC_{50} \pm SD$	$IC_{50} \pm SD$	$IC_{50} \pm SD$		$IC_{50} \pm SD$	$IC_{50} \pm SD$
1	0.012 ± 0.002	0.201 ± 0.113	1.566 ± 0.454	7.8	0.103 ± 0.015	0.195 ± 0.025
2	0.010 ± 0.002	0.021 ± 0.006	0.398 ± 0.075	19.0	0.011 ± 0.001	0.114 ± 0.072
3	0.014 ± 0.002	0.017 ± 0.004	0.145 ± 0.021	8.6	0.024 ± 0.003	0.223 ± 0.032
4	0.009 ± 0.001	0.010 ± 0.003	0.063 ± 0.012	6.3	0.010 ± 0.001	0.016 ± 0.001
5	0.008 ± 0.003	0.011 ± 0.005	0.065 ± 0.009	6.2	0.010 ± 0.001	0.017 ± 0.001
6	0.009 ± 0.000	0.011 ± 0.002	0.063 ± 0.007	5.8	0.009 ± 0.001	0.043 ± 0.036
7	0.009 ± 0.001	0.014 ± 0.005	0.098 ± 0.026	7.1	0.009 ± 0.001	0.153 ± 0.035
8	0.009 ± 0.001	0.011 ± 0.003	0.068 ± 0.002	6.0	0.009 ± 0.001	0.031 ± 0.022
9	0.010 ± 0.001	0.191 ± 0.158	1.555 ± 0.386	8.1	0.080 ± 0.007	0.197 ± 0.022
10	0.010 ± 0.001	1.107 ± 0.907	8.079 ± 1.788	7.3	0.085 ± 0.008	0.156 ± 0.022
11	0.069 ± 0.011	2.754 ± 2.058	18.816 ± 3.262	6.8	0.158 ± 0.038	1.441 ± 0.251
12	0.009 ± 0.001	0.042 ± 0.012	0.562 ± 0.141	13.3	0.012 ± 0.002	0.139 ± 0.001
13	0.010 ± 0.002	0.250 ± 0.135	2.987 ± 1.062	11.9	0.083 ± 0.008	0.135 ± 0.001
14	0.009 ± 0.001	0.011 ± 0.006	0.064 ± 0.014	6.0	0.008 ± 0.001	0.110 ± 0.064
Cisplatin	10.700 ± 0.753	3.767 ± 0.390	3.033 ± 0.637	0.8	6.367 ± 1.413	8.600 ± 2.923
Doxorubicin	0.386 ± 0.118	0.681 ± 0.633	8.187 ± 1.409	12.0	0.258 ± 0.044	1.012 ± 0.868

resistance index (*RI*) for LoVo/DX versus LoVo cells are also shown.

The IC_{50} value is defined as the concentration at which 50% growth inhibition is observed. The following cell lines were used: human lung adenocarcinoma (A549), human breast adenocarcinoma (MCF-7), human colon adenocarcinoma (LoVo) and doxorubicin resistant subline (LoVo/DX), normal murine embryonic fibroblast (BALB/3T3).

The RI (Resistance Index) indicates fold-resistance relative to parental cell line. The RI was calculated for each compound using the formula: $RI = IC_{50} \text{ for LoVoDX} / IC_{50} \text{ for LoVo}$ cell line. $RI < 1$, MDR cells are more sensitive; $RI = 1-2$, no or very low level of resistance; $RI = 2-10$, moderate resistance; $RI > 10$, strong drug-resistance.

6.1.7 Statistical analysis

Unpaired *t* test with Welch's correction was performed for the significance and *p* values of <0.05 were considered significant.

6.1.8 Immunofluorescence microscopy

MCF-7 (0.4×10^6 cells/dish) or HeLa (0.2×10^6 cells/dish) cells were seeded on cover slips in 10 mm diameter tissue culture dishes (353001, Falcon) and cultured for 48 h (MCF-7) or 24 h (HeLa) at 37°C in a humidified 5% CO₂ incubator before adding compounds. In order to prevent contamination, cover slips and dishes were sterilized under UV light for 1 h before seeding cells. After pre-incubation, the medium was replaced and the cells were treated with either 0.1% DMSO (vehicle), 100 nM vincristine (positive control) or compounds **1** (120 nM) or **5** (80 nM) (concentrations equal to $10 \times IC_{50}$ values determined *via* cell viability assay on MCF-7 cell line, Table 6-1). The experiment was performed in duplicate. After 12 h incubation the cells were fixed with ice-cold methanol, permeabilized with 5% bovine serum albumin (BSA), 0.2% Triton X-100, 0.00125% sodium azide in PBS. Cells were stained with β -tubulin antibody (T-4026, Sigma) (1:300) and Cy-5 conjugated AffinPure Donkey anti-mouse secondary antibody (715-175-150, Jackson ImmunoResearch Laboratories), diluted 1:100. Cells were visualized using a Zeiss LSM410 confocal microscope.

6.2 Results and discussion

6.2.1 Chemistry

Syntheses of the designed colchicine derivatives coupled to **3**, with the structurally different urethane moiety, were followed by investigation of their biological effects. The synthetic route to the novel compounds encompassed two traditional synthetic modifications and a new type of chemical modification, which is depicted in Figure 6-1. The first two steps of this synthesis are well described in literature. The first step was the preparation of thiocolchicine from the starting material (colchicine) according to the reported procedure [29]. Thiocolchicine (**2**) (see Figure 6-1) has been readily available from colchicine by treatment with sodium methanethiolate [29], and is a potent inhibitor of tubulin polymerization resulting in the arrest of cell growth and cell

division. Notably, thiocolchicine binds to tubulin more rapidly than colchicine [30]. Hydrolysis of **2** with 20% HCl yielded 7-deacetyl-10-thiocolchicine (**3**) [29].

In recent years, much attention has been focused on the synthesis of carbamates using chloroformates as key intermediates. Carbamate synthesis through the chloroformate route has been achieved using various reaction conditions, such as the use of organic and inorganic bases. This method is not adequate for our designed thiocolchicine derivatives because the respective chloroformate are not commercially available and some of them cannot be synthesized [31]. Therefore, we searched for a cleaner and more efficient reaction. After reviewing the available literature, triphosgene [bis(trichloromethyl) carbonate, BTC], a solid and safe surrogate of phosgene [32], appeared as the reagent of choice for preparing carbamates.

Subsequently, our one-pot synthesis of eleven carbamates **4–14** was achieved through the reaction of amine **3** with a respective alcohol using triphosgene as the source of carbonyl equivalent. Carbamates **4–14** (Figure 6-1) were readily prepared from (**3**) and 1 equiv. of triphosgene (3 fold molar excess of phosgene) in THF in the presence of triethylamine (10 equiv.) and then reacted with suitable primary or secondary alcohols (10 equiv.) to provide a respective carbamate **4–14** with good yields in the range 41–90% (Figure 6-1). To facilitate the structural activity relationship analysis (SAR), we chose the primary and secondary alcohol with different substituents such as: saturated alkyl chains (**4–8**), alkyl chains containing additional OH group (**9–11**), alkyl chains containing oxygen atoms (**10–13**), alkyl chains containing fluorine atoms (**14**). All obtained compound were easily isolated in pure form after dry column vacuum chromatography on silica gel.

The structures of all products **2–14** were determined using EI MS, FT-IR, ^1H and ^{13}C NMR methods and are shown in Appendix E and discussed below. The characteristic signal of the OCH_3 group at the C(10) position of (**1**) in the ^{13}C and ^1H NMR spectra was observed at 56.1 ppm and as a singlet at 4.03 ppm, respectively. These signals vanish completely (see spectra of compounds **2–14**) after the reaction of (**1**) with sodium

methanethiolate proving the replacement of OCH₃ group with SCH₃ substitute at C(10) position in the tropolone ring of **1**. The signals of thiomethyl group in C(10) positions in the ¹³C NMR and ¹H NMR spectra of compounds **2–14** are present at 15.1 ppm and approximately 2.45 ppm, respectively. The characteristic ¹³C NMR signals assigned to the carbon atoms in the acetamide group at C(7) position of unmodified **1** are observed at 170.3 ppm, and 22.7 ppm, respectively. These signals are no longer observed in the ¹³C NMR spectrum of compound **3**, which confirms hydrolysis of the acetyl group. The NH₂ group of compound **3** reacts easily with triphosgene and the primary or secondary alcohols giving products **4–14** whose structures are confirmed by the presence of the ¹³C NMR signal assigned to the carbon atom of the urethane group at 153.6–155.9 ppm and additionally by a series of signals assigned to the aliphatic carbon atoms of the alcohol. In the ¹³C NMR spectra of compounds **2–14** a signal assigned to C(7) carbon atom of B ring was observed at 56.0–56.1 ppm, while in the spectrum of **1** it was observed at 52.8 ppm. The EI mass spectrometry confirmed the structure of the obtained compounds by the presence of an *m/z* signal assigned to the molecular ion of these compounds. The products of the chemo-selective one-pot reaction **3** with triphosgene and alcohol were very well identified using also the FT-IR spectroscopic method. The band assigned to the ν(C=O) vibrations (amide I band) of the acetamide group in the spectrum of **2** at 1660 cm⁻¹, vanishes completely in the spectrum of **3**, indicating the absence of acetamide group with the formation of respective amine **3**. The bands assigned to the ν(C=O) vibrations of urethane group in the FT-IR spectra of **4–13** are present in the range of 1710–1727 cm⁻¹. Only for compound **14** was this band shifted toward 1740 cm⁻¹ due to a strong inductive effect in the CH₂CF₃ moiety.

6.2.2 Inhibition of human cancer cell line growth

The synthesized 7-deacetyl-10-thiocolchicine derivatives **4–14** and starting compounds **1–3** were evaluated for their *in vitro* antiproliferative effect towards both

normal and cancer cells. Each compound was tested towards four human cancer cell lines, namely lung adenocarcinoma (A549), breast adenocarcinoma (MCF-7), colon adenocarcinoma cell line (LoVo) and its doxorubicin resistant subline (LoVo/DX). Antiproliferative effects were also studied using a normal murine embryonic fibroblast cell line (BALB/3T3) in order to obtain insight into their selectivity for cancer versus normal cells. IC₅₀ values of the tested compounds are presented in Table 6-1. To evaluate the activity against the cells with MDR (multidrug resistance) phenotype, LoVo/DX cells were also tested and the indices of resistance (RI) were calculated (see Table 6-1). The RI values indicate how many times more resistant is the subline in comparison to its parental cell line.

Most of the obtained urethane derivatives of 7-deacetyl-10-thiocolchicine were more potent, i.e. had lower IC₅₀ values, than unmodified **1**, intermediate compounds **2** and **3**, as well as doxorubicin and cisplatin, currently widely used as antitumor agents in cancer chemotherapy. From the set of tested substances, the most active compounds against MCF-7, LoVo, LoVo/DX and A549 tumor cell lines were **4–8** and **14** (IC₅₀ = 0.009–0.010 μM). Compound (**11**) showed the weakest activity against all cancer cell lines tested.

The calculated values of RI (Table 6-1) showed that the doxorubicin-resistant subline (LoVo/DX) showed various levels of resistance to the parent compound and all of its derivatives, which was consistent with them acting as substrates for MDR1-mediated drug transport. These cells also exhibited resistance to doxorubicin, another MDR1 substrate, but were actually slightly more sensitive to cisplatin than the parental cells (RI = 0.8), which was consistent with cisplatin not acting as a substrate for MDR1-mediated transport [33].

Selectivity index (SI) is a major challenge in drug discovery, because it defines the ability of a particular compound to preferentially kill tumor cells in relation to normal cells. For this purpose, the obtained compounds were tested not only against tumor cells but also against normal murine embryonic fibroblast cell line (BALB/3T3). The best

values of the selectivity index (see Table 6-2) for the tested compounds were obtained towards MCF-7 cells (SI = 1.89–20.81). The best selectivity was observed for compound **7** which also showed high antiproliferative activity against the four tested human cancer cell lines. The preliminary structure-activity relationships (SARs) revealed that the type of substituent at C(7) position in ring B and the presence of SCH₃ group at C(10) position in ring C of colchicine (**1**) were of cardinal importance to the compounds' activity.

The compounds with saturated alkyl chains (**4–8**), and alkyl chains containing fluorine atoms (**14**) displayed more potent antiproliferative activities than those with alkyl chains containing an additional OH group (**9–11**) or alkyl chains containing oxygen atoms (**9–13**). Compounds **7** and **14** with short and branched substituent (isopropyl and trifluoroethyl) show the highest ability to inhibit proliferation of the cancer cell lines tested. Simultaneously, their activities are higher than those of the chemically unmodified colchicine and thiocolchicine as well as doxorubicin and cisplatin, commonly used as antitumor agents in cancer chemotherapy. To summarize these studies, all obtained derivatives have been found active, to varying degrees, in proliferation inhibition in a specified concentration range. Their activities depend on the tested cancer cell line. Compounds **7** and **14** with the best anti-proliferative properties and good selectivity towards cancer cells are promising anticancer candidates.

Table 6-2. Selectivity indexes.

Compound	Calculated selectivity index SI			
	MCF-7	LoVo/Dx	LoVo	A-549
1	16.71	0.12	0.98	1.90
2	11.85	0.29	5.45	10.08
3	15.71	1.54	13.21	9.25
4	1.89	0.26	1.63	1.63
5	2.07	0.26	1.63	1.78
6	4.94	0.68	3.95	4.94
7	16.28	1.56	11.11	16.28
8	3.37	0.45	2.74	3.37
9	19.28	0.13	1.03	2.45
10	15.80	0.02	0.14	1.84
11	20.81	0.08	0.52	9.09
12	15.82	0.25	3.29	11.33
13	13.99	0.05	0.54	1.63
14	11.70	1.72	10.38	13.74
Cisplatin	0.80	2.84	2.28	1.35
Doxorubicin	2.62	0.12	1.49	3.93

The SI (Selectivity Index) was calculated for each compound using the formula: $SI = IC_{50}$ for a normal cell line BALB3T3/ IC_{50} for a respective cancerous cell line. A beneficial SI > 1.0 indicates a drug with efficacy against tumor cells greater than the toxicity against normal cells.

6.2.3 Molecular docking: *in silico* determination of the molecular mode of action

In order to determine the molecular mode of action of the new thiocolchicine derivatives we performed computational modeling aimed at the ligand-protein interaction. As the target protein, we used the most common tubulin isoform, βI tubulin, which is one of the subunits of microtubules. The structures of the new thiocolchicine derivatives described above were docked into the βI tubulin colchicine binding site and ranked according to their binding affinity. More specifically, a combination of different computational methods was used to explore ligand-tubulin interactions. The ligand structures were first minimized and then fully optimized on the basis of the RHF/cc-

pVDZ level of theory in the GAMESS-US software, version 2010-10-01 (<https://www.msg.chem.iastate.edu/gamess/>). Since there is no crystal structure available of human β I tubulin (TBB5_HUMAN), we first obtained its amino acid sequence from UniProt (www.uniprot.org; ID: Q13509). Next, we used the Protein Data Bank (www.rcsb.org) to obtain the tubulin structure 1SA0.pdb as a template to construct a homology model for β I tubulin using the Molecular Operating Environment software (MOE, 2015, www.chemcomp.com). We then docked our thiocolchicine library of derivatives to the target protein using the Autodock 4.2 program (<http://autodock.scripps.edu/>) and applied flexible ligand and rigid receptor conditions. AutoDock 4.2 software is designed to predict how drug candidates bind to a receptor of a known 3D structure, and consists of two main programs: autodock that performs the docking of the ligand to a set of grids describing the target protein and autogrid that pre-calculates these grids.

Binding energies interactions (BE) between the 14 different thiocolchicine derivatives and β I tubulin and the estimated Moriguchi octanol-water partition coefficient, $M \log P$ for each colchicine derivative are shown in Table 6-3. In order to arrive at a structure-function relationship for the series of compounds obtained, we also calculated the molecular weight of each compound and the length of the corresponding aliphatic chain. Most importantly, the binding energy for each compound was determined and we presented graphically the ligand-protein interactions showing the amino acids of the protein and the atomic groups of the ligand that engage in physical and chemical interactions, whose graphical representation is explained in the legend of Table 6-3 where all the computational results are summarized.

It is clear from the results summarized in Table 6-3 that all these compounds show high affinity to the colchicine binding site on β tubulin. It should be mentioned that the values of binding energies are not absolute but relative, to establish a rank order of the compounds. The strongest binding compound is predicted to be **7**, followed closely by **4**, **5**, **6** and **8**. On the other end of the spectrum, compound **11** appears to be

the weakest binder to the target. The most interactive residues seem to be Lys 352, Lys 254, Asn 258, Leu 255, Leu 248, Met 259 and Cys 241 which appear consistently involved in the binding of the thicolchicine derivatives. To a less degree, Asp 251 and Thr 353 also appear to play a role in several cases.

In Figure 6-2 we show the mode of action of the compounds studied in this chapter for the compounds divided into two groups: (a) the ones that bind to tubulin with binding energies of -8 kcal/mol and higher and (b) the ones that bind to tubulin with binding energies lower than -8 kcal/mol.

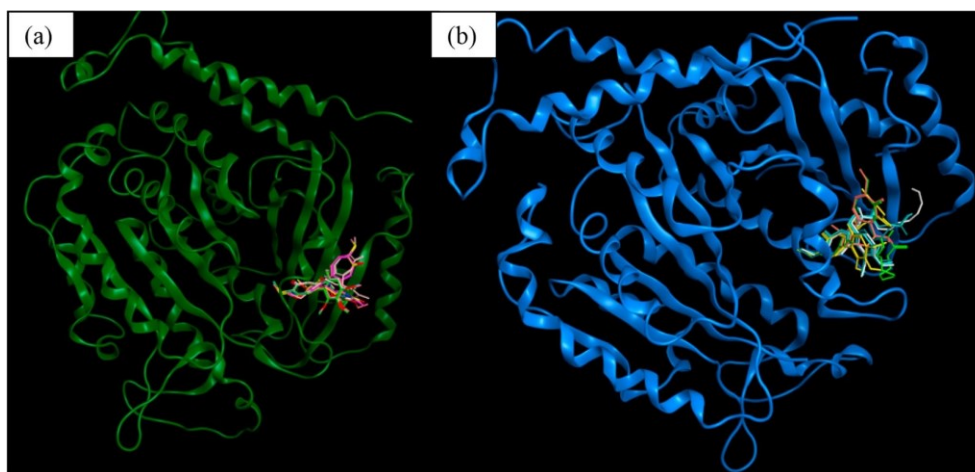
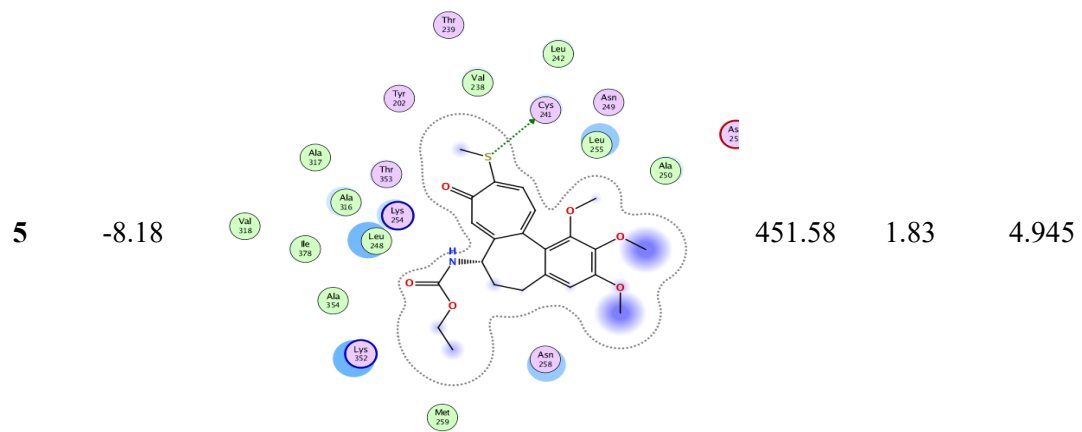
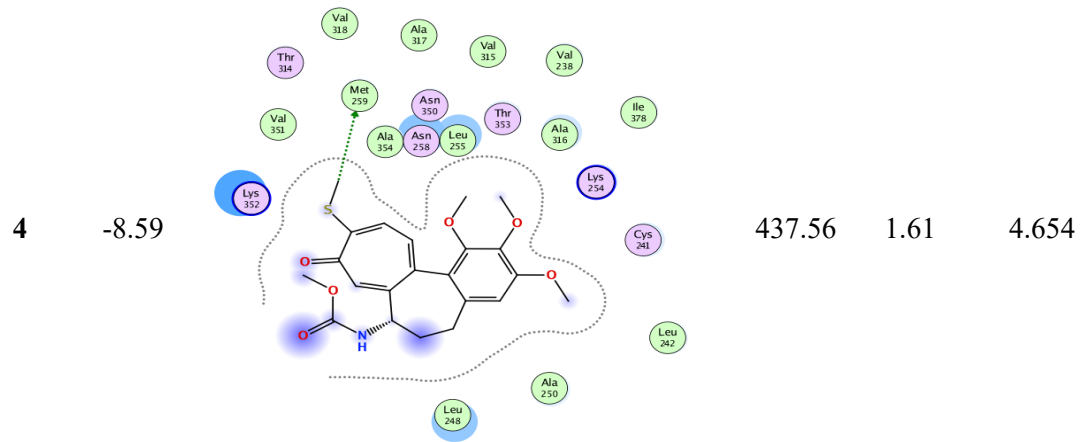
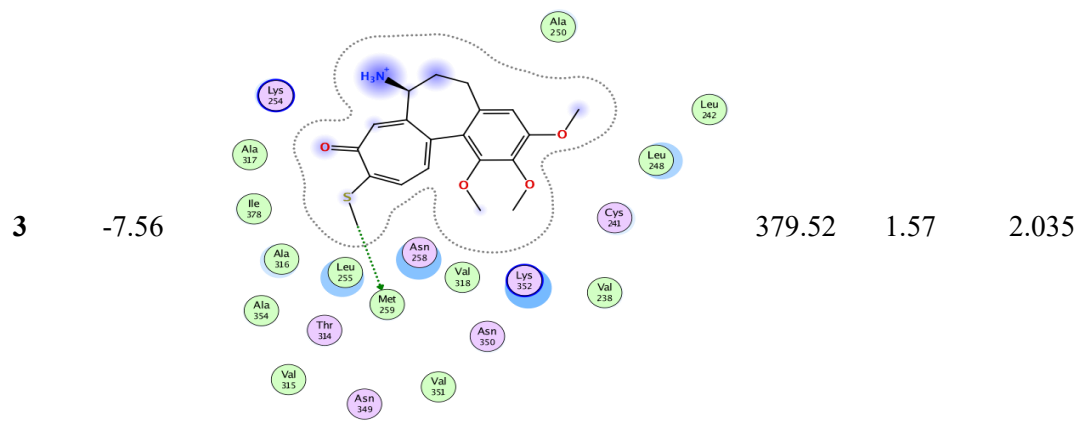


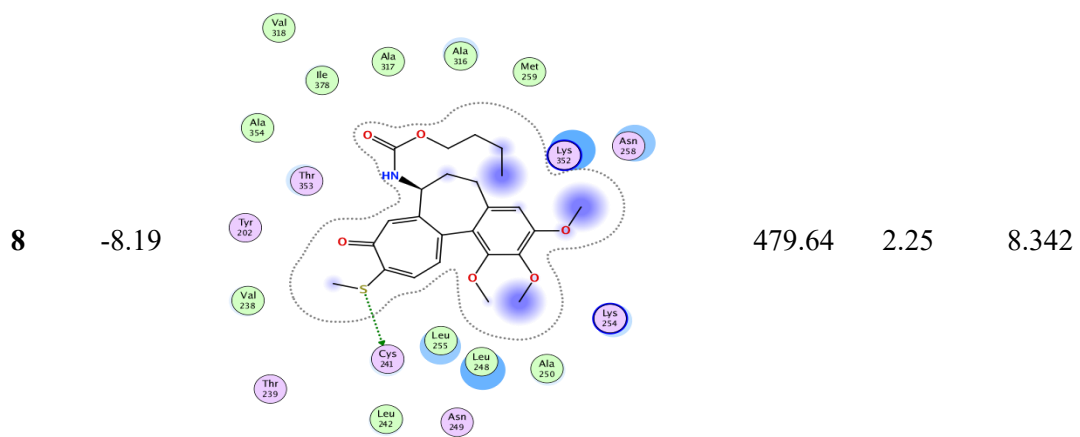
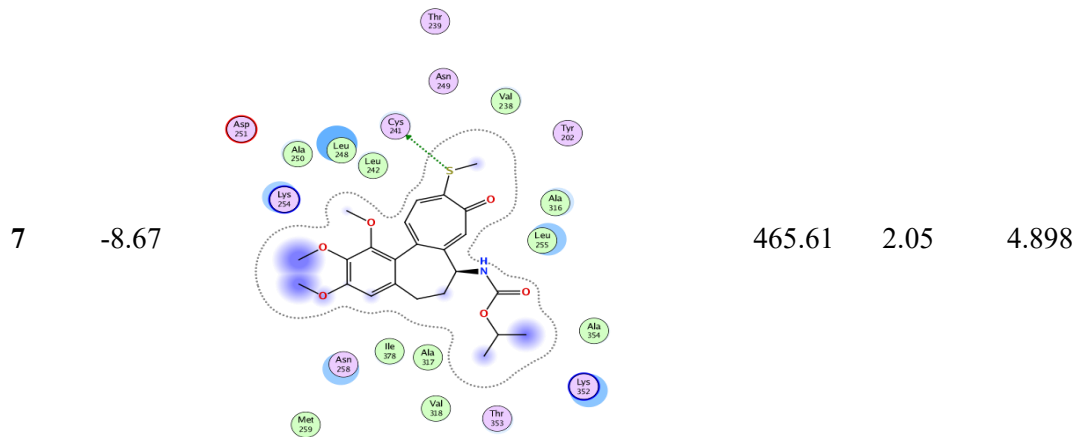
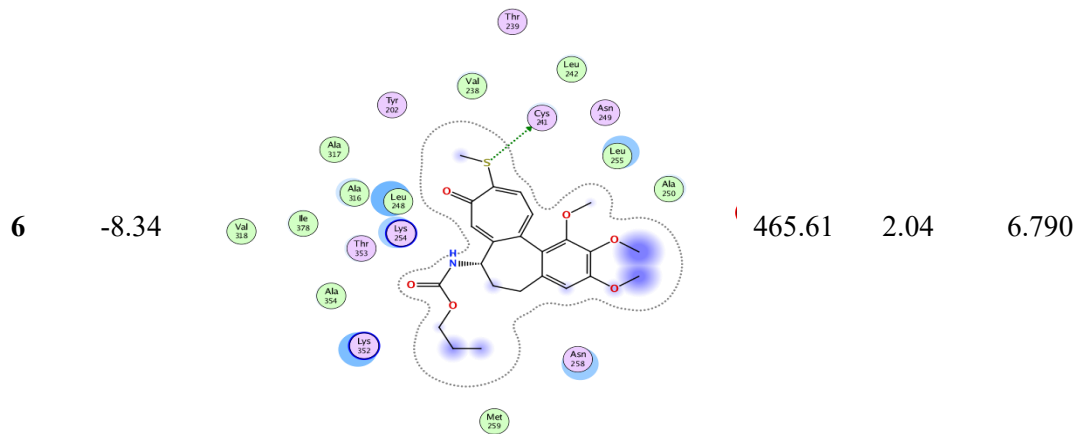
Figure 6-2. Illustration in 3D of the interaction modes of the tubulin β I structure with: (a) 8 thicolchicine derivatives with binding energies of -8 kcal/mol and higher; (b) with 6 thicolchicine derivatives with binding energies lower than -8 kcal/mol.

To better understand the structure-activity relationship for this series of compounds, we performed linear regression analysis with respect to the binding energy (Table 6-3) and $M \log P$ (Table 6-3) versus the experimentally determined values of IC_{50} (Table 6-1). The results of this analysis are shown in Appendix E, Figures E14–E18.

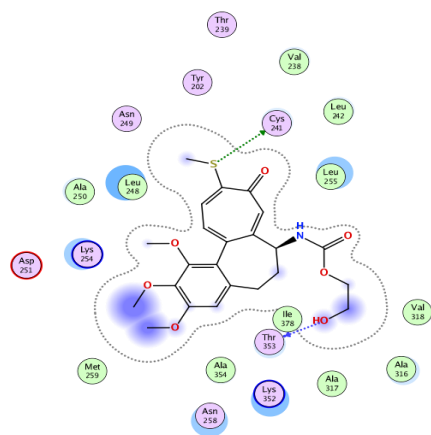
Table 6-3. Computational predictions of the interactions between thiocolchicine derivatives and β I tubulin. Binding energy values in kcal/mol, graphical representation of the ligand-protein interactions, molecular weight, partition coefficient and the length of the aliphatic chains involved are tabulated.

compound	Binding energy (kcal/mol)	Representations of the graphical interactions	MW	MlogP	Length of aliphatic chain
1	-8.09		399.45	1.37	5.841
2	-8.13		421.56	1.56	5.841



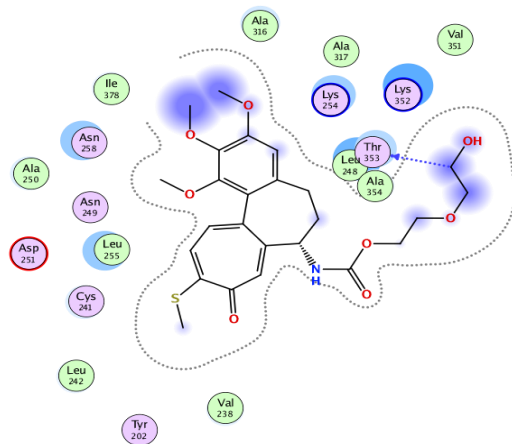


9 -7.91

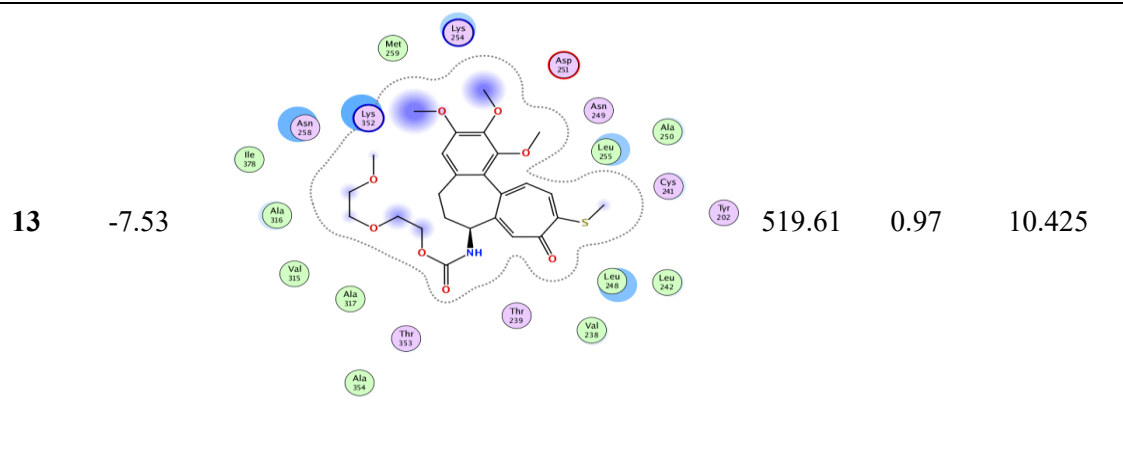
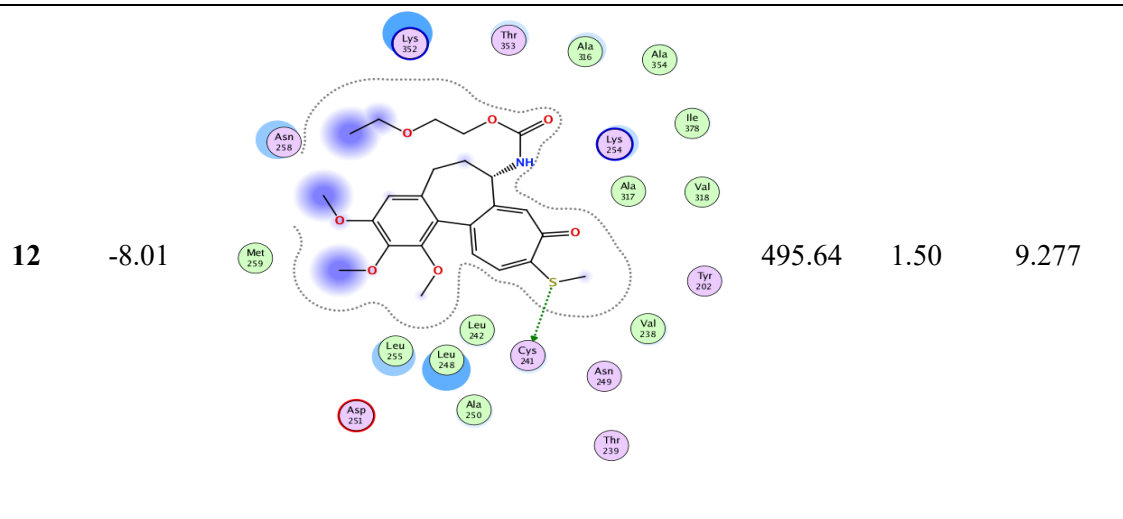
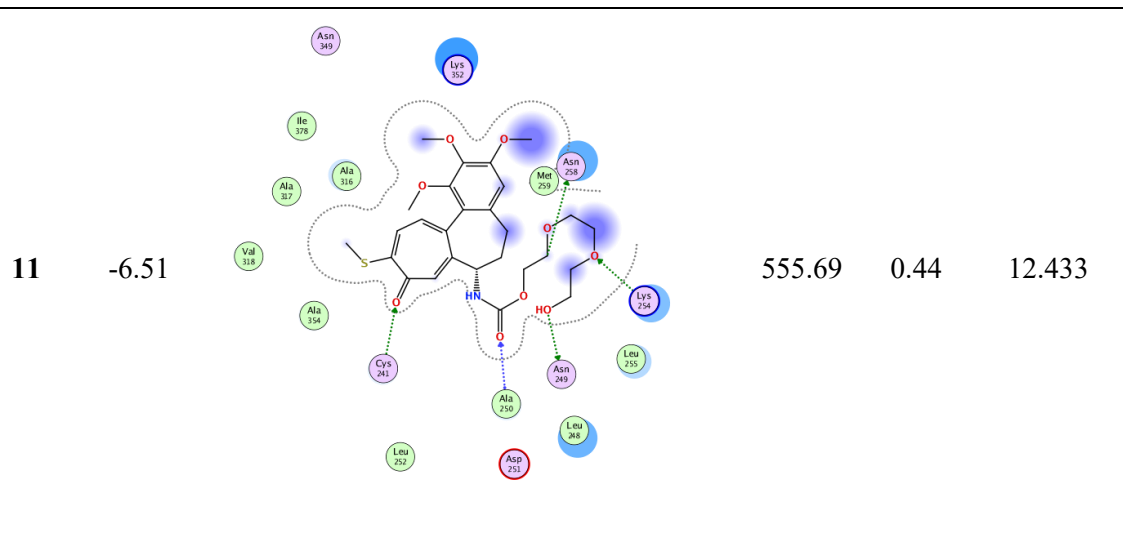


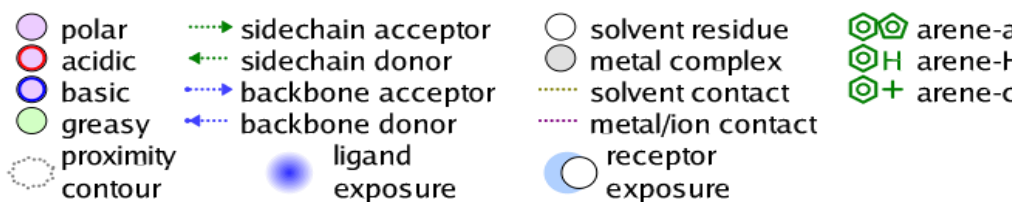
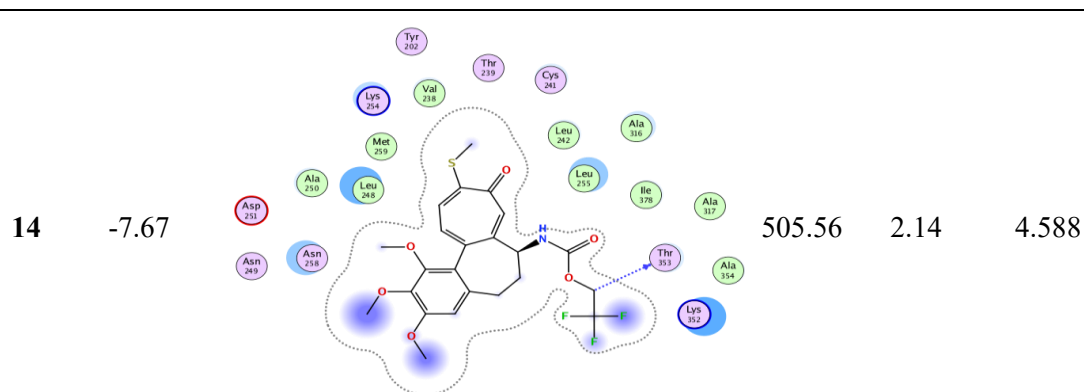
467.58 1.08 6.479

10 -7.36



511.64 0.76 8.645





The 3D plots indicate that there is a reasonable degree of correlation between the experimental activity data in terms of IC_{50} values for the cell lines studied and the computational prediction data expressed as the binding energy and partition coefficient. To quantify these relationships, in Table 6-4 we summarize the linear regression coefficients for these relationships for each cell line separately. The values of the regression coefficient (R^2) range from 0.43 for MCF-7 (which is a very aggressive breast cancer cell line) and 0.88 for LoVo/DX.

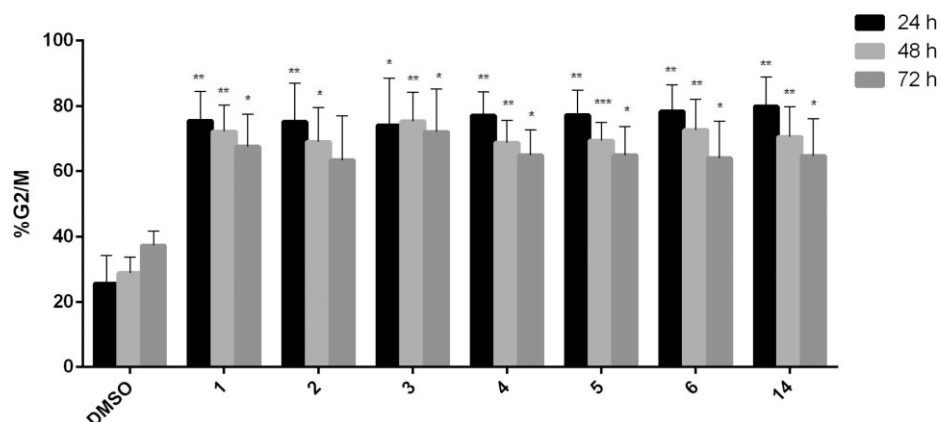


Figure 6-3. Colchicine (**1**), starting compounds (**2–3**) and derivatives (**4–6, 14**) induced G₂/M arrest in MCF-7 cells. MCF-7 cells were treated with the indicated compounds for 24, 48 or 72 h and subjected to propidium iodide staining and flow cytometry. Percent of cells with 4 N DNA (G₂/M phases) was determined (mean ± SD, n = 3). (**p < 0.01, *p < 0.05 vs. control). See Appendix E for a full set of representative data.

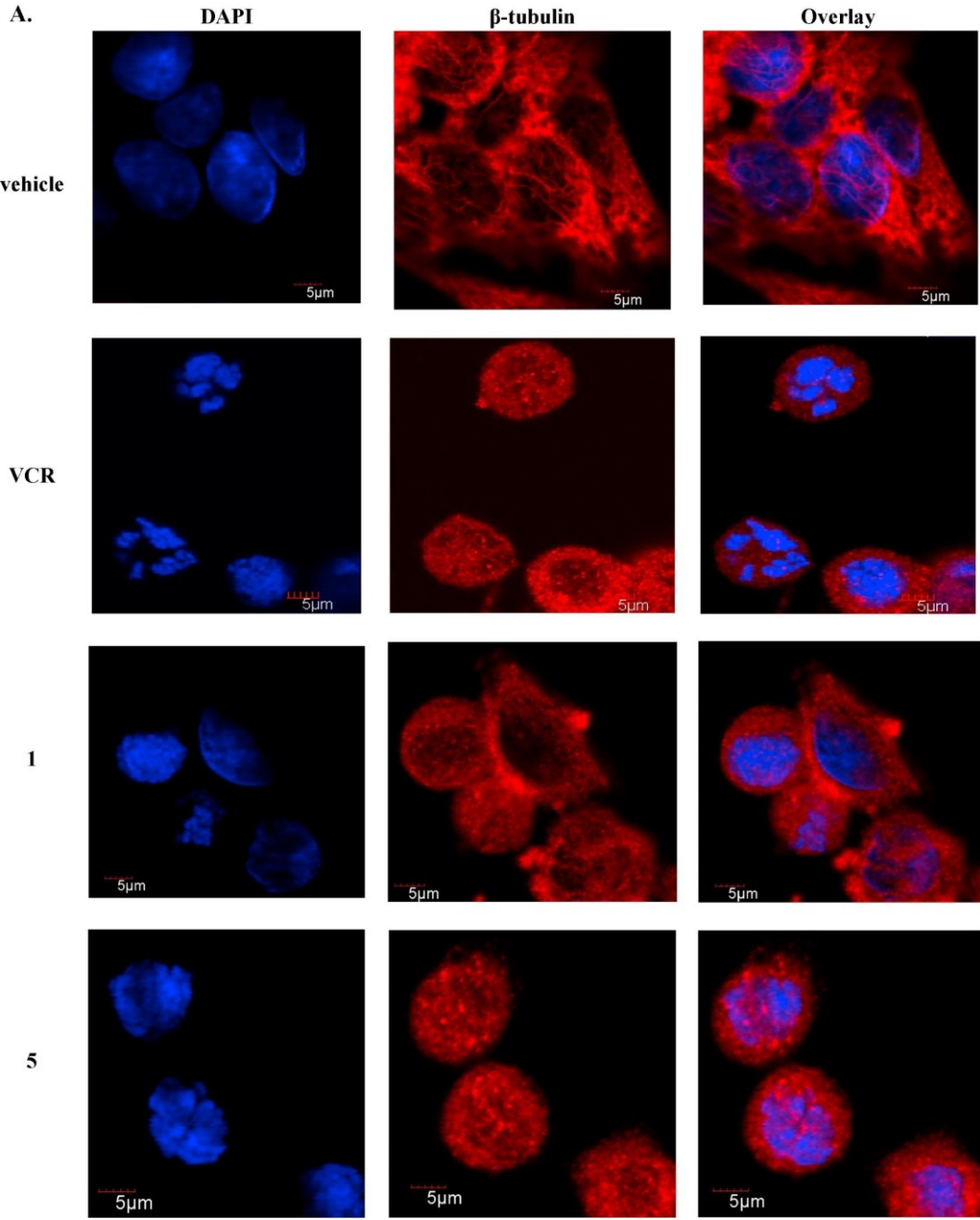
Table 6-4. Linear regressions two independent (binding energy and M log P) and log IC₅₀ [μM].

	MCF-7	LoVo/DX	LoVo	A-549	BALB/3T3
Linear regression (R ²)	0.43	0.88	0.86	0.74	0.55

6.2.4 Colchicine and its analogs induce G₂/M arrest in MCF-7 cells

In order to examine the effect of colchicine **1** and the most potent starting compounds **2–3** and derivatives **4–6** and **14** on the cell cycle progression, flow cytometric cell cycle analysis after propidium iodide staining was performed. MCF-7 cells were treated with 0.1% DMSO (vehicle) or compounds **1–6** and **14** at concentrations equal to 10 × IC₅₀ values determined *via* cell viability assay (Table 6-1) for 24, 48 and 72 h. The full set of representative cytograms is included in (Appendix E, Figure E19). A graphical representation of summarized percentage of cells in G₂/M phase of the cell cycle (n = 3) is shown in Figure 6-3. For all of the compounds studied, statistically significant G₂/M phase arrest was observed as early as 24 h after drug addition, with the level of arrested cells slightly decreasing after further incubation for

48 and 72 h Figure 6-3. The lack of significant sub-G1 DNA even after 72 h (Appendix E) suggests that cell death under these conditions may not involve DNA fragmentation. However, more assays would need to be performed in order to verify this hypothesis.



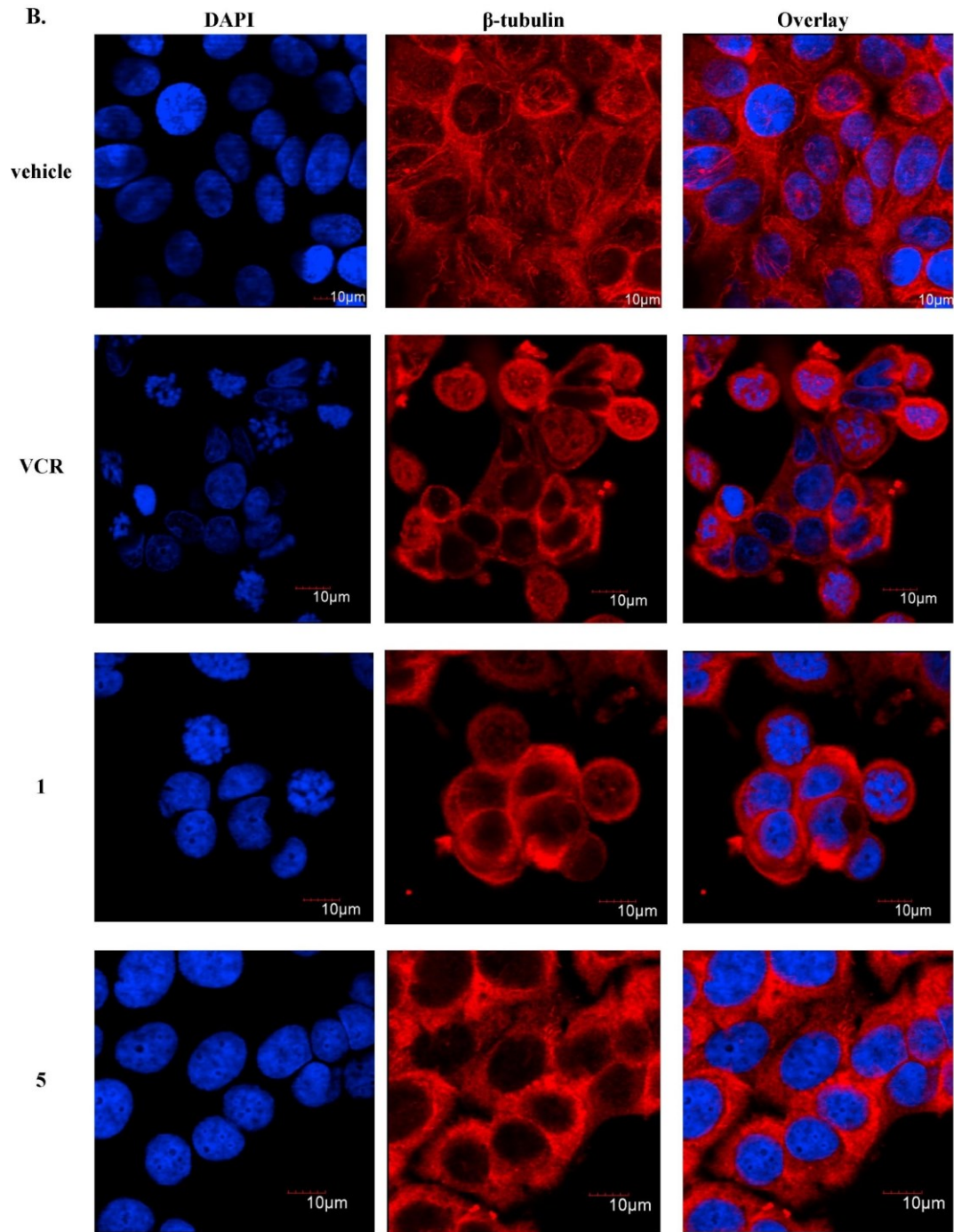


Figure 6-4. Effects of 1 and 5 on microtubule structures in HeLa (A) and MCF-7 (B) cells. HeLa and MCF-7 cells were incubated for 12 h without (vehicle, 0.1% DMSO) or with 1

(120 nM), **5** (80 nM) (concentrations corresponding with $10 \times IC_{50}$ values) or 100 nM VCR (positive control). Bar equals 5 μ m (A) or 10 μ m (B).

6.2.5 Effect of colchicine and compound 5 on microtubule depolymerization

Immunofluorescence staining for β -tubulin in MCF-7 cells was performed to investigate the effect of **1**) and compound **5** (selected based on having the lowest IC_{50} value for MCF-7 cells, Table 6-1) on microtubule integrity. HeLa cells treated with vincristine (VCR) served as a positive control for microtubule depolymerization, as demonstrated previously [34,35]. Untreated MCF-7 and HeLa cells exhibited distinct microtubule structures (Figure 6-4A and B, first row) and as expected after treatment with VCR both cell types exhibited diffuse β -tubulin staining with no detectable microtubules, which was consistent with depolymerization (Figure 6-4A and B, second row). Parent compound **1** and compound **5** also clearly induced microtubule depolymerization, similar to the effects of VCR, in both HeLa and MCF-7 cells (Figure 6-4A and B, third row and fourth row).

6.3 Conclusions

In conclusion, we designed and synthesized a new series of colchicine **1** derivatives based on modification of previously reported tubulin polymerization inhibitors such as thiocolchicine **2**. Compounds **4–14** were prepared from colchicine by an efficient three-step synthetic procedure including synthesis of **2** and its hydrolysis to 7-deacetyl-10-thiocolchicine **3**. Eleven target carbamates of 7-deacetyl-10-thiocolchicine (**4–14**) were obtained using a simple “one-pot reaction” of **3** with eleven different alcohols in the presence of triphosgene. When tested for antiproliferative activity, most of the derivatives were more potent than colchicine. An exception was compound **11**, which had a higher IC_{50} than colchicine against all tested cell lines. In

terms of selectivity for tumor versus normal cells, many of the derivatives were superior to colchicine. Compounds **7** and **14**, for example, were highly selective for three of the four tested cancer cell lines when compared to colchicine (Table 6-2) and were also more potent than colchicine against all cancer cell lines (Table 6-1). Compounds **7** and **14** in particular, therefore represent promising leads for further development. The results also reveal that the nature of the aliphatic chain at the urethane group and the nature of the heteroatom (F better than O) have a marked influence on the antiproliferative activity of the compounds. Generally, we observed also that the introduction of a functionalized alkyl chain in the urethane group, for example by an end-standing hydroxyl group i.e. **9**, **10**, **11**, decreased the anti-proliferative activity and also that long alkyl chain including oxygen atoms **12**, **13** did not improve this activity. Molecular docking was performed and revealed that all of the obtained compounds successfully dock in the colchicine binding site of tubulin. Therefore, these results suggest that carbamates of 7-deacetyl-10-thiocolchicine **4–14** are potential inhibitors of tubulin polymerization. This conclusion was supported by studies on select derivatives whose results showed that they caused mitotic arrest and promoted tubulin depolymerization, as displayed by colchicines [5-10,34]. Finally, these compounds are amenable to further structural modifications and could serve as useful pharmacophore templates for the generation of molecules as potential anticancer agents.

References

- [1] F. Roubille, E. Kritikou, D. Busseuil, S. Barrere-Lemaire, and J.-C. Tardif, “Colchicine: an old wine in a new bottle?,” *Antiinflamm. Antiallergy. Agents Med. Chem.*, vol. 12, no. 1, pp. 14–23, 2013, doi: 10.2174/1871523011312010004.
- [2] G. Cocco, D. C. C. Chu, and S. Pandolfi, “Colchicine in clinical medicine. A guide for internists.,” *Eur. J. Intern. Med.*, vol. 21, no. 6, pp. 503–8, Dec. 2010, doi: 10.1016/j.ejim.2010.09.010.
- [3] G. Sivakumar, “Colchicine semisynthetics: chemotherapeutics for cancer?,” *Curr. Med. Chem.*, vol. 20, no. 7, pp. 892–898, 2013.
- [4] L. Johnson et al., “Novel Colchicine Derivatives and their Anti-cancer Activity.,” *Curr. Top. Med. Chem.*, vol. 17, no. 22, pp. 2538–2558, 2017, doi: 10.2174/1568026617666170104143618.
- [5] A. Kumar, P. R. Sharma, and D. M. Mondhe, “Potential anticancer role of colchicine-based derivatives: an overview.,” *Anticancer. Drugs*, vol. 28, no. 3, pp. 250–262, 2017, doi: 10.1097/CAD.0000000000000464.
- [6] B. Bhattacharyya, D. Panda, S. Gupta, and M. Banerjee, “Anti-mitotic activity of colchicine and the structural basis for its interaction with tubulin.,” *Med. Res. Rev.*, vol. 28, no. 1, pp. 155–183, Jan. 2008, doi: 10.1002/med.20097.
- [7] Y. Lu, J. Chen, M. Xiao, W. Li, and D. D. Miller, “An overview of tubulin inhibitors that interact with the colchicine binding site.,” *Pharm. Res.*, vol. 29, no. 11, pp. 2943–71, Nov. 2012, doi: 10.1007/s11095-012-0828-z.
- [8] I. Spasevska et al., “Modeling the Colchicum autumnale Tubulin and a Comparison of Its Interaction with Colchicine to Human Tubulin.,” *Int. J. Mol. Sci.*, vol. 18, no. 8, Aug. 2017, doi: 10.3390/ijms18081676.
- [9] B. Kumar et al., “Synthesis and biological evaluation of pyrimidine bridged combretastatin derivatives as potential anticancer agents and mechanistic studies,” *Bioorg. Chem.*, vol. 78, pp. 130–140, 2018, doi: <https://doi.org/10.1016/j.bioorg.2018.02.027>.

- [10] B. Kumar, R. Kumar, I. Skvortsova, and V. Kumar, "Mechanisms of Tubulin Binding Ligands to Target Cancer Cells: Updates on their Therapeutic Potential and Clinical Trials," *Curr. Cancer Drug Targets*, vol. 17, no. 4, pp. 357–375, 2017, doi: 10.2174/15680096166666160928110818.
- [11] A. A. Ghawanmeh, K. F. Chong, S. M. Sarkar, M. A. Bakar, R. Othaman, and R. M. Khalid, "Colchicine prodrugs and codrugs: Chemistry and bioactivities," *Eur. J. Med. Chem.*, vol. 144, pp. 229–242, 2018, doi: <https://doi.org/10.1016/j.ejmech.2017.12.029>.
- [12] A. Huczyński et al., "Synthesis, antiproliferative activity and molecular docking of Colchicine derivatives," *Bioorg. Chem.*, vol. 64, pp. 103–112, 2016, doi: <https://doi.org/10.1016/j.bioorg.2016.01.002>.
- [13] V. Blasco et al., "Arylureas derived from colchicine: Enhancement of colchicine oncogene downregulation activity.," *Eur. J. Med. Chem.*, vol. 150, pp. 817–828, Apr. 2018, doi: 10.1016/j.ejmech.2018.03.039.
- [14] A. Marzo-Mas et al., "Interactions of long-chain homologues of colchicine with tubulin," *Eur. J. Med. Chem.*, vol. 126, pp. 526–535, 2017, doi: <https://doi.org/10.1016/j.ejmech.2016.11.049>.
- [15] A. Huczyński et al., "Synthesis, antiproliferative and antibacterial evaluation of C-ring modified colchicine analogues.," *Eur. J. Med. Chem.*, vol. 90, pp. 296–301, Jan. 2015, doi: 10.1016/j.ejmech.2014.11.037.
- [16] T. Kozaka et al., "Antitumor agents 273. Design and synthesis of N-alkyl-thiocolchicinoids as potential antitumor agents.," *Bioorg. Med. Chem. Lett.*, vol. 20, no. 14, pp. 4091–4, Jul. 2010, doi: 10.1016/j.bmcl.2010.05.081.
- [17] S.-H. Lee et al., "New synthetic thiocolchicine derivatives as lowtoxic anticancer agents.," *Arch. Pharm. (Weinheim).*, vol. 338, no. 12, pp. 582–589, Dec. 2005, doi: 10.1002/ardp.200500148.

- [18] G. T. Shiau, K. K. De, and R. E. Harmon, "Synthesis and evaluation of N-deacetyl-N-glycosylalkylthiocolchicines as antileukemic agents.," *J. Pharm. Sci.*, vol. 67, no. 3, pp. 394–397, Mar. 1978, doi: 10.1002/jps.2600670333.
- [19] A. K. Ghosh and M. Brindisi, "Organic carbamates in drug design and medicinal chemistry.," *J. Med. Chem.*, vol. 58, no. 7, pp. 2895–2940, Apr. 2015, doi: 10.1021/jm501371s.
- [20] A. Brossi and P. Kerekes, "Carbamates of colchicine for treatment of gout." Google Patents, Aug. 06, 1985.
- [21] T. H. Dunning, "Gaussian basis sets for use in correlated molecular calculations. I. The atoms boron through neon and hydrogen," *J. Chem. Phys.*, vol. 90, no. 2, pp. 1007–1023, Jan. 1989, doi: 10.1063/1.456153.
- [22] G. B. Rocha, R. O. Freire, A. M. Simas, and J. J. P. Stewart, "RM1: A reparameterization of AM1 for H, C, N, O, P, S, F, Cl, Br, and I," *J. Comput. Chem.*, vol. 27, no. 10, pp. 1101–1111, Jul. 2006, doi: 10.1002/jcc.20425.
- [23] M. W. Schmidt et al., "General atomic and molecular electronic structure system," *J. Comput. Chem.*, vol. 14, no. 11, pp. 1347–1363, Nov. 1993, doi: 10.1002/jcc.540141112.
- [24] M. S. Gordon and M. W. Schmidt, "Advances in electronic structure theory: GAMESS a decade later," in *Theory and Applications of Computational Chemistry*, C. E. Dykstra, G. Frenking, K. S. Kim, and G. E. Scuseria, Eds. Amsterdam: Elsevier, 2005, pp. 1167–1189.
- [25] G. M. J. Barca et al., "Recent developments in the general atomic and molecular electronic structure system.," *J. Chem. Phys.*, vol. 152, no. 15, p. 154102, Apr. 2020, doi: 10.1063/5.0005188.
- [26] W. G. Dirks et al., "Cell line cross-contamination initiative: an interactive reference database of STR profiles covering common cancer cell lines.," *International journal of cancer*, vol. 126, no. 1. United States, pp. 303–304, Jan. 2010, doi: 10.1002/ijc.24999.

- [27] A. Urbaniak, M. Delgado, M. Antoszczak, A. Huczyński, and T. C. Chambers, "Salinomycin derivatives exhibit activity against primary acute lymphoblastic leukemia (ALL) cells in vitro.," *Biomed. Pharmacother.*, vol. 99, pp. 384–390, Mar. 2018, doi: 10.1016/j.biopha.2018.01.081.
- [28] M. Antoszczak et al., "Biological activity of doubly modified salinomycin analogs - Evaluation in vitro and ex vivo.," *Eur. J. Med. Chem.*, vol. 156, pp. 510–523, Aug. 2018, doi: 10.1016/j.ejmech.2018.07.021.
- [29] Q. Shi, P. Verdier-Pinard, A. Brossi, E. Hamel, and K. H. Lee, "Antitumor Agents-CLXXV. Anti-tubulin action of (+)-thiocolchicine prepared by partial synthesis," *Bioorg. Med. Chem.*, vol. 5, no. 12, pp. 2277–2282, 1997, doi: 10.1016/S0968-0896(97)00171-5.
- [30] R. M. Chabin and S. B. Hastie, "Association of thiocolchicine with tubulin.," *Biochem. Biophys. Res. Commun.*, vol. 161, no. 2, pp. 544–550, Jun. 1989, doi: 10.1016/0006-291x(89)92633-8.
- [31] D. Chaturvedi, "Perspectives on the synthesis of organic carbamates," *Tetrahedron*, vol. 68, no. 1, pp. 15–45, 2012, doi: <https://doi.org/10.1016/j.tet.2011.10.001>.
- [32] L. Cotarca, T. Geller, and J. Répási, "Bis(trichloromethyl)carbonate (BTC, Triphosgene): A Safer Alternative to Phosgene?," *Org. Process Res. Dev.*, vol. 21, no. 9, pp. 1439–1446, Sep. 2017, doi: 10.1021/acs.oprd.7b00220.
- [33] D.-W. Shen, L. M. Pouliot, M. D. Hall, and M. M. Gottesman, "Cisplatin resistance: a cellular self-defense mechanism resulting from multiple epigenetic and genetic changes.," *Pharmacol. Rev.*, vol. 64, no. 3, pp. 706–721, Jul. 2012, doi: 10.1124/pr.111.005637.
- [34] M. A. Jordan, D. Thrower, and L. Wilson, "Mechanism of inhibition of cell proliferation by Vinca alkaloids.," *Cancer Res.*, vol. 51, no. 8, pp. 2212–2222, Apr. 1991.

[35] M. Delgado and T. C. Chambers, “Microtubules play an essential role in the survival of primary acute lymphoblastic leukemia cells advancing through G1 phase.,” *Cell Cycle*, vol. 17, no. 14, pp. 1784–1796, 2018, doi: 10.1080/15384101.2018.1496746.

Chapter 7:
Prediction of the Inhibitory
Concentrations of Colchicine
Derivatives for Specific Cancer Cell
Lines by 3D Quantitative Structure-
Activity Relationship (QSAR)
Modelling

7.1 Introduction

Microtubules are one of the major components of the cytoskeleton in eukaryotic cells. These filamentous intracellular structures play a critical role in maintaining cell structure, providing pathways for cellular transport *via* motor proteins and generating forces for mitosis. These cylindrical protein polymers are formed from heterodimers of α and β tubulin. Microtubules are one of the most well-known chemotherapeutic targets in cancer therapy. Even though there are multiple unique binding sites on a tubulin heterodimer, β tubulin is the main binding target for all major microtubule-binding drug families [1–3].

Depolymerization of microtubules can be triggered by inhibition of β tubulin *via* binding to a chemotropic agent such as colchicine, vinblastine, or taxol. Among them, colchicine, a well-known tropolone alkaloid extracted from *Colchicum autumnale* [4], is noteworthy due to its high-potency antimetabolic properties. Because of its distinctive mechanism of action, not only has colchicine played an important role in studies of mitosis, but it has also generated much interest in the potential use for chemotherapeutic treatments in the clinical setting [5–13]. However, colchicine itself has not been used as a successful drug in long-term cancer treatment because of its serious adverse side effects, and indeed, despite numerous pre-clinical and clinical studies, almost no colchicine derivatives have yet been able to successfully complete clinical trials [5–7]. Up to now, many structure-activity-relationship studies have been performed to elucidate the structural features required for tubulin binding. In practice, however, there are some limitations of *in vitro* approaches for testing chemotherapeutic agents, including the complexity of synthesis methods and problems related to compound solubility. Conversely, while by their nature highly approximate, computational methods are particularly promising in their ability to overcome these problems, at the same time elucidating crucial relationships between the chemical structure of compounds and functional consequences on their respective target.

In this study, 3-dimensional Quantitative Structure-Activity Relationship (QSAR) models were generated by the use of ADMET predictor software (Simulations Plus Inc.) to predict the response of two important cancer cell lines, A549 and MCF7, to treatment with a sizeable panel of novel colchicine derivatives. The biological assays used for these two cell lines exposed to the novel colchicine derivatives were quantified through IC₅₀ values, while the computational analysis was based on both the estimates of the interaction energies between inhibitors and the binding site of its well-studied target and the chemical descriptors of the considered compounds obtained from ADMET analysis. The goal in any QSAR modelling is to obtain the best mathematical expression to elucidate the relationship between chemistry and biology. The success rate of this approach depends on several factors, such as (a) accuracy of input data; (b) the selection of descriptors; (c) modelling and validation using statistical procedures [14].

The *in-silico* models developed in this work can be practical tools to optimize the experimental design pipeline of drug-cell response screenings by robustly predicting the IC₅₀ values of new colchicine derivatives rather than relying exclusively on their experimental measurements. Moreover, since personalized treatment is a major goal in modern oncology, the accurate prediction of the response of specific cancer cells to a given therapy might pave the way towards the achievement of this ambitious goal as well by using cell cultures obtained *ex vivo*.

All the compounds used in this study were extracted from previous work of Huczynski's group [15–21] on double- and triple-modified novel colchicine derivatives. The series of recently published papers focused on the synthesis of a novel library of these derivatives and the subsequent assessment on how the double modification in C-4 and C-10 positions and triple modification in C-4, C-7, and C-10 positions influences the activity and selectivity of colchicine derivatives as cytotoxic, tubulin-targeting agents. (Figure 7-1).

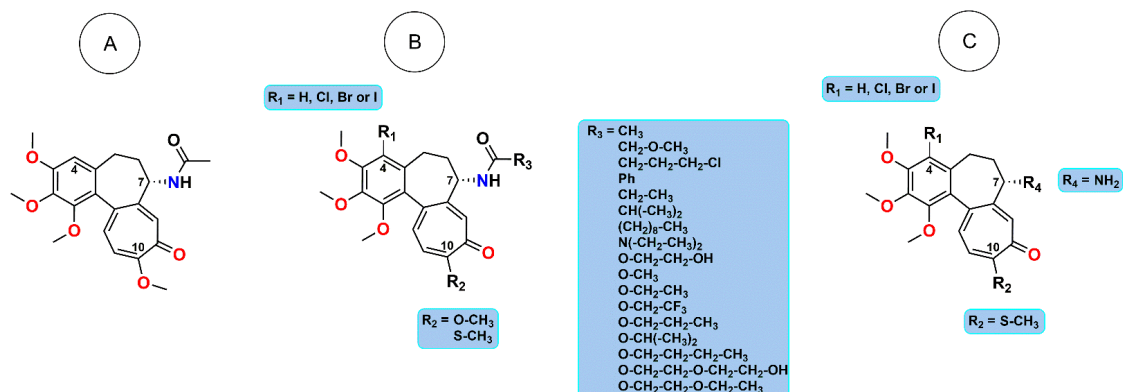


Figure 7-1. (A) Colchicine. (B) Double modification in C-4 and C-10 positions and triple modification in C-4, C-7 and C-10 positions on colchicine., $R_1 = H, Cl, I$ and Br , $R_3 =$ mentioned above and $R_2 = S-CH_3$ and $O-CH_3$. (C) Triple modification $R_1 = H, Cl, I$ and Br , $R_2 = S-CH_3$ and $R_4 = NH_3$

As mentioned above, the half-maximal inhibitory concentration of colchicine derivatives was tested *in vitro* using two cancer cell lines, namely human lung adenocarcinoma, A549, and human breast adenocarcinoma, MCF-7 (Table1).

Table 7-1. Novel colchicine derivatives were used in training and internal and external test sets. R_1, R_2 and R_3 represent the modification on for C_4, C_{10} , and C_7 respectively. pIC_{50} values for MCF7 and A549 cell lines are reported.

Training and internal test set

No.	R_1	R_2	R_3	$pIC_{50-A549}$	$pIC_{50-MCF7}$
1	H	O-CH ₃	CH ₃	-6.90	-7.26
2	Br	O-CH ₃	CH ₃	-6.98	-7.57
3	Br	S-CH ₃	CH ₃	-7.99	-7.83
4	Br	S-CH ₃	$R_4 = NH_2$	-6.94	-6.75
5	Br	S-CH ₃	CH ₂ -O-CH ₃	-7.99	-7.94
6	Br	S-CH ₃	CH ₂ -CH ₂ -CH ₂ -Cl	-7.26	-7.31
7	Br	S-CH ₃	Ph	-8.02	-7.94
8	Br	S-CH ₃	CH ₂ -CH ₃	-7.98	-7.95
9	Br	S-CH ₃	(CH ₂) ₈ -CH ₃	-6.05	-6.02
10	Br	S-CH ₃	N(-CH ₂ -CH ₃) ₂	-7.00	-7.01
11	Cl	O-CH ₃	CH ₃	-7.34	-7.64
12	Cl	S-CH ₃	CH ₃	-7.66	-7.66

13	Cl	S-CH ₃	R ₄ = NH ₂	-6.83	-6.65
14	Cl	S-CH ₃	O-CH ₂ -CH ₂ -OH	-7.09	-7.40
15	Cl	S-CH ₃	O-CH ₃	-7.68	-7.68
16	Cl	S-CH ₃	O-CH ₂ -CH ₃	-8.00	-7.68
17	Cl	S-CH ₃	O-CH ₂ -CF ₃	-8.04	-7.72
18	Cl	S-CH ₃	O-CH ₂ -CH ₂ -CH ₃	-8.00	-7.70
19	Cl	S-CH ₃	O-CH(-CH ₃) ₂	-7.70	-7.40
20	Cl	S-CH ₃	O-CH ₂ -CH ₂ -CH ₂ -CH ₃	-7.23	-7.01
21	Cl	S-CH ₃	O-CH ₂ -CH ₂ -O-CH ₂ -CH ₂ -OH	-7.03	-6.78
22	Cl	S-CH ₃	CH ₂ -O-CH ₃	-7.89	-7.89
23	Cl	S-CH ₃	CH ₂ -CH ₂ -CH ₂ -Cl	-7.54	-7.74
24	Cl	S-CH ₃	Ph	-7.96	-7.92
25	Cl	S-CH ₃	CH ₂ -CH ₃	-7.92	-7.92
26	Cl	S-CH ₃	CH(-CH ₃) ₂	-7.89	-7.89
27	Cl	S-CH ₃	(CH ₂) ₈ -CH ₃	-6.32	-6.09
28	Cl	S-CH ₃	N(-CH ₂ -CH ₃) ₂	-6.95	-6.97
29	I	O-CH ₃	CH ₃	-7.03	-7.01
30	I	S-CH ₃	CH ₃	-7.96	-7.77
31	I	S-CH ₃	R ₄ = NH ₂	-6.06	-5.77
32	I	S-CH ₃	O-CH ₂ -CH ₂ -OH	-7.00	-6.87
33	I	S-CH ₃	O-CH ₃	-7.11	-6.99
34	I	S-CH ₃	O-CH ₂ -CH ₃	-7.17	-7.03
35	I	S-CH ₃	O-CH ₂ -CF ₃	-7.05	-6.94
36	I	S-CH ₃	O-CH ₂ -CH ₂ -CH ₃	-7.07	-6.99
37	I	S-CH ₃	O-CH(-CH ₃) ₂	-6.96	-6.90
38	I	S-CH ₃	O-CH ₂ -CH ₂ -CH ₂ -CH ₃	-7.00	-6.92
39	I	S-CH ₃	O-CH ₂ -CH ² -O-CH ₂ -CH ₃	-7.00	-6.97
40	I	S-CH ₃	CH ₂ -O-CH ₃	-7.96	-7.96
41	I	S-CH ₃	CH ₂ -CH ₂ -CH ₂ -Cl	-7.08	-7.05
42	I	S-CH ₃	Ph	-7.89	-7.32
43	I	S-CH ₃	CH ₂ -CH ₃	-7.96	-7.96
44	I	S-CH ₃	CH(-CH ₃) ₂	-7.20	-7.43
45	I	S-CH ₃	(CH ₂) ₈ -CH ₃	-6.08	-6.07
46	I	S-CH ₃	N(-CH ₂ -CH ₃) ₂	-7.09	-7.02
47	H	S-CH ₃	CH ₃	-7.96	-8.00
48	H	S-CH ₃	R ₄ = NH ₂	-7.62	-7.85
49	H	S-CH ₃	CH ₂ -O-CH ₃	-7.89	-7.89
50	H	S-CH ₃	CH ₂ -CH ₂ -CH ₂ -Cl	-7.89	-7.92
51	H	S-CH ₃	Ph	-7.96	-7.96
52	H	S-CH ₃	CH ₂ -CH ₃	-7.89	-7.92
53	H	S-CH ₃	CH(-CH ₃) ₂	-7.80	-7.85
54	H	S-CH ₃	(CH ₂) ₈ -CH ₃	-7.57	-7.18
55	H	S-CH ₃	N(-CH ₂ -CH ₃) ₂	-6.88	-6.95

External Validation Set

56	Br	S-CH ₃	O-CH ₂ -CH ₂ -OH	-7.13	-7.24
57	Br	S-CH ₃	O-CH ₃	-8.00	-7.89
58	Br	S-CH ₃	O-CH ₂ -CH ₃	-7.92	-7.74
59	Br	S-CH ₃	O-CH ₂ -CF ₃	-7.52	-7.26
60	Br	S-CH ₃	O-CH ₂ -CH ₂ -CH ₃	-7.92	-7.57
61	Br	S-CH ₃	O-CH ₂ -CH ₂ -CH ₂ -CH ₃	-7.02	-6.90
62	Br	S-CH ₃	O-CH ₂ -CH ₂ -O-CH ₂ -CH ₂ -OH	-7.03	-6.90
63	H	S-CH ₃	O-CH ₂ -CH ₂ -OH	-7.10	-8.00
64	H	S-CH ₃	O-CH ₃	-8.00	-8.04
65	H	S-CH ₃	O-CH ₂ -CH ₃	-8.00	-8.10
66	H	S-CH ₃	O-CH ₂ -CF ₃	-8.10	-8.04
67	H	S-CH ₃	O-CH ₂ -CH ₂ -CH ₃	-8.04	-8.04
68	H	S-CH ₃	O-CH(-CH ₃) ₂	-8.04	-8.04
69	H	S-CH ₃	O-CH ₂ -CH ₂ -O-CH ₂ -CH ₂ -OH	-7.07	-8.00
70	H	S-CH ₃	O-CH ₂ -CH ₂ -O-CH ₂ -CH ₃	-7.92	-8.04

7.2 Materials and methods

7.2.1 Dataset collection

70 of the introduced double- and triple-modified derivatives with reported anticancer activity in terms of the corresponding IC₅₀ (nM) values [15–21] were selected to develop 3-dimensional QSAR models and used to create an *ad hoc* library. To ensure data consistency among the different compounds in the library, we included in the latter only those compounds for which the synthesis and the measurements of IC₅₀ values have been carried out within the same experimental setting, both in terms of personnel and methodologies, and within a limited time frame [15–21]. The models were thus designed to predict specific anticancer activity – as IC₅₀ values – of colchicine derivatives against two different commonly studied human cancer cell lines, specifically A549 and MCF7.

The two-dimensional (2D) chemical structures were transformed into three-dimensional (3D) structures through the use of QMMM (quantum mechanics/molecular mechanics) software package GAMESS-US (Version 2010-10-01) [22–24].

Specifically, the derivatives' structures were fully optimized based on the RHF/ cc-pVDZ level of theory [25].

In this work, the *in vitro* biological activities of these compounds based on the inhibition of tubulin polymerization were retrieved from previously published work [15–21] and converted into the corresponding pIC₅₀ (-log IC₅₀) values (Table 7-1), which were used as dependent variables in the 3D-QSAR model we developed in the present study.

7.2.2 Docking

In the context of choosing the best descriptors to accurately predict IC₅₀ values of colchicine derivatives against the two cancer cell lines, binding and electrostatic energies between the novel colchicine derivatives and β II isotype of tubulin were calculated by the use of docking methodology. To perform docking, we employed AutoDock4 software [26], which is designed to predict how drug candidates bind to the 3D structure of a target receptor. Briefly, the protocol we used to perform docking is the following: first, a grid of size 44 x 44 x 60 Å³ and spacing of 0.375 Å was built and centered on the colchicine binding site using the AutoGrid tool; subsequently the AutoDock program was used to perform the docking of each of the 70 derivatives, as well as of colchicine, with the following settings: The genetic algorithm was run 100 times on β II tubulin and the novel library with explicit hydrogens. The partial charges of the system were applied using the Gasteiger method.

To overcome the obstacle of not having an experimental crystal structure for human β II tubulin (gene TBB2B), we first built a homology model of the latter. First, the sequence of β II tubulin was obtained from UniProt [27] (code Q9BVA1) in fasta format. Software package MOE2018 (Molecular Operating Environment, Inc) [28] was used to construct the homology model of β II tubulin using the entry 1SA0 from the Protein Data Bank [29], which is an experimental structure of colchicine-bound, bovine

tubulin with resolution of 3.58 Å, as a template. Twelve homology models were created based on the maximum number of independent models that is set to 10. To optimize ionization states and proton placement in the final model, Protonate 3D application was used before the final refinement step at pH value being set at 7 and the salt concentration at 0.15 M. The quality of the final homology model was assessed through the lowest RMSD alignment with the template structure and the lowest heavy atom RMSD of each model to the average position of all of the intermediate models. The homology model was then energy minimized with periodic boundaries using the AMBER 14:EHT force field.

The flexible ligands were then docked to the rigid protein using the Autodock4 program with the protocol described above. Finally, the binding affinities of docked colchicine itself and its seventy derivatives were ranked and used as descriptors (Table 7-2). Electrostatic energies between the modified derivatives and β II tubulin were also collected and used as a second descriptor.

7.2.3 Descriptor Calculations

A total of 500 descriptors has been calculated for each of the training set compounds. The conventional descriptors were grouped into molecular and atomic descriptors. Two sets of atomic descriptors were developed by Hall and Kier (1991; 1995) [30,31] and were calculated for all the compounds. Besides these standard atomic descriptors, an advanced set of reactivity descriptors and proprietary atomic charges are implemented in the ADMET Predictor software [32,33] which are derived from the analysis of over 1000 diverse multifunctional molecules. These were also calculated for the investigated compounds, and included in the dataset. GAMESS calculations were carried out at the B3LYP/6-311G(d,p) level of theory [34–38] and natural population analysis (NPA) was subsequently conducted to extract atomic charges [39,40]. For the extraction of separate sigma and pi components of the partial atomic charges, a special

protocol was employed using natural bond orbitals (NBO) [39,40]. All ADMET charge-based descriptors are aggregate functions of the above atomic descriptors [41].

Molecular descriptors are the second major class of descriptors that are functions of the overall molecular structure (e.g., bond and ring counts, etc.). The standard molecular descriptors are divided into two sub-models. The first one includes the constitutional descriptors that capture various aspects of molecular size and uniformity of composition and the second one is electron topological state descriptors that were devised by Kier and Hall and have been widely used in QSAR applications [41,42].

The standard molecular descriptors have been explained in detail elsewhere [43]. The recommended molecular descriptors generated by ADMET Predictor are 341 molecular descriptors from 2D structures with an additional 36 from 3D structures.

To select the best subset of descriptors, highly correlated descriptors, maximum absolute correlation of 0.98, were excluded. A cell-based genetic algorithm was employed to explore different descriptor combinations, evaluating each based on its ability to model the training set: the final subset of descriptors chosen by ADMET Predictor to generate the models included binding energies, electrostatic energies, polarizability calculated by Miller's method [44] and sum of absolute values of Hückel pi atomic charges on O atoms.

7.2.4 3-Dimensional Quantitative-Structure-Activity-Relationship

Models

To attempt to build a robust QSAR model, the experimental dataset was divided into a training set (38 compounds) and an internal test set (17 compounds). When splitting a given dataset into a training set and a test set, a general rule of thumb in Machine Learning is that the latter should consist of 20-30% of the original data, and should cover the range of features present in the training set. As such, the test set

compounds were chosen randomly from the dataset and represented around 30% of the original data [45].

A Kohonen map, an unsupervised self-organizing machine learning technique that classifies sampling of structures, was used to select the test set: the QSAR models were developed based on an artificial neural network method (ANN) [41]. 14 inputs and 10 neurons were used to build our ensemble models, each of which includes 50 models. As a result, 64 models were generated by desired descriptors and the two best models were chosen for each of the cell lines. Finally, the prediction of the two chosen models was tested with an external test set (15 compounds).

7.2.5 Statistical Evaluation/Validation of the Model

Statistical validation is a very important process for robust QSAR model development. In this work, three different statistical parameters were employed to assess the quality of the models on the training set and on the test set: (a) the square of the Pearson correlation coefficient, R^2 , which ranges from 0 to 1. Models with R^2 greater than 0.6 can generally be regarded as of good quality [45]; (b) the value of the coefficient of determination, q^2 , which has the same range as R^2 . A value greater than 0.5 is considered as an indicator of good predictive capability of the model [46]; (c) Root mean square error (RMSE) and mean absolute error (MAE).

RMSE and MAE are two other important parameters besides R^2 and q^2 that should be used to assess the robustness of the QSAR model. Unlike the R^2 and q^2 values, there is no general consensus on RMSE and MAE values to be universally regarded as indicative of high-quality models; rather, the general criterion is that smaller values indicate better models. More importantly, the values of both RMSE and MAE should not be inconsistent between the training and test sets. Indeed, a discrepancy in the form of low RMSE and MAE in the training set and significantly higher values in the test set indicates an overfitted model [46].

7.2.6 External Validation

Golbraikh and Tropsha proposed a set of statistical guidelines for the external test set [45], validated by Tropsha, Gramatica and Chirico to be used for external test validation [47–50]. First, the R^2 of the external validation set should be larger than 0.6 where R^2 is the squared correlation coefficient between the predicted and observed values of the activity. Second, $\frac{R^2 - R_0^2}{R^2} < 0.1$ or $\frac{R^2 - R_0'^2}{R^2} < 0.1$ where R_0^2 and $R_0'^2$ are the squared correlation coefficients calculated by using regression through the origin (RTO) for graphs of predicted versus observed activities and observed versus predicted activities, respectively. The slope of these graphs, K and K' should be as close to 1 as possible, $0.85 < K$ or $K' < 1.15$. More specifically RTO referred to linear regression by the least-squares method without a constant term [46]. Uncertainty estimates are also useful in validating model performance since they allow to distinguish marginal disagreements with observation values from substantive ones.

Numerical modelling uncertainty analysis put into operation several techniques to investigate various sources of uncertainty in model input and design. Uncertainty analysis is a trending approach to determine the accuracy and reliability of the prediction of the models.

ADMET Predictor generalized gamma distributions are fitted to the cumulative distributions of squared error and ensemble standard deviation of the training set points to build an uncertainty model. It can be shown, based on the properties of the cumulative gamma distribution, that the greater the separation between the predicted cumulative squared error distribution and predicted cumulative standard deviation distribution, the stronger is the dependence of the predictive uncertainty on the standard deviation of the sub-model predictions. An uncertainty model can estimate the regression uncertainty associated with a prediction. Uncertainty estimates are computed from the standard deviation of predictions from individual models that make up the ensemble model.

Higher standard deviations lead to higher uncertainty estimates and lower standard deviations lead to lower uncertainty estimates [41].

The RMSU metric is another valuable parameter to assess the quality of the uncertainty model. It is analogous to RMSE except the calculation uses the estimated uncertainty for each model prediction instead of the observed error.

The protocol used to build an uncertainty model usually results in the RMSU for the training set being very close to the training set RMSE. Thus, the similarity of the RMSU to the RMSE for the training set is generally not an informative indicator of the quality of the uncertainty model. Conversely, the same similarity between RMSU and RMSE for the test set is indeed indicative of a good uncertainty model. It shows that the mean squared uncertainty over a reasonably sized dataset is a good estimate of the predictive model's mean squared error over the same data set.

A quantile-quantile plot (Q-Q plot) is a graphical method for comparing two probability distributions by plotting their quantiles against each other [51]. The Q-Q plots are a better representative plot to illustrate the difference between the observed and predicted statistics [41].

7.3 Results and Discussion

7.3.1 3D-QSAR Model Development and Validation

Two statistical nonlinear regression QSAR models were developed and studied for their ability to predict the IC₅₀ values of colchicine derivatives against the two different cell lines A549, associated with lung cancer, and MCF7 associated with breast cancer (Figure 7-2).

In a previous study [15,17,20], a good correlation between predicted binding energies of the mentioned library with β II tubulin and experimental IC₅₀ values was achieved [15–20,52]. This result suggests the hypothesis that binding energies should be a good candidate descriptor for 3D Quantitative Structure-Activity Relationship models

(QSAR) to predict the antiproliferative efficacy of such compounds. At the same time, due to the dominantly electrostatic nature of hydrogen bonding, electrostatic energies between ligands and β II tubulins were chosen as a further descriptor to be included in the model. Lastly, polarizability and sum of absolute values of Hückel pi atomic charges on O atoms were also chosen by ADMET Predictor software as two conventional atomic descriptors to be included in the model as well. The calculated values of the four mentioned descriptors are reported in Table 7-2 for each compound in the training set and internal test set, as well as in the external validation set.

Table 7-2. Binding energies (kcal/mol) and electrostatic energies (kcal/mol) between β II tubulin and referred derivatives, polarizability (\AA^3) and sum of absolute values of Hückel pi atomic charges on O atoms, used to build two QSAR models for MCF7 and A549 cells.

Compound	Descriptors values for training and internal test set			
	Hückel pi atomic charges on O atoms	Polarizability	Binding Energies	Electrostatic energy
1	42.2	1.68	-7.06	-0.04
2	44.9	1.68	-6.89	-0.04
3	47.3	1.46	-7.05	-0.06
4	43.5	0.99	-7.01	-0.12
5	49.8	1.46	-5.71	0.05
6	52.9	1.47	-5.04	0.05
7	55.7	1.49	-7.25	0.01
8	49.1	1.47	-7.49	0.03
9	61.0	1.47	-6.47	-0.04
10	54.2	1.56	-4.38	-0.01
11	44.6	1.68	-6.80	-0.05
12	46.7	1.47	-6.89	-0.06
13	42.8	0.99	-6.99	-0.16
14	49.7	1.63	-6.19	-0.12
15	47.2	1.63	-7.31	-0.05
16	49.0	1.63	-6.54	-0.05
17	48.6	1.63	-5.99	0.00
18	50.9	1.63	-6.72	-0.06
19	50.9	1.62	-5.76	0.03
20	52.7	1.63	-6.67	-0.07
21	54.0	1.63	-6.89	-0.10
22	49.0	1.46	-6.07	0.05
23	52.1	1.47	-6.18	0.02
24	54.3	1.48	-7.25	0.00

25	48.4	1.47	-7.51	0.04
26	50.2	1.46	-7.34	0.04
27	61.2	1.47	-6.71	-0.02
28	53.5	1.56	-4.53	-0.01
29	46.8	1.68	-6.79	0.03
30	49.2	1.47	-7.04	-0.06
31	45.4	0.99	-7.03	-0.12
32	52.4	1.63	-5.11	-0.01
33	49.9	1.64	-7.06	-0.06
34	51.7	1.63	-6.77	-0.00
35	51.4	1.63	-6.45	-0.00
36	53.5	1.63	-6.68	-0.00
37	53.5	1.62	-7.02	-0.07
38	55.3	1.63	-6.85	-0.07
39	56.0	1.63	-6.18	-0.06
40	51.7	1.46	-5.55	-0.11
41	54.8	1.47	-5.48	0.08
42	56.9	1.48	-7.13	0.00
43	51.0	1.47	-7.24	0.02
44	52.8	1.47	-7.09	0.02
45	63.8	1.47	-6.44	0.02
46	56.1	1.57	-4.79	-0.01
47	44.7	1.47	-6.68	-0.05
48	40.9	0.99	-6.66	-0.11
49	47.1	1.46	-6.68	0.04
50	50.2	1.47	-7.15	0.07
51	52.5	1.48	-7.36	0.00
52	46.5	1.47	-6.95	0.05
53	48.3	1.47	-6.58	0.05
54	59.4	1.47	-7.35	-0.01
55	51.9	1.56	-5.70	-0.20
<hr/>				
Descriptors values for external test set				
56	50.4	1.63	-6.14	-0.08
57	48.0	1.63	-7.31	-0.06
58	49.8	1.63	-7.28	-0.05
59	49.5	1.63	-5.32	0.03
60	51.6	1.63	-6.63	-0.06
61	53.4	1.63	-6.74	-0.06
62	54.8	1.63	-6.89	-0.10
63	47.7	1.63	-5.83	-0.06
64	45.3	1.64	-7.03	-0.05
65	47.1	1.63	-6.62	-0.04
66	46.6	1.63	-6.74	-0.01
67	49.0	1.63	-6.62	-0.05
68	49.0	1.62	-6.89	-0.05

69	52.1	1.63	-7.56	-0.10
70	51.4	1.63	-6.35	-0.03

The analysis produced 64 models with good R^2 values between 0.7 to 0.9 for both training and test sets. The Kohonen map technique that was employed to cluster input samples by their structures typically gives good results for medium-sized data sets. Artificial Neural Network (ANN) was used to generate the models. ANN models are nonlinear ensemble models, with hidden neurons between the inputs and output [41].

48 and 16 models were generated for A549 and MCF7 cell lines, respectively. However, most of the models were discarded due to overfitting on the training set or poor estimation of the IC_{50} values on the external test set. Out of the 64 models generated in total, two successfully passed the validation on the training set, internal test set and validation set (Figure 7-2), one for each cell line. These models featured R^2 values larger than 0.75 (0.88 for MCF7 and 0.76 for A549) and RMSE values were consistent between the training and test sets (0.21 for MCF7 and 0.28 for A549 cancer cell lines).

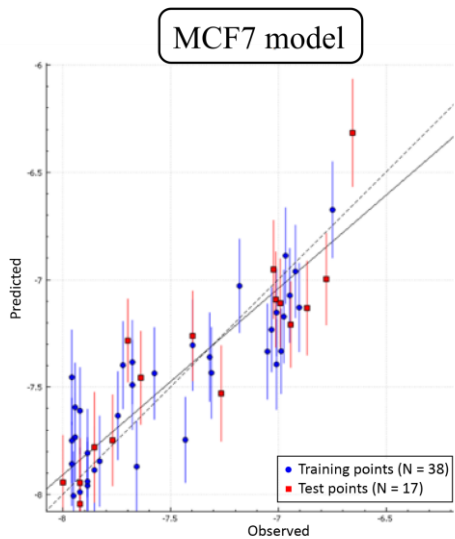
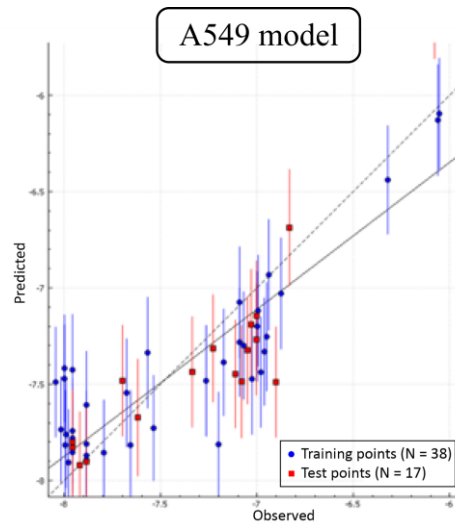


Figure 7-2. Linear regression graph of predicted vs observed values of IC_{50} for both A549 and MCF7 cancer cell lines for training and internal test sets.

In Table 7-3, values of R^2 , RMSE, RMSU, and MAE were reported for each of the training and internal test sets of model 1 (for MCF7 cell line) and model 2 (for A459 cell line).

Table 7-3. Values of R², RMSE, RMSU, and MAE were reported for each of the training and internal test sets of model 1 (for MCF7 cell line) and model 2 (for A459cell line).

MCF7 Model validations					
	RMSU	MAE	RMSE	Q²	R²
Training set	0.21	0.17	0.21	0.868	0.88
Internal test set	0.22	0.18	0.21	0.843	0.86
A459 Model validations					
Training set	0.28	0.22	0.28	0.75	0.76
Internal test set	0.29	0.21	0.28	0.70	0.77

7.3.2 External Validation

The two finalized 3D-QSAR models for the prediction of IC₅₀ values for both A549 and MCF7 cancer cell lines were tested with an external independent dataset (Figure 7-3). The purpose of the external validation is to evaluate the robustness of generated models and assess if they can generalize to unseen data without significant loss of predictive power. The prediction values of an independent validation set can thus quantitatively determine the quality of the developed model [46]. The mentioned models pass the statistical guidelines for the external validation set proposed by Golbraikh and Tropsha Table 7-4) [45]. The R² values of both candidate models are higher than 0.6, while the slope of the regression through the origin (RTO), K, is larger than 0.8 and smaller than 1.15. The criterion $\frac{R^2 - R_0^2}{R^2} \leq 0.1$ defined before is also satisfied for both models [45,46].

Table 7-4. validation parameters for the external test on A549 and MCF7 models: R^2 , the squared correlation coefficient of predicted versus observed activities; R_0^2 the squared correlation coefficient calculated by using regression through the origin (RTO) for graphs of predicted versus observed activities; K, the slope of the regression through the origin (RTO).

	R^2	R_0^2	K
A549 model	0.69	0.62	1.05
MCF7 model	0.60	0.54	1.06

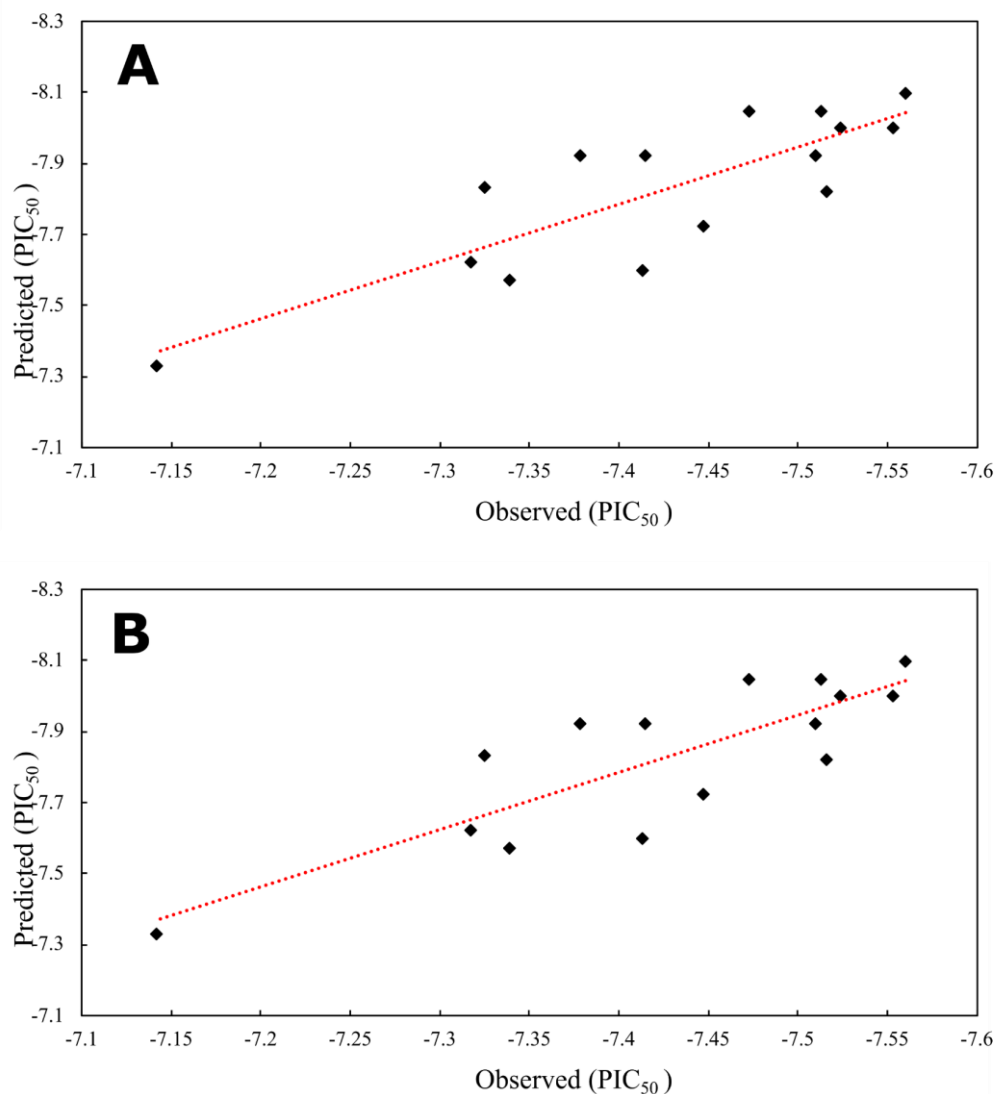


Figure 7-3. (A) Linear regression graph of predicted vs observed values of pIC_{50} for A549 cancer cell lines in external test sets. (B) Linear regression graph of predicted vs observed values of pIC_{50} for MCF7 cancer cell lines in external test sets.

7.3.3 Regression Uncertainty

Two associated regression uncertainty models generated starting from our models are shown in Figure 7-4. The blue and red dashed lines represent the squared error and standard deviation of the predictions, respectively. The dashed lines allow us

to assess the quality of how well the generalized gamma distributions are fitted to the cumulative distributions of squared error and ensemble standard deviation of the training set points [41]. The failure to get a satisfactory level on uncertainty for a regression model may be indicative of overtraining or of bias in dataset selection.

The predictive uncertainty on the standard deviation of the sub-model predictions is strongly dependent on the extent of the separation between the predicted cumulative squared error distribution and predicted cumulative standard deviation distribution. As seen in Figure 7-4, the red and blue dashed lines are perfectly fitted in both of our uncertainty models [41].

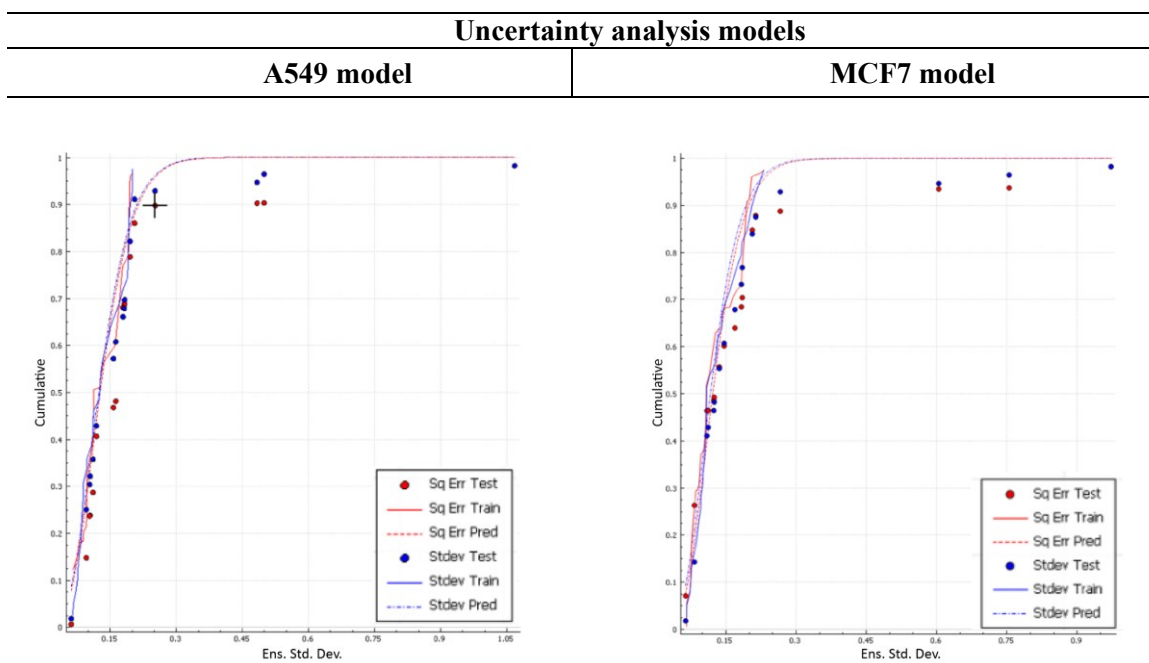
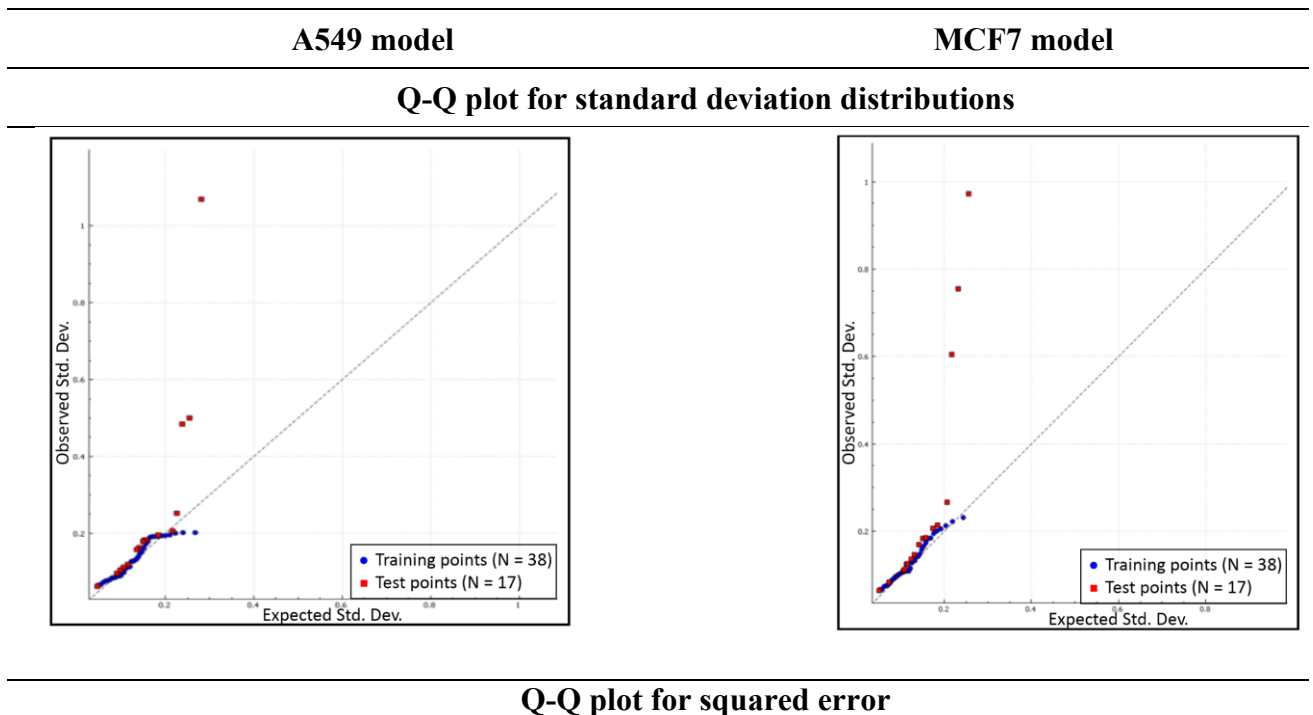


Figure 7-4. Associated regression uncertainty models of 3D-QSAR model both A549 and MCF7 cancer cell lines.

Moreover, as mentioned in the Methods section, the closeness of values of the RMSU and RMSE of test sets is a characteristic of a good uncertainty model that is achieved for both models in Figure 7-4.

Quantile-Quantile Plots

In Figure 7-5, Q-Q plots are shown for the squared error and standard deviation distributions. Each of the models for both cancer cell lines shows four outliers that belong to the test set.



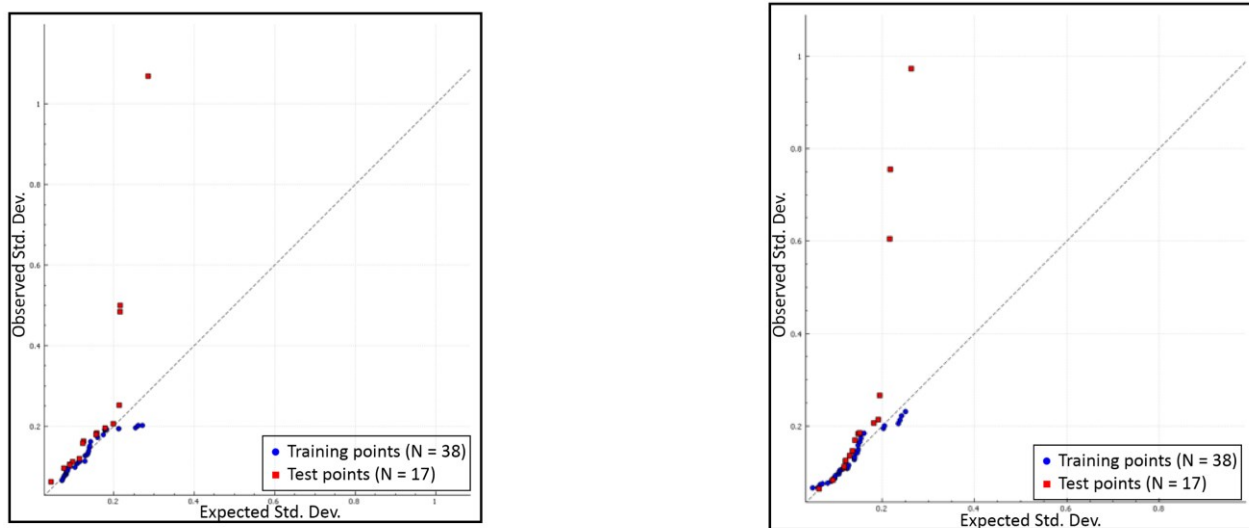


Figure 7-5. Associated squared error and standard deviation distributions Q-Q plots of 3D-QSAR models for A549 and MCF7 cancer cell lines.

Compounds 13, 48, and 45 are three out of four unfitted structures of Q-Q plots for both A549 and MCF7 cancer cell line (Figure 7-6). Being able to distinguish the outlier of the input data gives us a chance to improve our models by eliminating the mentioned structures in the future or redo the measurement of their IC_{50} to assure the robustness of the experimental data. Also, the details of the interaction between these compounds and the colchicine binding site might be worth investigating in greater detail, both experimentally and computationally through techniques such as molecular dynamics.

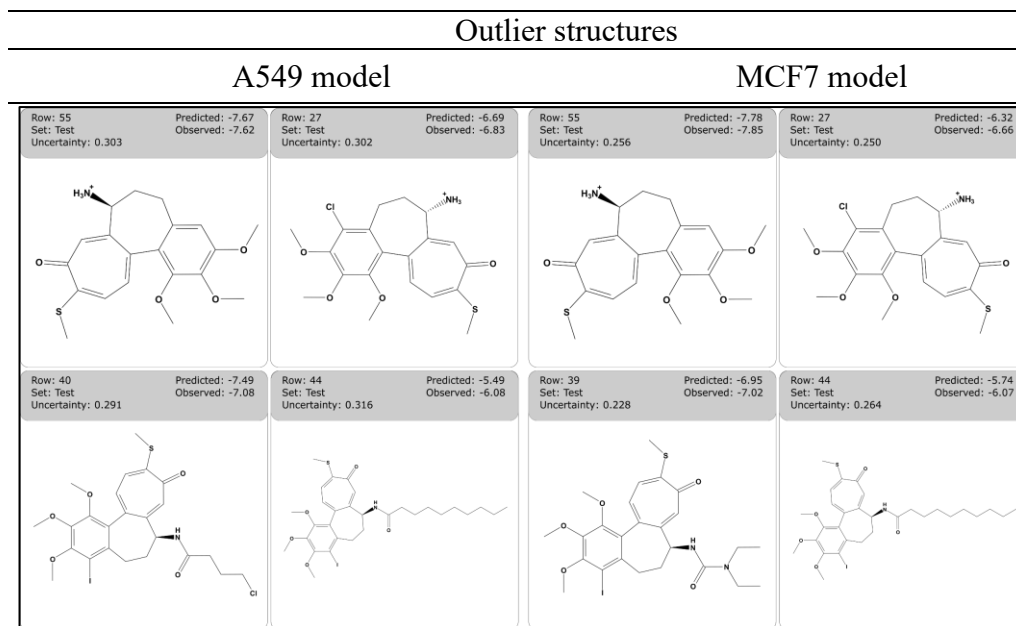


Figure 7-6. Outlier structures of internal test sets of 3D-QSAR models for A549 and MCF7 cancer cell lines.

7.4 Conclusions

Microtubules are well-known and commonly used molecular targets for cancer therapy, and it is widely accepted that both drug-induced stabilization and depolymerization of microtubules could play a critical role in cancer treatment. Colchicine, a unique tubulin-targeting inhibitor which prevents microtubule polymerization, has to this date been unable to make it through clinical trials for cancer chemotherapy, mainly due to its high systemic toxicity. The extensive effort of designing and optimizing colchicine derivatives has not yet yielded desirable results, due to the difficulty in the synthesis of compounds exhibiting both specificity and selectivity for their molecular targets. In this context, we aimed to generate two 3D QSAR models to predict the missing IC_{50} values for 70 novel colchicine derivatives against two commonly-used breast and lung cancer lines, namely MCF7 and A549. The

chemical structure of 50 new compounds was used as input data along with their corresponding *in vitro* activity (IC₅₀ values) to build two models for the aforementioned cell lines. A method based on Kohonen maps was applied to split the input data into training and test sets. 15 independent compounds were subsequently used as an external independent validation set. The binding and electrostatic energies between the mentioned library of derivatives and β II tubulin were estimated by docking and then used as two novel descriptors, along with two conventional ones, namely polarizability and sum of absolute values of Hückel pi atomic charges on O atoms. A widely used Artificial Neural Network was deployed to generate our models. Based on the calculations and analysis presented in this chapter, our two finalized QSAR models for both A549 and MCF7 cancer cell lines, not only showed good performance on the test set, assessed through the high value of q^2 and R^2 , but also show predictive ability and good generalization on the independent validation set of compounds. Moreover, the produced models proved sufficiently robust according to the restrictive criteria that were suggested by Golbraikh and Tropsha [45]. Analysis of the associated uncertainty models of our robust models also illustrate how RMSU values are consistent with RMSE for the test set for both of our QSAR models, which further confirms the quality of the uncertainty models.

References

- [1] J. Torin Huzil, R. F. Ludueña, and J. Tuszynski, “Comparative modelling of human β tubulin isotypes and implications for drug binding.,” *Nanotechnology*, vol. 17, no. 4, pp. S90–S100, Feb. 2006, doi: 10.1088/0957-4484/17/4/014.
- [2] S. Ravanbakhsh, M. Gajewski, R. Greiner, and J. A. Tuszynski, “Determination of the optimal tubulin isotype target as a method for the development of individualized cancer chemotherapy.,” *Theor. Biol. Med. Model.*, vol. 10, no. 29, p. 29, May 2013, doi: 10.1186/1742-4682-10-29.
- [3] B. Kumar, R. Kumar, I. Skvortsova, and V. Kumar, “Mechanisms of Tubulin Binding Ligands to Target Cancer Cells: Updates on their Therapeutic Potential and Clinical Trials.,” *Curr. Cancer Drug Targets*, vol. 17, no. 4, pp. 357–375, 2017, doi: 10.2174/1568009616666160928110818.
- [4] J. S. Hyams and H. Stebbings, “The mechanism of microtubule associated cytoplasmic transport. Isolation and preliminary characterisation of a microtubule transport system.,” *Cell Tissue Res.*, vol. 196, no. 1, pp. 103–16, Jan. 1979, doi: 10.1007/BF00236351.
- [5] N. G. Vindya, N. Sharma, M. Yadav, and K. R. Ethiraj, “Tubulins - the target for anticancer therapy.,” *Curr. Top. Med. Chem.*, vol. 15, no. 1, pp. 73–82, 2015, doi: 10.2174/1568026615666150112115805.
- [6] J. Seligmann and C. Twelves, “Tubulin: an example of targeted chemotherapy.,” *Future Med. Chem.*, vol. 5, no. 3, pp. 339–52, Mar. 2013, doi: 10.4155/fmc.12.217.
- [7] C. D. Katsetos and P. Dráber, “Tubulins as therapeutic targets in cancer: from bench to bedside.,” *Curr. Pharm. Des.*, vol. 18, no. 19, pp. 2778–92, 2012, doi: 10.2174/138161212800626193.
- [8] C. Avendaño and J. C. Menendez, *Medicinal chemistry of anticancer drugs*, 2nd ed. Elsevier, 2015.
- [9] A. Slobodnick, B. Shah, M. H. Pillinger, and S. Krasnokutsky, “Colchicine: old and new.,” *Am. J. Med.*, vol. 128, no. 5, pp. 461–70, May 2015, doi: 10.1016/j.amjmed.2014.12.010.
- [10] N. Nerlekar, A. Beale, and R. W. Harper, “Colchicine--a short history of an ancient drug.,” *Med. J. Aust.*, vol. 201, no. 11, pp. 687–8, Dec. 2014, doi: 10.5694/mja14.00846.
- [11] I. Grattagliano, L. Bonfrate, V. Ruggiero, G. Scaccianoce, G. Palasciano, and P. Portincasa, “Novel therapeutics for the treatment of familial Mediterranean fever:

- from colchicine to biologics.,” *Clin. Pharmacol. Ther.*, vol. 95, no. 1, pp. 89–97, Jan. 2014, doi: 10.1038/clpt.2013.148.
- [12] G. Cocco, D. C. C. Chu, and S. Pandolfi, “Colchicine in clinical medicine. A guide for internists.,” *Eur. J. Intern. Med.*, vol. 21, no. 6, pp. 503–8, Dec. 2010, doi: 10.1016/j.ejim.2010.09.010.
- [13] L. P. H. Yang, “Oral colchicine (Colcris): in the treatment and prophylaxis of gout.,” *Drugs*, vol. 70, no. 12, pp. 1603–13, Aug. 2010, doi: 10.2165/11205470-000000000-00000.
- [14] A. Tropsha, P. Gramatica, and V. Gombar, “The Importance of Being Earnest: Validation is the Absolute Essential for Successful Application and Interpretation of QSPR Models,” *QSAR Comb. Sci.*, vol. 22, no. 1, pp. 69–77, Apr. 2003, doi: 10.1002/qsar.200390007.
- [15] U. Majcher *et al.*, “Synthesis, antiproliferative activity and molecular docking of thiocolchicine urethanes.,” *Bioorg. Chem.*, vol. 81, pp. 553–566, 2018, doi: 10.1016/j.bioorg.2018.09.004.
- [16] U. Majcher *et al.*, “Antiproliferative Activity and Molecular Docking of Novel Double-Modified Colchicine Derivatives.,” *Cells*, vol. 7, no. 11, p. 192, Nov. 2018, doi: 10.3390/cells7110192.
- [17] U. Majcher *et al.*, “Synthesis and Biological Evaluation of Novel Triple-Modified Colchicine Derivatives as Potent Tubulin-Targeting Anticancer Agents.,” *Cells*, vol. 7, no. 11, Nov. 2018, doi: 10.3390/cells7110216.
- [18] G. Klejborowska *et al.*, “Synthesis, antiproliferative activity, and molecular docking studies of 4-chlorothiocolchicine analogues,” *Chem. Biol. Drug Des.*, vol. 95, no. 1, pp. 182–191, Jan. 2020, doi: 10.1111/cbdd.13618.
- [19] G. Klejborowska *et al.*, “Synthesis, biological evaluation and molecular docking studies of new amides of 4-bromothiocolchicine as anticancer agents.,” *Bioorg. Med. Chem.*, vol. 27, no. 23, p. 115144, 2019, doi: 10.1016/j.bmc.2019.115144.
- [20] G. Klejborowska *et al.*, “Synthesis, biological evaluation and molecular docking studies of new amides of 4-chlorothiocolchicine as anticancer agents.,” *Bioorg. Chem.*, vol. 97, p. 103664, 2020, doi: 10.1016/j.bioorg.2020.103664.
- [21] G. Klejborowska *et al.*, “Synthesis, anticancer activity and molecular docking studies of N-deacetylthiocolchicine and 4-iodo-N-deacetylthiocolchicine derivatives.,” *Bioorg. Med. Chem.*, vol. 32, p. 116014, Feb. 2021, doi: 10.1016/j.bmc.2021.116014.
- [22] M. W. Schmidt *et al.*, “General atomic and molecular electronic structure system,” *J. Comput. Chem.*, vol. 14, no. 11, pp. 1347–1363, Nov. 1993, doi:

10.1002/jcc.540141112.

- [23] M. S. Gordon and M. W. Schmidt, “Advances in electronic structure theory: GAMESS a decade later,” in *Theory and Applications of Computational Chemistry*, C. E. Dykstra, G. Frenking, K. S. Kim, and G. E. Scuseria, Eds. Amsterdam: Elsevier, 2005, pp. 1167–1189.
- [24] G. M. J. Barca *et al.*, “Recent developments in the general atomic and molecular electronic structure system.,” *J. Chem. Phys.*, vol. 152, no. 15, p. 154102, Apr. 2020, doi: 10.1063/5.0005188.
- [25] T. H. Dunning, “Gaussian basis sets for use in correlated molecular calculations. I. The atoms boron through neon and hydrogen,” *J. Chem. Phys.*, vol. 90, no. 2, pp. 1007–1023, Jan. 1989, doi: 10.1063/1.456153.
- [26] G. M. Morris *et al.*, “AutoDock4 and AutoDockTools4: Automated docking with selective receptor flexibility.,” *J. Comput. Chem.*, vol. 30, no. 16, pp. 2785–91, Dec. 2009, doi: 10.1002/jcc.21256.
- [27] G. Y. Cederquist *et al.*, “An inherited TUBB2B mutation alters a kinesin-binding site and causes polymicrogyria, CFEMO and axon dysinnervation.,” *Hum. Mol. Genet.*, vol. 21, no. 26, pp. 5484–99, Dec. 2012, doi: 10.1093/hmg/ddc393.
- [28] *Autodock*. Chemical Computing Group ULC, Montreal, Canada, 2018.
- [29] R. B. G. Ravelli *et al.*, “Insight into tubulin regulation from a complex with colchicine and a stathmin-like domain.,” *Nature*, vol. 428, no. 6979, pp. 198–202, Mar. 2004, doi: 10.1038/nature02393.
- [30] L. H. Hall, B. Mohney, and L. B. Kier, “The electrotopological state: structure information at the atomic level for molecular graphs,” *J. Chem. Inf. Model.*, vol. 31, no. 1, pp. 76–82, Feb. 1991, doi: 10.1021/ci00001a012.
- [31] L. H. Hall and L. B. Kier, “Electrotopological State Indices for Atom Types: A Novel Combination of Electronic, Topological, and Valence State Information,” *J. Chem. Inf. Comput. Sci.*, vol. 35, no. 6, pp. 1039–1045, Nov. 1995, doi: 10.1021/ci00028a014.
- [32] *Simulations Plus, Inc. ADMET Predictor, Version 9.5: ADMET Property Estimation and Model Building*. Simulations Plus, Inc. Lancaster, CA, 2019.
- [33] M. F. Sanner, “Python: a programming language for software integration and development.,” *J. Mol. Graph. Model.*, vol. 17, no. 1, pp. 57–61, Feb. 1999.
- [34] A. D. Becke, “Density-functional thermochemistry. I. The effect of the exchange-only gradient correction,” *J. Chem. Phys.*, vol. 96, no. 3, pp. 2155–2160, Feb. 1992, doi: 10.1063/1.462066.
- [35] A. D. Becke, “Density-functional thermochemistry. II. The effect of the Perdew–

- Wang generalized-gradient correlation correction,” *J. Chem. Phys.*, vol. 97, no. 12, pp. 9173–9177, Dec. 1992, doi: 10.1063/1.463343.
- [36] A. D. Becke, “Density-functional thermochemistry. III. The role of exact exchange,” *J. Chem. Phys.*, vol. 98, no. 7, pp. 5648–5652, Apr. 1993, doi: 10.1063/1.464913.
- [37] Lee, Yang, and Parr, “Development of the Colle-Salvetti correlation-energy formula into a functional of the electron density.,” *Phys. Rev. B. Condens. Matter*, vol. 37, no. 2, pp. 785–789, Jan. 1988, doi: 10.1103/physrevb.37.785.
- [38] R. Krishnan, J. S. Binkley, R. Seeger, and J. A. Pople, “Self-consistent molecular orbital methods. XX. A basis set for correlated wave functions,” *J. Chem. Phys.*, vol. 72, no. 1, pp. 650–654, Jan. 1980, doi: 10.1063/1.438955.
- [39] J. P. Foster and F. Weinhold, “Natural hybrid orbitals,” *J. Am. Chem. Soc.*, vol. 102, no. 24, pp. 7211–7218, Nov. 1980, doi: 10.1021/ja00544a007.
- [40] A. E. Reed, L. A. Curtiss, and F. Weinhold, “Intermolecular interactions from a natural bond orbital, donor-acceptor viewpoint,” *Chem. Rev.*, vol. 88, no. 6, pp. 899–926, Sep. 1988, doi: 10.1021/cr00088a005.
- [41] *Admet predictor, ver. 9.5. (2019) User manual*. Simulations Plus, Inc, Lancaster, CA, USA, 2019.
- [42] K. Roy and I. Mitra, “Electrotopological state atom (E-state) index in drug design, QSAR, property prediction and toxicity assessment,” *Curr. Comput. Aided. Drug Des.*, vol. 8, no. 2, pp. 135–158, 2012, doi: 10.2174/157340912800492366.
- [43] V. C. Roberto Todeschini, *Handbook of Molecular Descriptors*, vol. 11. Wiley, 2008.
- [44] K. J. Miller and J. Savchik, “A new empirical method to calculate average molecular polarizabilities,” *J. Am. Chem. Soc.*, vol. 101, no. 24, pp. 7206–7213, Nov. 1979, doi: 10.1021/ja00518a014.
- [45] A. Golbraikh and A. Tropsha, “Beware of $q^2!$,” *J. Mol. Graph. Model.*, vol. 20, no. 4, pp. 269–276, Jan. 2002, doi: 10.1016/s1093-3263(01)00123-1.
- [46] A. Shayanfar and S. Shayanfar, “Is regression through origin useful in external validation of QSAR models?,” *Eur. J. Pharm. Sci.*, vol. 59, pp. 31–5, Aug. 2014, doi: 10.1016/j.ejps.2014.03.007.
- [47] N. Chirico and P. Gramatica, “Real external predictivity of QSAR models: how to evaluate it? Comparison of different validation criteria and proposal of using the concordance correlation coefficient.,” *J. Chem. Inf. Model.*, vol. 51, no. 9, pp. 2320–35, Sep. 2011, doi: 10.1021/ci200211n.
- [48] P. Gramatica, “On the development and validation of QSAR models.,” *Methods*

- Mol. Biol.*, vol. 930, pp. 499–526, 2013, doi: 10.1007/978-1-62703-059-5_21.
- [49] A. Tropsha, “Recent Advances in Development, Validation, and Exploitation of QSAR Models,” in *Burger’s Medicinal Chemistry and Drug Discovery*, Hoboken, NJ, USA: John Wiley & Sons, Inc., 2010, pp. 505–534.
- [50] T. Le, V. C. Epa, F. R. Burden, and D. A. Winkler, “Quantitative structure-property relationship modeling of diverse materials properties.,” *Chem. Rev.*, vol. 112, no. 5, pp. 2889–919, May 2012, doi: 10.1021/cr200066h.
- [51] G. Blom, *Statistical estimates and transformed beta-variables*. Almqvist & Wiksell, 1958.
- [52] Y.-L. Zhang *et al.*, “Synthesis, anticancer activity and molecular docking studies on 1,2-diarylbenzimidazole analogues as anti-tubulin agents.,” *Bioorg. Chem.*, vol. 92, p. 103219, 2019, doi: 10.1016/j.bioorg.2019.103219.

Chapter 8:
Computational Prediction and
Experimental Validation of the Unique
Molecular Mode of Action of
Scoulerine

Introduction

Natural products have played a dominant role in traditional medicine in over the previous centuries. In recent years, in spite of major advances in the computational drug discovery and total synthesis areas, there has been a growing interest in using natural products for the development of anti-cancer therapeutics [1]. Some of these pharmaceutical agents have shown promising results in the prevention or treatment of cancer [2]. Scoulerine (also known as discretamine and aequaline) is a natural product isolated from *Corydalis* plants and belongs to one of the largest groups of natural compounds known as isoquinoline alkaloids [3]. Isoquinoline alkaloids are biogenetically derived from phenylalanine and tyrosine, having a basic structure of an isoquinoline or a tetrahydroisoquinoline ring in their scaffold [4]. The scoulerine molecule consists of two tetrahydroisoquinoline rings with two hydroxyls and two methoxyl functional groups (Figure 8-1). This molecule has shown a broad range of pharmacological properties such as antiemetic, antitussive, anti-bacterial, and anti-inflammatory activities [3]. It has also been demonstrated to have an anti-proliferative and pro-apoptotic function in cancer cells [5]. In addition, it is a precursor in the biosynthesis of noscapine, another natural compound with anti-mitotic properties that has been extensively tested in the cancer chemotherapy space [6–9].

Scoulerine inhibits β -site amyloid precursor protein cleaving enzyme 1 (BACE1), which is a very favourable target for Alzheimer's treatment [10]. It has been also recently reported that scoulerine exhibits effective antimitotic activity, which leads to microtubule disruption suggesting this molecule as a promising candidate for suppression of cancer cell growth [5].

Microtubules are ubiquitous filamentous structures found in the cytoskeleton of all eukaryotic cells. They polymerize from α and β tubulin heterodimers. Microtubules are dynamic polymers in kinetic equilibrium with the α , β tubulin heterodimers in solution which is achieved through polymerization and depolymerization cycles [11].

Microtubules play a crucial role in the development and maintenance of cell shape. They are also importantly involved in mitosis and cellular movements [12]. Microtubules have been one of the most commonly considered targets for tubulin-targeting chemotherapeutic agents. The α , β tubulin heterodimers and microtubules have several different binding domains. Some of the well-studied inhibitors and their binding pockets are: the colchicine-binding domain, vinca-binding domain, laulimalide-binding domain, and taxol-binding domain, to list the most important few [11]. Most of the binding sites are not exclusive to primary inhibitors and can be targeted by other compounds. The mechanism of action of a large number of chemically diverse inhibitors of microtubules can be classified into two categories: they can act as either stabilizers or destabilizers. Microtubule-stabilizing agents stabilize the polymer by obstructing depolymerization and inducing the polymerization of tubulin [13]. Microtubule-destabilizing agents bind to the tubulin dimers and destabilize microtubules by halting polymerization of tubulin [14]. Despite the known effects of scoulerine on microtubules, a precise mechanism of action of this molecule is still unclear and further research is required [5].

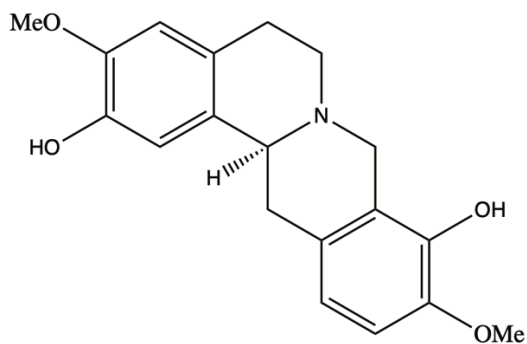


Figure 8-1. Scoulerine structure

The present study aims to address the mode of action of scoulerine by means of computational prediction studies. For this purpose, blind docking was used to predict

binding pockets for scoulerine. An evaluation scheme based on binding affinities and root mean square deviation (RMSD) between the crystallographic and the docked ligand conformations leads to valuable initial information. For an expanded investigation into predicted binding sites for scoulerine, molecular dynamic (MD) simulations were used. The complex systems of scoulerine bound in the potential binding pockets were designed and analyzed by RMSD and clustering analysis. All of the above-mentioned steps were followed to predict the stability of the binding interactions and closeness of the inhibitor to the potential scoulerine binding sites.

8.1 Materials and methods

8.1.1 3D structure preparation of the ligand.

The two-dimensional (2D) chemical structure of scoulerine was converted into a corresponding three-dimensional (3D) structure. The 3D scoulerine structure was first minimized and then fully optimized based on the RHF/ccpVDZ level of theory using the GAMESS-US software package (Version 2010-10-01) [31–34]. To investigate protonation of nitrogen in the scoulerine structure, the total energies of protonated and non-protonated scoulerine were calculated in the presence of hydronium and hydroxy ions in vacuum and water environments, respectively. The restricted Hartree-Fock method was used with the Dunning cc- pVDZ basis set for the above-mentioned calculations [31].

8.1.2 Blind docking

The optimized structure of scoulerine was blindly docked to the 1SA0 Protein Data Bank (PDB) structure of α and β tubulin *via* AutoDock4 software [16]. To do so, the maximum size of the grid box used was $126 \times 126 \times 126 \text{ \AA}^3$, which then divided

each of tubulin monomers into three parts and docking procedure was subsequently applied.

8.1.3 3D structure preparation of complexes for MD simulation

Scoulerine in the colchicine binding

The complex designed in the first part of the present study consists of scoulerine bound in the colchicine-binding pocket of human α and β I tubulin heterodimers. A homology model allows overcoming the obstacle of not having a valid crystal structure for human α (TBA1A_HUMAN) and β I tubulin (TBB5_HUMAN). The software package MOE2018 (Molecular Operating Environment, Inc) [35] was used to construct the procedure. The 1SA0 PDB crystal structure [36] was used as a structural template to create human α and β I tubulin heterodimers based on the corresponding sequence (UniProt: P07437) for human β I and (UniProt: Q71U36) for human α tubulin. The scoulerine structure was optimized by quantum mechanics molecular mechanics (QMMM) calculations. The pose of the drug was taken from the docked scoulerine to the colchicine binding site of the 1SA0 PDB crystal structure.

Scoulerine in the laulimalide binding sites of microtubule

The model used in the second part of the present study consists of scoulerine bound between two adjacent heterodimers. The homology models of human β I tubulin (TBB5_HUMAN) sequence (UniProt: P07437) and human α tubulin (TBA1A_HUMAN) sequence (UniProt: Q71U36) were generated by taking tubulin structures in 4O4H as a template [26]. The protofilament arrangement was based on the 2XRP crystal structure, which combined 8 Å resolution cryo-electron microscopy data with the 4O4H crystal structure, which has a resolution of 2.1 Å to obtain a microtubule structure at atomic resolution [26,37]. The scoulerine pose was taken from the docked scoulerine to laulimalide binding site on 4O4H.

8.1.4 Molecular dynamic simulation

In both complexes, parameters for the scoulerine were compatible with the general Amber force field (GAFF) and calculated *via* the antechamber suite of Amber 18 [38]. The Amber ff12SB force field was used to describe tubulin components. Each complex was solvated in an octahedral box of TIP3P water molecules [39] extending 12 Å from the solute. To obtain a 0.15 M ion concentration, sodium and chloride ions were added to neutralize the systems. The systems were gradually heated up to 310 K over 200 ps and maintained at 310 K for another 100 ps under constant volume conditions (NVT). The Langevin thermostat was used with a time collision frequency of 2 ps. Non-bonded terms were calculated within a 10 Å cut-off, except for long-range electrostatics, which was calculated with the particle mesh Ewald method [40]. During simulations, the SHAKE algorithm was used [41].

8.1.5 Clustering analysis

RMSD-based clustering was used to extract protein and ligand structures to represent the overall closeness and stability of a new inhibitor in the binding site. The movement trajectory of the complex was broken down into clusters of similar sampled conformations during the MD simulation. The mass-weighted RMSD of the tubulin components was calculated with respect to the structure at 0 ns. The heavy atoms of the backbone of the protein were fitted for RMSD. The clustering analysis was performed on each system, which was structurally equilibrated after 43 ns using the average linkage. The average-linkage is one of the bottom-up algorithms, in AmberTools18 (Figure 8-6 and 12) [42]. Several studies have discussed and validated the use of hierarchical algorithms in MD simulations [23,24]. A representative structure was extracted for each cluster and used for comparative analyses [43].

8.1.6 Binding affinities and pose analysis of potential scoulerine binding sites

To obtain numerical representatives for illustration of how close the potential binding sites are to the available colchicine and laulimalide binding sites, the RMSD values of scoulerine in S₁ and S₂ were calculated with respect to the reference crystal structures of colchicine, CN2 (the colchicine derivative) and laulimalide from 5NM5, 1SA0 and 4O4H PDB files, respectively.

The RMSD values of 3.5 and 3.4 Å between blind-docked scoulerine in S₁ and crystal structure of colchicine (5MN5) and CN2 (1SA0) support the assumption and illustrate that the colchicine might share its binding site with scoulerine. Moreover, the RMSD values of 1.6 Å display even more adjacency between docked scoulerine in S₂ and the crystal structure of laulimalide (4O4H). To put to a test the strength of interactions between scoulerine and residues of the above-mentioned binding sites, colchicine and scoulerine were docked specifically to the colchicine binding site (1SA0) by Autodock and their binding affinities were then compared (Table 8-1). The same method was applied to calculate and compare the binding affinities of laulimalide and scoulerine to the only crystal structure that is available for laulimalide binding site (4O4H). The fact that a laulimalide docked between microtubule protofilaments and perhaps has two binding sites on β tubulin should not be overlooked (Table 8-1).

The binding affinity of -9.23 kcal/mol for colchicine versus -7.96 kcal/mol for scoulerine in the same binding site of β tubulin predicts weaker interactions between scoulerine and colchicine binding site of β tubulin. Scoulerine is a new chemotherapeutic drug and most of the biological aspects of the drug still need to be evaluated. In 2018, the Habartova group used 20 μM of scoulerine to disrupt microtubule function in the A549 lung cancer cell line where nocodazole, another

colchicine binding site inhibitor (CBSI), was used as control [6]. Nocodazole, at a concentration of 5 μ M was shown to be as effective as scoulerine [5,19]. Binding affinity of -7.50 kcal/mol for laulimalide versus -6.87 kcal/mol for scoulerine in the same binding site of β tubulin also predicted weaker binding interactions between scoulerine and β tubulin in the laulimalide binding sites of the 4O4H PDB crystal structure.

Table 8-1. (A) Binding energies of scoulerine and colchicine docked in the colchicine binding site (1SA0). (B) scoulerine and laulimalide docked in the laulimalide binding site (4O4H).

Name	Colchicine binding site A		Laulimalide binding site B	
	Colchicine	scoulerine	Laulimalide	scoulerine
B.A (kcal/mol)	-9.23	- 7.96	-7.50	- 6.87

The steps described below were followed to evaluate the three potential binding sites of β tubulin and identify which one might be the most probable binding site for scoulerine. First, visualization of the docked poses of scoulerine was done. Next, analysis of the interacting residues of each binding site of β tubulin with scoulerine was carried out. Finally, results of molecular dynamics simulations of scoulerine in the colchicine and laulimalide binding pockets were inspected.

Table 8-2. RMSD values for scoulerine in S1 and S2 with respect to the reference of crystal structures of colchicine, colchicine derivative, CN2 and laulimalide form 5NM5,1SA0 and 4O4H PDB files respectively.

Crystal structure (Reference)	Docked scoulerine	RMSD (\AA)
CN2 (1SA0)	S ₁	3.4
5NM5 (Colchicine)	S ₁	3.5
Laulimalide (4O4H)	S ₂	1.6

8.1.7 Microscale thermophoresis

Microscale thermophoresis analyses were carried out using a Monolith NT.115 instrument (Nano Temper Technologies, Germany). Lyophilized tubulin powder was purchased from commercial sources (Cytoskeleton Inc, Denver, CO, USA; T240) and reconstituted as previously described (Kalra et al., 2020). Briefly, 180 μ L of GTP (guanosine triphosphate) supplemented BRB80 (80 mM PIPES pH 6.9, 2 mM $MgCl_2$, 0.5 mM EGTA, 1mM GTP) was first added to 20 μ L of microtubule cushion buffer (BRB80T in 60 % glycerol). This solution was added to 1 g of lyophilized tubulin powder for reconstitution, aliquoted and stored at $-80^\circ C$. Rhodamine labelled tubulin (Cytoskeleton Inc, Denver, CO, USA; TL590m; 20 μ g) was reconstituted by adding 70 μ L of unlabelled tubulin solution (described above) to 5 μ L of microtubule cushion buffer. All experiments were carried out at 23 $^\circ C$ in Monolith NT.115 Premium capillaries (Nano Temper Technologies, cat# MO-L011), with 95% LED power (fluorescence lamp intensity) and 60% microscale thermophoresis power (IR-laser intensity). Scoulerine was diluted into the assay buffer containing 80 mM PIPES-KOH, pH 6.9, 2 mM $MgCl_2$ and 0.5 mM EGTA, with titration range of 50 μ M to 12.2 nM. Experiments were performed in two replicates, data were analyzed by Monolith Affinity Analysis v2.2.6 software, exported to excel and plotted with GraphPad Prism 7.0.

8.2 Result and discussion

8.2.1 Protonated or deprotonated scoulerine in cancer cell

The first step to investigate the mechanism of action of scoulerine is to distinguish the proper structure for the ligand in the cancer cell environment. Scoulerine has a nitrogen atom in its ring that can be protonated in a sufficiently acidic environment. The acidity of cancer cells is slightly different from normal cells. *In vivo*, the

extracellular matrix of tumours shows acidity of 6.2 to 6.9 pH. However, the intracellular matrix of tumours is alkaline, having a pH range of 7.12 to 7.65 [15]. With the help of quantum mechanical calculations, the total energies of scoulerine and protonated nitrogen scoulerine in acidic (H_3O^+) and basic (OH^-) environment, in vacuum and in the presence of water, were calculated and compared (Table 8-3). The total energies of -3050122 kJ/mol. for scoulerine and H_2O versus -3049860 kJ/mol. for deprotonated scoulerine with hydroxy indicate that nitrogen of scoulerine stays deprotonated in the alkaline cancer cell environment.

Table 8-3. Total energy of protonated and non-protonated scoulerine by quantum mechanical calculations in 8 different systems. (A) scoulerine and hydronium in vacuum and water. (B) protonated scoulerine with H_2O in water and vacuum. (C) scoulerine with H_2O in water and vacuum. (D) protonated scoulerine with hydroxy in water and vacuum.

A	E_{Scoul} (kJ/mol)	$E_{\text{H}_3\text{O}^+}$ (kJ/mol)	E_{Total} (kJ/mol)	B	$E_{\text{H}^+ \text{Scoul}}$ (kJ/mol)	$E_{\text{H}_2\text{O}}$ (kJ/mol)	E_{Total} (kJ/mol)
Shifted by	-2850	-2009	-3051		-2851	-1996	-3051
Vac	-453	-56	-409	Vac	-529	-170	-120
H_2O	-506	-56	-461	H_2O	-711	-170	-330
C	E_{Scoul} (kJ/mol)	$E_{\text{H}_2\text{O}}$ (kJ/mol)	E_{Total} (kJ/mol)	D	$E_{\text{H}^+ \text{scoul}}$ (kJ/mol)	E_{HO^-} (kJ/mol)	E_{Total} (kJ/mol)
Vac	-453	1283	930	Vac	-529	-1821	1692
H_2O	-506	1257	878	H_2O	-713	-1428	1140

8.2.2 Analysis of potential scoulerine binding sites on β tubulin

The AutoDock software package was used [16] to test whether it is possible to find the potential binding sites and binding modes of flexible scoulerine on α and β tubulin monomers without any prior knowledge of their location and conformation. The

AutoDock based blind docking (BD) approach [16] searches the entire surface of proteins for finding binding sites while simultaneously optimizing the conformations and the pose of the docked ligands. AutoDock is an appropriate tool for such a test because of its parameter set, based on the AMBER force field [17], and the capability of using flexible torsions for the ligands during the docking process. The protocol for docking procedures in different software packages is slightly different. In Autodock4, first the auto-grid program maps the target protein and then the auto-dock program docks the desired ligands to the set of grids of the mentioned protein [16].

Three potential binding sites were predicted as a result of blind docking of deprotonated scoulerine to 1SA0 PDB structure from Protein Data Bank (Figure 8-2). All of the three estimated binding sites found were on β tubulin. To investigate whether any of the predicted binding sites matched with the known binding sites of β tubulin, 41 Protein Data Bank files were superimposed on the 1SA0 PDB structure with scoulerine docked to the three predicted binding sites. Vinca alkaloids, colchicine, taxol, epothilone, and laulimalide sites are the major binding sites for most stabilizing and destabilizing tubulin inhibitors bind to prevent the dynamics of microtubules [18].

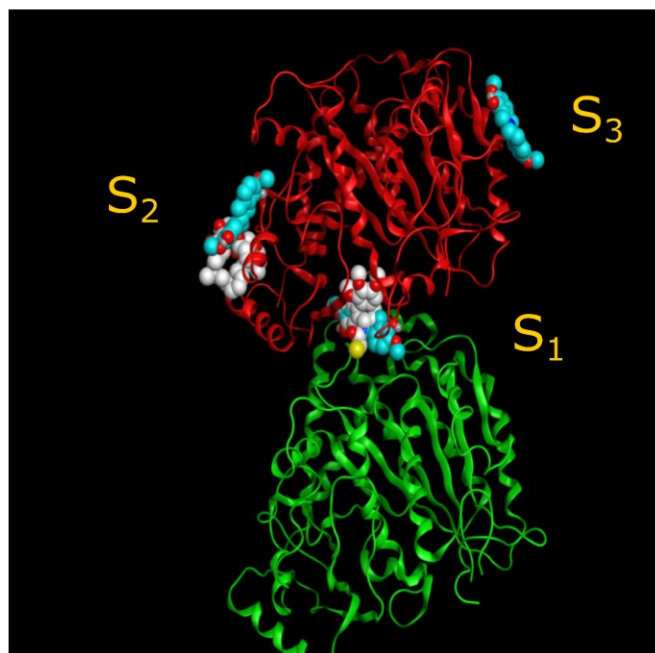


Figure 8-2. S_1 , S_2 and S_3 represent the three predicted potential binding sites by blink docking of scoulerine (blue) to α (green) and β (red) tubulins of 1SA0 PDB structure. Colchicine derivative from 1SA0 in S_1 and Laulimalide from 404H in S_2 shown in white.

CN2, a colchicine derivative, from 1SA0 and colchicine from 5NM5, were found to be close to the docked scoulerine location in S_1 . This observation suggests S_1 site has the potential to be a colchicine binding site. Laulimalide from 404H was also found to be close to the docked scoulerine location in S_2 . Based on the analysis, the S_2 site can also potentially be a laulimalide binding pocket. For S_3 , However, none of the available inhibitors were close enough to the docked scoulerine.

8.2.3 Colchicine site

The colchicine binding site on tubulin is a well-studied binding pocket and to date, many crystal structures of inhibitors have been found to dock in the colchicine binding site [20,21]. Seven pharmacophoric points were distinguished for CBSIs and are displayed in Figure 8-3. Based on previous work done on the subject, none of the

known structures of CBSIs contains all seven pharmacophore groups [20,21]. Three hydrogen bond acceptors of pharmacophoric points are labelled as A1, A2 and A3 in Figure 8-3. The backbone nitrogen of Val α 179 of the colchicine binding pocket is in contact with A1. The sulfur atom of Cys β 239 interacts with A2. Finally, A3 forms one contact mainly with the backbone nitrogen of Ala β 248, Asp β 249, and Leu β 250. Hydrogen bond donor of pharmacophoric points, D1, interacts with the backbone oxygen of Thr α 177. H1 and H2 are the two hydrophobic centers of pharmacophoric points. H1 point reacts to the side chains of Val α 179 and Met β 257. H2 interacts with side chains of Leu β 255, Ala β 316, Val β 318 and Ile β 378. The last pharmacophoric points, R1, belong to one planar group (Figure 8-3) [20,21].

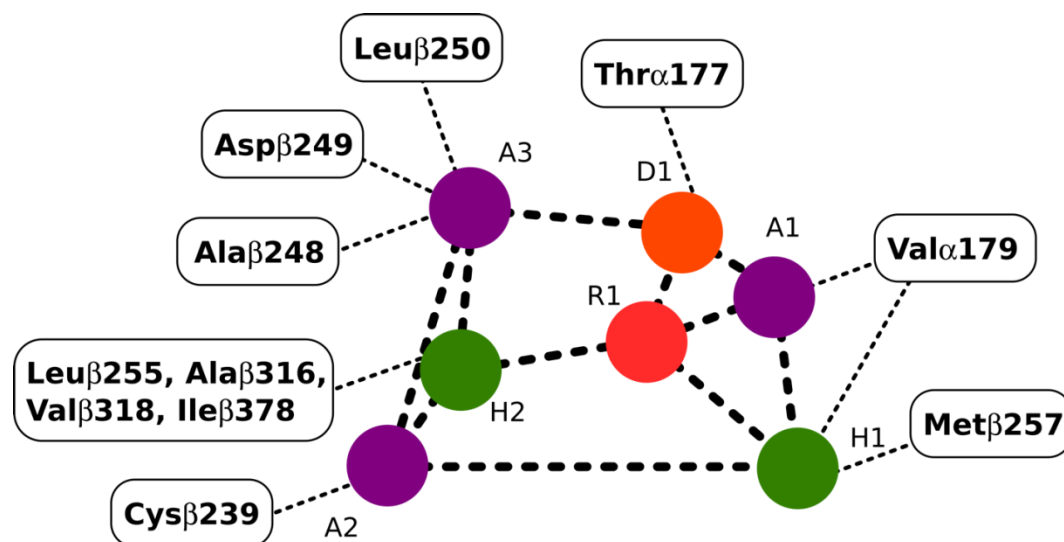


Figure 8-3. Interactions between the pharmacophoric points and the tubulin structure [21].

8.2.4 Potential scoulerine binding site (S_1)

In Figure 8-4A, a two-dimensional interaction scheme of the superimposed colchicine crystal structure from 5NM5 PDB file (green) on scoulerine in the S_1 site (red) illustrates the pose of scoulerine in comparison to the pose of colchicine. Even

though the pose of the colchicine crystal structure overlaps with the pose of scoulerine in the S_1 (Figure 8-4A), analyzing the adaptation of scoulerine with seven pharmacophore groups of colchicine binding site inhibitors was essential. The two-dimensional interaction scheme (Figure 8-4B) displays interactions between scoulerine and potentially a binding pocket, S_1 . Scoulerine has the A1 pharmacophoric point of CBSI ligands because of the hydrogen acceptor interaction between a sulfur atom of Cys239 with N of scoulerine. The A3 pharmacophoric point of CBSI ligands is supposed to have a hydrogen acceptor by the backbone nitrogen of Ala248 or Leu250. However, the distance between the backbone nitrogen of Ala248 or Leu250 and scoulerine is 4.2 Å that translates into weak electrostatic interactions. Taking into consideration that the pose of scoulerine is the result of wide blind docking, there is a possibility that a small adjustment might lead to the hydrogen bonding with either Ala248 or Leu250 (Figure 8-4B). The third pharmacophoric point of CBSI, H2, is a hydrophobic center that interacts with side chains of Leu255, Ala316, Val318, and Ile378. The green color of the above-mentioned residues in the 2-dimensional interaction scheme in Figure 8-4B means greasy that refer to hydrophobic nature of the residues. The blue circles show the ligand exposure to the solvent and the dotted line around the ligand shows the proximity contour. The closer is the ligand to the contour in the scheme, the deeper the ligand is in the cavity of the binding pocket of the protein. To put it in a better perspective, Figure 8-4C is generated to show the hydrophobic surface of protein in the S_1 site that wraps the hydrophobic center, H2, of the scoulerine.

Scoulerine also has planar group to fit the pharmacophoric R1 point. D1 and A1 of the pharmacophoric points of CBSI interact with Thr177 and Val178 of α tubulin. However, the closest residue of α tubulin in the Figure 8-4B is Ser178.

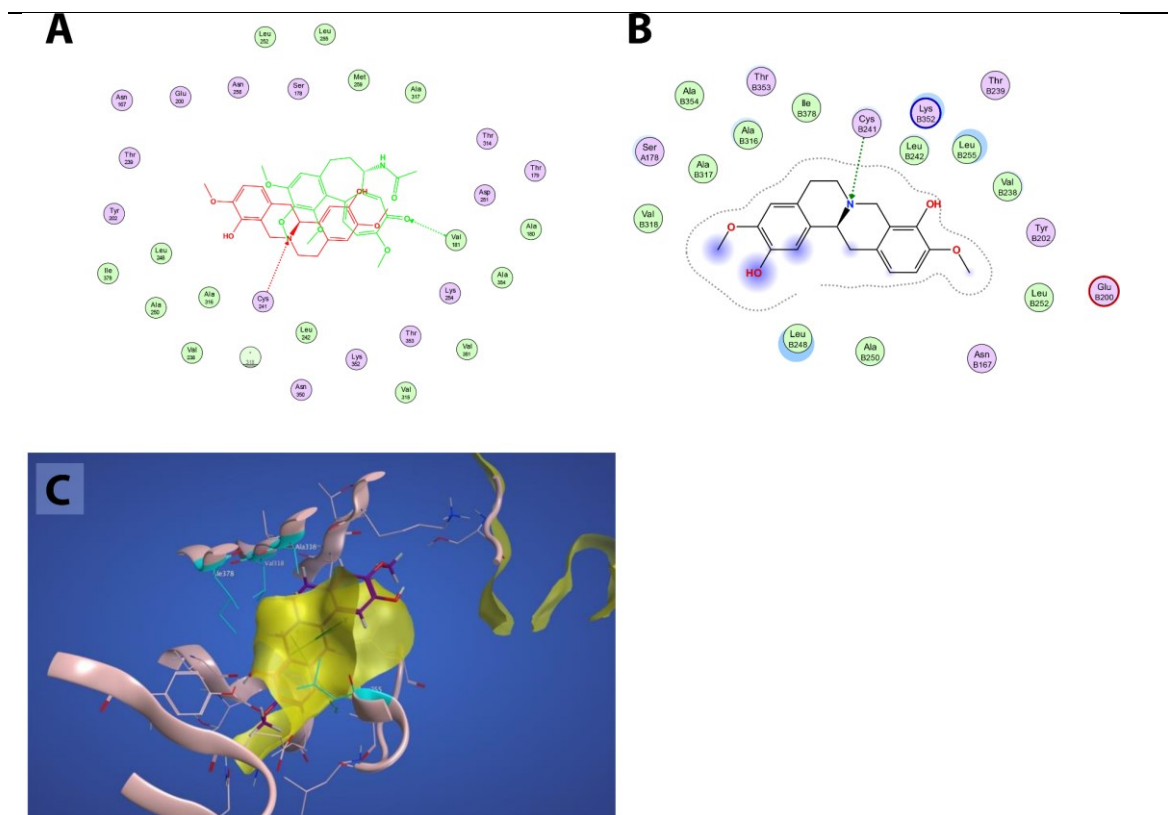


Figure 8-4. (A) 2D-interaction scheme of superimposed colchicine crystal structure from 5NM5 PDB file (green) on scoulerine in the S_1 site (red). (B) 2D-interaction scheme of scoulerine in the S_1 site. (C) Surface patches identifying regions of hydrophobicity (yellow) around scoulerine. Residues Leu255, Ala316, Val318, and Ile378 of β tubulin that involve in hydrophobic interaction colored in teal.

8.2.5 Conformational analysis

RMSD analysis on S_1 site

Homology model of human α and β I tubulin based on 1SA0 template was performed. Scoulerine was specifically docked to colchicine binding site. Molecular dynamic simulation of the system was performed for 120 ns. The RMSD values of scoulerine to the backbone of colchicine binding site were calculated during the simulation. In order to assess the equilibration of the system, the plot of total energies

of the system versus time was plotted and compared to the RMSD plot. The system appeared to be equilibrated after 43 ns. The RMSD value of 2.2 to 2.3 Å for 77 ns of simulation after the equilibration verified that the interactions between scoulerine and residues of colchicine binding site are strong enough to keep the ligand close to binding pocket Figure 8-5.

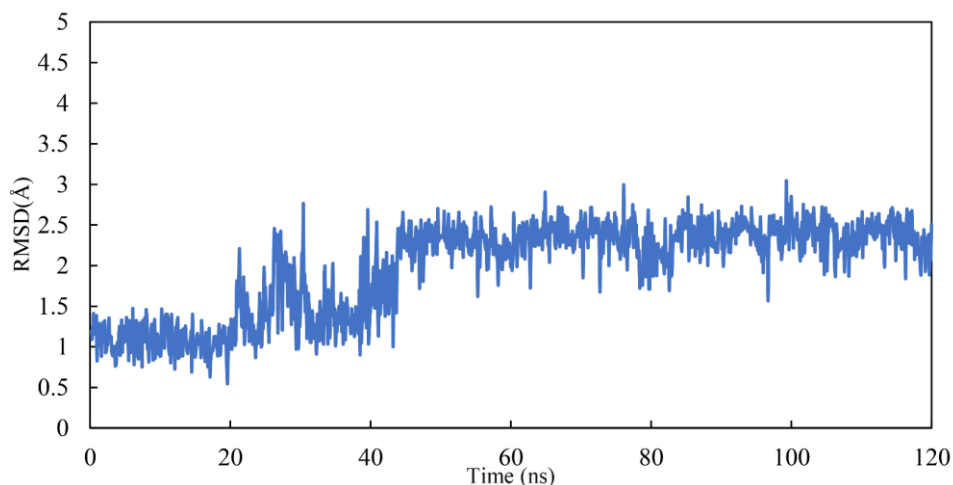


Figure 8-5. RMSD of scoulerine to the colchicine binding site (S₁-ISA0).

Clustering analysis

Clustering analysis was carried out with the hierarchical agglomerative algorithm [22]. Several studies have discussed and validated the use of hierarchical algorithms in MD simulations [23,24]. The frames of 77 ns were clustered as reported by binding site closeness. To be specific, this closeness was sorted based on the mass-weighted RMSD of the binding-site atoms, which includes scoulerine and residues having atoms within 8 Å of scoulerine. The centroid structures have the smallest RMSD relative to all the other members of the same cluster.

The algorithm generates representative structures, centroid structures, of scoulerine poses in the colchicine binding site throughout the 77 ns simulation. The

trajectory frames were partitioned into clusters A, B, and C (Figure 8-6). Cluster B of the graph indicates more than 50 percent of occupancy during the simulation. In Figure 8-7A, the pose of the representative structure of dominant cluster B was displayed with the pose of colchicine's crystal structure (Figure 8-7D) of 5NM5 structure. The representative structure (centroid) for each cluster was extracted and displayed in (Figure 8-7C).

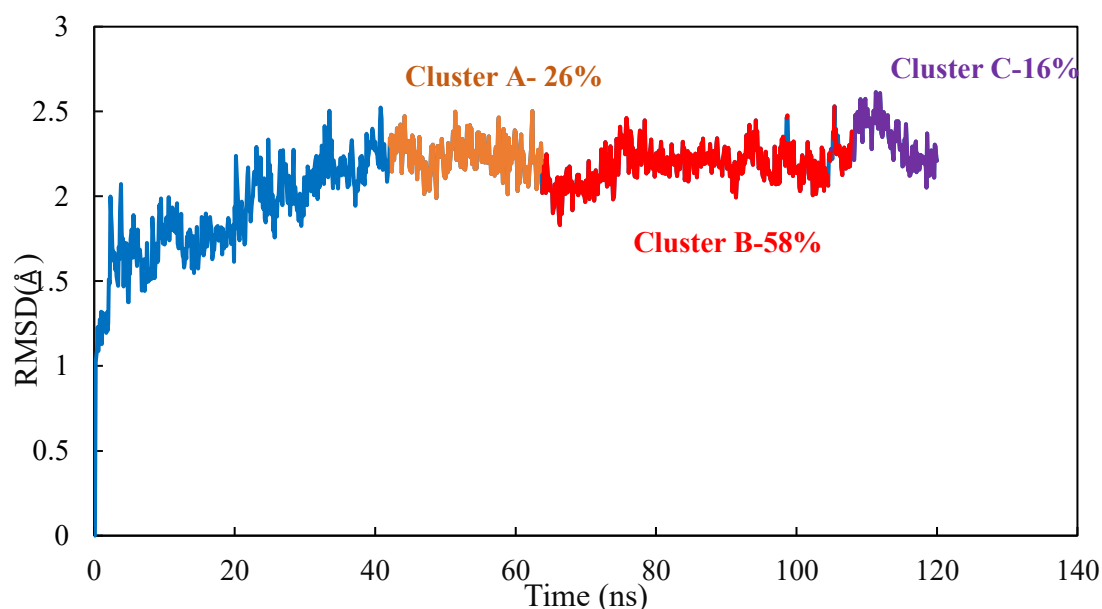


Figure 8-6. Mass-weighted root mean squared deviation (\AA) of the binding site of colchicine to tubulin, classified according to cluster number, with occupancy indicated. The binding site includes scoulerine and residues having atoms within 8 \AA of scoulerine. The dark blue part of the graph illustrates the equilibration.

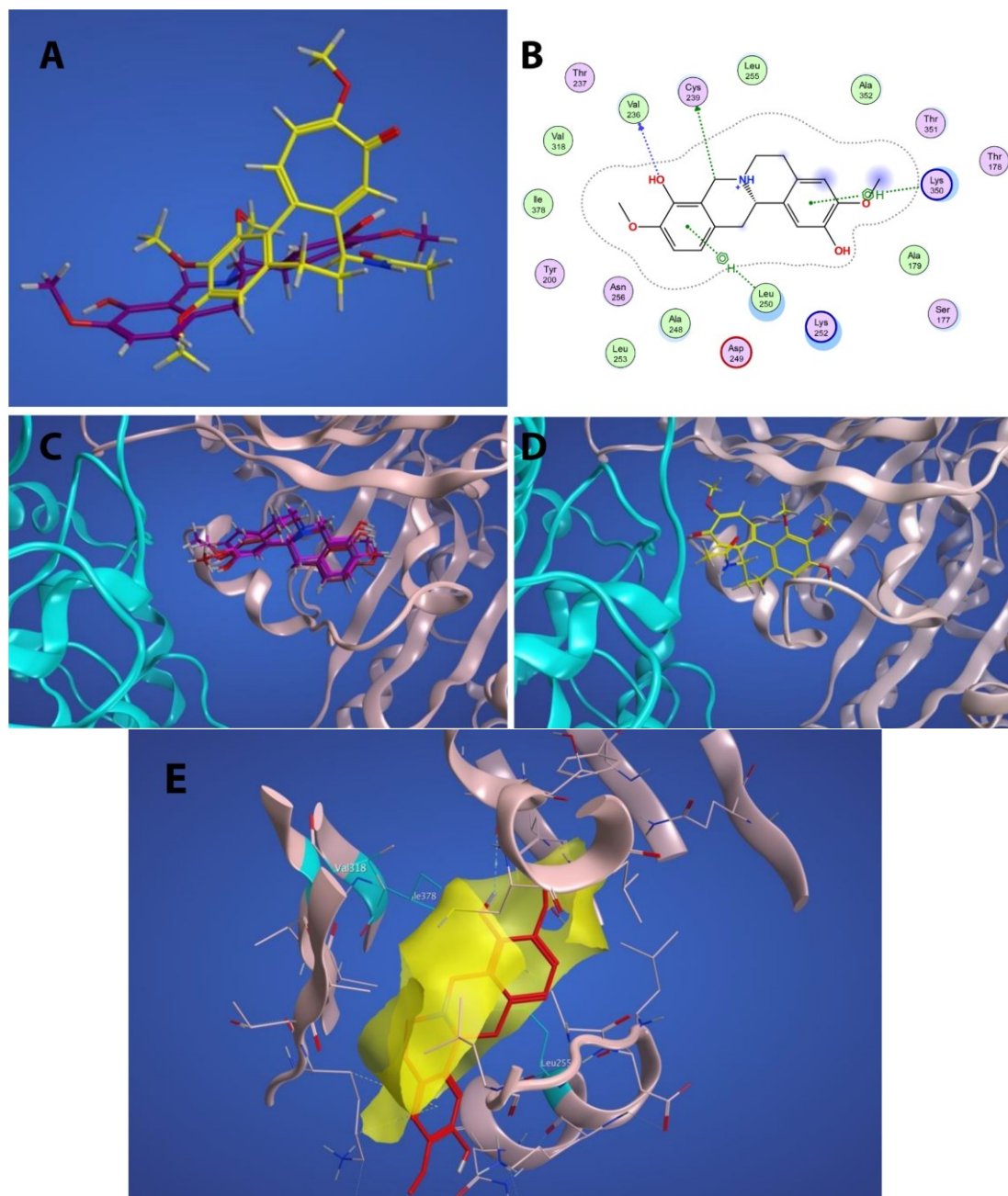


Figure 8-7. (A) Representative structures of scoulerine in cluster B (purple) versus colchicine (yellow) (B) 2D- interaction scheme of scoulerine in colchicine binding site. (C) Representative structures of cluster A (red), cluster B (purple) and cluster C (dark pink) in colchicine binding site, α tubulin colored in teal and β I tubulin colored in light pink. (D) Colchicine (yellow) in colchicine binding site, α tubulin colored in teal and β I tubulin colored in light pink. (E) surface patches identifying regions of hydrophobicity (yellow) around scoulerine, residues Leu255, Val318, and Ile378 of β tubulin that involve in hydrophobic interaction colored in teal.

As displayed in Figure 8-7C, the sulfur atom of Cys β 239 still has a hydrogen acceptor with scoulerine (A2). As predicted before, the backbone nitrogen of Leu β 250 now is sufficiently close to make a hydrogen binding with scoulerine (A3). Hydrophobic interactions between scoulerine (H2) with side chains of Leu255, Val318, and Ile378 still occurred as illustrated in Figure 8-7E. The hydrogen bond donor D1 pharmacophoric point of colchicine binding site inhibitors did not appear in the interaction diagram of blindly docked scoulerine to α and β tubulin. D1 interacts with the backbone oxygen of Thr α 177. However, the interaction diagram of the most dominant representative structure of scoulerine docked to colchicine binding site of human α and β I tubulin over 77 ns of MD simulation shows Thr α 177 near enough to the ligand to demonstrate weak electrostatic interaction.

8.2.6 Laulimalide sites on β tubulin

Laulimalide is a novel microtubule stabilizer that binds between two protofilaments of a microtubule, which has been in the spotlight because of its unique mode of action. Despite computational studies which attempted to identify the laulimalide binding site, the first crystal structure of laulimalide bound to tubulin was captured by X-ray diffraction in 2014. The binding pocket is formed by residues Gln293, Phe296, Pro307, Arg308, Tyr312, Val335, Asn339, Tyr342, Ser298, Asp297, and Phe343 of tubulin (Figure 8-8). Gln293, Ser298, Asp297, and Asn339 are the residues that form hydrogen bonds with laulimalide [22,25,26].

Computational studies on the mode of action of laulimalide discovered Gln293, Phe296, and Asn 339 residues of β tubulin as the most stabilizing residues [22,25,26]. The computational analyses also showed that Lys122, Glu125, Ser126, and Arg121 residues of β tubulin of adjacent protofilament bind to laulimalide but they have smaller stabilizing contribution [22,25,26].

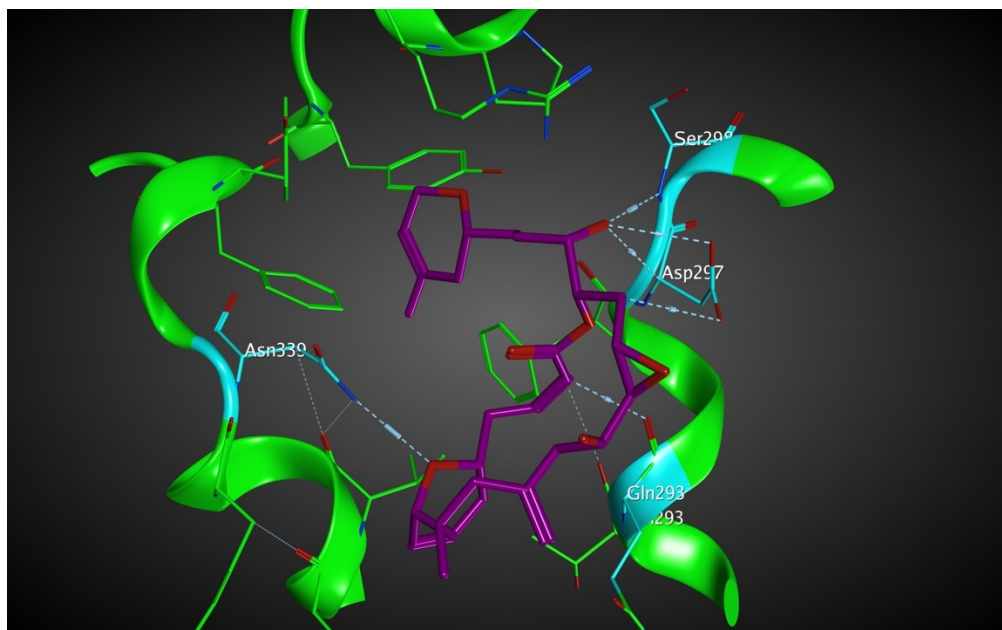


Figure 8-8. Laulimalide in the laulimalide binding site of β tubulin (green) in 4O4H PDB file. Residues in blue have hydrogen bonding interaction with laulimalide (purple).

Similar to colchicine binding pocket, laulimalide is not the only inhibitor that binds to laulimalide binding sites. Peloruside (4O4L PDB) is another drug that binds to the laulimalide binding site of β tubulin and has been identified by X-ray diffraction. The binding mode of peloruside and laulimalide to tubulin is similar. In this case, Ser298, Asp297, Arg308, Gln293, and Tyr312 residues of tubulin formed hydrogen bonds with peloruside. Gln293, Ser298, and Asp297 residues are special since they make hydrogen bonding with both of the inhibitors, i.e., laulimalide and peloruside [26].

8.2.7 Potential scoulerine binding site (S₂)

Based on blind docking results, the O37 of the hydroxyl group of scoulerine in the binding site S₂, similar to laulimalide and peloruside, makes hydrogen-donor bonds with the side chains of Gln293 (Figure 8-9A). Asp297 of the laulimalide binding pocket

also forms hydrogen bonds with laulimalide and peloruside. However, in the interaction of scoulerine with the residues of the S₂ site, Asp297 shows an electrostatic interaction instead. Pro307, Arg308, Val335, Lys338, Phe296, and Asn339 are other interactive residues of the S₂ site that are held in common with the residues of the laulimalide binding site. In Figure 8-9B, a two-dimensional interaction scheme of superimposed laulimalide crystal structure from 4O4H PDB file (green) on scoulerine in the S₂ site (red) illustrates the pose of scoulerine in comparison with the pose of laulimalide. The computational analyses also showed that Lys122, Glu125, Ser126, and Arg121 residues of β tubulin of the adjacent protofilament bind to laulimalide but they have a smaller stabilizing contribution.

The S₃ site primarily appears by blind docking of scoulerine to 1SA0 PDB structure and did not show any compatibility with available binding sites of β tubulin by crystallography (Figure 8-9C). The residues of the S₃ site, Arg123, Lys124, Glu127, and Ser128, are very similar to the residues of the second binding site of laulimalide on β tubulin of the adjacent protofilament, namely Lys122, Glu125, Ser126, and Arg121.

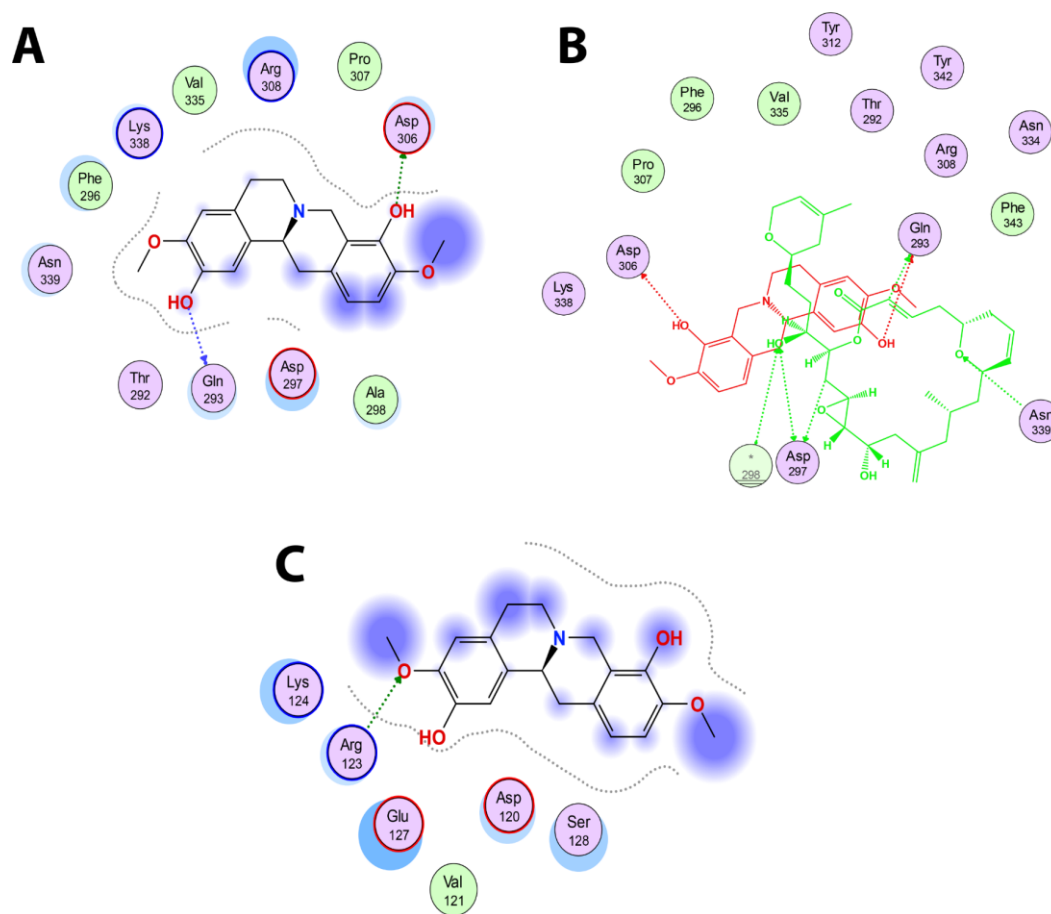


Figure 8-9. (A) 2D-interaction scheme of scoulerine in the S_2 site *via* blind docking. (B) 2D-interaction scheme of superimposed laulimalide crystal structure from 4O4H PDB file (green) on scoulerine (red) in the S_2 site. (C) 2D-interaction scheme of scoulerine in the S_3 site *via* blind docking.

8.2.8 Conformational analysis

RMSD analysis on scoulerine bound between protofilament (laulimalide binding sites)

Homology model of human α and β I tubulins was performed based on 4O4H crystal structure combined with the 2XRP crystal structure to arrange two adjacent

protofilament. The scoulerine pose was taken from the docked scoulerine to laulimalide binding site on 4O4H [26].

Molecular dynamics simulation of the system was performed for 160 ns. The RMSD values of scoulerine to the backbone of the laulimalide binding site were calculated during the simulation (Figure 8-10). In order to assess the system's equilibration, the plot of total energies of the system versus time was graphed and compared to the RMSD plot. The system appeared to be equilibrated after 10 ns but since substantial structural equilibration (45 ns) is necessary to stabilize the lateral contacts between tubulin heterodimers, production data were collected for 115 ns after equilibration. The RMSD value of 3.1 to 3.3 Å for 115 ns of simulation verified that the interactions between scoulerine and residues of the scoulerine binding site are strong enough to keep the ligand close to the binding pocket.

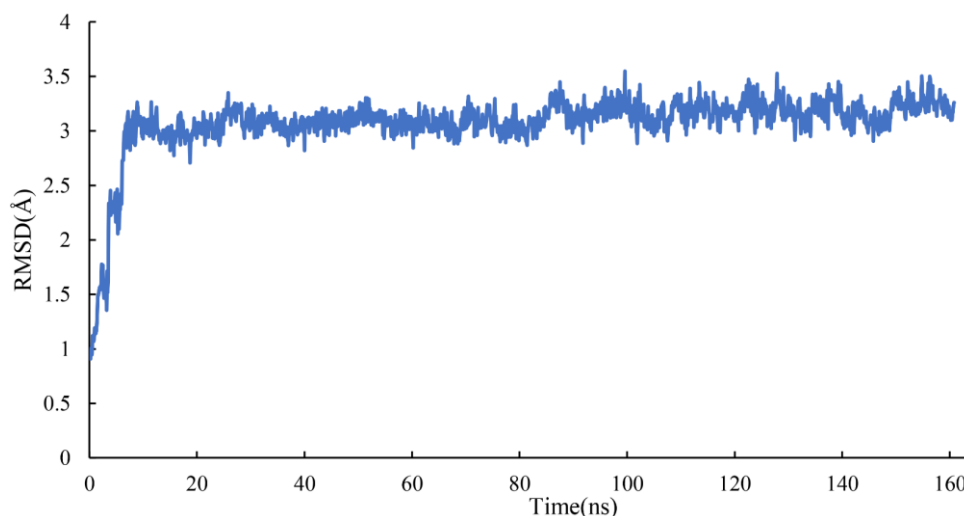


Figure 8-10. RMSD of scoulerine to the laulimalide binding site (S1-1SA0).

Clustering Analysis

The same as for the colchicine binding site, clustering analysis was also conducted for the frames of the last 115 ns of the simulation to show the stability of the system to keep the ligand in the binding pocket. The mass-weighted RMSD of the binding-site atoms throughout the trajectory frames of 115 ns were classified after equilibration to two clusters. To be specific, the binding-site atoms include scoulerine and residues having atoms within 8 Å of scoulerine, while water and ions are excluded. The algorithm also generates two representative structures of scoulerine poses in the laulimalide binding sites between the protofilament for each of the clusters (Figure 8-11). Cluster A of the graph indicates more than 67 percent of occupancy during the simulation.

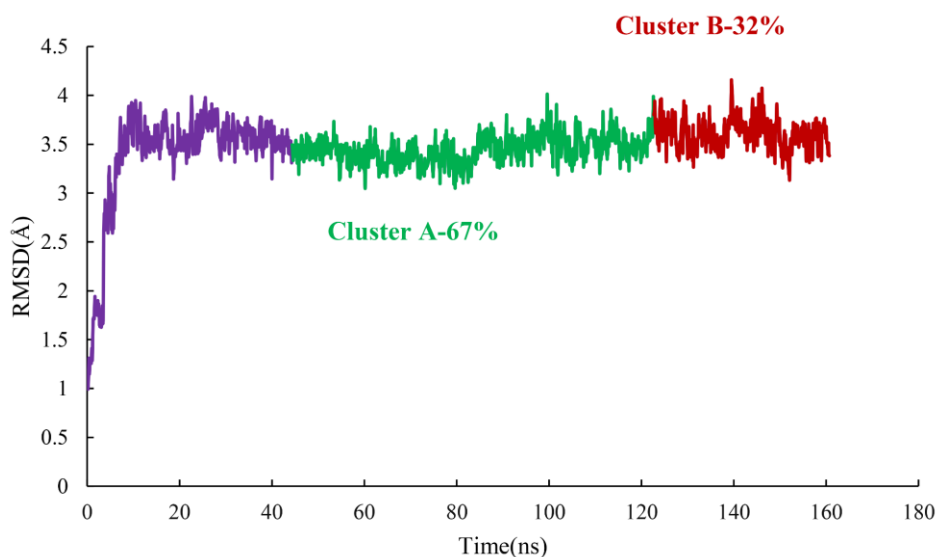


Figure 8-11. Mass-weighted root mean squared deviation (Å) of the binding sites of laulimalide to tubulin, classified according to cluster number, with occupancy indicated. The binding site includes scoulerine and residues having atoms within 8 Å of scoulerine. The purple part of the graph illustrates the equilibration.

Representative structures of scoulerine between $\alpha_A \beta_A$ and $\alpha_B \beta_B$ tubulins of two adjacent protofilaments are displayed in Figure 8-12C. Representative structures for cluster A are shown in purple and in dark pink for cluster B.

In Figure 8-12A, the representative structure of dominant cluster A was displayed with superimposed laulimalide of the 4O4H crystal structure. The residues of laulimalide's binding pocket of β_B tubulin are highlighted in light green. The computational study illustrated the residues of the second binding site of laulimalide on the adjacent β_A tubulin and they are coloured dark green in Figure 8-12A [22]. The 2D interaction scheme of the most dominant representative structure of the system shows that scoulerine can also bind between β tubulins of two adjacent protofilaments (Figure 8-12B). The hydrogen acceptor between the nitrogen of the scoulerine and Gln293 of β_B tubulin and the π -hydrogen interaction between a ring of scoulerine and Ser125 of β_A tubulin, are the two most important binding interactions between scoulerine and residues of the laulimalide binding pockets. Gln293, Phe296, and Asn339 residues of β tubulin are the most important stabilizer residues in the binding interaction between laulimalides and residues of its binding sites. The involvement of all three residues in the interaction scheme of scoulerine with laulimalide binding sites [22,25] raised the possibility that scoulerine might be a new inhibitor to bind between microtubules. Val335 and Phe296 residues of laulimalide binding site also showed weak electrostatic interaction with scoulerine. As shown in Figure 8-12A, scoulerine has smaller-scale structure compared to laulimalide. Thus, the new drug shifted from the first binding pocket of laulimalide on β_B tubulin, the crystal structure of laulimalide binding site 4O4H PDB, toward the second one on β_A tubulin to be able to bind to both binding sites. Lys122, Glu125, and Ser126 are the most important residues on laulimalide binding pocket on β_A tubulin [22,25] which also interact with scoulerine (Figure 8-12A and B).

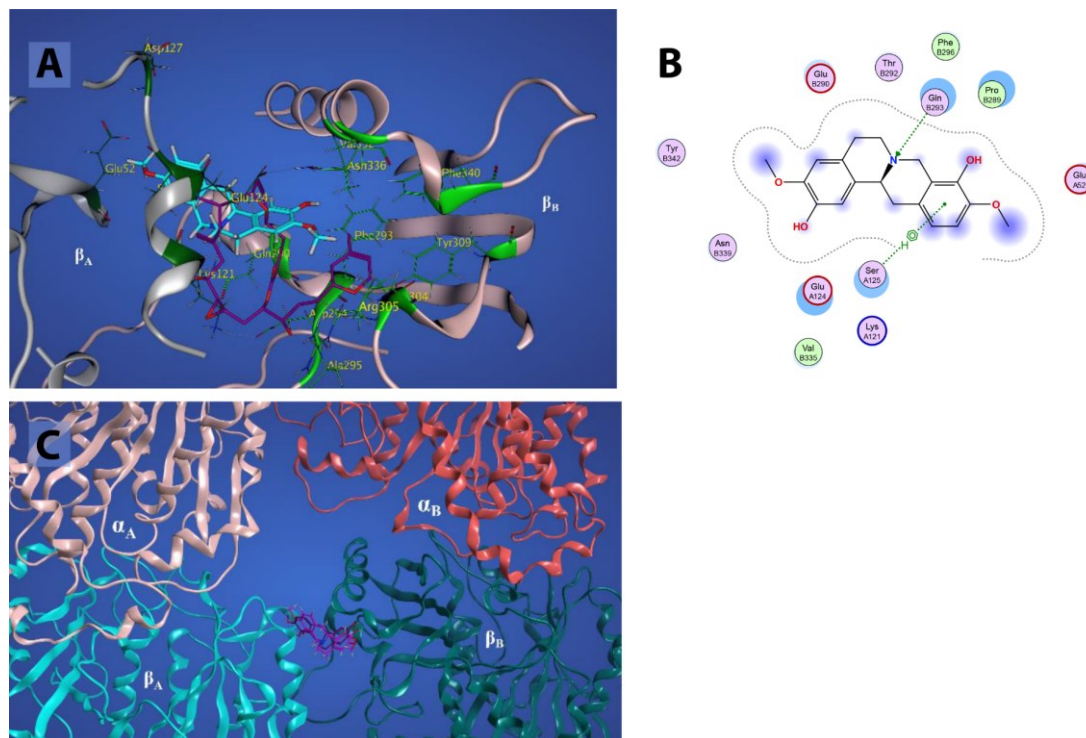


Figure 8-12. (A) 3D-interaction scheme of scoulerine (blue) and superimposed laulimalide crystal structure from 4O4H PDB file (purple) between microtubules. Residues in light green are in laulimalides's site on β_A tubulin and residues in dark green are in laulimalides's site on β_B tubulin. (B) 2D-interaction scheme of Scoulerine in laulimalide binding sites on β_A tubulin and β_B tubulin. (C) Representative structures of cluster A (purple) and cluster B (pink) in laulimalide binding sites. α_A and α_B tubulins colored in light and dark pink and β_A and β_B tubulins colored in light and dark green respectively.

Experimental validation

Based on the computational prediction, scoulerine potentially should be able to bind to both colchicine and laulimalide binding sites. However, based on docking results, the binding affinities might not be as strong as for colchicine or laulimalide.

To evaluate the predictions, the dissociation constant of scoulerine bound to free α and β tubulin dimers and microtubules were measured by the microscale thermophoresis method. The K_d values of 35.9×10^{-6} M and 431×10^{-6} M were reported

for scoulerine bound to labelled free α and β tubulin dimers and labelled microtubules, respectively (Figure 8-13A)

The range of values for the reported dissociation constants confirms the computational results and indicates that scoulerine can bind to both free tubulin dimers and microtubules. Consequently, it has a dual mechanism of action.

The dissociation constant, K_d , of the well-studied colchicine bound to free α and β tubulin dimers were also measured to use as a reference. The K_d value of 67.6×10^{-6} M shows that colchicine's binding affinity is stronger than that of the scoulerine in the interaction with tubulin dimers (Figure 8-13B). The binding affinities calculated *via* docking were reported to be -9.32, -7.96, and -6.87 kcal/mol for colchicine and scoulerine in colchicine and laulimalide binding sites, respectively (Table 8-1). Unfortunately, due to extreme difficulty in obtaining samples of laulimalide, we have not been able to test its binding affinity for tubulin in microtubules in this assay but it has been reported elsewhere [27]. The range of values of binding affinities agrees with dissociation constant values.

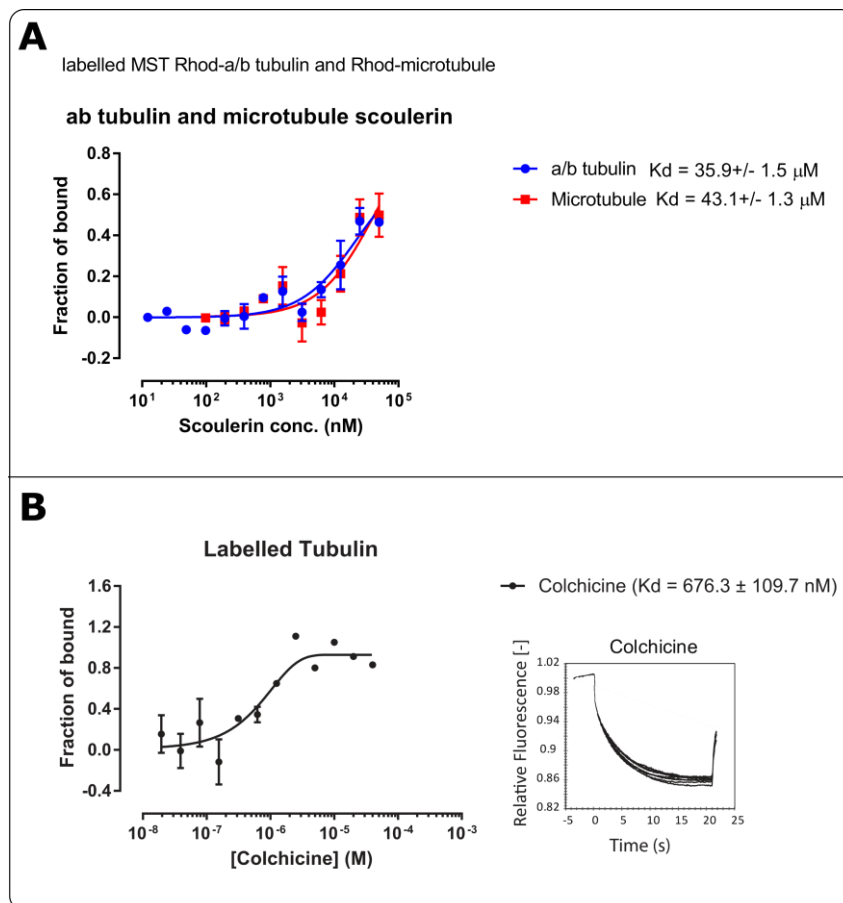


Figure 8-13. (A) K_d values for scoulerin bound to labelled α and β tubulin (colchicine binding site) and microtubule (laulimalide binding site) obtained by microscale thermophoresis. (B) K_d value of colchicine bound to labelled α and β tubulin (colchicine binding site) used as a control.

8.3 Conclusions

Scoulerine is a natural drug in the family of isoquinoline alkaloids that can be extracted from *Croton flavens* [28], *Corydalis dubia* [29], and *Corydalis cava* [10,30]. New research on scoulerine has revealed a range of effects, including anti-proliferative and pro-apoptotic properties, as well as antimetabolic activity that disrupts microtubules [5,6]. The listed properties of scoulerine make it a possible candidate for use in cancer

treatment. However, the mode of action of the scoulerine is still unclear to date. The present work attempted to predict the mechanism of action of this new chemotherapeutic agent by computational approach. A combination of blind docking and molecular dynamics provides a useful approach to acquire new, detailed information about the interactions between scoulerine and β tubulin within a microtubule. Three potential binding sites were found on β tubulin of a microtubule *via* the blind docking method. With the help of the RMSD between the crystallographic structure of inhibitors of β tubulin and the docked ligand conformations, three possible binding sites have been discovered and labelled S₁, S₂, and S₃ (Figure 8-2). The residues of the discovered S₁ binding site on β tubulin are mostly the same as the colchicine binding pocket.

Laulimalide is a unique stabilizer of the microtubule that can bind to β tubulins of adjacent protofilament [22]. The residues of estimated S₂ and S₃ binding sites of β tubulins have similarities with the laulimalide binding site on β tubulins of adjacent protofilament. Two improved models of scoulerine binding to $\alpha\beta$ tubulin heterodimers were designed and investigated by molecular dynamics simulations. The first one consists of scoulerine located between α and β tubulins in the crystallographic colchicine binding sites based on 1SA0 PDB. In the second one, scoulerine is placed between two adjacent $\alpha\beta$ heterodimers and bound to a crystallographic laulimalide binding site based on 4O4H PDB. The cluster analyses were calculated for both of the systems. The structures of the smallest RMSD of each of the clusters were also presented. The 3D interaction scheme of the representative structure of the highest cluster for both systems is also displayed. The results showed scoulerine can bind between both α and β tubulin of a heterodimer. It can also bind between β tubulins of two adjacent heterodimers. The mentioned prediction was put to the test by measuring the dissociation constant between scoulerine bound to labelled free and tubulin dimers and labelled microtubules. The K_d values of 35.9×10^{-6} M and 431×10^{-6} M were reported for scoulerine bound to labelled free α and β tubulin dimers and labelled

microtubules. The similarity between the values of the K_d for both systems confirmed the computational estimations and illustrated that scoulerine might have a dual mechanism of action both as microtubule stabilizer in the laulimalide binding sites and an inhibitor of microtubule polymerization which binds in the colchicine binding site. This places scoulerine in a unique category of tubulin-binding agents.

References

- [1] G. M. Cragg and J. M. Pezzuto, "Natural Products as a Vital Source for the Discovery of Cancer Chemotherapeutic and Chemopreventive Agents," *Med. Princ. Pract.*, vol. 25, no. 2, pp. 41–59, 2016, doi: 10.1159/000443404.
- [2] D. Liu, X. Meng, D. Wu, Z. Qiu, and H. Luo, "A Natural Isoquinoline Alkaloid With Antitumor Activity: Studies of the Biological Activities of Berberine.," *Front. Pharmacol.*, vol. 10, p. 9, 2019, doi: 10.3389/fphar.2019.00009.
- [3] J. Tian *et al.*, "Scoulerine promotes cell viability reduction and apoptosis by activating ROS-dependent endoplasmic reticulum stress in colorectal cancer cells.," *Chem. Biol. Interact.*, vol. 327, p. 109184, Aug. 2020, doi: 10.1016/j.cbi.2020.109184.
- [4] W. A. Kukula-Koch and J. Widelski, "Alkaloids," in *Pharmacognosy*, S. Badal and R. Delgoda, Eds. Boston: Elsevier, 2017, pp. 163–198.
- [5] K. Habartova *et al.*, "Scoulerine affects microtubule structure, inhibits proliferation, arrests cell cycle and thus culminates in the apoptotic death of cancer cells.," *Sci. Rep.*, vol. 8, no. 1, p. 4829, 2018, doi: 10.1038/s41598-018-22862-0.
- [6] J. M. Hagel *et al.*, "Transcriptome analysis of 20 taxonomically related benzyloisoquinoline alkaloid-producing plants.," *BMC Plant Biol.*, vol. 15, p. 227, Sep. 2015, doi: 10.1186/s12870-015-0596-0.
- [7] L. Alisaraie and J. A. Tuszynski, "Determination of noscapine's localization and interaction with the tubulin- α/β heterodimer.," *Chem. Biol. Drug Des.*, vol. 78, no. 4, pp. 535–546, Oct. 2011, doi: 10.1111/j.1747-0285.2011.01189.x.
- [8] P. E. Ghaly, R. M. Abou El-Magd, C. D. M. Churchill, J. A. Tuszynski, and F. G. West, "A new antiproliferative noscapine analogue: chemical synthesis and biological evaluation.," *Oncotarget*, vol. 7, no. 26, pp. 40518–40530, Jun. 2016, doi: 10.18632/oncotarget.9642.
- [9] P. E. Ghaly *et al.*, "Synthesis and biological evaluation of structurally simplified noscapine analogues as microtubule binding agents," *Can. J. Chem.*, vol. 95, no. 6, pp. 649–655, 2017, doi: 10.1139/cjc-2016-0649.
- [10] J. Chlebek *et al.*, "Application of BACE1 immobilized enzyme reactor for the characterization of multifunctional alkaloids from *Corydalis cava* (Fumariaceae) as Alzheimer's disease targets.," *Fitoterapia*, vol. 109, pp. 241–7, Mar. 2016, doi: 10.1016/j.fitote.2016.01.008.
- [11] B. Kumar, R. Kumar, I. Skvortsova, and V. Kumar, "Mechanisms of Tubulin Binding Ligands to Target Cancer Cells: Updates on their Therapeutic Potential and

- Clinical Trials.,” *Curr. Cancer Drug Targets*, vol. 17, no. 4, pp. 357–375, 2017, doi: 10.2174/1568009616666160928110818.
- [12] P. Dustin, “The Role of MT in Mitosis,” in *Microtubules*, Springer, 1978, pp. 340–397.
- [13] C. C. Rohena and S. L. Mooberry, “Recent progress with microtubule stabilizers: new compounds, binding modes and cellular activities.,” *Nat. Prod. Rep.*, vol. 31, no. 3, pp. 335–55, Mar. 2014, doi: 10.1039/c3np70092e.
- [14] A. E. Prota *et al.*, “A new tubulin-binding site and pharmacophore for microtubule-destabilizing anticancer drugs.,” *Proc. Natl. Acad. Sci. U. S. A.*, vol. 111, no. 38, pp. 13817–21, Sep. 2014, doi: 10.1073/pnas.1408124111.
- [15] T. Koltai, “Cancer: fundamentals behind pH targeting and the double-edged approach.,” *Onco. Targets. Ther.*, vol. 9, pp. 6343–6360, 2016, doi: 10.2147/OTT.S115438.
- [16] G. M. Morris *et al.*, “AutoDock4 and AutoDockTools4: Automated docking with selective receptor flexibility.,” *J. Comput. Chem.*, vol. 30, no. 16, pp. 2785–91, Dec. 2009, doi: 10.1002/jcc.21256.
- [17] W. D. Cornell *et al.*, “A Second Generation Force Field for the Simulation of Proteins, Nucleic Acids, and Organic Molecules,” *J. Am. Chem. Soc.*, vol. 117, no. 19, pp. 5179–5197, May 1995, doi: 10.1021/ja00124a002.
- [18] P. G. Morris and M. N. Fornier, “Microtubule active agents: beyond the taxane frontier.,” *Clin. Cancer Res.*, vol. 14, no. 22, pp. 7167–72, Nov. 2008, doi: 10.1158/1078-0432.CCR-08-0169.
- [19] Y. Wang *et al.*, “Structures of a diverse set of colchicine binding site inhibitors in complex with tubulin provide a rationale for drug discovery.,” *FEBS J.*, vol. 283, no. 1, pp. 102–11, Jan. 2016, doi: 10.1111/febs.13555.
- [20] Y. Lu, J. Chen, M. Xiao, W. Li, and D. D. Miller, “An overview of tubulin inhibitors that interact with the colchicine binding site.,” *Pharm. Res.*, vol. 29, no. 11, pp. 2943–71, Nov. 2012, doi: 10.1007/s11095-012-0828-z.
- [21] N. M. O’Boyle *et al.*, “Synthesis and evaluation of azetidinone analogues of combretastatin A-4 as tubulin targeting agents.,” *J. Med. Chem.*, vol. 53, no. 24, pp. 8569–84, Dec. 2010, doi: 10.1021/jm101115u.
- [22] C. D. M. Churchill, M. Klobukowski, and J. A. Tuszynski, “The Unique Binding Mode of Laulimalide to Two Tubulin Protofilaments.,” *Chem. Biol. Drug Des.*, vol. 86, no. 2, pp. 190–9, Aug. 2015, doi: 10.1111/cbdd.12475.

- [23] Ö. Demir *et al.*, “Ensemble-based computational approach discriminates functional activity of p53 cancer and rescue mutants.,” *PLoS Comput. Biol.*, vol. 7, no. 10, p. e1002238, Oct. 2011, doi: 10.1371/journal.pcbi.1002238.
- [24] J. Shao, S. W. Tanner, N. Thompson, and T. E. Cheatham, “Clustering Molecular Dynamics Trajectories: 1. Characterizing the Performance of Different Clustering Algorithms.,” *J. Chem. Theory Comput.*, vol. 3, no. 6, pp. 2312–34, Nov. 2007, doi: 10.1021/ct700119m.
- [25] C. D. M. Churchill, M. Klobukowski, and J. A. Tuszynski, “Analysis of the binding mode of laulimalide to microtubules: Establishing a laulimalide-tubulin pharmacophore.,” *J. Biomol. Struct. Dyn.*, vol. 34, no. 7, pp. 1455–69, Jul. 2016, doi: 10.1080/07391102.2015.1078115.
- [26] A. E. Prota *et al.*, “Structural basis of microtubule stabilization by laulimalide and peloruside A.,” *Angew. Chem. Int. Ed. Engl.*, vol. 53, no. 6, pp. 1621–5, Feb. 2014, doi: 10.1002/anie.201307749.
- [27] D. E. Pryor *et al.*, “The microtubule stabilizing agent laulimalide does not bind in the taxoid site, kills cells resistant to paclitaxel and epothilones, and may not require its epoxide moiety for activity.,” *Biochemistry*, vol. 41, no. 29, pp. 9109–9115, Jul. 2002, doi: 10.1021/bi020211b.
- [28] W. J. Eisenreich, G. Höfner, and F. Bracher, “Alkaloids from *Croton flavens* L. and their affinities to GABA-receptors.,” *Nat. Prod. Res.*, vol. 17, no. 6, pp. 437–40, Dec. 2003, doi: 10.1080/1478641031000111516.
- [29] P. Wangchuk, P. A. Keller, S. G. Pyne, A. C. Willis, and S. Kamchonwongpaisan, “Antimalarial alkaloids from a Bhutanese traditional medicinal plant *Corydalis dubia*.,” *J. Ethnopharmacol.*, vol. 143, no. 1, pp. 310–3, Aug. 2012, doi: 10.1016/j.jep.2012.06.037.
- [30] J. Chlebek, K. Macáková, L. Cahlíková, M. Kurfürst, J. Kuneš, and L. Opletal, “Acetylcholinesterase and Butyrylcholinesterase Inhibitory Compounds from *Corydalis Cava* (Fumariaceae).,” *Nat. Prod. Commun.*, vol. 6, no. 5, pp. 607–610, May 2011, doi: 10.1177/1934578X1100600507.
- [31] T. H. Dunning, “Gaussian basis sets for use in correlated molecular calculations. I. The atoms boron through neon and hydrogen,” *J. Chem. Phys.*, vol. 90, no. 2, pp. 1007–1023, Jan. 1989, doi: 10.1063/1.456153.
- [32] M. W. Schmidt *et al.*, “General atomic and molecular electronic structure system,” *J. Comput. Chem.*, vol. 14, no. 11, pp. 1347–1363, Nov. 1993, doi: 10.1002/jcc.540141112.

- [33] M. S. Gordon and M. W. Schmidt, “Advances in electronic structure theory: GAMESS a decade later,” in *Theory and Applications of Computational Chemistry*, C. E. Dykstra, G. Frenking, K. S. Kim, and G. E. Scuseria, Eds. Amsterdam: Elsevier, 2005, pp. 1167–1189.
- [34] G. M. J. Barca *et al.*, “Recent developments in the general atomic and molecular electronic structure system,” *J. Chem. Phys.*, vol. 152, no. 15, p. 154102, Apr. 2020, doi: 10.1063/5.0005188.
- [35] *Autodock*. Chemical Computing Group ULC, Montreal, Canada, 2018.
- [36] R. B. G. Ravelli *et al.*, “Insight into tubulin regulation from a complex with colchicine and a stathmin-like domain,” *Nature*, vol. 428, no. 6979, pp. 198–202, Mar. 2004, doi: 10.1038/nature02393.
- [37] F. J. Fourniol *et al.*, “Template-free 13-protofilament microtubule-MAP assembly visualized at 8 Å resolution,” *J. Cell Biol.*, vol. 191, no. 3, pp. 463–70, Nov. 2010, doi: 10.1083/jcb.201007081.
- [38] J. Wang, R. M. Wolf, J. W. Caldwell, P. A. Kollman, and D. A. Case, “Development and testing of a general amber force field,” *J. Comput. Chem.*, vol. 25, no. 9, pp. 1157–74, Jul. 2004, doi: 10.1002/jcc.20035.
- [39] W. L. Jorgensen, J. Chandrasekhar, J. D. Madura, R. W. Impey, and M. L. Klein, “Comparison of simple potential functions for simulating liquid water,” *J. Chem. Phys.*, vol. 79, no. 2, pp. 926–935, Jul. 1983, doi: 10.1063/1.445869.
- [40] U. Essmann, L. Perera, M. L. Berkowitz, T. Darden, H. Lee, and L. G. Pedersen, “A smooth particle mesh Ewald method,” *J. Chem. Phys.*, vol. 103, no. 19, pp. 8577–8593, Nov. 1995, doi: 10.1063/1.470117.
- [41] J.-P. Ryckaert, G. Ciccotti, and H. J. Berendsen, “Numerical integration of the cartesian equations of motion of a system with constraints: molecular dynamics of n-alkanes,” *J. Comput. Phys.*, vol. 23, no. 3, pp. 327–341, Mar. 1977, doi: 10.1016/0021-9991(77)90098-5.
- [42] T. A. D. D.A. Case, I.Y. Ben-Shalom, S.R. Brozell, D.S. Cerutti, T.E. Cheatham, III, V.W.D. Cruzeiro, Y. H. R.E. Duke, D. Ghoreishi, M.K. Gilson, H. Gohlke, A.W. Goetz, D. Greene, R Harris, N. Homeyer, D. J. S. Izadi, A. Kovalenko, T. Kurtzman, T.S. Lee, S. LeGrand, P. Li, C. Lin, J. Liu, T. Luchko, R. Luo, R. Mermelstein, K.M. Merz, Y. Miao, G. Monard, C. Nguyen, H. Nguyen, I. Omelyan, A. Onufriev, F. Pan, and P. A. K. Qi, D.R. Roe, A. Roitberg, C. Sagui, S. Schott-Verdugo, J. Shen, C.L. Simmerling, J. Smith, R. SalomonFerrer, J. Swails, R.C. Walker, J. Wang, H. Wei, R.M. Wolf, X. Wu, L. Xiao, D.M. York, *AMBER 2018*, University of California, San Francisco. 2018.

[43] M. G. Lepre, S. I. Omar, G. Grasso, U. Morbiducci, M. A. Deriu, and J. A. Tuszynski, "Insights into the Effect of the G245S Single Point Mutation on the Structure of p53 and the Binding of the Protein to DNA.," *Molecules*, vol. 22, no. 8, Aug. 2017, doi: 10.3390/molecules22081358.

Chapter 9:

Major conclusions

9.1 Conclusion

The main goal of this thesis was to use computational approaches to identify a suitable substitute for colchicine that is as effective as the inhibitor, while having lower cytotoxicity and less antimitotic effect on healthy cells. Toward fulfilling this goal, the free binding energies of various libraries of colchicine derivatives and their effect on β tubulin were investigated. Computational studies on colchicine derivatives included as follows:

1. Molecular docking studies on a set of novel double- and triple-modified colchicine derivatives including 7-deacetyl-10-thiocolchicine and 4-iodo-7-deacetyl-10-thiocolchicine analogues in the colchicine-binding site. This study led to identification of derivatives with stronger β -binding energies with β -tubulin. These results, combined with *in vitro* studies, showed that this set of colchicine analogues constitute promising lead compounds as chemotherapy agents against several types of cancer such as A549, MCF-7, LoVo, and LoVo/DX.
2. Computational studies on three double-modified colchicine derivatives, where colchicine structure was chemically modified in C-4 and C-10 positions. Docking methods were used to calculate the binding affinities of these colchicine derivatives against eight different isotypes of human β -tubulin. Moreover, the computational data were compared by IC_{50} values of the mentioned compounds against the A549, MCF-7, LoVo, and LoVo/DX cancer cell lines.
3. The mode of binding of a series of novel triple-modified 4-chloro-7-carbamatethiocolchicines to β -tubulin was evaluated *in silico* by docking study. The results were compared with experimental data against four human tumour cell lines (A549, MCF-7, LoVo, and LoVo/DX). To consider permeability and solubility of the ligands, the Moriguchi octanol-water partition coefficients (MLogP) of novel derivatives were calculated. Good regression coefficients between experimental and computational data were found for LoVo/DX and A549 cancer cell lines.

4. In a following study (addressed in chapter 5), a series of novel triple-modified colchicine derivatives were investigated. The mode of binding of the synthesized compounds was evaluated *in silico* using molecular docking to a 3D structure of β -tubulin based on crystallographic data from the Protein Data Bank and homology methodology. Binding free energy estimates, binding poses, and MlogP values of the compounds were obtained. These studies were conducted against four human tumour cell lines (A549, MCF-7, LoVo, and LoVo/DX), and resulted in a very good correlation of 0.66 and 0.84 involving log IC₅₀ for LoVo and LoVo/DX cell lines, respectively.
5. A group of thiocolchicine derivatives have been obtained in a simple reaction of 7-deacetyl-10-thiocolchicine **3** with eleven different alcohols in the presence of triphosgene. The mentioned derivatives were modified at the B ring. Their mechanism has been confirmed as colchicine binding site inhibition (CBSI) using molecular docking. Molecular simulations provided rational tubulin-binding models for the tested compounds.

As mentioned above, large libraries of colchicine derivatives were studied computationally as part of the scope of this thesis, and experimentally with a Polish collaborating group. In this thesis, using linear regression and the R² method, the experimental and computational results were compared to have a more comprehensive understanding of the derivatives that might be used as lead compounds. Nonetheless, there was another modified large library that was unable to make experimental assessments due to the complexity of synthesis.

Furthermore, due to the lack of IC₅₀ values, it was not possible to estimate the relationship between experimental data and computational data. In order to solve the problem, the seventh chapter reports the generation of 3D QSAR models with the ability to predict IC₅₀ values for 70 novel colchicine derivatives against two commonly-used breast and lung cancer lines, namely MCF7 and A549. The chemical structure of 50 new compounds was used as input data along with their corresponding *in vitro* activity values

(IC₅₀ values) to build two models for the aforementioned cell lines. A method based on Kohonen maps was applied to split the input data into training and test sets. 15 independent compounds were subsequently used as an external independent validation set. The binding and electrostatic energies between the mentioned library of derivatives and β II tubulin were estimated by docking and then used as two novel descriptors, along with two conventional ones, namely polarizability and sum of absolute values of Hückel pi atomic charges on O atoms. A widely used Artificial Neural Network was deployed to generate our models. Based on the calculations and analysis presented in this chapter, our two finalized QSAR models for both A549 and MCF7 cancer cell lines, not only showed good performance on the test set, assessed through the high value of q^2 and R^2 , but also show predictive ability and good generalization on the independent validation set of compounds.

In commitment to expand the library of novel compounds that can potentially be a good lead for discovery of a new chemotherapeutic agent, the mode of action of scoulerine was studied in the eighth chapter. Scoulerine is a natural compound that is known to bind to tubulin and has anti-mitotic properties demonstrated in various cancer cells. Its molecular mode of action has not been precisely known. In this work we perform computational prediction and experimental validation of the mode of action of scoulerine. Based on the existing data in the Protein Data Bank (PDB) and using homology modeling we create human tubulin structures corresponding to both free tubulin dimers and tubulin in a microtubule. We then perform docking of the optimized structure of scoulerine and find the highest affinity binding sites located in both the free tubulin and in a microtubule. We conclude that binding in the vicinity of the colchicine binding site and near the laulimalide binding site are the most likely locations for scoulerine interacting with tubulin. Thermophoresis assays using scoulerine and tubulin in both free and polymerized form confirm these computational predictions. We conclude that scoulerine exhibits a unique property of a dual mode of action with both

microtubule stabilization and tubulin polymerization inhibition, both of which have similar affinity values.

9.2 Future work

With the results of analysis on currently built QSAR models, the applicability domain of the QSAR models can be improved by adding more input compounds, specifically more colchicine derivatives with high IC_{50} values. The models can be tested against more external libraries to evaluate the accuracy and robustness of their prediction. The variety of different β isotypes is diverse in cancer cell lines. With the use of binding energies between β II tubulin and colchicine derivatives as a descriptor, two QSAR models were built for MCF7 (breast cancer) cell lines and A549 (lung cancer cell lines). β IVa and β IVb isotypes are dominant in LoVo (colon cancer) cell lines. Based on the mentioned knowledge, an attempt to build a QSAR model for the LoVo cancer cell line with binding energies between β IVa or β IVb tubulin and colchicine derivatives as a descriptor is a good strategy for future work.

For the last chapter, With the knowledge of the multi-modal activity, the modification of the scoulerine can lead to synthesizing the scoulerine derivatives that are as effective as currently used chemotherapeutic agents. The scoulerine has two hydroxyl groups that can be substituted with more active functional groups.

References

Chapter 1

- [1] R. W. Ruddon, *Cancer Biology*. Oxford University Press, USA, 2007.
- [2] D. Hanahan and R. A. Weinberg, “Hallmarks of Cancer: The Next Generation,” *Cell*, vol. 144, no. 5, pp. 646–674, Mar. 2011, doi: 10.1016/j.cell.2011.02.013.
- [3] H. F. M. Kamel and H. S. B. Al-Amodi, “Cancer Biomarkers,” in *Role of Biomarkers in Medicine*, InTech, 2016.
- [4] H. Sung *et al.*, “Global cancer statistics 2020: GLOBOCAN estimates of incidence and mortality worldwide for 36 cancers in 185 countries,” *CA. Cancer J. Clin.*, p. caac.21660, Feb. 2021, doi: 10.3322/caac.21660.
- [5] A. A. Demers, D. R. Brenner, L. Smith, and A. Shaw, “At-a-glance, Cancer trends in Canada, 1984 to 2015,” *Heal. Promot. Chronic Dis. Prev. Canada*, vol. 39, no. 11, pp. 310–314, Nov. 2019, doi: 10.24095/hpcdp.39.11.04.
- [6] S. Pilleron *et al.*, “Estimated global cancer incidence in the oldest adults in 2018 and projections to 2050,” *Int. J. Cancer*, vol. 148, no. 3, pp. 601–608, Feb. 2021, doi: 10.1002/ijc.33232.
- [7] H. Lodish *et al.*, *Molecular Cell Biology*, 8th ed. W. H. Freeman, 2016.
- [8] S. Chakraborty and T. Rahman, “The difficulties in cancer treatment,” *Ecancermedicalscience*, vol. 6, p. ed16, 2012, doi: 10.3332/ecancer.2012.ed16.
- [9] D. Schaefer and W. H. McBride, “Opportunities and challenges of radiotherapy for treating cancer,” *Nat. Rev. Clin. Oncol.*, vol. 12, no. 9, pp. 527–40, Sep. 2015, doi: 10.1038/nrclinonc.2015.120.
- [10] E. Bidram *et al.*, “A concise review on cancer treatment methods and delivery systems,” *J. Drug Deliv. Sci. Technol.*, vol. 54, p. 101350, Dec. 2019, doi: 10.1016/j.jddst.2019.101350.
- [11] P. M. Gunjal, G. Schneider, A. A. Ismail, S. S. Kakar, M. Kucia, and M. Z. Ratajczak, “Evidence for induction of a tumor metastasis-receptive

- microenvironment for ovarian cancer cells in bone marrow and other organs as an unwanted and underestimated side effect of chemotherapy/radiotherapy.,” *J. Ovarian Res.*, vol. 8, p. 20, Mar. 2015, doi: 10.1186/s13048-015-0141-7.
- [12] S. Charmsaz, D. M. Collins, A. S. Perry, and M. Prencipe, “Novel Strategies for Cancer Treatment: Highlights from the 55th IACR Annual Conference.,” *Cancers (Basel)*., vol. 11, no. 8, Aug. 2019, doi: 10.3390/cancers11081125.
- [13] V. Emuss, “The Molecular Biology of Cancer,” *Br. J. Cancer*, vol. 95, no. 8, pp. 1128–1128, Oct. 2006, doi: 10.1038/sj.bjc.6603379.
- [14] Komala M, Sathesh Kumar S, and Padmavathy J, “Novel Drug Formulation for the Treatment of Hepatic Cancer- A Review,” *Int. J. Res. Pharm. Sci.*, vol. 11, no. 3, pp. 4395–4401, Jul. 2020, doi: 10.26452/ijrps.v11i3.2658.
- [15] P. Ravi, Z. Bakouny, A. Schmidt, and T. K. Choueiri, “Novel Therapeutic Approaches and the Evolution of Drug Development in Advanced Kidney Cancer.,” *Cancer J.*, vol. 26, no. 5, pp. 464–470, doi: 10.1097/PPO.0000000000000477.
- [16] U. Hani *et al.*, “Recent advances in novel drug delivery systems and approaches for management of breast cancer: A comprehensive review,” *J. Drug Deliv. Sci. Technol.*, vol. 56, p. 101505, Apr. 2020, doi: 10.1016/j.jddst.2020.101505.
- [17] B. Alberts, *Molecular Biology of the Cell*. W.W. Norton, 2017.
- [18] J. Zhou and P. Giannakakou, “Targeting microtubules for cancer chemotherapy.,” *Curr. Med. Chem. Anticancer. Agents*, vol. 5, no. 1, pp. 65–71, Jan. 2005, doi: 10.2174/1568011053352569.
- [19] E. Nogales, S. G. Wolf, and K. H. Downing, “Structure of the alpha beta tubulin dimer by electron crystallography.,” *Nature*, vol. 391, no. 6663, pp. 199–203, Jan. 1998, doi: 10.1038/34465.
- [20] M. Auer, “Three-dimensional electron cryo-microscopy as a powerful structural tool in molecular medicine.,” *J. Mol. Med. (Berl)*., vol. 78, no. 4, pp. 191–202, 2000, doi: 10.1007/s001090000101.

- [21] T. Allen, *Introduction to electron microscopy for biologists*. Elsevier Science, 2008.
- [22] Y. Fujiyoshi, “Structural physiology based on electron crystallography.,” *Protein Sci.*, vol. 20, no. 5, pp. 806–17, May 2011, doi: 10.1002/pro.621.
- [23] J. Torin Huzil, R. F. Ludueña, and J. Tuszynski, “Comparative modelling of human β tubulin isotypes and implications for drug binding.,” *Nanotechnology*, vol. 17, no. 4, pp. S90–S100, Feb. 2006, doi: 10.1088/0957-4484/17/4/014.
- [24] M. P. M. H. Benoit, A. B. Asenjo, and H. Sosa, “Cryo-EM reveals the structural basis of microtubule depolymerization by kinesin-13s.,” *Nat. Commun.*, vol. 9, no. 1, p. 1662, Apr. 2018, doi: 10.1038/s41467-018-04044-8.
- [25] E. Nogales, M. Whittaker, R. A. Milligan, and K. H. Downing, “High-resolution model of the microtubule.,” *Cell*, vol. 96, no. 1, pp. 79–88, Jan. 1999, doi: 10.1016/s0092-8674(00)80961-7.
- [26] H. Sosa *et al.*, “A model for the microtubule-Ncd motor protein complex obtained by cryo-electron microscopy and image analysis.,” *Cell*, vol. 90, no. 2, pp. 217–24, Jul. 1997, doi: 10.1016/s0092-8674(00)80330-x.
- [27] F. J. Fourniol *et al.*, “Template-free 13-protofilament microtubule-MAP assembly visualized at 8 Å resolution.,” *J. Cell Biol.*, vol. 191, no. 3, pp. 463–70, Nov. 2010, doi: 10.1083/jcb.201007081.
- [28] G. M. Alushin, G. C. Lander, E. H. Kellogg, R. Zhang, D. Baker, and E. Nogales, “High-Resolution Microtubule Structures Reveal the Structural Transitions in $\alpha\beta$ -Tubulin upon GTP Hydrolysis,” *Cell*, vol. 157, no. 5, pp. 1117–1129, May 2014, doi: 10.1016/j.cell.2014.03.053.
- [29] K. M. Yip, N. Fischer, E. Paknia, A. Chari, and H. Stark, “Atomic-resolution protein structure determination by cryo-EM.,” *Nature*, vol. 587, no. 7832, pp. 157–161, Nov. 2020, doi: 10.1038/s41586-020-2833-4.
- [30] A. Bartesaghi *et al.*, “2.2 Å resolution cryo-EM structure of β -galactosidase in complex with a cell-permeant inhibitor.,” *Science*, vol. 348, no. 6239, pp. 1147–

51, Jun. 2015, doi: 10.1126/science.aab1576.

- [31] E. Binshtein and M. D. Ohi, “Cryo-electron microscopy and the amazing race to atomic resolution.,” *Biochemistry*, vol. 54, no. 20, pp. 3133–41, May 2015, doi: 10.1021/acs.biochem.5b00114.
- [32] D. Bhella, “Cryo-electron microscopy: an introduction to the technique, and considerations when working to establish a national facility.,” *Biophysical reviews*, vol. 11, no. 4, pp. 515–519, Aug. 2019, doi: 10.1007/s12551-019-00571-w.
- [33] J. A. Tuszynski and M. Kurzynski, *Introduction to Molecular Biophysics*. CRC Press, 2003.
- [34] T. Mitchison and M. Kirschner, “Dynamic instability of microtubule growth,” *Nature*, vol. 312, no. 5991, pp. 237–242, 1984, doi: 10.1038/312237a0.
- [35] R. A. Walker *et al.*, “Dynamic instability of individual microtubules analyzed by video light microscopy: rate constants and transition frequencies.,” *J. Cell Biol.*, vol. 107, no. 4, pp. 1437–48, Oct. 1988, doi: 10.1083/jcb.107.4.1437.
- [36] B. Alberts *et al.*, *Essential Cell Biology*, 6th ed. Garland Science, 2009.
- [37] L. R. B. Eldra P. Solomon, Diana W. Martin, *Biology*, 8th ed. Brooks/Cole, 2007.
- [38] J. J. Blow and T. U. Tanaka, “The chromosome cycle: coordinating replication and segregation. Second in the cycles review series.,” *EMBO Rep.*, vol. 6, no. 11, pp. 1028–34, Nov. 2005, doi: 10.1038/sj.embor.7400557.
- [39] S. Ruchaud, M. Carmena, and W. C. Earnshaw, “Chromosomal passengers: conducting cell division.,” *Nat. Rev. Mol. Cell Biol.*, vol. 8, no. 10, pp. 798–812, Oct. 2007, doi: 10.1038/nrm2257.
- [40] J. Zhou, D. Panda, J. W. Landen, L. Wilson, and H. C. Joshi, “Minor alteration of microtubule dynamics causes loss of tension across kinetochore pairs and activates the spindle checkpoint.,” *J. Biol. Chem.*, vol. 277, no. 19, pp. 17200–8, May 2002, doi: 10.1074/jbc.M110369200.
- [41] C. L. Rieder and R. E. Palazzo, “Colcemid and the mitotic cycle.,” *J. Cell Sci.*,

- vol. 102 (Pt 3, pp. 387–392, Jul. 1992.
- [42] O. J. Eigsti and P. Dustin, *Colchicine in agriculture, medicine, biology, and chemistry*. Ames,: Iowa State College Press, 1955.
- [43] A. Musacchio and E. D. Salmon, “The spindle-assembly checkpoint in space and time.,” *Nat. Rev. Mol. Cell Biol.*, vol. 8, no. 5, pp. 379–93, May 2007, doi: 10.1038/nrm2163.
- [44] M. A. Jordan and K. Kamath, “How do microtubule-targeted drugs work? An overview.,” *Curr. Cancer Drug Targets*, vol. 7, no. 8, pp. 730–742, 2007, doi: 10.2174/156800907783220417.
- [45] Q. Shi, K. Chen, S. L. Morris-Natschke, and K. H. Lee, “Recent progress in the development of tubulin inhibitors as antimitotic antitumor agents.,” *Curr. Pharm. Des.*, vol. 4, no. 3, pp. 219–248, Jun. 1998.
- [46] K.-S. Chan, C.-G. Koh, and H.-Y. Li, “Mitosis-targeted anti-cancer therapies: where they stand.,” *Cell Death Dis.*, vol. 3, no. 10, p. e411, Oct. 2012, doi: 10.1038/cddis.2012.148.
- [47] B. Bhattacharyya, D. Panda, S. Gupta, and M. Banerjee, “Anti-mitotic activity of colchicine and the structural basis for its interaction with tubulin.,” *Med. Res. Rev.*, vol. 28, no. 1, pp. 155–183, Jan. 2008, doi: 10.1002/med.20097.
- [48] B. A. Weaver, “How Taxol/paclitaxel kills cancer cells.,” *Mol. Biol. Cell*, vol. 25, no. 18, pp. 2677–2681, Sep. 2014, doi: 10.1091/mbc.E14-04-0916.
- [49] U. Majcher *et al.*, “Synthesis, antiproliferative activity and molecular docking of thiocolchicine urethanes.,” *Bioorg. Chem.*, vol. 81, pp. 553–566, 2018, doi: 10.1016/j.bioorg.2018.09.004.
- [50] M. A. Jordan and L. Wilson, “Microtubules as a target for anticancer drugs.,” *Nat. Rev. Cancer*, vol. 4, no. 4, pp. 253–65, Apr. 2004, doi: 10.1038/nrc1317.
- [51] C. Dumontet and M. A. Jordan, “Microtubule-binding agents: a dynamic field of cancer therapeutics.,” *Nat. Rev. Drug Discov.*, vol. 9, no. 10, pp. 790–803, Oct. 2010, doi: 10.1038/nrd3253.

- [52] J. J. Field, J. F. Díaz, and J. H. Miller, “The binding sites of microtubule-stabilizing agents.,” *Chem. Biol.*, vol. 20, no. 3, pp. 301–15, Mar. 2013, doi: 10.1016/j.chembiol.2013.01.014.
- [53] E. Mukhtar, V. M. Adhami, and H. Mukhtar, “Targeting microtubules by natural agents for cancer therapy.,” *Mol. Cancer Ther.*, vol. 13, no. 2, pp. 275–284, Feb. 2014, doi: 10.1158/1535-7163.MCT-13-0791.
- [54] K. E. Arnst *et al.*, “Current advances of tubulin inhibitors as dual acting small molecules for cancer therapy.,” *Med. Res. Rev.*, vol. 39, no. 4, pp. 1398–1426, Jul. 2019, doi: 10.1002/med.21568.
- [55] A. R. Ranade *et al.*, “Characterizing the Epothilone Binding Site on β -Tubulin by Photoaffinity Labeling: Identification of β -Tubulin Peptides TARGSQY and TSRGSQQY as Targets of an Epothilone Photoprobe for Polymerized Tubulin.,” *J. Med. Chem.*, vol. 59, no. 7, pp. 3499–514, Apr. 2016, doi: 10.1021/acs.jmedchem.6b00188.
- [56] L. A. Amos, “What tubulin drugs tell us about microtubule structure and dynamics.,” *Semin. Cell Dev. Biol.*, vol. 22, no. 9, pp. 916–26, Dec. 2011, doi: 10.1016/j.semcdb.2011.09.014.
- [57] Y. Lu, J. Chen, M. Xiao, W. Li, and D. D. Miller, “An overview of tubulin inhibitors that interact with the colchicine binding site.,” *Pharm. Res.*, vol. 29, no. 11, pp. 2943–71, Nov. 2012, doi: 10.1007/s11095-012-0828-z.
- [58] M. O. Steinmetz and A. E. Prota, “Microtubule-Targeting Agents: Strategies To Hijack the Cytoskeleton.,” *Trends Cell Biol.*, vol. 28, no. 10, pp. 776–792, Oct. 2018, doi: 10.1016/j.tcb.2018.05.001.
- [59] L. M. West, P. T. Northcote, and C. N. Battershill, “Peloruside A: a potent cytotoxic macrolide isolated from the new zealand marine sponge *Mycale* sp.,” *J. Org. Chem.*, vol. 65, no. 2, pp. 445–449, Jan. 2000, doi: 10.1021/jo991296y.
- [60] D. G. Corley, R. Herb, R. E. Moore, P. J. Scheuer, and V. J. Paul, “Laulimalides. New potent cytotoxic macrolides from a marine sponge and a nudibranch

- predator,” *J. Org. Chem.*, vol. 53, no. 15, pp. 3644–3646, Jul. 1988, doi: 10.1021/jo00250a053.
- [61] A. Kanakkanthara, M. R. Rowe, J. J. Field, P. T. Northcote, P. H. Teesdale-Spittle, and J. H. Miller, “ β I-tubulin mutations in the laulimalide/peloruside binding site mediate drug sensitivity by altering drug–tubulin interactions and microtubule stability,” *Cancer Lett.*, vol. 365, no. 2, pp. 251–260, Sep. 2015, doi: 10.1016/j.canlet.2015.06.001.
- [62] T. N. Gaitanos *et al.*, “Peloruside A does not bind to the taxoid site on beta-tubulin and retains its activity in multidrug-resistant cell lines.,” *Cancer Res.*, vol. 64, no. 15, pp. 5063–5067, Aug. 2004, doi: 10.1158/0008-5472.CAN-04-0771.
- [63] D. E. Pryor *et al.*, “The microtubule stabilizing agent laulimalide does not bind in the taxoid site, kills cells resistant to paclitaxel and epothilones, and may not require its epoxide moiety for activity.,” *Biochemistry*, vol. 41, no. 29, pp. 9109–9115, Jul. 2002, doi: 10.1021/bi020211b.
- [64] E. H. Kellogg *et al.*, “Insights into the Distinct Mechanisms of Action of Taxane and Non-Taxane Microtubule Stabilizers from Cryo-EM Structures,” *J. Mol. Biol.*, vol. 429, no. 5, pp. 633–646, 2017, doi: 10.1016/j.jmb.2017.01.001.
- [65] A. E. Prota *et al.*, “Structural basis of microtubule stabilization by laulimalide and peloruside A.,” *Angew. Chem. Int. Ed. Engl.*, vol. 53, no. 6, pp. 1621–5, Feb. 2014, doi: 10.1002/anie.201307749.
- [66] Y.-N. Cao, L.-L. Zheng, D. Wang, X.-X. Liang, F. Gao, and X.-L. Zhou, “Recent advances in microtubule-stabilizing agents.,” *Eur. J. Med. Chem.*, vol. 143, pp. 806–828, Jan. 2018, doi: 10.1016/j.ejmech.2017.11.062.
- [67] B. Dasgeb, D. Kornreich, K. McGuinn, L. Okon, I. Brownell, and D. L. Sackett, “Colchicine: an ancient drug with novel applications.,” *Br. J. Dermatol.*, vol. 178, no. 2, pp. 350–356, Feb. 2018, doi: 10.1111/bjd.15896.
- [68] M. I. Lopes *et al.*, “Beneficial effects of colchicine for moderate to severe COVID-19: a randomised, double-blinded, placebo-controlled clinical trial.,”

RMD open, vol. 7, no. 1, 2021, doi: 10.1136/rmdopen-2020-001455.

- [69] A. Kumar, P. R. Sharma, and D. M. Mondhe, “Potential anticancer role of colchicine-based derivatives: an overview.,” *Anticancer. Drugs*, vol. 28, no. 3, pp. 250–262, 2017, doi: 10.1097/CAD.0000000000000464.
- [70] Z.-Y. Lin, C.-H. Kuo, D.-C. Wu, and W.-L. Chuang, “Anticancer effects of clinically acceptable colchicine concentrations on human gastric cancer cell lines.,” *Kaohsiung J. Med. Sci.*, vol. 32, no. 2, pp. 68–73, Feb. 2016, doi: 10.1016/j.kjms.2015.12.006.
- [71] K. Larocque, P. Ovadje, S. Djurdjevic, M. Mehdi, J. Green, and S. Pandey, “Novel analogue of colchicine induces selective pro-death autophagy and necrosis in human cancer cells.,” *PLoS One*, vol. 9, no. 1, p. e87064, 2014, doi: 10.1371/journal.pone.0087064.
- [72] Y. Finkelstein *et al.*, “Colchicine poisoning: the dark side of an ancient drug.,” *Clin. Toxicol. (Phila)*, vol. 48, no. 5, pp. 407–14, Jun. 2010, doi: 10.3109/15563650.2010.495348.
- [73] R. B. G. Ravelli *et al.*, “Insight into tubulin regulation from a complex with colchicine and a stathmin-like domain.,” *Nature*, vol. 428, no. 6979, pp. 198–202, Mar. 2004, doi: 10.1038/nature02393.
- [74] J. Löwe, H. Li, K. . Downing, and E. Nogales, “Refined structure of $\alpha\beta$ -tubulin at 3.5 Å resolution 1 1Edited by I. A. Wilson,” *J. Mol. Biol.*, vol. 313, no. 5, pp. 1045–1057, Nov. 2001, doi: 10.1006/jmbi.2001.5077.
- [75] A. Dorléans, B. Gigant, R. B. G. Ravelli, P. Mailliet, V. Mikol, and M. Knossow, “Variations in the colchicine-binding domain provide insight into the structural switch of tubulin.,” *Proc. Natl. Acad. Sci. U. S. A.*, vol. 106, no. 33, pp. 13775–9, Aug. 2009, doi: 10.1073/pnas.0904223106.
- [76] M.-J. Pérez-Pérez, E.-M. Priego, O. Bueno, M. S. Martins, M.-D. Canela, and S. Liekens, “Blocking Blood Flow to Solid Tumors by Destabilizing Tubulin: An Approach to Targeting Tumor Growth.,” *J. Med. Chem.*, vol. 59, no. 19, pp.

- 8685–8711, 2016, doi: 10.1021/acs.jmedchem.6b00463.
- [77] A. Massarotti, A. Coluccia, R. Silvestri, G. Sorba, and A. Brancale, “The tubulin colchicine domain: a molecular modeling perspective.,” *ChemMedChem*, vol. 7, no. 1, pp. 33–42, Jan. 2012, doi: 10.1002/cmdc.201100361.
- [78] A. Akhmanova and M. O. Steinmetz, “Control of microtubule organization and dynamics: two ends in the limelight.,” *Nat. Rev. Mol. Cell Biol.*, vol. 16, no. 12, pp. 711–26, Dec. 2015, doi: 10.1038/nrm4084.
- [79] G. Sliwoski, S. Kothiwale, J. Meiler, and E. W. J. Lowe, “Computational methods in drug discovery.,” *Pharmacol. Rev.*, vol. 66, no. 1, pp. 334–395, 2014, doi: 10.1124/pr.112.007336.
- [80] D. B. Kitchen, H. Decornez, J. R. Furr, and J. Bajorath, “Docking and scoring in virtual screening for drug discovery: methods and applications.,” *Nat. Rev. Drug Discov.*, vol. 3, no. 11, pp. 935–949, Nov. 2004, doi: 10.1038/nrd1549.
- [81] C. J. Cramer, *Essentials of Computational Chemistry Theories and Models*. Wiley, 2004.
- [82] S. A. Adcock and J. A. McCammon, “Molecular Dynamics: Survey of Methods for Simulating the Activity of Proteins,” *Chem. Rev.*, vol. 106, no. 5, pp. 1589–1615, May 2006, doi: 10.1021/cr040426m.
- [83] M. Karplus and J. A. McCammon, “Molecular dynamics simulations of biomolecules,” *Nat. Struct. Biol.*, vol. 9, no. 9, pp. 646–652, Sep. 2002, doi: 10.1038/nsb0902-646.
- [84] I. N. Levine, *Quantum chemistry*. Englewood Cliffs, NJ: Prentice Hall, 1991.
- [85] F. Jensen, *Introduction to Computational Chemistry*. Hoboken: John Wiley and Sons Ltd, 2006.
- [86] R. A. Friesner, “Ab initio quantum chemistry: Methodology and applications,” *Proceedings of the National Academy of Sciences*, vol. 102, no. 19, pp. 6648–6653, 2005.

[87] J. Verma, V. M. Khedkar, and E. C. Coutinho, “3D-QSAR in drug design--a review.,” *Curr. Top. Med. Chem.*, vol. 10, no. 1, pp. 95–115, 2010, doi: 10.2174/156802610790232260.

Chapter 2

- [1] S. L. Wallace, “Colchicine,” *Semin. Arthritis Rheum.*, vol. 3, no. 4, pp. 369–381, 1974, doi: [https://doi.org/10.1016/0049-0172\(74\)90006-7](https://doi.org/10.1016/0049-0172(74)90006-7).
- [2] E. S. Shchegravina, D. I. Knyazev, I. P. Beletskaya, E. V. Svirshchevskaya, H.-G. Schmalz, and A. Y. Fedorov, “Synthesis of Nonracemic Pyrrolo-allocholchicinoids Exhibiting Potent Cytotoxic Activity,” *European J. Org. Chem.*, vol. 2016, no. 34, pp. 5620–5623, 2016, doi: <https://doi.org/10.1002/ejoc.201601069>.
- [3] D. Zemer, A. Livneh, Y. L. Danon, M. Pras, and E. Sohar, “Long-term colchicine treatment in children with familial Mediterranean fever.,” *Arthritis Rheum.*, vol. 34, no. 8, pp. 973–7, Aug. 1991, doi: 10.1002/art.1780340806.
- [4] M. Imazio *et al.*, “Colchicine for recurrent pericarditis (CORP): a randomized trial.,” *Ann. Intern. Med.*, vol. 155, no. 7, pp. 409–414, Oct. 2011, doi: 10.7326/0003-4819-155-7-201110040-00359.
- [5] E. Ben-Chetrit and M. Levy, “Colchicine prophylaxis in familial Mediterranean fever: Reappraisal after 15 years,” *Semin. Arthritis Rheum.*, vol. 20, no. 4, pp. 241–246, 1991, doi: [https://doi.org/10.1016/0049-0172\(91\)90019-V](https://doi.org/10.1016/0049-0172(91)90019-V).
- [6] C. Cerquaglia, M. Diaco, G. Nucera, M. La Regina, M. Montalto, and R. Manna, “Pharmacological and clinical basis of treatment of Familial Mediterranean Fever (FMF) with colchicine or analogues: an update.,” *Curr. Drug Targets. Inflamm. Allergy*, vol. 4, no. 1, pp. 117–124, Feb. 2005, doi: 10.2174/1568010053622984.
- [7] K. Masuda, A. Nakajima, A. Urayama, K. Nakae, M. Kogure, and G. Inaba, “Double-masked trial of cyclosporin versus colchicine and long-term open study of cyclosporin in Behçet’s disease.,” *Lancet (London, England)*, vol. 1, no. 8647, pp. 1093–1096, May 1989, doi: 10.1016/s0140-6736(89)92381-7.

- [8] M. M. Kaplan, “New strategies needed for treatment of primary biliary cirrhosis?,” *Gastroenterology*, vol. 104, no. 2. United States, pp. 651–653, Feb. 1993, doi: 10.1016/0016-5085(93)90440-n.
- [9] Y. Gong and C. Gluud, “Colchicine for primary biliary cirrhosis: a Cochrane Hepato-Biliary Group systematic review of randomized clinical trials.,” *Am. J. Gastroenterol.*, vol. 100, no. 8, pp. 1876–1885, Aug. 2005, doi: 10.1111/j.1572-0241.2005.41522.x.
- [10] R. J. McKendry, G. Kraag, S. Seigel, and A. al-Awadhi, “Therapeutic value of colchicine in the treatment of patients with psoriatic arthritis.,” *Ann. Rheum. Dis.*, vol. 52, no. 11, pp. 826–828, Nov. 1993, doi: 10.1136/ard.52.11.826.
- [11] R. A. Kyle *et al.*, “A trial of three regimens for primary amyloidosis: colchicine alone, melphalan and prednisone, and melphalan, prednisone, and colchicine.,” *N. Engl. J. Med.*, vol. 336, no. 17, pp. 1202–1207, Apr. 1997, doi: 10.1056/NEJM199704243361702.
- [12] M. Imazio and F. Gaita, “Colchicine for cardiovascular medicine.,” *Future Cardiol.*, vol. 12, no. 1, pp. 9–16, Jan. 2016, doi: 10.2217/fca.15.59.
- [13] R. C. Weisenberg, G. G. Borisy, and E. W. Taylor, “The colchicine-binding protein of mammalian brain and its relation to microtubules.,” *Biochemistry*, vol. 7, no. 12, pp. 4466–4479, Dec. 1968, doi: 10.1021/bi00852a043.
- [14] J. Seligmann and C. Twelves, “Tubulin: an example of targeted chemotherapy.,” *Future Med. Chem.*, vol. 5, no. 3, pp. 339–52, Mar. 2013, doi: 10.4155/fmc.12.217.
- [15] C. D. Katsetos and P. Dráber, “Tubulins as therapeutic targets in cancer: from bench to bedside.,” *Curr. Pharm. Des.*, vol. 18, no. 19, pp. 2778–92, 2012, doi: 10.2174/138161212800626193.
- [16] C. Avendaño and J. C. Menéndez, “Chapter 1 - Introduction,” in *Medicinal Chemistry of Anticancer Drugs*, C. Avendaño and J. C. Menéndez, Eds. Amsterdam: Elsevier, 2008, pp. 1–8.

- [17] X. Zhang *et al.*, “Design, synthesis and biological evaluation of colchicine derivatives as novel tubulin and histone deacetylase dual inhibitors,” *Eur. J. Med. Chem.*, vol. 95, pp. 127–135, 2015, doi: <https://doi.org/10.1016/j.ejmech.2015.03.035>.
- [18] K. C. Nicolaou, R. A. Valiulin, J. K. Pokorski, V. Chang, and J. S. Chen, “Bio-inspired synthesis and biological evaluation of a colchicine-related compound library,” *Bioorg. Med. Chem. Lett.*, vol. 22, no. 11, pp. 3776–3780, 2012, doi: <https://doi.org/10.1016/j.bmcl.2012.04.007>.
- [19] D.-J. Chang *et al.*, “Design, synthesis and identification of novel colchicine-derived immunosuppressant,” *Bioorg. Med. Chem. Lett.*, vol. 19, no. 15, pp. 4416–4420, 2009, doi: <https://doi.org/10.1016/j.bmcl.2009.05.054>.
- [20] A. Marzo-Mas *et al.*, “Interactions of long-chain homologues of colchicine with tubulin,” *Eur. J. Med. Chem.*, vol. 126, pp. 526–535, 2017, doi: <https://doi.org/10.1016/j.ejmech.2016.11.049>.
- [21] L. Johnson *et al.*, “Novel Colchicine Derivatives and their Anti-cancer Activity.,” *Curr. Top. Med. Chem.*, vol. 17, no. 22, pp. 2538–2558, 2017, doi: [10.2174/1568026617666170104143618](https://doi.org/10.2174/1568026617666170104143618).
- [22] B. Kumar *et al.*, “Synthesis and biological evaluation of pyrimidine bridged combretastatin derivatives as potential anticancer agents and mechanistic studies,” *Bioorg. Chem.*, vol. 78, pp. 130–140, 2018, doi: <https://doi.org/10.1016/j.bioorg.2018.02.027>.
- [23] A. Kumar, P. R. Sharma, and D. M. Mondhe, “Potential anticancer role of colchicine-based derivatives,” *Anticancer. Drugs*, vol. 28, no. 3, pp. 250–262, Mar. 2017, doi: [10.1097/CAD.0000000000000464](https://doi.org/10.1097/CAD.0000000000000464).
- [24] E. S. Shchegravina *et al.*, “Synthesis and biological evaluation of novel non-racemic indole-containing allocolchicinoids,” *Eur. J. Med. Chem.*, vol. 141, pp. 51–60, 2017, doi: <https://doi.org/10.1016/j.ejmech.2017.09.055>.
- [25] D. Bartusik, B. Tomanek, E. Lattová, H. Perreault, J. Tuszynski, and G. Fallone,

- “Derivatives of thiocolchicine and its applications to CEM cells treatment using 19F Magnetic Resonance ex vivo,” *Bioorg. Chem.*, vol. 38, no. 1, pp. 1–6, 2010, doi: <https://doi.org/10.1016/j.bioorg.2009.10.002>.
- [26] G. Raspaglio *et al.*, “Thiocolchicine dimers: a novel class of topoisomerase-I inhibitors,” *Biochem. Pharmacol.*, vol. 69, no. 1, pp. 113–121, 2005, doi: <https://doi.org/10.1016/j.bcp.2004.09.004>.
- [27] T. Kozaka *et al.*, “Antitumor agents 273. Design and synthesis of N-alkyl-thiocolchicinoids as potential antitumor agents.,” *Bioorg. Med. Chem. Lett.*, vol. 20, no. 14, pp. 4091–4, Jul. 2010, doi: 10.1016/j.bmcl.2010.05.081.
- [28] K. Nakagawa-Goto *et al.*, “Antitumor agents. Part 236: Synthesis of water-soluble colchicine derivatives.,” *Bioorg. Med. Chem. Lett.*, vol. 15, no. 1, pp. 235–238, Jan. 2005, doi: 10.1016/j.bmcl.2004.07.098.
- [29] N. Yasobu *et al.*, “Design, Synthesis, and Antitumor Activity of 4-Halocolchicines and Their Pro-drugs Activated by Cathepsin B.,” *ACS Med. Chem. Lett.*, vol. 2, no. 5, pp. 348–352, May 2011, doi: 10.1021/ml100287y.
- [30] N. Hiroyuki *et al.*, “Synthesis and biological evaluation of 4-chlorocolchicine derivatives as potent anticancer agents with broad effective dosage ranges,” *Medchemcomm*, vol. 3, pp. 1500–1504, 2012.
- [31] A. Huczyński *et al.*, “Synthesis, antiproliferative and antibacterial evaluation of C-ring modified colchicine analogues.,” *Eur. J. Med. Chem.*, vol. 90, pp. 296–301, Jan. 2015, doi: 10.1016/j.ejmech.2014.11.037.
- [32] A. Huczyński *et al.*, “Synthesis, antiproliferative activity and molecular docking of Colchicine derivatives,” *Bioorg. Chem.*, vol. 64, pp. 103–112, 2016, doi: <https://doi.org/10.1016/j.bioorg.2016.01.002>.
- [33] U. Majcher *et al.*, “Antiproliferative Activity and Molecular Docking of Novel Double-Modified Colchicine Derivatives.,” *Cells*, vol. 7, no. 11, p. 192, Nov. 2018, doi: 10.3390/cells7110192.
- [34] U. Majcher *et al.*, “Synthesis and Biological Evaluation of Novel Triple-Modified

- Colchicine Derivatives as Potent Tubulin-Targeting Anticancer Agents.,” *Cells*, vol. 7, no. 11, Nov. 2018, doi: 10.3390/cells7110216.
- [35] U. Majcher *et al.*, “Synthesis, antiproliferative activity and molecular docking of thiocolchicine urethanes.,” *Bioorg. Chem.*, vol. 81, pp. 553–566, 2018, doi: 10.1016/j.bioorg.2018.09.004.
- [36] J. Kurek *et al.*, “7-Deacetyl-10-alkylthiocolchicine derivatives-new compounds with potent anticancer and fungicidal activity,” *Medchemcomm*, vol. 9, no. 10, pp. 1708–1714, 2018, doi: 10.1039/C8MD00352A.
- [37] H. Alkadi, M. J. Khubeiz, and R. Jbeily, “Colchicine: A Review on Chemical Structure and Clinical Usage.,” *Infect. Disord. Drug Targets*, vol. 18, no. 2, pp. 105–121, 2018, doi: 10.2174/1871526517666171017114901.
- [38] A. A. Ghawanmeh, K. F. Chong, S. M. Sarkar, M. A. Bakar, R. Othaman, and R. M. Khalid, “Colchicine prodrugs and codrugs: Chemistry and bioactivities,” *Eur. J. Med. Chem.*, vol. 144, pp. 229–242, 2018, doi: <https://doi.org/10.1016/j.ejmech.2017.12.029>.
- [39] A. A. Ghawanmeh, H. M. Al-Bajalan, M. M. Mackeen, F. Q. Alali, and K. F. Chong, “Recent developments on (–)-colchicine derivatives: Synthesis and structure-activity relationship,” *Eur. J. Med. Chem.*, vol. 185, p. 111788, 2020, doi: <https://doi.org/10.1016/j.ejmech.2019.111788>.
- [40] I. A. Gracheva, E. S. Shchegravina, H.-G. Schmalz, I. P. Beletskaya, and A. Y. Fedorov, “Colchicine Alkaloids and Synthetic Analogues: Current Progress and Perspectives.,” *J. Med. Chem.*, vol. 63, no. 19, pp. 10618–10651, Oct. 2020, doi: 10.1021/acs.jmedchem.0c00222.
- [41] A. Brossi *et al.*, “Biological effects of modified colchicines. 2. Evaluation of catecholic colchicines, colchifolines, colchicide, and novel N-acyl- and N-aroyldeacetylcolchicines.,” *J. Med. Chem.*, vol. 26, no. 10, pp. 1365–1369, Oct. 1983, doi: 10.1021/jm00364a006.
- [42] P. Kerekes, P. N. Sharma, A. Brossi, C. F. Chignell, and F. R. Quinn, “Synthesis

and biological effects of novel thiocolchicines. 3. Evaluation of N-acyldeacetylthiocolchicines, N-(alkoxycarbonyl) deacetylthiocolchicines, and O-ethyl-demethylthiocolchicines. New synthesis of thiodemecolcine and antileukemic effects of 2-deme,” *J. Med. Chem.*, vol. 28, no. 9, pp. 1204–1208, Sep. 1985, doi: 10.1021/jm00147a014.

- [43] L. Sun, E. Hamel, C. M. Lin, S. B. Hastie, A. Pyluck, and K. H. Lee, “Antitumor agents. 141. Synthesis and biological evaluation of novel thiocolchicine analogs: N-acyl-, N-aroyl-, and N-(substituted benzyl)deacetylthiocolchicines as potent cytotoxic and antimetabolic compounds,” *J. Med. Chem.*, vol. 36, no. 10, pp. 1474–1479, May 1993, doi: 10.1021/jm00062a021.
- [44] G. Klejborowska *et al.*, “Synthesis, antiproliferative activity, and molecular docking studies of 4-chlorothiocolchicine analogues,” *Chem. Biol. Drug Des.*, vol. 95, no. 1, pp. 182–191, Jan. 2020, doi: 10.1111/cbdd.13618.
- [45] G. Klejborowska *et al.*, “Synthesis, biological evaluation and molecular docking studies of new amides of 4-chlorothiocolchicine as anticancer agents,” *Bioorg. Chem.*, vol. 97, p. 103664, 2020, doi: 10.1016/j.bioorg.2020.103664.
- [46] G. Klejborowska *et al.*, “Synthesis, biological evaluation and molecular docking studies of new amides of 4-bromothiocolchicine as anticancer agents,” *Bioorg. Med. Chem.*, vol. 27, no. 23, p. 115144, 2019, doi: 10.1016/j.bmc.2019.115144.
- [47] Q. Shi, P. Verdier-Pinard, A. Brossi, E. Hamel, and K. H. Lee, “Antitumor agents-CLXXV. Anti-tubulin action of (+)-thiocolchicine prepared by partial synthesis,” *Bioorg. Med. Chem.*, vol. 5, no. 12, pp. 2277–2282, Dec. 1997, doi: 10.1016/s0968-0896(97)00171-5.
- [48] B. A. Nijmeijer *et al.*, “Long-term culture of primary human lymphoblastic leukemia cells in the absence of serum or hematopoietic growth factors,” *Exp. Hematol.*, vol. 37, no. 3, pp. 376–385, Mar. 2009, doi: 10.1016/j.exphem.2008.11.002.
- [49] A. Kothari, W. N. Hittelman, and T. C. Chambers, “Cell Cycle-Dependent

Mechanisms Underlie Vincristine-Induced Death of Primary Acute Lymphoblastic Leukemia Cells,” *Cancer Res.*, vol. 76, no. 12, pp. 3553–3561, Jun. 2016, doi: 10.1158/0008-5472.CAN-15-2104.

- [50] W. G. Dirks *et al.*, “Cell line cross-contamination initiative: an interactive reference database of STR profiles covering common cancer cell lines.,” *International journal of cancer*, vol. 126, no. 1. United States, pp. 303–304, Jan. 2010, doi: 10.1002/ijc.24999.
- [51] P. Skehan *et al.*, “New colorimetric cytotoxicity assay for anticancer-drug screening.,” *J. Natl. Cancer Inst.*, vol. 82, no. 13, pp. 1107–1112, Jul. 1990, doi: 10.1093/jnci/82.13.1107.
- [52] D. Nevozhay, “Cheburator software for automatically calculating drug inhibitory concentrations from in vitro screening assays.,” *PLoS One*, vol. 9, no. 9, p. e106186, 2014, doi: 10.1371/journal.pone.0106186.
- [53] M. C. Alley *et al.*, “Feasibility of drug screening with panels of human tumor cell lines using a microculture tetrazolium assay.,” *Cancer Res.*, vol. 48, no. 3, pp. 589–601, Feb. 1988.
- [54] O. Trott and A. J. Olson, “AutoDock Vina: Improving the speed and accuracy of docking with a new scoring function, efficient optimization, and multithreading,” *J. Comput. Chem.*, vol. 31, no. 2, pp. 455–461, Jan. 2009, doi: 10.1002/jcc.21334.
- [55] T. H. Dunning, “Gaussian basis sets for use in correlated molecular calculations. I. The atoms boron through neon and hydrogen,” *J. Chem. Phys.*, vol. 90, no. 2, pp. 1007–1023, Jan. 1989, doi: 10.1063/1.456153.
- [56] M. W. Schmidt *et al.*, “General atomic and molecular electronic structure system,” *J. Comput. Chem.*, vol. 14, no. 11, pp. 1347–1363, Nov. 1993, doi: 10.1002/jcc.540141112.
- [57] M. S. Gordon and M. W. Schmidt, “Advances in electronic structure theory: GAMESS a decade later,” in *Theory and Applications of Computational Chemistry*, C. E. Dykstra, G. Frenking, K. S. Kim, and G. E. Scuseria, Eds.

Amsterdam: Elsevier, 2005, pp. 1167–1189.

- [58] G. M. J. Barca *et al.*, “Recent developments in the general atomic and molecular electronic structure system.,” *J. Chem. Phys.*, vol. 152, no. 15, p. 154102, Apr. 2020, doi: 10.1063/5.0005188.
- [59] M. A. Jordan and L. Wilson, “Microtubules as a target for anticancer drugs.,” *Nat. Rev. Cancer*, vol. 4, no. 4, pp. 253–65, Apr. 2004, doi: 10.1038/nrc1317.
- [60] M. Delgado, A. Urbaniak, and T. C. Chambers, “Contrasting effects of microtubule destabilizers versus stabilizers on induction of death in G1 phase of the cell cycle.,” *Biochem. Pharmacol.*, vol. 162, pp. 213–223, Apr. 2019, doi: 10.1016/j.bcp.2018.12.015.
- [61] R. U. Jänicke, M. L. Sprengart, M. R. Wati, and A. G. Porter, “Caspase-3 is required for DNA fragmentation and morphological changes associated with apoptosis.,” *J. Biol. Chem.*, vol. 273, no. 16, pp. 9357–9360, Apr. 1998, doi: 10.1074/jbc.273.16.9357.
- [62] M. Antoszczak *et al.*, “Biological activity of doubly modified salinomycin analogs - Evaluation in vitro and ex vivo.,” *Eur. J. Med. Chem.*, vol. 156, pp. 510–523, Aug. 2018, doi: 10.1016/j.ejmech.2018.07.021.
- [63] A. Urbaniak, M. Delgado, M. Antoszczak, A. Huczyński, and T. C. Chambers, “Salinomycin derivatives exhibit activity against primary acute lymphoblastic leukemia (ALL) cells in vitro.,” *Biomed. Pharmacother.*, vol. 99, pp. 384–390, Mar. 2018, doi: 10.1016/j.biopha.2018.01.081.
- [64] P. G. Morris and M. N. Fornier, “Microtubule active agents: beyond the taxane frontier.,” *Clin. Cancer Res.*, vol. 14, no. 22, pp. 7167–72, Nov. 2008, doi: 10.1158/1078-0432.CCR-08-0169.
- [65] L. J. Leandro-García *et al.*, “Tumoral and tissue-specific expression of the major human beta-tubulin isoforms.,” *Cytoskeleton (Hoboken)*, vol. 67, no. 4, pp. 214–223, Apr. 2010, doi: 10.1002/cm.20436.
- [66] S. Mons *et al.*, “The interaction between lipid derivatives of colchicine and

tubulin: consequences of the interaction of the alkaloid with lipid membranes.,” *Biochim. Biophys. Acta*, vol. 1468, no. 1–2, pp. 381–395, Sep. 2000, doi: 10.1016/s0005-2736(00)00279-0.

Chapter 3

- [1] J. Hyams and H. Stebbings, “The mechanism of microtubule associated cytoplasmic transport,” *Cell Tissue Res.*, vol. 196, no. 1, Jan. 1979, doi: 10.1007/BF00236351.
- [2] P. Dustin, Ed., *Microtubules*, 2nd ed. Berlin: Springer-Verlag, 1984.
- [3] M. A. Jordan and L. Wilson, “Microtubules as a target for anticancer drugs.,” *Nat. Rev. Cancer*, vol. 4, no. 4, pp. 253–65, Apr. 2004, doi: 10.1038/nrc1317.
- [4] S. K. Dutcher, “The tubulin fraternity: alpha to eta,” *Curr. Opin. Cell Biol.*, vol. 13, no. 1, pp. 49–54, Feb. 2001, doi: 10.1016/S0955-0674(00)00173-3.
- [5] N. G. Vindya, N. Sharma, M. Yadav, and K. R. Ethiraj, “Tubulins - the target for anticancer therapy.,” *Curr. Top. Med. Chem.*, vol. 15, no. 1, pp. 73–82, 2015, doi: 10.2174/1568026615666150112115805.
- [6] J. Seligmann and C. Twelves, “Tubulin: an example of targeted chemotherapy.,” *Future Med. Chem.*, vol. 5, no. 3, pp. 339–52, Mar. 2013, doi: 10.4155/fmc.12.217.
- [7] C. D. Katsetos and P. Dráber, “Tubulins as therapeutic targets in cancer: from bench to bedside.,” *Curr. Pharm. Des.*, vol. 18, no. 19, pp. 2778–92, 2012, doi: 10.2174/138161212800626193.
- [8] J. Torin Huzil, R. F. Ludueña, and J. Tuszynski, “Comparative modelling of human β tubulin isotypes and implications for drug binding.,” *Nanotechnology*, vol. 17, no. 4, pp. S90–S100, Feb. 2006, doi: 10.1088/0957-4484/17/4/014.
- [9] S. Ravanbakhsh, M. Gajewski, R. Greiner, and J. A. Tuszynski, “Determination of the optimal tubulin isotype target as a method for the development of

- individualized cancer chemotherapy.,” *Theor. Biol. Med. Model.*, vol. 10, no. 29, p. 29, May 2013, doi: 10.1186/1742-4682-10-29.
- [10] B. Kumar, R. Kumar, I. Skvortsova, and V. Kumar, “Mechanisms of Tubulin Binding Ligands to Target Cancer Cells: Updates on their Therapeutic Potential and Clinical Trials.,” *Curr. Cancer Drug Targets*, vol. 17, no. 4, pp. 357–375, 2017, doi: 10.2174/1568009616666160928110818.
- [11] C. Avendaño and J. C. Menéndez, *Medicinal Chemistry of Anticancer Drugs*. 2008.
- [12] A. Slobodnick, B. Shah, M. H. Pillinger, and S. Krasnokutsky, “Colchicine: old and new.,” *Am. J. Med.*, vol. 128, no. 5, pp. 461–70, May 2015, doi: 10.1016/j.amjmed.2014.12.010.
- [13] N. Nerlekar, A. Beale, and R. W. Harper, “Colchicine — a short history of an ancient drug,” *Med. J. Aust.*, vol. 201, no. 11, pp. 687–688, Dec. 2014, doi: 10.5694/mja14.00846.
- [14] I. Grattagliano, L. Bonfrate, V. Ruggiero, G. Scaccianoce, G. Palasciano, and P. Portincasa, “Novel therapeutics for the treatment of familial Mediterranean fever: from colchicine to biologics.,” *Clin. Pharmacol. Ther.*, vol. 95, no. 1, pp. 89–97, Jan. 2014, doi: 10.1038/clpt.2013.148.
- [15] G. Cocco, D. C. C. Chu, and S. Pandolfi, “Colchicine in clinical medicine. A guide for internists.,” *Eur. J. Intern. Med.*, vol. 21, no. 6, pp. 503–8, Dec. 2010, doi: 10.1016/j.ejim.2010.09.010.
- [16] L. P. H. Yang, “Oral Colchicine (Colcrys®),” *Drugs*, vol. 70, no. 12, pp. 1603–1613, 2010, doi: 10.2165/11205470-000000000-00000.
- [17] J. Marangon *et al.*, “Tools for the rational design of bivalent microtubule-targeting drugs,” *Biochem. Biophys. Res. Commun.*, vol. 479, no. 1, pp. 48–53, 2016, doi: <https://doi.org/10.1016/j.bbrc.2016.09.022>.

- [18] A. Huczyński *et al.*, “Synthesis, antiproliferative and antibacterial evaluation of C-ring modified colchicine analogues,” *Eur. J. Med. Chem.*, vol. 90, pp. 296–301, Jan. 2015, doi: 10.1016/j.ejmech.2014.11.037.
- [19] A. Huczyński *et al.*, “Synthesis, antiproliferative activity and molecular docking of Colchicine derivatives,” *Bioorg. Chem.*, vol. 64, pp. 103–112, 2016, doi: <https://doi.org/10.1016/j.bioorg.2016.01.002>.
- [20] A. Kumar, P. R. Sharma, and D. M. Mondhe, “Potential anticancer role of colchicine-based derivatives,” *Anticancer. Drugs*, vol. 28, no. 3, pp. 250–262, Mar. 2017, doi: 10.1097/CAD.0000000000000464.
- [21] E. S. Shchegravina *et al.*, “Synthesis and biological evaluation of novel non-racemic indole-containing allocolchicinoids,” *Eur. J. Med. Chem.*, vol. 141, pp. 51–60, 2017, doi: <https://doi.org/10.1016/j.ejmech.2017.09.055>.
- [22] D. Bartusik, B. Tomanek, E. Lattová, H. Perreault, J. Tuszynski, and G. Fallone, “Derivatives of thiocolchicine and its applications to CEM cells treatment using 19F Magnetic Resonance ex vivo,” *Bioorg. Chem.*, vol. 38, no. 1, pp. 1–6, 2010, doi: <https://doi.org/10.1016/j.bioorg.2009.10.002>.
- [23] G. Raspaglio *et al.*, “Thiocolchicine dimers: a novel class of topoisomerase-I inhibitors,” *Biochem. Pharmacol.*, vol. 69, no. 1, pp. 113–121, 2005, doi: <https://doi.org/10.1016/j.bcp.2004.09.004>.
- [24] T. Kozaka *et al.*, “Antitumor agents 273. Design and synthesis of N-alkyl-thiocolchicinoids as potential antitumor agents,” *Bioorg. Med. Chem. Lett.*, vol. 20, no. 14, pp. 4091–4094, 2010, doi: 10.1016/j.bmcl.2010.05.081.
- [25] K. Nakagawa-Goto *et al.*, “Antitumor agents. Part 236: Synthesis of water-soluble colchicine derivatives,” *Bioorg. Med. Chem. Lett.*, vol. 15, no. 1, pp. 235–238, Jan. 2005, doi: 10.1016/j.bmcl.2004.07.098.
- [26] N. Yasobu *et al.*, “Design, Synthesis, and Antitumor Activity of 4-Halocolchicines and Their Pro-drugs Activated by Cathepsin B,” *ACS Med. Chem. Lett.*, vol. 2, no. 5, pp. 348–352, May 2011, doi: 10.1021/ml100287y.

- [27] E. S. Shchegravina, D. I. Knyazev, I. P. Beletskaya, E. V. Svirshchevskaya, H.-G. Schmalz, and A. Y. Fedorov, "Synthesis of Nonracemic Pyrrolo-allocolchicinoids Exhibiting Potent Cytotoxic Activity," *European J. Org. Chem.*, vol. 2016, no. 34, pp. 5620–5623, 2016, doi: <https://doi.org/10.1002/ejoc.201601069>.
- [28] X. Zhang *et al.*, "Design, synthesis and biological evaluation of colchicine derivatives as novel tubulin and histone deacetylase dual inhibitors," *Eur. J. Med. Chem.*, vol. 95, pp. 127–135, 2015, doi: <https://doi.org/10.1016/j.ejmech.2015.03.035>.
- [29] K. C. Nicolaou, R. A. Valiulin, J. K. Pokorski, V. Chang, and J. S. Chen, "Bio-inspired synthesis and biological evaluation of a colchicine-related compound library," *Bioorg. Med. Chem. Lett.*, vol. 22, no. 11, pp. 3776–3780, 2012, doi: <https://doi.org/10.1016/j.bmcl.2012.04.007>.
- [30] D.-J. Chang *et al.*, "Design, synthesis and identification of novel colchicine-derived immunosuppressant," *Bioorg. Med. Chem. Lett.*, vol. 19, no. 15, pp. 4416–4420, 2009, doi: <https://doi.org/10.1016/j.bmcl.2009.05.054>.
- [31] A. Marzo-Mas *et al.*, "Interactions of long-chain homologues of colchicine with tubulin," *Eur. J. Med. Chem.*, vol. 126, pp. 526–535, 2017, doi: <https://doi.org/10.1016/j.ejmech.2016.11.049>.
- [32] L. Johnson *et al.*, "Novel Colchicine Derivatives and their Anti-cancer Activity.," *Curr. Top. Med. Chem.*, vol. 17, no. 22, pp. 2538–2558, 2017, doi: [10.2174/1568026617666170104143618](https://doi.org/10.2174/1568026617666170104143618).
- [33] B. Kumar *et al.*, "Synthesis and biological evaluation of pyrimidine bridged combretastatin derivatives as potential anticancer agents and mechanistic studies," *Bioorg. Chem.*, vol. 78, pp. 130–140, 2018, doi: <https://doi.org/10.1016/j.bioorg.2018.02.027>.
- [34] Q. Shi, P. Verdier-Pinard, A. Brossi, E. Hamel, and K. H. Lee, "Antitumor Agents-CLXXV. Anti-tubulin action of (+)-thiocolchicine prepared by partial

- synthesis,” *Bioorg. Med. Chem.*, vol. 5, no. 12, pp. 2277–2282, 1997, doi: 10.1016/S0968-0896(97)00171-5.
- [35] A. Banerjee, L. T. Kasmala, E. Hamel, L. Sun, and K.-H. Lee, “Interaction of Novel Thiocolchicine Analogs with the Tubulin Isoforms from Bovine Brain 1,” vol. 337, pp. 334–337, 1999, doi: 10.1006/bbrc.1998.9943.
- [36] P. B. Prajapati, K. B. Bodiwala, and B. P. Marolia, “Oxidative Degradation Kinetic Study of Thiocolchicoside using Stability Indicating High Performance Thin Layer Chromatographic Method,” *Pharm. Methods*, vol. 5, no. 2, pp. 1–10, 2014, doi: 10.5530/phm.2014.2.5.
- [37] P. Skehan et al., “New colorimetric cytotoxicity assay for anticancer-drug screening,” *J. Natl. Cancer Inst.*, vol. 82, no. 13, pp. 1107–1112, Jul. 1990, doi: 10.1093/jnci/82.13.1107.
- [38] D. Nevozhay, “Cheburator software for automatically calculating drug inhibitory concentrations from in vitro screening assays,” *PLoS One*, vol. 9, no. 9, p. e106186, 2014, doi: 10.1371/journal.pone.0106186.
- [39] T. H. Dunning, “Gaussian basis sets for use in correlated molecular calculations. I. The atoms boron through neon and hydrogen,” *J. Chem. Phys.*, vol. 90, no. 2, pp. 1007–1023, Jan. 1989, doi: 10.1063/1.456153.
- [40] M. W. Schmidt et al., “General atomic and molecular electronic structure system,” *J. Comput. Chem.*, vol. 14, no. 11, pp. 1347–1363, Nov. 1993, doi: 10.1002/jcc.540141112.
- [41] M. S. Gordon and M. W. Schmidt, “Advances in electronic structure theory: GAMESS a decade later,” in *Theory and Applications of Computational Chemistry*, C. E. Dykstra, G. Frenking, K. S. Kim, and G. E. Scuseria, Eds. Amsterdam: Elsevier, 2005, pp. 1167–1189.
- [42] G. M. J. Barca et al., “Recent developments in the general atomic and molecular electronic structure system,” *J. Chem. Phys.*, vol. 152, no. 15, p. 154102, Apr. 2020, doi: 10.1063/5.0005188.

- [43] U. Majcher et al., "Synthesis, antiproliferative activity and molecular docking of thiocolchicine urethanes," *Bioorg. Chem.*, vol. 81, pp. 553–566, 2018, doi: 10.1016/j.bioorg.2018.09.004.
- [44] H. Devalapally, A. Chakilam, and M. M. Amiji, "Role of nanotechnology in pharmaceutical product development.," *J. Pharm. Sci.*, vol. 96, no. 10, pp. 2547–2565, Oct. 2007, doi: 10.1002/jps.20875.
- [45] R. F. Ludueña, "Multiple Forms of Tubulin: Different Gene Products and Covalent Modifications," in *International review of cytology* vol. 173, 1st Editio., Academic Press, 1997, pp. 207–275.
- [46] L. J. Leandro-García et al., "Tumoral and tissue-specific expression of the major human beta-tubulin isotypes," *Cytoskeleton*, vol. 67, no. 4, pp. 214–223, 2010, doi: 10.1002/cm.20436.
- [47] S. Mozzetti et al., "Class III beta-tubulin overexpression is a prominent mechanism of paclitaxel resistance in ovarian cancer patients.," *Clin. Cancer Res.*, vol. 11, no. 1, pp. 298–305, Jan. 2005.
- [48] P. Sève and C. Dumontet, "Is class III β -tubulin a predictive factor in patients receiving tubulin-binding agents?," *Lancet Oncol.*, vol. 9, no. 2, pp. 168–175, Feb. 2008, doi: 10.1016/S1470-2045(08)70029-9.
- [49] L. Hiser et al., "Comparison of beta-tubulin mRNA and protein levels in 12 human cancer cell lines," *Cell Motil. Cytoskeleton*, vol. 63, no. 1, pp. 41–52, 2006, doi: 10.1002/cm.20109.
- [50] A. Davis, S. Martinez, D. Nelson, and K. Middleton, "A tubulin polymerization microassay used to compare ligand efficacy," in *Methods in Cell Biology*, First edit., vol. 95, no. C, L. Wilson and J. J. Correia, Eds. Elsevier, 2010, pp. 331–351.
- [51] C. Y. Tseng et al., "Quantitative analysis of the effect of tubulin isotype expression on sensitivity of cancer cell lines to a set of novel colchicine

- derivatives,” *Mol. Cancer*, vol. 9, pp. 1–19, 2010, doi: 10.1186/1476-4598-9-131.
- [52] C. Dumontet and M. A. Jordan, “Microtubule-binding agents: a dynamic field of cancer therapeutics,” *Nat. Rev. Drug Discov.*, vol. 9, no. 10, pp. 790–803, Oct. 2010, doi: 10.1038/nrd3253.
- [53] Y. H. Choi and A.-M. Yu, “ABC transporters in multidrug resistance and pharmacokinetics, and strategies for drug development,” *Curr. Pharm. Des.*, vol. 20, no. 5, pp. 793–807, 2014.

Chapter 4

- [1] E. Ben-Chetrit and M. Levy, “Colchicine prophylaxis in familial Mediterranean fever: Reappraisal after 15 years,” *Semin. Arthritis Rheum.*, vol. 20, no. 4, pp. 241–246, 1991, doi: [https://doi.org/10.1016/0049-0172\(91\)90019-V](https://doi.org/10.1016/0049-0172(91)90019-V).
- [2] C. Cerquaglia, M. Diaco, G. Nucera, M. La Regina, M. Montalto, and R. Manna, “Pharmacological and clinical basis of treatment of Familial Mediterranean Fever (FMF) with colchicine or analogues: an update,” *Curr. Drug Targets. Inflamm. Allergy*, vol. 4, no. 1, pp. 117–124, Feb. 2005, doi: 10.2174/1568010053622984.
- [3] Y. Gong and C. Gluud, “Colchicine for primary biliary cirrhosis: a Cochrane Hepato-Biliary Group systematic review of randomized clinical trials,” *Am. J. Gastroenterol.*, vol. 100, no. 8, pp. 1876–1885, Aug. 2005, doi: 10.1111/j.1572-0241.2005.41522.x.
- [4] M. Imazio and F. Gaita, “Colchicine for cardiovascular medicine,” *Future Cardiol.*, vol. 12, no. 1, pp. 9–16, Jan. 2016, doi: 10.2217/fca.15.59.
- [5] M. Imazio *et al.*, “Colchicine for recurrent pericarditis (CORP): a randomized trial,” *Ann. Intern. Med.*, vol. 155, no. 7, pp. 409–414, Oct. 2011, doi: 10.7326/0003-4819-155-7-201110040-00359.

- [6] M. M. Kaplan, “New strategies needed for treatment of primary biliary cirrhosis?,” *Gastroenterology*, vol. 104, no. 2. United States, pp. 651–653, Feb. 1993, doi: 10.1016/0016-5085(93)90440-n.
- [7] R. A. Kyle *et al.*, “A Trial of Three Regimens for Primary Amyloidosis: Colchicine Alone, Melphalan and Prednisone, and Melphalan, Prednisone, and Colchicine,” *N. Engl. J. Med.*, vol. 336, no. 17, pp. 1202–1207, Apr. 1997, doi: 10.1056/NEJM199704243361702.
- [8] K. Masuda, A. Nakajima, A. Urayama, K. Nakae, M. Kogure, and G. Inaba, “Double-masked trial of cyclosporin versus colchicine and long-term open study of cyclosporin in Behçet’s disease.,” *Lancet (London, England)*, vol. 1, no. 8647, pp. 1093–1096, May 1989, doi: 10.1016/s0140-6736(89)92381-7.
- [9] R. J. McKendry, G. Kraag, S. Seigel, and A. al-Awadhi, “Therapeutic value of colchicine in the treatment of patients with psoriatic arthritis.,” *Ann. Rheum. Dis.*, vol. 52, no. 11, pp. 826–828, Nov. 1993, doi: 10.1136/ard.52.11.826.
- [10] E. S. Shchegravina, D. I. Knyazev, I. P. Beletskaya, E. V Svirshchevskaya, H.-G. Schmalz, and A. Y. Fedorov, “Synthesis of Nonracemic Pyrrolo-allocholchicinoids Exhibiting Potent Cytotoxic Activity,” *European J. Org. Chem.*, vol. 2016, no. 34, pp. 5620–5623, 2016, doi: <https://doi.org/10.1002/ejoc.201601069>.
- [11] D. Zemer, A. Livneh, Y. L. Danon, M. Pras, and E. Sohar, “Long-term colchicine treatment in children with familial mediterranean fever,” *Arthritis & Rheum.*, vol. 34, no. 8, pp. 973–977, 1991, doi: <https://doi.org/10.1002/art.1780340806>.
- [12] C. Avendaño and J. C. Menéndez, “Chapter 1 - Introduction,” in *Medicinal Chemistry of Anticancer Drugs*, C. Avendaño and J. C. Menéndez, Eds. Amsterdam: Elsevier, 2008, pp. 1–8.
- [13] C. D. Katsetos and P. Dráber, “Tubulins as therapeutic targets in cancer: from bench to bedside.,” *Curr. Pharm. Des.*, vol. 18, no. 19, pp. 2778–92, 2012, doi: 10.2174/138161212800626193.

- [14] J. Seligmann and C. Twelves, "Tubulin: an example of targeted chemotherapy.," *Future Med. Chem.*, vol. 5, no. 3, pp. 339–52, Mar. 2013, doi: 10.4155/fmc.12.217.
- [15] A. Banerjee, L. T. Kasmala, E. Hamel, L. Sun, and K. H. Lee, "Interaction of novel thiocolchicine analogs with the tubulin isoforms from bovine brain.," *Biochem. Biophys. Res. Commun.*, vol. 254, no. 2, pp. 334–337, Jan. 1999, doi: 10.1006/bbrc.1998.9943.
- [16] D. Bartusik, B. Tomanek, E. Lattová, H. Perreault, J. Tuszynski, and G. Fallone, "Derivatives of thiocolchicine and its applications to CEM cells treatment using 19F Magnetic Resonance ex vivo," *Bioorg. Chem.*, vol. 38, no. 1, pp. 1–6, 2010, doi: <https://doi.org/10.1016/j.bioorg.2009.10.002>.
- [17] A. Huczyński *et al.*, "Synthesis, antiproliferative activity and molecular docking of Colchicine derivatives," *Bioorg. Chem.*, vol. 64, pp. 103–112, 2016, doi: <https://doi.org/10.1016/j.bioorg.2016.01.002>.
- [18] T. Kozaka *et al.*, "Antitumor agents 273. Design and synthesis of N-alkyl-thiocolchicinoids as potential antitumor agents.," *Bioorg. Med. Chem. Lett.*, vol. 20, no. 14, pp. 4091–4, Jul. 2010, doi: 10.1016/j.bmcl.2010.05.081.
- [19] J. Marangon *et al.*, "Tools for the rational design of bivalent microtubule-targeting drugs," *Biochem. Biophys. Res. Commun.*, vol. 479, no. 1, pp. 48–53, 2016, doi: <https://doi.org/10.1016/j.bbrc.2016.09.022>.
- [20] P. B. Prajapati, K. B. Bodiwala, and B. P. Marolia, "Oxidative Degradation Kinetic Study of Thiocolchicoside using Stability Indicating High Performance Thin Layer Chromatographic Method," *Pharm. Methods*, vol. 5, no. 2, pp. 1–10, 2014, doi: 10.5530/phm.2014.2.5.
- [21] G. Raspaglio *et al.*, "Thiocolchicine dimers: a novel class of topoisomerase-I inhibitors," *Biochem. Pharmacol.*, vol. 69, no. 1, pp. 113–121, 2005, doi: <https://doi.org/10.1016/j.bcp.2004.09.004>.

- [22] N. Yasobu *et al.*, “Design, Synthesis, and Antitumor Activity of 4-Halocolchicines and Their Pro-drugs Activated by Cathepsin B,” *ACS Med. Chem. Lett.*, vol. 2, no. 5, pp. 348–352, May 2011, doi: 10.1021/ml100287y.
- [23] N. Hiroyuki *et al.*, “Synthesis and biological evaluation of 4-chlorocolchicine derivatives as potent anticancer agents with broad effective dosage ranges,” *Medchemcomm*, vol. 3, pp. 1500–1504, 2012.
- [24] Q. Shi *et al.*, “Discovery of a (19)F MRI sensitive salinomycin derivative with high cytotoxicity towards cancer cells,” *Chem. Commun. (Camb)*., vol. 52, no. 29, pp. 5136–5139, Apr. 2016, doi: 10.1039/c6cc01508e.
- [25] U. Majcher *et al.*, “Antiproliferative Activity and Molecular Docking of Novel Double-Modified Colchicine Derivatives,” *Cells*, vol. 7, no. 11, p. 192, Nov. 2018, doi: 10.3390/cells7110192.
- [26] U. Majcher *et al.*, “Synthesis, antiproliferative activity and molecular docking of thiocolchicine urethanes,” *Bioorg. Chem.*, vol. 81, pp. 553–566, 2018, doi: 10.1016/j.bioorg.2018.09.004.
- [27] U. Majcher *et al.*, “Synthesis and Biological Evaluation of Novel Triple-Modified Colchicine Derivatives as Potent Tubulin-Targeting Anticancer Agents,” *Cells*, vol. 7, no. 11, Nov. 2018, doi: 10.3390/cells7110216.
- [28] B. R. Smith, C. M. Eastman, and J. T. Njardarson, “Beyond C, H, O, and N! Analysis of the elemental composition of U.S. FDA approved drug architectures,” *J. Med. Chem.*, vol. 57, no. 23, pp. 9764–9773, Dec. 2014, doi: 10.1021/jm501105n.
- [29] R. B. G. Ravelli *et al.*, “Insight into tubulin regulation from a complex with colchicine and a stathmin-like domain,” *Nature*, vol. 428, no. 6979, pp. 198–202, Mar. 2004, doi: 10.1038/nature02393.
- [30] H. Devalapally, A. Chakilam, and M. M. Amiji, “Role of nanotechnology in pharmaceutical product development,” *J. Pharm. Sci.*, vol. 96, no. 10, pp. 2547–2565, Oct. 2007, doi: 10.1002/jps.20875.

Chapter 5

- [1] A. Slobodnick, B. Shah, M. H. Pillinger, and S. Krasnokutsky, “Colchicine: old and new.,” *Am. J. Med.*, vol. 128, no. 5, pp. 461–70, May 2015, doi: 10.1016/j.amjmed.2014.12.010.
- [2] E. S. Shchegravina, D. I. Knyazev, I. P. Beletskaya, E. V. Svirshchevskaya, H.-G. Schmalz, and A. Y. Fedorov, “Synthesis of Nonracemic Pyrrolo-allocolchicinoids Exhibiting Potent Cytotoxic Activity,” *European J. Org. Chem.*, vol. 2016, no. 34, pp. 5620–5623, 2016, doi: <https://doi.org/10.1002/ejoc.201601069>.
- [3] D. Zemer, A. Livneh, Y. L. Danon, M. Pras, and E. Sohar, “Long-term colchicine treatment in children with familial Mediterranean fever.,” *Arthritis Rheum.*, vol. 34, no. 8, pp. 973–7, Aug. 1991, doi: 10.1002/art.1780340806.
- [4] E. Ben-Chetrit and M. Levy, “Colchicine prophylaxis in familial Mediterranean fever: reappraisal after 15 years.,” *Semin. Arthritis Rheum.*, vol. 20, no. 4, pp. 241–6, Feb. 1991.
- [5] C. Cerquaglia, M. Diaco, G. Nucera, M. La Regina, M. Montalto, and R. Manna, “Pharmacological and clinical basis of treatment of Familial Mediterranean Fever (FMF) with colchicine or analogues: an update.,” *Curr. Drug Targets. Inflamm. Allergy*, vol. 4, no. 1, pp. 117–124, Feb. 2005, doi: 10.2174/1568010053622984.
- [6] K. Masuda, A. Nakajima, A. Urayama, K. Nakae, M. Kogure, and G. Inaba, “Double-masked trial of cyclosporin versus colchicine and long-term open study of cyclosporin in Behçet’s disease.,” *Lancet (London, England)*, vol. 1, no. 8647, pp. 1093–1096, May 1989, doi: 10.1016/s0140-6736(89)92381-7.
- [7] M. M. Kaplan, “New strategies needed for treatment of primary biliary cirrhosis?,” *Gastroenterology*, vol. 104, no. 2, pp. 651–653, Feb. 1993, doi: 10.5555/URI:PII:001650859390440N.

- [8] Y. Gong and C. Gluud, "Colchicine for primary biliary cirrhosis: a Cochrane Hepato-Biliary Group systematic review of randomized clinical trials.," *Am. J. Gastroenterol.*, vol. 100, no. 8, pp. 1876–1885, Aug. 2005, doi: 10.1111/j.1572-0241.2005.41522.x.
- [9] R. J. McKendry, G. Kraag, S. Seigel, and A. al-Awadhi, "Therapeutic value of colchicine in the treatment of patients with psoriatic arthritis.," *Ann. Rheum. Dis.*, vol. 52, no. 11, pp. 826–828, Nov. 1993, doi: 10.1136/ard.52.11.826.
- [10] R. A. Kyle *et al.*, "A Trial of Three Regimens for Primary Amyloidosis: Colchicine Alone, Melphalan and Prednisone, and Melphalan, Prednisone, and Colchicine," *N. Engl. J. Med.*, vol. 336, no. 17, pp. 1202–1207, Apr. 1997, doi: 10.1056/NEJM199704243361702.
- [11] M. Imazio and F. Gaita, "Colchicine for cardiovascular medicine.," *Future Cardiol.*, vol. 12, no. 1, pp. 9–16, Jan. 2016, doi: 10.2217/fca.15.59.
- [12] M. Imazio *et al.*, "Colchicine for recurrent pericarditis (CORP): a randomized trial.," *Ann. Intern. Med.*, vol. 155, no. 7, pp. 409–414, Oct. 2011, doi: 10.7326/0003-4819-155-7-201110040-00359.
- [13] J. Seligmann and C. Twelves, "Tubulin: an example of targeted chemotherapy.," *Future Med. Chem.*, vol. 5, no. 3, pp. 339–52, Mar. 2013, doi: 10.4155/fmc.12.217.
- [14] C. D. Katsetos and P. Dráber, "Tubulins as therapeutic targets in cancer: from bench to bedside.," *Curr. Pharm. Des.*, vol. 18, no. 19, pp. 2778–92, 2012, doi: 10.2174/138161212800626193.
- [15] C. Avendaño and J. C. Menéndez, *Medicinal Chemistry of Anticancer Drugs*. 2008.
- [16] T. Kozaka *et al.*, "Antitumor agents 273. Design and synthesis of N-alkylthiocolchicinoids as potential antitumor agents.," *Bioorg. Med. Chem. Lett.*, vol. 20, no. 14, pp. 4091–4, Jul. 2010, doi: 10.1016/j.bmcl.2010.05.081.

- [17] G. Raspaglio *et al.*, “Thiocolchicine dimers: a novel class of topoisomerase-I inhibitors,” *Biochem. Pharmacol.*, vol. 69, no. 1, pp. 113–121, 2005, doi: <https://doi.org/10.1016/j.bcp.2004.09.004>.
- [18] D. Bartusik, B. Tomanek, E. Lattová, H. Perreault, J. Tuszynski, and G. Fallone, “Derivatives of thiocolchicine and its applications to CEM cells treatment using 19F Magnetic Resonance ex vivo,” *Bioorg. Chem.*, vol. 38, no. 1, pp. 1–6, 2010, doi: <https://doi.org/10.1016/j.bioorg.2009.10.002>.
- [19] P. B. Prajapati, K. B. Bodiwala, and B. P. Marolia, “Oxidative Degradation Kinetic Study of Thiocolchicoside using Stability Indicating High Performance Thin Layer Chromatographic Method,” *Pharm. Methods*, vol. 5, no. 2, pp. 1–10, 2014, doi: 10.5530/phm.2014.2.5.
- [20] A. Banerjee, L. T. Kasmala, E. Hamel, L. Sun, and K. H. Lee, “Interaction of novel thiocolchicine analogs with the tubulin isoforms from bovine brain,” *Biochem. Biophys. Res. Commun.*, vol. 254, no. 2, pp. 334–337, Jan. 1999, doi: 10.1006/bbrc.1998.9943.
- [21] J. Marangon *et al.*, “Tools for the rational design of bivalent microtubule-targeting drugs,” *Biochem. Biophys. Res. Commun.*, vol. 479, no. 1, pp. 48–53, 2016, doi: <https://doi.org/10.1016/j.bbrc.2016.09.022>.
- [22] N. Yasobu *et al.*, “Design, Synthesis, and Antitumor Activity of 4-Halocolchicines and Their Pro-drugs Activated by Cathepsin B,” *ACS Med. Chem. Lett.*, vol. 2, no. 5, pp. 348–352, May 2011, doi: 10.1021/ml100287y.
- [23] U. Majcher *et al.*, “Synthesis, antiproliferative activity and molecular docking of thiocolchicine urethanes,” *Bioorg. Chem.*, vol. 81, pp. 553–566, 2018, doi: 10.1016/j.bioorg.2018.09.004.
- [24] Q. Shi, P. Verdier-Pinard, A. Brossi, E. Hamel, and K. H. Lee, “Antitumor Agents-CLXXV. Anti-tubulin action of (+)-thiocolchicine prepared by partial synthesis,” *Bioorg. Med. Chem.*, vol. 5, no. 12, pp. 2277–2282, 1997, doi: 10.1016/S0968-0896(97)00171-5.

- [25] P. Kerkes, P. N. Sharma, A. Brossi, C. F. Chignell, and F. R. Quinn, "Synthesis and biological effects of novel thiocolchicines. 3. evaluation of N-acyldeacetylthiocolchicines, N-(alkoxycarbonyl)deacetylthiocolchicines, and O-ethyl-demethylthiocolchicines. New synthesis of thiodemecolcine and antileukemic effects of 2-demeth," *J. Med. Chem.*, vol. 28, no. 9, pp. 1204–1208, Sep. 1985, doi: 10.1021/jm00147a014.
- [26] P. Skehan *et al.*, "New colorimetric cytotoxicity assay for anticancer-drug screening," *J. Natl. Cancer Inst.*, vol. 82, no. 13, pp. 1107–1112, Jul. 1990, doi: 10.1093/jnci/82.13.1107.
- [27] D. Nevozhay, "Cheburator software for automatically calculating drug inhibitory concentrations from in vitro screening assays," *PLoS One*, vol. 9, no. 9, p. e106186, 2014, doi: 10.1371/journal.pone.0106186.
- [28] T. H. Dunning, "Gaussian basis sets for use in correlated molecular calculations. I. The atoms boron through neon and hydrogen," *J. Chem. Phys.*, vol. 90, no. 2, pp. 1007–1023, Jan. 1989, doi: 10.1063/1.456153.
- [29] M. W. Schmidt *et al.*, "General atomic and molecular electronic structure system," *J. Comput. Chem.*, vol. 14, no. 11, pp. 1347–1363, Nov. 1993, doi: 10.1002/jcc.540141112.
- [30] M. S. Gordon and M. W. Schmidt, "Advances in electronic structure theory: GAMESS a decade later," in *Theory and Applications of Computational Chemistry*, C. E. Dykstra, G. Frenking, K. S. Kim, and G. E. Scuseria, Eds. Amsterdam: Elsevier, 2005, pp. 1167–1189.
- [31] G. M. J. Barca *et al.*, "Recent developments in the general atomic and molecular electronic structure system," *J. Chem. Phys.*, vol. 152, no. 15, p. 154102, Apr. 2020, doi: 10.1063/5.0005188.
- [32] G. M. Morris *et al.*, "AutoDock4 and AutoDockTools4: Automated docking with selective receptor flexibility," *J. Comput. Chem.*, vol. 30, no. 16, pp. 2785–91, Dec. 2009, doi: 10.1002/jcc.21256.

- [33] L. J. Leandro-García et al., “Tumoral and tissue-specific expression of the major human β -tubulin isotypes,” *Cytoskeleton*, vol. 67, no. 4, pp. 214–223, 2010, doi: 10.1002/cm.20436.
- [34] H. Devalapally, A. Chakilam, and M. M. Amiji, “Role of nanotechnology in pharmaceutical product development.,” *J. Pharm. Sci.*, vol. 96, no. 10, pp. 2547–2565, Oct. 2007, doi: 10.1002/jps.20875.
- [35] M. M. Niu et al., “Tubulin inhibitors: Pharmacophore modeling, virtual screening and molecular docking,” *Acta Pharmacol. Sin.*, vol. 35, no. 7, pp. 967–979, 2014, doi: 10.1038/aps.2014.34.
- [36] “Update on activities at the Universal Protein Resource (UniProt) in 2013.,” *Nucleic Acids Res.*, vol. 41, no. Database issue, pp. D43-7, Jan. 2013, doi: 10.1093/nar/gks1068.
- [37] R. B. G. Ravelli et al., “Insight into tubulin regulation from a complex with colchicine and a stathmin-like domain.,” *Nature*, vol. 428, no. 6979, pp. 198–202, Mar. 2004, doi: 10.1038/nature02393.
- [38] R. Salomon-Ferrer, D. A. Case, and R. C. Walker, “An overview of the Amber biomolecular simulation package,” *WIREs Comput. Mol. Sci.*, vol. 3, no. 2, pp. 198–210, 2013, doi: <https://doi.org/10.1002/wcms.1121>.
- [39] D. R. Roe and T. E. 3rd Cheatham, “PTRAJ and CPPTRAJ: Software for Processing and Analysis of Molecular Dynamics Trajectory Data.,” *J. Chem. Theory Comput.*, vol. 9, no. 7, pp. 3084–3095, Jul. 2013, doi: 10.1021/ct400341p.
- [40] O. Trott and A. J. Olson, “AutoDock Vina: Improving the speed and accuracy of docking with a new scoring function, efficient optimization, and multithreading,” *J. Comput. Chem.*, vol. 31, no. 2, pp. 455–461, Jan. 2009, doi: 10.1002/jcc.21334.
- [41] J. Preto, P. Gentile, P. Winter, C. Churchill, S. Omar, and J. A. Tuszynski, “Molecular Dynamics and Related Computational Methods with Applications to

Drug Discovery,” in Workshop on Coupled Mathematical Models for Physical and Nanoscale Systems and their Applications, 2016, pp. 267–285.

- [42] T. Hou, J. Wang, Y. Li, and W. Wang, “Assessing the performance of the MM/PBSA and MM/GBSA methods. 1. The accuracy of binding free energy calculations based on molecular dynamics simulations.,” *J. Chem. Inf. Model.*, vol. 51, no. 1, pp. 69–82, Jan. 2011, doi: 10.1021/ci100275a.
- [43] I. Spasevska et al., “Modeling the Colchicum autumnale Tubulin and a Comparison of Its Interaction with Colchicine to Human Tubulin.,” *Int. J. Mol. Sci.*, vol. 18, no. 8, Aug. 2017, doi: 10.3390/ijms18081676.
- [44] A. Onufriev, D. Bashford, and D. A. Case, “Exploring protein native states and large-scale conformational changes with a modified generalized Born model.,” *Proteins*, vol. 55, no. 2, pp. 383–394, May 2004, doi: 10.1002/prot.20033.

Chapter 6

- [1] F. Roubille, E. Kritikou, D. Busseuil, S. Barrere-Lemaire, and J.-C. Tardif, “Colchicine: an old wine in a new bottle?,” *Antiinflamm. Antiallergy. Agents Med. Chem.*, vol. 12, no. 1, pp. 14–23, 2013, doi: 10.2174/1871523011312010004.
- [2] G. Cocco, D. C. C. Chu, and S. Pandolfi, “Colchicine in clinical medicine. A guide for internists.,” *Eur. J. Intern. Med.*, vol. 21, no. 6, pp. 503–8, Dec. 2010, doi: 10.1016/j.ejim.2010.09.010.
- [3] G. Sivakumar, “Colchicine semisynthetics: chemotherapeutics for cancer?,” *Curr. Med. Chem.*, vol. 20, no. 7, pp. 892–898, 2013.
- [4] L. Johnson et al., “Novel Colchicine Derivatives and their Anti-cancer Activity.,” *Curr. Top. Med. Chem.*, vol. 17, no. 22, pp. 2538–2558, 2017, doi: 10.2174/1568026617666170104143618.

- [5] A. Kumar, P. R. Sharma, and D. M. Mondhe, "Potential anticancer role of colchicine-based derivatives: an overview.," *Anticancer. Drugs*, vol. 28, no. 3, pp. 250–262, 2017, doi: 10.1097/CAD.0000000000000464.
- [6] B. Bhattacharyya, D. Panda, S. Gupta, and M. Banerjee, "Anti-mitotic activity of colchicine and the structural basis for its interaction with tubulin.," *Med. Res. Rev.*, vol. 28, no. 1, pp. 155–183, Jan. 2008, doi: 10.1002/med.20097.
- [7] Y. Lu, J. Chen, M. Xiao, W. Li, and D. D. Miller, "An overview of tubulin inhibitors that interact with the colchicine binding site.," *Pharm. Res.*, vol. 29, no. 11, pp. 2943–71, Nov. 2012, doi: 10.1007/s11095-012-0828-z.
- [8] I. Spasevska et al., "Modeling the *Colchicum autumnale* Tubulin and a Comparison of Its Interaction with Colchicine to Human Tubulin.," *Int. J. Mol. Sci.*, vol. 18, no. 8, Aug. 2017, doi: 10.3390/ijms18081676.
- [9] B. Kumar et al., "Synthesis and biological evaluation of pyrimidine bridged combretastatin derivatives as potential anticancer agents and mechanistic studies," *Bioorg. Chem.*, vol. 78, pp. 130–140, 2018, doi: <https://doi.org/10.1016/j.bioorg.2018.02.027>.
- [10] B. Kumar, R. Kumar, I. Skvortsova, and V. Kumar, "Mechanisms of Tubulin Binding Ligands to Target Cancer Cells: Updates on their Therapeutic Potential and Clinical Trials.," *Curr. Cancer Drug Targets*, vol. 17, no. 4, pp. 357–375, 2017, doi: 10.2174/1568009616666160928110818.
- [11] A. A. Ghawanmeh, K. F. Chong, S. M. Sarkar, M. A. Bakar, R. Othaman, and R. M. Khalid, "Colchicine prodrugs and codrugs: Chemistry and bioactivities," *Eur. J. Med. Chem.*, vol. 144, pp. 229–242, 2018, doi: <https://doi.org/10.1016/j.ejmech.2017.12.029>.
- [12] A. Huczyński et al., "Synthesis, antiproliferative activity and molecular docking of Colchicine derivatives," *Bioorg. Chem.*, vol. 64, pp. 103–112, 2016, doi: <https://doi.org/10.1016/j.bioorg.2016.01.002>.

- [13] V. Blasco et al., "Arylureas derived from colchicine: Enhancement of colchicine oncogene downregulation activity.," *Eur. J. Med. Chem.*, vol. 150, pp. 817–828, Apr. 2018, doi: 10.1016/j.ejmech.2018.03.039.
- [14] A. Marzo-Mas et al., "Interactions of long-chain homologues of colchicine with tubulin," *Eur. J. Med. Chem.*, vol. 126, pp. 526–535, 2017, doi: <https://doi.org/10.1016/j.ejmech.2016.11.049>.
- [15] A. Huczyński et al., "Synthesis, antiproliferative and antibacterial evaluation of C-ring modified colchicine analogues.," *Eur. J. Med. Chem.*, vol. 90, pp. 296–301, Jan. 2015, doi: 10.1016/j.ejmech.2014.11.037.
- [16] T. Kozaka et al., "Antitumor agents 273. Design and synthesis of N-alkylthiocolchicinoids as potential antitumor agents.," *Bioorg. Med. Chem. Lett.*, vol. 20, no. 14, pp. 4091–4, Jul. 2010, doi: 10.1016/j.bmcl.2010.05.081.
- [17] S.-H. Lee et al., "New synthetic thiocolchicine derivatives as lowtoxic anticancer agents.," *Arch. Pharm. (Weinheim).*, vol. 338, no. 12, pp. 582–589, Dec. 2005, doi: 10.1002/ardp.200500148.
- [18] G. T. Shiau, K. K. De, and R. E. Harmon, "Synthesis and evaluation of N-deacetyl-N-glycosylalkylthiocolchicines as antileukemic agents.," *J. Pharm. Sci.*, vol. 67, no. 3, pp. 394–397, Mar. 1978, doi: 10.1002/jps.2600670333.
- [19] A. K. Ghosh and M. Brindisi, "Organic carbamates in drug design and medicinal chemistry.," *J. Med. Chem.*, vol. 58, no. 7, pp. 2895–2940, Apr. 2015, doi: 10.1021/jm501371s.
- [20] A. Brossi and P. Kerekes, "Carbamates of colchicine for treatment of gout." Google Patents, Aug. 06, 1985.
- [21] T. H. Dunning, "Gaussian basis sets for use in correlated molecular calculations. I. The atoms boron through neon and hydrogen," *J. Chem. Phys.*, vol. 90, no. 2, pp. 1007–1023, Jan. 1989, doi: 10.1063/1.456153.

- [22] G. B. Rocha, R. O. Freire, A. M. Simas, and J. J. P. Stewart, "RM1: A reparameterization of AM1 for H, C, N, O, P, S, F, Cl, Br, and I," *J. Comput. Chem.*, vol. 27, no. 10, pp. 1101–1111, Jul. 2006, doi: 10.1002/jcc.20425.
- [23] M. W. Schmidt et al., "General atomic and molecular electronic structure system," *J. Comput. Chem.*, vol. 14, no. 11, pp. 1347–1363, Nov. 1993, doi: 10.1002/jcc.540141112.
- [24] M. S. Gordon and M. W. Schmidt, "Advances in electronic structure theory: GAMESS a decade later," in *Theory and Applications of Computational Chemistry*, C. E. Dykstra, G. Frenking, K. S. Kim, and G. E. Scuseria, Eds. Amsterdam: Elsevier, 2005, pp. 1167–1189.
- [25] G. M. J. Barca et al., "Recent developments in the general atomic and molecular electronic structure system.," *J. Chem. Phys.*, vol. 152, no. 15, p. 154102, Apr. 2020, doi: 10.1063/5.0005188.
- [26] W. G. Dirks et al., "Cell line cross-contamination initiative: an interactive reference database of STR profiles covering common cancer cell lines.," *International journal of cancer*, vol. 126, no. 1. United States, pp. 303–304, Jan. 2010, doi: 10.1002/ijc.24999.
- [27] A. Urbaniak, M. Delgado, M. Antoszczak, A. Huczyński, and T. C. Chambers, "Salinomycin derivatives exhibit activity against primary acute lymphoblastic leukemia (ALL) cells in vitro.," *Biomed. Pharmacother.*, vol. 99, pp. 384–390, Mar. 2018, doi: 10.1016/j.biopha.2018.01.081.
- [28] M. Antoszczak et al., "Biological activity of doubly modified salinomycin analogs - Evaluation in vitro and ex vivo.," *Eur. J. Med. Chem.*, vol. 156, pp. 510–523, Aug. 2018, doi: 10.1016/j.ejmech.2018.07.021.
- [29] Q. Shi, P. Verdier-Pinard, A. Brossi, E. Hamel, and K. H. Lee, "Antitumor Agents-CLXXV. Anti-tubulin action of (+)-thiocolchicine prepared by partial synthesis," *Bioorg. Med. Chem.*, vol. 5, no. 12, pp. 2277–2282, 1997, doi: 10.1016/S0968-0896(97)00171-5.

- [30] R. M. Chabin and S. B. Hastie, "Association of thiocolchicine with tubulin.," *Biochem. Biophys. Res. Commun.*, vol. 161, no. 2, pp. 544–550, Jun. 1989, doi: 10.1016/0006-291x(89)92633-8.
- [31] D. Chaturvedi, "Perspectives on the synthesis of organic carbamates," *Tetrahedron*, vol. 68, no. 1, pp. 15–45, 2012, doi: <https://doi.org/10.1016/j.tet.2011.10.001>.
- [32] L. Cotarca, T. Geller, and J. Répási, "Bis(trichloromethyl)carbonate (BTC, Triphosgene): A Safer Alternative to Phosgene?," *Org. Process Res. Dev.*, vol. 21, no. 9, pp. 1439–1446, Sep. 2017, doi: 10.1021/acs.oprd.7b00220.
- [33] D.-W. Shen, L. M. Pouliot, M. D. Hall, and M. M. Gottesman, "Cisplatin resistance: a cellular self-defense mechanism resulting from multiple epigenetic and genetic changes.," *Pharmacol. Rev.*, vol. 64, no. 3, pp. 706–721, Jul. 2012, doi: 10.1124/pr.111.005637.
- [34] M. A. Jordan, D. Thrower, and L. Wilson, "Mechanism of inhibition of cell proliferation by Vinca alkaloids.," *Cancer Res.*, vol. 51, no. 8, pp. 2212–2222, Apr. 1991.
- [35] M. Delgado and T. C. Chambers, "Microtubules play an essential role in the survival of primary acute lymphoblastic leukemia cells advancing through G1 phase.," *Cell Cycle*, vol. 17, no. 14, pp. 1784–1796, 2018, doi: 10.1080/15384101.2018.1496746

Chapter 7

- [1] J. Torin Huzil, R. F. Ludueña, and J. Tuszynski, "Comparative modelling of human β tubulin isotypes and implications for drug binding.," *Nanotechnology*, vol. 17, no. 4, pp. S90–S100, Feb. 2006, doi: 10.1088/0957-4484/17/4/014.
- [2] S. Ravanbakhsh, M. Gajewski, R. Greiner, and J. A. Tuszynski, "Determination of the optimal tubulin isotype target as a method for the development of individualized cancer chemotherapy.," *Theor. Biol. Med. Model.*, vol. 10, no. 29,

p. 29, May 2013, doi: 10.1186/1742-4682-10-29.

- [3] B. Kumar, R. Kumar, I. Skvortsova, and V. Kumar, “Mechanisms of Tubulin Binding Ligands to Target Cancer Cells: Updates on their Therapeutic Potential and Clinical Trials.,” *Curr. Cancer Drug Targets*, vol. 17, no. 4, pp. 357–375, 2017, doi: 10.2174/1568009616666160928110818.
- [4] J. S. Hyams and H. Stebbings, “The mechanism of microtubule associated cytoplasmic transport. Isolation and preliminary characterisation of a microtubule transport system.,” *Cell Tissue Res.*, vol. 196, no. 1, pp. 103–16, Jan. 1979, doi: 10.1007/BF00236351.
- [5] N. G. Vindya, N. Sharma, M. Yadav, and K. R. Ethiraj, “Tubulins - the target for anticancer therapy.,” *Curr. Top. Med. Chem.*, vol. 15, no. 1, pp. 73–82, 2015, doi: 10.2174/1568026615666150112115805.
- [6] J. Seligmann and C. Twelves, “Tubulin: an example of targeted chemotherapy.,” *Future Med. Chem.*, vol. 5, no. 3, pp. 339–52, Mar. 2013, doi: 10.4155/fmc.12.217.
- [7] C. D. Katsetos and P. Dráber, “Tubulins as therapeutic targets in cancer: from bench to bedside.,” *Curr. Pharm. Des.*, vol. 18, no. 19, pp. 2778–92, 2012, doi: 10.2174/138161212800626193.
- [8] C. Avendaño and J. C. Menendez, *Medicinal chemistry of anticancer drugs*, 2nd ed. Elsevier, 2015.
- [9] A. Slobodnick, B. Shah, M. H. Pillinger, and S. Krasnokutsky, “Colchicine: old and new.,” *Am. J. Med.*, vol. 128, no. 5, pp. 461–70, May 2015, doi: 10.1016/j.amjmed.2014.12.010.
- [10] N. Nerlekar, A. Beale, and R. W. Harper, “Colchicine--a short history of an ancient drug.,” *Med. J. Aust.*, vol. 201, no. 11, pp. 687–8, Dec. 2014, doi: 10.5694/mja14.00846.
- [11] I. Grattagliano, L. Bonfrate, V. Ruggiero, G. Scaccianoce, G. Palasciano, and P. Portincasa, “Novel therapeutics for the treatment of familial Mediterranean fever:

- from colchicine to biologics.,” *Clin. Pharmacol. Ther.*, vol. 95, no. 1, pp. 89–97, Jan. 2014, doi: 10.1038/clpt.2013.148.
- [12] G. Cocco, D. C. C. Chu, and S. Pandolfi, “Colchicine in clinical medicine. A guide for internists.,” *Eur. J. Intern. Med.*, vol. 21, no. 6, pp. 503–8, Dec. 2010, doi: 10.1016/j.ejim.2010.09.010.
- [13] L. P. H. Yang, “Oral colchicine (Colcris): in the treatment and prophylaxis of gout.,” *Drugs*, vol. 70, no. 12, pp. 1603–13, Aug. 2010, doi: 10.2165/11205470-000000000-00000.
- [14] A. Tropsha, P. Gramatica, and V. Gombar, “The Importance of Being Earnest: Validation is the Absolute Essential for Successful Application and Interpretation of QSPR Models,” *QSAR Comb. Sci.*, vol. 22, no. 1, pp. 69–77, Apr. 2003, doi: 10.1002/qsar.200390007.
- [15] U. Majcher *et al.*, “Synthesis, antiproliferative activity and molecular docking of thiocolchicine urethanes.,” *Bioorg. Chem.*, vol. 81, pp. 553–566, 2018, doi: 10.1016/j.bioorg.2018.09.004.
- [16] U. Majcher *et al.*, “Antiproliferative Activity and Molecular Docking of Novel Double-Modified Colchicine Derivatives.,” *Cells*, vol. 7, no. 11, p. 192, Nov. 2018, doi: 10.3390/cells7110192.
- [17] U. Majcher *et al.*, “Synthesis and Biological Evaluation of Novel Triple-Modified Colchicine Derivatives as Potent Tubulin-Targeting Anticancer Agents.,” *Cells*, vol. 7, no. 11, Nov. 2018, doi: 10.3390/cells7110216.
- [18] G. Klejborowska *et al.*, “Synthesis, antiproliferative activity, and molecular docking studies of 4-chlorothiocolchicine analogues,” *Chem. Biol. Drug Des.*, vol. 95, no. 1, pp. 182–191, Jan. 2020, doi: 10.1111/cbdd.13618.
- [19] G. Klejborowska *et al.*, “Synthesis, biological evaluation and molecular docking studies of new amides of 4-bromothiocolchicine as anticancer agents.,” *Bioorg. Med. Chem.*, vol. 27, no. 23, p. 115144, 2019, doi: 10.1016/j.bmc.2019.115144.
- [20] G. Klejborowska *et al.*, “Synthesis, biological evaluation and molecular docking

- studies of new amides of 4-chlorothiocolchicine as anticancer agents.," *Bioorg. Chem.*, vol. 97, p. 103664, 2020, doi: 10.1016/j.bioorg.2020.103664.
- [21] G. Klejborowska *et al.*, "Synthesis, anticancer activity and molecular docking studies of N-deacetylthiocolchicine and 4-iodo-N-deacetylthiocolchicine derivatives.," *Bioorg. Med. Chem.*, vol. 32, p. 116014, Feb. 2021, doi: 10.1016/j.bmc.2021.116014.
- [22] M. W. Schmidt *et al.*, "General atomic and molecular electronic structure system," *J. Comput. Chem.*, vol. 14, no. 11, pp. 1347–1363, Nov. 1993, doi: 10.1002/jcc.540141112.
- [23] M. S. Gordon and M. W. Schmidt, "Advances in electronic structure theory: GAMESS a decade later," in *Theory and Applications of Computational Chemistry*, C. E. Dykstra, G. Frenking, K. S. Kim, and G. E. Scuseria, Eds. Amsterdam: Elsevier, 2005, pp. 1167–1189.
- [24] G. M. J. Barca *et al.*, "Recent developments in the general atomic and molecular electronic structure system.," *J. Chem. Phys.*, vol. 152, no. 15, p. 154102, Apr. 2020, doi: 10.1063/5.0005188.
- [25] T. H. Dunning, "Gaussian basis sets for use in correlated molecular calculations. I. The atoms boron through neon and hydrogen," *J. Chem. Phys.*, vol. 90, no. 2, pp. 1007–1023, Jan. 1989, doi: 10.1063/1.456153.
- [26] G. M. Morris *et al.*, "AutoDock4 and AutoDockTools4: Automated docking with selective receptor flexibility.," *J. Comput. Chem.*, vol. 30, no. 16, pp. 2785–91, Dec. 2009, doi: 10.1002/jcc.21256.
- [27] G. Y. Cederquist *et al.*, "An inherited TUBB2B mutation alters a kinesin-binding site and causes polymicrogyria, CFEOM and axon dysinnervation.," *Hum. Mol. Genet.*, vol. 21, no. 26, pp. 5484–99, Dec. 2012, doi: 10.1093/hmg/dds393.
- [28] *Autodock*. Chemical Computing Group ULC, Montreal, Canada, 2018.
- [29] R. B. G. Ravelli *et al.*, "Insight into tubulin regulation from a complex with colchicine and a stathmin-like domain.," *Nature*, vol. 428, no. 6979, pp. 198–202,

- Mar. 2004, doi: 10.1038/nature02393.
- [30] L. H. Hall, B. Mohney, and L. B. Kier, "The electrotopological state: structure information at the atomic level for molecular graphs," *J. Chem. Inf. Model.*, vol. 31, no. 1, pp. 76–82, Feb. 1991, doi: 10.1021/ci00001a012.
- [31] L. H. Hall and L. B. Kier, "Electrotopological State Indices for Atom Types: A Novel Combination of Electronic, Topological, and Valence State Information," *J. Chem. Inf. Comput. Sci.*, vol. 35, no. 6, pp. 1039–1045, Nov. 1995, doi: 10.1021/ci00028a014.
- [32] *Simulations Plus, Inc. ADMET Predictor, Version 9.5: ADMET Property Estimation and Model Building*. Simulations Plus, Inc. Lancaster, CA, 2019.
- [33] M. F. Sanner, "Python: a programming language for software integration and development.," *J. Mol. Graph. Model.*, vol. 17, no. 1, pp. 57–61, Feb. 1999.
- [34] A. D. Becke, "Density-functional thermochemistry. I. The effect of the exchange-only gradient correction," *J. Chem. Phys.*, vol. 96, no. 3, pp. 2155–2160, Feb. 1992, doi: 10.1063/1.462066.
- [35] A. D. Becke, "Density-functional thermochemistry. II. The effect of the Perdew–Wang generalized-gradient correlation correction," *J. Chem. Phys.*, vol. 97, no. 12, pp. 9173–9177, Dec. 1992, doi: 10.1063/1.463343.
- [36] A. D. Becke, "Density-functional thermochemistry. III. The role of exact exchange," *J. Chem. Phys.*, vol. 98, no. 7, pp. 5648–5652, Apr. 1993, doi: 10.1063/1.464913.
- [37] Lee, Yang, and Parr, "Development of the Colle-Salvetti correlation-energy formula into a functional of the electron density.," *Phys. Rev. B. Condens. Matter*, vol. 37, no. 2, pp. 785–789, Jan. 1988, doi: 10.1103/physrevb.37.785.
- [38] R. Krishnan, J. S. Binkley, R. Seeger, and J. A. Pople, "Self-consistent molecular orbital methods. XX. A basis set for correlated wave functions," *J. Chem. Phys.*, vol. 72, no. 1, pp. 650–654, Jan. 1980, doi: 10.1063/1.438955.
- [39] J. P. Foster and F. Weinhold, "Natural hybrid orbitals," *J. Am. Chem. Soc.*, vol.

- 102, no. 24, pp. 7211–7218, Nov. 1980, doi: 10.1021/ja00544a007.
- [40] A. E. Reed, L. A. Curtiss, and F. Weinhold, “Intermolecular interactions from a natural bond orbital, donor-acceptor viewpoint,” *Chem. Rev.*, vol. 88, no. 6, pp. 899–926, Sep. 1988, doi: 10.1021/cr00088a005.
- [41] *Admet predictor, ver. 9.5. (2019) User manual*. Simulations Plus, Inc, Lancaster, CA, USA, 2019.
- [42] K. Roy and I. Mitra, “Electrotopological state atom (E-state) index in drug design, QSAR, property prediction and toxicity assessment,” *Curr. Comput. Aided. Drug Des.*, vol. 8, no. 2, pp. 135–158, 2012, doi: 10.2174/157340912800492366.
- [43] V. C. Roberto Todeschini, *Handbook of Molecular Descriptors*, vol. 11. Wiley, 2008.
- [44] K. J. Miller and J. Savchik, “A new empirical method to calculate average molecular polarizabilities,” *J. Am. Chem. Soc.*, vol. 101, no. 24, pp. 7206–7213, Nov. 1979, doi: 10.1021/ja00518a014.
- [45] A. Golbraikh and A. Tropsha, “Beware of q^2 !,” *J. Mol. Graph. Model.*, vol. 20, no. 4, pp. 269–276, Jan. 2002, doi: 10.1016/s1093-3263(01)00123-1.
- [46] A. Shayanfar and S. Shayanfar, “Is regression through origin useful in external validation of QSAR models?,” *Eur. J. Pharm. Sci.*, vol. 59, pp. 31–5, Aug. 2014, doi: 10.1016/j.ejps.2014.03.007.
- [47] N. Chirico and P. Gramatica, “Real external predictivity of QSAR models: how to evaluate it? Comparison of different validation criteria and proposal of using the concordance correlation coefficient,” *J. Chem. Inf. Model.*, vol. 51, no. 9, pp. 2320–35, Sep. 2011, doi: 10.1021/ci200211n.
- [48] P. Gramatica, “On the development and validation of QSAR models,” *Methods Mol. Biol.*, vol. 930, pp. 499–526, 2013, doi: 10.1007/978-1-62703-059-5_21.
- [49] A. Tropsha, “Recent Advances in Development, Validation, and Exploitation of QSAR Models,” in *Burger’s Medicinal Chemistry and Drug Discovery*, Hoboken, NJ, USA: John Wiley & Sons, Inc., 2010, pp. 505–534.

- [50] T. Le, V. C. Epa, F. R. Burden, and D. A. Winkler, "Quantitative structure-property relationship modeling of diverse materials properties.," *Chem. Rev.*, vol. 112, no. 5, pp. 2889–919, May 2012, doi: 10.1021/cr200066h.
- [51] G. Blom, *Statistical estimates and transformed beta-variables*. Almqvist & Wiksell, 1958.
- [52] Y.-L. Zhang *et al.*, "Synthesis, anticancer activity and molecular docking studies on 1,2-diarylbenzimidazole analogues as anti-tubulin agents.," *Bioorg. Chem.*, vol. 92, p. 103219, 2019, doi: 10.1016/j.bioorg.2019.103219.

Chapter 8

- [1] G. M. Cragg and J. M. Pezzuto, "Natural Products as a Vital Source for the Discovery of Cancer Chemotherapeutic and Chemopreventive Agents," *Med. Princ. Pract.*, vol. 25, no. 2, pp. 41–59, 2016, doi: 10.1159/000443404.
- [2] D. Liu, X. Meng, D. Wu, Z. Qiu, and H. Luo, "A Natural Isoquinoline Alkaloid With Antitumor Activity: Studies of the Biological Activities of Berberine.," *Front. Pharmacol.*, vol. 10, p. 9, 2019, doi: 10.3389/fphar.2019.00009.
- [3] J. Tian *et al.*, "Scoulerine promotes cell viability reduction and apoptosis by activating ROS-dependent endoplasmic reticulum stress in colorectal cancer cells.," *Chem. Biol. Interact.*, vol. 327, p. 109184, Aug. 2020, doi: 10.1016/j.cbi.2020.109184.
- [4] W. A. Kukula-Koch and J. Widelski, "Alkaloids," in *Pharmacognosy*, S. Badal and R. Delgoda, Eds. Boston: Elsevier, 2017, pp. 163–198.
- [5] K. Habartova *et al.*, "Scoulerine affects microtubule structure, inhibits proliferation, arrests cell cycle and thus culminates in the apoptotic death of cancer cells.," *Sci. Rep.*, vol. 8, no. 1, p. 4829, 2018, doi: 10.1038/s41598-018-22862-0.

- [6] J. M. Hagel *et al.*, “Transcriptome analysis of 20 taxonomically related benzyloisoquinoline alkaloid-producing plants,” *BMC Plant Biol.*, vol. 15, p. 227, Sep. 2015, doi: 10.1186/s12870-015-0596-0.
- [7] L. Alisaraie and J. A. Tuszynski, “Determination of noscapine’s localization and interaction with the tubulin- α/β heterodimer,” *Chem. Biol. Drug Des.*, vol. 78, no. 4, pp. 535–546, Oct. 2011, doi: 10.1111/j.1747-0285.2011.01189.x.
- [8] P. E. Ghaly, R. M. Abou El-Magd, C. D. M. Churchill, J. A. Tuszynski, and F. G. West, “A new antiproliferative noscapine analogue: chemical synthesis and biological evaluation,” *Oncotarget*, vol. 7, no. 26, pp. 40518–40530, Jun. 2016, doi: 10.18632/oncotarget.9642.
- [9] P. E. Ghaly *et al.*, “Synthesis and biological evaluation of structurally simplified noscapine analogues as microtubule binding agents,” *Can. J. Chem.*, vol. 95, no. 6, pp. 649–655, 2017, doi: 10.1139/cjc-2016-0649.
- [10] J. Chlebek *et al.*, “Application of BACE1 immobilized enzyme reactor for the characterization of multifunctional alkaloids from *Corydalis cava* (Fumariaceae) as Alzheimer’s disease targets,” *Fitoterapia*, vol. 109, pp. 241–7, Mar. 2016, doi: 10.1016/j.fitote.2016.01.008.
- [11] B. Kumar, R. Kumar, I. Skvortsova, and V. Kumar, “Mechanisms of Tubulin Binding Ligands to Target Cancer Cells: Updates on their Therapeutic Potential and Clinical Trials,” *Curr. Cancer Drug Targets*, vol. 17, no. 4, pp. 357–375, 2017, doi: 10.2174/1568009616666160928110818.
- [12] P. Dustin, “The Role of MT in Mitosis,” in *Microtubules*, Springer, 1978, pp. 340–397.
- [13] C. C. Rohena and S. L. Mooberry, “Recent progress with microtubule stabilizers: new compounds, binding modes and cellular activities,” *Nat. Prod. Rep.*, vol. 31, no. 3, pp. 335–55, Mar. 2014, doi: 10.1039/c3np70092e.

- [14] A. E. Prota *et al.*, “A new tubulin-binding site and pharmacophore for microtubule-destabilizing anticancer drugs.,” *Proc. Natl. Acad. Sci. U. S. A.*, vol. 111, no. 38, pp. 13817–21, Sep. 2014, doi: 10.1073/pnas.1408124111.
- [15] T. Koltai, “Cancer: fundamentals behind pH targeting and the double-edged approach.,” *Onco. Targets. Ther.*, vol. 9, pp. 6343–6360, 2016, doi: 10.2147/OTT.S115438.
- [16] G. M. Morris *et al.*, “AutoDock4 and AutoDockTools4: Automated docking with selective receptor flexibility.,” *J. Comput. Chem.*, vol. 30, no. 16, pp. 2785–91, Dec. 2009, doi: 10.1002/jcc.21256.
- [17] W. D. Cornell *et al.*, “A Second Generation Force Field for the Simulation of Proteins, Nucleic Acids, and Organic Molecules,” *J. Am. Chem. Soc.*, vol. 117, no. 19, pp. 5179–5197, May 1995, doi: 10.1021/ja00124a002.
- [18] P. G. Morris and M. N. Fornier, “Microtubule active agents: beyond the taxane frontier.,” *Clin. Cancer Res.*, vol. 14, no. 22, pp. 7167–72, Nov. 2008, doi: 10.1158/1078-0432.CCR-08-0169.
- [19] Y. Wang *et al.*, “Structures of a diverse set of colchicine binding site inhibitors in complex with tubulin provide a rationale for drug discovery.,” *FEBS J.*, vol. 283, no. 1, pp. 102–11, Jan. 2016, doi: 10.1111/febs.13555.
- [20] Y. Lu, J. Chen, M. Xiao, W. Li, and D. D. Miller, “An overview of tubulin inhibitors that interact with the colchicine binding site.,” *Pharm. Res.*, vol. 29, no. 11, pp. 2943–71, Nov. 2012, doi: 10.1007/s11095-012-0828-z.
- [21] N. M. O’Boyle *et al.*, “Synthesis and evaluation of azetidinone analogues of combretastatin A-4 as tubulin targeting agents.,” *J. Med. Chem.*, vol. 53, no. 24, pp. 8569–84, Dec. 2010, doi: 10.1021/jm101115u.
- [22] C. D. M. Churchill, M. Klobukowski, and J. A. Tuszynski, “The Unique Binding Mode of Laulimalide to Two Tubulin Protofilaments.,” *Chem. Biol. Drug Des.*, vol. 86, no. 2, pp. 190–9, Aug. 2015, doi: 10.1111/cbdd.12475.

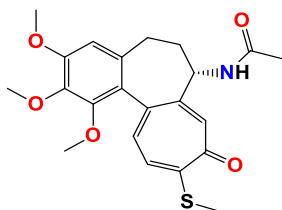
- [23] Ö. Demir *et al.*, “Ensemble-based computational approach discriminates functional activity of p53 cancer and rescue mutants.,” *PLoS Comput. Biol.*, vol. 7, no. 10, p. e1002238, Oct. 2011, doi: 10.1371/journal.pcbi.1002238.
- [24] J. Shao, S. W. Tanner, N. Thompson, and T. E. Cheatham, “Clustering Molecular Dynamics Trajectories: 1. Characterizing the Performance of Different Clustering Algorithms.,” *J. Chem. Theory Comput.*, vol. 3, no. 6, pp. 2312–34, Nov. 2007, doi: 10.1021/ct700119m.
- [25] C. D. M. Churchill, M. Klobukowski, and J. A. Tuszynski, “Analysis of the binding mode of laulimalide to microtubules: Establishing a laulimalide-tubulin pharmacophore.,” *J. Biomol. Struct. Dyn.*, vol. 34, no. 7, pp. 1455–69, Jul. 2016, doi: 10.1080/07391102.2015.1078115.
- [26] A. E. Prota *et al.*, “Structural basis of microtubule stabilization by laulimalide and peloruside A.,” *Angew. Chem. Int. Ed. Engl.*, vol. 53, no. 6, pp. 1621–5, Feb. 2014, doi: 10.1002/anie.201307749.
- [27] D. E. Pryor *et al.*, “The microtubule stabilizing agent laulimalide does not bind in the taxoid site, kills cells resistant to paclitaxel and epothilones, and may not require its epoxide moiety for activity.,” *Biochemistry*, vol. 41, no. 29, pp. 9109–9115, Jul. 2002, doi: 10.1021/bi020211b.
- [28] W. J. Eisenreich, G. Höfner, and F. Bracher, “Alkaloids from *Croton flavens* L. and their affinities to GABA-receptors.,” *Nat. Prod. Res.*, vol. 17, no. 6, pp. 437–40, Dec. 2003, doi: 10.1080/1478641031000111516.
- [29] P. Wangchuk, P. A. Keller, S. G. Pyne, A. C. Willis, and S. Kamchonwongpaisan, “Antimalarial alkaloids from a Bhutanese traditional medicinal plant *Corydalis dubia*.,” *J. Ethnopharmacol.*, vol. 143, no. 1, pp. 310–3, Aug. 2012, doi: 10.1016/j.jep.2012.06.037.
- [30] J. Chlebek, K. Macáková, L. Cahlíková, M. Kurfürst, J. Kuneš, and L. Opletal, “Acetylcholinesterase and Butyrylcholinesterase Inhibitory Compounds from

- Corydalis Cava (Fumariaceae),” *Nat. Prod. Commun.*, vol. 6, no. 5, pp. 607–610, May 2011, doi: 10.1177/1934578X1100600507.
- [31] T. H. Dunning, “Gaussian basis sets for use in correlated molecular calculations. I. The atoms boron through neon and hydrogen,” *J. Chem. Phys.*, vol. 90, no. 2, pp. 1007–1023, Jan. 1989, doi: 10.1063/1.456153.
- [32] M. W. Schmidt *et al.*, “General atomic and molecular electronic structure system,” *J. Comput. Chem.*, vol. 14, no. 11, pp. 1347–1363, Nov. 1993, doi: 10.1002/jcc.540141112.
- [33] M. S. Gordon and M. W. Schmidt, “Advances in electronic structure theory: GAMESS a decade later,” in *Theory and Applications of Computational Chemistry*, C. E. Dykstra, G. Frenking, K. S. Kim, and G. E. Scuseria, Eds. Amsterdam: Elsevier, 2005, pp. 1167–1189.
- [34] G. M. J. Barca *et al.*, “Recent developments in the general atomic and molecular electronic structure system,” *J. Chem. Phys.*, vol. 152, no. 15, p. 154102, Apr. 2020, doi: 10.1063/5.0005188.
- [35] *Autodock*. Chemical Computing Group ULC, Montreal, Canada, 2018.
- [36] R. B. G. Ravelli *et al.*, “Insight into tubulin regulation from a complex with colchicine and a stathmin-like domain,” *Nature*, vol. 428, no. 6979, pp. 198–202, Mar. 2004, doi: 10.1038/nature02393.
- [37] F. J. Fourniol *et al.*, “Template-free 13-protofilament microtubule-MAP assembly visualized at 8 Å resolution,” *J. Cell Biol.*, vol. 191, no. 3, pp. 463–70, Nov. 2010, doi: 10.1083/jcb.201007081.
- [38] J. Wang, R. M. Wolf, J. W. Caldwell, P. A. Kollman, and D. A. Case, “Development and testing of a general amber force field,” *J. Comput. Chem.*, vol. 25, no. 9, pp. 1157–74, Jul. 2004, doi: 10.1002/jcc.20035.
- [39] W. L. Jorgensen, J. Chandrasekhar, J. D. Madura, R. W. Impey, and M. L. Klein, “Comparison of simple potential functions for simulating liquid water,” *J. Chem. Phys.*, vol. 79, no. 2, pp. 926–935, Jul. 1983, doi: 10.1063/1.445869.

- [40] U. Essmann, L. Perera, M. L. Berkowitz, T. Darden, H. Lee, and L. G. Pedersen, “A smooth particle mesh Ewald method,” *J. Chem. Phys.*, vol. 103, no. 19, pp. 8577–8593, Nov. 1995, doi: 10.1063/1.470117.
- [41] J.-P. Ryckaert, G. Ciccotti, and H. J. . Berendsen, “Numerical integration of the cartesian equations of motion of a system with constraints: molecular dynamics of n-alkanes,” *J. Comput. Phys.*, vol. 23, no. 3, pp. 327–341, Mar. 1977, doi: 10.1016/0021-9991(77)90098-5.
- [42] T. A. D. D.A. Case, I.Y. Ben-Shalom, S.R. Brozell, D.S. Cerutti, T.E. Cheatham, III, V.W.D. Cruzeiro, Y. H. R.E. Duke, D. Ghoreishi, M.K. Gilson, H. Gohlke, A.W. Goetz, D. Greene, R Harris, N. Homeyer, D. J. S. Izadi, A. Kovalenko, T. Kurtzman, T.S. Lee, S. LeGrand, P. Li, C. Lin, J. Liu, T. Luchko, R. Luo, R. Mermelstein, K.M. Merz, Y. Miao, G. Monard, C. Nguyen, H. Nguyen, I. Omelyan, A. Onufriev, F. Pan, and P. A. K. Qi, D.R. Roe, A. Roitberg, C. Sagui, S. Schott-Verdugo, J. Shen, C.L. Simmerling, J. Smith, R. SalomonFerrer, J. Swails, R.C. Walker, J. Wang, H. Wei, R.M. Wolf, X. Wu, L. Xiao, D.M. York, *AMBER 2018, University of California, San Francisco*. 2018.
- [43] M. G. Lepre, S. I. Omar, G. Grasso, U. Morbiducci, M. A. Deriu, and J. A. Tuszynski, “Insights into the Effect of the G245S Single Point Mutation on the Structure of p53 and the Binding of the Protein to DNA.,” *Molecules*, vol. 22, no. 8, Aug. 2017, doi: 10.3390/molecules22081358.

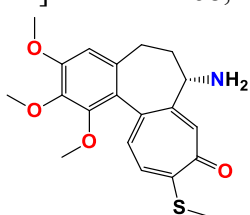
Appendix A.

Supplementary material for chapter 2



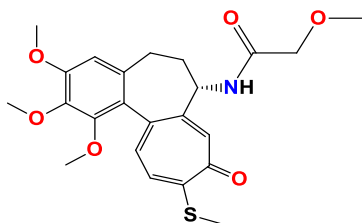
Chemical formula of 2: C₂₂H₂₅NO₅S, MW = 415.5 g/mol

¹H-NMR (403 MHz, CDCl₃) δ 7.92 (s, 1H), 7.46 (s, 1H), 7.33 (d, J = 10.4 Hz, 1H), 7.10 (d, J = 10.5 Hz, 1H), 6.55 (s, 1H), 4.72–4.64 (m, 1H), 3.95 (s, 3H), 3.91 (s, 3H), 3.67 (s, 3H), 2.54 (dd, J = 13.0, 5.8 Hz, 1H), 2.45 (s, J = 5.7 Hz, 3H), 2.43–2.26 (m, 2H), 1.99 (s, 3H), 1.94 (dd, J = 11.8, 5.5 Hz, 1H) ppm. ¹³C-NMR (101 MHz, CDCl₃) δ 182.4, 170.0, 158.1, 153.6, 151.8, 151.1, 141.6, 138.6, 134.8, 134.4, 128.3, 126.7, 125.6, 107.3, 61.6, 61.4, 56.1, 52.3, 36.4, 29.9, 22.8, 15.1 ppm. FT-IR (KBr pellet): 3283, 2935, 1660, 1605, 1541, 1485, 1461, 1425, 1404, 1349, 1321, 1286, 1236, 1195, 1155, 1138, 1095, 1023 cm⁻¹. ESI-MS (m/z): [M + H]⁺ calcd. 416, found 416, [M + Na]⁺ calcd. 438, found 438, [M + K]⁺ calcd. 454 found 454, [2M + Na]⁺ calcd. 853, found 853, [3M + Na]⁺ calcd. 1268, found 1268.



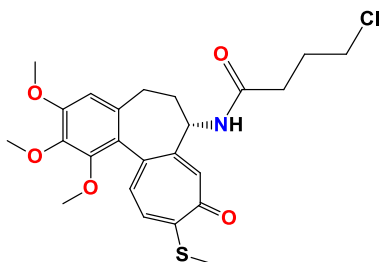
Chemical formula of 3: C₂₀H₂₃NO₄S, MW = 373.5 g/mol.

¹³C NMR (101 MHz, CDCl₃) δ 182.5, 157.8, 153.7, 153.4, 150.6, 141.1, 138.1, 135.2, 134.1, 129.3, 125.9, 125.4, 106.9, 61.1, 61.0, 56.0, 53.6, 40.2, 30.5, 15.1 ppm. ¹H NMR (403 MHz, CDCl₃) δ 7.58 (s, 1H), 7.19 (d, J = 10.3 Hz, 1H), 7.03 (d, J = 10.7 Hz, 1H), 6.54 (s, 1H), 3.91 (s, 3H), 3.91 (s, 3H), 3.75 – 3.69 (m, 1H), 3.66 (s, 3H), 2.52 – 2.26 (m, 6H), 1.65 – 1.57 (m, 3H) ppm. FT-IR (KBr pellet): 3365, 3293, 2931, 2852, 2838, 1603, 1546, 1485, 1458, 1422, 1402, 1347, 1318, 1138, 1094, 1017 cm⁻¹. ESI-MS (m/z): [M+H]⁺ calcd 374, found 374.



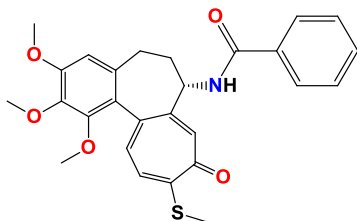
Chemical formula of 4: C₂₃H₂₇NO₆S, MW = 445.5 g/mol

¹H NMR (403 MHz, CDCl₃) δ 7.26 (d, J = 10.3 Hz, 1H), 7.18 (s, 1H), 7.09 (d, J = 7.5 Hz, 1H), 7.02 (d, J = 10.6 Hz, 1H), 6.52 (s, 1H), 4.65 (dt, J = 11.8, 6.9 Hz, 1H), 3.92 (s, 3H), 3.88 (s, 3H), 3.83 (d, J = 4.3 Hz, 2H), 3.63 (s, 3H), 3.41 (s, 3H), 2.59 – 2.51 (m, 1H), 2.48 – 2.37 (m, 4H), 2.22 (tt, J = 13.0, 6.6 Hz, 1H), 1.88 (ddd, J = 11.9, 8.9, 5.8 Hz, 1H) ppm. ¹³C NMR (101 MHz, CDCl₃) δ 182.3, 167.0, 158.2, 153.5, 151.2, 150.0, 141.6, 137.7, 134.4, 134.1, 128.5, 126.1, 125.6, 107.3, 71.6, 61.4, 61.3, 59.1, 56.0, 51.2, 36.8, 29.8, 15.1 ppm. FT-IR: 3287, 2937, 1672, 1607, 1552, 1486, 1462, 1426, 1403, 1350, 1323, 1287, 1264, 1236, 1195, 1154, 1138, 1096, 1022 cm⁻¹. ESI-MS (m/z): [M+Na]⁺ calcd 468, found 468.



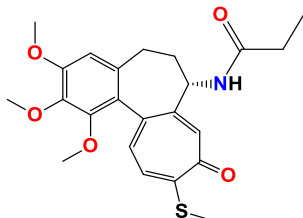
Chemical formula of 5: C₂₄H₂₈ClNO₅S, MW = 478.0 g/mol

¹H NMR (403 MHz, CDCl₃) δ 7.55 (d, J = 7.4 Hz, 1H), 7.45 (s, 1H), 7.34 – 7.29 (m, 1H), 7.08 (d, J = 10.8 Hz, 1H), 6.53 (s, 1H), 4.70 (dt, J = 11.8, 6.9 Hz, 1H), 3.94 (s, 3H), 3.90 (s, 3H), 3.66 (s, 3H), 3.51 (td, J = 6.6, 1.1 Hz, 2H), 2.55 – 2.47 (m, 1H), 2.45 – 2.33 (m, 6H), 2.26 (dt, J = 18.6, 6.3 Hz, 1H), 2.08 – 1.99 (m, 2H), 1.94 – 1.86 (m, 1H) ppm. ¹³C NMR (101 MHz, CDCl₃) δ 182.4, 171.5, 158.2, 153.6, 151.5, 151.1, 141.6, 138.4, 134.7, 134.3, 128.6, 126.6, 125.6, 107.3, 61.6, 61.4, 56.1, 51.9, 44.4, 36.8, 33.0, 30.0, 28.1, 15.12 ppm. FT-IR: 3273, 2937, 1669, 1604, 1531, 1486, 1461, 1428, 1403, 1368, 1346, 1320, 1282, 1234, 1194, 1156, 1138, 1092, 1020 cm⁻¹. ESI-MS (m/z): [M+Na]⁺ calcd 500, found 500.



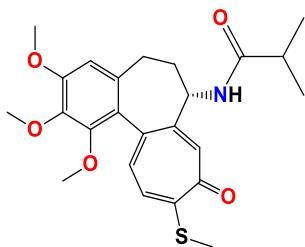
Chemical formula of 6: C₂₇H₂₇NO₅S, MW = 477.6 g/mol

¹H NMR (403 MHz, CDCl₃) δ 7.83 – 7.79 (m, 2H), 7.68 (d, J = 7.3 Hz, 1H), 7.49 (s, 1H), 7.40 – 7.28 (m, 4H), 7.08 (d, J = 10.8 Hz, 1H), 6.56 (s, 1H), 4.91 (dt, J = 11.7, 6.8 Hz, 1H), 3.96 (s, 3H), 3.91 (s, 3H), 3.74 (s, 3H), 2.57 (dd, J = 13.3, 5.9 Hz, 1H), 2.50 – 2.40 (m, 4H), 2.35 (td, J = 12.4, 6.2 Hz, 1H), 2.07 (td, J = 11.7, 5.4 Hz, 1H) ppm. ¹³C NMR (101 MHz, CDCl₃) δ 182.2, 166.8, 158.2, 153.6, 151.2, 141.6, 138.3, 134.6, 134.4, 133.5, 131.5, 128.7, 128.4, 127.1, 126.4, 125.7, 107.3, 61.7, 61.4, 56.1, 52.5, 36.6, 30.0, 15.1 ppm. FT-IR: 3334, 2937, 1658, 1605, 1545, 1528, 1485, 1461, 1424, 1404, 1350, 1322, 1287, 1235, 1195, 1154, 1137, 1095, 1020 cm⁻¹. ESI-MS (m/z): [M+H]⁺ calcd 478, found 478, [M+Na]⁺ calcd 500, found 500.



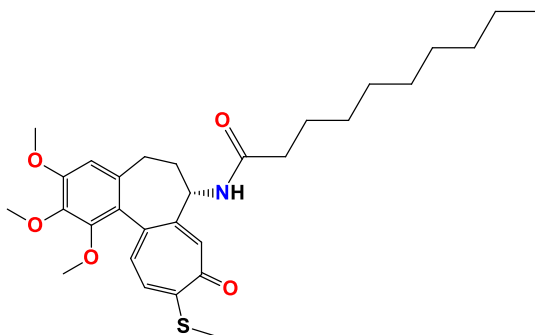
Chemical formula of 7: C₂₃H₂₇NO₅S, MW = 429.5 g/mol

¹H NMR (403 MHz, CDCl₃) δ 7.39 (s, 1H), 7.30 (d, J = 10.3 Hz, 1H), 7.07 (d, J = 10.6 Hz, 1H), 6.52 (s, J = 4.6 Hz, 1H), 4.67 (dt, J = 11.8, 6.7 Hz, 1H), 3.93 (s, 3H), 3.89 (s, 3H), 3.66 (s, 3H), 2.51 (dd, J = 13.3, 6.2 Hz, 1H), 2.45 – 2.33 (m, 4H), 2.30 – 2.22 (m, 3H), 1.95 – 1.84 (m, 1H), 1.09 (t, J = 7.6 Hz, 3H) ppm. ¹³C NMR (101 MHz, CDCl₃) δ 182.4, 173.6, 158.1, 153.5, 151.6, 151.1, 141.6, 138.4, 134.6, 134.4, 128.4, 126.6, 125.7, 107.3, 61.7, 61.3, 56.1, 51.9, 36.6, 29.9, 29.2, 15.1, 9.5 ppm. FT-IR: 3303, 2937, 1660, 1607, 1543, 1486, 1462, 1425, 1404, 1349, 1321, 1283, 1235, 1196, 1154, 1138, 1096, 1022 cm⁻¹. ESI-MS (m/z): [M+H]⁺ calcd 430, found 430, [M+Na]⁺ calcd 552, found 552 [M+K]⁺ calcd 468, found 468.



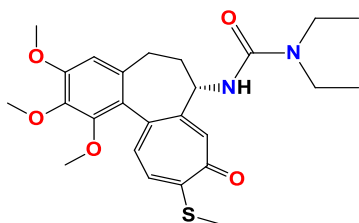
Chemical formula of 8: C₂₄H₂₉NO₅S, MW = 443.6 g/mol

¹H NMR (403 MHz, CDCl₃) δ 7.45 (s, 1H), 7.41 (d, J = 7.6 Hz, 1H), 7.32 – 7.28 (m, 1H), 7.06 (d, J = 10.8 Hz, 1H), 6.52 (s, 1H), 4.69 (dt, J = 11.8, 7.0 Hz, 1H), 3.93 (s, 3H), 3.89 (s, 3H), 3.67 (s, 3H), 2.51 (dt, J = 13.5, 6.8 Hz, 2H), 2.44 – 2.32 (m, 4H), 2.25 (dt, J = 18.6, 6.3 Hz, 1H), 1.89 (td, J = 11.8, 6.1 Hz, 1H), 1.12 (dd, J = 6.9, 4.0 Hz, 6H). ¹³C NMR (101 MHz, CDCl₃) δ 182.3, 176.8, 158.0, 153.5, 151.7, 151.2, 141.6, 138.4, 134.5, 134.4, 128.6, 126.5, 125.7, 107.3, 61.7, 61.3, 56.1, 51.5, 36.7, 35.2, 30.0, 19.5, 19.5, 15.1 ppm. FT-IR: 3312, 2968, 2935, 1669, 1607, 1544, 1486, 1461, 1425, 1404, 1349, 1322, 1283, 1235, 1196, 1154, 1137, 1096, 1021 cm⁻¹. ESI-MS (m/z): [M+Na]⁺ calcd 466, found 466.



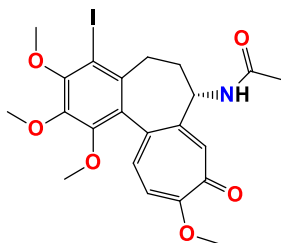
Chemical formula of 9: C₃₀H₄₁NO₅S, MW = 527.7 g/mol

¹H NMR (403 MHz, CDCl₃) δ 7.56 (d, J = 7.4 Hz, 1H), 7.45 (s, 1H), 7.31 (d, J = 10.4 Hz, 1H), 7.08 (d, J = 10.8 Hz, 1H), 6.54 (s, 1H), 4.71 (dt, J = 11.8, 6.9 Hz, 1H), 3.95 (s, 3H), 3.91 (s, 3H), 3.67 (s, 3H), 2.52 (dd, J = 13.3, 6.1 Hz, 1H), 2.46 – 2.34 (m, 4H), 2.30 – 2.21 (m, 3H), 1.89 (td, J = 11.9, 6.2 Hz, 1H), 1.58 (dd, J = 14.6, 7.2 Hz, 2H), 1.30 – 1.19 (m, 12H), 0.86 (t, J = 6.9 Hz, 3H) ppm. ¹³C NMR (101 MHz, CDCl₃) δ 182.3, 173.0, 158.0, 153.5, 151.7, 151.1, 141.5, 138.4, 134.6, 134.4, 128.6, 126.5, 125.7, 107.3, 61.6, 61.3, 56.0, 51.8, 36.6, 36.3, 31.8, 30.0, 29.3, 29.3, 29.2, 29.2, 25.5, 22.6, 15.1, 14.0 ppm. FT-IR: 3298, 2927, 2853, 1655, 1607, 1543, 1485, 1461, 1425, 1404, 1348, 1321, 1282, 1235, 1195, 1154, 1137, 1097, 1022 cm⁻¹. ESI-MS (m/z): [M+Na]⁺ calcd 550, found 550.



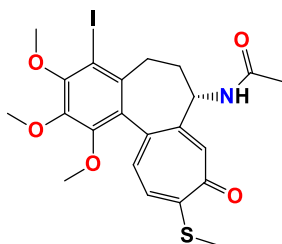
Chemical formula of 10: C₂₅H₃₂N₂O₅S, MW = 472.6 g/mol

¹H NMR (403 MHz, CDCl₃) δ 7.48 (s, 1H), 7.26 (d, J = 10.4 Hz, 1H), 7.03 – 6.99 (d, J = 10.8 Hz, 1H), 6.50 (s, 1H), 5.90 (d, J = 7.1 Hz, 1H), 4.66 (dt, J = 11.7, 6.7 Hz, 1H), 3.91 (s, 3H), 3.87 (s, 3H), 3.67 (s, 3H), 3.32 – 3.25 (m, 4H), 2.48 (dd, J = 13.3, 5.7 Hz, 1H), 2.41 – 2.20 (m, 5H), 1.97 – 1.86 (m, 1H), 1.11 (t, J = 7.1 Hz, 6H) ppm. ¹³C NMR (101 MHz, CDCl₃) δ 182.2, 157.8, 156.0, 153.3, 152.6, 151.1, 141.5, 138.4, 134.6, 134.3, 129.2, 126.2, 125.8, 107.2, 61.7, 61.3, 56.0, 53.1, 40.9, 37.2, 30.2, 15.0, 13.9 ppm. FT-IR: 3372, 2970, 2935, 1641, 1607, 1550, 1523, 1486, 1460, 1425, 1404, 1349, 1322, 1282, 1269, 1236, 1195, 1152, 1138, 1096, 1021 cm⁻¹. ESI-MS (m/z): [M+H]⁺ calcd 473, found 473, [M+Na]⁺ calcd 495, found 495, [M+K]⁺ calcd 511, found 511.



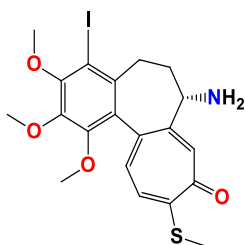
Chemical formula of 11: C₂₂H₂₄INO₆, MW = 525.3 g/mol

¹H NMR (403 MHz, CDCl₃) δ 8.22 (d, J = 5.6 Hz, 1H), 7.61 (s, 1H), 7.30 (d, J = 10.7 Hz, 1H), 6.89 (d, J = 11.2 Hz, 1H), 4.55 – 4.47 (m, 1H), 4.04 (s, 3H), 3.97 (s, 3H), 3.95 (s, 3H), 3.63 (s, 3H), 3.21 – 3.15 (m, 1H), 2.40 (dd, J = 12.7, 5.0 Hz, 1H), 1.99 (s, 3H), 1.87 – 1.81 (m, 1H) ppm. ¹³C NMR (101 MHz, CDCl₃) δ 179.5, 170.2, 164.4, 153.4, 152.0, 151.4, 145.6, 136.7, 136.2, 135.6, 130.1, 129.5, 112.5, 92.1, 61.5, 61.3, 60.7, 56.5, 52.6, 34.4, 34.4, 22.7 ppm. FT-IR (KBr pellet): 3274, 2934, 1662, 1617, 1588, 1563, 1461, 1406, 1393, 1346, 1318, 1266, 1249, 1171, 1136, 1078, 1015 cm⁻¹. ESI-MS (m/z): [M+H]⁺ calcd 526, found 526 [M+Na]⁺ calcd 548, found 548.



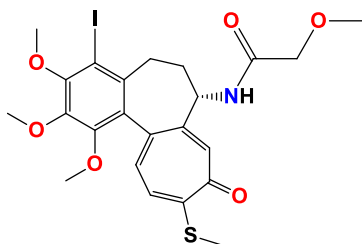
Chemical formula of 12: C₂₂H₂₄INO₅S, MW = 541.4 g/mol

¹H NMR (403 MHz, CDCl₃) δ 7.75 (d, J = 6.9 Hz, 1H), 7.42 (s, 1H), 7.25 (d, J = 10.3 Hz, 1H), 7.09 (d, J = 10.8 Hz, 1H), 4.58 – 4.50 (m, 1H), 3.97 (s, 3H), 3.95 (s, 3H), 3.63 (s, 3H), 3.18 (dd, J = 13.7, 5.0 Hz, 1H), 2.46 (s, 3H), 2.40 (dd, J = 13.6, 6.2 Hz, 1H), 2.32 – 2.23 (m, 1H), 2.01 (s, 3H), 1.85 – 1.79 (m, 1H) ppm. ¹³C NMR (101 MHz, CDCl₃) δ 182.4, 170.1, 159.1, 153.5, 151.4, 151.1, 145.6, 137.8, 136.8, 134.7, 129.7, 128.1, 126.3, 92.2, 61.6, 61.4, 60.8, 52.1, 34.5, 34.4, 22.9, 15.2 ppm. FT-IR (KBr pellet): 3288, 2936, 1660, 1607, 1547, 1461, 1406, 1346, 1318, 1288, 1262, 1197, 1138, 1081, 1019 cm⁻¹. ESI-MS (m/z): [M+H]⁺ calcd 542, found 542, [M+Na]⁺ calcd 564, found 564, [M+K]⁺ calcd 580, found 580.



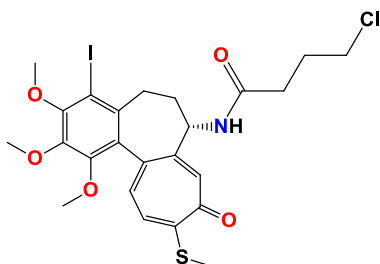
Chemical formula of 13: C₂₀H₂₂INO₄S, MW = 499.4 g/mol

¹H NMR (403 MHz, cdcl₃) δ 7.59 (s, 1H), 7.11 (d, J = 10.3 Hz, 1H), 7.01 (d, J = 10.7 Hz, 1H), 3.93 (s, 6H), 3.62 (s, 3H), 3.57 (dd, J = 10.8, 6.2 Hz, 1H), 3.15 – 3.08 (m, 1H), 2.48 – 2.39 (m, 4H), 2.33 – 2.24 (m, 1H), 1.53 – 1.46 (m, 3H) ppm. ¹³C NMR (101 MHz, cdcl₃) δ 182.5, 158.7, 153.4, 153.1, 150.9, 145.1, 137.7, 137.5, 133.8, 129.5, 129.2, 125.5, 91.7, 61.2, 61.0, 60.8, 53.4, 38.2, 35.1, 15.1 ppm. FT-IR (KBr pellet): 3375, 3309, 2932, 1605, 1553, 1460, 1405, 1343, 1313, 1246, 1195, 1136, 1081, 1014 cm⁻¹. ESI-MS (m/z): [M+H]⁺ calcd 500, found 500.



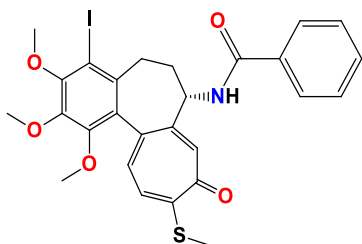
Chemical formula of 14: C₂₃H₂₆INO₆S, MW = 571.4 g/mol

¹H NMR (403 MHz, CDCl₃) δ 7.20 (d, J = 7.6 Hz, 1H), 7.19 (s, 1H), 7.16 (d, J = 6.6 Hz, 1H), 7.03 (d, J = 10.6 Hz, 1H), 4.53 (dt, J = 11.8, 6.9 Hz, 1H), 3.97 (s, 3H), 3.94 (s, 3H), 3.87 (q, J = 15.0 Hz, 2H), 3.62 (s, 3H), 3.43 (s, 3H), 3.20 (dd, J = 13.9, 5.1 Hz, 1H), 2.52 – 2.42 (m, 4H), 2.28 – 2.17 (m, 1H), 1.80 (td, J = 12.0, 6.5 Hz, 1H) ppm. ¹³C NMR (101 MHz, CDCl₃) δ 182.2, 169.2, 159.2, 153.4, 151.5, 149.4, 145.6, 137.0, 136.6, 134.3, 129.7, 128.3, 125.7, 92.1, 71.6, 61.4, 61.3, 60.7, 59.1, 51.1, 34.8, 34.4, 15.1 ppm. FT-IR: 3339, 2998, 2929, 1674, 1605, 1547, 1516, 1465, 1449, 1425, 1408, 1373, 1347, 1316, 1292, 1262, 1190, 1156, 1134, 1107, 1081, 1056, 1018 cm⁻¹. ESI-MS (m/z): [M+Na]⁺ calcd 594, found 594.



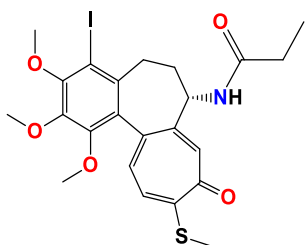
Chemical formula of 15: C₂₄H₂₇ClINO₅S, MW = 603.9 g/mol

¹H NMR (403 MHz, CDCl₃) δ 7.47 (d, J = 7.3 Hz, 1H), 7.42 (s, 1H), 7.23 (d, J = 10.4 Hz, 1H), 7.07 (d, J = 10.7 Hz, 1H), 4.57 (dt, J = 11.8, 6.9 Hz, 1H), 3.96 (s, 3H), 3.95 (s, 3H), 3.63 (s, 3H), 3.53 (t, J = 6.4 Hz, 2H), 3.16 (dd, J = 13.7, 5.0 Hz, 1H), 2.52 – 2.35 (m, 7H), 2.29 – 2.18 (m, 1H), 2.11 – 2.02 (m, 2H), 1.78 (td, J = 12.0, 5.6 Hz, 1H) ppm. ¹³C NMR (101 MHz, CDCl₃) δ 182.3, 171.7, 159.2, 153.5, 151.4, 150.8, 145.6, 137.6, 136.7, 134.7, 129.6, 128.4, 126.2, 92.2, 61.6, 61.4, 60.8, 51.7, 44.4, 34.8, 34.5, 33.0, 28.1, 15.2 ppm. FT-IR: 3301, 2937, 1674, 1607, 1544, 1461, 1406, 1346, 1318, 1283, 1262, 1244, 1196, 1154, 1137, 1081, 1054, 1019 cm⁻¹. ESI-MS (m/z): [M+Na]⁺ calcd 626, found 626.



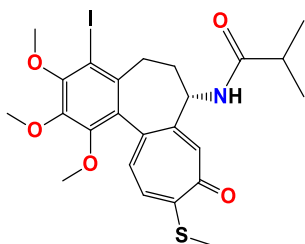
Chemical formula of 16: C₂₇H₂₆INO₅S, MW = 603.5 g/mol

¹H NMR (403 MHz, CDCl₃) δ 7.93 (d, J = 7.1 Hz, 1H), 7.81 (dt, J = 8.5, 1.7 Hz, 2H), 7.52 (s, 1H), 7.37 – 7.32 (m, 1H), 7.29 – 7.23 (m, 3H), 7.10 – 7.05 (m, 1H), 4.79 (dt, J = 11.8, 6.9 Hz, 1H), 3.98 (s, 3H), 3.95 (s, 3H), 3.71 (s, 3H), 3.20 (dd, J = 13.7, 4.8 Hz, 1H), 2.52 – 2.42 (m, 4H), 2.31 (dt, J = 17.1, 4.9 Hz, 1H), 2.05 – 1.96 (m, 1H) ppm. ¹³C NMR (101 MHz, CDCl₃) δ 182.2, 167.1, 159.2, 153.5, 151.5, 150.9, 145.6, 137.7, 136.9, 134.6, 133.3, 131.6, 129.8, 128.5, 128.4, 127.1, 126.1, 92.2, 61.7, 61.4, 60.8, 52.3, 34.7, 34.5, 15.2 ppm. FT-IR: 3323, 3058, 2935, 1659, 1606, 1549, 1487, 1461, 1406, 1346, 1319, 1289, 1262, 1197, 1152, 1081, 1019 cm⁻¹. ESI-MS (m/z): [M+H]⁺ calcd 604, found 604, [M+Na]⁺ calcd 626, found 626.



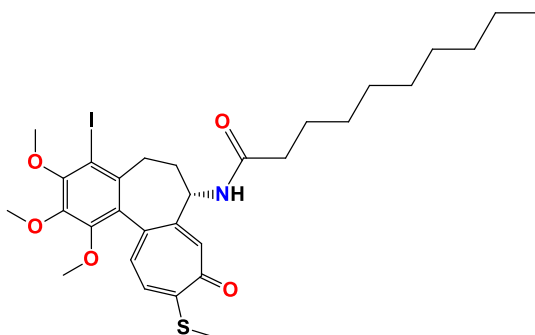
Chemical formula of 17: C₂₃H₂₆INO₅S, MW = 555.4 g/mol

¹H NMR (403 MHz, CDCl₃) δ 7.53 – 7.48 (m, 1H), 7.40 (s, 1H), 7.24 (dd, J = 9.1, 4.0 Hz, 1H), 7.10 – 7.05 (m, 1H), 4.56 (dt, J = 11.9, 6.8 Hz, 1H), 3.97 (s, 3H), 3.95 (s, 3H), 3.64 (s, 3H), 3.17 (dd, J = 14.0, 4.6 Hz, 1H), 2.49 – 2.37 (m, 4H), 2.35 – 2.20 (m, 3H), 1.79 (td, J = 12.0, 5.2 Hz, 1H), 1.11 (dd, J = 9.8, 5.3 Hz, 3H) ppm. ¹³C NMR (101 MHz, CDCl₃) δ 182.3, 173.8, 159.1, 153.4, 151.4, 151.0, 145.6, 137.7, 136.8, 134.6, 129.7, 128.2, 126.2, 92.2, 61.6, 61.4, 60.8, 51.7, 34.6, 34.5, 29.2, 15.2, 9.6 ppm. FT-IR: 3301, 2938, 1660, 1608, 1567, 1462, 1406, 1346, 1319, 1283, 1262, 1231, 1198, 1138, 1081, 1019 cm⁻¹. ESI-MS (m/z): [M+H]⁺ calcd 556, found 556, [M+Na]⁺ calcd 578, found 578.



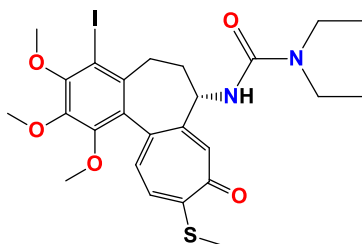
Chemical formula of 18: C₂₄H₂₈INO₅S, MW = 569.5 g/mol

¹H NMR (403 MHz, CDCl₃) δ 7.47 (d, J = 8.3 Hz, 2H), 7.23 (d, J = 10.3 Hz, 1H), 7.06 (d, J = 10.6 Hz, 1H), 4.58 (dt, J = 11.8, 7.0 Hz, 1H), 3.97 (s, 3H), 3.95 (s, 3H), 3.65 (s, 3H), 3.16 (dd, J = 13.8, 5.1 Hz, 1H), 2.55 (dt, J = 13.8, 6.9 Hz, 1H), 2.48 – 2.36 (m, 4H), 2.28 – 2.16 (m, 1H), 1.80 (td, J = 11.9, 5.3 Hz, 1H), 1.16 (dd, J = 6.9, 3.6 Hz, 6H) ppm. ¹³C NMR (101 MHz, CDCl₃) δ 182.2, 177.0, 159.0, 153.4, 151.5, 151.1, 145.6, 137.7, 136.8, 134.5, 129.7, 128.5, 126.1, 92.2, 61.7, 61.3, 60.8, 51.3, 35.2, 34.7, 34.6, 19.5, 19.4, 15.1 ppm. FT-IR: 3331, 2970, 2935, 1669, 1608, 1552, 1461, 1406, 1345, 1319, 1284, 1262, 1239, 1198, 1153, 1137, 1081, 1019 cm⁻¹. ESI-MS (m/z): [M+H]⁺ [M+Na]⁺ calcd 592, found 592.



Chemical formula of 19: C₃₀H₄₀INO₅S, MW = 653.6 g/mol

¹H NMR (403 MHz, CDCl₃) δ 7.40 (s, 1H), 7.23 (d, J = 10.3 Hz, 1H), 7.15 (d, J = 7.1 Hz, 1H), 7.06 (d, J = 10.8 Hz, 1H), 4.57 (dt, J = 11.9, 7.0 Hz, 1H), 3.97 (s, 3H), 3.95 (s, 3H), 3.63 (s, 3H), 3.17 (dd, J = 13.9, 5.0 Hz, 1H), 2.47 – 2.18 (m, 7H), 1.75 (td, J = 12.0, 5.2 Hz, 1H), 1.60 (td, J = 14.8, 7.3 Hz, 2H), 1.35 – 1.20 (m, 12H), 0.86 (t, J = 7.2 Hz, 3H) ppm. ¹³C NMR (101 MHz, CDCl₃) δ 182.3, 173.2, 159.1, 153.4, 151.5, 150.9, 145.6, 137.6, 136.7, 134.5, 129.7, 128.3, 126.2, 92.2, 61.6, 61.3, 60.8, 51.6, 36.4, 34.8, 34.5, 31.8, 29.4, 29.3, 29.3, 29.2, 25.5, 22.6, 15.1, 14.1 ppm. FT-IR: 3298, 2927, 2856, 1656, 1607, 1547, 1461, 1406, 1346, 1319, 1283, 1262, 1246, 1198, 1154, 1138, 1081, 1019 cm⁻¹. ESI-MS (m/z): [M+H]⁺ calcd 654, found 654.



Chemical formula of 20: C₂₅H₃₁N₂O₅S, MW = 598.5 g/mol

¹H NMR (403 MHz, CDCl₃) δ 7.48 (s, 1H), 7.21 – 7.17 (m, 1H), 7.03 – 6.99 (m, 1H), 5.89 – 5.85 (m, 1H), 4.53 (dt, J = 11.7, 6.7 Hz, 1H), 3.94 (s, 3H), 3.92 (s, 3H), 3.64 (s, 3H), 3.30 (q, J = 7.1 Hz, 4H), 3.12 (dd, J = 13.8, 4.7 Hz, 1H), 2.44 – 2.33 (m, 4H), 2.28 – 2.18 (m, 1H), 1.81 (td, J = 12.0, 5.3 Hz, 1H), 1.12 (t, J = 7.1 Hz, 6H) ppm. ¹³C NMR (101 MHz, CDCl₃) δ 182.2, 158.8, 156.0, 153.2, 152.1, 151.4, 145.5, 137.6, 137.0, 134.3, 129.9, 128.9, 125.9, 92.1, 61.7, 61.3, 60.7, 52.9, 41.0, 35.2, 34.8, 15.1, 13.9 ppm. FT-IR: 3383, 2973, 2935, 1639, 1608, 1553, 1525, 1492, 1460, 1425, 1406, 1344, 1318, 1284, 1264, 1216, 1183, 1152, 1137, 1080, 1018 cm⁻¹. ESI-MS (m/z): [M+H]⁺ calcd 599, found 599, [M+Na]⁺ calcd 621, found 621.

Exemplary NMR spectra

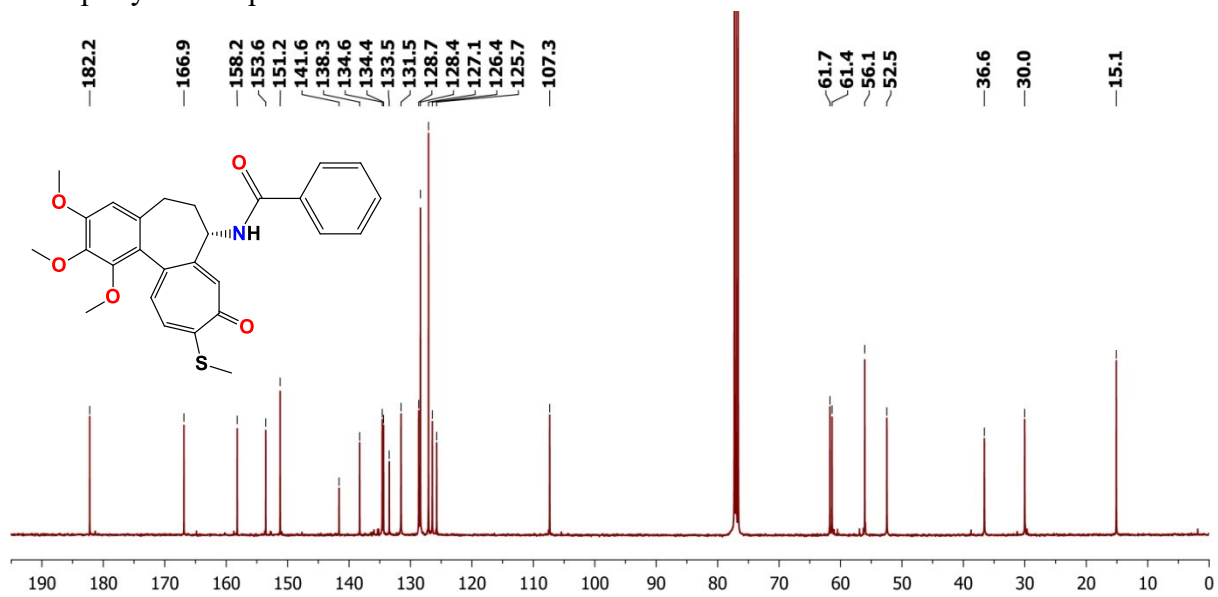


Figure A-1. The ¹³C-NMR spectrum of 6 in CDCl₃.

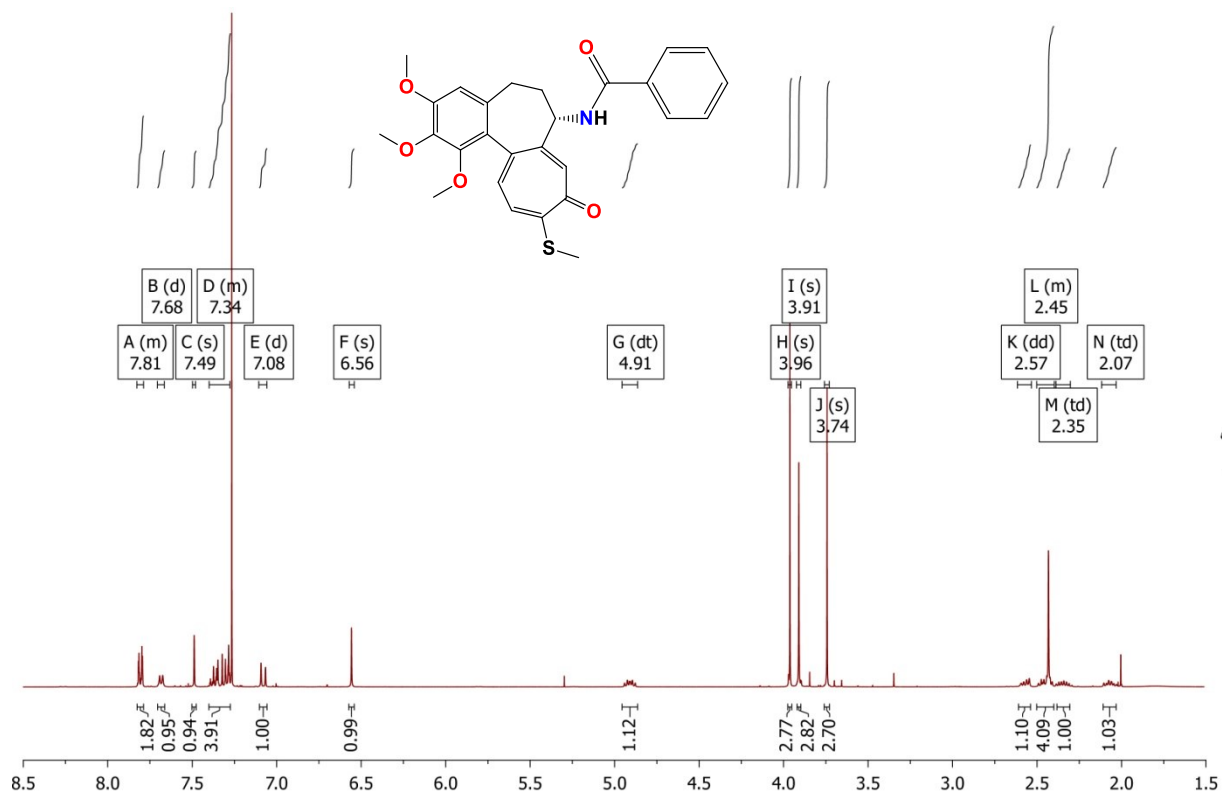


Figure A-2. The ^1H -NMR spectrum of 6 in CDCl_3 .

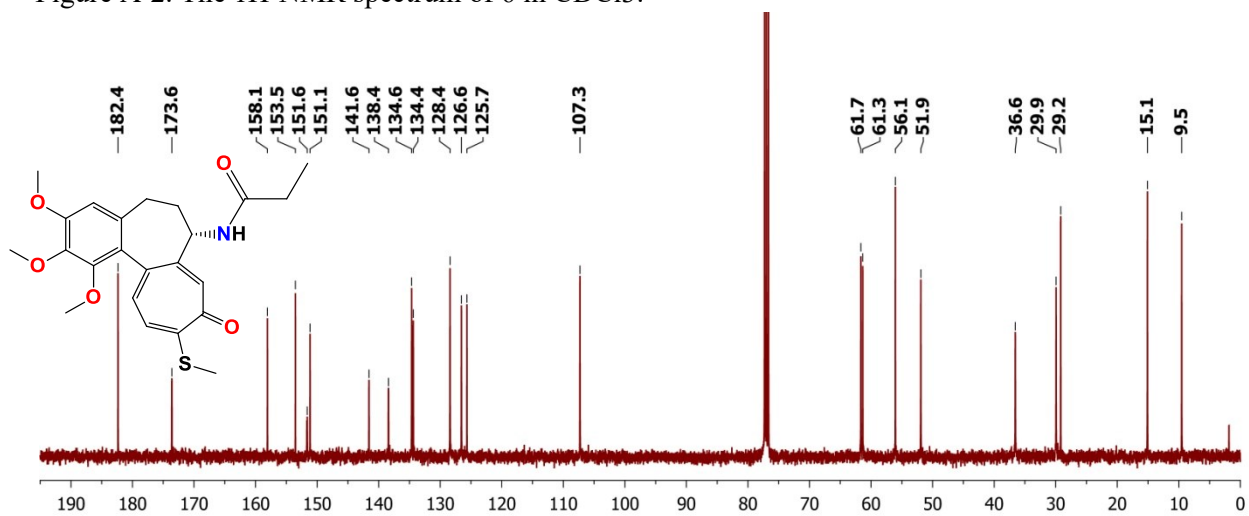


Figure A-3. The ^{13}C -NMR spectrum of 7 in CDCl_3 .

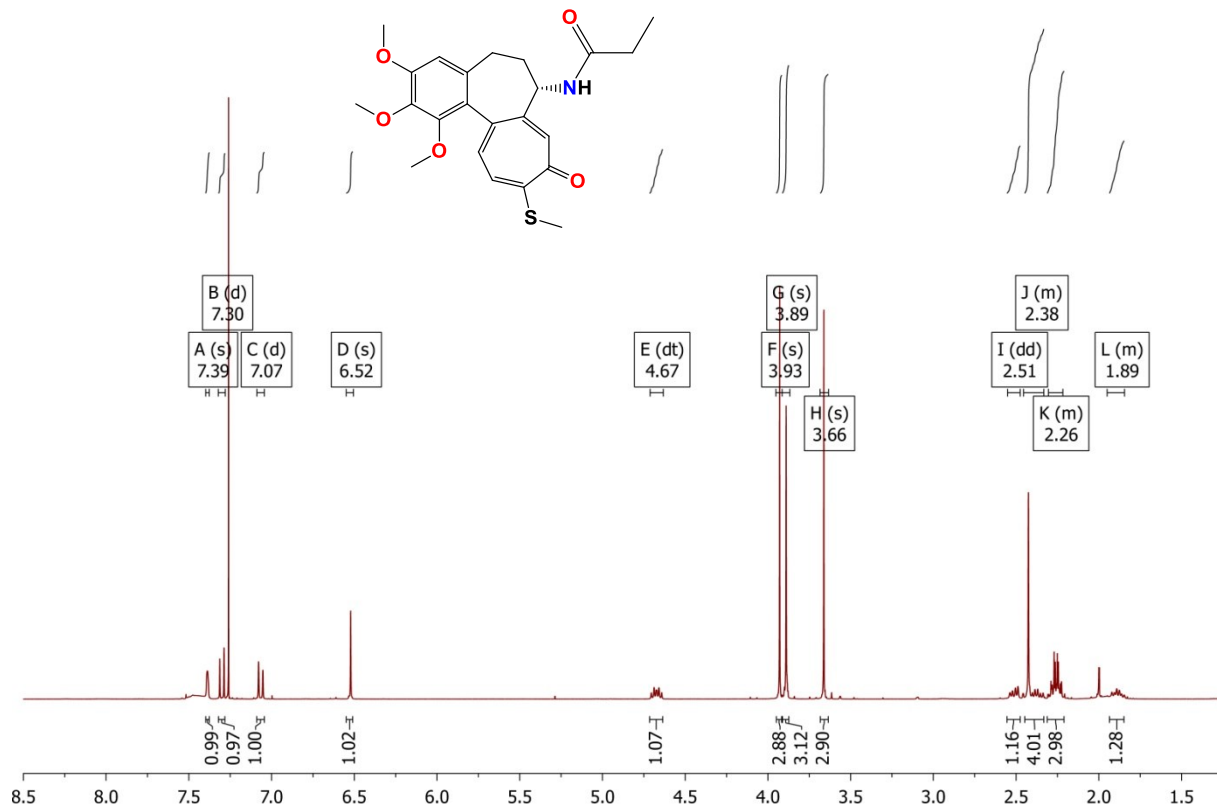


Figure A-4. The ¹H-NMR spectrum of 7 in CDCl₃.

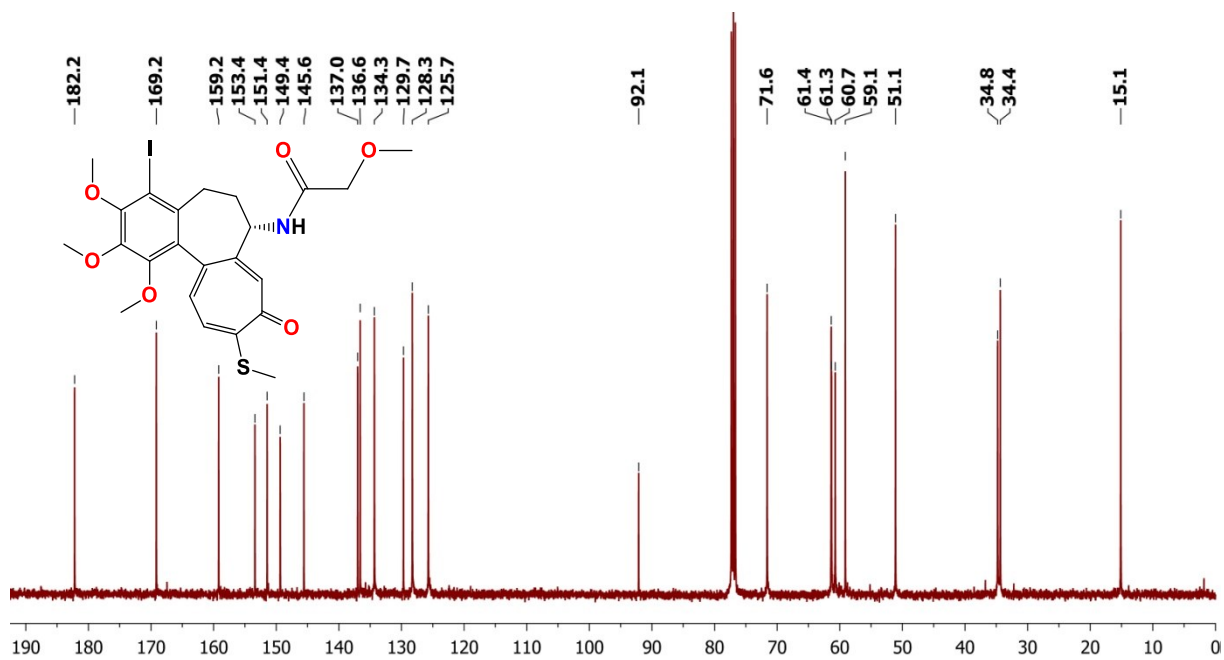


Figure A-5. The ¹³C-NMR spectrum of 14 in CDCl₃.

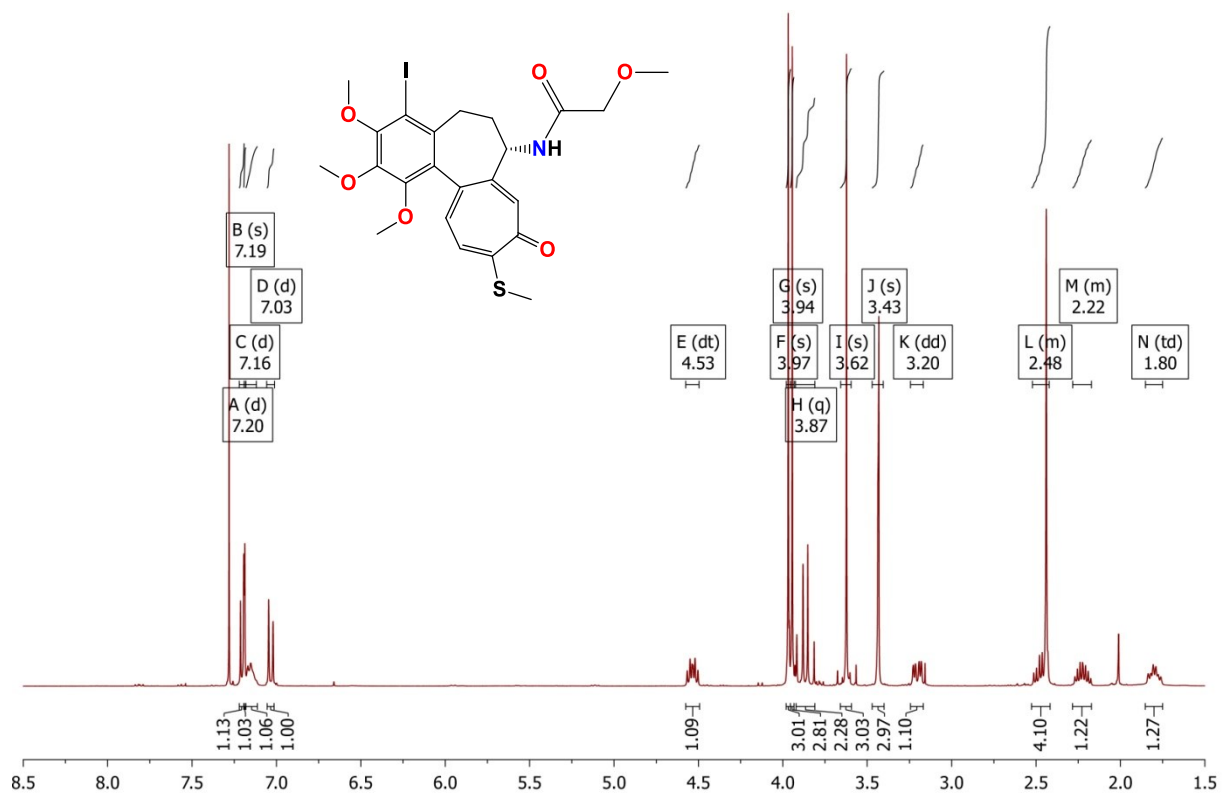


Figure A-6. The ¹H-NMR spectrum of 14 in CDCl₃.

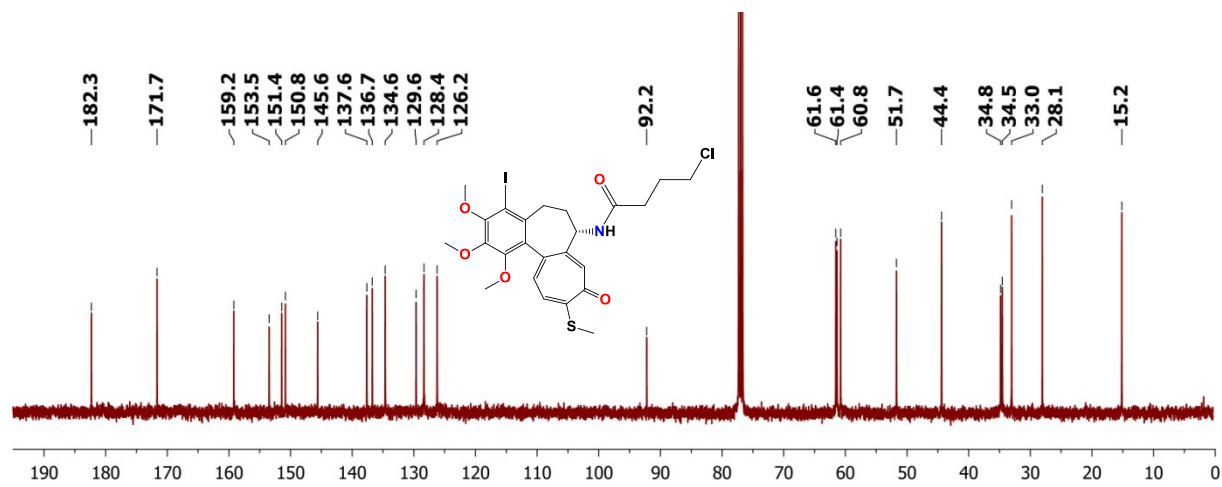


Figure A-7. The ¹³C-NMR spectrum of 15 in CDCl₃.

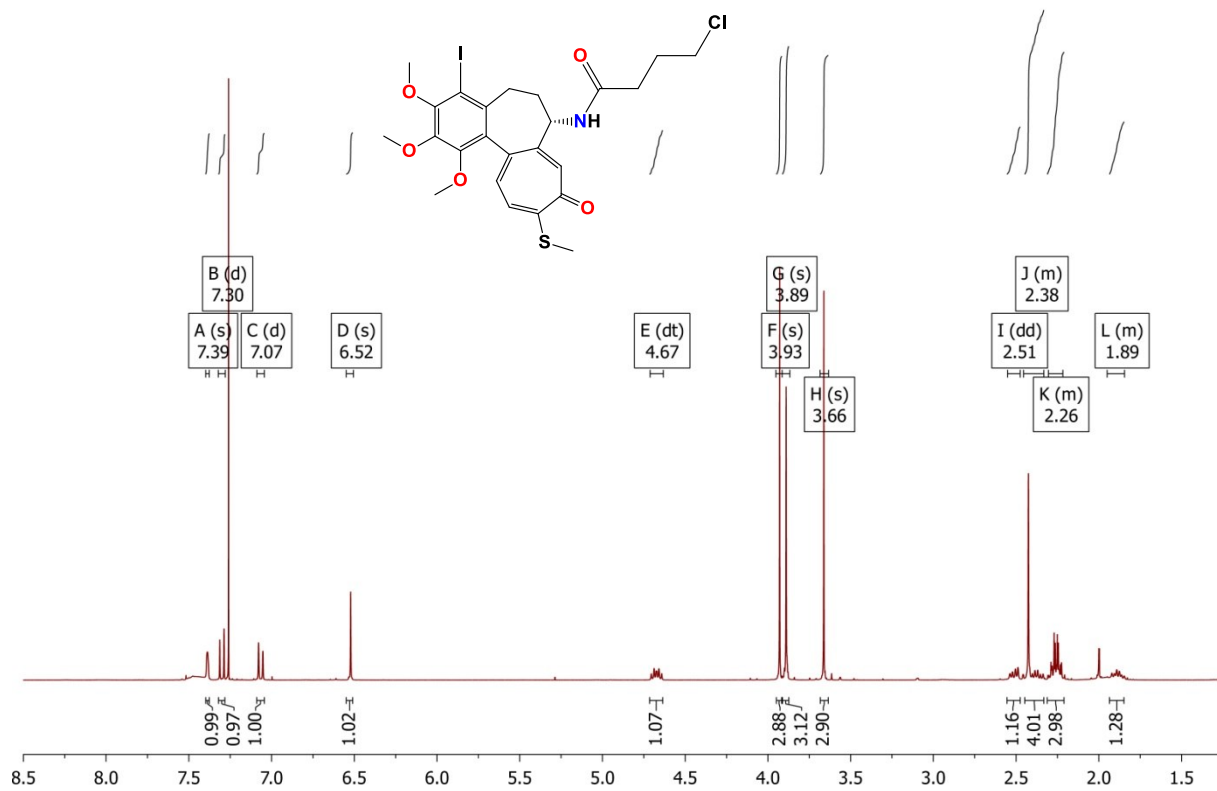
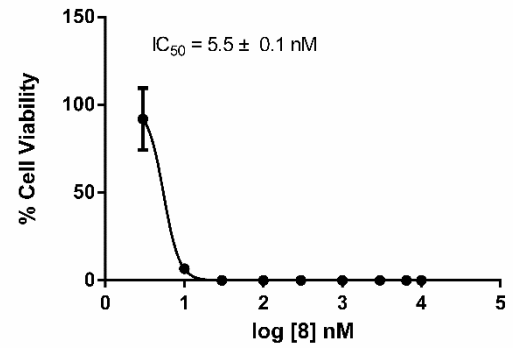
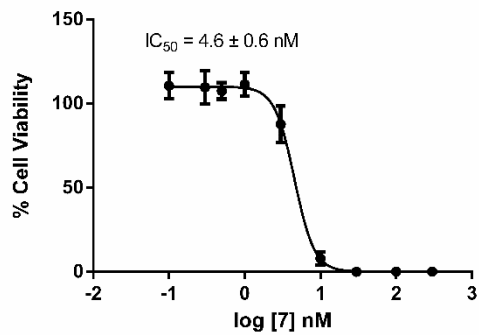
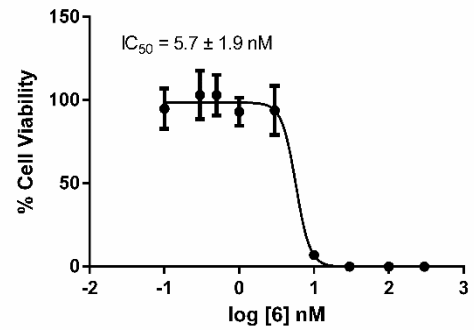
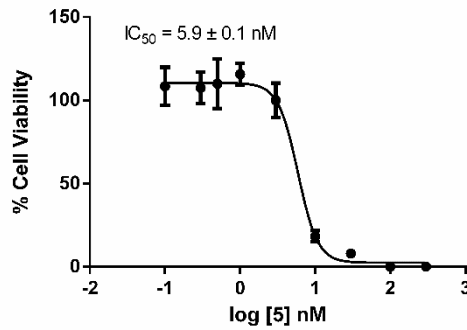
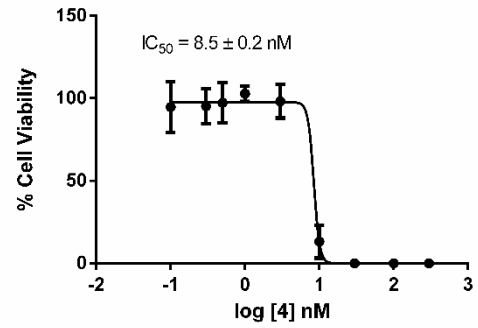
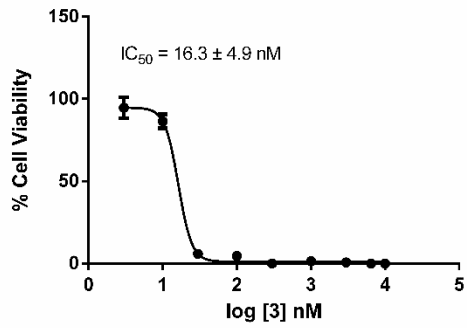
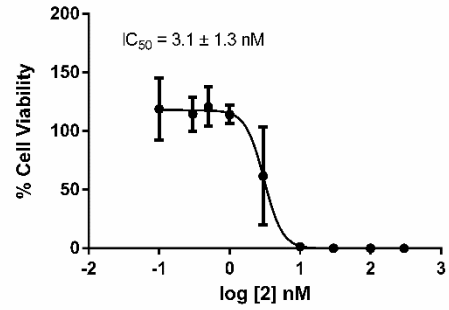
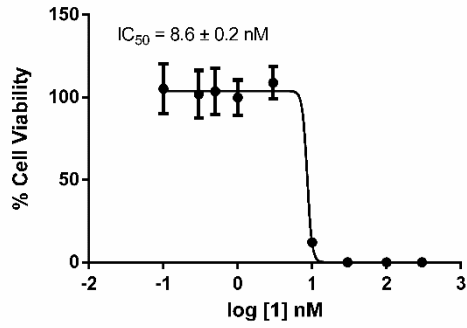
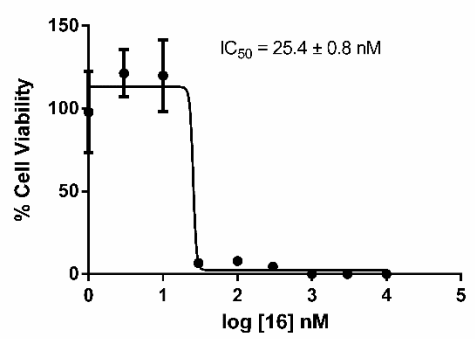
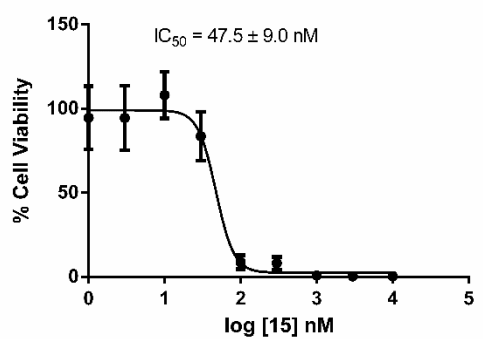
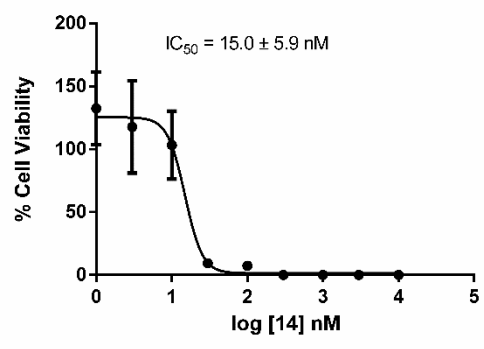
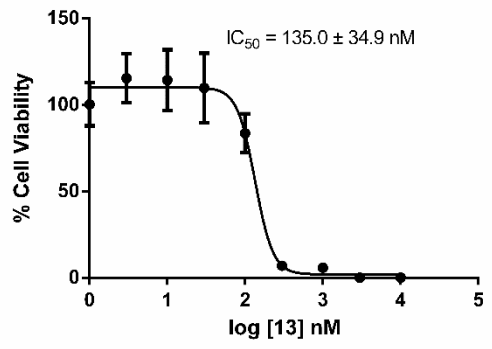
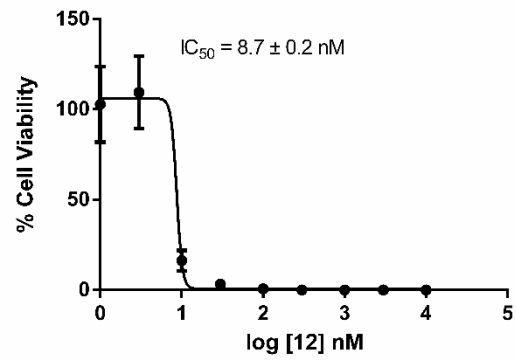
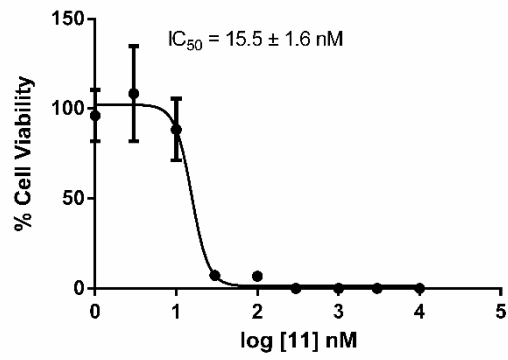
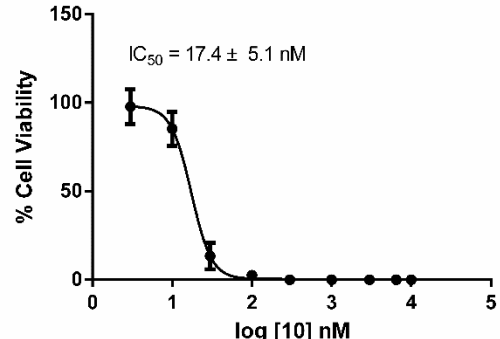
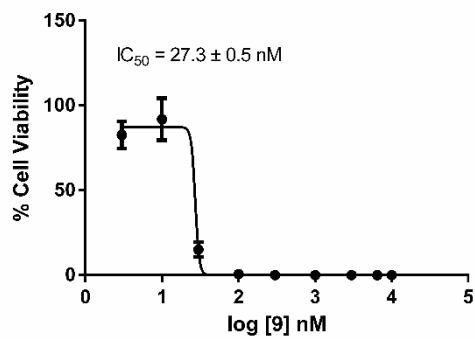


Figure A-8. The ¹H-NMR spectrum of 15 in CDCl₃.





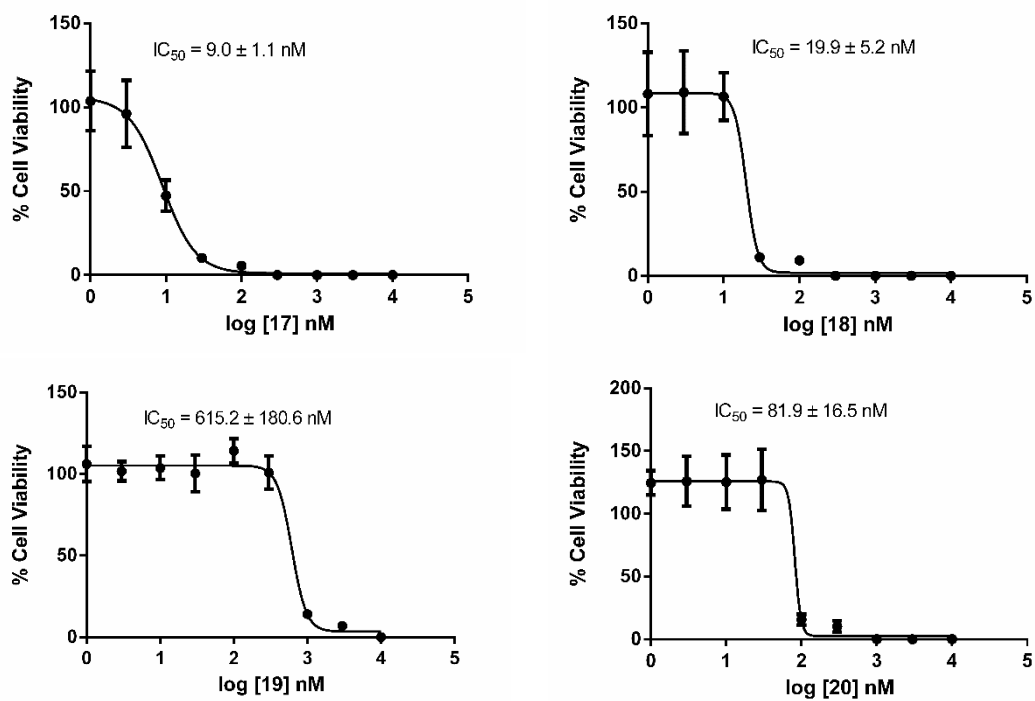
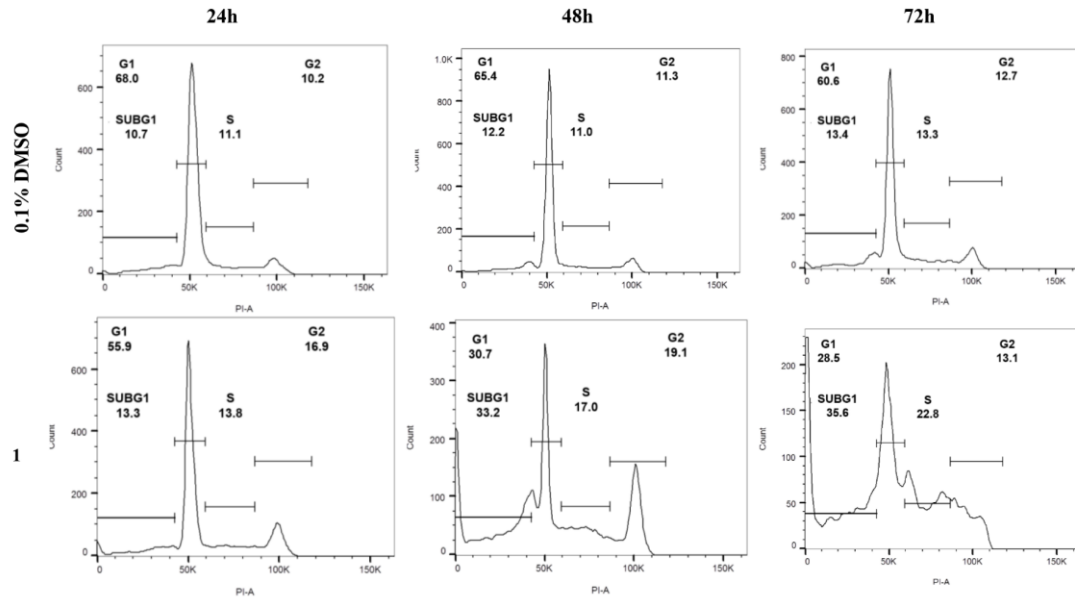
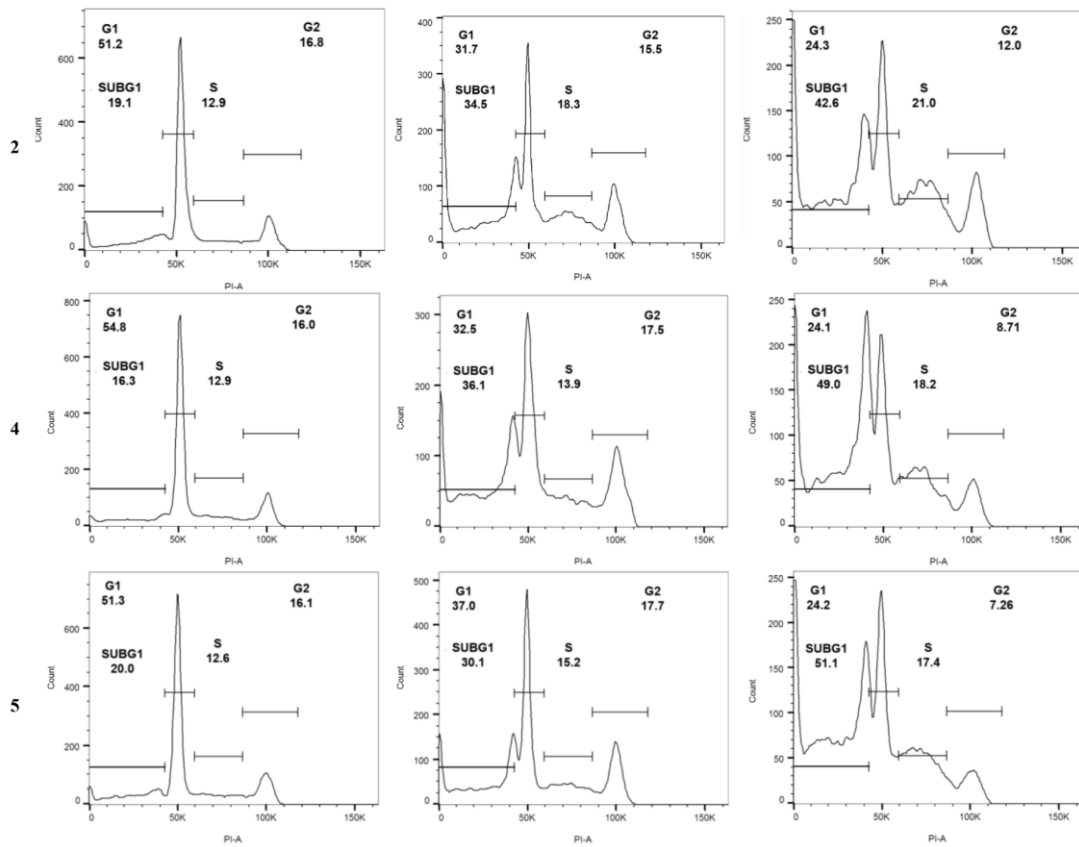
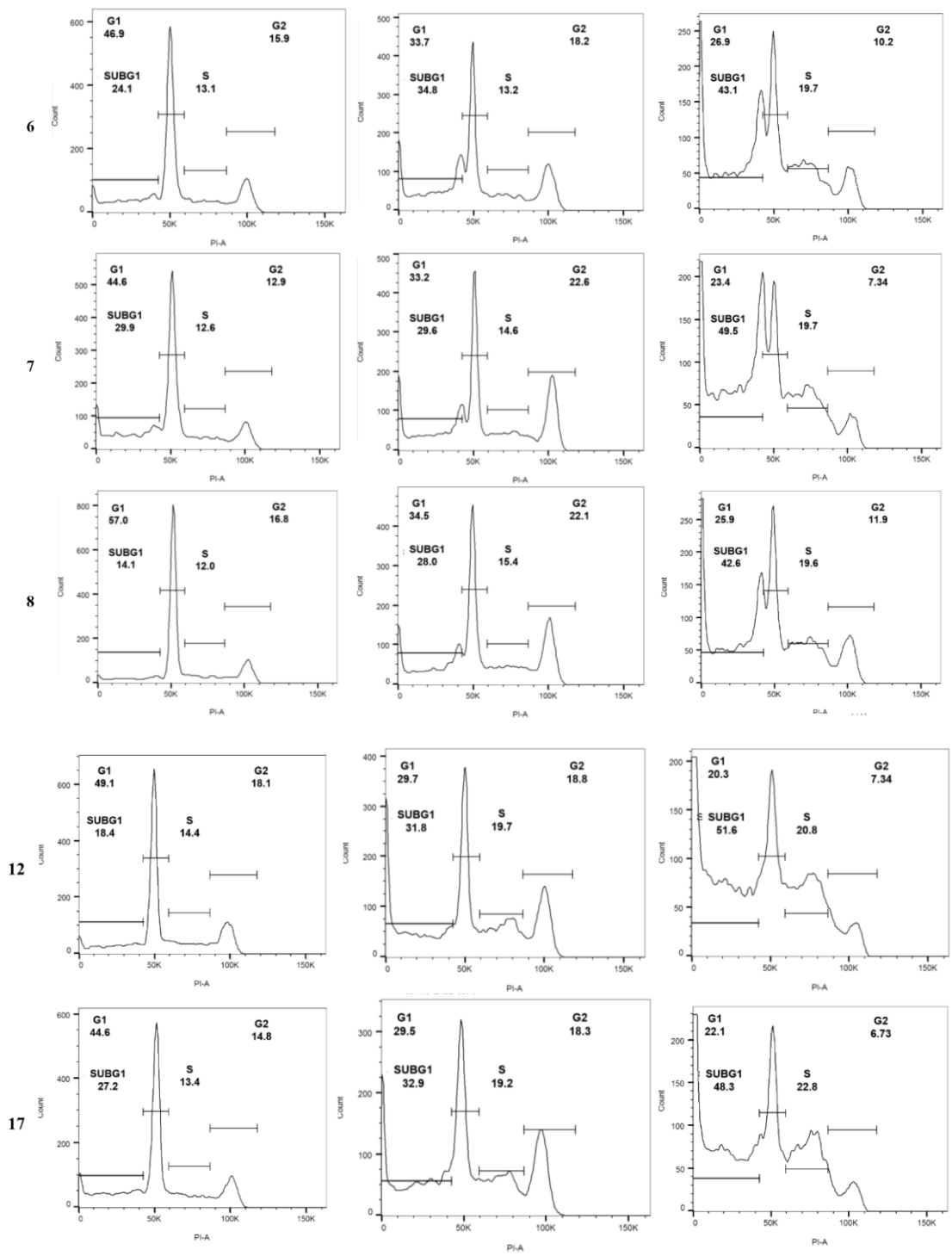


Figure A-9. Sensitivity of primary ALL cells to 1 and its derivatives. Cell viability was assessed by MTT assay employing ALL-5 cells. Cells were treated with vehicle (100% viability) or increasing concentrations of investigated compounds for 120 h. Results are given as mean \pm SD ($n = 4$) and IC₅₀ values are indicated. See Figure 1 for structures.

A.







B.

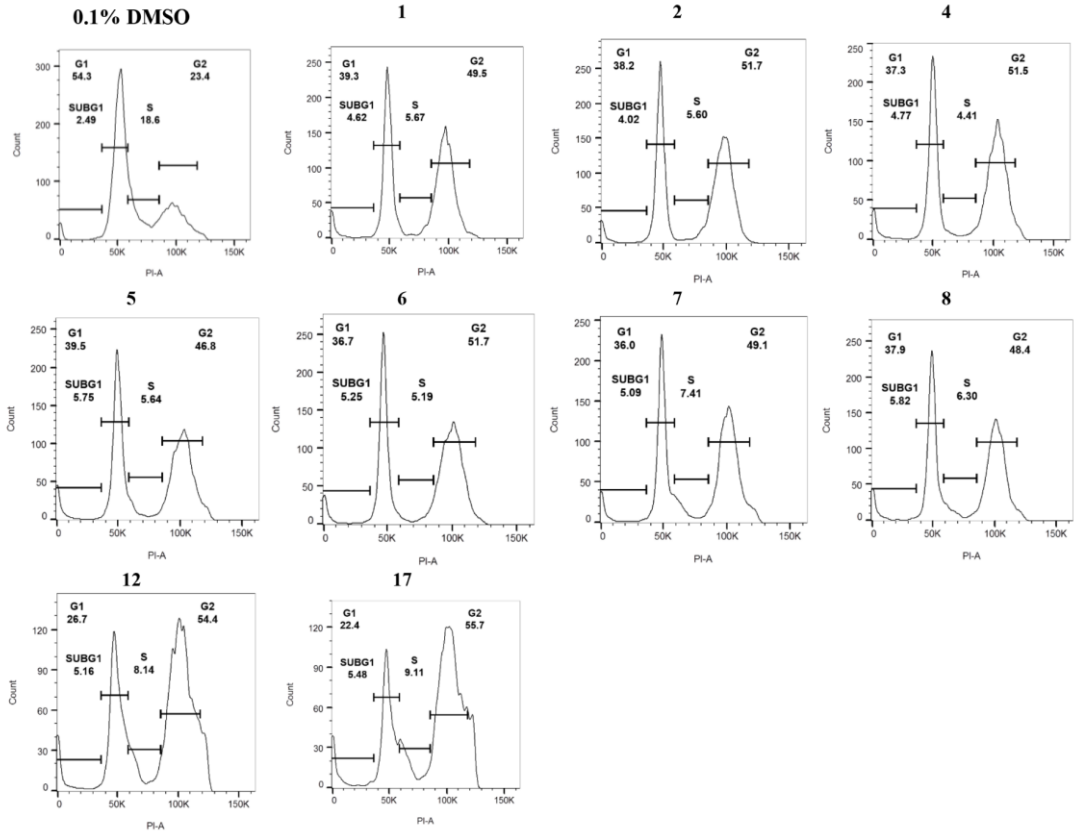


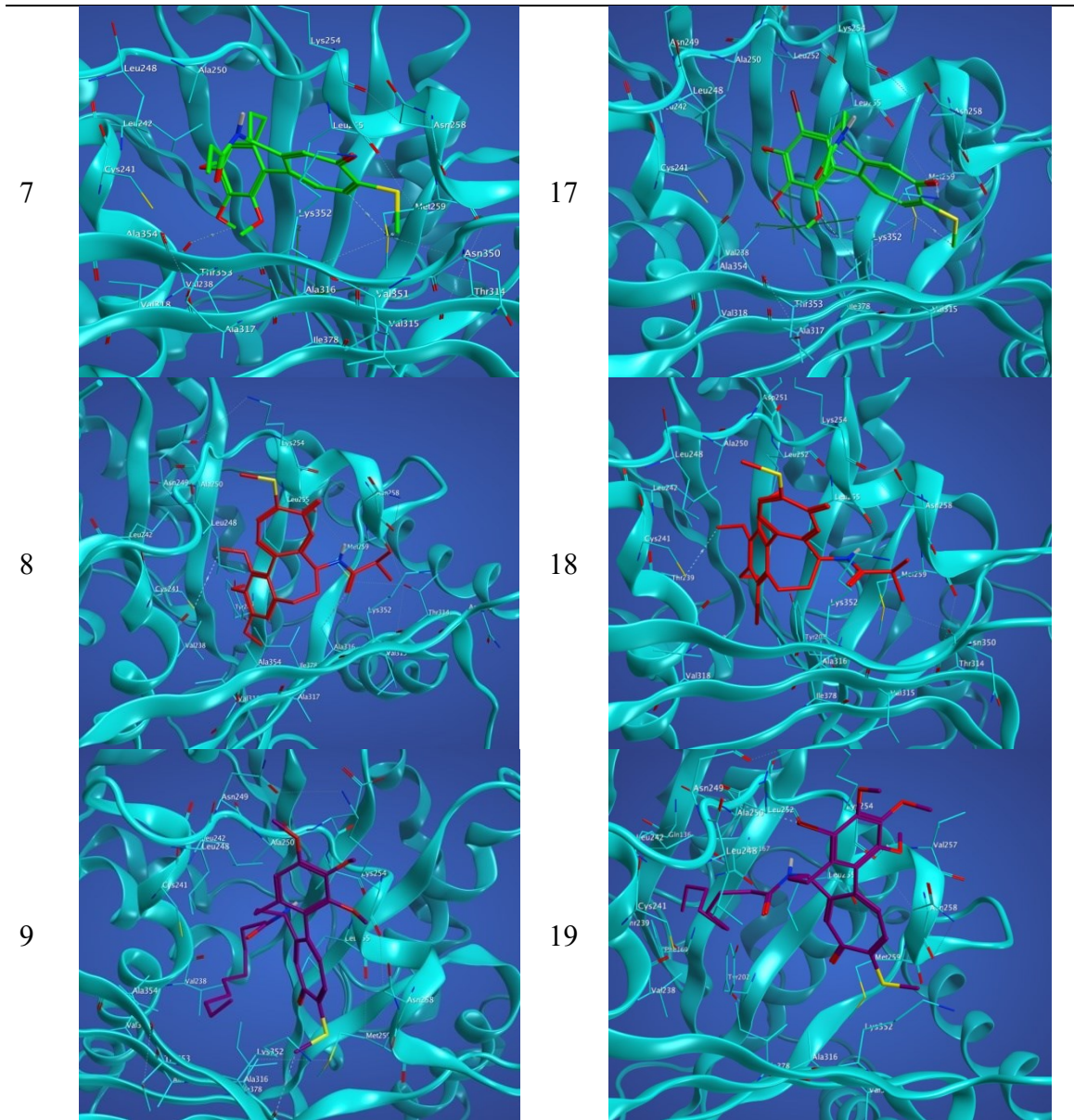
Figure A-10. DNA content of treated cells. ALL-5 (A) or MCF-7 (B) cells were treated with 5 x IC₅₀ values of 1, its analogs or 0.1% of DMSO (vehicle) for 24, 48 or 72 h (panel A, ALL-5, as indicated) or 72 h (panel B, MCF-7), and subjected to propidium iodide staining and flow cytometry, as described in Materials and Methods. The proportion of cells in different cell cycle phases or with sub-G1 DNA is indicated numerically and by the bars. Data shown are representative of three independent experiments.

Table A-1. 2D interaction diagrams for the interactions between β I tubulin and N-deacetylthiocolchicine and 4-iodo-N-deacetylthiocolchicine analogues.

Compound	2D-interaction	Compound	2D-interaction	2D-interaction of overlay
1		11		
2		12		
3		13		

Table A-2. 3D interaction diagrams for the interactions between β I tubulin and N-deacetylthiocolchicine and 4-iodo-N-deacetylthiocolchicine analogues.

Compound	3D-interaction	Compound	3D-interaction
1		11	
2		12	
3		13	



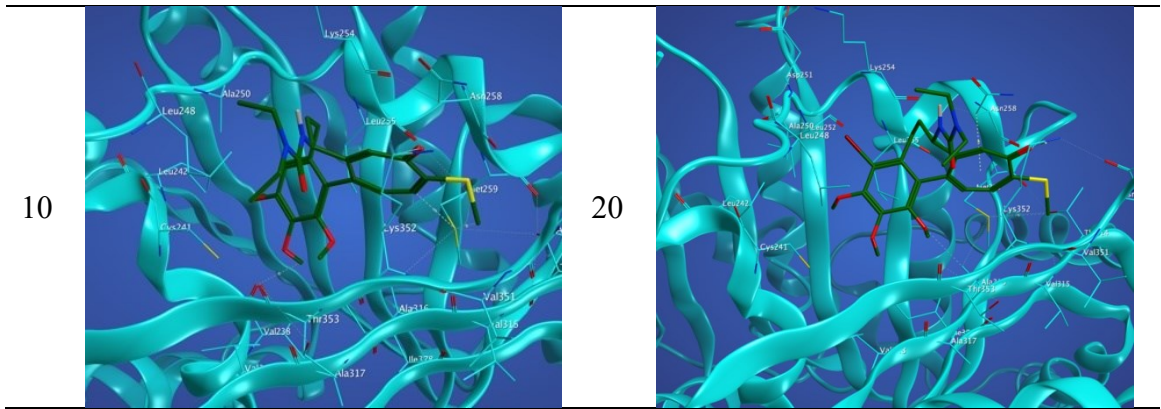
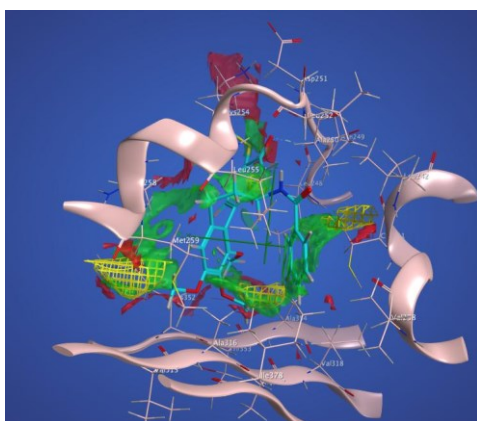


Table A-3. RMSD values of the 20 colchicine derivatives with respect to the X-ray structure of colchicine (5NM5).

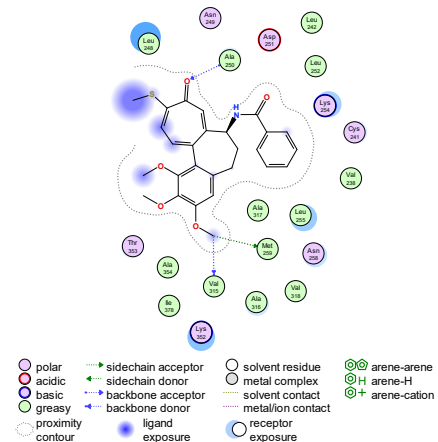
Compound	RMSD with respect to the Colchicine's X-ray structure
Colchicine (1)	0.980
2	0.491
3	0.407
4	0.448
5	5.601
6	5.222
7	0.765
8	4.077
9	4.588
10	0.530
11	4.248
12	0.874
13	5.131
14	4.327
15	0.946
16	5.178
17	0.897
18	3.557
19	4.728
20	0.952

Table A-4. A. contact preference map to predict non-bonded contact preferences, the preferred locations of hydrophobic and hydrophilic ligand atoms (hyd green, HPL red) and electrostatic feature maps that predict the electrostatically preferred locations of hydrophobic from the solutions of the Poisson-Boltzmann equation (yellow) B. 2D scheme of ligand-protein interaction C. The protein-ligand interaction fingerprints (PLIF) based on surface contact interactions between each of our derivatives and beta-tubulin (H: hydrophobic surface contact Q: charged surface contact and P: partial hydrophobic contact).

A. contact preference map



B. 2D scheme of ligand-protein interaction



C. Protein-ligand interaction fingerprints

entry	molecule	248	252
1	Beta1-pocket	-	H
2	Derivative-6	P	-

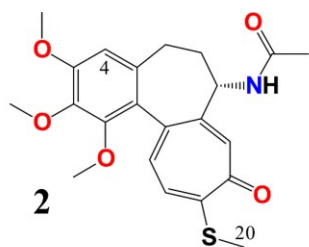
Table A-5. Values of H-bonding, atomic charges, solubility, etc calculated for the colchicine derivatives by ADMET predictors.

	MWt	S+logP	S+logD	S+Peff	S+S_pH	LogBB	N_FrRotB	F_SgleB	F_TpleB	F_AromB	T_RDmtr	T_Rgrav	T_Rgeom	T_Radmax	T_Rada	T_Radb	T_Radc
1	399,447	1,069	1,069	2,759	0,501	-0,952	6	0,516	0	0,419	0,379	3,815	3,7	6,018	8,112	6,263	3,864
2	415,511	1,734	1,734	3,33	0,076	-0,931	6	0,516	0	0,419	0,379	3,858	3,7	5,966	8,127	6,279	3,879
3	373,474	1,9	1,262	1,773	0,864	-0,751	4	0,5	0	0,464	0,423	3,601	3,432	5,72	8,23	4,945	3,84
4	445,538	1,598	1,598	2,518	0,174	-0,89	8	0,545	0	0,394	0,387	4,152	3,992	7,295	8,517	6,886	3,847
5	478,01	2,932	2,932	3,225	0,025	-0,703	9	0,559	0	0,382	0,406	4,542	4,186	7,771	9,005	7,019	3,848
6	477,583	3,053	3,053	3,508	0,015	-0,729	6	0,432	0	0,514	0,382	4,435	4,34	7,843	9,49	6,966	3,794
7	429,538	2,061	2,061	3,529	0,059	-0,864	7	0,531	0	0,406	0,367	3,982	3,828	6,493	8,24	6,638	3,868
8	443,565	2,432	2,432	3,658	0,045	-0,746	7	0,545	0	0,394	0,355	4,084	3,934	6,296	8,419	6,82	3,849
9	527,727	5,6	5,6	1,782	0,002	-0,58	14	0,615	0	0,333	0,486	5,586	5,468	11,762	12,508	6,885	3,767
10	472,607	2,356	2,355	3,319	0,054	-0,901	9	0,571	0	0,371	0,364	4,337	4,194	6,956	9,06	6,968	3,807
11	525,343	1,756	1,756	2,86	0,29	-0,938	6	0,531	0	0,406	0,367	3,757	3,71	6,628	8,146	6,227	4,025
12	541,407	2,445	2,445	3,433	0,049	-0,91	6	0,531	0	0,406	0,367	3,818	3,71	6,463	8,161	6,242	4,04
13	499,37	2,631	1,941	1,767	0,717	-0,706	4	0,517	0	0,448	0,407	3,577	3,447	6,467	8,251	4,966	3,963
14	571,434	2,259	2,259	2,604	0,112	-0,877	8	0,559	0	0,382	0,375	4,092	3,999	7,762	8,537	6,861	4,002
15	603,906	3,669	3,669	3,283	0,023	-0,662	9	0,571	0	0,371	0,394	4,465	4,19	8,334	9,01	7,008	3,997
16	603,479	3,825	3,825	3,637	0,012	-0,689	6	0,447	0	0,5	0,371	4,371	4,346	8,392	9,493	6,965	3,94
17	555,434	2,786	2,786	3,633	0,04	-0,837	7	0,545	0	0,394	0,355	3,934	3,837	6,913	8,272	6,603	4,027
18	569,461	3,18	3,18	3,764	0,031	-0,711	7	0,559	0	0,382	0,344	4,033	3,942	6,748	8,445	6,792	4,005
19	653,624	6,387	6,387	1,921	0,002	-0,522	14	0,625	0	0,325	0,474	5,452	5,463	12,511	12,485	6,903	3,893
20	598,503	3,004	3,004	3,417	0,044	-0,891	9	0,583	0	0,361	0,353	4,28	4,2	7,471	9,069	6,959	3,958

	T HydroR	T Dipole	HBDH	HBA	HBAo	HBAo	NPA MaxQ	NPA Q1	EEM XFon	Pi MaxQ	Pi Q1	Pi FPI1	Elephity	F NLP
1	6,03	1,993	1	7	6	1	0,709	-1,471	1,384	0,245	-0,128	21,016	110,086	0,448
2	6,046	1,959	1	6	5	1	0,706	-1,802	1,374	0,245	-0,165	22,732	109,319	0,448
3	5,606	1,546	2	5	4	1	0,417	-0,458	1,432	0,203	-0,111	20,605	99,769	0,393
4	6,36	2,21	1	7	6	1	0,68	-1,141	1,387	0,248	-0,161	22,74	117,112	0,484
5	6,557	2,2	1	6	5	1	0,699	-1,307	1,315	0,246	-0,164	22,735	127,442	0,406
6	6,669	2,073	1	6	5	1	0,622	-1,146	1,345	0,236	-0,165	29,594	125,074	0,382
7	6,198	1,857	1	6	5	1	0,7	-1,375	1,395	0,246	-0,164	22,736	113,268	0,433
8	6,307	1,804	1	6	5	1	0,694	-1,179	1,416	0,248	-0,162	22,741	117,409	0,419
9	7,538	3,84	1	6	5	1	0,689	-0,366	1,48	0,246	-0,164	22,741	140,924	0,351
10	6,542	2,076	1	7	5	2	0,702	-1,337	1,42	0,23	-0,131	24,522	127,736	0,424
11	6,086	2,068	1	7	6	1	0,709	-1,517	1,376	0,245	-0,132	23,17	110,704	0,433
12	6,101	2,023	1	6	5	1	0,706	-1,848	1,366	0,245	-0,17	25,074	109,937	0,433
13	5,664	1,598	2	5	4	1	0,417	-0,504	1,423	0,203	-0,115	22,946	100,387	0,378
14	6,414	2,273	1	7	6	1	0,679	-1,187	1,379	0,248	-0,165	25,083	117,73	0,469
15	6,609	2,261	1	6	5	1	0,699	-1,353	1,309	0,246	-0,168	25,077	128,061	0,394
16	6,723	2,068	1	6	5	1	0,622	-1,191	1,338	0,236	-0,17	31,936	125,693	0,371
17	6,253	1,908	1	6	5	1	0,7	-1,42	1,387	0,246	-0,168	25,078	113,887	0,419
18	6,362	1,84	1	6	5	1	0,694	-1,225	1,408	0,248	-0,166	25,082	118,027	0,406
19	7,585	3,728	1	6	5	1	0,689	-0,411	1,474	0,246	-0,168	25,081	141,543	0,342
20	6,597	2,1	1	7	5	2	0,702	-1,382	1,413	0,23	-0,136	26,864	128,354	0,412

Appendix B.

Supplementary material for chapter 3



Chemical Formula: C₂₂H₂₅NO₅S
Exact Mass: 415,15

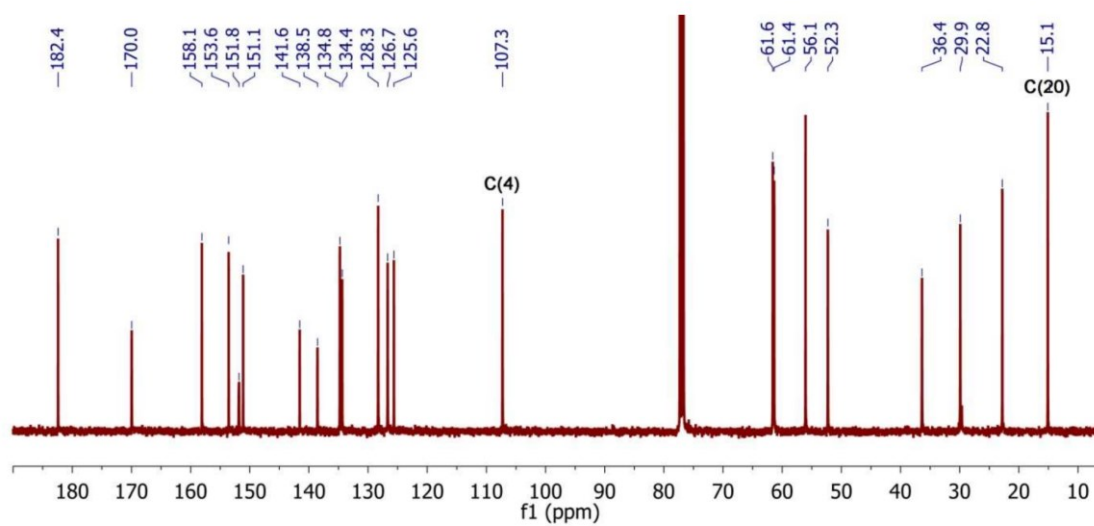


Figure B-1. The ¹³C NMR spectrum of **2** in CDCl₃.

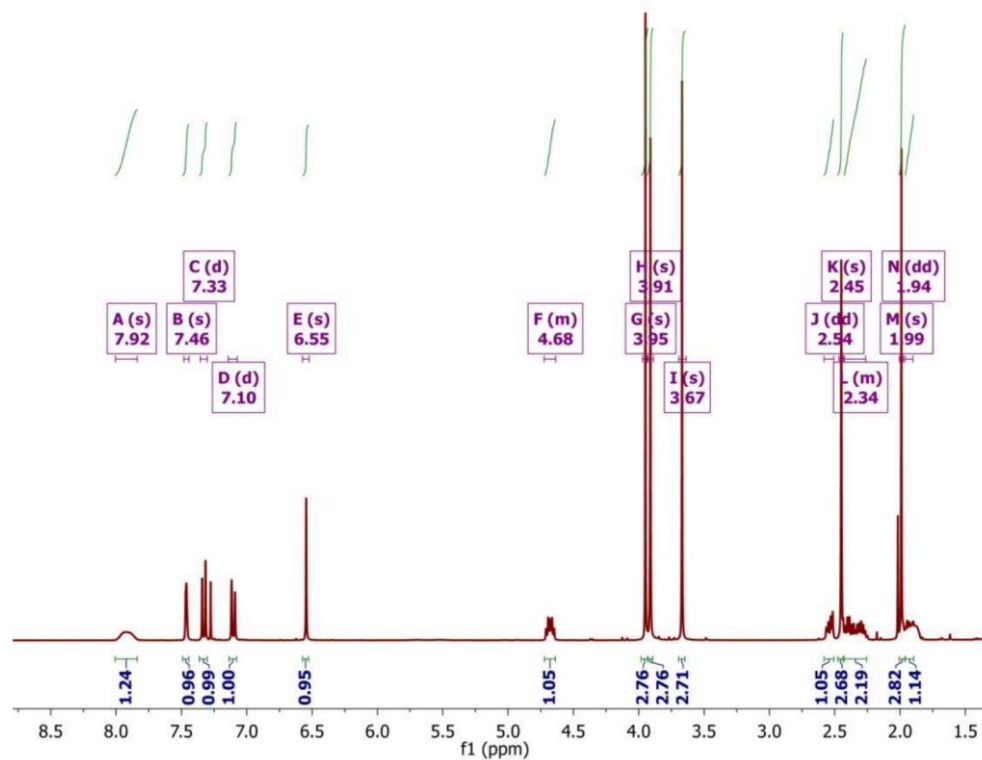


Figure B-2. The ^1H NMR spectrum of **2** in CDCl_3

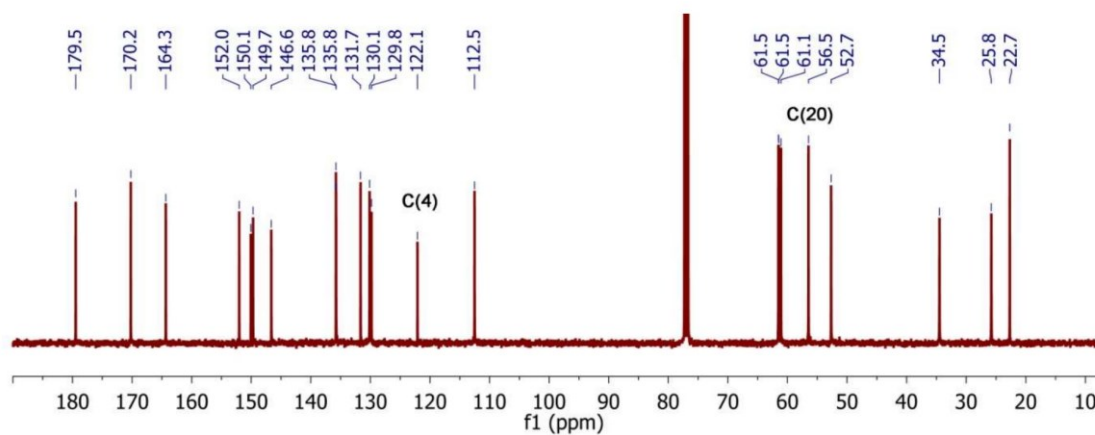
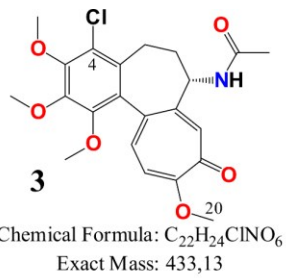


Figure B-3. The ^{13}C NMR spectrum of **3** in $CDCl_3$

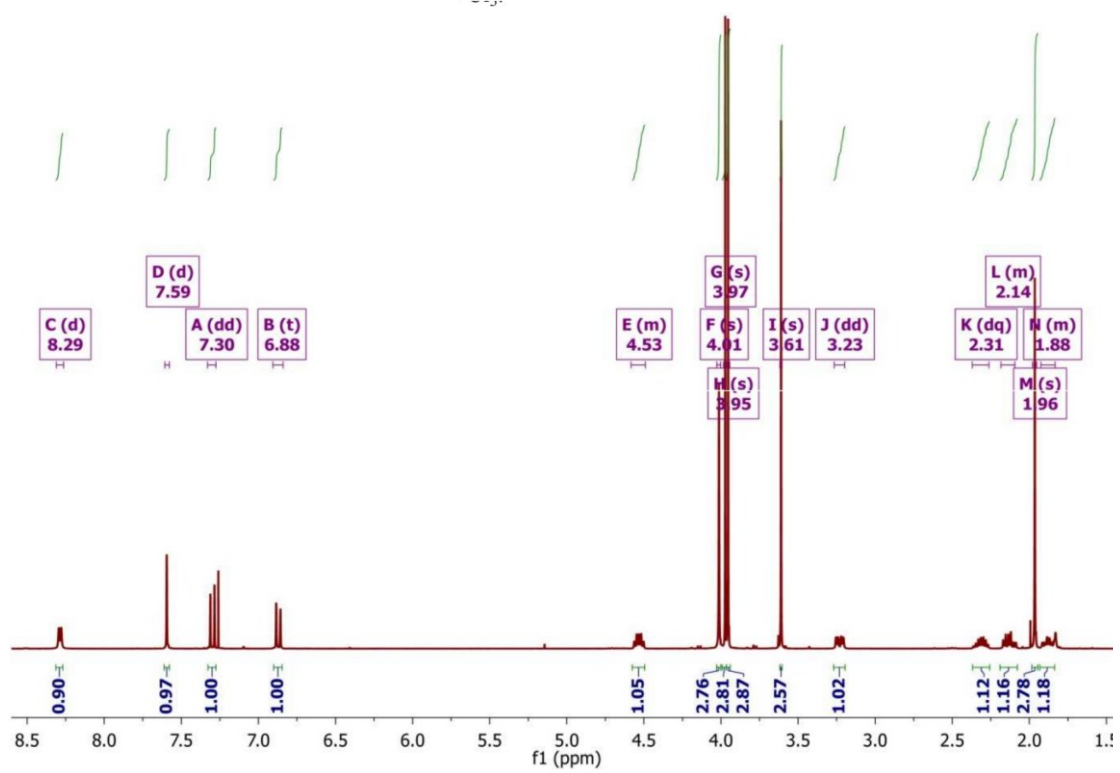


Figure B-4. The ^1H NMR spectrum of **3** in CDCl_3

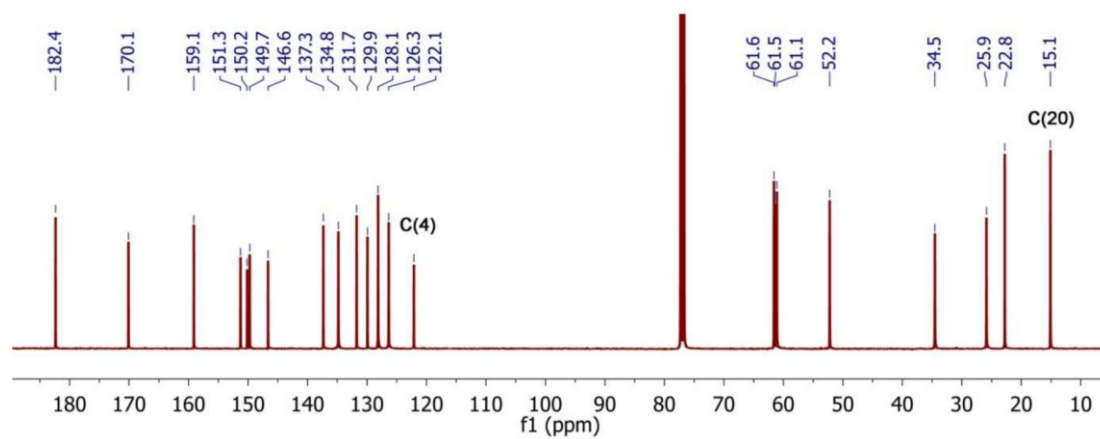
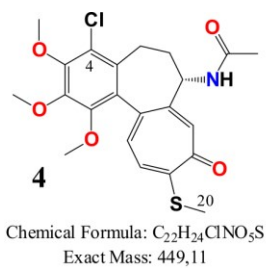


Figure B-5. The ¹³C NMR spectrum of 4 in CDCl₃

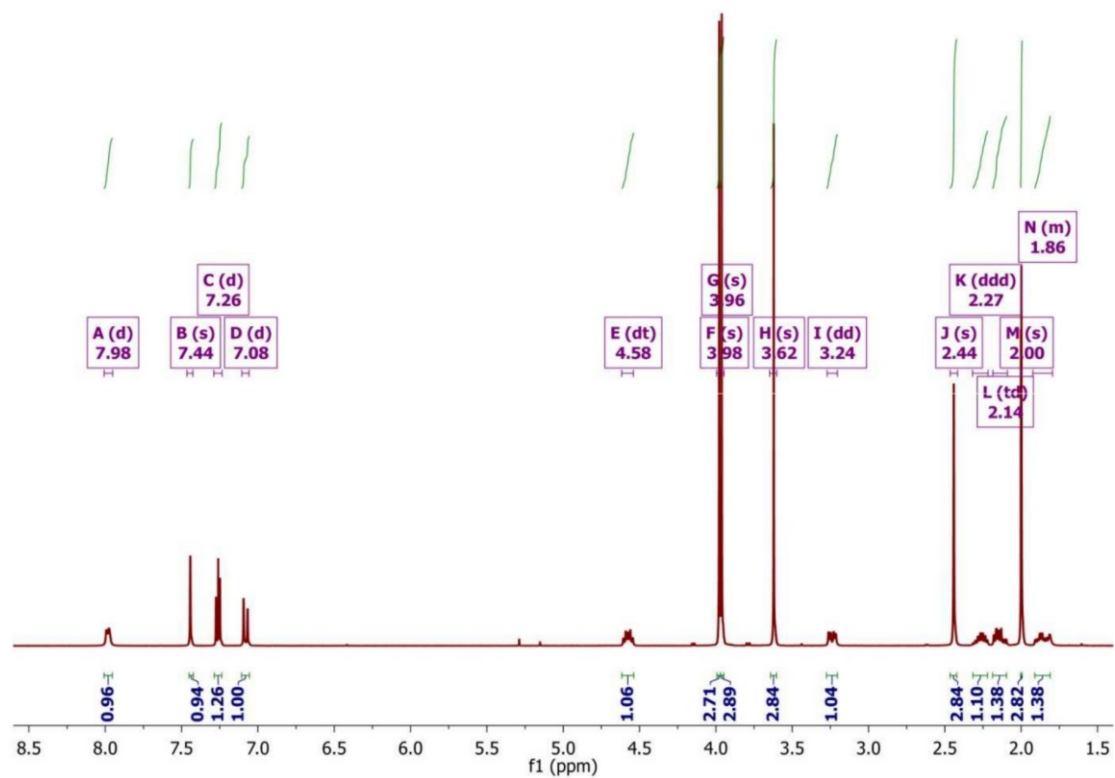


Figure B-6. The ^1H NMR spectrum of **4** in CDCl_3

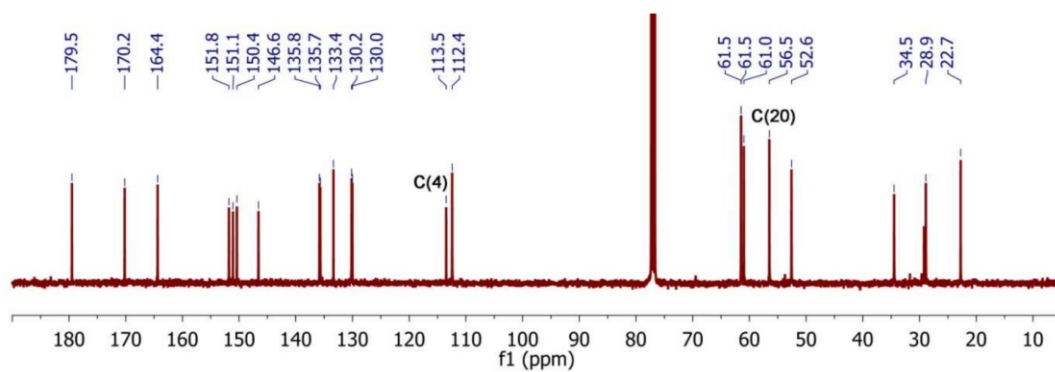
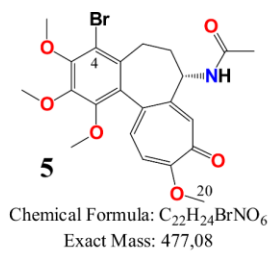


Figure B-7. The ^{13}C NMR spectrum of **5** in $CDCl_3$

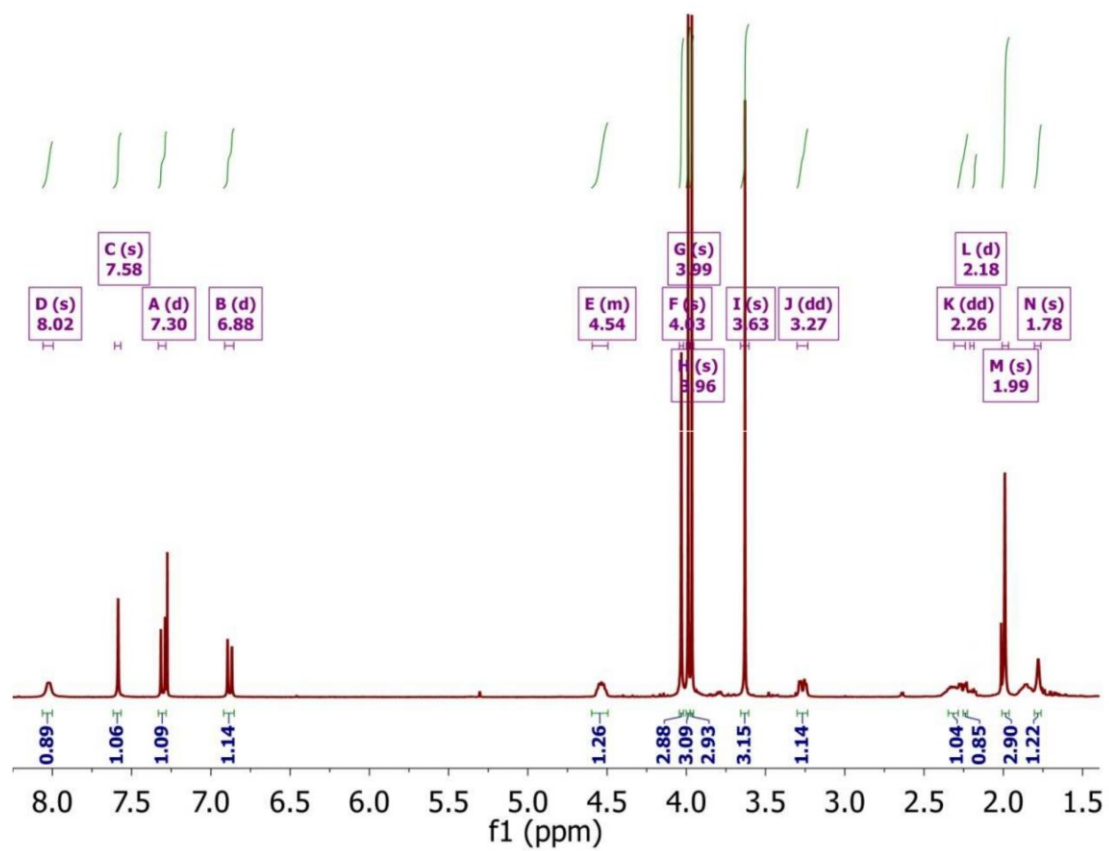


Figure B-8. The ^1H NMR spectrum of **5** in CDCl_3

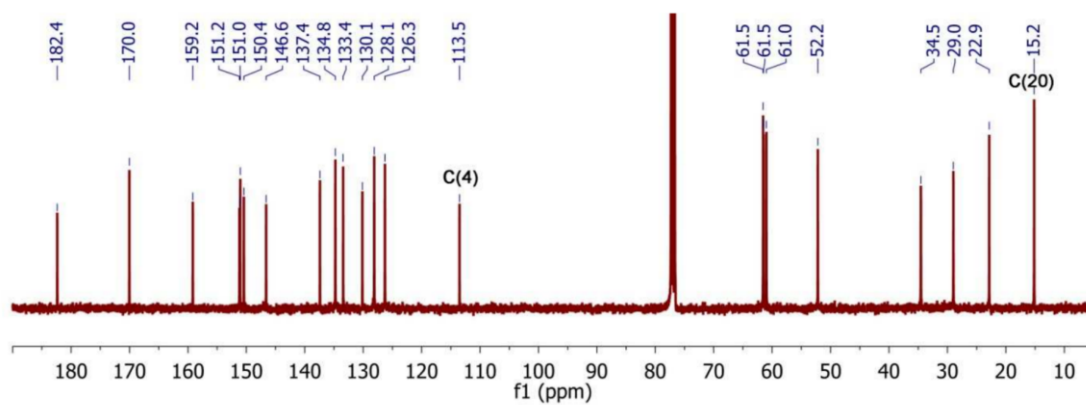
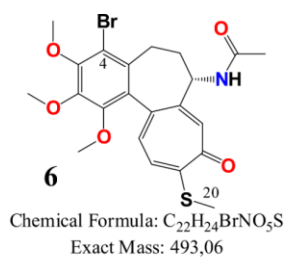


Figure B-9. The ^{13}C NMR spectrum of **6** in $CDCl_3$

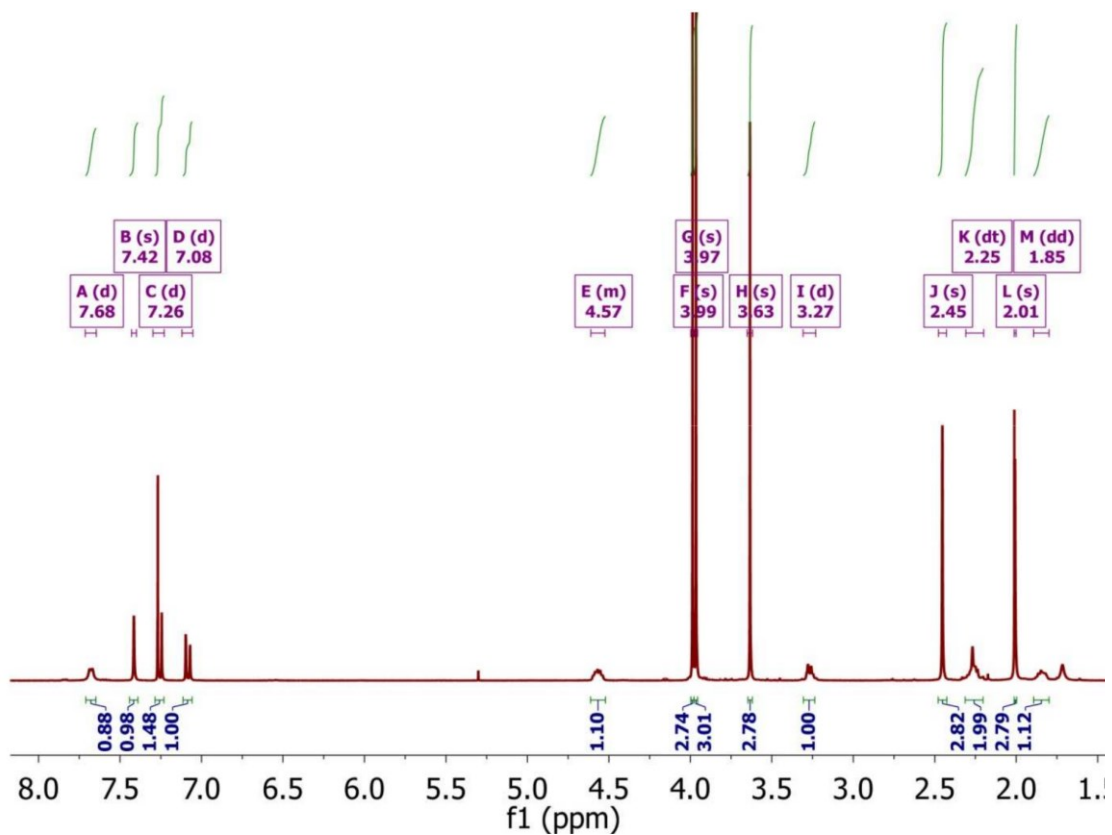


Figure B-10. The ^1H NMR spectrum of **6** in CDCl_3

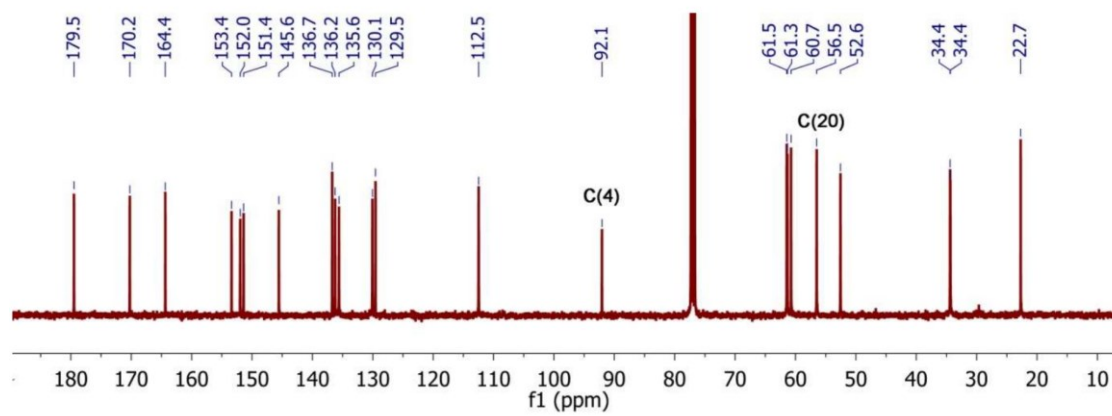
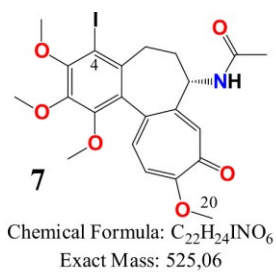


Figure B-11. The ^{13}C NMR spectrum of **7** in $CDCl_3$

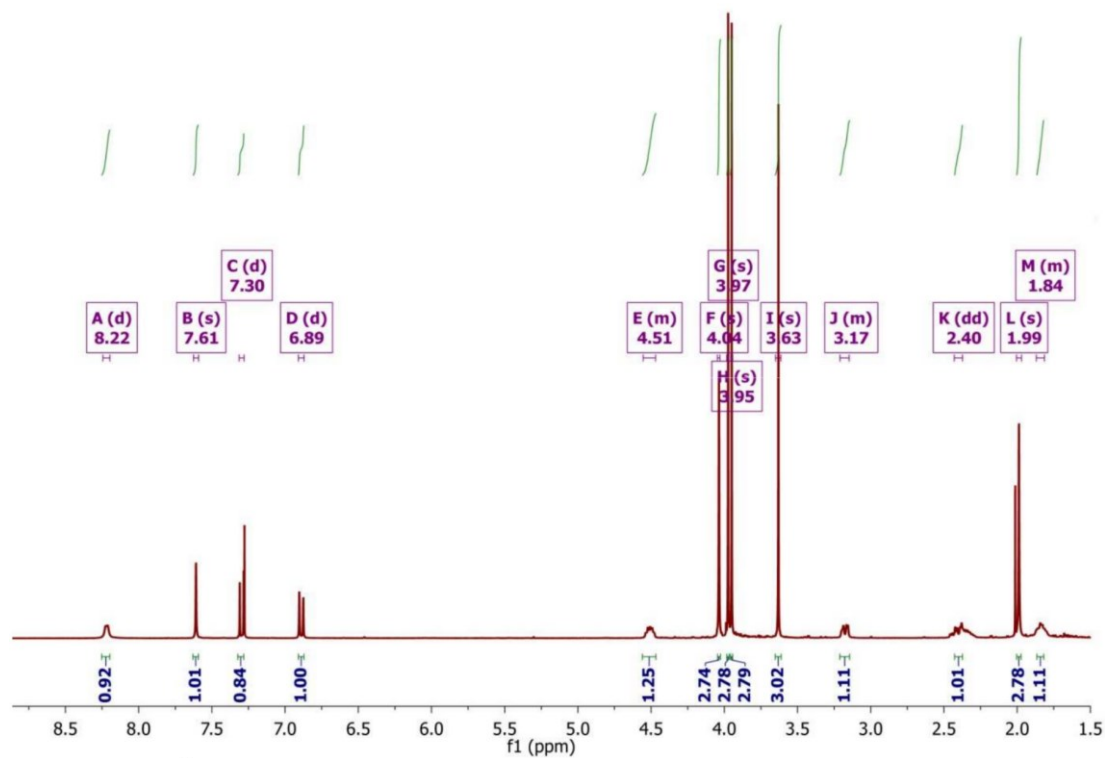


Figure B-12. The ^1H NMR spectrum of **7** in CDCl_3

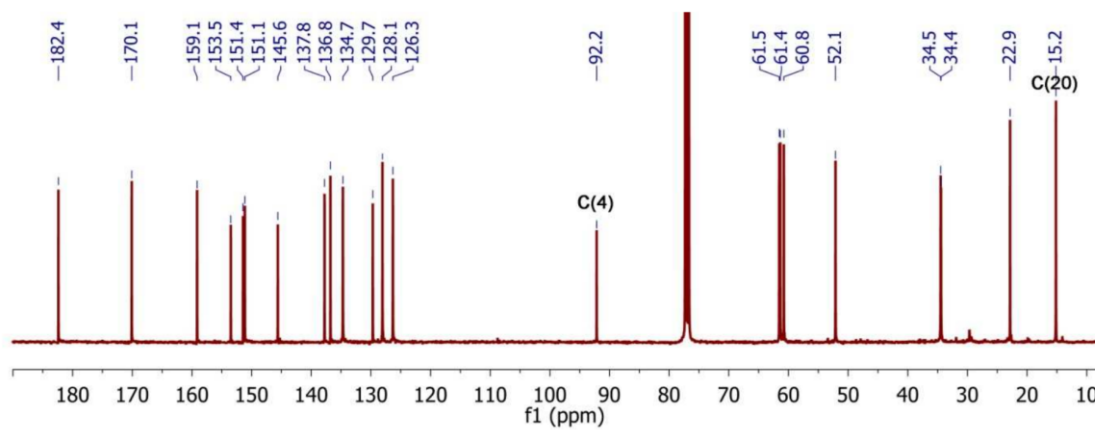
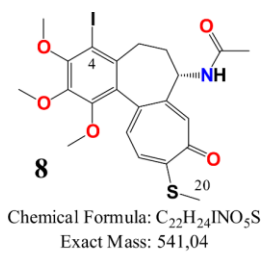


Figure B-13. The ^{13}C NMR spectrum of **8** in $CDCl_3$

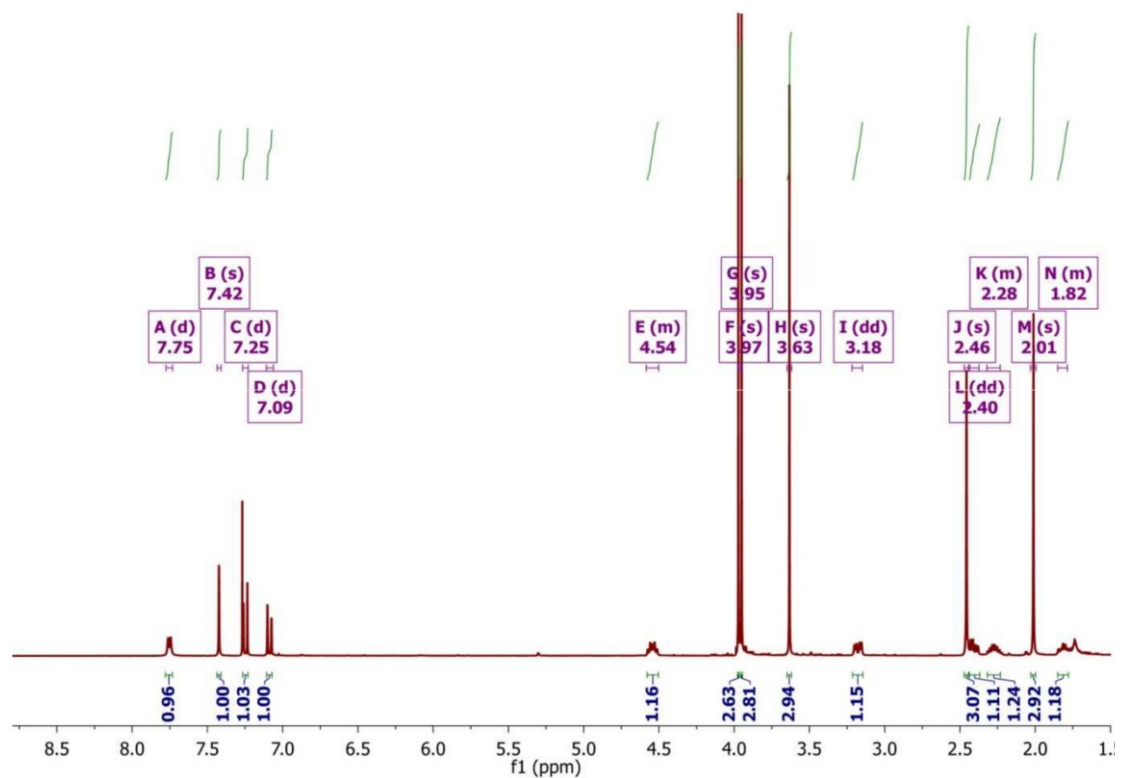


Figure B-14. The ^1H NMR spectrum of **8** in CDCl_3

Appendix C.

Supplementary material for chapter 4

Materials

All precursors for the synthesis and solvents were obtained from Sigma Aldrich (Merck KGaA, Saint Louis, MO, USA) and were used as received without further purification. CDCl₃ spectral grade solvent was stored over 3 Å molecular sieves for several days. TLC was carried out on precoated plates (TLC silica gel 60 F254, Aluminium Plates Merck, Merck KGaA, Saint Louis, MO, USA) and spots were detected by illumination with an UV lamp. All the solvents used in flash chromatography were of HPLC grade (CHROMASOLV from Sigma Aldrich, Merck KGaA, Saint Louis, MO, USA) and were used as received. The elemental analysis of compounds was carried out on Vario ELIII (Elementar, Langenselbold, Germany).

Spectroscopic measurements

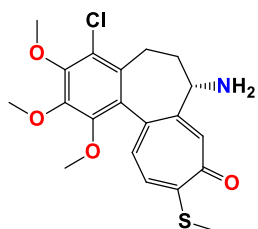
The ¹H, ¹³C spectra were recorded on a Varian VNMR-S 400 MHz spectrometer (Varian, Inc., Palo Alto, CA, USA). ¹H NMR measurements of **1-9** (0.07 mol dm⁻³) in CDCl₃ were carried out at the operating frequency 402.64 MHz. The error of the chemical shift value was 0.01 ppm. The ¹³C NMR spectra were recorded at the operating frequency 101.25 MHz. The error of chemical shift value was 0.1 ppm. All spectra were locked to deuterium resonance of CDCl₃. The ¹H and ¹³C NMR spectra are shown in the Supplementary Materials.

The FT-IR spectra of **1-9** in the mid infrared region were recorded in KBr. The spectra were taken with an IFS 113v FT-IR spectrophotometer (Bruker, Karlsruhe, Germany) equipped with a DTGS detector; resolution 2 cm⁻¹, NSS = 64. The Happ-Genzel apodization function was used.

The ESI (Electrospray Ionisation) mass spectra were recorded also on a Waters/Micromass (Waters Corporation, Manchester, UK) ZQ mass spectrometer

equipped with a Harvard Apparatus syringe pump. The samples were prepared in dry acetonitrile ($5 \times 10^{-5} \text{ mol dm}^{-3}$). The sample was infused into the ESI source using a Harvard pump at a flow rate of 20 ml min^{-1} . The ESI source potentials were: capillary 3 kV, lens 0.5 kV, extractor 4 V. The standard ESI mass spectra were recorded at the cone voltages: 10 and 30 V. The source temperature was 120°C and the desolvation temperature was 300°C . Nitrogen was used as the nebulizing and desolvation gas at flow-rates of $100 \text{ dm}^3 \text{ h}^{-1}$. Mass spectra were acquired in the positive ion detection mode with unit mass resolution at a step of 1 m/z unit. The mass range for ESI experiments was from $m/z = 100$ to $m/z = 1000$, as well as from $m/z = 200$ to $m/z = 1500$.

Synthesis and spectroscopic data of **1**



Compound **1** was prepared from 4-chlorothiocolchicine by hydrolysis with 2 N HCl. To a solution of compound 4-chlorothiocolchicine (500 mg, 1.11 mmol) in MeOH (3 ml), the 2 N HCl solution (5 ml) was added. The mixture was stirred at 90°C for 72 h. Reaction time was determined by TLC. After that time the reaction mixture was quenched by the addition of water (100 ml). The whole mixture was extracted four times with CH_2Cl_2 , and the combined organic layers were dried over MgSO_4 , filtered, and evaporated under reduced pressure. The residue was purified by CombiFlash[®] (EtOAc/MeOH, increasing concentration gradient) to give **1** ($\text{C}_{20}\text{H}_{22}\text{ClNO}_4\text{S}$, MW = 407.9 g/mol) with yield 88% [1].

^{13}C NMR (101 MHz, CDCl_3) δ 182.4, 158.7, 153.1, 150.1, 149.2, 146.2, 137.0, 134.0, 132.6, 129.8, 129.2, 125.5, 121.8, 61.3, 61.1, 53.5, 38.3, 26.5, 15.1 ppm.

^1H NMR (403 MHz, CDCl_3) δ 7.59 (s, 1H), 7.16 – 7.12 (m, 1H), 7.03 (dd, $J = 10.2, 5.1$ Hz, 1H), 3.97 (s, 3H), 3.96 (s, 3H), 3.66 – 3.60 (m, 4H), 3.22 – 3.16 (m, 1H), 2.44 (s, 3H), 2.29 (ddd, $J = 17.8, 12.0, 5.9$ Hz, 1H), 2.21 – 2.12 (m, 1H), 1.58 – 1.53 (m, 1H) ppm.

FT-IR (KBr pellet): 3378, 2936, 1606, 1556, 1464, 1412, 1401, 1348, 1253, 1197, 1141, 1086, 1021 cm^{-1} .

ESI-MS (m/z): $[\text{M}+\text{H}]^+$ calcd 408, found 408, $[\text{M}+\text{Na}]^+$ calcd 430, found 430, $[\text{2M}+\text{H}]^+$ calcd 815, found 815, $[\text{2M}+\text{Na}]^+$ calcd 837, found 837.

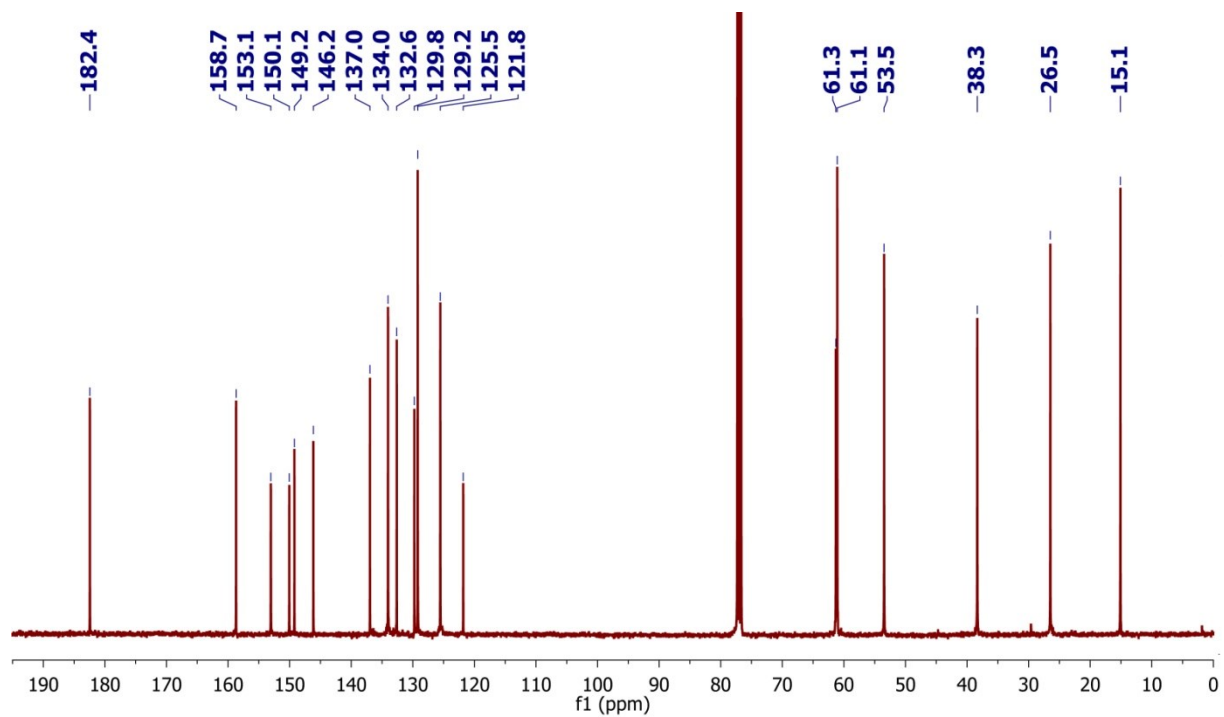


Figure C-1. The ^{13}C NMR spectrum of **1** in CDCl_3

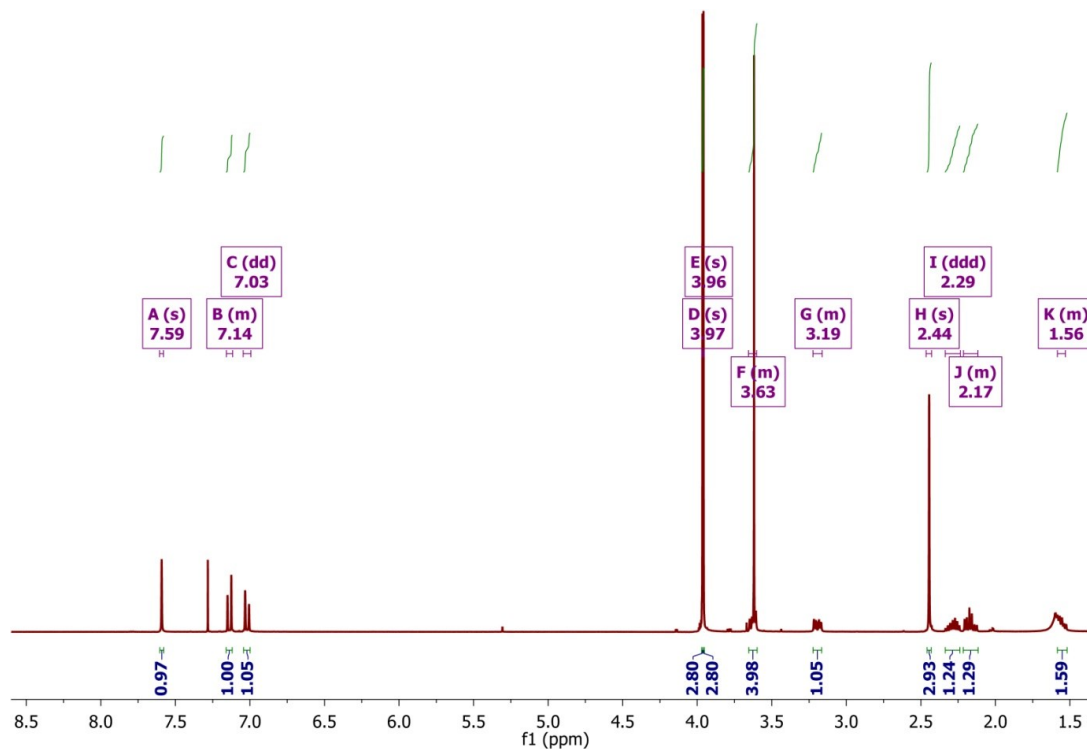


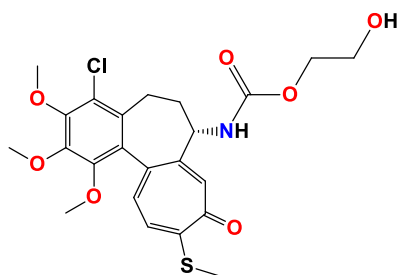
Figure C-2. The ^1H NMR spectrum of **1** in CDCl_3 .

General procedure for the synthesis of colchicine derivatives (2-9)

Compounds **2-9** were obtained directly from compound **1**. To a solution of compound **1** (100 mg, 0.25 mmol) in tetrahydrofuran (5 ml) cooled to 0°C , the following compounds were added: Et_3N (1 ml, 7 mmol), triphosgene (78 mg, 0.26 mmol). The mixture was first stirred at 0°C for 20 min and then for the next 20 min at RT. After that time respective alcohol (11 mmol) was added and the mixture was stirred at RT for the next 48 h. Reaction time was determined by TLC. The solution was filtered to remove triethylamine hydrochloride. The THF was evaporated and the residue was quenched by the addition of CH_2Cl_2 (100 ml) and was washed sequentially with a solution of HCl (aq) (0.5 M) and then with water. The organic layer was evaporated to dryness under reduced

pressure and purified by CombiFlash[®] (hexane/ethyl acetate, increasing concentration gradient) to give respective compounds as amorphous yellow solids (**2-9**).

Spectroscopic data of **2**



C₂₃H₂₆ClNO₇S, MW = 496.0 g/mol;

¹³C NMR (101 MHz, CDCl₃) δ 182.5, 159.2, 155.9, 150.7, 150.2, 149.7, 146.6, 137.0, 134.8, 131.8, 129.8, 128.5, 126.3, 122.2, 66.9, 61.5, 61.4, 61.1, 61.1, 53.8, 35.0, 25.9, 15.1 ppm.

¹H NMR (403 MHz, CDCl₃) δ 7.43 (s, 1H), 7.27 – 7.23 (d, *J* = 10.4 Hz, 1H), 7.09 (d, *J* = 10.5 Hz, 1H), 6.56 (d, *J* = 7.3 Hz, 1H), 4.34 (dt, *J* = 13.4, 6.8 Hz, 1H), 4.09 (dddd, *J* = 15.6, 11.7, 8.6, 4.5 Hz, 2H), 3.99 (s, 3H), 3.98 (s, 3H), 3.69 (t, *J* = 4.2 Hz, 2H), 3.60 (s, 3H), 3.26 (dd, *J* = 13.5, 4.8 Hz, 1H), 2.45 (s, 3H), 2.29 (ddd, *J* = 17.7, 12.0, 5.9 Hz, 2H), 2.22 – 2.12 (m, 1H), 1.85 (td, *J* = 11.8, 5.2 Hz, 1H) ppm.

FT-IR (KBr pellet): 3290, 2937, 1712, 1607, 1545, 1462, 1410, 1349, 1326, 1284, 1253, 1198, 1153, 1085, 1063, 1023 cm⁻¹.

ESI-MS (*m/z*): [M+Na]⁺ calcd 518, found 518, [2M+Na]⁺ calcd 1013, found 1013.

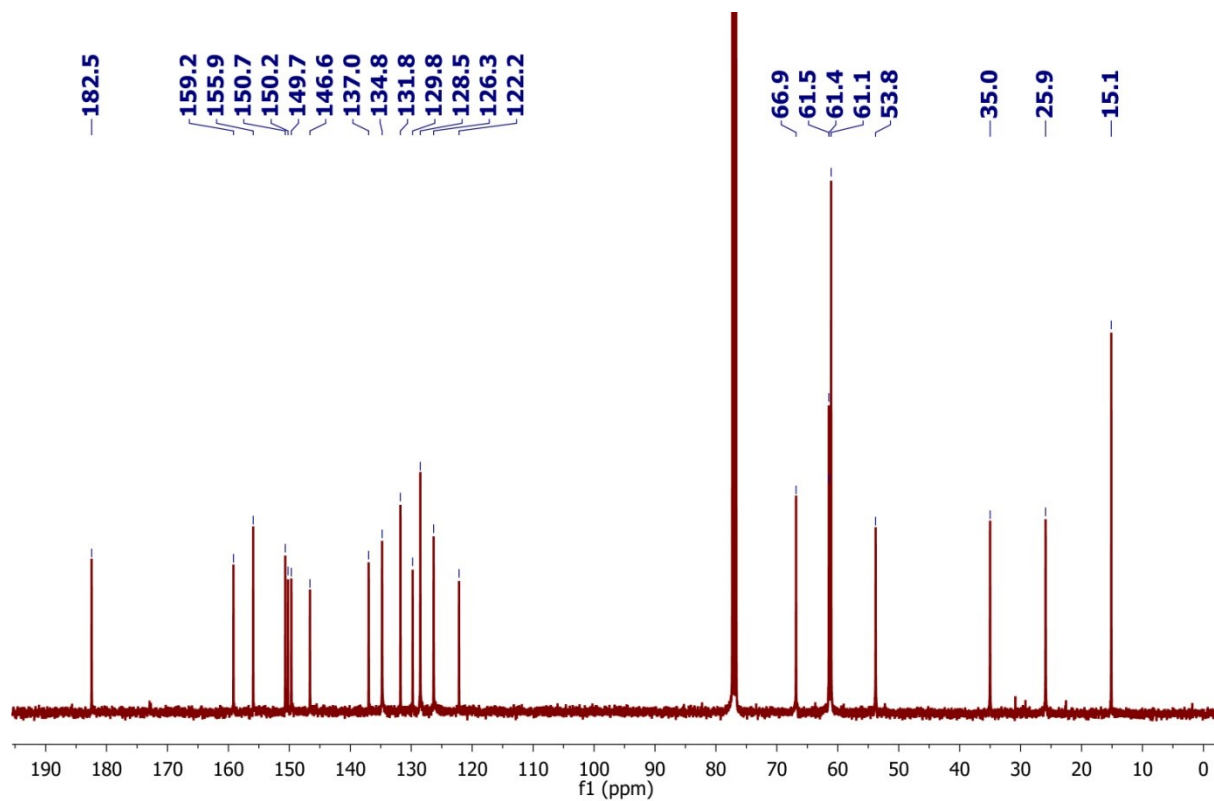


Figure C-3. The ^{13}C NMR spectrum of **2** in CDCl_3

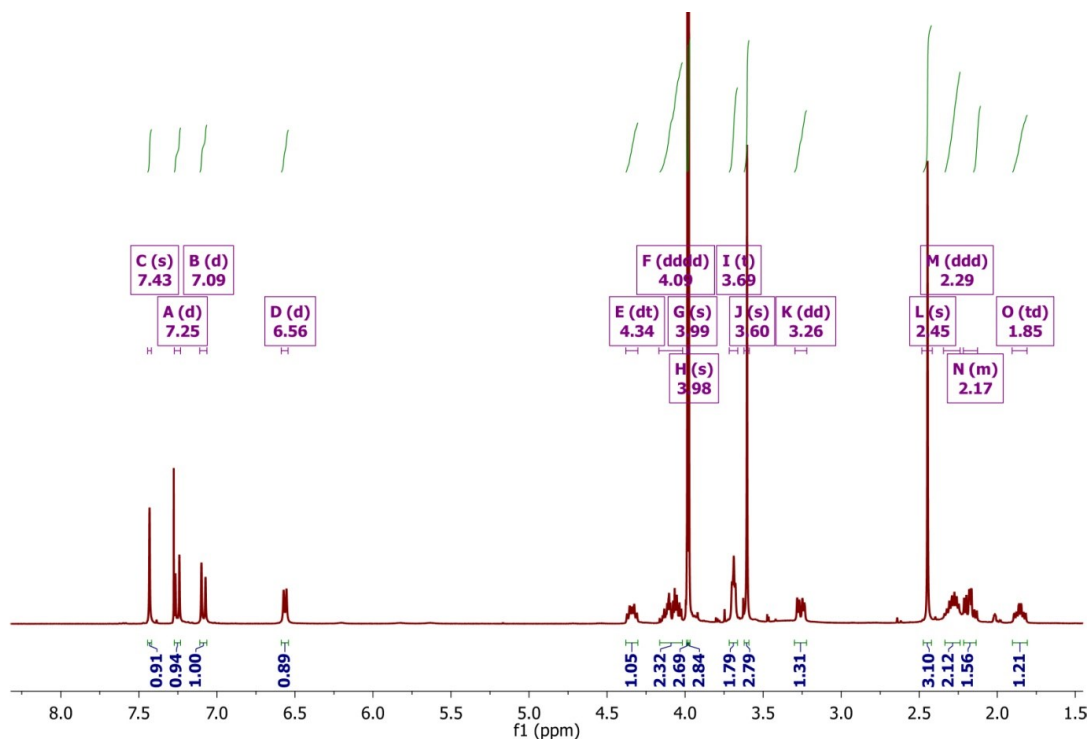
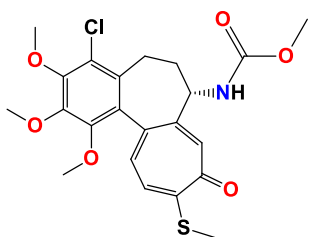


Figure C-4. The ^1H NMR spectrum of **2** in CDCl_3 .

Spectroscopic data of compound **3**



Chemical formula: $\text{C}_{22}\text{H}_{24}\text{ClNO}_6\text{S}$, MW = 466.0

g/mol;

^{13}C NMR (101 MHz, CDCl_3) δ 182.3, 159.2, 156.0, 150.1, 149.9, 149.7, 146.7, 136.5, 134.5, 131.7, 129.9, 128.5, 125.9, 122.1, 61.5, 61.4, 61.1, 53.6, 52.3, 35.2, 25.9, 15.2

ppm.

^1H NMR (403 MHz, CDCl_3) δ 7.34 (s, 1H), 7.22 (d, $J = 10.3$ Hz, 1H), 7.04 (d, $J = 10.5$ Hz, 1H), 5.65 (d, $J = 6.3$ Hz, 1H), 4.35 (dt, $J = 13.1, 6.7$ Hz, 1H), 3.99 (s, $J = 3.9$

Hz, 3H), 3.97 (s, 3H), 3.61 (s, 3H), 3.60 (s, 3H), 3.25 (dd, $J = 13.2, 4.3$ Hz, 1H), 2.44 (s, 3H), 2.33 – 2.12 (m, 2H), 1.75 (td, $J = 11.7, 5.7$ Hz, 1H) ppm.

FT-IR (KBr pellet): 3249, 2936, 1726, 1607, 1544, 1456, 1407, 1347, 1250, 1195, 1151, 1086, 1026 cm^{-1} .

ESI-MS (m/z): $[M+H]^+$ calcd 466, found 466, $[M+Na]^+$ calcd 488, found 488, $[2M+H]^+$ calcd 931, found 931, $[2M+Na]^+$ calcd 953, found 953.

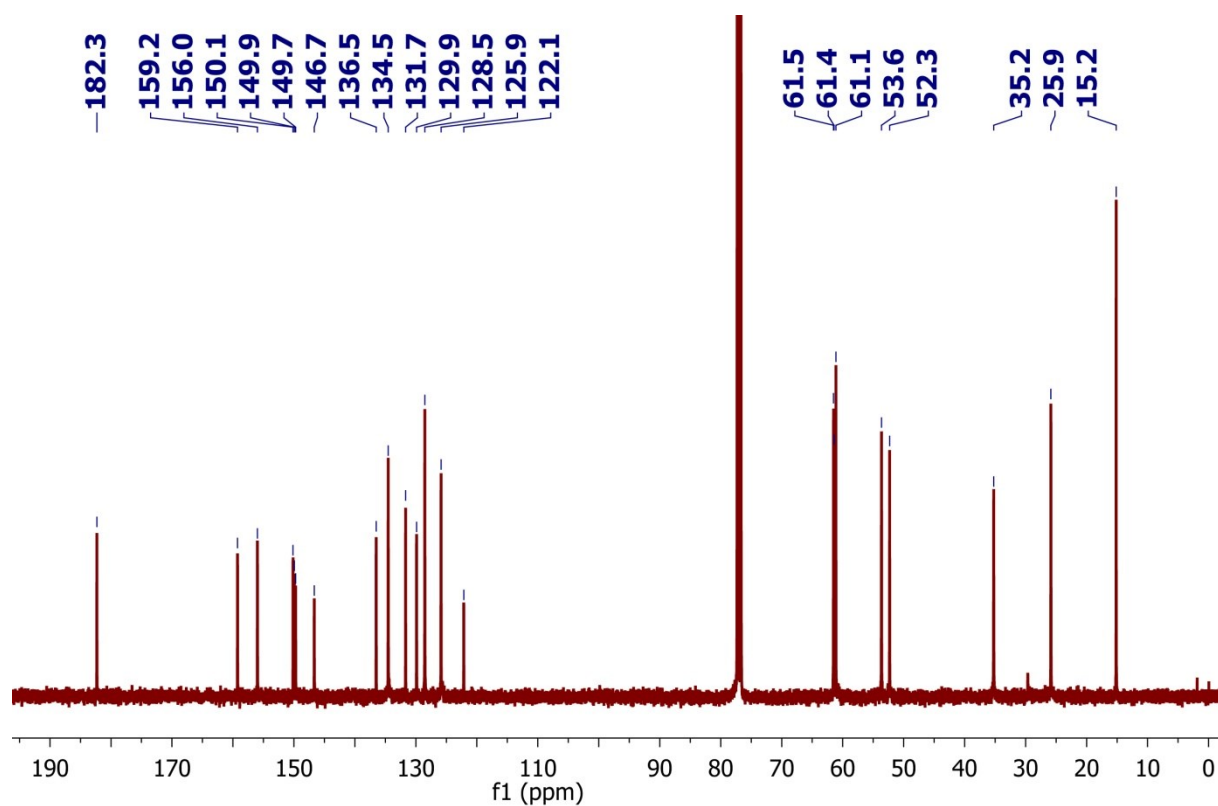


Figure C-5. The ^{13}C NMR spectrum of **3** in CDCl_3

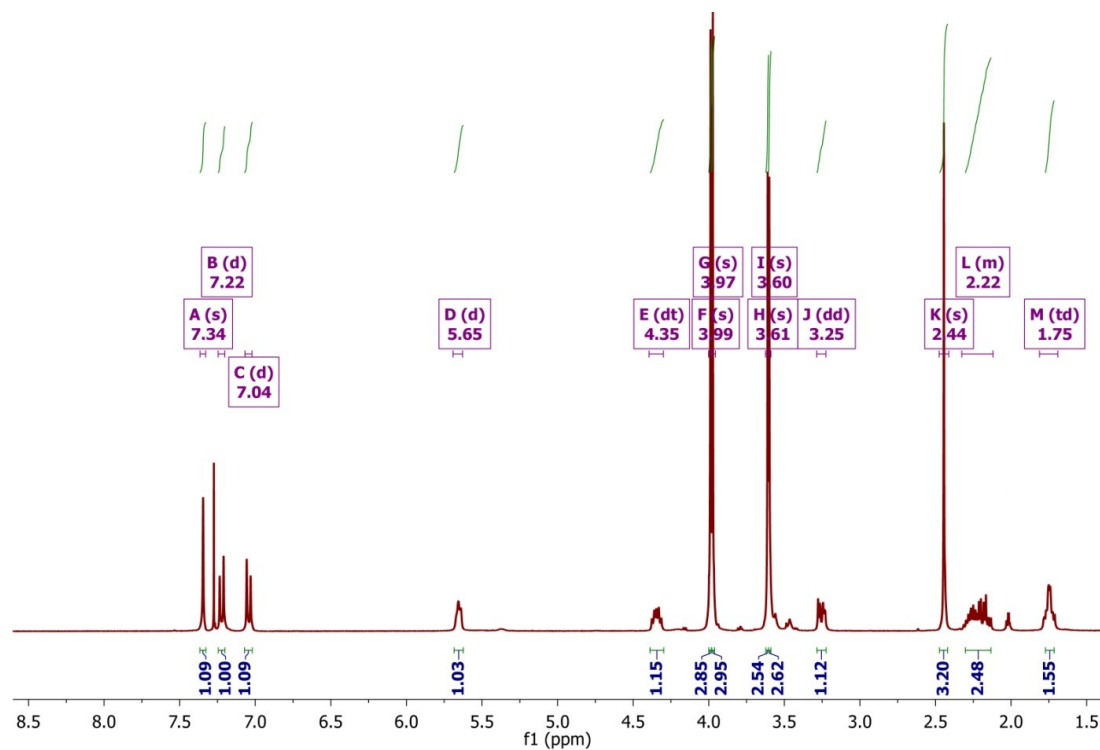
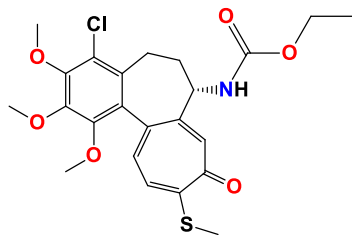


Figure C-6. The ^1H NMR spectrum of **3** in CDCl_3 .

Spectroscopic data of compound **4**



Chemical formula: $\text{C}_{23}\text{H}_{26}\text{ClNO}_6\text{S}$, MW = 480.0

g/mol;

^{13}C NMR (101 MHz, CDCl_3) δ 182.4, 159.2, 155.5, 150.2, 149.9, 149.7, 146.7, 136.5, 134.5, 131.7, 129.9, 128.6, 125.8, 122.1, 61.5, 61.4, 61.2, 61.1, 53.5, 35.4, 25.9, 15.2, 14.4 ppm.

^1H NMR (403 MHz, CDCl_3) δ 7.33 (s, 1H), 7.22 (d, J = 10.3 Hz, 1H), 7.04 (d, J = 10.5 Hz, 1H), 5.40 (d, J = 7.3 Hz, 1H), 4.34 (dt, J = 13.3, 6.7 Hz, 1H), 4.04 – 4.00 (m,

1H), 3.99 (s, 3H), 3.97 (s, 3H), 3.61 (s, 3H), 3.29 – 3.22 (m, 1H), 2.44 (s, 3H), 2.22 (dtd, $J = 31.8, 13.2, 6.1$ Hz, 2H), 1.77 – 1.70 (m, 2H), 1.19 (t, $J = 7.1$ Hz, 3H) ppm.

FT-IR (KBr pellet): 3293, 2933, 1715, 1608, 1549, 1462, 1409, 1349, 1326, 1249, 1198, 1151, 1086, 1023 cm^{-1} .

ESI-MS (m/z): $[\text{M}+\text{H}]^+$ calcd 480, found 480, $[\text{M}+\text{Na}]^+$ calcd 502, found 502, $[\text{2M}+\text{H}]^+$ calcd 959, found 959, $[\text{2M}+\text{Na}]^+$ calcd 981, found 981.

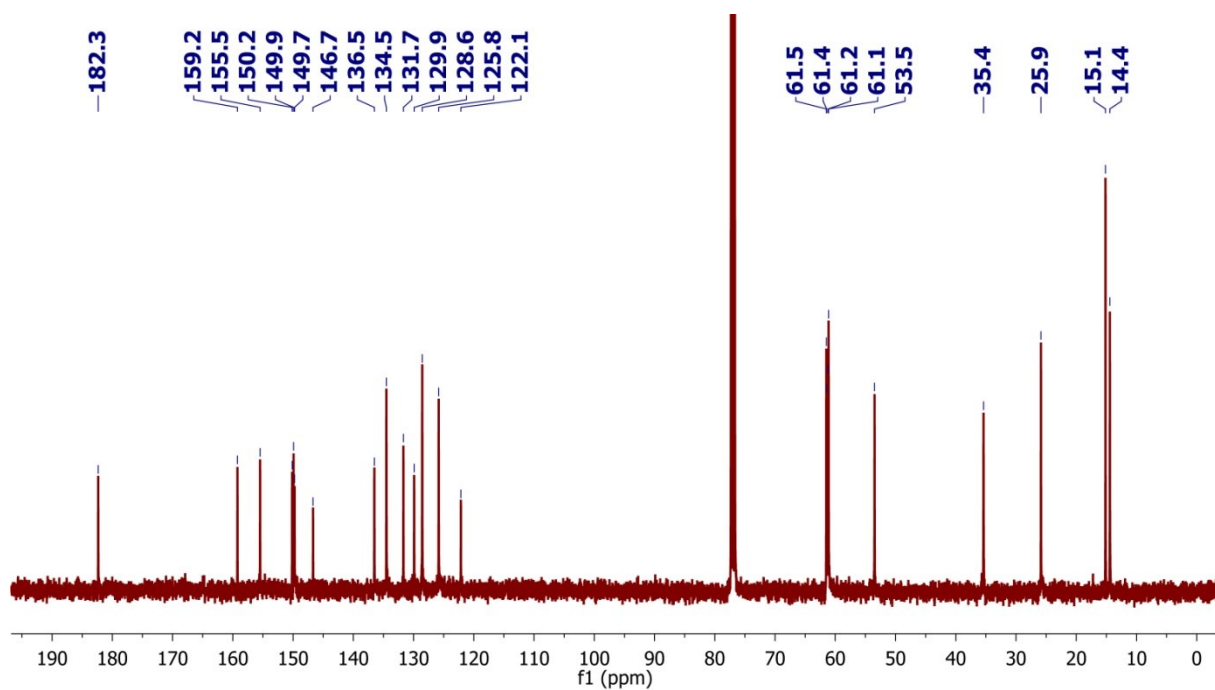


Figure C-7. The ^{13}C NMR spectrum of **4** in CDCl_3

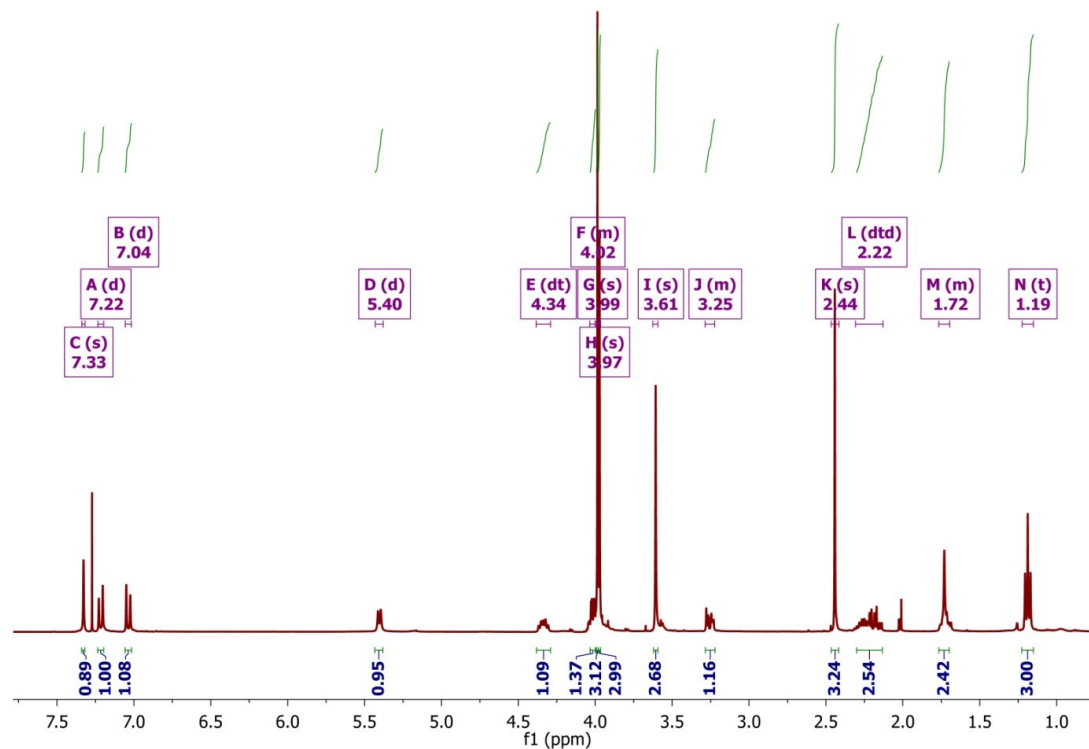
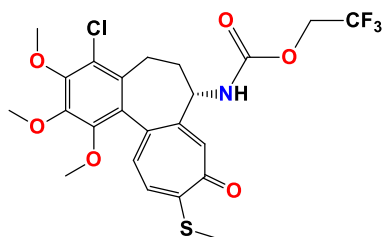


Figure C-8. The ^1H NMR spectrum of **4** in CDCl_3 .

Spectroscopic data of compound **5**



Chemical formula: $\text{C}_{23}\text{H}_{23}\text{ClF}_3\text{NO}_6\text{S}$, MW = 534.0 g/mol

^{13}C NMR (101 MHz, CDCl_3) δ 182.4, 159.5, 153.6, 150.3, 149.7, 149.6, 146.7, 136.5, 134.8, 131.7, 129.7, 128.6, 126.1, 124.2, 122.3, 121.4, 61.5, 61.3, 61.1, 61.1, 60.7, 54.1, 35.2, 25.9, 15.2 ppm.

^1H NMR (403 MHz, CDCl_3) δ 7.44 (s, 1H), 7.27 – 7.24 (m, 1H), 7.09 (d, $J = 10.6$ Hz, 1H), 6.55 (s, 1H), 4.48 (dq, $J = 12.7, 8.5$ Hz, 1H), 4.36 (dt, $J = 11.9, 6.9$ Hz, 1H), 4.07 (dq, $J = 12.7, 8.4$ Hz, 1H), 3.99 (s, 3H), 3.98 (s, 3H), 3.59 (s, 3H), 3.29 (dd, J

= 13.7, 5.0 Hz, 1H), 2.45 (s, 3H), 2.35 (ddd, $J = 18.0, 12.2, 6.0$ Hz, 1H), 2.20 (td, $J = 13.5, 6.3$ Hz, 1H), 1.91 (td, $J = 11.8, 5.9$ Hz, 1H) ppm.

^{19}F NMR (379 MHz, CDCl_3) δ -74.8 ppm.

FT-IR (KBr pellet): 3231, 2940, 1737, 1609, 1545, 1464, 1411, 1351, 1283, 1245, 1163, 1086, 1024 cm^{-1} .

ESI-MS (m/z): $[\text{M}+\text{H}]^+$ calcd 534, found 534, $[\text{M}+\text{Na}]^+$ calcd 556, found 556, $[2\text{M}+\text{Na}]^+$ calcd 1089, 1091, found 1091.

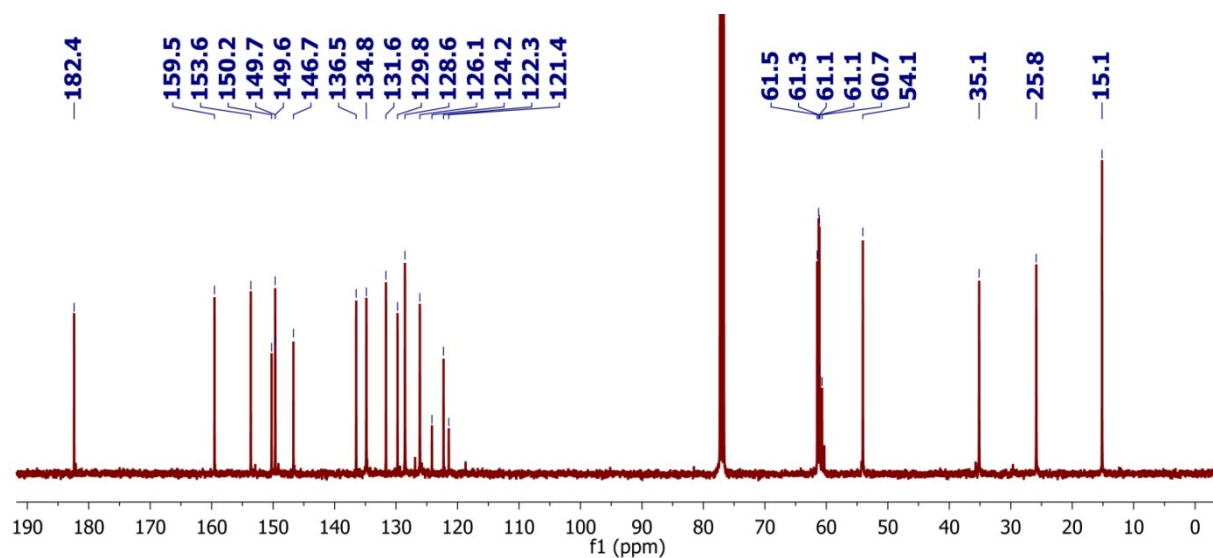


Figure C-9. The ^{13}C NMR spectrum of **5** in CDCl_3 .

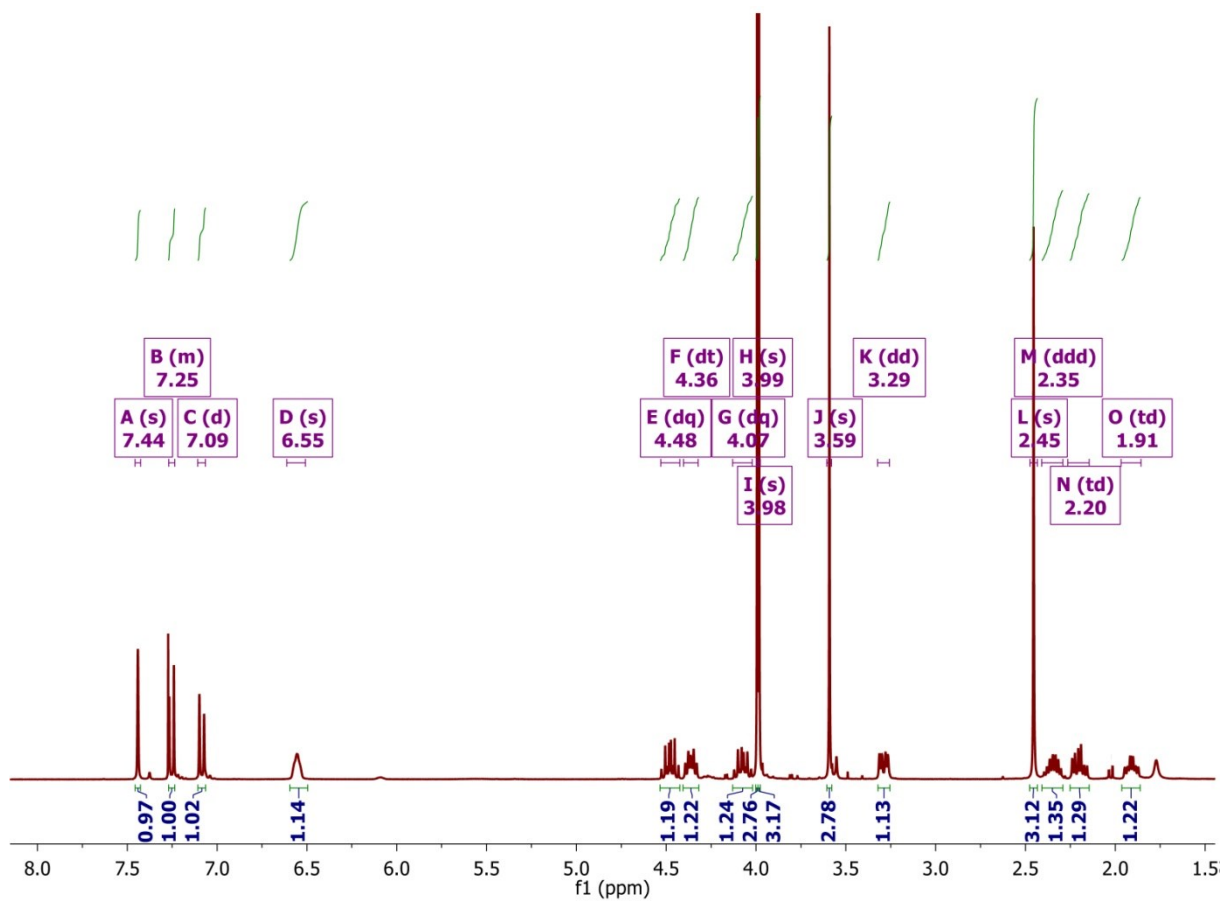


Figure C-10. The ^1H NMR spectrum of **5** in CDCl_3

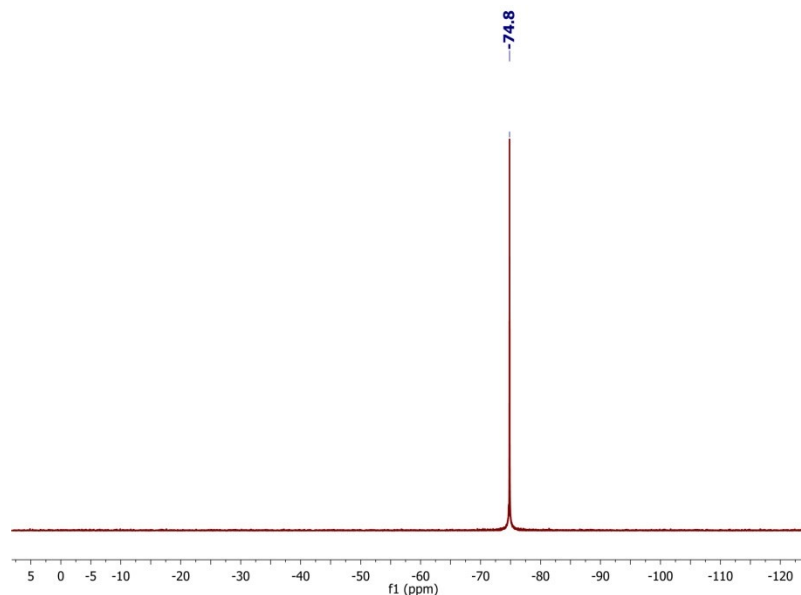
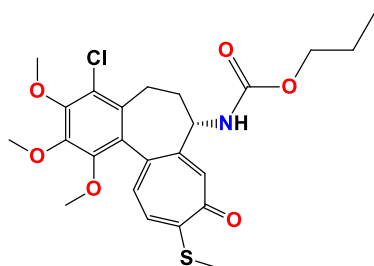


Figure C-11. The ^{19}F NMR spectrum of **5** in CDCl_3 .

Spectroscopic data of compound **6**



Chemical formula: $\text{C}_{24}\text{H}_{28}\text{ClNO}_6\text{S}$, MW = 494.0

g/mol;

^{13}C NMR (101 MHz, CDCl_3) δ 182.3, 159.2, 155.6, 150.2, 149.9, 149.7, 146.7, 136.5, 134.5, 131.7, 129.9, 128.5, 125.8, 122.1, 66.9, 61.5, 61.4, 61.1, 53.5,

35.4, 25.9, 22.1, 15.1, 10.2 ppm.

^1H NMR (403 MHz, CDCl_3) δ 7.33 (s, 1H), 7.22 (d, $J = 10.3$ Hz, 1H), 7.04 (d, $J = 10.5$ Hz, 1H), 5.41 (d, $J = 7.1$ Hz, 1H), 4.34 (dt, $J = 13.2, 6.7$ Hz, 1H), 3.99 (s, 3H), 3.97 (s, 3H), 3.95 – 3.89 (m, 2H), 3.61 (s, 3H), 3.29 – 3.22 (m, 1H), 2.44 (s, 3H), 2.24 (ddd, $J = 16.7, 12.6, 7.2$ Hz, 2H), 1.74 (s, 1H), 1.58 (dd, $J = 14.2, 7.1$ Hz, 2H), 0.89 (t, $J = 7.4$ Hz, 3H) ppm.

FT-IR (KBr pellet): 3290, 2935, 1714, 1608, 1550, 1462, 1409, 1349, 1248, 1151, 1085, 1023 cm^{-1} .

ESI-MS (m/z): [M+H]⁺ calcd 494, found 494, [M+Na]⁺ calcd 516, found 516, [2M+H]⁺ calcd 987, found 987.

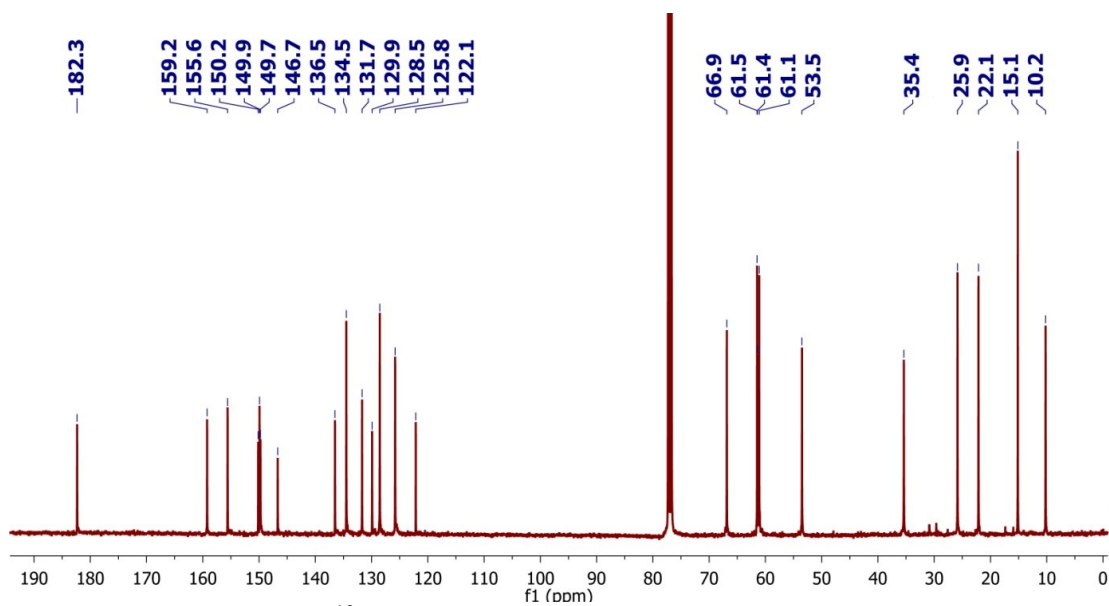


Figure C-12. The ¹³C NMR spectrum of **6** in CDCl₃.

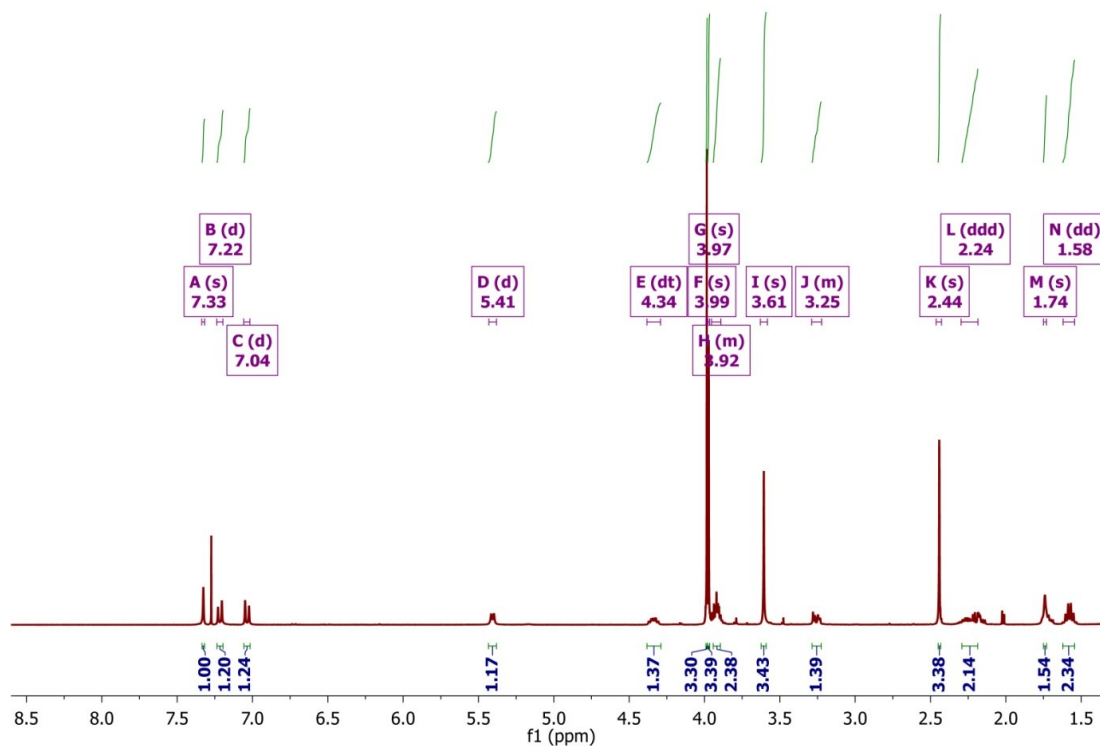
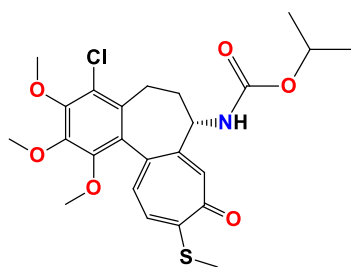


Figure C-13. The ^1H NMR spectrum of **6** in CDCl_3

Spectroscopic data of compound **7**



Chemical formula: $\text{C}_{24}\text{H}_{28}\text{ClNO}_6\text{S}$, MW = 494.0

g/mol;

^{13}C NMR (101 MHz, CDCl_3) δ 182.4, 159.2, 155.0, 150.2, 149.9, 149.8, 146.7, 136.5, 134.5, 131.7, 129.9, 128.5, 125.8, 122.1, 68.7, 61.5, 61.5, 61.1, 53.4, 35.5, 25.9, 22.1, 22.1, 15.2 ppm.

^1H NMR (403 MHz, CDCl_3) δ 7.30 (s, 1H), 7.21 (d, $J = 10.4$ Hz, 1H), 7.03 (d, $J = 10.5$ Hz, 1H), 5.20 (d, $J = 7.3$ Hz, 1H), 4.78 (dt, $J = 12.5, 6.3$ Hz, 1H), 4.33 (dt, $J = 13.4, 6.8$ Hz, 1H), 3.99 (s, 3H), 3.97 (s, 3H), 3.61 (s, 3H), 3.29 – 3.22 (m, 1H), 2.44 (s,

3H), 2.31 – 2.19 (m, 2H), 1.67 (dd, $J = 12.2, 5.4$ Hz, 1H), 1.18 (dd, $J = 8.6, 6.3$ Hz, 6H) ppm.

FT-IR (KBr pellet): 3304, 2978, 2936, 1711, 1608, 1551, 1462, 1408, 1349, 1251, 1147, 1086, 1023 cm^{-1} .

ESI-MS (m/z): $[M+H]^+$ calcd 494, found 494, $[M+Na]^+$ calcd 516, found 516, $[2M+H]^+$ calcd 987, found 987.

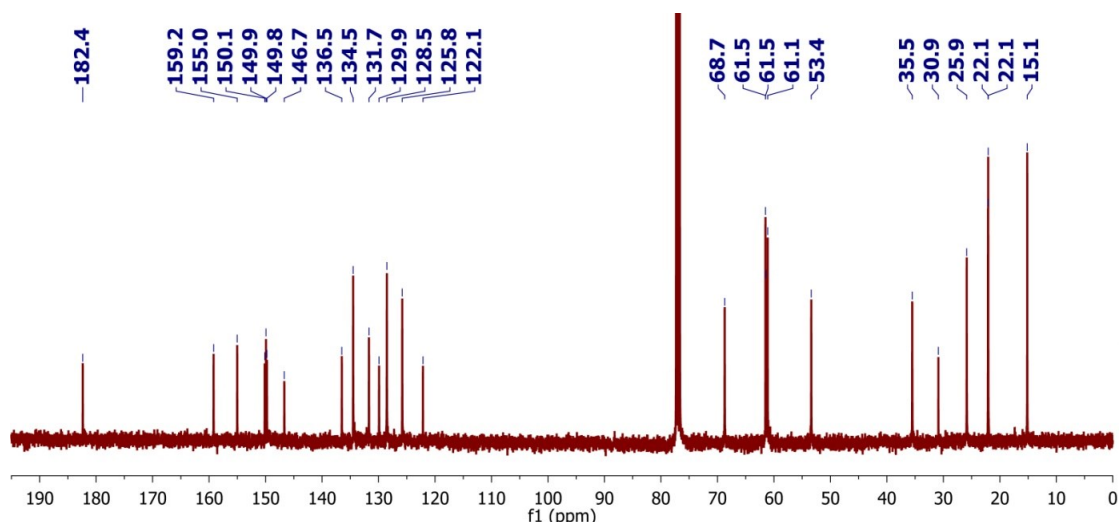


Figure C-14. The ^{13}C NMR spectrum of **7** in CDCl_3 .

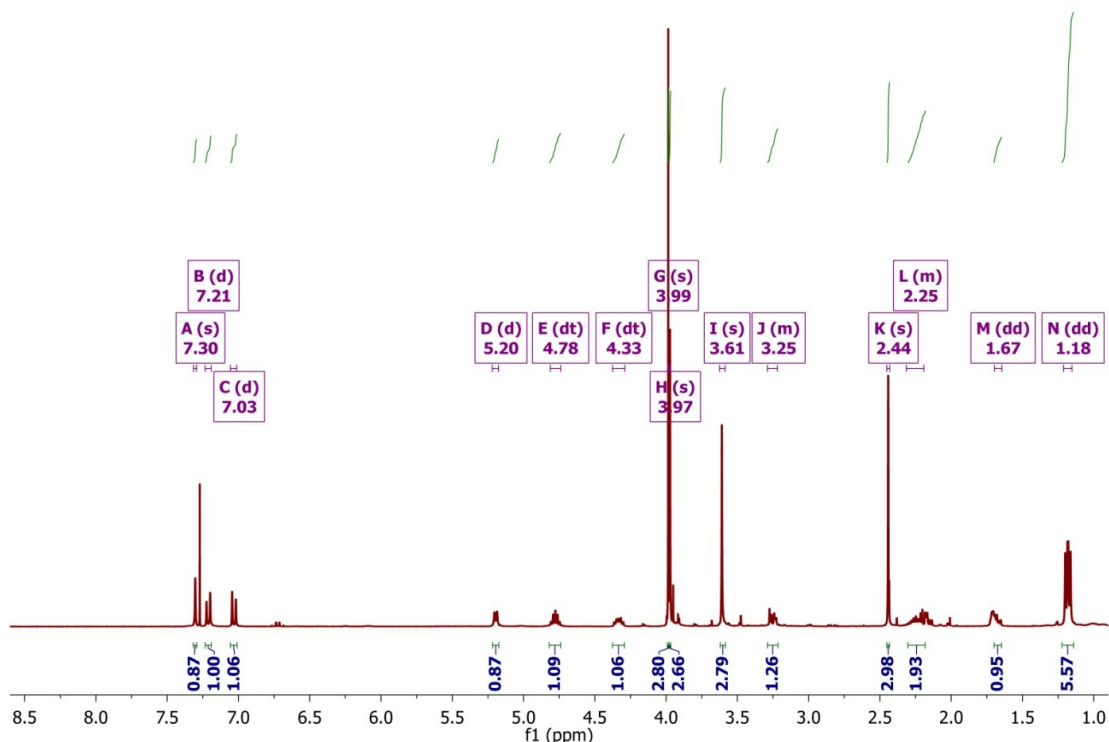
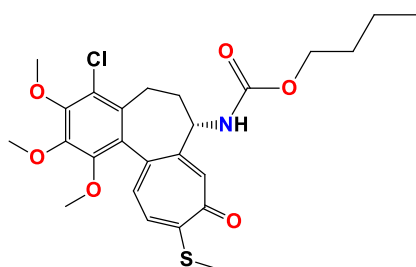


Figure C-15. The ^1H NMR spectrum of **7** in CDCl_3 .

Spectroscopic data of compound **8**



Chemical formula: $\text{C}_{25}\text{H}_{30}\text{ClNO}_6\text{S}$, MW = 508.0 g/mol

^{13}C NMR (101 MHz, CDCl_3) δ 182.3, 159.2, 155.6, 150.1, 150.0, 149.7, 146.7, 136.5, 134.5, 131.7, 129.9, 128.6, 125.8, 122.1, 65.1, 61.5, 61.4, 61.1, 53.5, 35.4, 30.8, 25.9, 19.0, 15.1, 13.6 ppm.

^1H NMR (403 MHz, CDCl_3) δ 7.33 (s, 1H), 7.22 (d, $J = 10.3$ Hz, 1H), 7.04 (d, $J = 10.5$ Hz, 1H), 5.46 (d, $J = 7.3$ Hz, 1H), 4.34 (dt, $J = 13.2, 6.7$ Hz, 1H), 3.99 (s, 3H), 3.97 (s, 3H), 3.95 – 3.91 (m, 2H), 3.61 (s, 3H), 3.29 – 3.23 (m, 1H), 2.44 (s, 3H), 2.32 –

2.18 (m, 2H), 1.73 (dd, $J = 12.2, 6.2$ Hz, 1H), 1.58 – 1.49 (m, 2H), 1.31 (tt, $J = 12.6, 6.5$ Hz, 2H), 0.89 (t, $J = 7.4$ Hz, 3H) ppm.

FT-IR (KBr pellet): 3286, 2935, 1715, 1608, 1549, 1462, 1408, 1349, 1249, 1150, 1085, 1024 cm^{-1} .

ESI-MS (m/z): $[\text{M}+\text{H}]^+$ calcd 508, found 508, $[\text{M}+\text{Na}]^+$ calcd 530, found 530, $[\text{2M}+\text{H}]^+$ calcd 1015, found 1015, $[\text{2M}+\text{Na}]^+$ calcd 1037, found 1037.

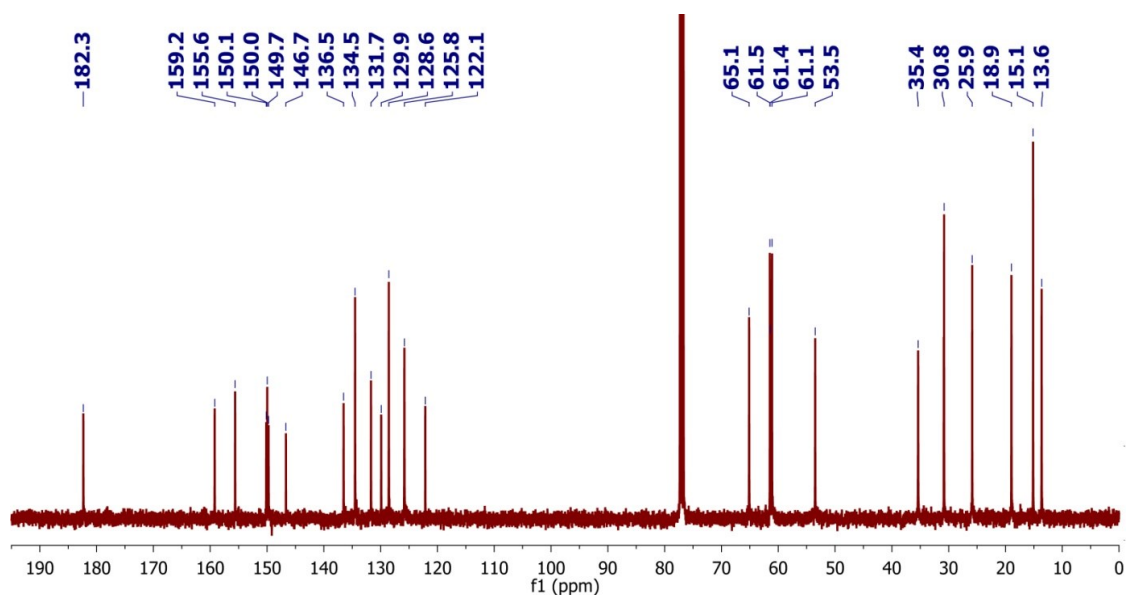


Figure C-16. The ^{13}C NMR spectrum of **8** in CDCl_3 .

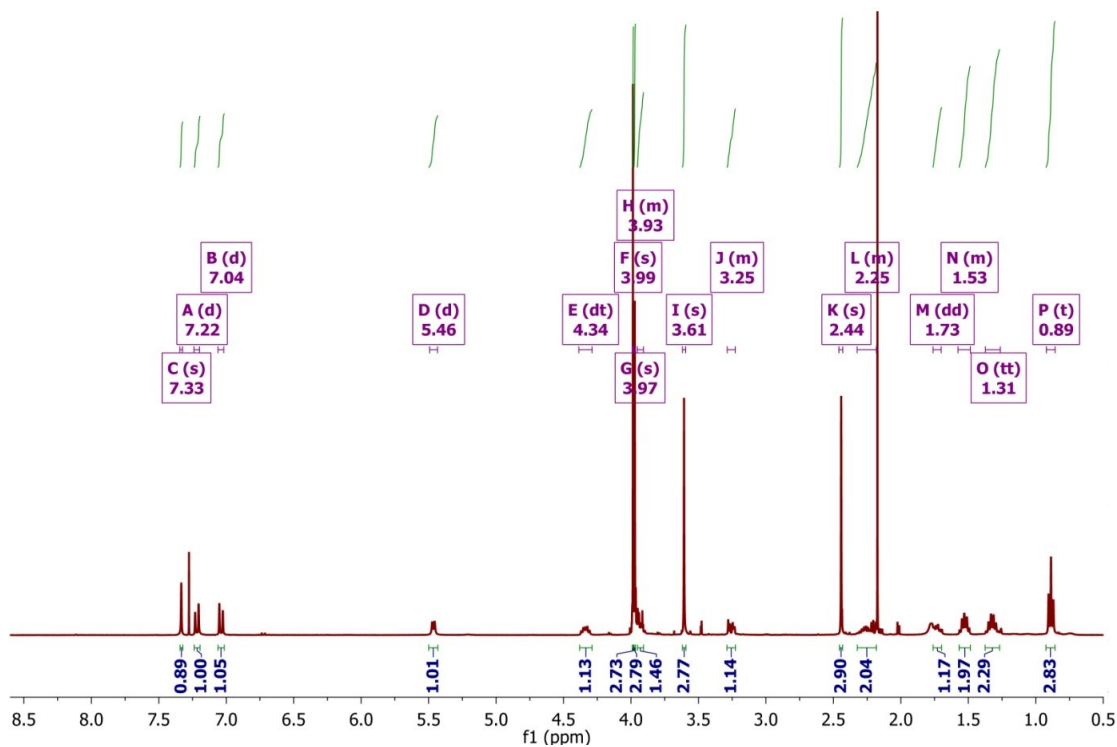
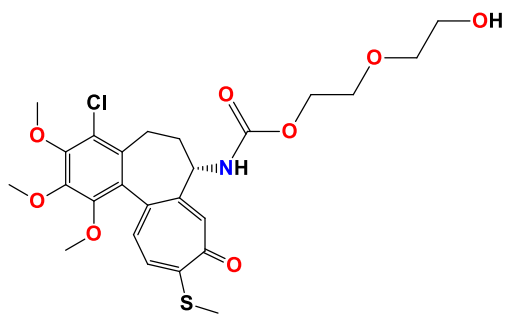


Figure C-17. The ^1H NMR spectrum of **8** in CDCl_3 .

Spectroscopic data of compound **9**



Chemical formula: $\text{C}_{25}\text{H}_{30}\text{ClNO}_8\text{S}$,
MW = 540.0 g/mol;

^{13}C NMR (101 MHz, CDCl_3) δ 182.4,
159.3, 155.4, 150.2, 150.2, 149.7, 146.6,
136.7, 134.7, 131.7, 129.8, 128.3, 126.1,
122.1, 72.5, 69.1, 64.2, 61.5, 61.4, 61.4, 61.1,

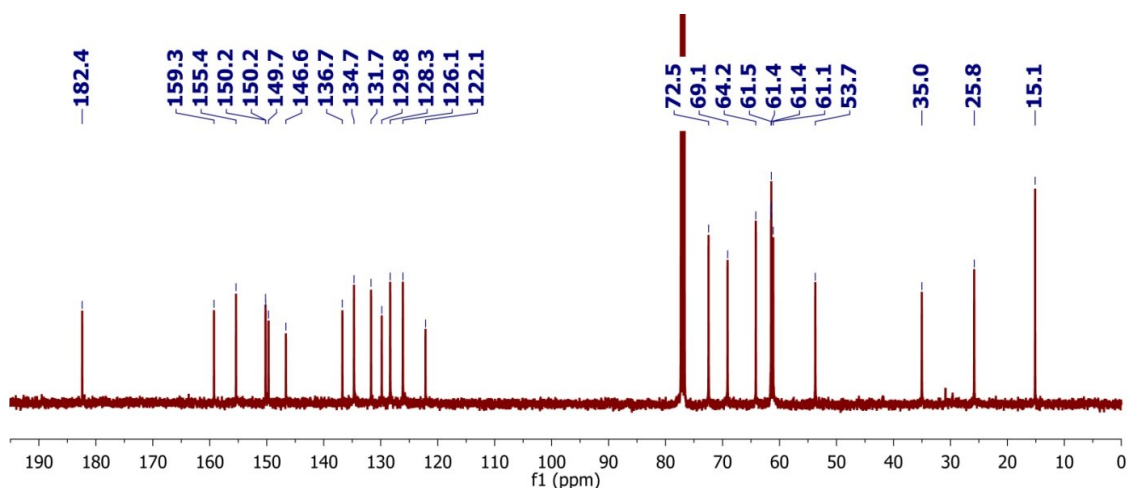
53.7, 35.0, 25.8, 15.1 ppm.

^1H NMR (403 MHz, CDCl_3) δ 7.36 (s, 1H), 7.25 – 7.21 (m, 1H), 7.06 (d, J = 10.6 Hz, 1H), 6.04 (d, J = 7.2 Hz, 1H), 4.36 – 4.21 (m, 2H), 4.08 (ddd, J = 13.6, 7.1, 4.1 Hz, 1H), 3.99 (s, 3H), 3.97 (s, 3H), 3.73 (ddd, J = 11.8, 8.8, 4.1 Hz, 2H), 3.64 (dd, J =

5.7, 3.5 Hz, 2H), 3.61 – 3.57 (m, 5H), 3.29 – 3.23 (m, 1H), 2.44 (d, $J = 5.8$ Hz, 3H), 2.34 – 2.19 (m, 2H), 1.77 (td, $J = 11.4, 4.8$ Hz, 1H) ppm.

FT-IR (KBr pellet): 3285, 2937, 1715, 1607, 1547, 1461, 1409, 1350, 1253, 1136, 1083, 1023 cm^{-1} .

ESI-MS (m/z): $[\text{M}+\text{H}]^+$ calcd 540, found 540, $[\text{M}+\text{Na}]^+$ calcd 562, found 562, $[2\text{M}+\text{Na}]^+$ calcd 1101, found 1101.



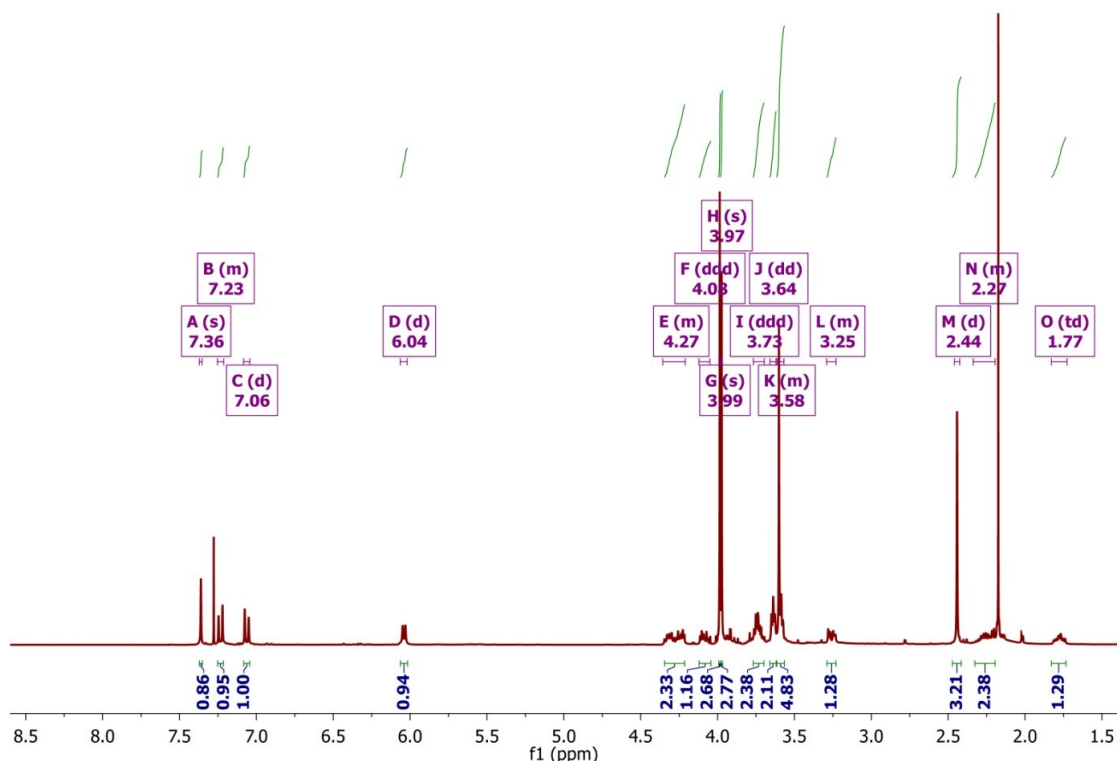


Figure C-19. The ^1H NMR spectrum of **9** in CDCl_3 .

Antiproliferative activity of colchicine and its derivatives

Four human cancer cell lines and one murine normal cell line were used to evaluate antiproliferative activity of colchicine and its derivatives (**1-9**): human lung adenocarcinoma (A549), human breast adenocarcinoma (MCF-7), human colon adenocarcinoma cell lines sensitive and resistant to doxorubicin (LoVo) and (LoVo/DX) respectively, and also normal murine embryonic fibroblast cell line (BALB/3T3). The BALB/3T3 cell line was purchased from the American Type Culture Collection (ATCC Manassas, VA, USA), A549 and MCF-7 cell lines – from European Collection of Authenticated Cell Cultures (Salisbury, UK), LoVo cell line was purchased from the American Type Culture Collection (ATCC, Manassas, VA, USA), and LoVo/DX by courtesy of Prof. E. Borowski (Technical University of Gdańsk, Gdańsk, Poland). All

the cell lines are maintained in the Institute of Immunology and Experimental Therapy (IET), Wrocław, Poland. Human lung adenocarcinoma cell line was cultured in mixture of OptiMEM and RPMI 1640 (1:1) medium (IET, Wrocław, Poland), supplemented with 5% foetal bovine serum (GE Healthcare, Logan UT, USA) and 2 mM L-glutamine (Sigma-Aldrich, Merck KGaA, Saint Louis, MO, USA). Human breast adenocarcinoma cell line was cultured in mixture of Eagle medium (IET, Wrocław, Poland), supplemented with 10% foetal bovine serum, 2 mM L-glutamine, 8 µg/ml insulin and 1% amino-acids (Sigma-Aldrich, Merck KGaA, Saint Louis, MO, USA). Human colon adenocarcinoma cell lines were cultured in mixture of OptiMEM and RPMI 1640 (1:1) medium (IET, Wrocław, Poland), supplemented with 5% foetal bovine serum (GE Healthcare, Logan, UT, USA), 2 mM L-glutamine, 1 mM sodium pyruvate (Sigma-Aldrich, Merck KGaA, Saint Louis, MO, USA) and 10 µg/100 ml doxorubicin for LoVo/DX (Sigma-Aldrich, Merck KGaA, Saint Louis, MO, USA). Murine embryonic fibroblast cells were cultured in Dulbecco medium (Life Technologies Limited, Paisley, UK), supplemented with 10% foetal bovine serum (GE Healthcare, Logan, UT, USA) and 2 mM glutamine (Sigma-Aldrich, Merck KGaA, Saint Louis, MO, USA). All culture media contained antibiotics: 100 U/ml penicillin and 100 µg/ml streptomycin (Polfa-Tarchomin, Warsaw, Poland). All cell lines were cultured during entire experiment in humid atmosphere at 37°C and 5% CO₂. Cells were tested for mycoplasma contamination by mycoplasma detection kit for conventional PCR: Venor GeM Classic (Minerva Biolabs GmbH, Berlin, Germany) and negative results was obtained. The mycoplasma contamination test is repeated once a year or after thawing in case of less frequently used lines.

The antiproliferative assay *in vitro*

Twenty-four hours before adding the tested compounds, all cell lines were seeded in 96-well plates (Sarstedt, Nümbrecht, Germany) in appropriate media with 10⁴ cells per well. All cell lines were exposed to each tested agent at four different

concentrations in the range 100 – 0.001 µg/ml for 72 h. Cells were also exposed to the reference drug cisplatin (Teva Pharmaceuticals Polska, Warsaw, Poland) and doxorubicin (Accord Healthcare Limited, Middlesex, UK). Additionally, all cell lines were exposed to DMSO (solvent used for tested compounds) (POCh, Gliwice, Poland) at concentrations corresponding to these present in tested agents' dilutions. After 72 h sulforhodamine B assay (SRB) was performed [2]. Compounds at each concentration were tested in triplicates in a single experiment and each experiment was repeated at least three times independently.

SRB

After 72 h of incubation with the tested compounds, cells were fixed in situ by gently adding of 50 µl per well of cold 50% trichloroacetic acid TCA (POCh, Gliwice, Poland) and were incubated at 4°C for one hour. Following, wells were washed four times with water and air dried. Next, 50 µl of 0.1% solution of sulforhodamine B (Sigma–Aldrich, Merck KGaA, Saint Louis, MO, USA) in 1% acetic acid (POCh, Gliwice, Poland) were added to each well and plates were incubated at room temperature for 0.5 h. After incubation time, unbound dye was removed by washing plates four times with 1% acetic acid whereas stain bound to cells was solubilized with 10 mM Tris base (Sigma–Aldrich, Merck KGaA, Saint Louis, MO, USA). Absorbance of each solution was read at Synergy H4 Hybrid Multi-Mode Microplate Reader (BioTek Instruments, Inc., Winooski VT, USA) at the 540 nm wavelength.

Results are presented as mean IC₅₀ (concentration of the tested compound, that inhibits cell proliferation by 50%) ± standard deviation. IC₅₀ values were calculated in Cheburator 0.4, Dmitry Nevozhay software (version 1.2.0 software by Dmitry Nevozhay, 2004–2014, <http://www.cheburator.nevozhay.com>, freely available) for each experiment [3]. Compounds at each concentration were tested in triplicates in a single experiment and each experiment was repeated at least three times independently.

Molecular docking simulations

Molecular docking was combined with other computational methods to explore ligand-tubulin interactions for the compounds discussed in this chapter. AutoDock4 software [4] is one of the molecular docking software packages, which consists of two main modules: (i) autodock, which performs the docking of the ligand to a set of grids describing the target protein; and (ii) autogrid, which pre-calculates these grids. In this article, flexible ligand and rigid receptor conditions were used to dock a small library of the investigated colchicine derivatives to the target protein structure (see Table 5-2). The ligand structures were then fully optimized on the basis of the RHF/cc-pVDZ [5] level of theory implemented in the software package GAMESS-US, version 2010-10-01 [6-8]. Since there is no crystal structure for human β I tubulin (UniProt ID: P07437) available in the Protein Data Bank (PDB), the bovine tubulin structure 1SA0.pdb was used as a template to construct the homology model for human β I tubulin using the software package MOE2015.

The Moriguchiocanol-water partition coefficient (MLogP), a useful factor in estimating and comparing the distribution of the drugs within the cells, organs and the body was calculated using the software package called ADMET Predictor 8.0 (ADMET Predictor, Simulations Plus, Lancaster, CA, USA).

To build a 3D model for the α - β I tubulin heterodimer, The Molecular Operating Environment (MOE) software package was used [9]. The protein amino acid sequence UniProt ID [10]: P07437 and UniProt ID: Q71U36 corresponding to the respective gene TUBB and gene TUBA1A was used to represent human β -tubulin and α -tubulin, respectively. The best model was chosen by setting the number of generated models to 10 and by selecting the final model based on MOE's Generalized Born/Volume Integral (GB/VI) scoring function *via* homology modelling. The crystallographic structure of α - β IIb tubulin isotype complexed with colchicine (PDB ID: 1SA0) was applied as a template [11]. The final model was eventually protonated at neutral pH and minimized using a MOE's built-in protocol. It should also be mentioned that cofactors including

GTP, GDP, colchicine and the magnesium ion located at the interface between α - and β -monomers were taken as part of the molecular environment during the modelling exercise.

Molecular dynamics (MD) simulations were run using Amber14 to equilibrate the final model and to obtain representative conformations [12]. In order to generate MD parameters - e.g. partial charges, force constants, *etc.*, for the four cofactors from the Gasteiger charge method, Amber's antechamber utility was used. TIP3P water was selected as a solvent *via* Amber's tleap program. Minimization of the structure was carried out in two steps which both use the steepest descent and conjugate gradient methods. A 2 ps minimization on solvent atoms only was performed, by restraining the protein-ligand complex. Next, minimization was run without restraint for 10 ps. A 20 and 40 ps equilibration was performed on the system in an NVT and NPT ensemble, respectively. The temperature was set to 298K and 1 bar pressure was applied. Finally, MD production was run for 70 ns. The root-mean-square deviation (RMSD) of both the entire tubulin structure and the colchicine-binding site were found to plateau after 40 ns.

In order to identify representative conformations of the tubulin dimer, clustering analysis was made by Amber's cpptraj program for the last 30 ns of the generated MD trajectory [13] Using the RMSD of atoms in the colchicine-binding site as a metric, clustering was carried out *via* a hierarchical agglomerative and an RMSD cutoff of 1.0 Å, which led to three representative structures of the tubulin dimer. The structures were further used as a rigid target for the screening of 4-chlorothiocolchicine derivatives.

Docking binding energies were calculated for 4-chlorothiocolchicinederivatives using the AutoDockVina program, which makes use of an iterated local search global optimizer [14]. A cubic box with size 30.0 Å centred at the centre of mass of the bound colchicine derivative was used for our docking simulations. Our calculation was run separately between each of the three tubulin representative structures and our colchicine derivative library. Here, the best pose was used as the initial configuration for MM/PBSA computations for each compound/tubulin isotype pair.

The free energy associated with binding of 4-chlorothiocolchicine derivatives was calculated by the Molecular Mechanics Poisson–Boltzmann Surface Area (MM/PBSA) technique [15,16]. This method is based on molecular mechanics that consider solvents as continuum solvation models. The binding free energy is estimated as $\Delta G_{bind} = \langle \Delta E_{MM} \rangle - T\Delta S + \Delta G_{solv}$, where $\langle \Delta E_{MM} \rangle - T\Delta S$ can be regarded as the change in the free energy of the system in vacuum (gas phase). It includes the change in the molecular mechanics energy $\langle \Delta E_{MM} \rangle = \langle E_{MM} \rangle_{bound} - \langle E_{MM} \rangle_{unbound}$ and the change in the conformational entropy ΔS due to the binding. Since the difference in the structure of our colchicine derivatives is small, it is assumed that they provide comparable ΔS values so the calculation of ΔS is not necessary when calculating ΔG_{bind} . The value of ΔG_{solv} represents the difference in solvation free energies because of binding, which is given as $\Delta G_{solv} = \Delta G_{solv}^{complex} - \Delta G_{solv}^{lig} - \Delta G_{solv}^{prot}$ where each term on the right-hand side is the sum of polar and nonpolar contributions. Either the Generalized-Born (GB) model or the Poisson-Boltzmann (PB) equation can be used for the calculations of the polar parts. The nonpolar terms are estimated from a linear relation to the solvent accessible surface area (SASA). The values of $\langle \Delta E_{MM} \rangle$ and ΔG_{solv} are generally computed as ensemble averages requiring a short MD trajectory of the solvated complexed system as the input of the MM/PBSA method. In this article, an MD simulation was run for each of the best docking poses of ligand-beta tubulin isotypes in TIP3P water for 1ns using Amber14 and 200 frames of each MD trajectory were collected for the subsequent MM/PBSA and MM/GBSA calculations. For PB calculations, an ionic strength of 0.0 nM (istrng=0.0) and a solvent probe radius of 1.6 Å (prbrad=1.6) were used. For GBSA calculations, the igb parameter was set to 5 that corresponds to a modified GB model equivalent to model II in reference [17].

References

- [1] Kerkes, P.; Sharma, P. N.; Brossi, A.; Chignell, C. F.; Quinn, F. R. Synthesis and biological effects of novel thiocolchicines. 3. evaluation of N-acyldeacetylthiocolchicines, N-(alkoxycarbonyl)deacetylthiocolchicines, and O-ethyl-demethylthiocolchicines. New synthesis of thiodemecolcine and antileukemic effects of 2-demethyl- and 3-demethylthiocolchicine. *J. Med. Chem.* 1985, 28, 1204–1208, doi:10.1021/jm00147a014.
- [2] Skehan, P.; Storeng, R.; Scudiero, D.; Monks, A.; McMahon, J.; Vistica, D.; Warren, J. T.; Bokesch, H.; Kenney, S.; Boyd, M. R. New colorimetric cytotoxicity assay for anticancer-drug screening. *J. Natl. Cancer Inst.* 1990, 82, 1107–12.
- [3] Nevozhay, D. Cheburator Software for Automatically Calculating Drug Inhibitory Concentrations from *In vitro* Screening Assays. *PLoS One* 2014, 9, e106186, doi:10.1371/journal.pone.0106186.
- [4] Morris, G. M.; Huey, R.; Lindstrom, W.; Sanner, M. F.; Belew, R. K.; Goodsell, D. S.; Olson, A. J. AutoDock4 and AutoDockTools4: Automated docking with selective receptor flexibility. *J. Comput. Chem.* 2009, 30, 2785–2791, doi:10.1002/jcc.21256.
- [5] T. H. Dunning, “Gaussian basis sets for use in correlated molecular calculations. I. The atoms boron through neon and hydrogen,” *J. Chem. Phys.*, vol. 90, no. 2, pp. 1007–1023, Jan. 1989, doi: 10.1063/1.456153.
- [6] M. W. Schmidt *et al.*, “General atomic and molecular electronic structure system,” *J. Comput. Chem.*, vol. 14, no. 11, pp. 1347–1363, Nov. 1993, doi: 10.1002/jcc.540141112.
- [7] M. S. Gordon and M. W. Schmidt, “Advances in electronic structure theory: GAMESS a decade later,” in *Theory and Applications of Computational Chemistry*, C. E. Dykstra, G. Frenking, K. S. Kim, and G. E. Scuseria, Eds. Amsterdam: Elsevier, 2005, pp. 1167–1189.
- [8] G. M. J. Barca *et al.*, “Recent developments in the general atomic and molecular electronic structure system,” *J. Chem. Phys.*, vol. 152, no. 15, p. 154102, Apr. 2020, doi: 10.1063/5.0005188.
- [9] Niu, M. M.; Qin, J. Y.; Tian, C. P.; Yan, X. F.; Dong, F. G.; Cheng, Z. Q.; Fida, G.; Yang, M.; Chen, H.; Gu, Y. Q. Tubulin inhibitors: Pharmacophore modeling, virtual screening and molecular docking. *Acta Pharmacol. Sin.* 2014, 35, 967–979, doi:10.1038/aps.2014.34.
- [10] Consortium, T. U. Update on activities at the Universal Protein Resource

- (UniProt) in 2013. *Nucleic Acids Res.* 2013, 41, D43–D47, doi:10.1093/nar/gks1068.
- [11] Ravelli, R. B. G.; Gigant, B.; Curmi, P. A.; Jourdain, I.; Lachkar, S.; Sobel, A.; Knossow, M. Insight into tubulin regulation from a complex with colchicine and a stathmin-like domain. *Nature* 2004, 428, 198–202, doi:10.1038/nature02393.
- [12] Salomon-Ferrer, R.; Case, D. A.; Walker, R. C. An overview of the Amber biomolecular simulation package. *Wiley Interdiscip. Rev. Comput. Mol. Sci.* 2013, 3, 198–210, doi:10.1002/wcms.1121.
- [13] Roe, D. R.; Cheatham, T. E. PTRAJ and CPPTRAJ: Software for Processing and Analysis of Molecular Dynamics Trajectory Data. *J. Chem. Theory Comput.* 2013, 9, 3084–3095, doi:10.1021/ct400341p.
- [14] Trott, O.; Olson, A. J. AutoDock Vina: Improving the speed and accuracy of docking with a new scoring function, efficient optimization, and multithreading. *J. Comput. Chem.* 2009, 31, NA-NA, doi:10.1002/jcc.21334.
- [15] Hou, T.; Wang, J.; Li, Y.; Wang, W. Assessing the Performance of the MM/PBSA and MM/GBSA Methods. 1. The Accuracy of Binding Free Energy Calculations Based on Molecular Dynamics Simulations. *J. Chem. Inf. Model.* 2011, 51, 69–82, doi:10.1021/ci100275a.
- [16] Spasevska, I.; Ayoub, A. T.; Winter, P.; Preto, J.; Wong, G. K. S.; Dumontet, C.; Tuszynski, J. A. Modeling the *Colchicum autumnale* tubulin and a comparison of its interaction with colchicine to human tubulin. *Int. J. Mol. Sci.* 2017, 18, doi:10.3390/ijms18081676.
- [17] Onufriev, A.; Bashford, D.; Case, D. A. Exploring protein native states and large-scale conformational changes with a modified generalized Born model. *Proteins Struct. Funct. Bioinforma.* 2004, 55, 383–394, doi:10.1002/prot.20033.

Appendix D.

Supplementary material for chapter 5



Chemical formula: C₂₂H₂₄BrNO₆, MW = 478.3 g/mol

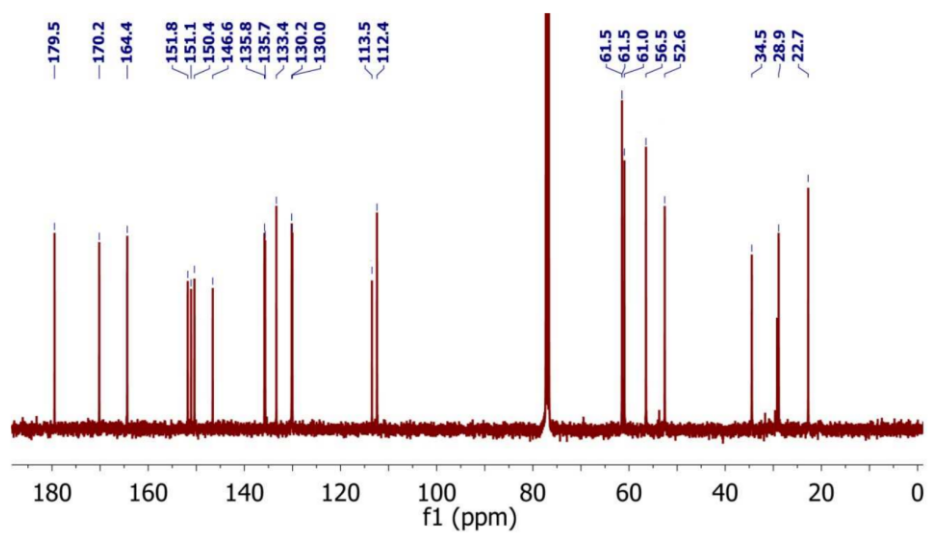


Figure D-1. The ¹³C NMR spectrum of **2** in CDCl₃

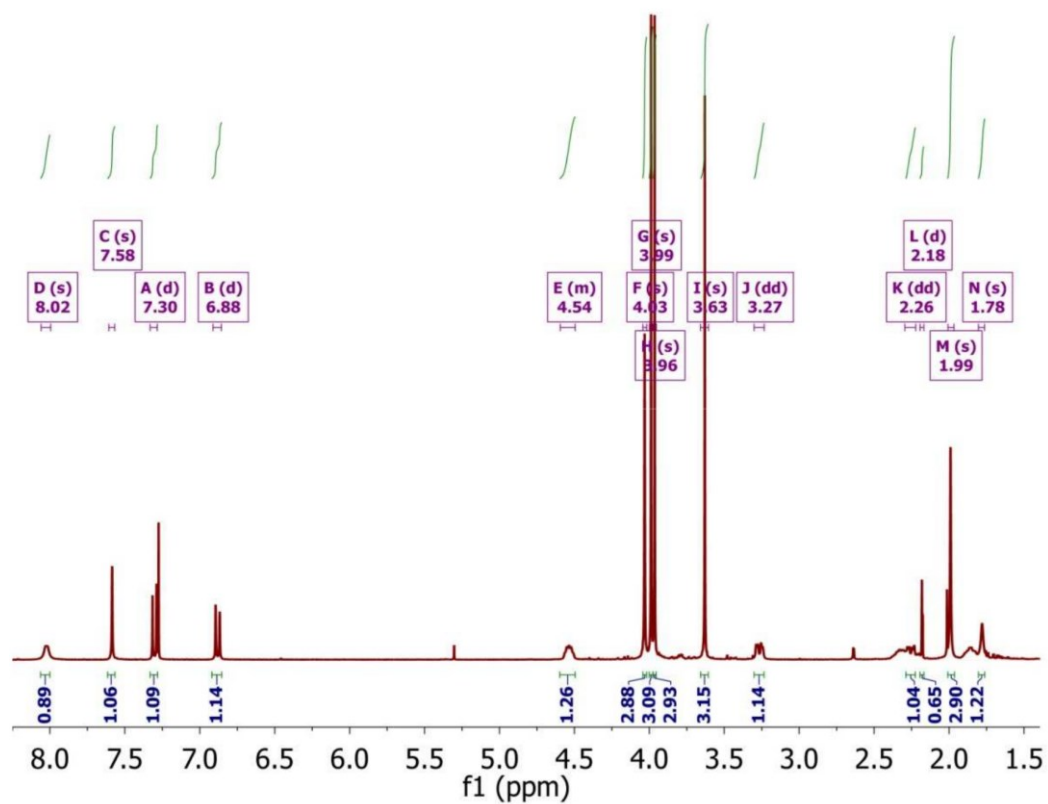
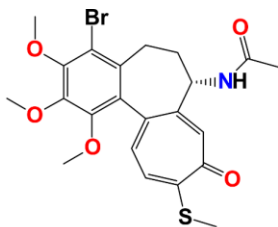


Figure D-2. The ^1H NMR spectrum of **2** in CDCl_3



Chemical formula: C₂₂H₂₄BrNO₅S, MW = 494.4 g/mol

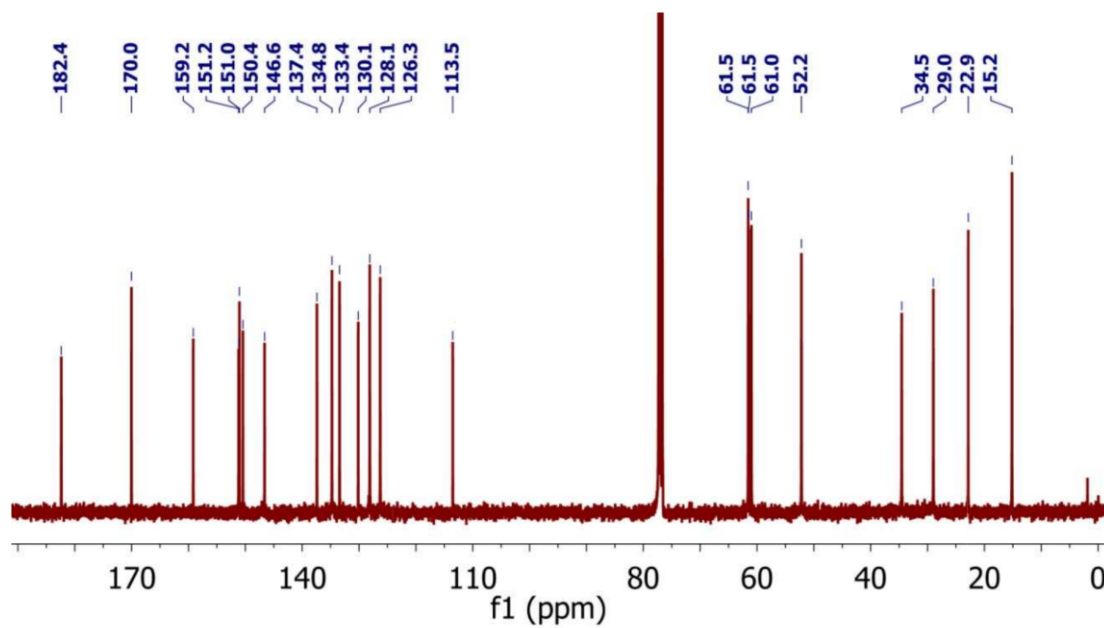


Figure D-3. The ¹³C NMR spectrum of **3** in CDCl₃

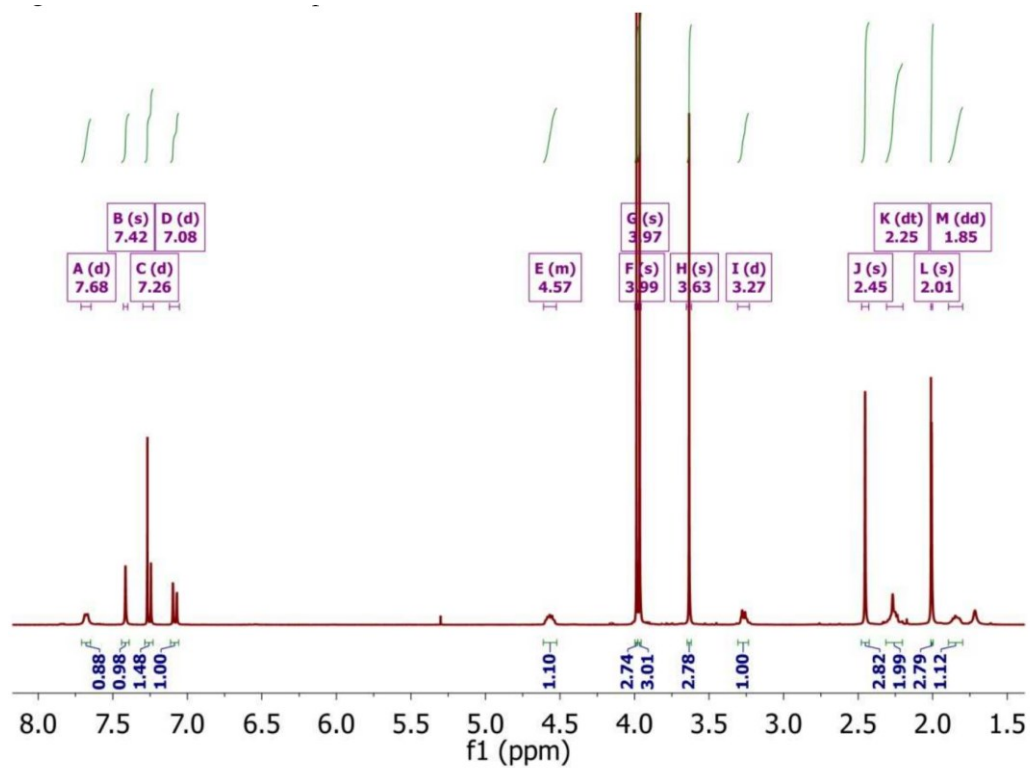
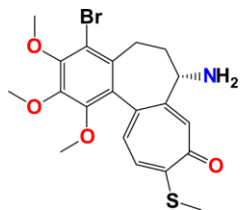


Figure D-4. The ^1H NMR spectrum of **3** in CDCl_3



Chemical formula: C₂₀H₂₂BrNO₄S, MW = 452.4 g/mol

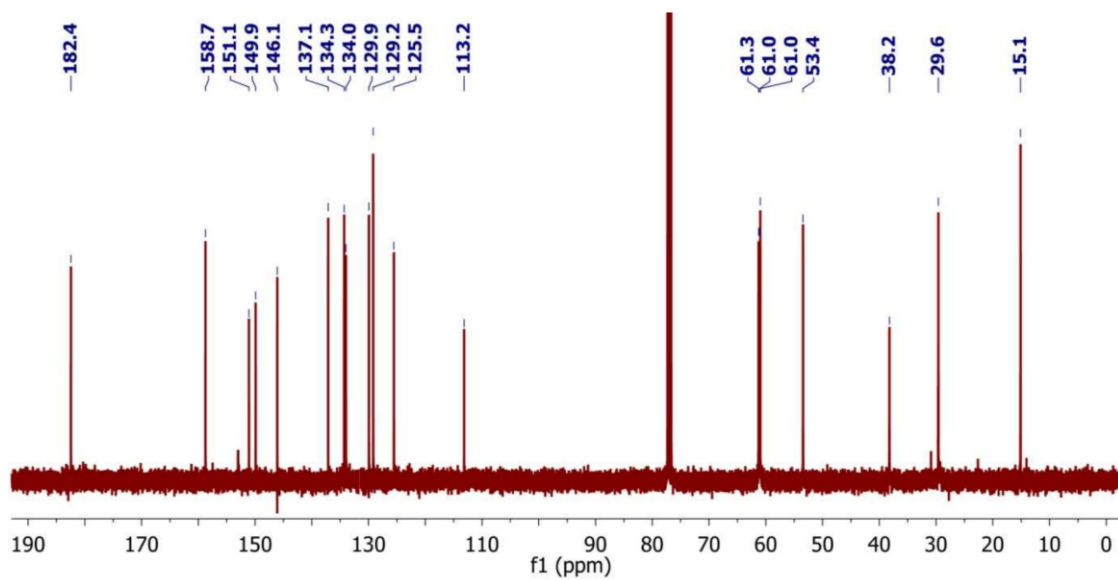


Figure D-5. The ¹³C NMR spectrum of **4** in CDCl₃

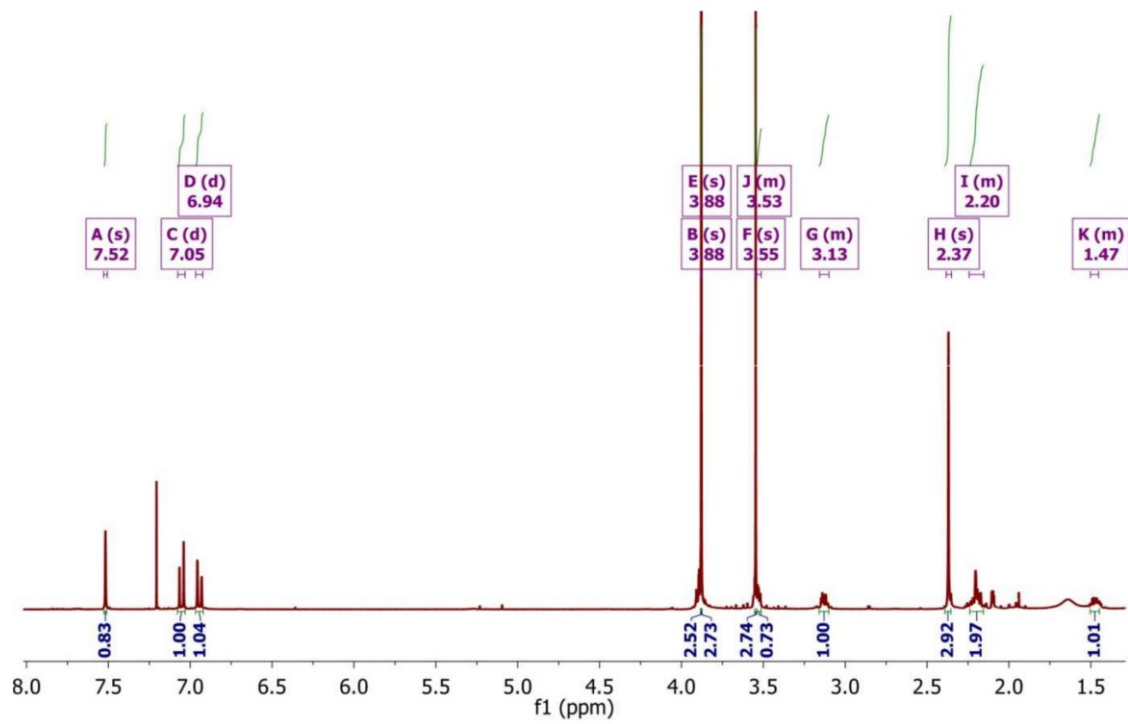
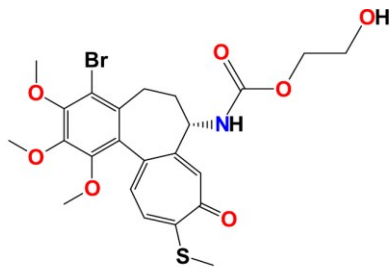


Figure D-6. The ¹H NMR spectrum of 4 in CDCl₃



Chemical formula: $C_{23}H_{26}BrNO_7S$, MW = 539.1 g/mol

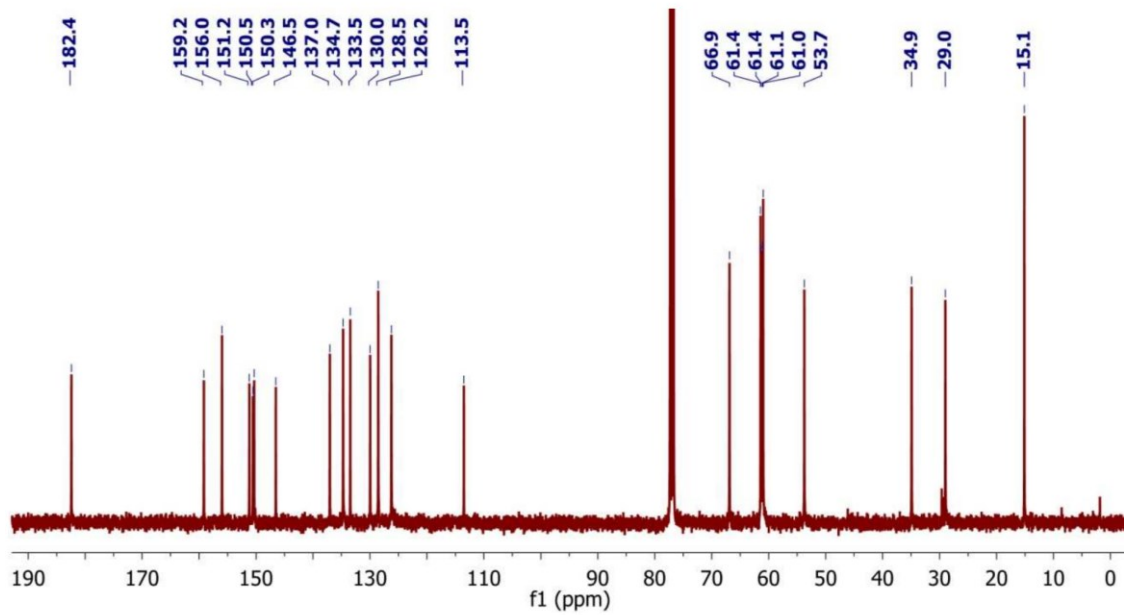


Figure D-7. The ^{13}C NMR spectrum of **5** in $CDCl_3$

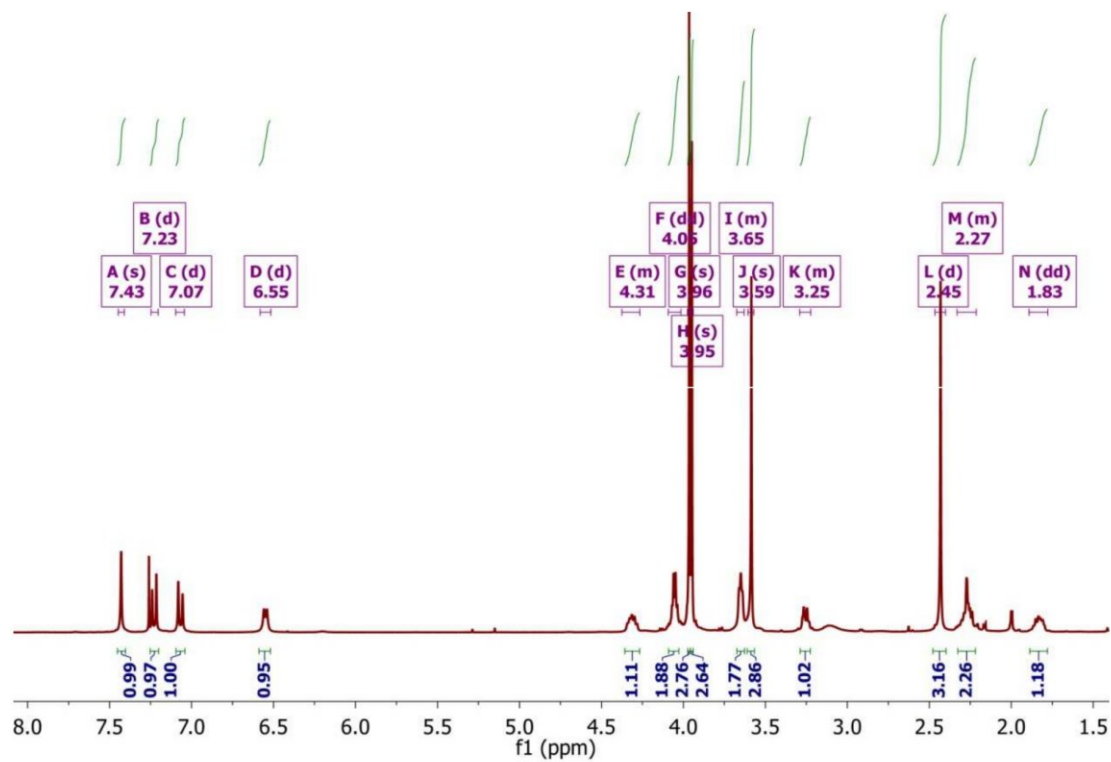
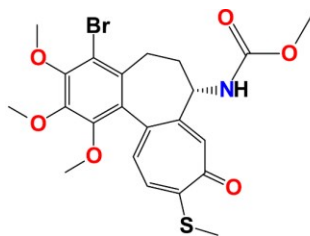


Figure D-8. The ¹H NMR spectrum of **5** in CDCl₃



Chemical formula: $C_{22}H_{24}BrNO_6S$, MW = 509.1 g/mol

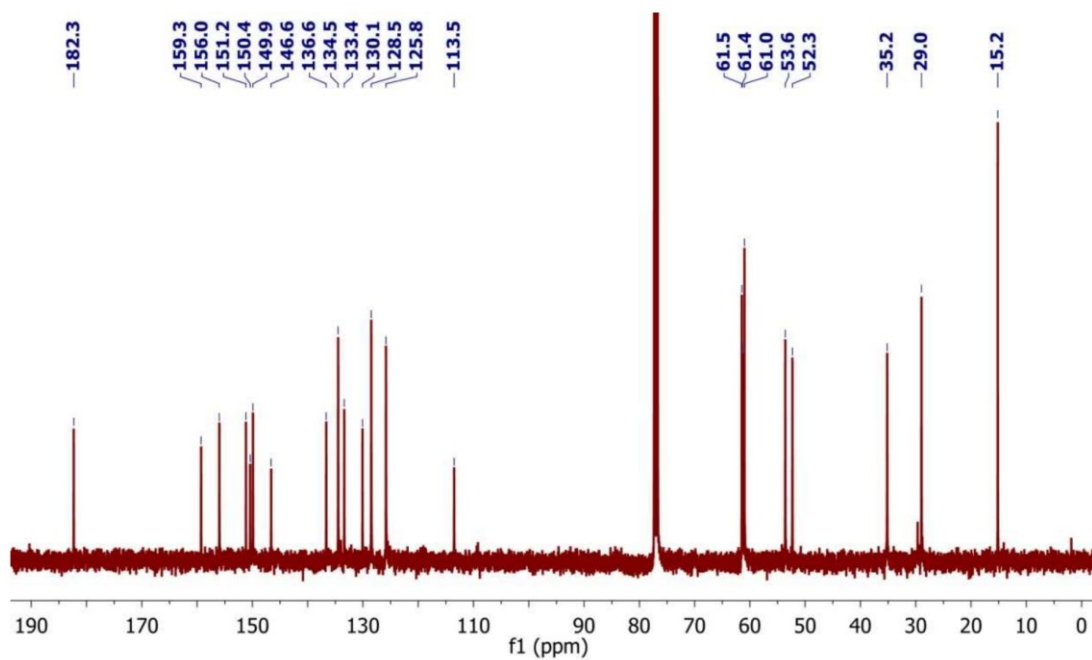


Figure D-9. The ^{13}C NMR spectrum of **6** in $CDCl_3$

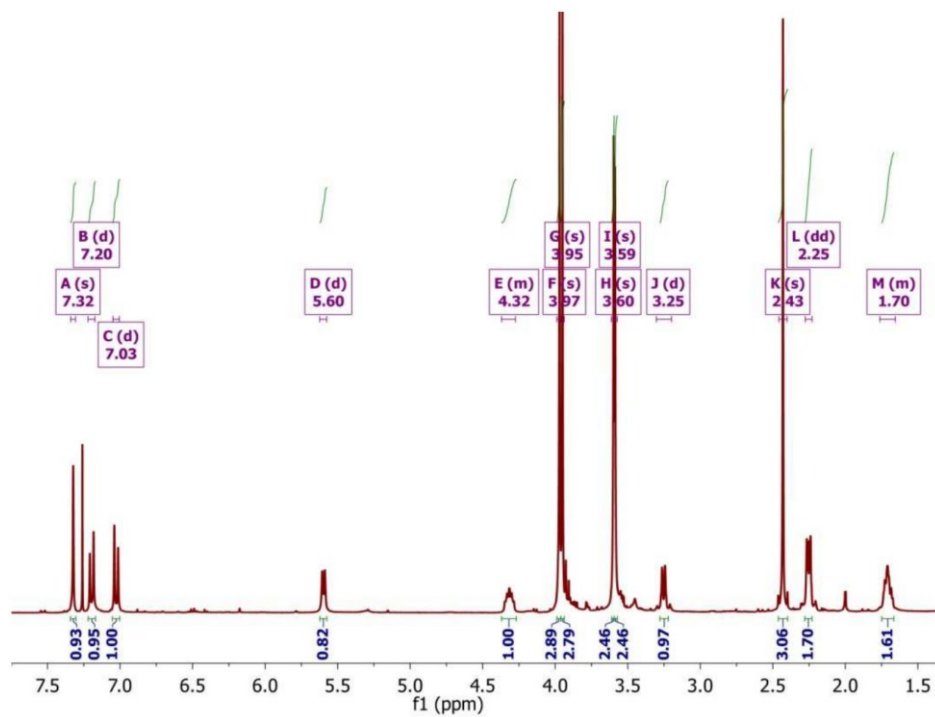
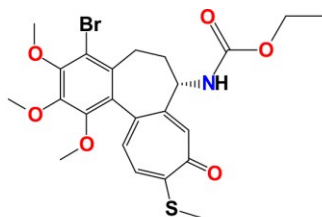


Figure D-10. The ^1H NMR spectrum of **6** in CDCl_3



Chemical formula: $C_{23}H_{26}BrNO_6S$, MW = 524.4 g/mol

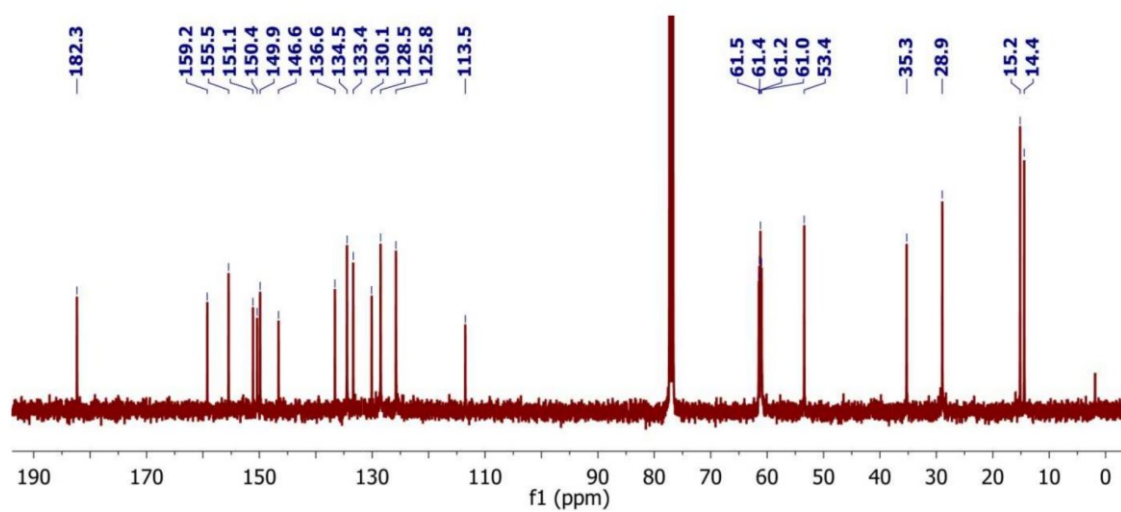


Figure D-11. The ^{13}C NMR spectrum of **7** in $CDCl_3$

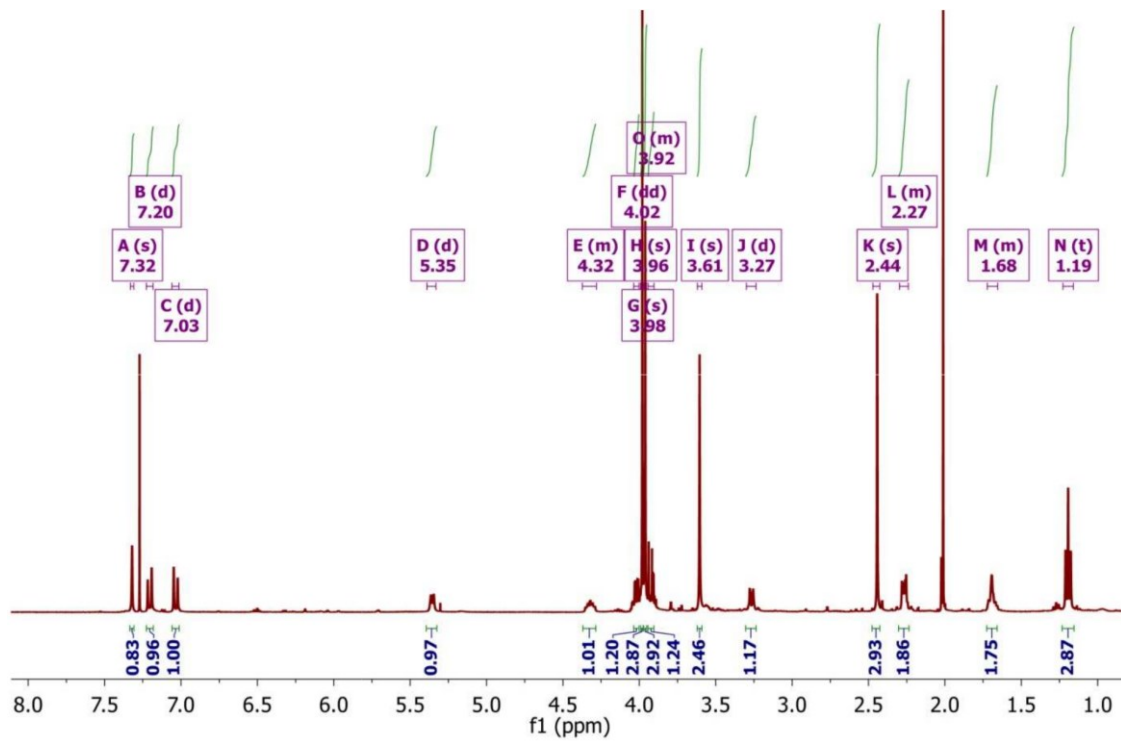
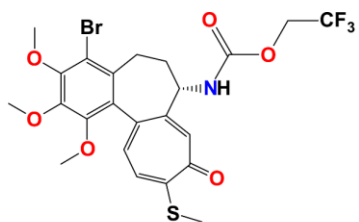


Figure D-12. The ^1H NMR spectrum of 7 in CDCl_3



Chemical formula: $C_{23}H_{23}BrF_3NO_6S$, MW = 578.4 g/mol

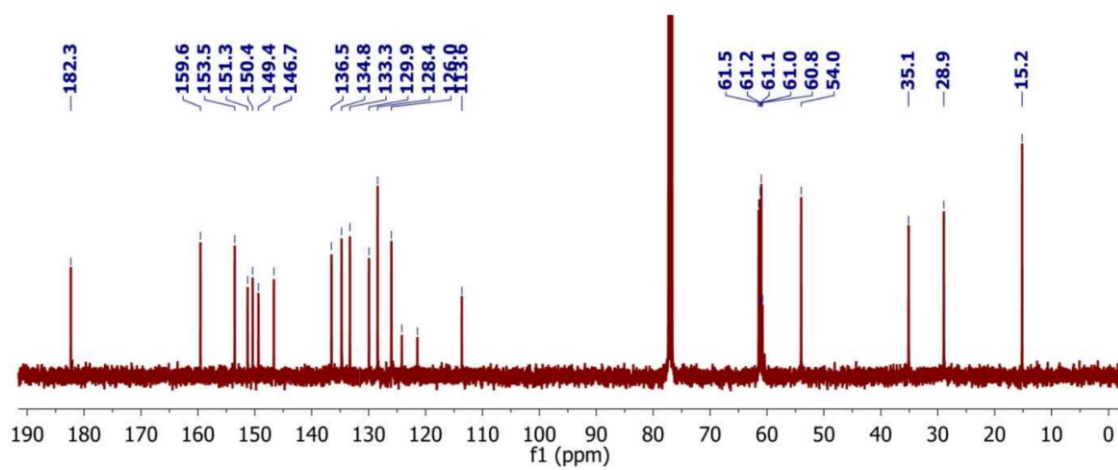


Figure D-13. The ^{13}C NMR spectrum of **8** in $CDCl_3$

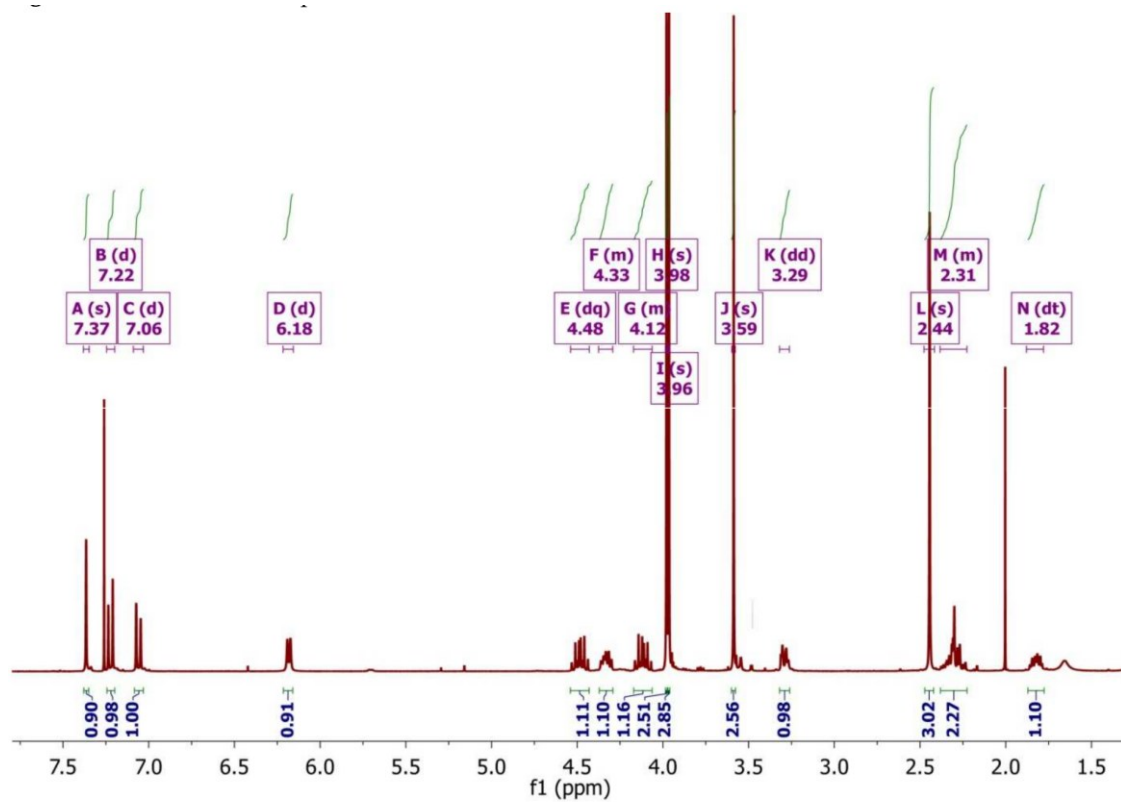


Figure D-14. The ¹H NMR spectrum of **8** in CDCl₃

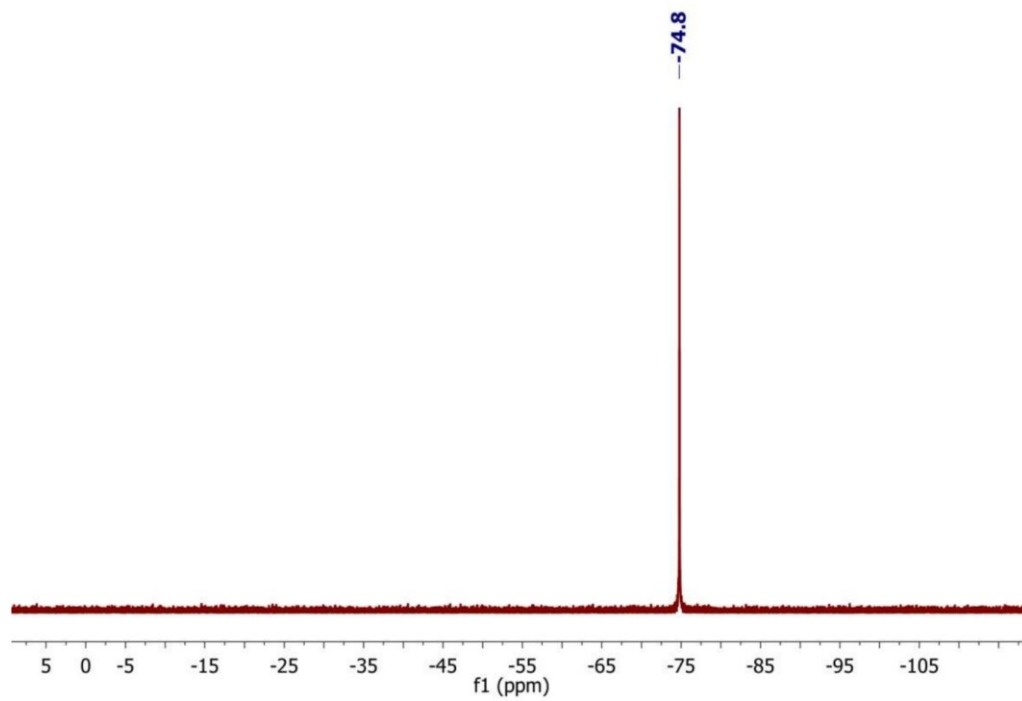
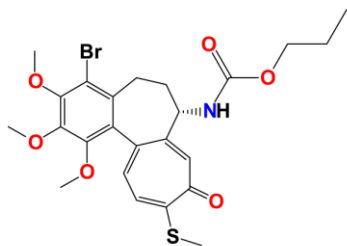


Figure D-15. The ^{19}F NMR spectrum of **8** in CDCl_3



Chemical formula: $C_{24}H_{28}BrNO_6S$, MW = 538.5 g/mol

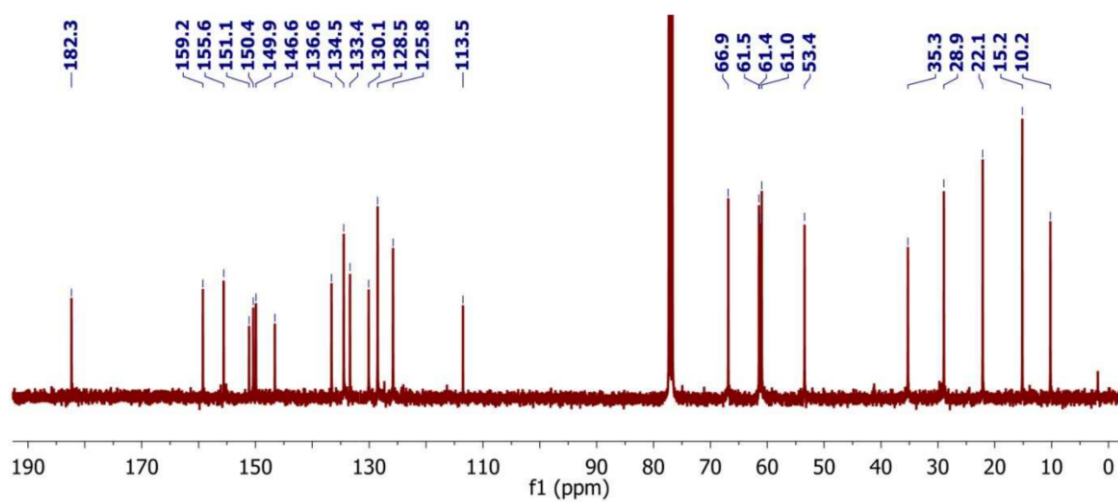


Figure D-16. The ^{13}C NMR spectrum of **9** in $CDCl_3$

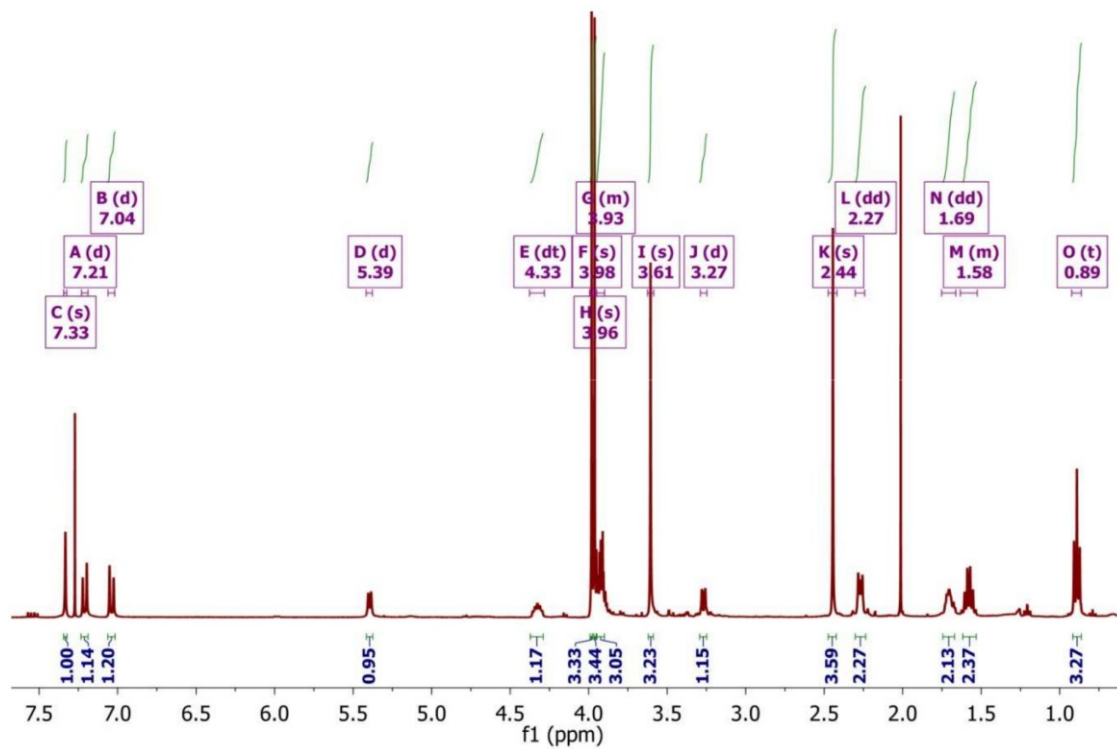


Figure D-17. The ^1H NMR spectrum of **9** in CDCl_3



Chemical formula: $C_{24}H_{28}BrNO_6S$, MW = 538.5 g/mol

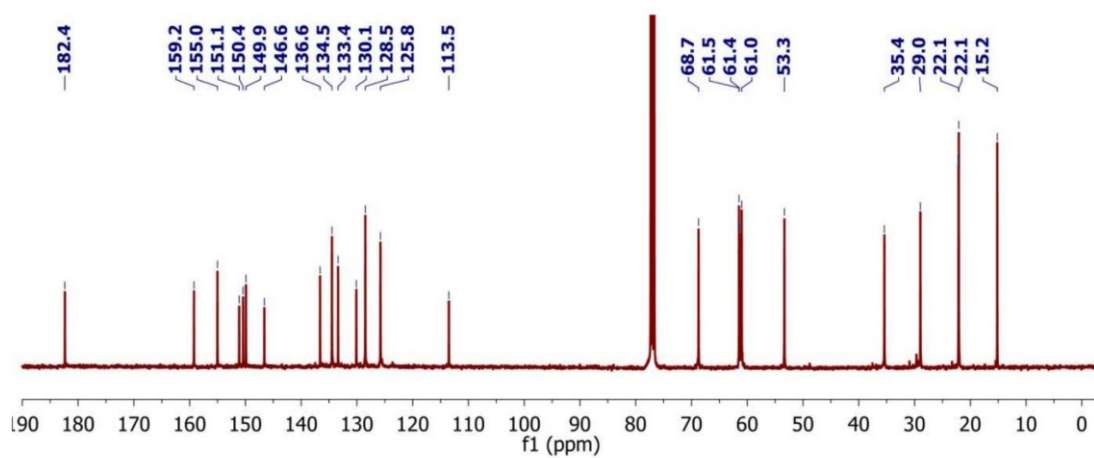


Figure D-18. The ^{13}C NMR spectrum of **10** in $CDCl_3$

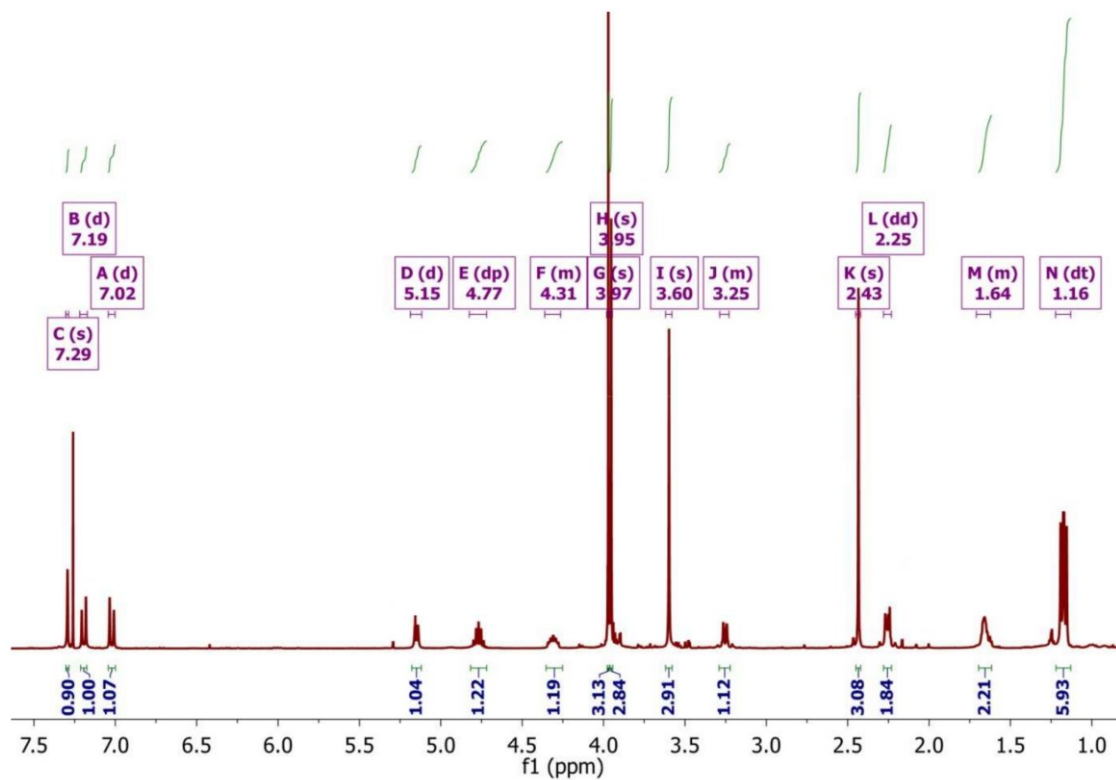
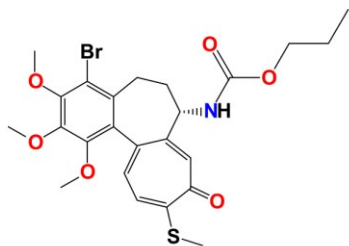


Figure D-19. The ^1H NMR spectrum of in **10** CDCl_3



Chemical formula: C₂₅H₃₀BrNO₆S, MW = 551.1 g/mol

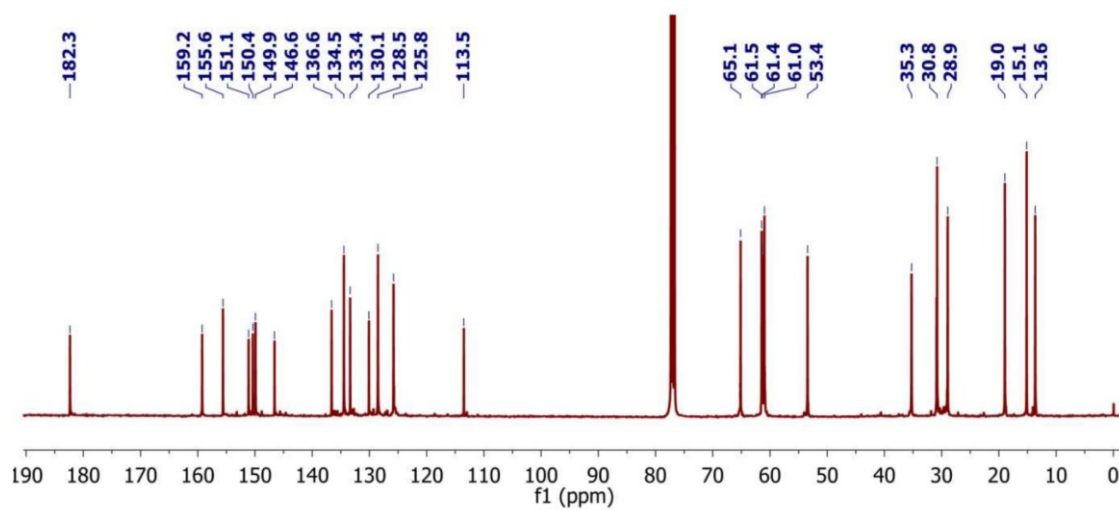


Figure D-20. The ¹³C NMR spectrum of **11** in CDCl₃

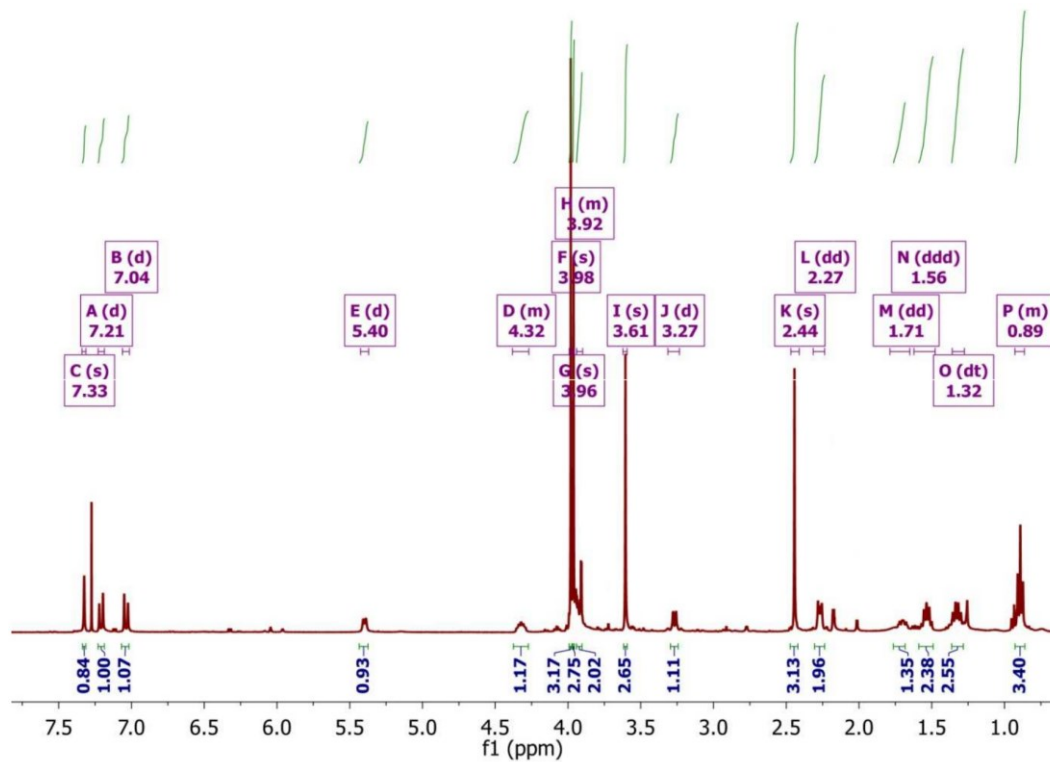
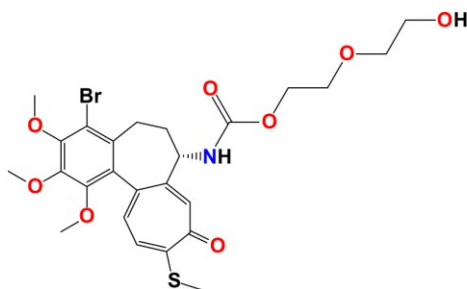


Figure D-21. The ^1H NMR spectrum of **11** in CDCl_3



Chemical formula: $C_{25}H_{30}BrNO_8S$, MW = 584.5 g/mol

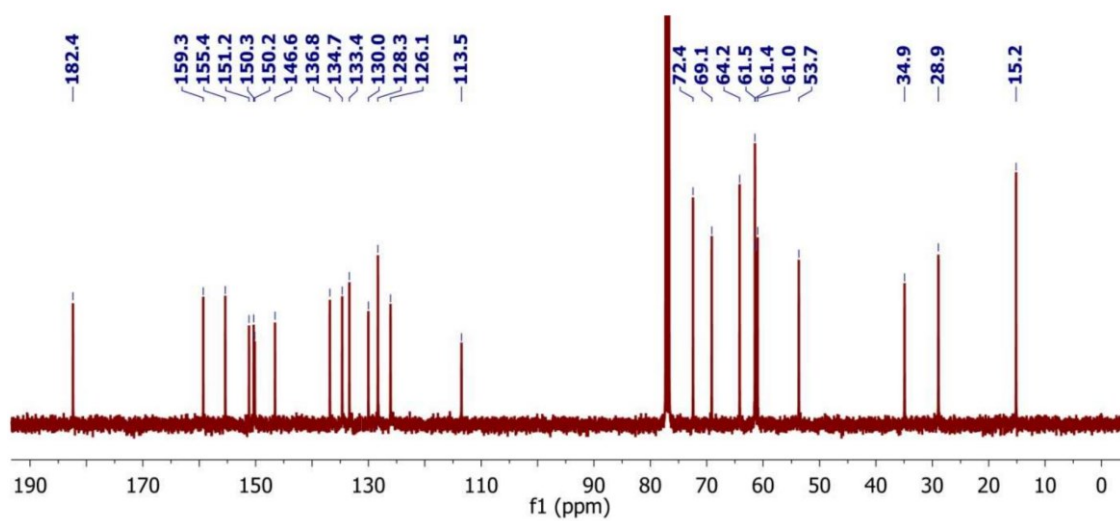


Figure D-22. The ^{13}C NMR spectrum of **12** in $CDCl_3$

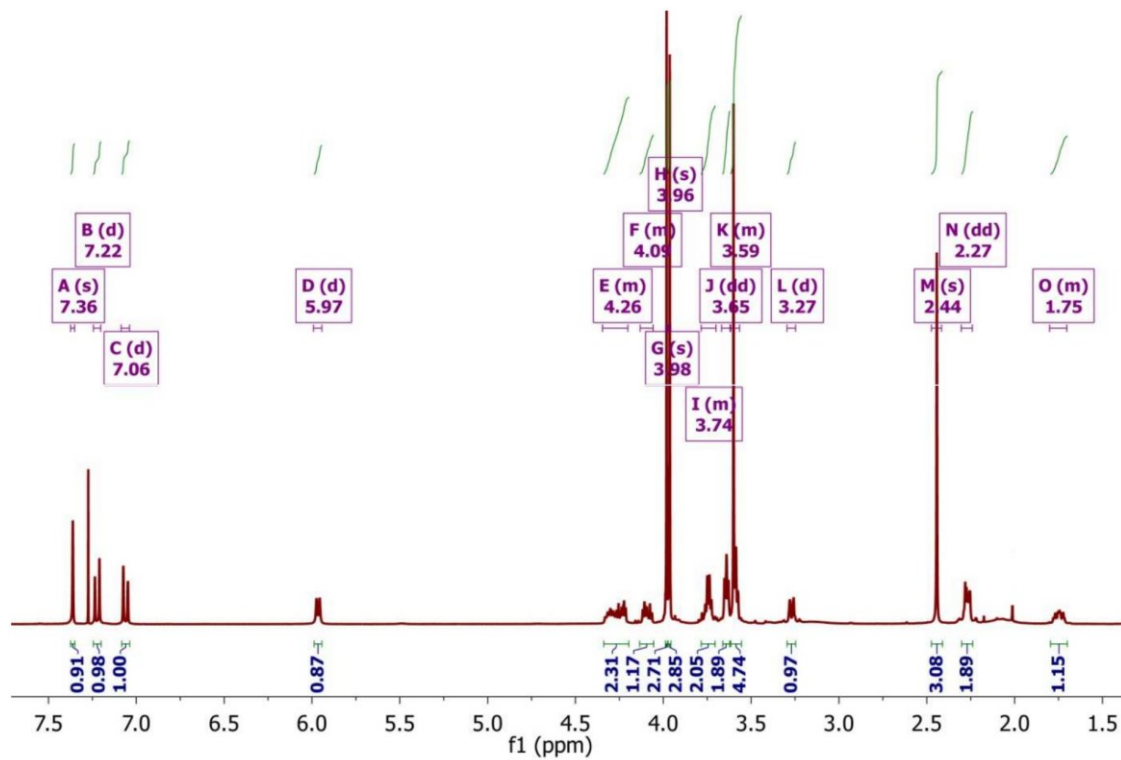


Figure D-23. The ^1H NMR spectrum of **12** in CDCl_3

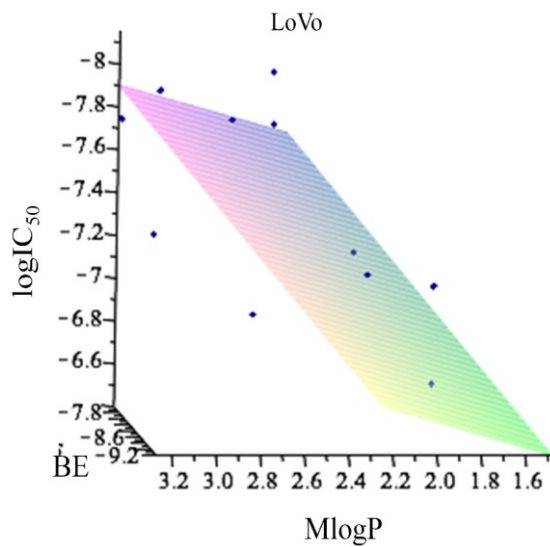


Figure D-24. 3D plots of the linear regression results for the binding energies (BE) vs $MlogP$ vs $\log IC_{50}$ [μM] values for LoVo cell line.

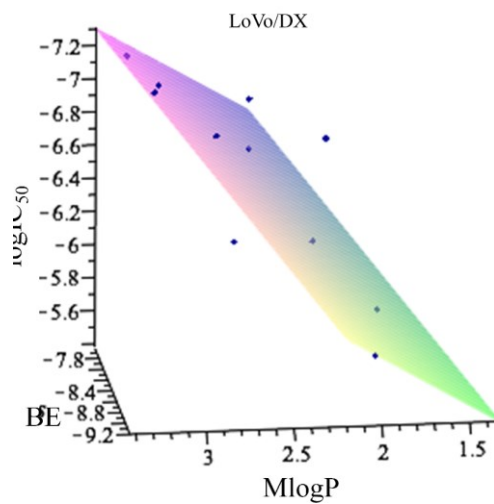


Figure D-25. 3D plots of the linear regression results for the binding energies (BE) vs $MlogP$ vs $\log IC_{50}$ [μM] values for LoVo/DX cell line.

Appendix E.

Supplementary material for chapter 6

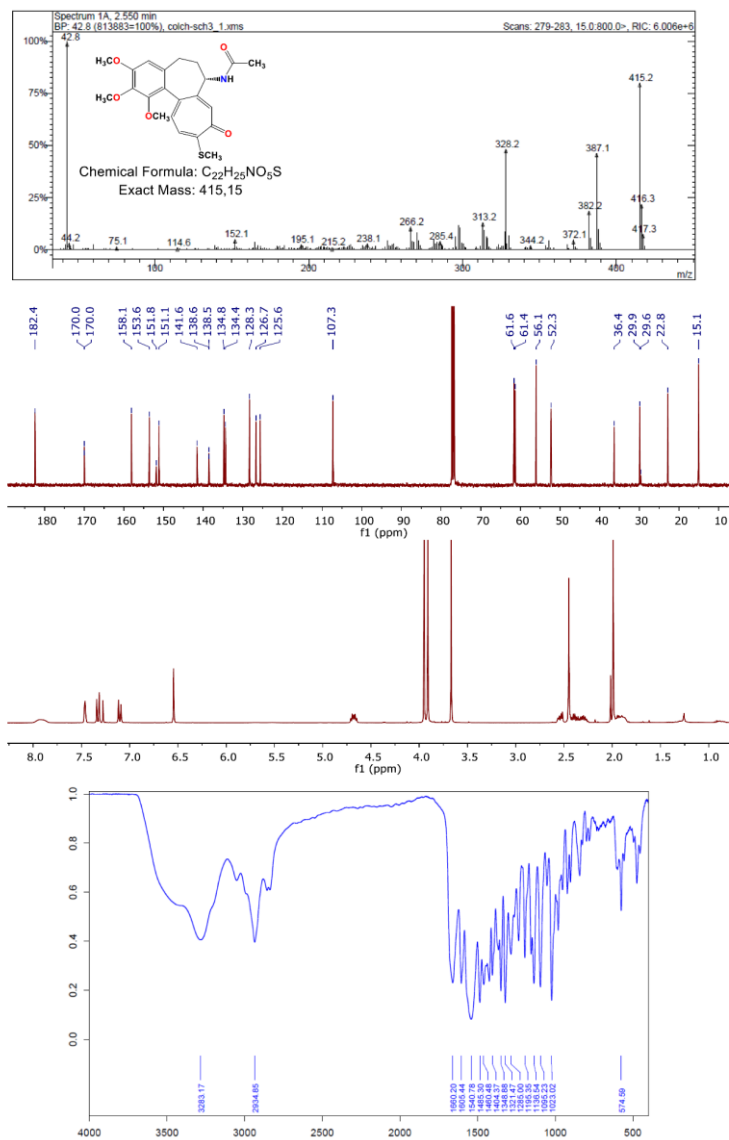


Figure E-1. Spectroscopic characterization of compound 2.

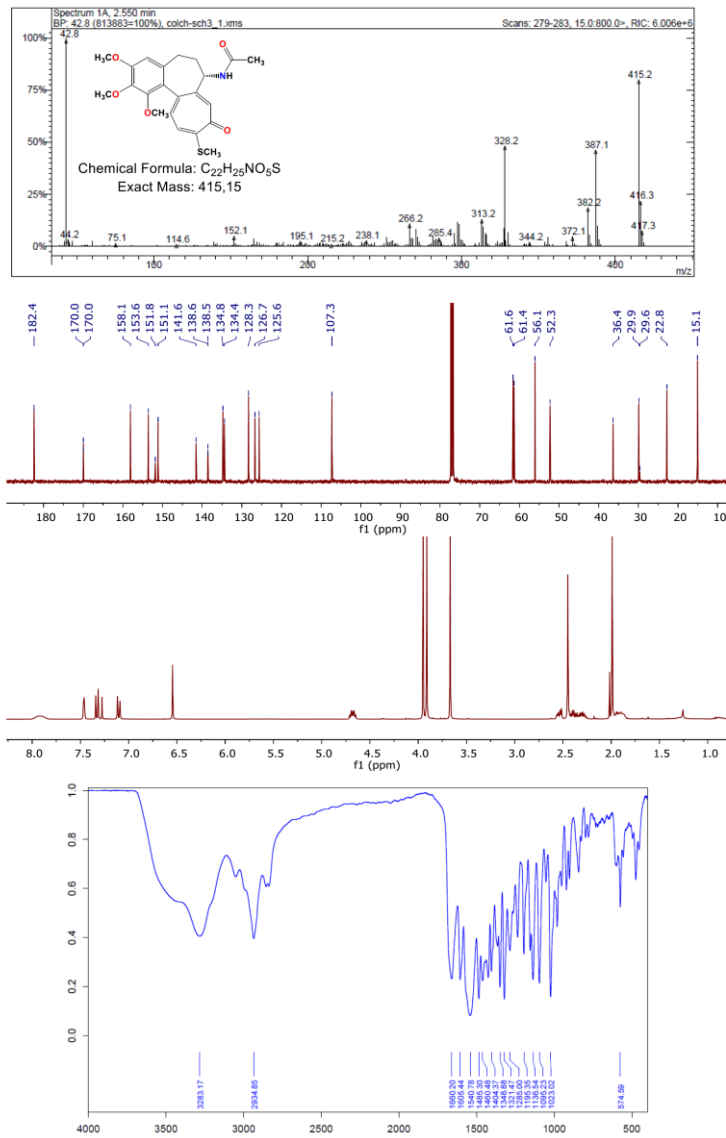


Figure E-2. Spectroscopic characterization of compound 3.

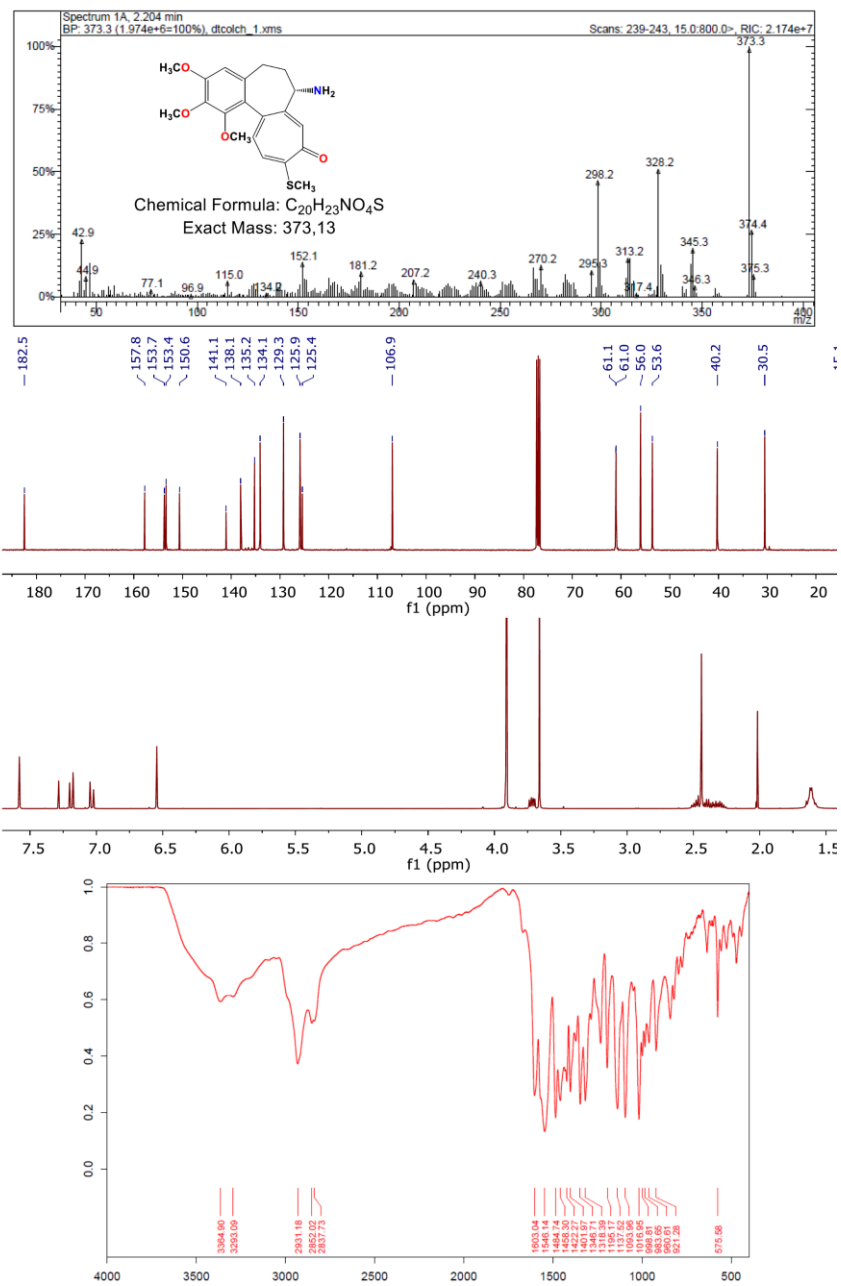


Figure E-3. Spectroscopic characterization of compound 3.

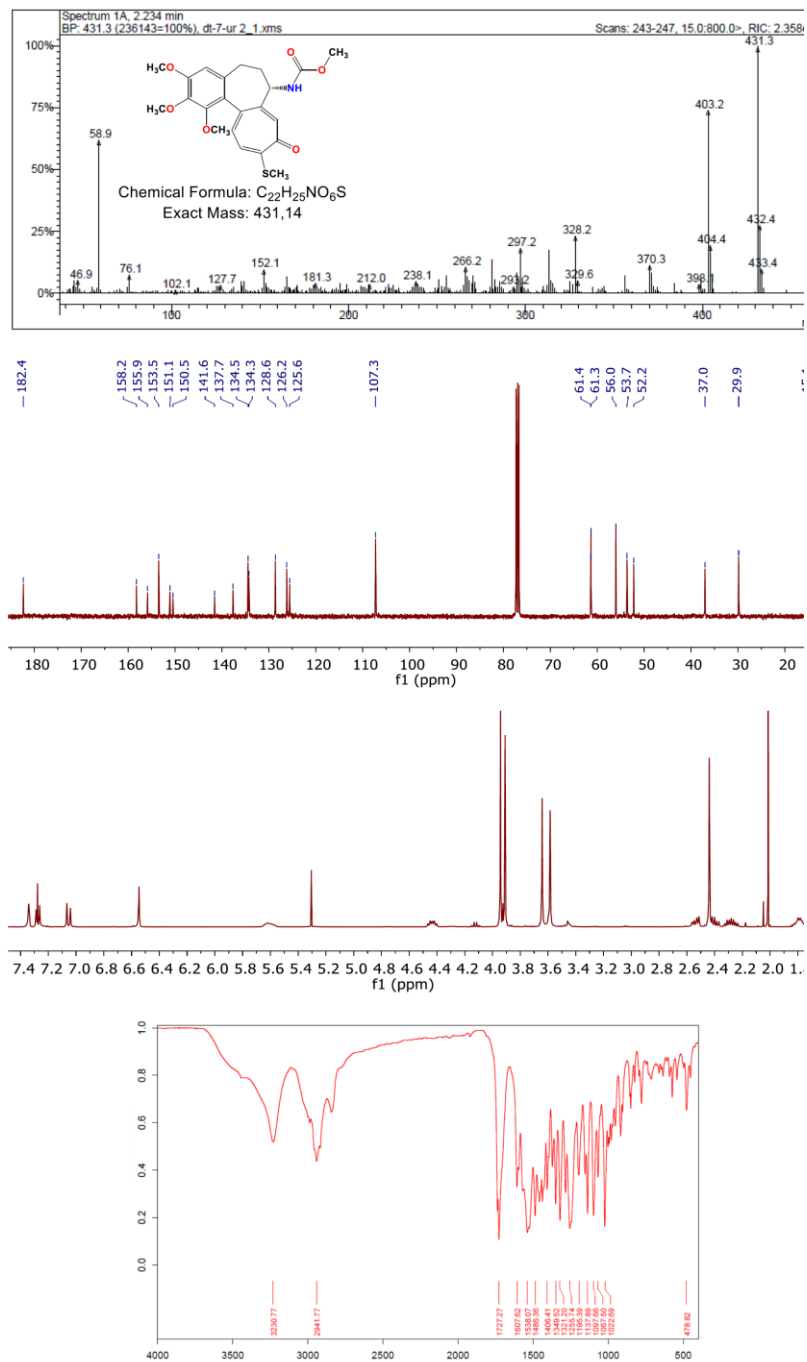


Figure E-4. Spectroscopic characterization of compound 4.

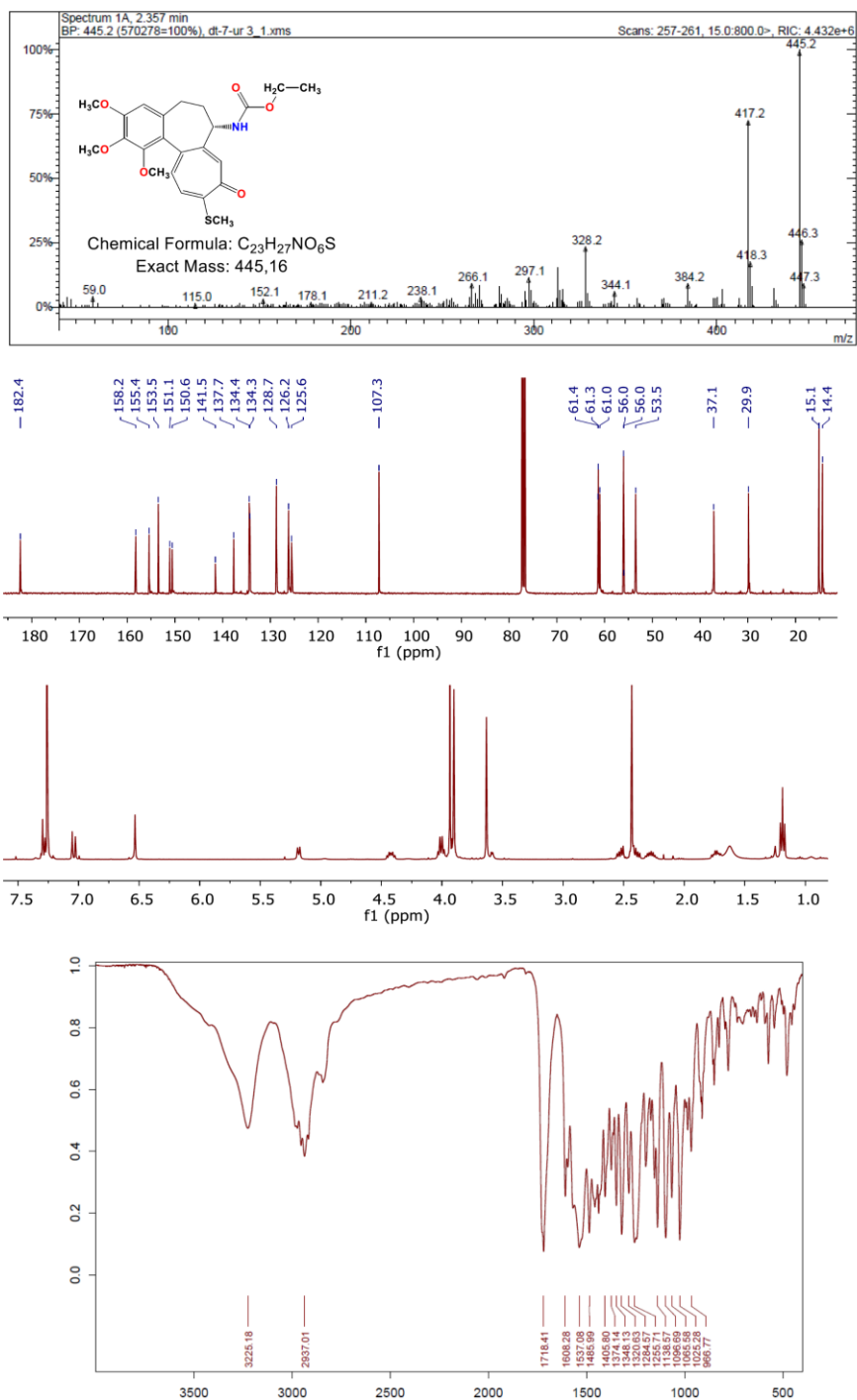


Figure E-5. Spectroscopic characterization of compound 5.

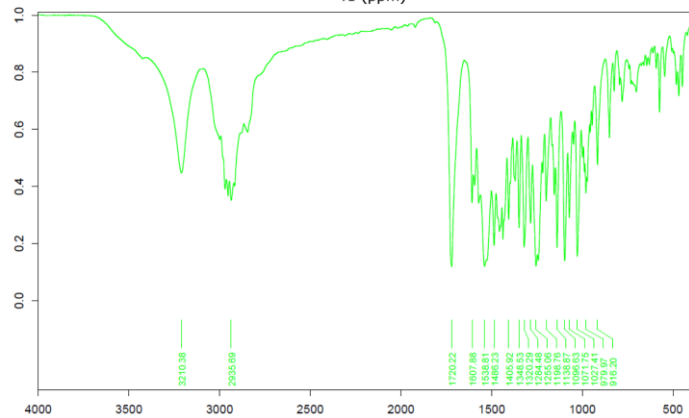
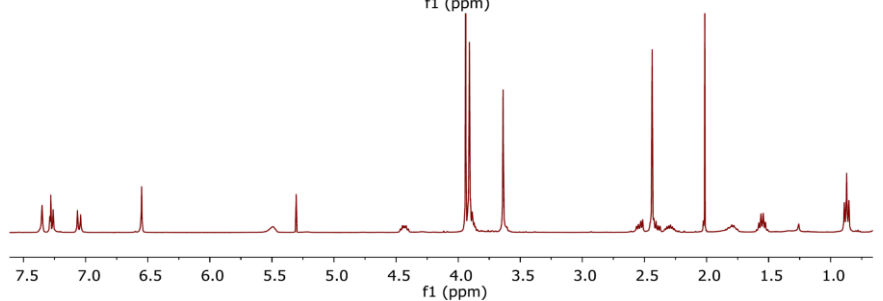
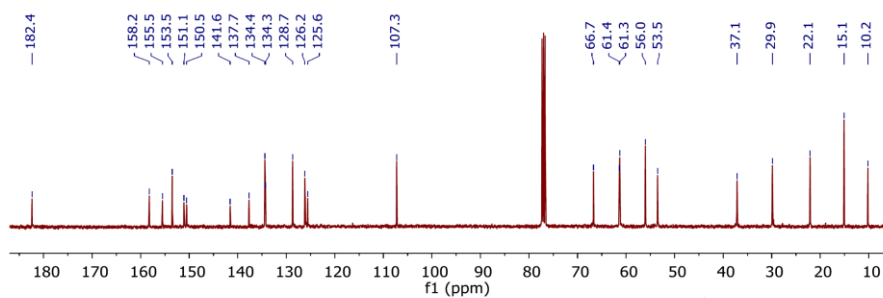
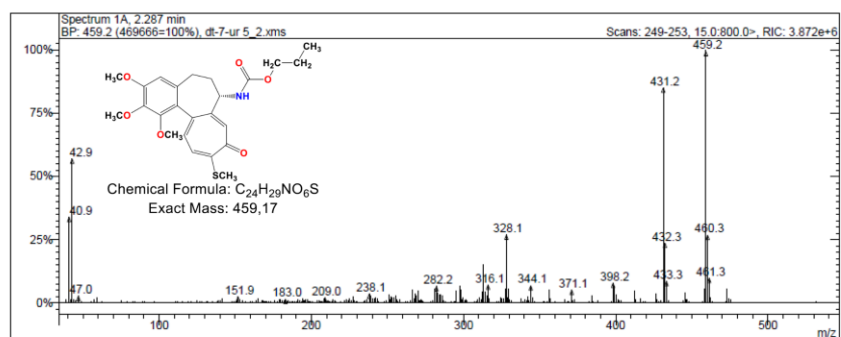


Figure E-6. Spectroscopic characterization of compound **6**.

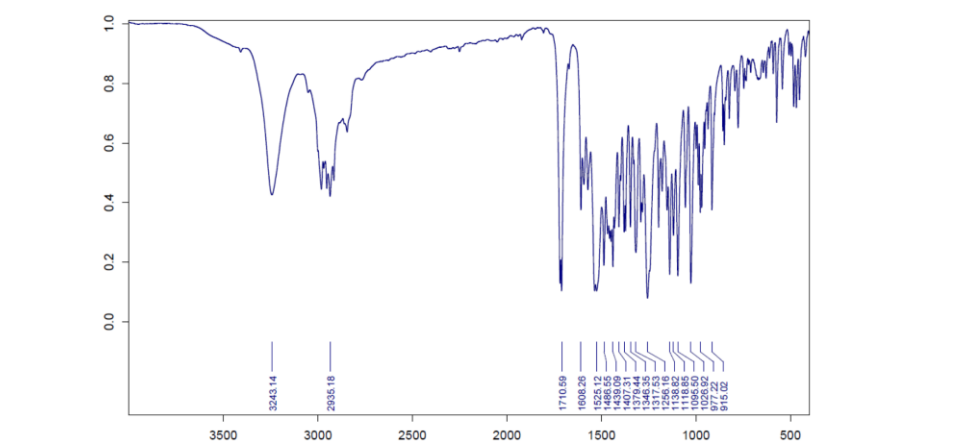
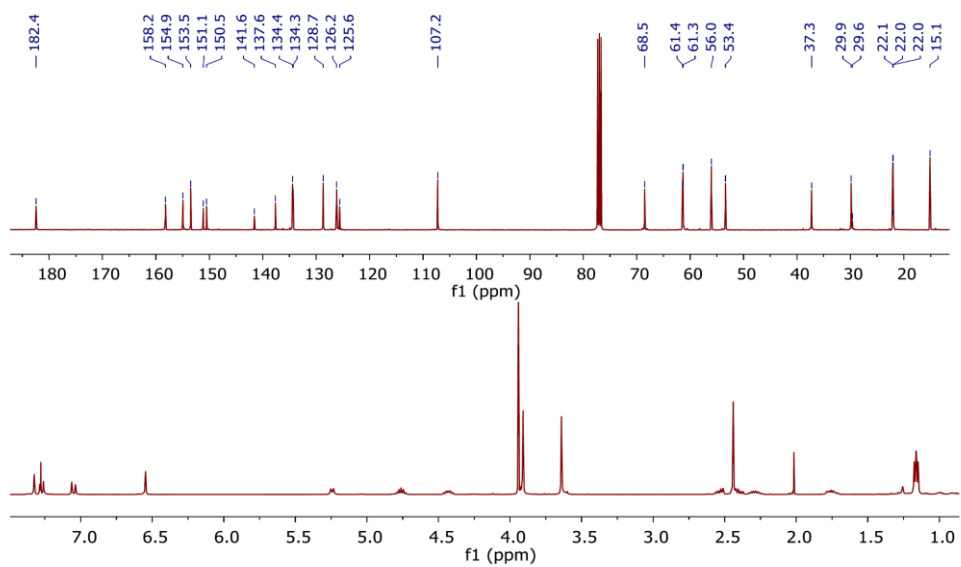
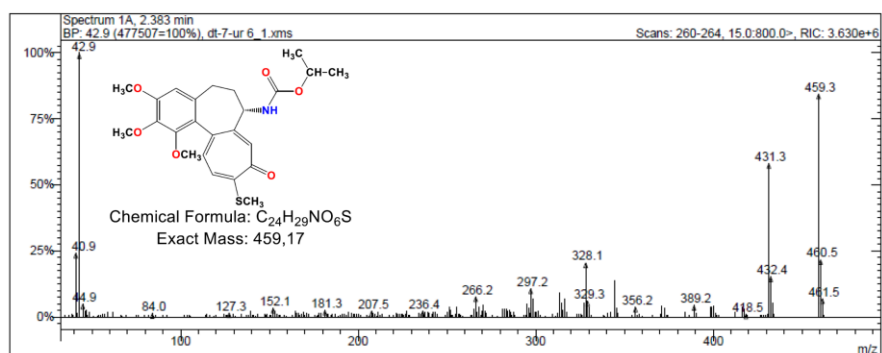


Figure E-7. Spectroscopic characterization of compound 7.

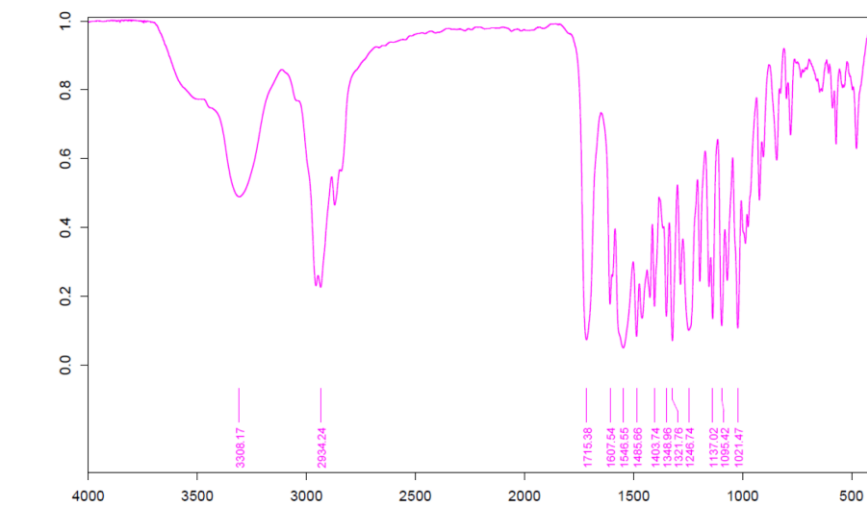
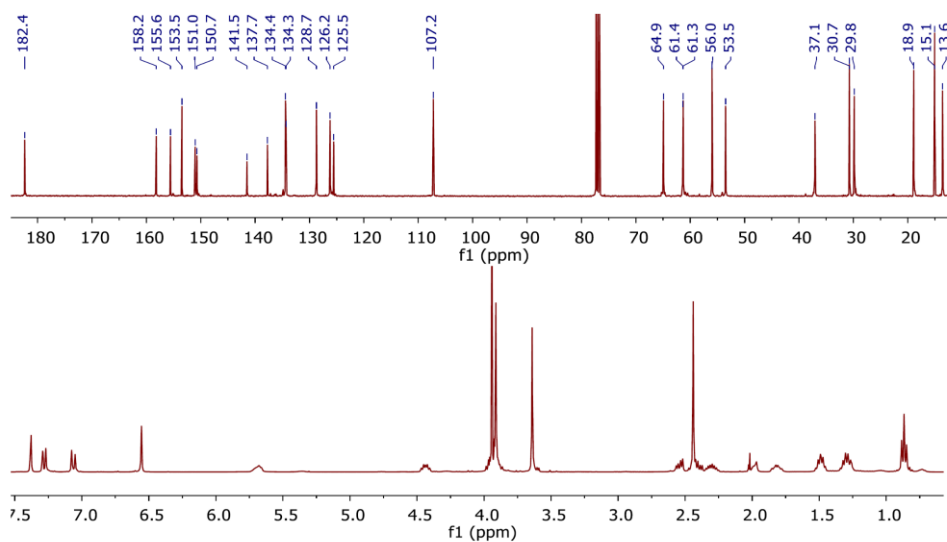
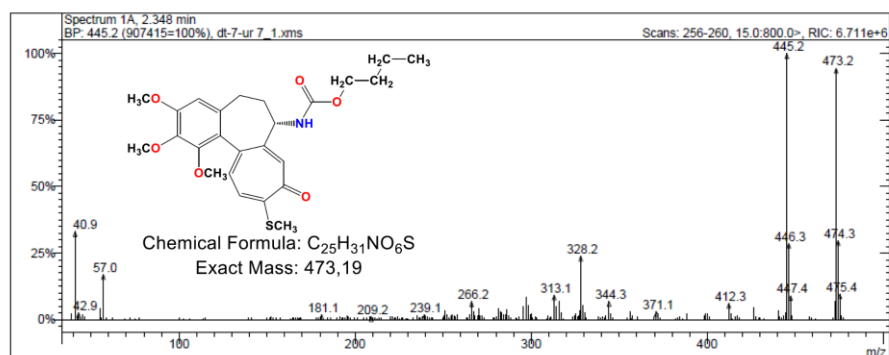


Figure E-8. Spectroscopic characterization of compound 8.

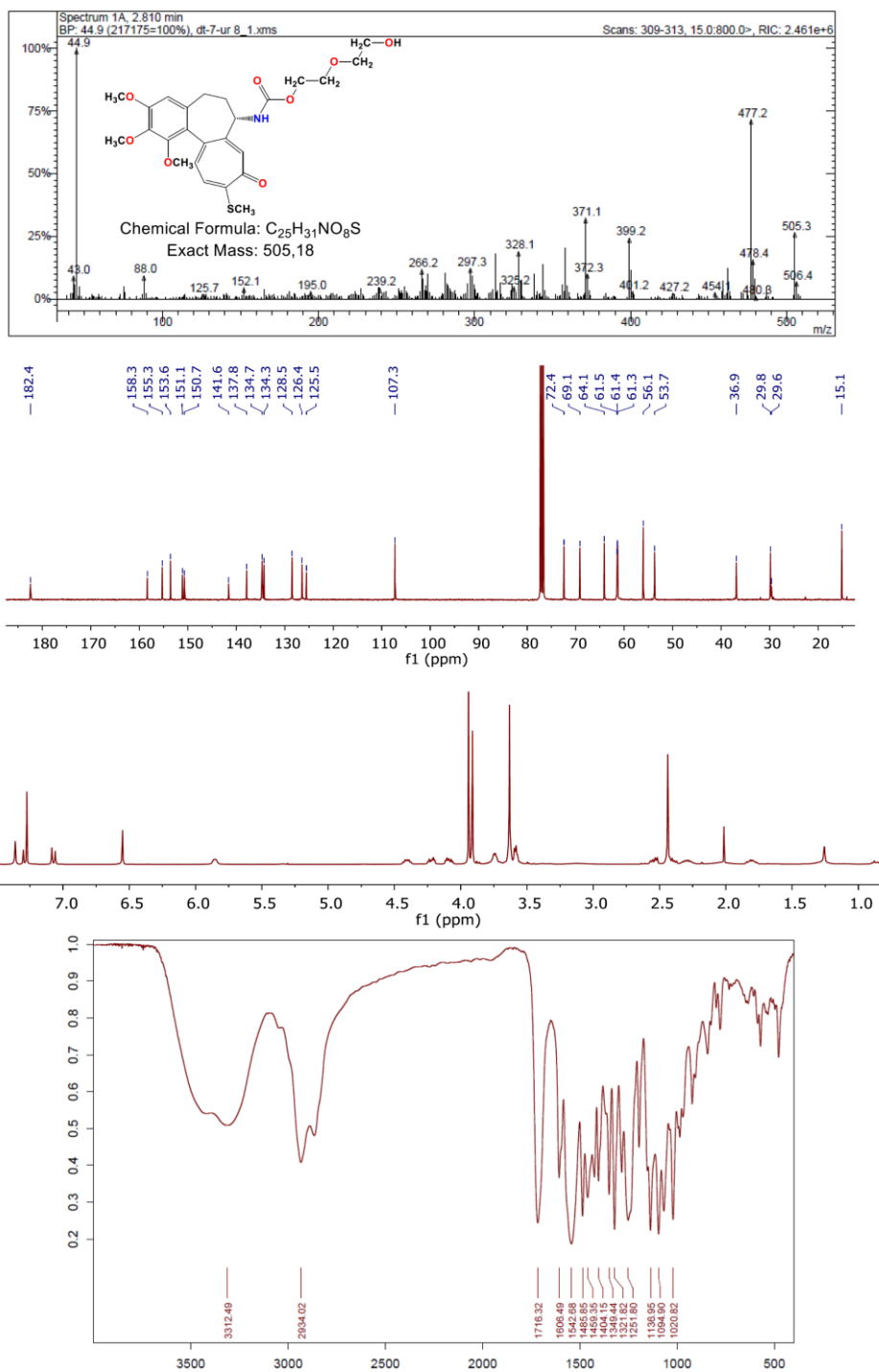


Figure E-10. Spectroscopic characterization of compound 10.

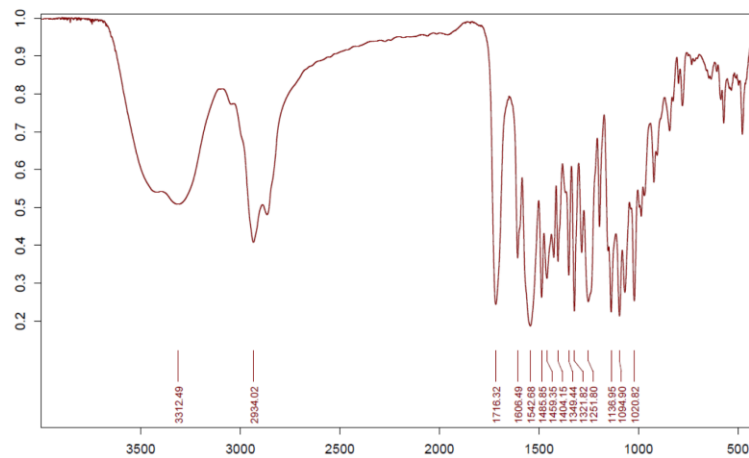
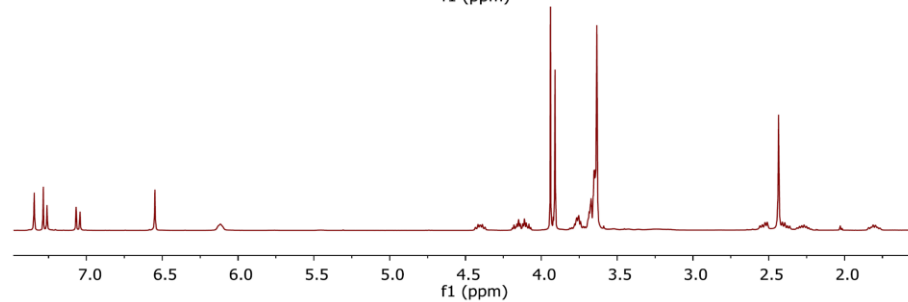
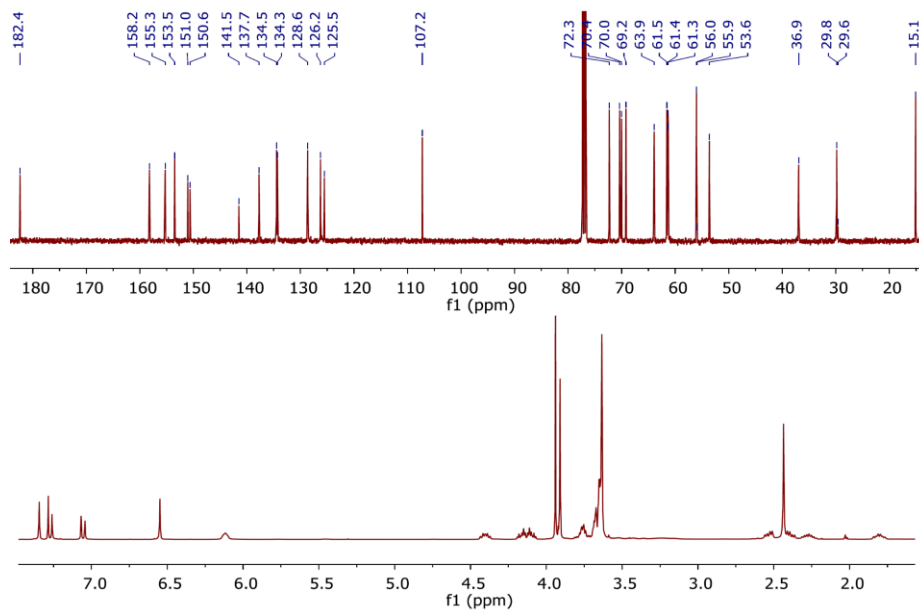
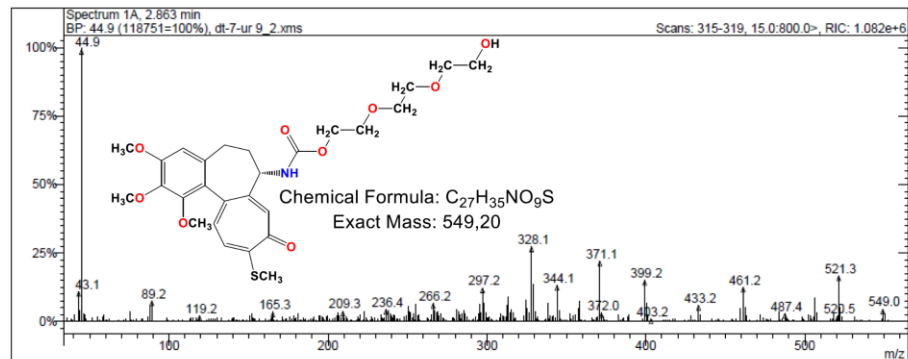


Figure E-11. Spectroscopic characterization of compound 11.

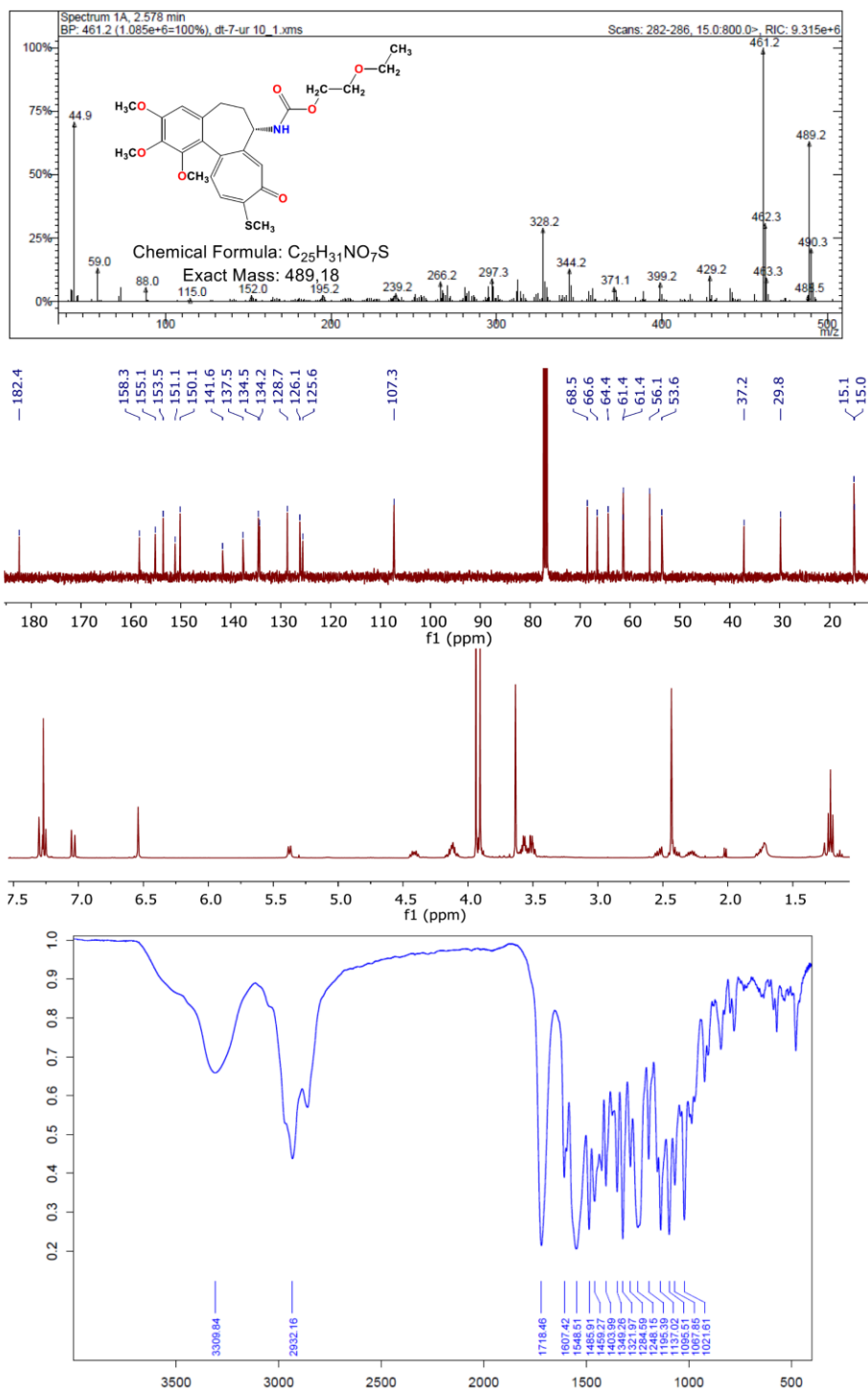


Figure E-12. Spectroscopic characterization of compound 12.

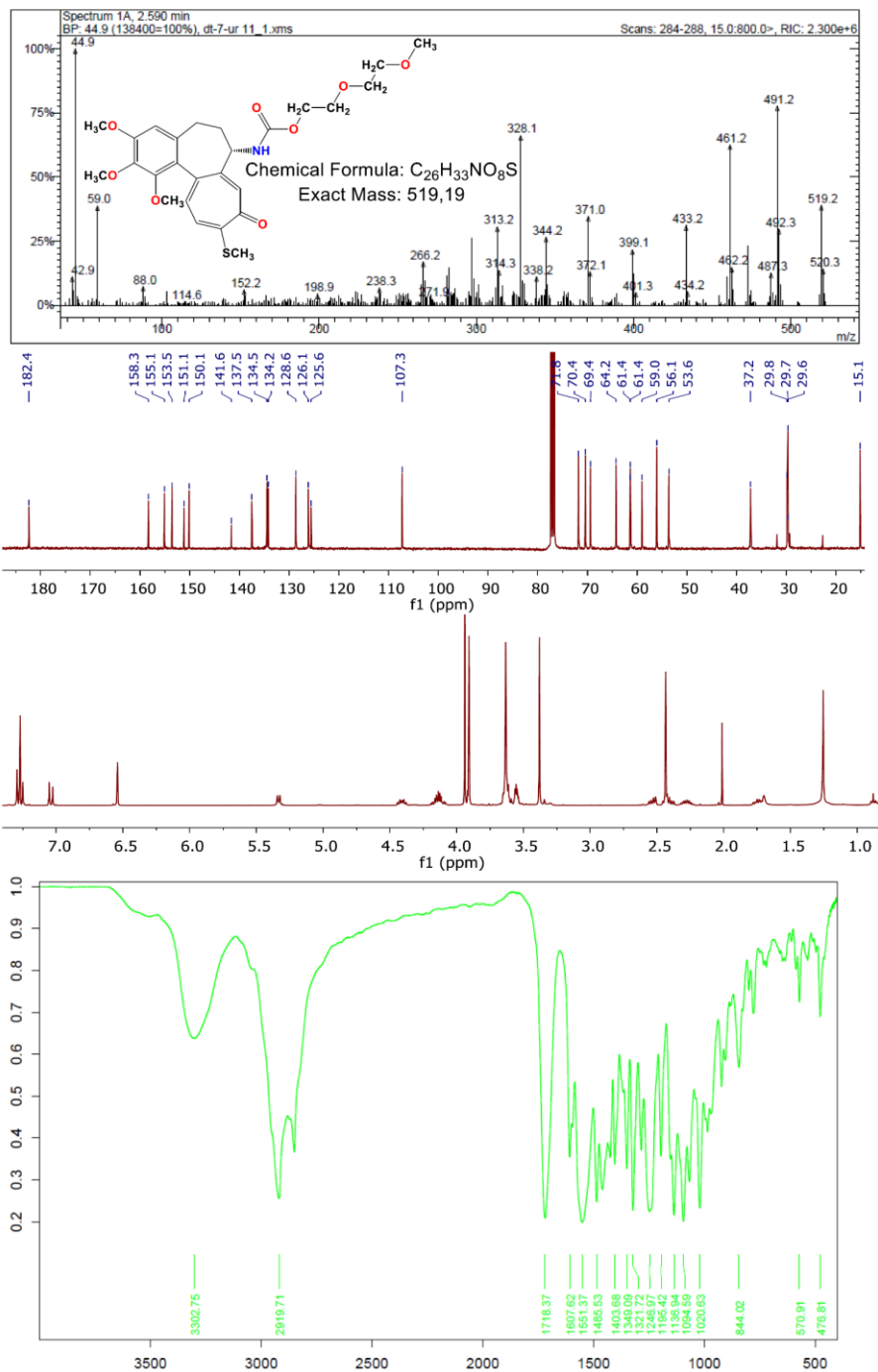


Figure E-13. Spectroscopic characterization of compound 13.

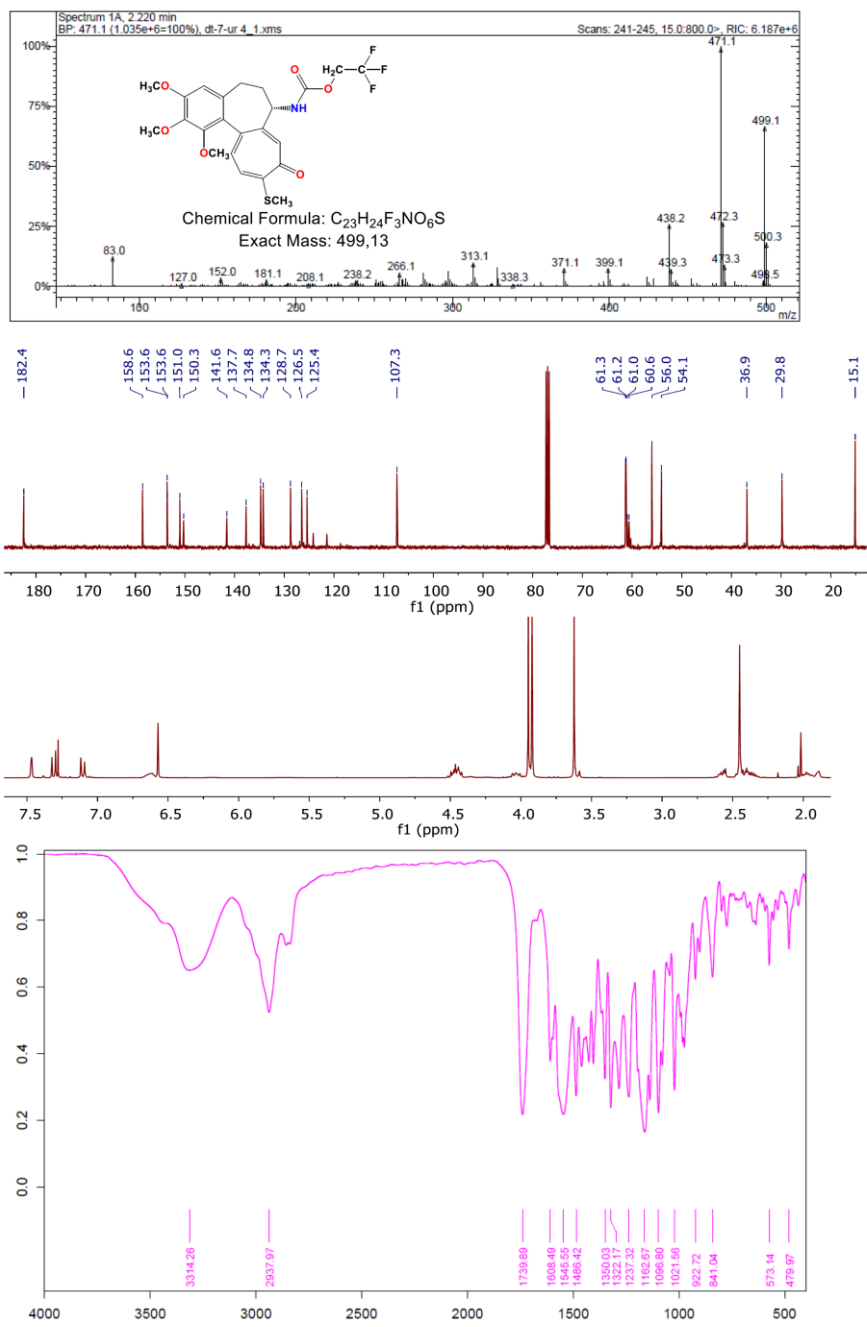


Figure E-14. Spectroscopic characterization of compound 14.

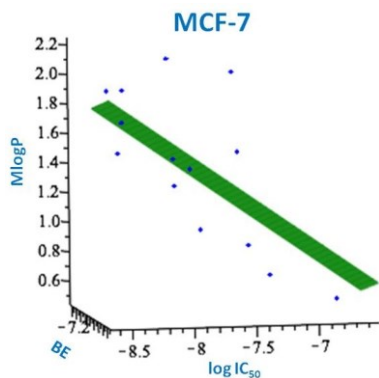


Figure E-15. 3D plots of the linear regression results for the binding energies (BE) vs MlogP vs $\log IC_{50}$ [μM] values for MCF-7 cell line.

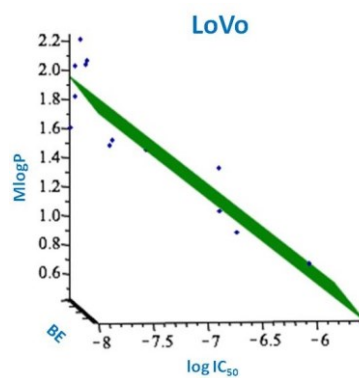


Figure E-16. 3D plots of the linear regression results for the binding energies (BE) vs MlogP vs $\log IC_{50}$ [μM] values for LoVo cell line.

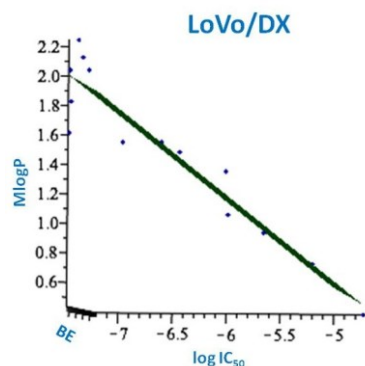


Figure E-17. 3D plots of the linear regression results for the binding energies (BE) vs MlogP vs $\log IC_{50}$ [μM] values for LoVo/DX cell line.

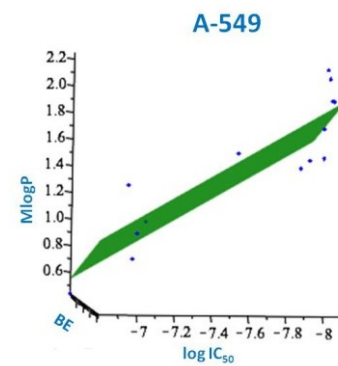


Figure E-18. 3D plots of the linear regression results for the binding energies (BE) vs MlogP vs $\log IC_{50}$ [μM] values for A-549 cell line.

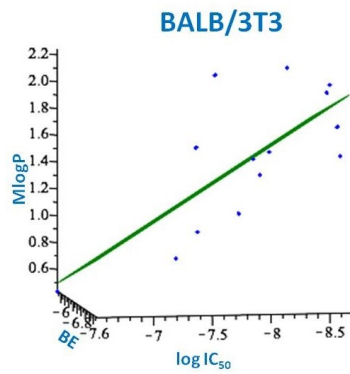
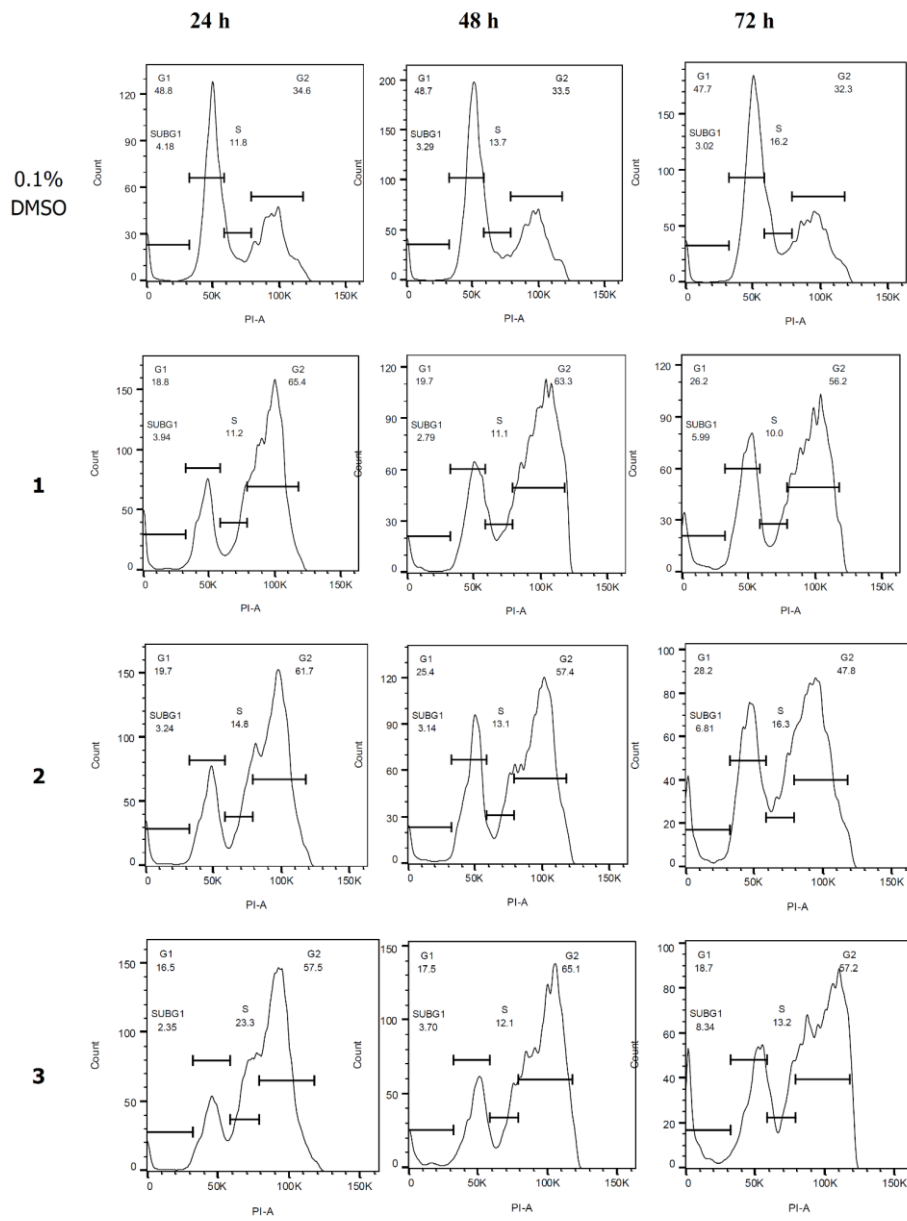


Figure E-19. 3D plots of the linear regression results for the binding energies (BE) vs MlogP vs $\log IC_{50}$ [μM] values for BALB/3T3 cell line.



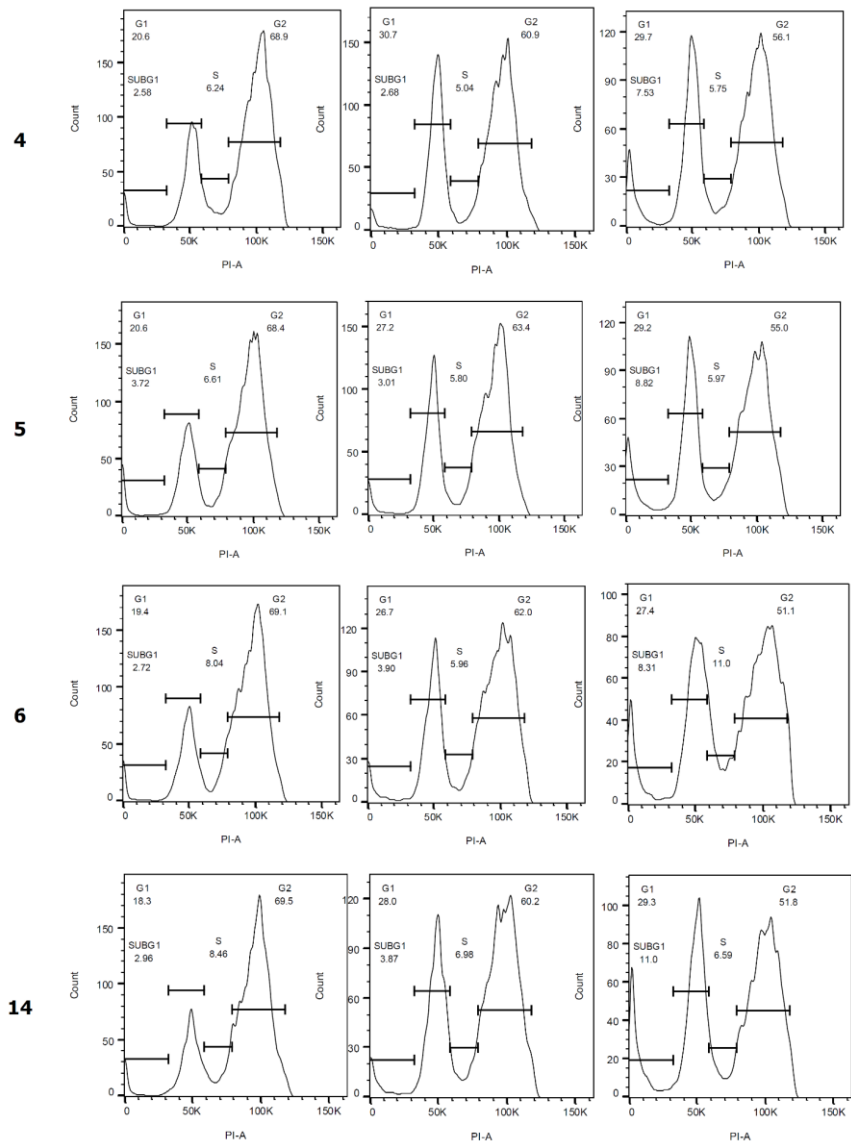


Figure E-20. Colchicine and its analogs, induce G₂/M phase arrest. MCF-7 cells were treated with 10 x IC₅₀ values of the indicated compounds, for 24, 48 or 72 h, and subjected to propidium iodide staining and flow cytometry, as described in Experimental section. The proportion of cells in different cell cycle phases or with sub-G1 DNA is indicated numerically and by the bars. Data shown are representative of three independent experiments.